Current Topics in Microbiology and Immunology

Esteban Domingo
Peter Schuster *Editors*

Quasispecies: From Theory to Experimental Systems

Springer

Current Topics in Microbiology and Immunology

Volume 392

More information about this series at http://www.springer.com/series/82

Esteban Domingo · Peter Schuster
Editors

Quasispecies: From Theory to Experimental Systems

Responsible Series Editor: Michael B.A. Oldstone

Springer

Editors
Esteban Domingo
Centro de Biología Molecular Severo Ochoa (CSIC-UAM)
Campus de Cantoblanco
Madrid
Spain

Peter Schuster
Institut für Theoretische Chemie
Universität Wien
Vienna
Austria

and

The Santa Fe Institute
Santa Fe, NM
USA

ISSN 0070-217X ISSN 2196-9965 (electronic)
Current Topics in Microbiology and Immunology
ISBN 978-3-319-23897-5 ISBN 978-3-319-23898-2 (eBook)
DOI 10.1007/978-3-319-23898-2

Library of Congress Control Number: 2016930545

Printed on acid-free paper

This Springer imprint is published by SpringerNature
The registered company is Springer International Publishing AG Switzerland

In memory of
Christof Biebricher and
Emmanuel Tannenbaum

Foreword

The concept of the quasispecies will soon be 50 years old. This term I introduced in the late 1960s in my considerations on self-organization of matter and the evolution of biological macromolecules.

The idea of heterogeneous populations has been quite uncommon in biology. Population biology considered mutation as a rare event and even in the absence of selective differences Kimura's theory of neutral evolution predicted a very low fraction of mutants. Molecular biology, on the other hand, was showing that correct reproduction and mutation are parallel reaction channels, which inevitably result in a distribution of genotypes. Heterogeneity in populations of bacteriophages has been verified experimentally in the laboratory of Charles Weissmann at about the same time. Chemical kinetics of replication and mutation built a firm bridge from molecular biology to evolutionary theory and provided the basis for the design of evolution experiments in the test tube. These included the work of Sol Spiegelman and his group as well as that of Christof Biebricher, who conducted research on replication of RNA from the bacteriophage Qβ in my laboratory. Biebricher's fundamental experiments on exploring the chemical kinetics of in vitro evolution laid the foundation for the forthcoming applications of the theory in evolutionary biotechnology and antiviral pharmacology. Without his careful and detailed work on Qβ-phage RNA, we would not now be able to understand Darwinian evolution in the test tube.

The dedication of the volume to the memory of Christof Biebricher recognizes his pioneering research on quasispecies. Esteban Domingo and Peter Schuster present fourteen selected chapters written by experts who revisit the concept of quasispecies, review the current status in theory and experiment, and provide an overview of its application to virus evolution. This book should find a place in every Life Science collection.

Göttingen
July 2015

Manfred Eigen

Preface

Quasispecies theory has come of age, and regular updates of the concept of mutation-caused diversity of populations are appropriate in order to provide straightforward access to information on recent progress in theory and applications to the real-world problems. Among a great variety of other applications, the concept of viral quasispecies, the limitation of sustainable mutation rates through error thresholds, and its usage in the development of antiviral therapies are most prominent. Indeed viral infection of hosts, epidemic spread of viral diseases as well as evolution of virus species can hardly be understood in depth without the notion of quasispecies and sufficient knowledge on their evolutionary dynamics.

Within the last decade, progress in the theory of quasispecies came mainly from two developments: (i) the accessibility of real fitness landscapes due to the enormous technical improvements in sequencing and high-throughput techniques and (ii) the exploitation of the formal mathematical analogy of quasispecies dynamics and statistical mechanics of classical and quantum spin systems. In the latter case, Eigen's quasispecies concept and Crow and Kimura's mutation-selection model give rise to identical mathematical problems, and therefore, the distinction between the two approaches is often not made with sufficient clarity: Mutation in the quasispecies theory is a parallel process to correct replication and happens during reproduction, whereas mutation and replication are entirely two separate processes in the Crow–Kimura model and occur at different instants. In virus reproduction, the former case applies and, accordingly, only the quasispecies concept is the appropriate model. Another important issue concerns the mechanism of mutagen-induced extinction of viral populations. A change in the mutation rate through certain pharmaceutical compounds, notably nucleotide analogues, is considered as the causing principle. This antiviral mechanism has been popularized under the name "lethal mutagenesis." Quasispecies theory predicts a maximal error rate that is compatible with a stable virus population. The antiviral strategy is to destabilize and extinguish the virus population by a drug-induced increase of the mutation rate that generates defective genomes that drive the virus population through the error threshold. There is also a second mechanism of extinction which

consists in increasing the fraction of lethal variants in the population above the maximum required for survival. As shown in several chapters of this book, both mechanisms are in operation and by now the interplay of error threshold phenomena and lethal mutagenesis is well established.

Since the CTMI volume 299 on Quasispecies published in 2006, major progress has been based in developments on the scope of applicability of quasispecies theory, the implementation of ultra-deep sequencing to analyze mutant spectra of viral populations, and the confirmation of the profound biological effects that changes in replication fidelity have on virus behavior. John Holland wrote in the 2006 volume the closing chapter on a historical perspective of major transitions in the understanding of RNA viruses. He emphasized the recognition of viral quasispecies dynamics as a major development in RNA virology. Sadly, John passed away on October 11, 2013. As people convinced of the role of viral dynamics to understand viral disease, we were very fortunate that John's laboratory became involved in this area of research, after a long and productive career that resulted in fundamental contributions in virology. Indeed, John Holland established the concept of cellular receptors as determinants of tissue tropism and did pioneering work on viral polyprotein synthesis and processing, and in the characterization and biological activities of defective interfering (DI) RNAs and particles (see the "In Memoriam" note by K.R. Spindler and B.L. Semler in Journal of Virology 88: 5903–5905, 2014). He recognized high mutation rates as key to the understanding of competition dynamics between vesicular stomatitis virus and its DIs. Expanding on this, his laboratory made key contributions to measurements of viral mutation rates, to the understanding of viral quasispecies, and to establish connections between quasispecies and several concepts from classic population genetics. His work permeates most of the chapters on experimental quasispecies in the present volume, with a number of topics which are now pursued with the new experimental, theoretical, and bioinformatic tools that have become available over the last years.

The present volume consists of fourteen chapters. Chapter "What Is a Quasispecies? Historical Origins and Current Scope" provides an introduction into the concept of quasispecies and its applications. The next chapter "The Nucleation of Semantic Information in Prebiotic Matter" deals with the concept of semantic information and its origin in biology. The simplest systems that can be studied by both extensive computation and in vitro experiments showing adaptation and evolution are small RNA molecules that are described in chapter "Evolution of RNA-Based Networks." The interplay of fitness landscapes and mutation-selection dynamics in particular with respect to quasispecies formation and the existence of error thresholds is treated in chapter "Quasispecies on Fitness Landscapes." Chapter "Mathematical Models of Quasispecies Theory and Exact Results for the Dynamics" deals with the application of methods from quantum statistical mechanics to derive solutions for the quasispecies concept and the Crow–Kimura mutation-selection model. The quasispecies concept can be extended to much more complex reproduction mechanisms than asexual reproduction and mutation as is shown in chapter "Theoretical Models of Generalized Quasispecies." Chapter "Theories of Lethal Mutagenesis: From Error Catastrophe to Lethal Defection" reviews models of lethal

mutagenesis, with a critical assessment of their relevance to experimental observations. Chapter "Estimating Fitness of Viral Quasispecies from Next-Generation Sequencing Data" reveals how new developments in deep sequencing can provide an increasingly accurate picture of viral population structure, and fitness landscapes based on the quasispecies model. Chapter "Getting to Know Viral Evolutionary Strategies: Towards the Next Generation of Quasispecies Models" discusses the difficulties of capturing the implications of complex mutant spectra, and the need to integrate theoretical and experimental approaches. In chapter "Cooperative Interaction Within RNA Virus Mutant Spectra," the fundamental issue of biological implications of interactions among components of a mutant spectrum is addressed. In chapter "Arenavirus Quasispecies and Their Biological Implications," replication of the important group of arenavirus pathogens is dissected at the molecular level to reveal the impact of genome variation; this chapter is a paradigm of the multiple facets of genome variation in viral pathogenesis and how to approach the problem experimentally. Chapter "Models of Viral Population Dynamics" connects theory and observation in the important area of dynamics of drug resistance in viral populations, centered on research on HIV-1. Chapter "Fidelity Variants and RNA Quasispecies" reviews the increasingly important field of copying fidelity mutants in viruses, and the book closes with chapter "Antiviral Strategies Based on Lethal Mutagenesis and Error Threshold" which is a review of recent developments on antiviral treatment designs based on lethal mutagenesis. We have tried to bring to the reader an updated account of quasispecies theory and experiment, and to reduce the gap between these two branches of research.

Madrid
Vienna
March 2016

Esteban Domingo
Peter Schuster

Contents

What Is a Quasispecies? Historical Origins and Current Scope 1
Esteban Domingo and Peter Schuster

The Nucleation of Semantic Information in Prebiotic Matter 23
Bernd-Olaf Küppers

Evolution of RNA-Based Networks 43
Peter F. Stadler

Quasispecies on Fitness Landscapes 61
Peter Schuster

Mathematical Models of Quasi-Species Theory and Exact Results for the Dynamics 121
David B. Saakian and Chin-Kun Hu

Theoretical Models of Generalized Quasispecies 141
Nathaniel Wagner, Yoav Atsmon-Raz and Gonen Ashkenasy

Theories of Lethal Mutagenesis: From Error Catastrophe to Lethal Defection 161
Héctor Tejero, Francisco Montero and Juan Carlos Nuño

Estimating Fitness of Viral Quasispecies from Next-Generation Sequencing Data 181
David Seifert and Niko Beerenwinkel

Getting to Know Viral Evolutionary Strategies: Towards the Next Generation of Quasispecies Models 201
Susanna Manrubia and Ester Lázaro

Cooperative Interaction Within RNA Virus Mutant Spectra 219
Yuta Shirogane, Shumpei Watanabe and Yusuke Yanagi

Arenavirus Quasispecies and Their Biological Implications 231
Ana Grande-Pérez, Veronica Martin, Hector Moreno
and Juan C. de la Torre

Models of Viral Population Dynamics 277
Pranesh Padmanabhan and Narendra M. Dixit

Fidelity Variants and RNA Quasispecies 303
Antonio V. Bordería, Kathryn Rozen-Gagnon and Marco Vignuzzi

Antiviral Strategies Based on Lethal Mutagenesis and Error Threshold 323
Celia Perales and Esteban Domingo

Author Index 341

Subject Index 351

What Is a Quasispecies? Historical Origins and Current Scope

Esteban Domingo and Peter Schuster

Abstract The quasispecies concept is introduced by means of a simple theoretical model that uses as little chemical kinetics and mathematics as possible but fully in the spirit of Albert Einstein who said: "Things should be made as simple as possible but not simpler." More elaborate treatments follow in the forthcoming chapters. It is shown that the most important results of the theory, in particular the existence of error thresholds, are not dependent on simplifying assumptions concerning the distribution of fitness values. Error thresholds are regularly found on landscapes with large and irregular scatter of fitness. After the introduction to theory, it will be shown how experimental data on the evolution of molecules or viruses may be fit to the theoretical model.

Contents

1 Evolution on the Cross-Road of Chemistry and Biology 2
2 A Few Quantitative Relations 6
3 What Happens Beyond Error Threshold? 8
4 Origin of the Experimental Quasispecies Concept 10
5 Quasispecies Theory and Experimental RNA Virus Quasispecies 12

E. Domingo (✉)
Centro de Biología Molecular "Severo Ochoa" (CSIC-UAM), Consejo Superior de Investigaciones Científicas (CSIC), Campus de Cantoblanco, 28049 Madrid, Spain
e-mail: edomingo@cbm.csic.es

E. Domingo
Centro de Investigación Biomédica en Red de Enfermedades Hepáticas y Digestivas (CIBERehd), Barcelona, Spain

P. Schuster (✉)
Institut für Theoretische Chemie der Universität Wien, Währingerstraβe 17, 1090 Vienna, Austria
e-mail: pks@tbi.univie.ac.at

P. Schuster
The Santa Fe Institute, 1399 Hyde Park Road, Santa Fe, NM 87501, USA

Current Topics in Microbiology and Immunology (2016) 392: 1–22
DOI 10.1007/82_2015_453

Published Online: 30 August 2015

6 Extensions of Quasispecies to Non-viral Systems 15
7 Limitations and Strengths of the Quasispecies Concept 18
References 19

1 Evolution on the Cross-Road of Chemistry and Biology

A theory of evolution at the molecular level was conceived by Manfred Eigen (Eigen 1971; Eigen and Schuster 1977, 1978a, 1978b) through merging population dynamics with the knowledge of molecular biology. In this way, evolution could be integrated into chemical kinetics without losing the characteristic features of biology, in particular the role of genetic information stored in nucleic acid molecules and the nature of mutations were fully preserved. The key to evolution is reproduction, and at the level of DNA or RNA, reproduction is replication, which can be simply understood as copying of genetic information, which is error prone in general but can be error free or correct in a particular replication event. Modeling the basic property of molecular copying mechanisms, correct replication and mutation are parallel chemical reaction channels (Fig. 1) and accordingly, the same model assumptions hold for low and high mutation rates. The assumption that mutation is a byproduct of replication is straightforward for virus populations. One important consequence of this assumption is the factorization of fitness and mutation effects that is indispensable for the fitness landscape concept, which turned out to be very useful in understanding viral infection (see, e.g., Kouyos et al. 2012). In population genetics, for particular in the Crow–Kimura model of asexual evolution (Crow and Kimura 1970, p. 265), replication and mutation are considered as independent events, but there an entirely different mechanism is assumed: Mutation is not related to reproduction and occurs by external action during the whole lifetime of the organism. In order to be able to study evolution of molecules, environmental conditions may be kept constant in the model, but the extension to changing condition is straightforward.

General results derived from the theory of molecular evolution in constant environment are as follows:

(i) In error-free replication,

$$\mathbf{A} + \mathbf{X}_k \rightarrow 2\mathbf{X}_k; \quad k = 1, 2, \ldots \mathrm{n}, \tag{1}$$

selection in the sense of Charles Darwin's survival of the fittest results from chemical reactions approaching a stable stationary state, and is a straightforward consequence of the reaction mechanism. The approach toward stationarity is accompanied by optimization of the mean fitness of the population. Accordingly, the mean fitness of the population $\bar{f}$ is steadily increasing during the selection process, the selected molecular species $\mathbf{X}_m$ is the one with the highest fitness value: $f_m = \max(f_1, f_2, \ldots, f_n)$, and survival of the fittest is

tantamount to optimization of the fitness of the entire population. The final result of selection is unique, a stationary homogeneous population containing only the fittest molecular species $\mathbf{X}_m$, no matter what the initial sequence distribution in the population was (provided it contained $\mathbf{X}_m$ at some, maybe very small amount).

(ii) Errors occurring during the replication process,

$$\mathbf{A} + \mathbf{X}_k \rightarrow \mathbf{X}_j + \mathbf{X}_k; \quad j,k = 1,2,\ldots n;\ j \neq k, \tag{2}$$

produce mutations (Fig. 1) and change the features of correct replication kinetics discussed in (i). After sufficiently long time, the replication–mutation process approaches a stationary state, which does not consist of not a single fittest species $\mathbf{X}_m$ only but is a collective of replicating variants, symbolized by γ. The name "quasispecies" has been coined for this longtime sequence distribution in order to point at the fact that asexual reproduction like sexual reproduction forms genetic reservoirs, which provide pools of variants for future evolution. For a given parameter set, the quasispecies is unique: No matter what the population looked like initially the same longtime sequence distribution will result. The question of fitness optimization is more subtle than in the previous case (i): For most initial conditions, fitness will increase during the replication–mutation process and selection of the quasispecies γ is

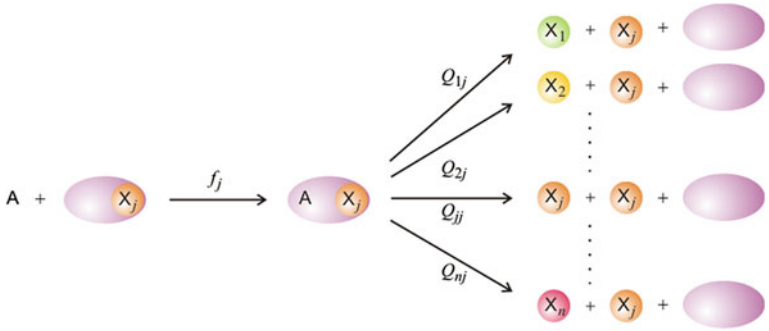

Fig. 1 A molecular view of replication and mutation. The replication device **E** (*violet*), commonly a single replicase molecule—as in polymerase chain reaction (PCR) or in many examples of simple viruses—or a multienzyme complex binds the template DNA or RNA molecule ($\mathbf{X}_j$, *orange*) in order to form a replication complex $\mathbf{E} \cdot \mathbf{X}_j$ and replicates with a rate parameter f_j. During the template-copying process, reaction channels leading to mutations are opened through replication errors. The reaction leads to a correct copy with frequency Q_{jj} and to a mutant $\mathbf{X}_k$ with frequency Q_{kj}. Commonly, we have $Q_{jj} \gg Q_{kj}$ for all $k \neq j$. In other words, correct replication dominates mutant formation. Stoichiometry of replication requires $\sum_{i=1}^{n} Q_{ij} = 1$, since the product has to be either correct or incorrect. The reaction is terminated by full dissociation of the replication complex. The sum of all activated monomers is denoted by **A**. A consequence of the model is factorization of the contributions from fitness and mutation: $w_{kj} = Q_{kj} \cdot f_j$

accompanied by an increase of the mean fitness $\bar{f}$ like in the mutation-free selection process. Nevertheless, situations are possible where this is not the case. Consider, for example, a homogeneous initial population consisting of the fittest genotype $\mathbf{X}_m$ only; then replication and mutation will create the quasispecies that contains other sequences too; these sequences have lower fitness; and mean fitness of the population is doomed to decrease during quasispecies formation: The paradigm of fitness optimization is invalidated. More complex cases can be constructed by choosing appropriate initial conditions, and then, the mean fitness may even change non-monotonously and go through a maximum or minimum during the approach toward the quasispecies γ. Optimization of mean fitness is not a global property in replication–mutation systems, but it is confined to a certain region of initial conditions. This region, the optimization region, is by far the largest part of the space of all possible initial conditions, and accordingly, optimization is observed in the majority of all replication–mutation experiments, artificial or in nature. Consequently, the Darwinian principle is a very powerful heuristic in the replication–mutation system, despite not being a universal law.

(iii) The population structure of quasispecies shows some regularities that turn out to be important for applications. The distribution of mutants is centered around a most frequent sequence called the "master sequence" $\mathbf{X}_m$, which commonly but not always is the sequence with largest fitness. The frequency of a mutant $\mathbf{X}_k$ in the stationary distribution is determined by two quantities: (a) the minimum number of point mutations or the Hamming distance d_{km} separating $\mathbf{X}_k$ from the master $\mathbf{X}_m$, and (b) the difference in the fitness values of the two sequences, $f_m - f_k$. Quasispecies theory explains also an empirical fact: The mean sequence of a population called the consensus sequence coincides with the master sequence unless the mutation rate is very high.

(iv) Considering the quasispecies as a function of the mutation rate p, a threshold phenomenon is predicted by the theory: Error-free replication leads to a quasispecies that contains the master sequence exclusively; the relative amount of the master sequence decreases gradually with increasing mutation rate p until a maximum mutation rate $p_{\max}$ is reached above which no stationary population exists; and no stable transfer of genetic information from generation to generation is possible (Fig. 2).

Chemical kinetics of RNA replication by means of virus-specific replicases is a rather complicated multistep process, but as Christof Biebricher (Biebricher 1983; Biebricher et al. 1983) has shown, conditions can be found under which the mechanism follows to a good approximation the simple autocatalytic overall kinetics mentioned above (Eq. 2). The conditions for the occurrence of the simple kinetics are excess material for RNA synthesis, here denoted by **A**, and replicating enzyme an RNA-specific RNA polymerase in excess to the template polynucleotide $\mathbf{X}_k$. Few enzymes can support synthesis of infectious viral genomic RNA in the test

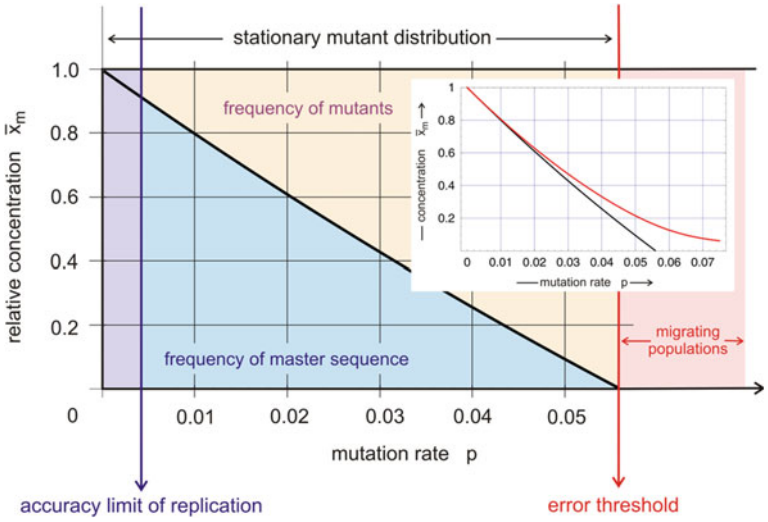

Fig. 2 The error threshold. The stationary frequency of the master sequence $\mathbf{X}_m$ is shown as a function of the local mutation rate p. In the approximation neglecting mutational backflow, the function $\overline{x_m}(p)$ is almost linear in the particular example shown here. In the insert, the approximation (*black*) is shown together with the exact solution (*red*). The error rate p has two natural limitations: (i) The physical accuracy limit of the replication process provides a lower bound for the mutation rate, and (ii) the error threshold defines a minimum accuracy of replication that is required to sustain inheritance and sets an upper bound for the mutation rate. Parameters used in the calculations: binary sequences, $l = 6$, $\sigma = 1.4131$

tube in the way Qβ replicase does (Biebricher 1983). Important advances in the enzymology of viral RNA replication have been made by Craig Cameron and his colleagues working with poliovirus polymerase. They devised simplified template-primer molecules that have allowed calculation of basic kinetic parameters for nucleotide incorporation, and the quantification of polymerase fidelity, an extremely important development, that will be discussed in several chapters of this book [(Castro et al. 2005) and references therein].

DNA replication involving some twenty or more proteins and enzymes is much more complex than RNA replication, but again suitable conditions can be found where the process can be approximated by simple autocatalysis (Eq. 2). Life cycles of viruses follow a complex multistep process with the overall stoichiometry $\mathbf{A} + \mathbf{X} \rightarrow n\,\mathbf{X}$ with n being the number of virions produced in one life cycle through the infection of a single cell. This process obeys the same laws as simple autocatalysis with the only difference that n reaction channels corresponding to n virions are chosen simultaneously rather than a single one (Fig. 1). Bacteria and more complex organisms adopt highly complex and perfectly controlled mechanisms of cell division that allow for modeling by simple autocatalysis since reproduction occurs at the level of cells rather than at the level of molecules. Simple autocatalysis (Eq. 2), direct or as overall kinetics, is the basis for the applicability of replication–mutation kinetics (Fig. 1) to the analysis of evolutionary phenomena sketched in the

next section. It is not unimportant to verify the overall mechanism of reproduction in order to make sure that quasispecies theory in the form presented here is applicable, particularly in the case of cell-free evolution of molecules.

2 A Few Quantitative Relations

The replication–mutation mechanism sketched in Fig. 1 can be cast into ordinary differential equations as used in conventional chemical kinetics:

$$\frac{\mathrm{d}x_j}{\mathrm{d}t} = \sum_{k=1}^{n} Q_{jk} f_k x_k - x_j \bar{f};\ j = 1, \ldots, n \quad \text{with} \quad \bar{f} = \sum_{i=1}^{n} f_i x_i \Big/ \sum_{i=1}^{n} x_i \tag{3}$$

The symbols used in this equation are as follows: The extensive variable $x_j = [\mathbf{X}_j]$ is the amount of species $\mathbf{X}_j$ present in the system expressed as concentration, but sometimes the usage of particle numbers $X_j = [\mathbf{X}_j]$ is of advantage, f_k is the fitness of species $\mathbf{X}_k$, $\bar{f}$ is the mean fitness of the population, and Q_{jk} finally is the frequency with which species $\mathbf{X}_j$ is produced as an error copy of $\mathbf{X}_k$ (Fig. 1). Considering the population as a whole, we introduce a total concentration or population size $c = \sum_{i=1}^{n} x_i$ and $\frac{\mathrm{d}c}{\mathrm{d}t} = \sum_{i=1}^{n} \frac{\mathrm{d}x_i}{\mathrm{d}t}$. Since all replication products are either correct or incorrect, we have a conservation relation $\sum_{j=1}^{n} Q_{jk} = 1$, the term $-\sum x_j \bar{f} = -c\bar{f}$ compensates exactly the population growth $\sum_{j=1}^{n} \sum_{k=1}^{n} Q_{jk} f_k x_k$, and the total concentration or population size is constant.

Exact solutions of Eq. (3) can be derived via an eigenvalue problem, and this implies that they are available in numerical form only (Jones et al. 1976; Eigen et al. 1989; Thompson and McBride 1974). For many purposes, however, approximations are perfect when they can be obtained in analytical form. We shall present here simple and illustrative expressions that are accurate enough for almost all practical purposes.

The most efficient approximation in this context is based on the assumption of "zero mutational backflow" (Eigen 1971): If the mutational flow from species $\mathbf{X}_k$ to species $\mathbf{X}_j$ is denoted by $\Phi_{k\to \mathrm{j}}$, we can symbolize the flow from the master to the mutation cloud by $\Phi_{m\to(\mathrm{j})}$ where (j) stands for $j = 1, \ldots, n; j \neq m$. Then, mutational backflow from the cloud to the master is written $\Phi_{m\leftarrow(\mathrm{j})}$. In other words, only mutations from the master sequence to the various mutants are allowed and all back mutations, $\mathbf{X}_j \rightarrow \mathbf{X}_m$, are forbidden. To be consistent, all mutations within the mutant cloud are neglected too. Equation (3) implies constant population size, and the modification of the mutation term requires a compensation in the flow term $-x_j\bar{f}$, which when introduced leads to a useful approximation for small mutation rates (see Chap. 4). Eigen leaves the flow term unchanged, and accordingly, the population size is no longer a constant. We shall denote this procedure that will turn out a posteriori as extremely successful as "phenomenological approach."

The mutation rate for single nucleotides, denoted by p, is assumed to be independent of the position on the sequence or, in other words, mutations are assumed to occur with the same frequency at each site. This approximation has been characterized as "uniform error rate" assumption, and it simplifies substantially the calculation of the mutation rates Q_{jk}. The probability to be copied correctly is the same for all sequences $\mathbf{X}_k$ and has the form

$$Q_{kk} = Q = (1-p)^l \quad \text{for all } k = 1, \ldots, n, \tag{4a}$$

where l is the chain length of the polynucleotide. This equation comprises the trivial fact that for error-free replication, $p = 0$, all copies are correct. Then, the fraction of correct replicas decreases monotonously with increasing mutation rate p (Fig. 2). The error containing copies $\mathbf{X}_j$ are obtained with the frequency

$$Q_{jk} = (1-p)^{l-d_{jk}} p^{d_{jk}} = Q\varepsilon^{d_{jk}} \quad \text{with} \quad \varepsilon = p/1-p \tag{4b}$$

The exponent d_{jk} is the Hamming distance between the two sequences $\mathbf{X}_j$ and $\mathbf{X}_k$. The Hamming distance is the (minimal) number of positions in which the two sequences differ. With these approximations and notations, it is straightforward to calculate the stationary concentration of the master sequence $\mathbf{X}_m$ that we denote by $\hat{x}_m^{(0)}$:

$$\hat{x}_m^{(0)} = \frac{Q - \sigma_m^{-1}}{1 - \sigma_m^{-1}}\hat{c} \quad \text{with } \sigma_m = \frac{f_m}{\bar{f}_{-m}} \quad \text{and} \quad \bar{f}_{-m} = \frac{\sum_{i=1, i\neq m}^{n} f_i \hat{x}_i^{(0)}}{\hat{c} - \hat{x}_m^{(0)}}, \tag{5a}$$

where $\hat{c} = \sum_{i=1}^{n} \hat{x}_i^{(0)}$ and where we indicate stationary concentrations by a hat and the zero mutational backflow approximation by the superscript "(0)". The mean fitness of all sequences except the master or, in other words, the mean fitness of the mutants is denoted by $\bar{f}_{-m}$, and finally, σ_m is the superiority of the master expressing the ratio of the fitness of the master and the mean fitness of the rest of the population. For the mutants $\mathbf{X}_j$, we obtain by the same token

$$\hat{x}_j^{(0)} = \varepsilon^{d_{jm}} \frac{f_m}{f_m - f_j} \hat{x}_m^{(0)} = \varepsilon^{d_{jm}} \frac{f_m^2 (Q - \sigma_m^{-1})}{(f_m - f_j)(f_m - \bar{f}_{-m})} \hat{c}. \tag{5b}$$

In essence, the frequency at which a mutant is present in the quasispecies depends on two quantities: (i) the Hamming distance d_{jm} between sequence $\mathbf{X}_j$ and the master $\mathbf{X}_m$—the closer related to the master a sequence is the higher is its share in the stationary distribution—and (ii) the fitness difference between $\mathbf{X}_m$ and $\mathbf{X}_j$—the higher the fitness of the mutant, the higher is its frequency in the quasispecies. Accordingly, a quasispecies is not some arbitrary collective of variants but a highly ordered distribution with a master sequence in the center and mutant cloud surrounding it in sequence space.

Within the phenomenological approach, the stationary concentration of the master sequence as well as the concentrations of the mutations contains a factor $(Q - \sigma_m^{-1})$, which expresses the dependence of the concentrations on the mutation rate p, and vanishes if the condition $Q = \sigma_m^{-1}$ is fulfilled. The mutation rate $p_{\max}$ at which this happens is easily calculated:

$$Q = (1 - p_{\max})^l = \sigma_m^{-1} \quad \text{leading to} \quad p_{\max} \approx \frac{\ln \sigma}{l} \quad \text{or } l_{\max} \approx \frac{\ln \sigma}{p}. \tag{6}$$

The notation $p_{\max}$ points already at the fact that a conventional quasispecies exists only in the range $0 \leq p < p_{\max}$. As discussed in the next paragraph, at mutation rates higher than the threshold value, we get no information on the nature of the longtime solution of the replication–mutation system from the phenomenological approach. The phenomenon of a maximal mutation rate as described by Eq. (6) has been called the "error threshold": In order to guarantee evolutionary stability of the genetic information stored in nucleic acid sequences, the inaccuracy of replication must not exceed some critical value, which is defined by the sequence length l and the superiority of the master sequence σ_m. Alternatively, when the replication accuracy is given by some replication machinery, the error threshold defines some polynucleotide chain length $l_{\max}$ that cannot be exceeded without jeopardizing inheritance of genetic information. A comparison of the genome lengths of organisms from viroids to higher eukaryotes with replication machineries of largely different copying fidelity (Gago et al. 2009) yields a clear cut inverse relation between mutation rates and genome sizes. The error threshold concept has inspired an active field of antiviral research termed "virus transition into error catastrophe" or "lethal mutagenesis", consisting in virus extinction through defective viral gene products induced by excess of mutations (Chaps. 7 and 14).

It is important to stress that the existence of error thresholds is not restricted to a few model landscapes of fitness values. On the contrary, and as outlined in Chap. 5, all fitness distributions with strong scatter of the individual values show the threshold phenomenon and the width of the transition depends on the broadness of the dispersion of fitness values.

3 What Happens Beyond Error Threshold?

Since almost all analytical expressions of the quasispecies theory that are used in applications were derived within the frame provided by the phenomenological approach, we shall have a closer look on this assumption here. In particular, the error threshold in Eq. (6) has been derived from the application of the zero mutational backflow approximation to the mutation term, and therefore, it is legitimate to ask whether this result is a real phenomenon or an artifact of the approximation. First, we compare with the exact solution of Eq. (3) and consider the correct stationary concentration of the master sequence, $\bar{x}_m$, and its

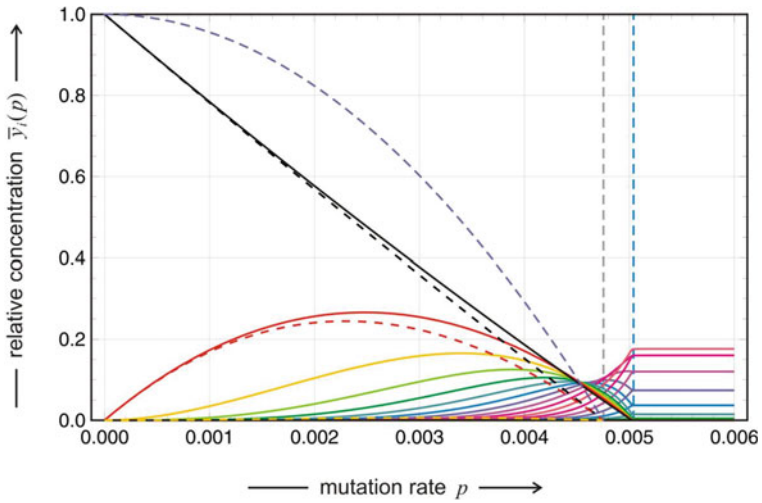

Fig. 3 The phenomenological approach. In the plot, the (*exact*) stationary solutions (*full lines*) are compared with the results derived from the phenomenological equations (*dashed lines*). The violet dashed line is the total relative concentration or population size in the phenomenological approach. The relative concentration of the master sequence (*black*) and the one-error class ($\bar{y}_1(p)$; *red*) agree well with the exact curves, whereas in case of all other error classes, the agreement is very poor (see, for example, $\bar{y}_2(p)$, *yellow*). The error threshold derived from the (*exact*) computation is $p_{\mathrm{cr}} = 0.00507$ (*dashed blue line* obtained from level-crossing and from class-merging as outlined in Chap. 5) and compares well to the value $p_{\mathrm{cr}} = 0.00475$ (*gray dashed line*) of the phenomenological approach. Choice of parameters: $l = 20$, single peak landscape with $f_m = 1.1$ and $f = 1.0$

approximation, $\hat{x}_m^{(0)}$. In order to facilitate the comparison, we assume that all sequences in a given error class have the same fitness. As illustrated in Fig. 3, there is little difference in the curves for master sequence and for the class of single point mutations. We remark that for sequences with two or more errors, this is not the case and the reasons for agreement and disagreement can be readily analyzed (Chap. 4 and Schuster 2012). Here, we use a plausibility argument: The dominant contribution to the mutational flow to one-error mutants comes from the master sequence, and it is taken into account correctly by the zero mutational backflow approximation. For mutants with two and more errors, the largest mutation flow comes from the mutants with one error less and mutations coming from other mutants are neglected. The take home lesson is that the phenomenological approach (5a) provides an excellent approximation for the master (5a) and the class of mutants carrying a single point mutation but only for them.

Whereas the stationary solution of the phenomenological approach is zero at the error threshold and becomes negative for $p > p_{\max}$ and thus no acceptable solution is available above threshold, the exact stationary solution becomes almost indistinguishable from the uniform distribution, which contains all variants—master sequence and mutants—at the same concentrations: $\bar{x}_m = \bar{x}_1 = \cdots = \bar{x}_n = \bar{c}/\kappa^l$, where κ denotes the size of the nucleotide alphabet. Numbers κ^l are

"hyperastronomical," for example, there are 3×10^{120} different sequences for the smallest viroid genome with the size $l \approx 200$ in the natural alphabet ($\kappa = 4$). Population sizes in evolution experiments with replicating molecules are the largest that can be achieved, they may be as large as 10^{15}, and this implies that in a sample with uniform concentrations, we would be dealing with values in the range $\bar{x} \approx 10^{-105}$. This result simply tells that uniform concentrations cannot exist, the only conceivable alternative are clonal populations migrating in the huge space of all sequences (Derrida and Peliti 1991; Huynen et al. 1996), and indeed no stationary population can exist for $p > p_{\max}$. The enormous size of sequence space has another consequence that will be important in several other contributions in this book: In practice, all realistic populations of viruses, viroids, or polynucleotide molecules are local in sequence space and no global solutions exist in reality. Under favorable circumstances like in case of the quasispecies, the global solutions coincide with some local solutions for all practical purposes. In other words, we can use the results of the quasispecies concepts up to a certain Hamming distance, and for mutants being further away from the master sequence, the results have no practical meaning. As described in several chapters of this book, many important phenotypic changes in viruses depend on one or few mutations. That is, the transitions between different phenotypes depend on short distance migrations (small Hamming distances) within the locally occupied sequence space.

4 Origin of the Experimental Quasispecies Concept

When the development of quasispecies theory and hypercyclic organization was well advanced (Eigen 1971; Eigen and Schuster 1979), Charles Weissmann and his colleagues were in the process of founding "reverse genetics", a term first proposed by Weissmann four decades ago (Weissmann et al. 1977). The principles of reverse genetics were established using the RNA *Escherichia coli* bacteriophage Qβ as model system. Sol Spiegelman had achieved replication of Qβ RNA in the test tube (in the absence of cells or cells extracts) by using Qβ RNA as template, purified Qβ replicase and a host factor protein as the replicative machinery, and nucleoside triphosphates under adequate ionic conditions (particulary the presence of Mg^{2+}). This reaction mixture supported efficient synthesis and many-fold amplification of genomic Qβ RNA (Mills et al. 1967). The experimental system allowed in vitro RNA evolution experiments by introducing selective pressures (intercalating dyes, ribonuclease, etc.) during RNA synthesis. The in vitro evolution experiments of Spiegelman were one of the incentives of Eigen to develop his first mathematical treatment of error-prone replication (Eigen 1971).

Weissmann and colleagues applied the in vitro Qβ RNA synthesis with the purpose of producing specific, site-directed mutants in bacteriophage Qβ and to analyze the biological consequences of the mutation introduced. Until then, the standard procedure in genetics was to generate mutations at random by chemical

mutagenesis and then select and study viruses (or cells) with a desired phenotypic trait. Hence, the term "reverse genetics" refers to the opposite strategy, to generate a precisely known mutation at a genomic site and to study its consequences.

One of the Qβ RNA genomic regions of interest at the time was the 3′-extracistronic (untranslated) region (3′-UTR) because of its conservation among related bacteriophages. Weissmann's team developed the procedure to generate specific 3′-UTR mutations taking advantage of a unique property of Qβ replicase that allowed a stepwise Qβ RNA synthesis (by limiting the types of nucleoside triphosphates made available to the replicase at each synthesis step) until a desired position at the growing minus (complementary) strand was reached. Then, a mutagenic nucleotide analogue was incorporated at the selected position, and the complementary strand synthesis completed by allowing the reaction to proceed with the four standard nucleotides (Flavell et al. 1974). While a first mutation introduced at 3′-UTR position 16 was not viable despite the RNA being efficiently replicated by Qβ replicase (Flavell et al. 1974), a mutant RNA with an A → G transition at position 40 (termed mutant 40) from the 3′-end yielded progeny virus upon transfection on *E. coli* spheroplasts (Domingo et al. 1976). However, the mutant reverted to the wild type with a kinetics sufficiently slow to permit quantifying the proportion of mutant 40 and true wild-type revertants as a function of passage number. Competition between wild type and mutant 40 Qβ phages in *E. coli*, and reversion of the mutant to wild type in the course of serial passages, allowed Eduard Batschelet to calculate a mutation rate for the G → A reversion of 10^{-4} substitutions per genome doubling (Batschelet et al. 1976). Despite the calculation referring to a single genomic site, the value obtained is quite representative of mutation rates for RNA viruses that were subsequently estimated by other procedures (Steinhauer and Holland 1986; Eigen and Biebricher 1988; Ward and Flanegan 1992; Drake 1993; Drake and Holland 1999; Sanjuan et al. 2010).

In the course of the experiments on site-directed mutagenesis, the RNA of many biological clones of bacteriophage Qβ was analyzed by T_1-oligonucleotide fingerprinting, a method of nucleotide sequence sampling used at the time because cDNA synthesis, molecular cloning, and rapid sequencing were not available. Martin Billeter had sequenced and mapped in the Qβ genome the large T_1-oligonucleotides so that changes in the fingerprints could be interpreted by the occurrence of point mutations in the RNA (Billeter 1978). The result of the survey of biological clones was astonishing: Virtually, the RNA of each biological clone from a multiply passaged phage population differed in one to two nucleotide positions from the average sequence of the corresponding parental population. Experiments in which individual biological clones were passaged to generate heterogeneous populations led to the following conclusion "A Qβ phage population is in a dynamic equilibrium, with viable mutants arising at a high rate on the one hand, and being strongly selected against on the other. The genome of Qβ phage cannot be described as a defined unique structure, but rather as a weighted average of a large number of individual sequences " (Domingo et al. 1978).

We know now that this statement applies to RNA viruses in general, as evidenced by work by many authors, initiated with foot-and-mouth disease virus (FMDV) by

Esteban Domingo and colleagues (Domingo et al. 1980; Sobrino et al. 1983) and vesicular stomatitis virus (VSV) by John Holland and colleagues (Holland et al. 1979, 1982). The early work on experimental quasispecies with bacterial, animal, and plant RNA viruses, as well as its impact for RNA genetics, was reviewed during the decade that followed the initial Qβ work (Domingo et al. 1985, 1988).

5 Quasispecies Theory and Experimental RNA Virus Quasispecies

During the 1970s, transdisciplinarity in science was less intense than today probably because of limited means of information exchange among practitioners of different scientific disciplines. Also, while theoretical physicists often asked general and fundamental issues of broad significance, experimental biologists focused on more detailed questions. Molecular biologists approached basic (but specific) problems of genome organization and expression, while virologists aimed at understanding viruses as disease agents. In the prevalent view at the time, disease mechanisms were unrelated to evolutionary concepts, a situation which is no longer tenable at present. Despite science compartmentalization, Manfred Eigen held a highly multidisciplinary Max Planck Winter Seminar at the Swiss village of Klosters, a stimulating scientific forum that continues until nowadays. In Winter 1978, Weissmann presented the experimental results on Qβ genome heterogeneity, and Eigen was thrilled to see the principles of quasispecies theory at work with a real virus. This key Klosters encounter and its impact have been described (Domingo et al. 1995, 2001; Holland 2006; Domingo et al. 2012), and it was the beginning of a stimulating collaboration between theoreticians and experimentalists that is partly responsible for the writing of the present book.

There is general agreement among theoretical biologists and experimental virologists that the Qβ population dynamics is directly connected with the generation of mutant distributions inherent to quasispecies theory. Nevertheless, a few population geneticists questioned the relevance of quasispecies theory for RNA viruses and some are still questioning it today. The main point in their argument goes as follows: RNA viruses are steadily evolving and cannot form stationary mutant distributions as required by quasispecies theory because there is not enough time for reaching a mutational equilibrium, and therefore, RNA virus populations cannot be seriously approached within the framework of quasispecies theory. Instead, the claim is raised that RNA virus heterogeneity is an extension of the classical concept of genetic polymorphism known in population biology since the 1960s, the only distinctive feature being that mutation rates of RNA viruses are orders of magnitude higher than standard mutation rates of cells. It is worth noting that classical population genetics is based on the assumption of small mutation rates, and in the classical concept of polymorphism, alleles that were not present in at least 10 % of individuals of a biological species were not counted as polymorphic sites (Spiess 1977). Deep sequencing applied to analyses of mutant spectra is

presently revealing the presence of many minority genomes at much lower levels (for example, at the 0.1–1 % level that is the current range of cutoff values for reliable mutant frequencies), which are relevant players in the continuous dynamics of replacement of some minority subpopulations by others. This dynamics can certainly not be identified with genetic polymorphism in the classical sense.

Two points must be added here regarding the suitability of quasispecies as a theoretical framework for viral population dynamics. First, quasispecies theory is an extension of populations dynamics in order to make it fit for the incorporations of molecular data, and therefore, it is not incompatible with the classical Wright–Fisher models of mutation–selection balance (Wilke 2005). In fact, quasispecies theory enables going one step further due to the internal interactions within a mutant spectrum that converts the entire viral quasispecies into a unit of selection. Intra-mutant spectrum interactions can be of complementation (individuals display lower replicative fitness than the ensemble) or interference (infectivity of fully infectious individuals can be suppressed by the mutant ensemble). Several chapters of this book deal with intra-mutant spectrum interactions that frequently occur through *trans*-acting proteins expressed from viral genomes (see Chaps. 10 and 14). In the mutant distributions of quasispecies theory, the critical element that permits the quasispecies to behave as a unit of selection is the connectivity among closely related genomes established through frequent mutation. Cross talk among genomes is very intense when genomes are close neighbors in sequence space although more distant interactions may be also established thanks to the high connectivity of sequence space (Eigen and Biebricher 1988) (Chap. 4). Selection does not pull an individual but a connected set of individuals.

The equilibrium argument is worth being considered in more detail. It is commonplace stating that nothing on the Earth is at thermodynamic equilibrium because our planet as such is exposed to a steady flow of energy and entropy that goes from sun into outer space but nevertheless, there exists a plentitude of phenomena that are perfectly described by quasi-equilibrium theories. The notion quasi-equilibrium expresses the fact that a system looks as if it were in an equilibrium state within a certain time span but is changing on longer time scales. What matters here is not the fact of change in the long run, but the validity of timescale separation. In rigorous mathematical terms, the problem is characterized as center manifold reduction (Carr et al. 1981). In a nutshell, it says that the final state is approached in two phases (i) a fast process leading from the initial conditions to the center manifold, and (ii) a slow process during which the population moves along the center manifold to some final state. The question whether or not a quasi-equilibrium hypothesis can be justified, boils down to the existence or non existence of a center manifold (see Chap. 4). Here, we illustrate the concept of center manifold reduction by addressing its meaning for viruses and virus evolution: (i) The fast process is the formation of a mutation-balanced clan of sequences consisting of the master sequence and its most frequent mutants that are, in essence, derived from single or at maximum double nucleotide exchange mutations, and (ii) the selection-based and neutral drift of the population through the appearance of

rare mutations and the occurrence of environmental changes. A necessary condition for the existence of center manifold and the meaningfulness of the quasispecies concept as well as any other quasi-equilibrium model is the formation of frequent mutants that occurs faster than the environment changes or, in other words, the environment is essentially constant during the formation of the mutation-balanced clans. In case of viroids and almost all RNA viruses, the postulation of a quasi-equilibrium seems to be on the safe side because the mutation rate is in the order of one per replication event (Gago et al. 2009). One remark about the frequency of mutations is important here: According to Eq. (4b), this frequency is proportional to the mutation rate raised to a power being the Hamming distance between the mutant sequence $\mathbf{X}_j$ and the master sequence $\mathbf{X}_m$, $\varepsilon^{d_{jm}}$. Since the mutation rate p—or $\varepsilon = p/(1 - p)$—is small and the Hamming distance between to virus genomes can vary enormously, we shall be always dealing with a core of frequent mutants being at quasi-equilibrium with the master sequence and a plethora of rare variants whose appearance are a stochastic events. Neutrality with respect to fitness is another biological phenomenon that requires notions of stationarity, which are more sophisticated than simple quasi-equilibria (see Chap. 4).

Extensions of quasispecies theory to finite populations and variable fitness landscapes have been developed by many authors, including Eigen himself (Nowak and Schuster 1989; Alves and Fontanari 1998; Eigen 2000; Wilke et al. 2001; Nowak 2006; Ochoa 2006; Saakian and Hu 2006; Saakian et al. 2006; Takeuchi and Hogeweg 2007; Saakian et al. 2009; Park et al. 2010; Schuster 2010a, 2010b). Finite quasispecies populations in variable fitness landscapes are further treated in Chaps. 3 and 4 of this book. In theoretical biology, it is quite frequent to develop a deterministic model in mathematically solvable terms and then to extend it to real situations by introducing stochastic components in the model formulation. The same schools that initially opposed quasispecies suggested also that the heterogeneity of mutant spectra had been overestimated due to misincorporations during the enzymatic procedures involved in the preparation of molecular clones for nucleotide sequencing. As discussed elsewhere (Arias et al. 2001; Domingo et al. 2004), these arguments have proven incorrect since the impact of artifactual mutations can be controlled, and they have not affected significantly the heterogeneity measurements. Application of deep sequencing methodologies has amply confirmed the extensive genomic heterogeneity of RNA virus populations (Chap. 8), in agreement with the results obtained by classic biological or molecular cloning and Sanger sequencing.

Thus, quasispecies theory (despite its limitations, see last section) has provided the theoretical framework to interpret key characteristics of RNA viral populations: extreme genetic heterogeneity, mutant ensembles acting as a unit of selection, evolution (both short-term or intra-host and long-term or inter-host) understood fundamentally as replacement of genome subpopulations by others, and movements in sequence space as the basis to generate new phenotypes which are extremely relevant to virus biology. These aspects are amply discussed in different chapters of the present volume.

Despite the overwhelming evidence of quasispecies dynamics for RNA viruses in their natural environment, a few geneticists still advocate using undefined terms such as "variation" (or similar) rather than quasispecies. Avoidance of the term quasispecies may be acceptable provided scientists are aware of the nature of viral populations. However, unexpected side effects can derive from ambiguous terms. Millions of dollars and euros have gone into projects on antiviral and vaccine strategies doomed to failure because quasispecies dynamics was not incorporated as a relevant feature prior to the designs. Thus, there are pressing scientific (and even economic!) arguments to incorporate the term quasispecies in the fields of experimental and clinical virology. Several chapters of this book cover relevant aspects.

Different definitions of quasispecies have been used in physics, chemistry, and biology. In physics, quasispecies has been defined as a cloud in sequence space. To chemists, quasispecies are mutant swarms composed of related, nonidentical genomic sequences, the definition most familiar to virologists. To biologists, quasispecies is the target of selection, without the term implying a modification of the species concept in biology. In connection with the present volume, the most widely used quasispecies definition in virology is as follows: "a collection of related viral genomes subjected to a continuous process of genetic variation, competition, and selection that act as a unit of selection" (Domingo et al. 2012). Interesting new developments outside virology may require some more general definition of quasispecies that render it applicable to non-replicative systems. Some such developments are summarized next.

6 Extensions of Quasispecies to Non-viral Systems

Replication with a regular production of error copies is not privative of viruses, but it is a feature shared by cellular and subcellular systems endowed with replicative machineries that display limited template-copying fidelity. Connections have been made between viral quasispecies and cellular collectivities in two aspects: (i) error-prone replication with its ensuing competition dynamics among cells and (ii) collective behavior arising from interacting cell ensembles [for review see (Mas et al. 2010; Ojosnegros et al. 2011; Domingo et al. 2012; Solé et al. 2014)].

Concerning the first aspect, error-prone replication is prominent in mutator bacteria (which are characterized by mutation rates which are 10^2- to 10^3-fold larger than standard bacterial mutation rates) as well as in cancer cells. In both cases, enhanced mutation rates provide a selective advantage to the cells, either to expand the range of phenotypes for increased adaptability or to enhance cellular proliferation. A difference with viral quasispecies is in place here. The capacity of exploration of the sequence space available to viruses is far greater than the capacity exhibited by cells. The main reason is the difference in genome size between cells and viruses in relation to the usual population size of viruses and cellular organisms in nature. As an example, a viral genome of 10,000 nucleotides has a maximum of 3×10^4 single mutants, a number which is lower than the population size of many

viruses, that can attain 10^{10} to 10^{12} particles per infected individual. All single mutants and many multiple mutants are potentially present (excluding fitness effects) in a viral population infecting a single host. In contrast, the potential number of single mutants in a mammalian genome will approach 10^{10}, a far larger value than the population size of mammalian species. These and other parameters [population heterogeneity, number of mutations needed for a biological change, and fecundity or the capacity to generate progeny; see further discussion in (Domingo et al. 2012)] render quasispecies a far more effective adaptive strategy for viruses than for cells, even if their population dynamics follow similar principles.

Cancer cell dynamics has been extensively studied both theoretically and from a clinical perspective. Martin Nowak reviewed the conceptual origins of cancer viewed as a genetic disease, the types of genetic lesions that render cancer cells an error-prone system that favors tumor progression, and the basic mathematics of tumor cell proliferation (Nowak 2006). Very early work emphasized the relevance of cancer cell heterogeneity, clonal evolution, and the consideration of tumor metastasis as an adaptive process (Nowell 1976; Nicolson 1987). Recent models view cancer as cell collectivities that have restricted their functional genetic information to that required for cell integrity and proliferation, but free of the constraints inherent to cellular differentiation (Gatenby and Frieden 2002; Solé et al. 2014). This is reminiscent of the result of evolution of Qβ RNA in the test tube (the classic Spiegelman–Weissmann passage experiments discussed earlier) in which maintenance of RNA infectivity was no longer needed, and the only remaining requirement to the RNA was to replicate. In the words of the authors: "What will happen to the RNA molecules if the only demand made is the Biblical injunction, multiply, with the biological proviso that they do so as rapidly as possible?" (Mills et al. 1967). The result was selection of RNAs with extensive deletions than were adapted to bind efficiently to the replicase and to undergo rapid replication; infectivity was rapidly lost.

The search for the minimum requirements for cancer cell proliferation may help providing the basis to produce an error catastrophe in cancer (Solé and Deisboeck 2004; Fox and Loeb 2010), following the strategy under investigation for viruses (Chaps. 7 and 14). Tumor cell heterogeneity is a determinant of adaptability and limits the efficacy of anticancer drugs, because of the ease of selection of drug-escape mutant cells through several molecular mechanisms. The problem of treatment failure due to selection of drug resistance within a tumor cell population is very similar to that faced in the case of viral infections (Chaps. 12 and 14), and strategies alternative to the standard anticancer chemotherapeutic protocols have been suggested (Gatenby et al. 2009; Luo et al. 2009). In the course of adaptive RNA virus evolution in natural environments, in particular during intra-host expansions of viral populations, mutation rates are expected to remain constant, except in rare cases in which a specific fidelity mutation may be incorporated in the viral polymerase gene and become dominant. In contrast, the cascade of molecular events during cancer progression, mainly mutations that increase the cell division rate and mutations that increase the cellular mutation rate (that include tumor suppressor genes, oncogenes and genetic instability genes), is more complex. As a

consequence, and interestingly, mutation rates are unlikely to remain constant through tumor progression. Evolutionary dynamics under constant versus increasing mutation rates deserves further theoretical and experimental investigation.

Concerning collective behavior due to cell to cell interactions, they have been also recognized within tumors, in particular regarding competition between fitter chemosensitive cells and less fit, drug-resistant cells during therapy (Gatenby et al. 2009). A parallel with the internal interactions among components of mutant spectra in viruses (Chaps. 10 and 14) has been also found in the behavior of bacterial collectivities [(Ojosnegros et al. 2011) and references therein]. In particular, quorum sensing in bacteria has been proposed as a factor to modulate virulence, so that an important biological trait is the result of cooperative interactions among individuals.

Recently, a striking conceptual parallelism has been established between the conformational heterogeneity of prions and viral quasispecies (Li et al. 2010; Weissmann et al. 2011; Weissmann 2012). Prions are infectious agents composed only of protein, without a nucleic acid. They are propagated through transmission of a misfolded form of a cell-coded protein (Castilla et al. 2008; Barria et al. 2009). Despite having the same amino acid sequence, distinguishable prion "strains" are characterized by different conformations. A "mutation" in a prion represents a change in conformation that may occur through environmental changes and confer altered pathogenic potential and drug sensitivity (Ghaemmaghami et al. 2009; Mahal et al. 2010). As in the case of viruses, both drug-resistant and drug-dependent prions can be selected (Oelschlegel and Weissmann 2013). Prion populations are heterogeneous in the sense that they include subsets of protein molecules with minority conformations, a parallel with the minority components of mutant spectra of viral quasispecies (Weissmann et al. 2011; Bateman and Wickner 2013; Vanni et al. 2014). Conformational variants can be either positively selected or remain in equilibrium with other variants (conformomers). In remarkable parallelism with viral quasispecies, the population size of a prion subjected to amplification can be a determinant of its evolution, and bottleneck transfers lead to reduced "replicative fitness" of prions (Vanni et al. 2014). How can such a parallel Darwinian behavior of a replicative and a non-replicative system originate? Mutations in genetic systems are the result of elementary molecular fluctuations events that determine base mispairings. Similar fluctuations may influence amino acid–amino acid interactions that determine protein conformation. A specific conformation may act as a nucleation point for the conversion of neighbor proteins into a similar conformation (Bernacki and Murphy 2009). Certainly, it would be extremely interesting to develop a theory for Darwinian evolution in non-genetic systems, search for protein transitional states and Darwinian behavior in proteins other than prions, and define the molecular basis of collective conformational transitions in protein ensembles. Such research may open new avenues for the control of neurological disease. Thus, the basic concepts emanating from quasispecies are permeating many domains of biological sciences, a demonstration of the experiment-provoking power of quasispecies theory.

7 Limitations and Strengths of the Quasispecies Concept

The concept of quasispecies refers to the level of populations in a homogeneous or mostly homogeneous environment, and this need not be realistic in case of real virus infections in heterogeneous host populations. In a sufficiently diverse population, for example, the master sequence in one host need not coincide with the master sequence in another host. Heterogeneity of environments may be important for many other reasons, but these are not quasispecies specific problems. Theoretical epidemiology is struggling with the effects of complex environments as well, and this for rather long time already.

In its current form, quasispecies theory does not account for stochastic effects. Small particle numbers up to several hundred infectious units can be important because of the autocatalytic nature of the replication process, and special stochastic effects such as incomplete packaging of genome segments in viruses with a segmented genome such as influenza A or early extinction due to replication accidents may need to be taken into account by virus-specific modeling. The major problem with stochastic modeling is not of principal nature. It concerns the numerical simulation techniques that are extremely time consuming even for medium-size systems and the unavailability of analytical methods for many component systems. The current best way to overcome this problem is to sacrifice generality and to construct virus group-specific stochastic models.

Although conceptually rooted in the same grounds as population genetics, the theory of the quasispecies has several advantages and can be more easily extended:

(i) The model is constructed at the molecular level, and this provides a frame that can be readily adapted to the desired level of details. The replication–mutation reaction (2) comprises the simplest conceivable mechanism. Provided one does not spare the effort, a detailed viral mechanism, for example, the RNA bacteriophage replication kinetics (Biebricher et al. 1983), could be introduced into the kinetic differential equations, and numerical analysis based on kinetic differential equations would be possible. By the same token, entirely different forms of reproduction can be incorporated, for example, the proliferation of prions (Weissmann et al. 2011) or mitosis of cancer cells (Gatenby and Frieden 2002; Gatenby et al. 2009). In the future, it will be desirable and possible to integrate complex regulation of gene expression into molecular models. Important examples are RNA-based epigenetic mechanisms.

(ii) Inherent in the molecular replication–mutation mechanism that understands mutation as a parallel reaction channel to correct copying is the possibility to factorize the selective value into one factor coming from the spectrum of fitness values and a second factor containing mutation frequencies. This handle on separability is not only an important tool for theoretical work but it also suggests to adopt two different strategies in the development of antiviral agents: reduction of fitness through interfering, for example, with the binding of the virus to the replication machinery or increase in mutation rate in order to drive the replicating virus beyond the error threshold.

(iii) The conventional quasispecies concept is based on the assumption that populations have reached a stationary or a quasi-stationary state. Although the validity of this assumption may be questionable, replication–mutation dynamics provides an appropriate tool for rigorous tests based on the center manifold theorem. The time a population system requires for a close approach to quasi-stationarity is well defined as a first passage time in the stochastic model and has been studied in the past [for an example with more references on this topic see the publication by Marin et al. (2012)]. Nevertheless, more detailed investigations are required to adapt the quasispecies theory questions concerning appropriate times, for example, the optimal duration of patient treatments.

(iv) Virus evolution is determined by the fitness landscape, which may be dynamic in a changing environment. Given a high degree of ruggedness as follows form empirical data, e.g., Kouyos et al. (2012) or the experience with biopolymer landscapes (Schuster 2006) quasispecies will commonly be unstable against changes in mutation rates. Quasispecies theory makes the prediction that migration into other regions in sequence space where "strong quasispecies" can be formed makes the population evolutionary stable (Chap. 4).

The application of quasispecies theory to the understanding of virus dynamics in infected organisms has opened the way to a rational design of antiviral interventions which until now have been basically an empirical endeavor. The increasing applicability of next generation, deep sequencing of viral populations as they replicate in their hosts, has unveiled the complexity of natural mutant spectra and estimates of relative fitness levels of minority genomes (Chap. 8). These analyses should permit personalized treatments with selected standard inhibitors and virus-specific mutagenic agents, used sequentially or in combination (Chap. 14). These are important practical consequences derived from the new understanding of viral populations that became clear when populations were examined under the focus of quasispecies theory.

Acknowledgments Peter Schuster wishes to acknowledge support by the University of Vienna, Wien, Austria and the Santa Fe Institute, Santa Fe, USA. Esteban Domingo acknowledges the support of grants BFU 2011-23604 and SAF2014-52400-R from Ministerio de Economía y Competitividad, grant S2013/ABI-2906 (PLATESA) from Comunidad Autónoma de Madrid, CIBERehd (Centro de Investigación Biomédica en Red de Enfermedades Hepáticas y Digestivas) which is funded by Instituto de Salud Carlos III, and Fundación Ramón Areces.

References

Alves D, Fontanari JF (1998) Error threshold in finite populations. Phys Rev E 57:7008–7013

Arias A, Lazaro E, Escarmis C, Domingo E (2001) Molecular intermediates of fitness gain of an RNA virus: characterization of a mutant spectrum by biological and molecular cloning. J Gen Virol 82:1049–1060

Barria MA, Mukherjee A, Gonzalez-Romero D, Morales R, Soto C (2009) De novo generation of infectious prions in vitro produces a new disease phenotype. PLoS Pathog 5(5):e1000421

Bateman DA, Wickner RB (2013) The [PSI+] prion exists as a dynamic cloud of variants. PLoS Genet 9(1):e1003257

Batschelet E, Domingo E, Weissmann C (1976) The proportion of revertant and mutant phage in a growing population, as a function of mutation and growth rate. Gene 1:27–32

Bernacki JP, Murphy RM (2009) Model discrimination and mechanistic interpretation of kinetic data in protein aggregation studies. Biophys J 96(7):2871–2887

Biebricher CK (1983) Darwinian selection of self-replicating RNA molecules. Evol Biol 16:1–52

Biebricher CK, Eigen M, Gardiner WC Jr (1983) Kinetics of RNA replication. Biochemistry 22:2544–2559

Billeter M (1978) Sequence and location of large RNase T_1 oligonucleotides in bacteriophage Qβ RNA. J Biol Chem 253:8381–8389

Carr J (1981) Applications of centre manifold theory. Springer, Berlin

Castilla J, Morales R, Saa P, Barria M, Gambetti P, Soto C (2008) Cell-free propagation of prion strins. EMBO J 27(19):2557–2566

Castro C, Arnold JJ, Cameron CE (2005) Incorporation fidelity of the viral RNA-dependent RNA polymerase: a kinetic, thermodynamic and structural perspective. Virus Res 107:141–149

Crow JF, Kimura M (1970) An introduction to population genetics theory. Harper & Row, New York (Reprinted at The Blackburn Press, Caldwell, NJ, 2009)

Derrida B, Peliti L (1991) Evolution in a flat fitness landscape. Bull Math Biol 53:355–382

Domingo E, Flavell RA, Weissmann C (1976) In vitro site-directed mutagenesis: generation and properties of an infectious extracistronic mutant of bacteriophage Qβ. Gene 1:3–25

Domingo E, Sabo D, Taniguchi T, Weissmann C (1978) Nucleotide sequence heterogeneity of an RNA phage population. Cell 13:735–744

Domingo E, Davila M, Ortin J (1980) Nucleotide sequence heterogeneity of the RNA from a natural population of foot-and-mouth-disease virus. Gene 11:333–346

Domingo E, Martínez-Salas E, Sobrino F, de la Torre JC, Portela A, Ortín J, López-Galindez C, Pérez-Breña P, Villanueva N, Nájera R, VandePol S, Steinhauer D, DePolo N, Holland JJ (1985) The quasispecies (extremely heterogeneous) nature of viral RNA genome populations: biological relevance–a review. Gene 40:1–8

Domingo E, Holland JJ, Ahlquist P (1988) RNA genetics. CRC Press, Boca Raton

Domingo E, Holland JJ, Biebricher C, Eigen M (1995) Quasispecies: the concept and the word. In: Gibbs A, Calisher C, García-Arenal F (eds) Molecular evolution of the viruses. Cambridge University Press, Cambridge, pp 171–180

Domingo E, Biebricher C, Eigen M, Holland JJ (2001) Quasispecies and RNA virus evolution: principles and consequences. Landes Bioscience, Austin

Domingo E, Ruiz-Jarabo CM, Arias A, Garcia-Arriaza JF, Escarmís C (2004) Quasispecies dynamics and evolution of foot-and-mouth disease virus. In: Sobrino F, Domingo E (eds) Foot-and-mouth disease. Horizon Bioscience, Wymondham

Domingo E, Sheldon J, Perales C (2012) Viral quasispecies evolution. Microbiol Mol Biol Rev 76:159–216

Drake JW (1993) Rates of spontaneous mutation among RNA viruses. Proc Natl Acad Sci USA 90:4171–4175

Drake JW, Holland JJ (1999) Mutation rates among RNA viruses. Proc Natl Acad Sci USA 96:13910–13913

Eigen M (1971) Self-organization of matter and the evolution of biological macromolecules. Die Naturwissenschaften 58:465–523

Eigen M (2000) Natural selection: a phase transition? Biophys Chem 85:101–123

Eigen M, Schuster P (1977) The hypercycle—a principle of natural self-organization. Part A: Emergence of the hypercycle. Naturwissenschaften 64:541–565

Eigen M, Schuster P (1978a) The hypercycle—a principle of natural self-organization. Part B: The abstract hypercycle. Naturwissenschaften 65:7–41

Eigen M, Schuster P (1978b) The hypercycle—a principle of natural self-organization. Part C: The realistic hypercycle. Naturwissenschaften 65:341–369

Eigen M, Schuster P (1979) The hypercycle. A principle of natural self-organization, Springer, Berlin
Eigen M, Biebricher CK (1988) Sequence space and quasispecies distribution. In: Domingo E, Ahlquist P, Holland JJ (eds) RNA genetics. CRC Press Inc, Boca Raton, FL., pp 211–245
Eigen M, McCaskill J, Schuster P (1989) The molecular quasispecies. Adv Chem Phys 75:149–263
Flavell RA, Sabo DL, Bandle EF, Weissmann C (1974) Site-directed mutagenesis: generation of an extracistronic mutation in bacteriophage Q beta RNA. J Mol Biol 89:255–272
Fox EJ, Loeb LA (2010) Lethal mutagenesis: targeting the phenotype in cancer. Semin Cancer Biol 20(5):353–359
Gago S, Elena SF, Flores R, Sanjuan R (2009) Extremely high mutation rate of a hammerhead viroid. Science 323:1308
Gatenby RA, Frieden BR (2002) Application of information theory and extreme physical information to carcinogenesis. Cancer Res 62(13):3675–3684
Gatenby RA, Silva AS, Gilles RJ, Frieden BR (2009) Adaptive therapy. Cancer Res 69(11):4894–4903
Ghaemmaghami S, Ahn M, Lessard P, Giles K, Legname G, DeArmond SJ, Prusiner SB (2009) Continuous quinacrine treatment results in the formation of drug-resistant prions. PLoS Pathog 5(11):e1000673
Holland JJ (2006) Transitions in understanding of RNA viruses: an historical perspective. Curr Top Microbiol Immunol 299:371–401
Holland JJ, Grabau EA, Jones CL, Semler BL (1979) Evolution of multiple genome mutations during long-term persistent infection by vesicular stomatitis virus. Cell 16:495–504
Holland JJ, Spindler K, Horodyski F, Grabau E, Nichol S, VandePol S (1982) Rapid evolution of RNA genomes. Science 215:1577–1585
Huynen MA, Stadler PF, Fontana W (1996) Smoothness within ruggedness: the role of neutrality in adaptation. Proc Natl Acad Sci USA 93:397–401
Jones BL, Enns RH, Rangnekar SS (1976) On the theory of selection of coupled macromolecular systems. Bull Math Biol 38:15–28
Kouyos RD, Leventhal GE, Hinkley T, Haddad M, Whitcomb JM, Petropoulos CJ, Bonhoeffer S (2012) Exploring the complexity of the HIV-1 fitness landscape. PLoS Genet 8:e1002551
Li J, Browning S, Mahal SP, Oelschlegel AM, Weissmann C (2010) Darwinian evolution of prions in cell culture. Science 327:869–872
Luo J, Solimini NL, Elledge SJ (2009) Principles of cancer therapy: oncogene and non-oncogene addiction. Cell 136(5):823–837
Mahal SP, Browning S, Li J, Suponitsky-Kroyter I, Weissmann C (2010) Transfer of a prion strain to different hosts leads to emergence of strain varriants. Proc Natl Acad Sci USA 107 (52):22653–22658
Marin A, Tejero H, Nuño JC, Montero F (2012) Characteristic time in quasispecies evolution. J Theor Biol 303:25–32
Mas A, Lopez-Galíndez C, Cacho I, Gomez J, Martínez MA (2010) Unfinished stories on viral quasispecies and Darwinian views of evolution. J Mol Biol 397(4):865–877
Mills DR, Peterson RL, Spiegelman S (1967) An extracellular Darwinian experiment with a self-duplicating nucleic acid molecule. Proc Natl Acad Sci USA 58:217–224
Nicolson GL (1987) Tumor cell instability, diversification, and progression to the metastatic phenotype. From oncogene to oncophetal expression. Cancer Res 47(6):1473–1487
Nowak MA (2006) Evolutionary Dynamics. The Belknap Press of Harvard University Press, Cambridge
Nowak M, Schuster P (1989) Error thresholds of replication in finite populations mutation frequencies and the onset of Muller's ratchet. J Theor Biol 137:375–395
Nowell P (1976) The clonal evolution of tumor cell populations. Science 194:23–28
Ochoa G (2006) Error thresholds in genetic algorithms. Evol Comput 14:157–182
Oelschlegel AM, Weissmann C (2013) Acquisition of drug resistance and dependence by prions. PLoS Pathog 9:e1003158

Ojosnegros S, Perales C, Mas A, Domingo E (2011) Quasispecies as a matter of fact: viruses and beyond. Virus Res 162:203–215
Park JM, Munoz E, Deem MW (2010) Quasispecies theory for finite populations. Phys Rev 81:011902
Saakian DB, Hu CK (2006) Exact solution of the Eigen model with general fitness functions and degradation rates. Proc Natl Acad Sci USA 103:4935–4939
Saakian DB, Munoz E, Hu CK, Deem MW (2006) Quasispecies theory for multiple-peak fitness landscapes. Phys Rev E 73:041913
Saakian DB, Biebricher CK, Hu CK (2009) Phase diagram for the Eigen quasispecies theory with a truncated fitness landscape. Phys Rev 79:041905
Schuster P (2006) Prediction of RNA secondary structures: from theory to models and real molecules. Rep Prog Phys 69:1419–1477
Sanjuan R, Nebot MR, Chirico N, Mansky LM, Belshaw R (2010) Viral mutation rates. J Virol 84:9733–9748
Schuster P (2010a) Genotypes and phenotypes in the evolution of molecules. In: Caetono-Anolles G (ed) Evolutionary genomics and systems biology. Wiley-Blackwell, New Jersey, pp 123–152
Schuster P (2010b) Mathematical modeling of evolution. Solved and open problems. Theory Biosci 130:71–89
Schuster P (2012) Evolution on 'realistic' fitness landscapes. Phase transitions, strong quasispecies, and neutrality. Santa Fe Institute working paper #12-06-006, Santa Fe Institute, Santa Fe
Sobrino F, Dávila M, Ortín J, Domingo E (1983) Multiple genetic variants arise in the course of replication of foot-and-mouth disease virus in cell culture. Virology 128:310–318
Solé RV, Deisboeck TS (2004) An error catastrophe in cancer? J Theor Biol 228(1):47–54
Solé RV, Valverde S, Rodriguez-Caso C, Sardanyés J (2014) Can a minimal replicating construct be identified as the embodiment of cancer? BioEssays 36:503–512
Spiess EB (1977) Genes in populations. Wiley, New York
Steinhauer DA, Holland JJ (1986) Direct method for quantitation of extreme polymerase error frequencies at selected single base sites in viral RNA. J Virol 57:219–228
Takeuchi N, Hogeweg P (2007) Error-threshold exists in fitness landscapes with lethal mutants. BMC Evol Biol 7(15):author reply 15
Thompson CJ, McBride JL (1974) On Eigen's theory of the self-organization of matter and the evolution of biological macromolecules. Math Biosci 21:127–142
Vanni I, Di Bari MA, Pirisinu L, D'Agostino C, Agrimi U, Nonno R (2014) In vitro replication highlights the mutability of prions. Prion 8:154–160
Ward CD, Flanegan JB (1992) Determination of the poliovirus RNA polymerase error frequency at eight sites in the viral genome. J Virol 66:3784–3793
Weissmann C (2012) Mutation and selection of prions. PLoS Pathog 8:e1002582
Weissmann C, Tanaguchi T, Domingo E, Sabo D, Flavell RA (1977) Site-directed mutagenesis as a tool in genetics. In: Schultz J, Brada Z (eds) Genetic manipulation as it affects the cancer problem. Academic Press, New York, pp 11–36
Weissmann C, Li J, Mahal SP, Browning S (2011) Prions on the move. EMBO Rep 12:1109–1117
Wilke CO (2005) Quasispecies theory in the context of population genetics. BMC Evol Biol 5:44
Wilke CO, Ronnewinkel C, Martinetz T (2001) Dynamic fitness landscapes in molecular evolution. Phys Rep 349:395–446

The Nucleation of Semantic Information in Prebiotic Matter

Bernd-Olaf Küppers

Abstract The analysis of the inherent context-dependence of genetic information suggests that there are evolutionary mechanisms which are independent of the processes of environmental adaptation and yet are able to push prebiotic matter towards functional complexity. In this regard, the extension of information space, by random prolongation of the primary structure of biological macromolecules, must have played a decisive role in the origin of life. On the one hand, the extension of information space is tantamount to an increase in the syntactic complexity of potential information carriers, which in turn is a prerequisite for the nucleation and evolution of semantic information. On the other hand, the increase in the dimensionality of information space expands the number of possible pathways of evolutionary optimisation and thereby improves the possible choices that can be made by progressive evolution. Alongside the optimisation of evolutionary optimisation itself, there are principles of evolutionary dynamics that direct the formation of functional order in prebiotic matter. Since these principles are constitutive for the proto-semantics of genetic information, they may be regarded as the elements of the semantic code of evolution.

Contents

1 Life = Matter + Information 24
2 Natural Selection of Information 26
3 Evolutionary Optimisation of Information 30
4 The Context-Dependence of Semantic Information 33
5 Overcoming Information Barriers 37
6 Deciphering the Semantic Code of Evolution 40
References 42

B.-O. Küppers (✉)
Friedrich Schiller Universität Jena, Jena, Germany
e-mail: bernd.kueppers@uni-jena.de

Current Topics in Microbiology and Immunology (2016) 392: 23–42
DOI 10.1007/82_2015_454

Published Online: 29 July 2015

1 Life = Matter + Information

The present-day understanding of living matter is based essentially on two fundamental assumptions, which are the epistemic guidelines of modern biology:

1. Living matter differs from non-living matter by its high degree of functional order. The transition from non-living to living matter is assumed to be a continuous one. This implies that there is no intrinsic difference between these two forms of matter.
2. The overarching concept for the understanding of living matter is the Darwinian theory of natural selection and evolution.

The claim that there is a continuous transition from non-living to living matter requires closer specification. First of all, we must think of it as a quasi-continuous transition, since matter itself is not a continuous substance. However, more important: Even if the transition is a quasi-continuous one, we still cannot draw a sharp borderline between non-living and living matter. For purely logical reasons, it is impossible to find a definition that expresses an intrinsic difference between the living and the non-living and which at the same time is free of tautology, i.e. of life-specific notions. Instead, the problem of defining life becomes a normative one; that is, the definition will always depend upon the particular paradigm that we regard as appropriate for an understanding of the phenomena of life (Küppers 2000).

The working hypothesis that the transition from non-living to living matter is a continuous one has also an important consequence for the methodology of modern biology. This is because it implies that in living matter the physical and chemical laws are valid, without any exceptions. Moreover, it follows that no additional laws are necessary for a deeper understanding of the phenomena of life. This, however, does not exclude the possibility that the laws of physics and chemistry operate in living matter as a special case—like for example Ohm's famous law, which is adhered to in an electrical circuit as a special case of the general laws of electrodynamics. "Special case" laws operate owing to the special organisation of matter, but they are not an inherent characteristic of matter itself. An important example from biology is the principle of natural selection (see below).

The consistent application of the idea that all life phenomena can in principle be reduced to the basic processes of physics and chemistry is known as the "reductionistic" research program of biology. Although this research program has been exceptionally successful in the past, it has been criticised again and again. Yet behind all the criticism hides a fundamental misunderstanding: the allegation that physics and chemistry still retain the naïve mechanistic view of Nature that was held at the end of the eighteenth century. However, this allegation is wrong. During the last two centuries, physics and chemistry have undergone perpetual change and have extended their theoretical concepts beyond a simple mechanistic understanding of matter.

One of the most important changes took place during the past decades during the development of the so-called structural sciences (Küppers 2000). This new branch

of science has arisen within the framework of the analysis of complex systems in Nature and society. The structural sciences pursue the goal of studying the abstract and overarching structures of reality, independently of the question of whether they are found in natural or artificial systems, in non-living or living matter. The best-known examples of this type of science are cybernetics, information theory, systems theory and game theory. Other disciplines—such as network theory, synergetics, complexity theory and the theory of fractals, to mention but a few—enrich the classical reservoir of structural sciences and are increasingly permeating the basic concepts of physics and chemistry as well.

Among all the structural sciences, the theory of information is of central importance for the theoretical understanding of biology, since all basic processes of life are instructed by information. Even the classical concept of Darwinian evolution received a firmer foundation under the influence of modern information theory, which makes the origin of life appear in a new light (Küppers 1990).

With regard to the all-encompassing role of information in living matter, it seems to be justified to rephrase the famous evolutionary dictum

> "Nothing in biology makes sense except in the light of evolution" (Dobzhansky 1973)

in the apodictic assertion

> "Nothing in biology makes sense except in the light of information" (Küppers 2000).

Although the concept of information has become the most important and successful concept for the theoretical understanding of living matter, it is very often called into question. Information, so the criticism, is a notion taken from our cultural world. It has its origin in human communication and can by no means be applied to natural objects. This is to say: matter and information are incommensurable notions and are essentially alien to each other.

However, the criticism does not hold. Information can perfectly well be reduced to physical terms and be applied to natural objects such as genes (Küppers 1992). To shed some light on this, we have to focus on the organisation of living matter. This organisation consists of a hierarchy of material boundaries at all levels of biological complexity (Küppers 1990). The notion of "boundaries" is borrowed from physics. In physics, the term "boundaries" normally denotes the constraints upon the system, like the walls of a gas container or the movement of a bead on a wire. In traditional physics, those boundaries are considered to be "contingent", i.e. they are neither random nor determined by laws. They can be as they are, but they could also have another form. If we change, for example, the walls of a gas container within moderate limits, this will not have any serious influence on the physical processes going on in the system. In contrast to systems of that kind, the boundaries of "functional" systems are exceptional in the sense that they are "non-contingent" properties of the system (Küppers 1992). This means that such systems are very critically dependent upon their boundaries, so that even a marginal change in the boundaries may lead to the collapse of the system's functional properties.

In other words, non-contingent boundaries are highly selective constraints upon the action of natural laws. They restrict all conceivable natural processes to those that are actually operating in the system. This is exactly the physical meaning of the notion of information in biology. It expresses the fact that all essential processes of a living system are instructed by specific physical boundaries, which are encoded in the detailed molecular structure of the genome.

From this point of view, a physical theory of the origin of life has to explain how under prebiotic conditions non-contingent physical boundaries could originate from contingent ones. Since the expectation value of a specific boundary condition—i.e. of the appearance of a macromolecule that carries biological information—is extremely small, specific boundary conditions could not originate by pure chance. However, the statistical analysis of this problem shows that such boundary conditions may appear through the selective self-organisation of matter (Küppers 1987). This suggests that the key for a physical understanding of the origin of genetic information may be sought in the physical foundation of the principle of natural selection.

2 Natural Selection of Information

For a long time, the Darwinian principle of natural selection seemed to be a physical riddle. Natural selection was considered either to be a tautology ("survival of the survivor") or to be a specific property of living matter that could not be reduced to the known principles of physics and chemistry. In fact, until the middle of the last century, the reproductive self-maintenance of living matter—obviously a necessary prerequisite for natural selection—was an unknown property in physics. The breakthrough came only with the epoch-making discovery of the molecular structure of DNA, which demonstrated that the capability of living beings to reproduce themselves is not an irreducible property of living matter, but rather a direct consequence of the physical and chemical properties of the genetic material. Two decades later, it was also demonstrated that Darwinian selection and evolution among molecules is in fact possible, and that such processes can even be simulated in the test tube under cell-free conditions (Mills et al. 1967).

These discoveries opened the door to a physical foundation of the principle of natural selection (Eigen 1971). Here, the first important step was to set up a model system, one that provides reproducible physical conditions for the investigation of the elementary processes of molecular evolution. Such a system has been termed an "evolution reactor". This is an experimental device that best can be compared to an idealised "prebiotic soup". The concept of the evolution reactor was initially a drawing-board idea that served the theoretical study of molecular evolution (Eigen and Schuster 1979; Küppers 1979, 1983). Later, it was also realised as a biotechnological instrument for the design of biochemical substances by means of artificial evolution.

The evolution reactor is essentially a chemical flow reactor, in which a population of self-reproducing biopolymers (e.g. nucleic acids) is competing for nutrients, i.e. energy-rich building-blocks (Fig. 1). Defined reaction conditions can be set up in the system by regulating the overall concentration of biopolymers as well as the supply of energy-rich building-blocks (monomers). Such conditions correspond largely to the experimental conditions under which Darwinian evolution among molecules has been demonstrated in the test tube (Kramer et al. 1974; Mills et al. 1967; Spiegelman 1971).

For a mathematical treatment of the selection process, one has to specify the model systems in more detail. Let us assume that the population inside the reactor consists of i different macromolecular sequences of equal chain length v, whose population numbers per unit volume we denote by x_i. We further assume that in the reactor vessel the total population $Z = \sum_i x_i$ is extremely small in comparison with the number n of all conceivable sequences. The assumption $Z \ll n$ complies with the conditions that presumably prevailed on the primitive Earth. Under this condition, the expectation value of a particular sequence is vanishingly small; it is therefore impossible that the initial distribution, existing in the system at the beginning, could have included all possible sequences.

Moreover, the reaction vessel is assumed to allow the inflow of energy-rich monomers and the outflow of energy-deficient monomers, as outlined in Fig. 1. In principle, there are two possibilities to exercise an experimental control over the

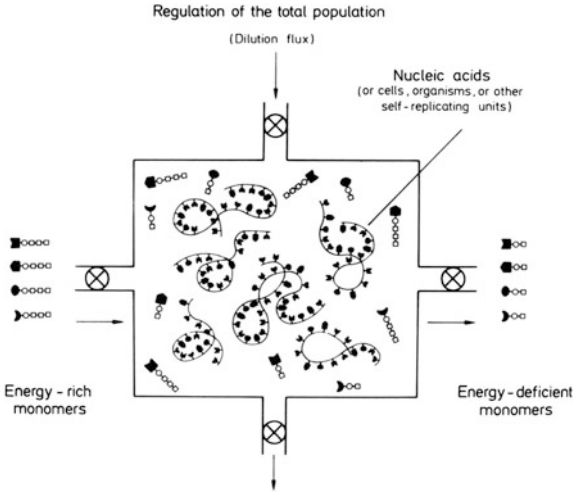

Fig. 1 A model system for the study of molecular self-organisation and precellular Darwinian evolution. In the reactor, there are biological macromolecules (nucleic acids) that are subject to permanent growth and decay. Growth takes place by the consumption of energy-rich monomers that are perpetually supplied to the system from outside (*left*). On the *right*, the energy-deficient decay products are perpetually removed from the system. A variable dilution flux (*top* to the *bottom*) allows the population to be adjusted and—for example—kept at a constant level. From Küppers (1990)

system by retarding or limiting its growth. One can either keep constant the overall population of macromolecules (CP conditions) or the flow rates of the various energy-rich materials (CF condition). In order to take into account Darwin's central idea of the selection mechanism, we introduce the CP assumption in our model system. Thus, the total population is held constant by a dilution flux that is unspecific, i.e. affects equally all substances present. We further assume separate rates of formation and decay of the various competing macromolecular species. In other words, we make the (in this case reasonable) approximation that the formation and decay of biological macromolecules are independent of one another.

We denote the amplification rate of the species x_i as A_i and its decay rate as D_i. The parameters A_i and D_i may depend on the concentrations x_j of other species. Finally we take account of mutability, in that we assume that only a part of the new copies of a particular sequence is error-free. The proportion of correct copies is expressed by a quality factor Q_i. This factor is dimensionless and lies by definition within the range $0 \leq Q_i \leq 1$.

The following equations (a full explanation can be found in Chaps. 1 and 3–5 of this book, as well as in Eigen 1971 and Küppers 1983) describe the change of the variables x_i:

$$\frac{\mathrm{d}x_i}{\mathrm{d}t} = (A_i Q_i - D_i)x_i - \sum_{j \neq i} \Phi_{ij} x_j - \bar{E}(t)x_i \quad (i,j = 1, \ldots, k), \tag{1}$$

where $\bar{E}(t)$, defined by

$$\bar{E}(t) = \sum_i (A_i Q_i - D_i)x_i / \sum_i x_i, \tag{2}$$

is the average rate of production of all molecular species.[1] In Eq. (1), $\bar{E}(t)x_i$ denotes a decay term that expresses the contribution made by the *i*th species to the turnover of individuals in the stationary state (Z = constant). The summed term $\sum_{j \neq i} \Phi_{ij} x_j$ is the contribution to the population number of the master sequence made by all mutant species $x_{j \neq i}$ as a consequence of "back mutation".

The set of Eq. (1) generally describes the kinetics of a reaction system characterised by the properties metabolism, self-reproduction and mutability.

1. *Metabolism* is expressed by the terms $\sum_i A_i x_i$ and $\sum_i D_i x_i$, which describe the turnover from energy-rich to energy-deficient monomers. In other words: The system is open with respect to a flow of matter and energy in the form of activated monomers.
2. *Self-reproduction* is expressed by the form of the reaction equations, in which the rate of formation of a molecular species x_i is proportional to its

[1] Strictly speaking, the $x_i(t)$ should be treated as discrete variables, and the differential equations should be replaced by difference equations. However, this would not alter the conclusions in any significant way, so for the sake of simplicity, we retain the continuous variables.

concentration, independently of how the kinetic parameters A_i and D_i depend on the concentrations x_j of the other species.

3. *Mutability* is expressed by the quality Q_i, which for real systems always fulfils the condition $0 < Q_i < 1$.

Metabolism, self-reproduction and mutability are all necessary conditions for a system being able to undergo evolution.

Let us take a closer look at the mechanism of selection and evolution. The parameters A_i, Q_i and D_i can be condensed into the quantity

$$W_i = A_i Q_i - D_i. \tag{3}$$

It is justified to denote W_i as the *selection value* of the species x_i. This is demonstrated by the following consideration, which is based on a simplification of Eq. (1). Let us assume that the reverse mutations $\sum_{j \neq i} \Phi_{ij} x_j$, which contribute to the species x_i, are negligible (as is the case for long chains). Making use of definition (3), we simplify the selection Eq. (1) and obtain

$$\frac{\mathrm{d}x_i}{\mathrm{d}t} = (W_i - \bar{E}(t))x_i \quad (i = 1, \ldots, k). \tag{4}$$

From this, the principle of natural selection follows directly as an extremum principle: All molecular species x_i whose selection value lies below $\bar{E}(t)$ are formed at a negative rate; that is, they die out. All species with a selection value above $\bar{E}(t)$ have positive rates of formation; that is, they increase in number. In consequence of this segregation process, the threshold $\bar{E}(t)$ is displaced to higher and higher levels. As a result, more and more species fall below the "threshold" value $\bar{E}(t)$ and die out. Selection equilibrium is reached when $\bar{E}(t)$ is equal to the greatest selection value in the population, that is,

$$\bar{E}(t) \rightarrow W_{\max}. \tag{5}$$

In selection equilibrium, $\bar{E}(t)$ is constant with respect to time:

$$\bar{E}(t) = W_{\max}. \tag{6}$$

Thus, the principle of selection is revealed within the framework of our model system as a physically justifiable extremum principle.

In the consideration above, the backflow terms $\sum_{j \neq i} \Phi_{ij} x_j$ have been neglected. However, we get the same results if we consider individual species not in isolation, but rather together with their accompanying mutant spectrum. In this case, the target of selection is not only the species with the greatest selection value (often called the "master sequence"), but rather the master sequence including its whole "tail" of mutants. This distribution is termed "quasi-species".

Mathematically, the selection equations of quasi-species are obtained by diagonalisation of the linear system of Eq. (1) after integrating factor transformation (for details see Chap. 3 of this book). If we denote the quasi-species by y_i and the corresponding eigenvalues by λ_i, then the selection kinetics are described by the following set of equations:

$$\frac{dy_i}{dt} = \left(\lambda_i - \bar{\lambda}(t)\right) y_i \quad (i = 1, \ldots, k). \tag{7}$$

This is structurally equivalent to the set of Eq. (4). However, in contrast to Eq. (4), which describes the selection kinetics of a single species x_i, Eq. (7) now describes the selection kinetics of the quasi-species y_i, i.e. the master sequence and its mutant distribution.

Ultimately, we come to the conclusion that the principle of natural selection is by no means an irreducible property of living matter. Rather, it is a consequence of physical and chemical laws, and it becomes manifest if matter has self-reproductive properties and is subject to limitation of growth. This result has also been verified by the extensive experimental investigations of the evolution of biological macromolecules in vitro (Kramer et al. 1974; Küppers 1979; Mills et al. 1967; Spiegelman 1971). These have demonstrated that a substantial part of the reductionist research program is sound.

3 Evolutionary Optimisation of Information

Let us consider the selection process described by Eq. (1) in more detail. For this purpose, it will be useful to introduce the concept of sequence space. This is a mathematical space whose coordinates cover all sequence alternatives of a given sequence of signs. In the abstract case, the signs are binary digits. In the present case, the signs are the monomers from which a biopolymer is composed. If we consider a biological macromolecule of length v, which is built up from μ classes of monomers, the total number of sequence alternatives n—and thus also the number of dimensions of the sequence space—is given by

$$n = \mu^v. \tag{8}$$

If population (or concentration) numbers are assigned to the "coordinates" of sequence space, one obtains the population (or concentration) profile. Alternatively, one can construct a "value profile" by assigning to each coordinate in sequence space the corresponding selection value W_i. The resulting "fitness landscape" is depicted in Fig. 2 in a greatly simplified manner. A precise mathematical description of the construction and the topological properties of sequence space can be found elsewhere (see for example Eigen 2013). From an information-theoretical point of view, sequence space may also be regarded as an information space, in which the selection of genetic information takes place.

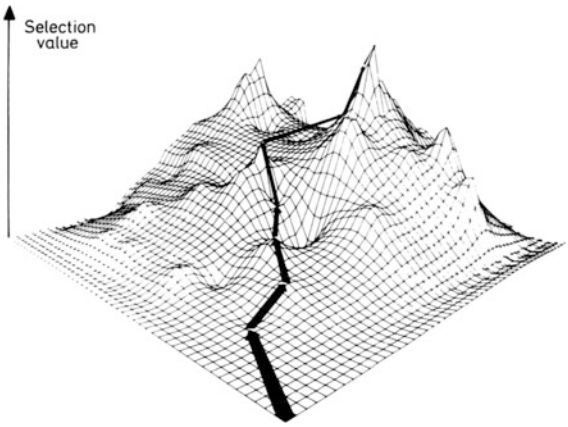

Fig. 2 Schematic representation of the adaptive surface in the sequence space. If all possible sequences n of a biological information carrier are represented as "coordinates" in sequence space and the selection value of the corresponding species is plotted over the appropriate coordinate, then an n-dimensional "mountain-range" profile is obtained, as shown here in a simplified, three-dimensional representation. The evolutionary origin of information then corresponds to a process of optimisation that leads from a low (local) peak to a higher (local) peak. From Küppers (1990)

Using this concept, we can describe the selection of a quasi-species as a condensation in information space (Eigen 2013). However, the resulting selection equilibrium is metastable. Whenever a species x_{i+1} appears that is selectively more favoured than the (hitherto) dominant species x_i, the original steady state collapses and a new selection equilibrium, characterised by the higher selection value of the now dominant species x_{i+1}, is attained. Thus, in the course of time, the system passes through a sequence of metastable selection equilibria, which can be described by a sequence of inequalities

$$W_{\max_1} < W_{\max_2} \cdots < W_{\text{opt}}. \tag{9}$$

Here, $W_{\max_i}$ is the selection value of the species x_i that dominates the selection equilibrium.

The physical significance of relation (9) can easily made clear by reference to a fitness landscape built upon sequence space (Fig. 2). Here the parameter $W_{\max_i}$ represents a local maximum of adaptation, that is, a peak in the value profile. Equation (9) restricts the evolutionary optimisation of the system, insofar as it defines a gradient in sequence space to which the route of optimisation is tied. In its evolutionary development, the system can only proceed along a route that takes it, starting from a local maximum, to a higher local maximum.[2]

[2]Strictly, this applies for the case of deterministic selection equations, in which fluctuations in the population are not taken into account.

From the foregoing discussion, we can draw the conclusion that the selection value of genetic information is clearly defined by the ability of a biological information-carrier to reproduce itself as fast as possible while maintaining high accuracy and stability. These are the conditions under which the selection value of a molecular species is maximised.

In the simplest case, W_i depends only upon the physical parameters P_k of the environment, such as temperature and energy flow. In a more general case, ecological coupling—such as the dependence upon the population size $x_{j\neq i}$ of other species—may appear. Thus, in general, W_i is a function that depends not only upon the parameters A_i, Q_i and D_i but also upon $x_{j\neq i}$ and P_k, that is:

$$W_i = W_i(x_{j\neq i}, P_k). \tag{10}$$

As expected, selection values reflect the complexity of living systems, including the complexity of their environment. It is therefore not surprising that the quantities W_i can only be specified physically for comparatively simple macromolecular systems. However, living systems are so complex—even at the lowest organisational levels—that their selection values can at best be given as phenomenological quantities.

The fact that selection values for living beings cannot be calculated explicitly has often given rise to the conjecture that Darwin's principle of the "survival of the fittest" is a mere tautology, because—it is said—the term "fittest" is defined alone by the fact of having survived ("survival of the survivor"). This is indeed the case for the non-Darwinian models of "neutral selection" (Kimura 1983). In these systems, in which all species are assumed to have the same selection values, a fluctuation in the population number of a certain species can amplify itself and finally reach the size of the whole population.

However, in the Darwinian model of natural selection, the situation is quite different. This becomes clear on examination of evolution in sequence space. The selection principle would be a tautology if the population profile, which represents the fact of "survival", and the value profile, which represents the "fitness" landscape, were to turn out to be identical. However, the physical analysis of Darwinian selection systems has shown that (as a rule) population profiles and value profiles possess different structures, which disproves the supposition of a tautology in the selection principle. This is seen, for example, in the case where one species in a population has the greatest selection value, but is present in a concentration lower than that of the mutant distribution arising from it. This is always the case when a dominant species reproduces itself with such a high error rate that just one copy is reproducibly preserved. At any moment, the stationary-state proportion of the selectively poorer mutants in the total population is greater than the proportion of the master copy, even though the mutants, seen as individuals, naturally die out again. The tautology asserted to lie behind the selection principle is thus falsified; its seeming existence is due to the extreme complexity of living systems and the resulting limits of their predictability.

The concept of sequence space allows further conclusions with regard to the origin and evolution of genetic information. In cases where selection values depend

only on environmental conditions, the structure of value space remains the same as long as the environment does not change. However, the assumption of a constant environment is an idealised condition: it cannot even be realised at the level of molecular evolution, since all individuals of a population of molecules contribute, with their physicochemical properties, to the environmental conditions of the population. Every change in the composition of a population must therefore lead to a change in the environment. In addition, the selection value of every single species will as a rule depend on the population variables of the other species taking part in selection, so that every evolutionary step changes the structure of the value profile (Eq. 10). This in turn means that goal and goal-directedness are interdependent. Since the elementary events (mutations) that lead to evolutionary changes are completely indeterminate, every evolutionary process is historically unique. This makes it clear that the molecular theory of evolution predicts only the *generation of genetic information as such*, but it does not predict the detailed outcome of evolution, as manifested in the *content of the genetic information*.

Equation (3), which defines the selection value, contains no details about the functional properties, which contribute to the parameters A_i, Q_i and D_i. Although it describes the "value" of an information carrier in a selection competition, its semantics are completely restricted to the aspect of selectivity. Yet the selection value, specified by Eq. (3), tells us nothing about the forces that determine the highly developed and differentiated semantics expressed in the functional complexity of living matter. For this reason, the semantics of genetic information are usually explained within the Darwinian theory of evolution a posteriori by appeal to plausibility. However, for a deeper understanding of the origin and evolution of genetic information, we need an approach to the semantic aspect of information that goes beyond the mere aspect of selectivity.

4 The Context-Dependence of Semantic Information

Semantic information is defined as "valued" information. The use of this expression already indicates that access to the semantic aspect of information must be sought by the receiver, which evaluates the information. In the widest sense, the receiver represents the "context" of the information. The context-dependence of information is a universal aspect of any kind of information. This is due to the fact that information in an absolute sense does not exist (Küppers 1995). Information obtains its meaning only in relation to its context. This is no less true of genetic information, which becomes operational—i.e. unfolds its meaningful content—only under certain physical and chemical conditions.

Because information in an absolute sense does not exist, each recipient needs some background information as a reference frame within which to evaluate the content of the information received. Even the task of identifying a piece of information "as" information requires some prior information, or prior knowledge, on the part of the recipient. This immediately raises a further question: How much

additional information is necessary in order to understand a given piece of (meaningful) information (Küppers 2013)?

At first glance, this question seems unanswerable, as it involves the problematic concept of "understanding". It is all the more surprising that an exact solution to this problem is nonetheless possible. However, to reach this solution one has to restrict the consideration to the minimum condition required for any kind of understanding (Küppers 2010). This minimum condition is the fact that the receiver must first register the information before the actual process of understanding can begin. This requirement is self-evident. It applies for every process of communication, independently of whether the communication takes place in a natural or an artificial system.

Let us analyse the consequences with regard to semantic information, written down in the letters of a human language. Even a superficial view of language reveals that any meaningful sequence of letters has an aperiodic structure. The reason for this is clear: only the use of aperiodic sequences opens up enough space for human language to code information and thus makes the unlimited richness of human language possible at all. If language were to use more or less periodic sequences of letters for coding information, the potential information space would be more or less empty.

This thought can be deepened by using the concept of algorithmic information theory, which has been developed within the framework of computer science. The core of algorithmic information theory is a measure of information that is linked to the "complexity" of a sequence of digits or symbols. A sequence of binary digits is to be considered as complex when the sequence cannot be compressed significantly, i.e. when there is no algorithm, shorter than the sequence itself, from which the sequence can be derived (see for example Chaitin 1987). According to this idea, the complexity K of a binary sequence s is given by the length L of the shortest program P of a computer C from which s can be generated:

$$K_{\mathrm{C}}(s) = \min_{C(P)=s} L(P). \tag{11}$$

In this definition, the complexity depends upon the *degree of incompressibility* of a sequence of binary digits. Two aspects of this definition must be emphasised: (1) The notion of "complexity", as introduced here, is completely equivalent to the notions of "aperiodicity" and "randomness". (2) The transition between non-complex sequences and complex sequences is obviously a continuous one.

Within algorithmic information theory, the measure of the information content of a message is its complexity, which in this case means the aperiodicity of its syntax. It is, as it were, the irreducible "bulk" of information that is contained in the message. If the complexity of a sequence of digits or symbols is at a maximum, then there is no algorithm that would be shorter than this sequence and by means of which the sequence or a missing part of it could be reconstructed. In this sense, the sequence is aperiodic or irregular. If, in contrast, the sequence is periodic (or largely periodic), then its inherent regularity would allow it to be compressed—or, if a part of the sequence were already known, this would allow the other part to be generated.

From this point of view, meaningful information in human language is always associated with aperiodic sequences. However, this statement should not be inverted! Not every aperiodic arrangement of letters in human language represents a meaningful sequence, nor does the aperiodicity of the syntax imply a random origin of the associated information. In short, the degree of aperiodicity is only a measure of the complexity of semantic information.

The assertion that semantic information is always encoded in aperiodic sequences will have important consequences for the recipient of this information (Küppers 2013). Since in this case there is no algorithm that allows the reconstruction of the whole sequence on the basis of a fragment of this sequence, the recipient must be in possession of the entire sequence, before the actual process of understanding its content can commence. In short, this means that the mere act of registration of an item of semantic information by a receiver demands that a certain quantity of information be already present with the recipient, and that this information has at least the same degree of complexity as the information that is to be understood.

This conclusion is generally valid. It remains unaffected by the fact that every language possesses syntactic rules according to which the words of the language are assembled into correctly formed sentences (Küppers 2013). Such rules only restrict the set of aperiodic sequences that can carry meaning at all. But they do not allow any inference to be made about the content itself. One can express this result in another way: semantic information cannot be compressed without loss of a part of its meaning. Of course, a piece of information may sometimes be reduced to its bare essentials, as done in telegram style or in boulevard newspapers, but some information is always lost in this process. In general, however, the loss of information is compensated for by a certain pre-knowledge of meaningful communication, which the receiver of this information possesses thanks to his cultural background, experience, prior agreements, etc.

The above conclusions rest totally on the assumption that semantic information is associated with random sequences. However, this is indeed a mere assumption, which we formulated on the basis of a plausibility consideration. We cannot prove it in any strict sense. Thus, it may be possible that there exist hidden algorithms that are able to generate a piece of semantic information, but which we have not discovered or identified so far. As soon as such a compact algorithm was found, however, our whole chain of arguments would break down.

Nevertheless, we can ascribe a high probability to our hypothesis by virtue of the fact that almost all binary sequences are random. It can easily be demonstrated in the following way. Let us consider all binary sequences of length v. Since the transition from random to non-random sequences is a continuous one, we must define a limit for randomness. Thus, we define all sequences with a complexity of—let us say—$K \geq v - 10$ as random. To this class of sequences belong all sequences which cannot be compressed by more than 10 bits.

We now ask how many sequences have a complexity below the threshold $K = v - 10$ and which could in principle be able to generate a sequence of complexity

$K \geq v - 10$. It is obvious that there are 2^1 sequences of complexity $K = 1$ with this property, 2^2 sequences of complexity $K = 2$, … and 2^{v-11} sequences of complexity $K = v - 11$. The number of all algorithms of complexity $K < v - 10$ thus adds up to

$$\sum_{i=1}^{v-11} 2^i = 2^{v-10} - 2. \tag{12}$$

As no algorithm with $K < v - 10$ can generate more than one binary sequence, there are fewer than 2^{v-10} ordered binary sequences. These make up one 2^{10}th of all v-membered binary sequences. This means that among all binary sequences of length v only about every thousandth sequence is non-random with a complexity $K < v - 10$. Thus, the overwhelming large fraction of all binary sequences indeed comprises random sequences.

To summarise the result: In order to understand a piece of information, one invariably needs a quantity of background information that has at least the same degree of complexity as the information that is to be understood. This finding gives the context-dependence of semantic information a highly precise form. It is generally valid, independently of the way in which the information is stored.

The foregoing conclusions can be applied immediately to the semantics of genetic information. This is not least because the sequence of nucleotides in the genome represents semantic information in the same way as the letters of a written text do.

As in the case of human language, a crucial feature of the genetic program is the aperiodicity of the sequence of nucleotides in the genome.[3] This in turn means that there are no hidden algorithms, i.e. no life-specific laws, that are able to order the monomers in a biological macromolecule in such a way that a piece of semantic information will originate (Küppers 1990). Since a random synthesis of meaningful information is excluded as well, only the Darwinian concept of evolution remains to explain the origin of semantic information in prebiotic matter (Küppers 1990).

In this regard, however, the Darwinian concept seems to leave an explanatory gap. This becomes clear if one takes into consideration the inherent context-dependence of information. Thus, from an information-theoretical point of view, evolution by adaptation must be regarded as a kind of communication between the sender and the receiver of information. The "sender" is the biological macromolecule with its information content, while the "receiver" of this information is the environment. The environment in turn represents an external source of information, which "evaluates" the content of genetic information according to the capability of the information carrier to survive under conditions of selection competition. However, within the Darwinian understanding of evolution, the

[3]That the aperiodicity must be the source for the complexity of living matter was already recognised at the dawn of molecular biology and led to the conjecture that chromosomes must have the structure of an "aperiodic crystal" (Schrödinger 1944).

environment, which directs the adaptation, is usually thought of as a *biotic* environment. Yet this environment is itself already enriched with semantic information. So where does this bulk of information come from? At the beginning of evolution no functional complexity, no meaningful information was present that could have provided a reference frame for progressive adaptation. The only environment that prevailed on the primordial earth was a world of physical laws and contingent boundaries. Thus, we must seek other principles of evolutionary dynamics—ones that act independently of the processes of adaptation and nevertheless push prebiotic matter towards the nucleation of functional complexity.

5 Overcoming Information Barriers

In the very early phase of the evolution of biological macromolecules, when a translation apparatus was not yet present, the target of selection could at best have been the phenotypic properties of the macromolecules themselves. This kind of selection, however, will most probably lead to a decrease of the chain length of potential information carriers, rather than to an increase. For, if there is no additional information encoded in the molecules, an increase in the chain length has no selective advantage under the constraint of fast reproduction. On the contrary, larger chain lengths would impede rapid reproduction and therefore lead to a selective disadvantage.

This conjecture was confirmed by the serial transfer experiment with the genome of the phage Q_β, where selection was aiming exclusively at the phenotypic properties of the genome (Mills et al. 1967). Thus, the chain length of the RNA was only preserved insofar, as it has to fulfil certain structural prerequisites for the reproduction by the enzyme. These are, in particular, the recognition signals of the template for the Q_β-replicase (Küppers and Sumper 1975). Consequently, the major part of the genetic information stored in the genome became eliminated in favour of fast reproduction.

Moreover, the serial transfer experiment underlines our previous conclusion that pure selection—i.e. selection decoupled from environmental adaptation—is not sufficient for the nucleation of semantic information. Instead, pre-existing semantic information may even become eliminated for the benefit of fast reproduction. Thus, in the early phase of molecular evolution, the nucleation of semantic information could only come about if there existed a principle that acted against the evolutionary tendency to reduce the complexity of macromolecular sequences.

In fact, alongside the mechanism of adaptation, there is a driving force of evolution that does not depend on the environment, but which nevertheless may lead to an increase in the chain lengths of biological macromolecules. This driving force turns out to be a special property of sequence space, in which information originates. It is related to the fact that, independently of the environmental conditions, the process of evolutionary optimisation becomes more effective in a

high-dimensional space than in a low-dimensional one. The reason for this is that a high-dimensional space opens up more possible pathways for optimisation than does a low-dimensional space, as is evident from Fig. 3. Consequently, in a high-dimensional space, there will be a greater probability of the evolutionary optimisation to avoid a dead end, where the system is captured in a local equilibrium of selection (Eigen 2013). This in turn means that any random extension of the chain length v of an information carrier will have a positive effect on the optimisation process itself. At the same time, an increase in the chain length of the sequences will lead to an increase in their capacity to encode meaningful information.

This finding is only apparently in contradiction to the result of the serial transfer experiment, in which under the constraints of fast reproduction, short RNA sequences have a selective advantage over long ones. In evolution it is quite common for antagonistic principles to act together in the evolutionary optimisation process without cancelling each other out. In fact, this kind of interaction seems to be indispensable for the nucleation of genetic information, as suggested by the concept of quasi-species (Eigen and Schuster 1979). During the very early stage of molecular self-organisation, when no proteins were present to catalyse the reproduction of potential information carriers, the quality of self-reproduction must be assumed to have been very low. This in turn places a fundamental limitation upon the amount of information that can be transferred reproducibly from one generation to the next.

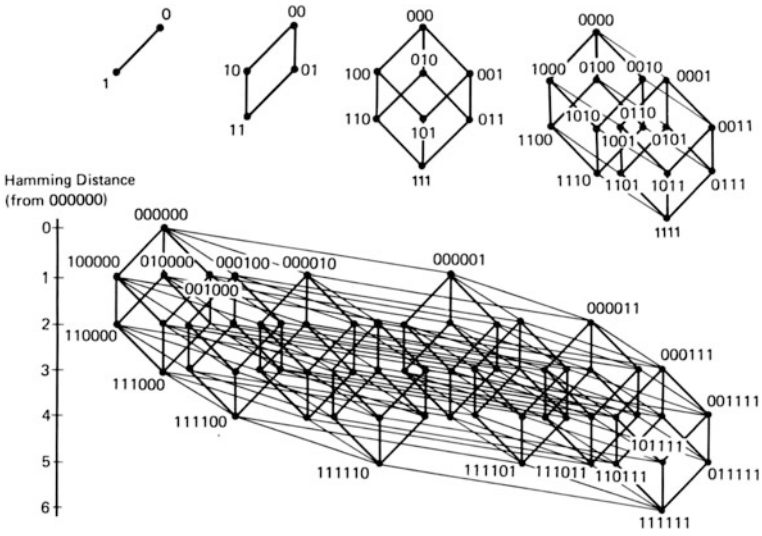

Fig. 3 Sequence space for binary sequences of chain length = 1, 2, 3, 4 and 6. The sequences are arranged according to the Hamming distance $d(ij)$, defined as the number of different positions between sequence i and sequence j. From Volkenstein (1994)

Detailed analysis of the error threshold has shown (Eigen and Schuster 1979) that, in a self-reproducing unit, the maximum number $\nu_{\max}$ of molecular symbols that can be transferred reproducibly across generations is given by equation

$$\nu_{\max} = \frac{\ln \sigma_m}{1 - \bar{q}_m}, \tag{13}$$

where $1 - \bar{q}_m$ is the average error rate per symbol and σ_m, defined by

$$\sigma_m = \frac{A_m}{\bar{E}_{k \neq m} + D_m}, \tag{14}$$

is the superiority factor of the species x_m, i.e. the advantage in growth of the master sequence x_m over its mutants $x_{k \neq m}$.

In the very early phase of prebiotic evolution, enzyme-free replication of RNA most probably involved per-digit error rates of 5×10^{-2}, which allows—depending on σ_m—the reproducible transfer of nucleic acid sequences between 14 and 60 nucleotides long (see Table 1). This amount of information is just enough to code for proteins with a rudimentary catalytic function, but is far from being sufficient for the formation of sophisticated functional order in prebiotic matter.

Thus, an important step in the solution of the problem of the origin of genetic information was the finding that the information barrier, which is a consequence of the error threshold, can be surmounted by the hypercyclic organisation of biological

Table 1 The amount of information ν_{max} that can be transferred reproducibly from one generation to the next, depending on the quality of the reproduction rate. From Eigen and Schuster (1979)

Digit error rate $1 - \bar{q}_m$	Superiority σ_m	Maximum digit content $\nu_{\max}$	Molecular mechanism and example in biology
5×10^{-2}	2	14	Enzyme-free RNA replication[a] t-RNA precursor, $\nu = 80$
	20	60	
	200	106	
5×10^{-4}	2	1386	Single-stranded RNA replication via specific replicases phage Q_β, $\nu = 4500$
	20	5991	
	200	10597	
1×10^{-6}	2	0.7×10^6	DNA replication via polymerases including proofreading by exonuclease *E. coli*, $\nu = 4 \times 10^6$
	20	3.0×10^6	
	200	5.3×10^6	
1×10^{-9}	2	0.7×10^9	DNA replication and recombination in eukaryotic cells vertebrates (man), $\nu = 3 \times 10^9$
	20	3.0×10^9	
	200	5.3×10^9	

[a]Uncatalyzed replication of RNA never has been observed to any satisfactory extent; however, catalysis at surfaces or via not specifically adapted proteinoids (as proposed by S.W. Fox) may involve error rates corresponding to the values quoted

macromolecules (Eigen 1971; Eigen and Schuster 1979). The cyclic coupling of self-reproducing information carriers into a hypercycle forces the competing information units to cooperate, which in turn leads to mutual stabilization of their information content and thereby to an increase in the total amount of information. The hypercycle, which combines competition with cooperation, is an important example of the balanced action of antagonistic principles in the early evolution of genetic information.

6 Deciphering the Semantic Code of Evolution

The hypercyclic organisation of nucleic acids and proteins must be considered as the archetype of genetic organisation, which is based on the principle of cooperation. With progressing evolution, other principles of evolutionary dynamics come into play, which refine the structure of genetic organisation. Besides cooperation, these principles include self-regulation, efficiency, recombination, flexibility, stability and others. They make possible the coexistence of information carriers, the overcoming of information barriers, resistance against perturbations and the integration of advantageous information. Although these principles are partly in conflict with each other, they act together in a well-balanced relationship, which allows the formation and evolutionary optimisation of functional order in prebiotic matter. They determine the proto-semantics of genetic information by fixing the functional frame for the development of genetic information. The detailed content of this information then emerges from the processes of adaptation to the environment.

In a certain sense, which is to be explained in more detail, the above principles can be conceived as elements ε_k of a semantic code of evolution C_{sem}, defined by

$$C_{\text{sem}} = \{\varepsilon_k\} \quad (k = 1, \ldots, n). \tag{15}$$

The general idea of a semantic code has been developed within the framework of structural sciences (Küppers 2013). It serves the purpose of getting a strict access to the semantic aspect of information. However, in contradistinction to the usual understanding of the notion of "code", the semantic code does not provide any rules for the assignment of symbols or sequences of symbols to another source of symbols. Instead, the semantic code represents the value scale that a recipient applies to a piece of information that he is going to decode in respect of its meaning.

Strictly speaking, the semantic code represents an evaluation scale that, by superimposition and specific weighting of its elements, restricts the value that the information has for the recipient and in this way becomes a measure of the meaning of the information. If the elements ε_k have the weights P_{jk} for the evaluation of a piece of information I_j by the recipient, then an adequate measure for the semantic value $\varepsilon(I_j)$ would be a linear combination of the weighted elements ε_k:

$$\varepsilon(I_j) = \sum_k p_{jk}\varepsilon_k \quad \text{with} \quad \sum_k p_{jk} = 1. \tag{16}$$

This measure, in turn, has the same mathematical structure as the entropy H of a message source $\{I_j\}$.

However, in place of the weighted messages, Eq. (16) now contains the weighted values ε_k of a chosen message I_j. In the limiting case, where the only value a recipient attaches to a message is its novelty, given by the expectation value of this message, Eq. (16) reduces to the information measure of classical information theory. At the same time, the number k is a measure of the fine structure of the evaluation scale: the greater k is, the sharper—i.e. the more highly differentiated—is the evaluation by the recipient.

The information value $\varepsilon(I_j)$ is a relative and subjective measure insofar as it depends upon the evaluation criteria applied by the recipient. However, for all recipients who use the same elements of the semantic code, and who for a given message I_j assign the same weights to these elements, $\varepsilon(I_j)$ is an objective quantity. Equation (16) describes the different value aspects, contributing to the overall value, which has some information for a receiver. In this abstract form, Eq. (16) applies to all systems in which semantic information is evaluated.

However, the evaluation of semantic information by a receiver requires some "pre-information". In human communication, the value scale is a highly specific one; it depends upon the recipient's prior knowledge, prejudices, desires and expectations. Therefore, the successful exchange of meaningful information requires standardisation of the framework of mutual understanding. This standardisation is achieved by precise co-ordination between the individuals of a community. However, in natural systems that exchange information, there is no explicit agreement about the value scale. Instead, the value scale is ultimately given—as in the case of Darwinian evolution—by the internal principles of evolutionary optimisation and the prevailing environmental conditions.

The semantic code, as introduced by Eq. (16), contains the elements that contribute (according to their weights) to the formation of functional organisation in prebiotic matter. The weights depend upon the type of organisation and the degree of evolutionary optimisation. Since the elements of the semantic code constitute the nucleation and improvement of genetic organisation itself, they epitomise in the true sense the creativity of natural evolution.

Finally, there arises the question of whether one can ascribe numbers to the weights of the different elements of the semantic code in the evolution of functional order. In view of the tremendous complexity of living matter and its physical boundaries, this seems to be an impossible task. Nevertheless, the elementary processes of natural evolution can be studied in the test tube under the idealised and reproducible conditions of controlled experiments. To this end, evolution reactors have been built, and these may also prove suitable for unravelling experimentally the semantic code of evolution and may thus lead to a deeper understanding of the general principles of the evolution of life.

References

Chaitin GJ (1987) Algorithmic information theory. Cambridge University Press, Cambridge
Dobzhansky T (1973) Nothing in biology makes sense except in the light of evolution. Am Biol Teach 25:125–129
Eigen M (1971) Selforganisation of matter and the evolution of biological macromolecules. Naturwissenschaften 58:465–523
Eigen M (2013) From strange simplicity to complex familiarity. Oxford University Press, Oxford
Eigen M, Schuster P (1979) The hypercycle. Springer, Berlin
Kimura M (1983) The neutral theory of molecular evolution. Cambridge University Press, Cambridge
Kramer FR, Mills DR, Cole PE, Nishihara T, Spiegelman S (1974) Evolution in vitro: sequence and phenotype of a mutant RNA resistant to ethidium bromide. J Mol Biol 89:719 (1974)
Küppers B-O (1979) Towards an experimental analysis of molecular self-organization and precellular Darwinian evolution. Naturwissenschaften 66:228–243
Küppers B-O (1983) Molecular theory of evolution. Springer, Berlin (reprinted 1985)
Küppers B-O (1987) On the prior probability of the existence of life. In: Gigerenzer G, Krüger L, Morgan MS (eds) The probabilistic revolution 1800-1930, vol 2. Probability in Modern Science, Cambridge/Mass, pp 355–369
Küppers B-O (1990) Information and the origin of life. MIT Press, Cambridge
Küppers B-O (1992) Understanding complexity. In: Beckermann A, Flohr H, Kim J (eds) Emergence or reduction. De Gruyter, Berlin, pp 241–256
Küppers B-O (1995) The context-dependence of biological information. In: Kornwachs K, Jacoby K (eds) Information. new questions to a multidisciplinary concept. De Gruyter, Berlin, pp 135–145
Küppers B-O (2000) The world of biological complexity: origin and evolution of life. In: Dick St. J (ed) Many worlds. Templeton Foundation Press, Pennsylvania, pp 31–43
Küppers B-O (2010) Information and communication in living matter. In: Davies P, Gregersen NH (eds) Information and the nature of reality. Cambridge University Press, Cambridge, pp 170–184
Küppers B-O (2013) Elements of a semantic code. In: Küppers B-O, Artmann S, Hahn U (eds) Evolution of semantic systems. Springer, Berlin, pp 67–85
Küppers B-O, Sumper M (1975) Minimal requirements for template recognition by bacteriophage Qß-replicase: approach to general RNA-dependent RNA synthesis. Proc Natl Acad Sci USA 72:2640–2643
Mills DR, Peterson RL, Spiegelman S (1967) An extracellular Darwinian experiment with a self-duplicating nucleic acid molecule. Proc Natl Acad Sci USA 58:217–224
Schrödinger E (1944) What is life? Cambridge University Press, Cambridge
Spiegelman S (1971) An approach to the experimental analysis of precellular evolution. Q Rev Biophys 4:213–253
Volkenstein MV (1994) Physical approaches to biological evolution. Springer, Berlin

Evolution of RNA-Based Networks

Peter F. Stadler

Abstract RNA molecules have served for decades as a paradigmatic example of molecular evolution that is tractable both in in vitro experiments and in detailed computer simulation. The adaptation of RNA sequences to external selection pressures is well studied and well understood. The de novo innovation or optimization of RNA aptamers and riboswitches in SELEX experiments serves as a case in point. Likewise, fitness landscapes building upon the efficiently computable RNA secondary structures have been a key toward understanding realistic fitness landscapes. Much less is known, however, on models in which multiple RNAs interact with each other, thus actively influencing the selection pressures acting on them. From a computational perspective, RNA–RNA interactions can be dealt with by same basic methods as the folding of a single RNA molecule, although many details become more complicated. RNA–RNA interactions are frequently employed in cellular regulation networks, e.g., as miRNA bases mRNA silencing or in the modulation of bacterial mRNAs by small, often highly structured sRNAs. In this chapter, we summarize the key features of networks of replicators. We highlight the differences between quasispecies-like models describing templates copied by an external replicase and hypercycle similar to autocatalytic replicators. Two aspects are of importance: the dynamics of selection within a population, usually described by conventional dynamical systems, and the evolution of replicating species in the space of chemical types. Product inhibition plays a key role in modulating selection dynamics from survival of the fittest to extinction of unfittest. The sequence evolution of replicators is rather well understood as approximate optimization in a fitness landscape for templates that is shaped by the sequence-structure map of

P.F. Stadler (✉)
Institute Für Informatik der Universität Leipzig, Härtelstraße 16-18,
04107 Leipzig, Germany
e-mail: peter.stadler@bioinf.uni-leipzig.de

P.F. Stadler
Max Planck Institute for Mathematics in the Sciences, Inselstraße 22,
04103 Leipzig, Germany

P.F. Stadler
The Santa Fe Institute, 1399 Hyde Park Road, Santa Fe, NM 87501, USA

Current Topics in Microbiology and Immunology (2016) 392: 43–59
DOI 10.1007/82_2015_470

Published Online: 04 September 2015

RNA. Some of the properties of this map, in particular shape space covering and extensive neutral networks, give rise to evolutionary patterns such as drift-like motion in sequence space, akin to the behavior of RNA quasispecies. In contrast, very little is known about the influence of sequence-structure maps on autocatalytic replication systems.

Contents

1 From Replication to Fitness Landscapes 44
1.1 The Quasispecies 44
1.2 Molecular Replicators 46
1.3 Quantifying Natural Fitness Landscapes 48
1.4 Computer Models of RNA Evolution 49
2 Autocatalytic Networks 52
2.1 The Bioinformatics of RNA–RNA Interactions 52
2.2 Replicator Networks 53
2.3 Evolution of Autocatalytic Networks 55
2.4 Distributed Autocatalysis 55
References 56

1 From Replication to Fitness Landscapes

1.1 The Quasispecies

The interplay of replication, selection, and mutation is the basis of Darwinian evolution. Replication can be interpreted as an autocatalytic chemical reaction that, in the simplest case, is of the form

$$\mathbf{A} + \mathbf{Y} \xrightarrow{k} 2\mathbf{Y}, \tag{1}$$

where **A** is the substrate that is used as building material for the autocatalyst **Y** that is required as template for its own formation. Mutation in the form of imprecise, or error-prone, reproduction represents the universal kind of variation, which occurs in all organisms and can be sketched by a single overall reaction step:

$$\mathbf{A} + \mathbf{Y} \xrightarrow{k_{xy}} \mathbf{Y} + \mathbf{X}. \tag{2}$$

Here, the mutant is denoted by **X,** and the rate parameters k and k_{xy} refer to two parallel reaction channels. Reaction rates depend explicitly on the *type* y of the replicator **Y**. These rate differences are the basis for selection due to the fact that the different templates compete for the common resource **A**.

In the case of RNA or protein molecules, y is simply the nucleotide sequence of the molecule **Y**. The production of a variant **X** from **Y**, in the simplest model, occurs with a probability $q_{xy} := \mathbb{P}[\mathbf{Y} \to \mathbf{X}]$, while **Y** undergoes the copying reaction with a rate $k_0(\mathbf{Y}) = \alpha f(y)$, where $\alpha := [\mathbf{A}]$ is the concentration of the building material **A**. Adding an unspecific outflow from the system, we arrive at a

$$\frac{\mathrm{d}[x]}{\mathrm{d}t} = \sum_y q_{xy}\alpha f(y)[y] - \varphi[x] \tag{3}$$

The dynamics of this system is thus described by two ingredients: the rate of copying of each type, $f(x)$, usually referred to as its *fitness*, and the probabilities of specific copying errors q_{xy}. The specific form of the flux φ plays little role for the overall dynamics as long as it is small enough not to completely drain all the replicating material from the system (Happel and Stadler 1999). In the simplest case, we may assume that the total concentration of all replicating types as well as the concentration of the building material is kept constant. This model, known as *constant organization*, yields the famous quasispecies equation as follows:

$$\frac{\mathrm{d}[x]}{\mathrm{d}t} = \sum_y q_{xy}f(y)[y] - \varphi[x] \quad \text{with} \quad \varphi = \sum_{x,y} q_{xy}f(y)[y] \tag{4}$$

i.e., φ equals the total production of replicating types.

Since the molecular types x and y are sequences, the most common model assumes that $\begin{pmatrix} q_{xy} = \\ ndp^d \end{pmatrix}$ where n is the sequence length, $d = d_{xy}$ is the number of sequence positions in which x and y differ, n is the common length of both sequences, and p is the probability of a point mutation, i.e., the exchange of a single letter, per copying event. Nearly all work on the quasispecies model has used this mutation model (Eigen 1971; Eigen et al. 1989; Eigen and Schuster 1977). Conceptually, it can be simplified further by ignoring the small probabilities of multiple mutations, simply setting $q_{xy} = 0$ if $x \neq y$ differ by more than a single mutation. Sequences are "easily accessible," i.e., adjacent, if they differ by a single (point) mutation only. This arranges the set X of sequences as the vertices of a graph, which is usually referred to as the *sequence space* (X, τ). The symbol τ denotes the accessibility structure, which here is just the edge set of graph but may, in general, be a more complicated topological structure (Flamm et al. 2007). Together with the fitness function $f : X \to \mathbb{R}$, that sequence space forms the *fitness landscape* (X, τ, f).

The dynamics of a population evolving according to Eq. (4) is governed by the underlying fitness landscape. Its stationary solution

$$\sum_y q_{xy}f(y)[y] = \varphi[x] \tag{5}$$

determines the equilibrium distribution of the variants in an evolved population. In the limit of small mutation rates, where $q_{xy} \approx 1 - pa_{xy}$ with $a_{xy} = 1$, if x and y are adjacent and $p \ll 1$, one can show that $[x]$ is concentrated around the fitness maximum (Eigen 1971). Chapters 1, 4, and 5 in this book are concerned with the relationships of the fitness landscape (X, τ, f) and the structure of the resulting quasispecies.

1.2 Molecular Replicators

A variety of in vitro systems embody self-replication of RNA or DNA. Although template-instructed ligation can also be achieved without enzymes, these are restricted to short and usually specialized sequences (Lee et al. 1996; von Kiedrowski 1986). All copy reactions of interestingly long and diverse templates known today, however, require elaborate enzymes.

The earliest system studied in detail was based on the RNA-dependent RNA polymerase of the bacteriophage Qβ, a Levivirus. Extensive studies on the reaction kinetics of this system (Biebricher and Eigen 1988) demonstrated that the kinetic data are consistent with a many-step reaction mechanism describing the stepwise addition of nucleotides. It can be coarse-grained to a Michaelis–Menten-like overall reaction of the form

$$\mathbf{A} + \mathbf{Y} + \mathbf{E} \leftrightharpoons \mathbf{A} + \mathbf{Y} \cdot \mathbf{E} \rightarrow \mathbf{Y} \cdot \mathbf{E} \cdot \mathbf{X} \leftrightharpoons \mathbf{Y} \cdot \mathbf{E} + \mathbf{X} \tag{6}$$

that still explains the observed three distinct regimes: exponential growth a low $[\mathbf{Y}]$, linear growth for intermediate replicator concentrations, and saturation by product inhibition at high concentrations. The rate constants depend strongly on the sequence of the template $\mathbf{Y}$ since Qβ replicase is well adapted to recognize the genomic RNA of the Qβ phage and to discriminate it from host cell sequences. Affinity to the replicase thus is an important determinant of fitness in in vitro evolution experiments with this system. Manipulation of the environment in this experimental setup has lead to the selection of widely different RNA molecules with surprising properties. SV11, for instance, is replicated from an extremely stable metastable conformation of the RNA (Biebricher and Luce 1992); a "drug-addicted" RNA was obtained in Kramer et al. (1974) by adding the intercalating dye ethidium bromide.

Enzymes that replicate nucleic acid templates effectively independent of their sequence have evolved in particular for genomic DNA templates. The discovery of the DNA polymerase chain reaction (PCR) (Mullis et al. 1986) was a milestone toward sequence independent amplification of DNA sequences in vitro. It requires, however, higher temperatures to separate the two strands of the double helical product. Since the product of template-directed replication or ligation is invariably a

double strand, product inhibition cannot be entirely avoided in most systems. The simplest replication system is thus better described by

$$\mathbf{A} + \mathbf{Y} + \mathbf{E} \rightarrow \mathbf{E} + \mathbf{Y} \cdot \mathbf{Y} \quad \text{and} \quad \mathbf{Y} \cdot \mathbf{Y} \leftrightharpoons 2\mathbf{Y} \tag{7}$$

Under the "quasi-steady state" approximation (Segel and Slemrod 1989), this model follows a modified kinetics (Wills et al. 1998)

$$\frac{\mathrm{d}[x]}{\mathrm{d}t} = [x](f(x)\psi(\beta(x)[x]c) - \varphi) \tag{8}$$

where $f(x)$ is the fitness measures at infinite dilution, i.e., for a total concentration of replicating material $c \rightarrow 0$, $\beta(x)$ is a constant derivable from the microscopic rate constants that describes the strength of product inhibition, and $\psi(u) = 2(\sqrt{u+1} - 1)/u$ is a function that decays like the square root of its argument. It reduces to the simple case for $\beta(x) \rightarrow 0$. A wide range of related mechanisms of template-directed ligation, including an experimentally studied systems based on DNA triple helices (Li and Nicolaou 1994), and the membrane-anchored mechanism suggested for the "Los Alamos Bug" artificial protocell project (Rasmussen et al. 2003) follow the same effective kinetic law. An approximation that replaces $\psi(u)$ by $\sqrt{u}$ was considered in Szathmáry and Gladkih (1989).

In contrast to the quasispecies-like models, which (apart from the mutant cloud around the "master sequence") effectively lead to "survival of the fittest" at least for small mutation rates, there is no selection in the parabolic growth model (Varga and Szathmáry 1997; Wills et al. 1998). More general systems with product inhibition, however, allow for cooperation of all replicators whose fitness exceeds a certain concentration-dependent threshold, which can be computed explicitly (Wills et al. 1998). Most of the experimental systems of self-replicating polymers without enzyme fall into this class, see, e.g., Plöger and Kiedrowski (2014) for a recent peptide nucleic acid system. Unless product inhibition is too strong (or concentrations become too large), these systems show selection by "extinction of the unfittest" rather than survival of the fittest. So far, their population-level dynamics have not been explored for complex, realistic fitness landscapes.

Several enzymatic systems have been well established to amplify nucleic acid sequences, most famously the PCR (Erlich 1989). Here the product inhibition problem is solved by "thermal cycling," i.e., a periodic increase in temperature to release product bound in duplices. An isothermal version based on T7 polymerase is the 3SR reaction (Fahy et al. 1991). A recently introduced alternative is the isothermal multiple displacement amplification (IMDA) (Luthra and Medeiros 2004). A common theme in these technologically highly relevant systems is that templates are amplified nearly independently of their sequence. This enables among other applications high-throughput DNA sequencing as well as artificial selection (Systematic Evolution of Ligands by EXponential Enrichment (SELEX)) (Ellington and Szostak 1990; Tuerk and Gold 1990). In the latter, amplification is alternated by an assay that enriches RNA or DNA molecules with desired properties, thereby

effectively implementing a user-defined fitness landscape. This allowed the creation of RNA and DNA sequences with a surprisingly wide variety of both binding and enzymatic properties. A detailed mathematical analysis of the SELEX procedure and its convergence properties can be found in Levine and Nilsen-Hamilton (2007).

1.3 *Quantifying Natural Fitness Landscapes*

Since the volume of sequence space increases exponentially with sequence length, it has long been impossible to obtain a comprehensive picture of fitness landscapes. Nevertheless, early attempts to empirically chart at least a neighborhood of the optimal or native sequence date back almost two decades (Aita et al. 2002; Aita et al. 2000; Hayashi et al. 2006; Reetz and Sanchis 2008).

The situation has changed with the advent of micro-arrays and then deep sequencing technologies. At least for very small model systems, it has become possible to measure the relative abundance of a very large number of sequences. Comparing the sequence distribution $p(x)$ with the distribution in the initial pool $p_0(x)$ immediately yields the estimated

$$f(x) \approx p(x)/p_0(x)\,. \tag{9}$$

It is worth noting that the fitness function cannot be inferred from the equilibrium quasispecies distribution since the latter is usually concentrated around the fittest member of the population, making it impossible to obtain data for more distant parts of the landscape.

Micro-arrays have provided a convenient means of measuring the fitness of larger samples in parallel (Lauring and Andino 2011). Instead of measuring fitness directly from an adapting population, equilibrium parameters such as RNA-protein binding constants also have been measured using micro-arrays (Rowe et al. 2010). Various sources of bias deriving from the ligation and sequencing steps must be measured and taken into account in the practical analysis of HTS-based surveys of landscapes, see, e.g., Jimenez et al. (2013) for details. Earlier work still targeted particular regions in sequence space. The fitness of all possible individual point mutants of a nine-amino acid region of yeast Hsp90 was determined in Hietpas et al. (2011). Pitt and Ferré d'Amaré (2010) mutagenized an artificial RNA ligase ribozyme and estimated the fitness in the neighborhood of the original ligase sequence from a reselected variant pool.

Various interpolation and machine learning schemes have been proposed to estimate the structure of fitness landscapes from sparse data (Romero et al. 2013; Woo and Reifman 2014). The issue, however, remains a difficult one and the problem is far from being solved. Most geometric and topological characteristics of the inferred fitness landscape, such as the number of monotonically increasing paths between ancestral and derived genotypes, the prevalence of sign epistasis, and the number of local fitness maxima, are distorted in the inferred landscape (Otwinowski and Plotkin 2014).

Most recently, small systems have been investigated in their entirety. An example is a survey the space of 24-mers selected for GTP binding (Jimenez et al. 2013), see also Athavale et al. (2014) for a recent review.

Empirical landscapes seem to differ substantially between different biological systems. DNA-protein binding landscapes (Rowe et al. 2010) have been found to be rugged, with many local optima. Protein landscape, on the other hand, seems to be at least locally smooth, "Mt. Fuji-like" (Aita et al. 2000; Lobkovsky et al. 2011) consistent with computational prediction from simple computational models (Babajide et al. 1997; Chan and Bornberg-Bauer 2002). Similar structures are observed for viral fitness landscapes, both experimentally (Lauring and Andino 2011; Woo and Reifman 2014) and in computational models (Kouyos et al. 2012). For RNA landscapes, however, there is an apparent discrepancy between the observed very rugged landscapes and the computationally predicted landscape structure (Athavale et al. 2014). We return to this issue in some detail in the next section.

A promising alternative to exhaustively covering sequence space is to associate fitness with a low-dimensional phenotype. Acevedo et al. (2014), for instance, mapped thousands of measured fitness values of mutants onto three-dimensional structures of viral proteins to explore the structure–function relationships.

1.4 Computer Models of RNA Evolution

RNA has turned out to be a particularly fruitful model to study fitness landscapes in computational models of evolution. On the one hand, it is intriguing catalytic activities and its crucial involvement in the core information metabolism of modern life forms, having lead up to the RNA world hypothesis of pre-biotic evolution (Gilbert 1986), justify detailed studies. On the other hand, nucleic acid structures have specific feature, not shared by polypeptides, which make them computationally tractable at a convenient coarse-grained resolution.

Nucleobases interact specifically through hydrogen bonding in a manner that established simple combinatorial rules of complementary base pairing (GC, AU, and GU). Paired bases form regular helical structures stabilized by π-electron interactions whose energetics are nearly perfectly additive in terms of the contributions of adjacent base pairs. The resulting secondary structures shown in Fig. 1 are thus *matchings* in the graph theoretical sense, which are further restricted by the *non-crossing* rule that excludes so-called "pseudoknots." These simplifications result in the combinatorial model of RNA secondary structures in which the *folding problem*, i.e., the prediction of structure from sequence, can be solved efficiently and completely by means of dynamic programming (Zuker and Stiegler 1981). This simple model, which has been parameterized by careful thermodynamic measurements (Turner and Mathews 2010), has proved its practical relevance in thousands of applications ranging from explaining and organizing structural features of RNAs to the prediction of effects of mutations and wholesale design of functional RNAs. Far from perfect, it nevertheless captures most of the energetics of RNA folding, it

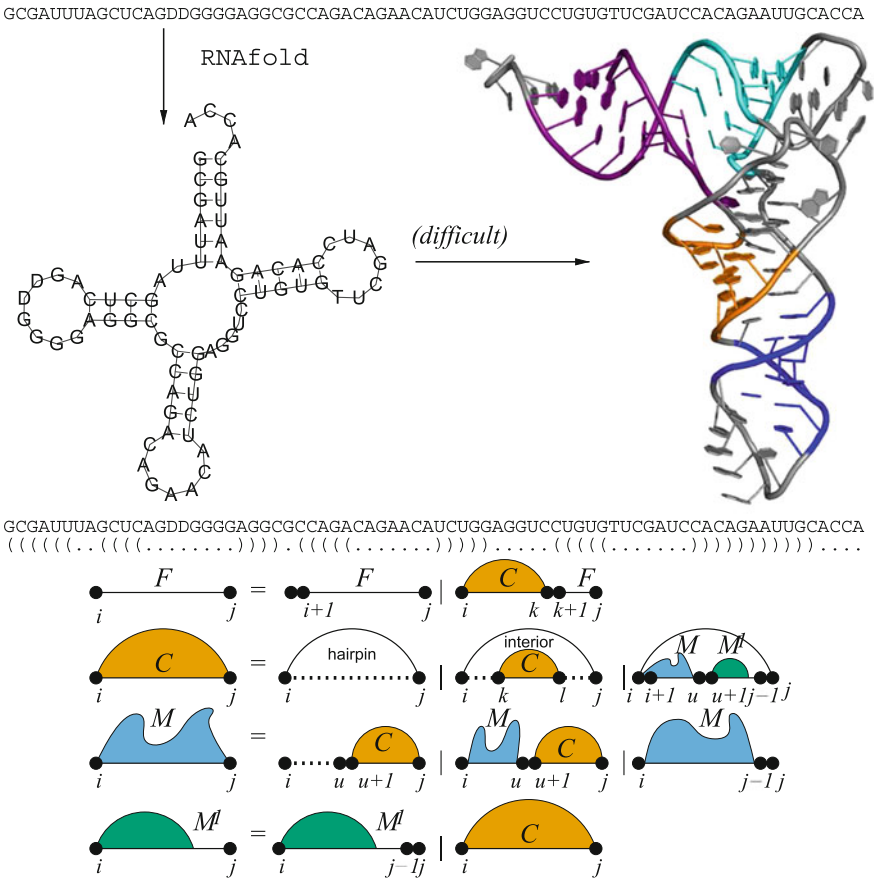

Fig. 1 RNA folding in a nutshell. *Top* Folding of the yeast tRNA-Phe. The secondary structure can be computed with little effort, while the 3D structure (shown here is the PDB crystal structure 5TNA) is not easily accessible by computational methods alone. *Below* The algorithm of RNA folding consists of fairly simple recursion relations that construct the energy (or partition function) of a substructure on a sequence interval from i to j from smaller components. An arbitrary structure (F) begins with either an unpaired base • or a substructure enclosed by a base pair (C). In both cases, it then continues with a correspondingly shorter unconstrained structure. The *second line* describes the decomposition of base pair enclosed structure (C) into the three major loop types: hairpin loops, interior loops (including stacked base pairs, $k = i + 1$ and $l = j - 1$), and multi-branch loops. The last three lines correspond to the recursion for multi-branch loops, see Lorenz et al. (2011); Zuker and Stiegler (1981) for details. For each possible decomposition step, the energy of the *l.h.s.* structure is the sum of the energies of the *r.h.s.* components. These recursions require quadratic memory and cubic time in terms of the input sequence length, providing a highly efficient and exact solution of the RNA folding problem

describes key features of RNA folding kinetics, and it explains many of the evolutionary patterns observed in RNA. We refer to a recent book on RNA bioinformatics for details on applications and limits of the model (Gorodkin and Ruzzo 2014).

Instead we concentrate here on a different aspect which was explored in substantial detail almost a quarter of a century ago (Schuster et al. 1994). The efficiency of structure prediction has made it feasible to explore the sequence-structure map of RNA as a proxy for genotype–phenotype maps. Starting from the insight that genotype (sequence) is acted upon by mutation and other genetic operators while the phenotype (structure) is subject to selection, it is appealing to model biologically relevant fitness landscapes as compositions

$$f(x) = \phi(\Phi(x)) \tag{10}$$

where $\Phi : X \rightarrow \mathbb{P}$ is the genotype–phenotype map and $\phi : \mathbb{P} \rightarrow \mathbb{R}$ is a fitness function that evaluates the phenotypes $y \in \mathbb{P}$ rather than the genotype. In the case of RNA secondary structures, Φ is simply RNA folding as implemented, e.g., by the `ViennaRNA` package (Lorenz et al. 2011) and $\mathbb{P}$ denotes the set of RNA secondary structures. In many circumstances, the properties of $f : X \rightarrow \mathbb{R}$ are essentially determined already by the genotype–phenotype map Φ, as in the case of RNA secondary structures.

Extensive computational studies (Fontana et al. 1991; Fontana et al. 1993; Fontana and Schuster 1998; Fontana et al. 1993; Gruener et al. 1996a, 1996b) showed the following:

1. A large fraction of point mutations are neutral in RNA molecules in the sense that the mutation does not change the base pairing pattern (secondary structure) of the ground state structure.
2. The pre-image $\Phi^{-1}(y)$, i.e., the sequences folding into a common RNA structure y, is to a first approximation homogeneously distributed among the sequences $C(y)$ that satisfy the base pairing constraints imposed by y. Note that $\Phi^{-1}(y) \subseteq C(y)$.
3. As a consequence of the high degree of neutrality (1) and the approximate homogeneity (2), there are extensive so-called "*neutral networks*" of sequences folding into the same ground state structure. These neutral networks "percolate" through sequence space and contain neutral paths that connect sequences without detectable sequence similarity.
4. The neutral networks tend to be connected or at least to decompose into only a small number of very large components.
5. The intersection theorem (Reidys et al. 1997) guarantees that the sets $C(y')$ and $C(y'')$ of sequences that are compatible with two arbitrary structures y' and y'' have non-empty intersection.
6. The neutral networks $\Phi^{-1}(y')$ and $\Phi^{-1}(y'')$ therefore come very close to each other, and the distance of an arbitrary sequence x_0 to a sequence $x \in \Phi^{-1}(y)$ folding into y is determined essentially by the violations of the base pairing constraints in x_0 only. This property is known as *shape space covering*.

This rather special structure of the RNA folding map implies a diffusion-like behavior of evolving populations of RNA molecules in sequence space, which conforms to Kimura's neutral theory (Huynen et al. 1996; Kimura 1983). It also implies constant rates of encountering novel variants along evolutionary trajectories (Huynen 1996). Thus, it explains the punctuated-equilibrium-like dynamics of RNA evolution characterized by long phases of diffusion on neutral networks interrupted by intermittent bursts of adaptive evolution when fitter mutants are encountered at the fringes of the neutral network (Huynen et al. 1996).

A beautiful illustration of these properties of the RNA folding map is the construction of a bistable ribozyme (Schultes and Bartel 2000): A single RNA folds into either of two evolutionarily unrelated ribozyme structures and catalyzes the corresponding reactions. Nevertheless, the bistable sequence has neighbors that are efficient catalysts for only one of the two alternative reactions and that are connected by neutral paths of the corresponding wild-type ribozyme.

Recent empirical work on very small RNA fitness landscapes defined by aptamer binding affinities, on the other hand, seems to be at odds with these observations and rather indicates as rugged structure without extensive paths (Athavale et al. 2014). The empirical aptamer binding landscape, however, focussed on the small subsequence actually involved in binding. This is indeed expected to be dominated by a few peaks corresponding to the best-binding motives. It forms a low-dimensional subspace that constrains the RNA molecules to those that have the binding motive but does not speak to the landscape defined by the large rest of the molecule. Computational studies indeed have shown that small sequence motives (as models of active sites or binding pockets) can be constrained without affecting the overall structure of the RNA folding map.

A different line of evidence for (nearly) neutral paths in RNA fitness landscapes comes from the comparative analysis homologous RNAs. Here we often observe a strong conservation of secondary structure while the sequence may have diverged already to beyond the detection limit (Torarinsson et al. 2006). Computational surveys with different methods have provided good evidence that this is not at all a rare phenomenon: More than 10 % of mammalian genomes are under stabilizing selection for RNA secondary structure elements, but more than 85 % of these elements are essentially unconstrained at sequence level (Smith et al. 2013). This provides a rather direct way to observe diffusive evolution on neutral networks.

2 Autocatalytic Networks

2.1 The Bioinformatics of RNA–RNA Interactions

Specific interactions among distinct RNA molecules are readily established by complementary base pairing, i.e., using the same principles that lead to the formation of intramolecular secondary structures. Conceptually straightforward (but

computationally at times difficult) extensions of the secondary structure model thus also incorporate RNA–RNA interactions. Since there is no local difference between intermolecular and intramolecular base pairs, even the same energy parameters can be used. For an in-depth discussion, we refer to Backofen (2014) for a recent review. An important issue is the concentration dependence. In thermodynamic equilibrium, setting is expressed as

$$\frac{[AB]}{[A][B]} = K_{AB} = \frac{Z'_{AB}}{Z_A Z_B} \tag{11}$$

where $[A]$, $[B]$, and $[AB]$ are the concentrations of monomers of two types of RNAs and their dimer, respectively. The key observation is that the equilibrium constant K_{AB} can be computed directly from the sequences using the partition function versions of `RNAfold` (Z_A, Z_B) and `RNAcofold` or `RIP` (Z_{AB}). The correct partition function for the duplex can be expressed as $Z'_{AB} = (Z_{AB} - Z_A Z_B)e^{-\beta e}$, where Z_{AB} is the partition function computed directly by a cofolding approach, which also contains non-interacting conformations, and e is an initialization energy parameter capturing the additional entropic effects of forming a duplex (Bernhart et al. 2006; Dimitrov and Zuker 2004).

RNA–RNA interactions by means of canonical base pairing play an important role in post-transcriptional regulation. For example, the interaction of microRNAs with messenger RNAs and of small nucleolar RNAs with ribosomal RNAs is of this type. Similarly, it is the preferred mode of action of bacterial small RNAs. Of course, product inhibition in model systems of replicating nucleic acids is also owed to RNA–RNA binding *in trans*.

2.2 Replicator Networks

Eigen and Schuster noticed already in the late 1970s that systems of replicating molecules behave qualitatively different depending on whether the catalyst **E** in Eq. (7) is considered part of the environment or whether the replicators also catalyze their—or each other's—replication (Eigen and Schuster 1979). The net reaction of such a system can be abstracted in the form

$$\mathbf{A} + 2\mathbf{Y} \xrightarrow{k} 3\mathbf{Y} \tag{12}$$

for a single self-replicator with perfect accuracy and

$$\mathbf{A} + \mathbf{Y} + \mathbf{Z} \xrightarrow{q_{xy}k_{yz}} \mathbf{Y} + \mathbf{Z} + \mathbf{X} \tag{13}$$

in the general case of cross-catalysis with imperfect copying. As in the quasispecies model, **Y** is the template, **X**, which may coincide with **Y,** is the product of the copy reaction, and **Z** is the ribozyme catalyst. The kinetic constants k_{yz} describe the rate of copying template **Y** by catalyst **Z**. Again q_{xy} is the mutation probability of producing the offspring **X** from the template **Y**.

The construction of an RNA replicase ribozyme that is capable of copying a broad range of templates, including itself, has been an open problem for decades, ever since the discovery that RNA molecules have catalytic activities akin to proteins. As proof of principle, an RNA ligase ribozyme (Paul and Joyce 2002) was obtained in 2002, the first RNA replicase followed in 2009 (Lincoln and Joyce 2009), and was improved stepwise (Ferretti and Joyce 2013). Earlier this year, Roberson and Joyce finally described a self-replicating ribozyme that can sustain exponential growth (Robertson and Joyce 2014). It also copies a partner ribozyme so that the coupled system is capable of Darwinian evolution. Autocatalytic self-replicators of this type are in principle capable of open-ended Darwinian evolution. Experimental exploration of the test tube models of a hypothetical RNA world comprising autonomous interacting self-replicating RNAs thus is becoming feasible.

The dynamics of such a system can again be derived from the reaction mechanism under the assumption of mass action kinetics. In the simplest instantiation, it is of the form (Stadler and Schuster 1992)

$$\frac{\mathrm{d}[x]}{\mathrm{d}t} = \underbrace{[x]\left(\sum_z k_{xz}[z] - \varphi\right)}_{\text{selection}} + \underbrace{\sum_{y,z}\left(q_{xy}k_{yz}[y][z] - q_{yx}k_{xz}[y][z]\right)}_{\text{mutation}} \tag{14}$$

Constant organization is enforced by balancing the flux with the net production in the system, i.e., $\varphi = \sum_{xz} k_{xz}[x][z]$, independent of the choice of the mutation rates q_{xy}. In the absence of mutation, $p \to 0$, the second term, which is proportional to the mutation rate p, vanishes. The remaining dynamical systems are known as the (quadratic) *replicator equation* (Schuster and Sigmund 1983). Maybe the most famous special case is the hypercycle model (Eigen and Schuster 1979). Second-order replicator equation also serves as a canonical model in game dynamics, and they are equivalent to the Lotka–Volterra equations, one of the first models of predator–prey interactions. They admit a rich mathematical theory with warrants books entirely dedicated to their analysis (Hofbauer and Sigmund 1998). More realistic reaction mechanisms again include variable levels of product inhibition. As in the quasispecies case, they are dominated by product inhibition for large total concentrations and eventually lead to global coexistence, i.e., the absence of selection. For moderate concentrations, however, complex dynamics described effectively by the catalyzed replication prevails Stadler et al. (2000).

2.3 Evolution of Autocatalytic Networks

Comparably, little is known about the evolution of sequences of autocatalytic networks. In Stadler (2002), the diffusion (in sequence space) of a population of interacting replicators has been studied. A major issue in models of this type is the assignment of the reaction rates k_{xy} as a function of sequences of template and catalyst. This problem is analogous to the assignment of fitness values to individual sequences in the quasispecies equation. It is even more challenging, however, since (1) we now have a quadratic number of coefficients to determine and (2) virtually nothing is known about the sequence dependence of the catalytic capabilities of nucleic acids. Very simple minimal models thus have been used: In Stadler (2002), k_{xy} is assumed to be dependent on the Hamming distance of x and y. In Forst (2000) and later in Stephan-Otto Attolini and Stadler (2006), the reaction rates were assumed to depend on the interaction structure of x and z as computed by `RNAcofold`. Neutrality in the interaction structure, i.e., of `RNAcofold` (x, z) w.r.t. mutation in either x or y, is important for evolvability in sequence space as well as the persistence of the population (Stephan-Otto Attolini and Stadler 2006). It remains unknown, however, whether this type of model is realistic even in a statistical sense. One would assume that the catalytic activity of a catalyst z on a template z depends on local interactions close to the processive site rather than on a conserved global structure.

2.4 Distributed Autocatalysis

Macromolecules that are directly self-replicating, i.e., that can copy a template including a second copy of themselves, are certainly the conceptually simplest building blocks of a self-propagating system. Since it has remained open for a long time whether RNA replicase enzymes can be constructed, alternative architectures have been explored at least theoretically. Assuming that copy machines are infeasible, systems of chemical reactions have been studied in which some of the chemical species also act as catalysts. Seminal work in this direction includes Stuart Kauffman's string concatenation model (Kauffman 1986) or Walter Fontana's artificial chemistry based on the lambda calculus (Fontana and Buss 1994). The key question is then to characterize closed, self-maintaining sets that collectively behave as an autocatalyst. Despite substantial progress in the mathematical and computational analysis of this class of models (Hordijk et al. 2012, 2014; Smith et al. 2014), it remains unclear whether and how they may have played a role in the origin of life. For example, it can be shown that in large chemical systems with n distinct molecular species, each molecule must catalyze $\propto \log n$ reaction in order to make it likely to find a collective autocatalytic set (Hordijk et al. 2011). At present, no plausible material instantiation appears to be known, and it remains to be seen whether the required abundance and specificity of catalytic activities are realistic for some kind of chemistry.

References

Acevedo A, Brodsky L, Andino R (2014) Mutational and fitness landscapes of an RNA virus revealed through population sequencing. Nature 505:686–690

Aita T, Hamamatsu N, Nomiya Y, Uchiyama H, Shibanaka Y, Husimi Y (2002) Surveying a local fitness landscape of a protein with epistatic sites for the study of directed evolution. Biopolymers 64:95–105

Aita T, Uchiyama H, Inaoka T, Nakajima M, Kokubo T, Husimi Y (2000) Analysis of a local fitness landscape with a model of the rough Mt. Fuji-type landscape: application to prolyl endopeptidase and thermolysin. Biopolymers 54:64–79

Athavale SS, Spicer B, Chen IA (2014) Experimental fitness landscapes to understand the molecular evolution of RNA-based life. Curr Opin Chem Biol 22C:35–39

Babajide A, Hofacker IL, Sippl MJ, Stadler PF (1997) Neutral networks in protein space: a computational study based on knowledge-based potentials of mean force. Fold Des 2:261–269

Backofen R (2014) Computational prediction of RNA–RNA interactions. Methods Mol Biol 1097:417–435

Bernhart SH, Tafer H, Mückstein U, Flamm C, Stadler PF, Hofacker IL (2006) Partition function and base pairing probabilities of RNA heterodimers. Algorithms Mol Biol 1:3 (epub)

Biebricher CK, Eigen M (1988) Kinetics of RNA replication by $Q\beta$ replicase. In: Domingo E, Holland JJ, Ahlquist P (eds) RNA genetics. RNA directed virus replication, vol I. CRC Press, Boca Raton, FL, pp 1–21

Biebricher CK, Luce R (1992) In vitro recombination and terminal elongation of RNA by $Q\beta$ replicase. EMBO J 11:5129–5135

Chan HS, Bornberg-Bauer E (2002) Perspectives on protein evolution from simple exact models. Appl Bioinf 1:121–144

Dimitrov RA, Zuker M (2004) Prediction of hybridization and melting for double-stranded nucleic acids. Biophys J 87:215–226

Eigen M (1971) Selforganization of matter and the evolution of macromolecules. Naturwissenschaften 58:465–523

Eigen M, McCaskill J, Schuster P (1989) The molecular quasispecies. Adv Chem Phys 75:149–263

Eigen M, Schuster P (1977) The hypercycle. A principle of natural self-organization. Part A: emergence of the hypercycle. Naturwissenschaften 64:541–565

Eigen M, Schuster P (1979) The hypercycle. Springer, New York

Ellington AD, Szostak JW (1990) In vitro selection of RNA molecules that bind specific ligands. Nature 346:818–822

Erlich HA (ed) (1989) PCR technology. Principles and applications for DNA amplification. Stockton Press, New York

Fahy E, Kwoh DY, Gingeras TR (1991) Self-sustained sequence replication (3SR): an isothermal transcription-based amplification system alternative to PCR. PCR Methods Appl 1:25–33

Ferretti AC, Joyce GF (2013) Kinetic properties of an RNA enzyme that undergoes self-sustained exponential amplification. Biochemistry 52:1227–1235

Flamm C, Stadler BMR, Stadler PF (2007) Saddles and barrier in landscapes of generalized search operators. In: Stephens CR, Toussaint M, Whitley D, Stadler PF (eds) Foundations of Genetic Algortithms IX. Lecture Notes Computer Science. 9th International Workshop, FOGA 2007, Mexico City, Mexico, vol 4436. Springer, Berlin, Heidelberg, 8–11 Jan 2007, pp 194–212

Fontana W, Buss LW (1994) What would be conserved "if the tape were played twice". Proc Natl Acad Sci USA 91:757–761

Fontana W, Griesmacher T, Schnabl W, Stadler PF, Schuster P (1991) Statistics of landscapes based on free energies, replication and degradation rate constants of RNA secondary structures. Monatsh Chem 122:795–819

Fontana W, Konings DAM, Stadler PF, Schuster P (1993a) Statistics of RNA secondary structures. Biopolymers 33:1389–1404

Fontana W, Schuster P (1998) Continuity in evolution: on the nature of transitions. Science 280:1451–1455
Fontana W, Stadler PF, Bornberg-Bauer EG, Griesmacher T, Hofacker IL, Tacker M, Tarazona P, Weinberger ED, Schuster P (1993b) RNA folding landscapes and combinatory landscapes. Phys Rev E 47:2083–2099
Forst CV (2000) Molecular evolution of catalysis. J Theor Biol 205:409–431
Gilbert W (1986) The RNA world. Nature 319:618
Gorodkin J, Ruzzo WL (2014) RNA sequence, structure, and function: computational and bioinformatic methods. Humana Press, New York City
Gruener W, Giegerich R, Strothmann D, Reidys C, Weber J, Hofacker IL, Stadler PF, Schuster P (1996a) Analysis of RNA sequence structure maps by exhaustive enumeration. I neutral networks. Monath Chem 127:355–374
Gruener W, Giegerich R, Strothmann D, Reidys C, Weber J, Hofacker IL, Stadler PF, Schuster P (1996b) Analysis of RNA sequence structure maps by exhaustive enumeration. II. structures of neutral networks and shape space covering. Monath Chem 127:375–389
Happel R, Stadler PF (1999) Autocatalytic replication in a CSTR and constant organization. J Math Biol 38:422–434
Hayashi Y, Aita T, Toyota H, Husimi Y, Urabe I, Yomo T (2006) Experimental rugged fitness landscape in protein sequence space. PLoS ONE 1:e96
Hietpas RT, Jensen JD, Bolon DN (2011) Experimental illumination of a fitness landscape. Proc Natl Acad Sci USA 108:7896–7901
Hofbauer J, Sigmund K (1998) Dynamical systems and the theory of evolution. Cambridge University Press, Cambridge
Hordijk W, Kauffman SA, Steel M (2011) Required levels of catalysis for emergence of autocatalytic sets in models of chemical reaction systems. Int J Mol Sci 12:3085–3101
Hordijk W, Steel M, Kauffman S (2012) The structure of autocatalytic sets: evolvability, enablement, and emergence. Acta Biotheor 60:379–392
Hordijk W, Wills PR, Steel MA (2014) Autocatalytic sets and biological specificity. Bull Math Biol 76:201–224
Huynen MA (1996) Exploring phenotype space through neutral evolution. J Mol Evol 43:165–169
Huynen MA, Stadler PF, Fontana W (1996) Smoothness within ruggedness: the role of neutrality in adaptation. Proc Natl Acad Sci (USA) 93:397–401
Jimenez JI, Xulvi-Brunet R, Campbell G, Turk-MacLeod R, Chen IA (2013) Comprehensive experimental fitness landscape and evolutionary network for small RNA. Proc Natl Acad Sci USA 110:14984–14989
Kauffman S (1986) Autocatalytic sets of proteins. J Theor Biol 119:1–24
Kimura M (1983) The neutral theory of molecular evolution. Cambridge University Press, Cambridge
Kouyos RD, Leventhal GE, Hinkley T, Haddad M, Whitcomb JM, Petropoulos CJ, Bonhoeffer S (2012) Exploring the complexity of the HIV-1 fitness landscape. PLoS Genet 8:e1002551
Kramer FR, Mills DR, Cole PE, Nishihara T, Spiegelman S (1974) Evolution in vitro: sequence and phenotype of a mutant RNA resistant to ethidium bromide. J Mol Biol 89:719–736
Lauring AS, Andino R (2011) Exploring the fitness landscape of an RNA virus by using a universal barcode microarray. J Virol 85:3780–3791
Lee DH, Granja JR, Martinez JA, Severin K, Ghadiri MR (1996) A self-replicating peptide. Nature 382:525–528
Levine HA, Nilsen-Hamilton M (2007) A mathematical analysis of SELEX. Comp Biol Chem 31:11–35
Li T, Nicolaou KC (1994) Chemical self-replication of palindromic duplex DNA. Nature 369:218–221
Lincoln TA, Joyce GF (2009) Self-sustained replication of an RNA enzyme. Science 323:1229–1232
Lobkovsky AE, Wolf Y, Koonin EV (2011) Predictability of evolutionary trajectories in fitness landscapes. PLoS Comput Biol 7:e1002302

Lorenz R, Bernhart SH, Höner zu Siederdissen C, Tafer H, Flamm C, Stadler PF, Hofacker IL (2011) ViennaRNA package 2.0. Alg Mol Biol 6:26
Luthra R, Medeiros LJ (2004) Isothermal multiple displacement amplification: a highly reliable approach for generating unlimited high molecular weight genomic DNA from clinical specimens. J Mol Diagn 6:236–242
Mullis KB, Faloona F, Scharf S, Saiki R, Horn G, Erlich H (1986) Specific enzymatic amplification of DNA in vitro: the polymerase chain reaction. Cold Spring Harb Symp Quant Biol 51(1):263–273
Otwinowski J, Plotkin JB (2014) Inferring fitness landscapes by regression produces biased estimates of epistasis. Proc Natl Acad Sci USA 111:E2301–E2309
Paul N, Joyce GF (2002) A self-replicating ligase ribozyme. Proc Natl Acad Sci USA 99:12733–12740
Pitt JN, Ferré-D'Amaré AR (2010) Rapid construction of empirical RNA fitness landscapes. Science 330:376–379
Plöger TA, Kiedrowski G (2014) A self-replicating peptide nucleic acid. Org Biomol Chem 12:6908–6914
Rasmussen S, Chen L, Nilsson M, Abe S (2003) Bridging nonliving to living matter. Artif Life 9:269–316
Reetz MT, Sanchis J (2008) Constructing and analyzing the fitness landscape of an experimental evolutionary process. ChemBioChem 9:2260–2267
Reidys C, Stadler PF, Schuster P (1997) Generic properties of combinatory maps: Neutral networks of RNA secondary structures. Bull Math Biol 59:339–397
Robertson MP, Joyce GF (2014) Highly efficient self-replicating RNA enzymes. Chem Biol 21:238–245
Romero PA, Krause A, Arnold FH (2013) Navigating the protein fitness landscape with Gaussian processes. Proc Natl Acad Sci USA 110:E193–E201
Rowe W, Platt M, Wedge DC, Day PJ, Kell DB, Knowles J (2010) Analysis of a complete DNA-protein affinity landscape. J R Soc Interface 7:397–408
Schultes EA, Bartel DP (2000) One sequence, two ribozymes: implications for the emergence of new ribozyme folds. Science 289:448–452
Schuster P, Fontana W, Stadler PF, Hofacker IL (1994) From sequences to shapes and back: a case study in RNA secondary structures. Proc Roy Soc Lond B 255:279–284
Schuster P, Sigmund K (1983) Replicator dynamics. J Theor Biol 100:533–538
Segel LA, Slemrod M (1989) The quasi-steady state assumption: a case study in perturbation. SIAM Rev 31:446–477
Smith JI, Steel M, Hordijk W (2014) Autocatalytic sets in a partitioned biochemical network. J Syst Chem 5:2
Smith MA, Gesell T, Stadler PF, Mattick JS (2013) Widespread purifying selection on RNA structure in mammals. Nucleic Acids Res 41:8220–8236
Stadler BMR (2002) Diffusion of a population of interacting replicators in sequence space. Adv Complex Syst 5(4):457–461
Stadler BMR, Stadler PF, Schuster P (2000) Dynamics of autocatalytic replicator networks based on higher order ligation reactions. Bull Math Biol 62:1061–1086
Stadler PF, Schuster P (1992) Mutation in autocatalytic networks—an analysis based on perturbation theory. J Math Biol 30:597–631
Stephan-Otto Attolini C, Stadler PF (2006) Evolving towards the hypercycle: a spatial model of molecular evolution. Physica D 217:134–141
Szathmáry E, Gladkih I (1989) Sub-exponential growth and coexistence of non-enzymatically replicating templates. J Theor Biol 138:55–58
Torarinsson E, Sawera M, Havgaard JH, Fredholm M, Gorodkin J (2006) Thousands of corresponding human and mouse genomic regions unalignable in primary sequence contain common RNA structure. Genome Res 16:885–889
Tuerk C, Gold L (1990) Systematic evolution of ligands by exponential enrichment: RNA ligands to bacteriophage T4 DNA polymerase. Science 249:505–510

Turner DH, Mathews DH (2010) NNDB: the nearest neighbor parameter database for predicting stability of nucleic acid secondary structure. Nucleic Acids Res 38D:280–282

Varga S, Szathmáry E (1997) An extremum principle for parabolic competition. Bull Math Biol 59:1145–1154

von Kiedrowski G (1986) A self-replicating hexadeoxynucleotide. Angew Chem Int Ed Engl 25:932–935

Wills PR, Kauffman SA, Stadler BM, Stadler PF (1998) Selection dynamics in autocatalytic systems: templates replicating through binary ligation. Bull Math Biol 60:1073–1098

Woo HJ, Reifman J (2014) Quantitative modeling of virus evolutionary dynamics and adaptation in serial passages using empirically inferred fitness landscapes. J Virol 88:1039–1050

Zuker M, Stiegler P (1981) Optimal computer folding of large RNA sequences using thermodynamics and auxiliary information. Nucleic Acids Res 9:133–148

Quasispecies on Fitness Landscapes

Peter Schuster

Abstract Selection–mutation dynamics is studied as adaptation and neutral drift on abstract fitness landscapes. Various models of fitness landscapes are introduced and analyzed with respect to the stationary mutant distributions adopted by populations upon them. The concept of quasispecies is introduced, and the error threshold phenomenon is analyzed. Complex fitness landscapes with large scatter of fitness values are shown to sustain error thresholds. The phenomenological theory of the quasispecies introduced in 1971 by Eigen is compared to approximation-free numerical computations. The concept of strong quasispecies understood as mutant distributions, which are especially stable against changes in mutations rates, is presented. The role of fitness neutral genotypes in quasispecies is discussed.

Contents

1 Fitness Landscapes 62
2 Sequence Structure Mappings 70
3 Mutations and Population Dynamics 75
4 Quasispecies and Error Thresholds 86
5 Conclusions and Perspectives 114
6 Color Code for Sequences and Classes 115
References 116

P. Schuster
Institut für Theoretische Chemie der Universität Wien,
Währingerstraße 17, 1090 Vienna, Austria

P. Schuster (✉)
The Santa Fe Institute, 1399 Hyde Park Road, Santa Fe, NM 87501, USA
e-mail: pks@tbi.univie.ac.at; pks@santafe.edu

Current Topics in Microbiology and Immunology (2016) 392: 61–120
DOI 10.1007/82_2015_469

Published Online: 24 November 2015

1 Fitness Landscapes

The idea of an *adaptive landscape* or *fitness landscape* is commonly attributed to Wright (1931, 1932, 1988) who introduced it as a metaphor underlying the illustration of evolution as hill-climbing on a multi-peak potential (hyper)surface.[1] According to McCoy (1979), the concept of evolution as an adaptive process on a fitness landscape has been used the first time much earlier by Janet (1895) in order to provide an explanation for the lack of intermediate forms of species in the fossil record. Wright's *shifting balance* model of evolution consists of three phases: (i) random genetic drift splitting the global population in subpopulations, (ii) selection within subpopulations, and (iii) selection between subpopulations. The mean fitness of the population is assumed to decrease during phase (i) and to increase during phases (ii) and (iii). Wright's illustration visualizes a genotype recombination space with several alleles per locus. Before Watson and Crick published their model of the molecular structure of DNA (Watson and Crick 1953), the process creating mutations was not an integral part of the theory of evolution, operated like a *deus ex machina* unseen in the background, and could not be systematically related to moves in genotype space. Wright's fitness landscape is mapped upon a two-dimensional sketch of genotype space and contains many local peaks upon which his model of evolution is approaching the highest fitness optimum. Wright's model and the metaphor have been heavily debated in the following years [see, e.g., Provine (1986), Ruse (1996), and for a more recent well-founded analysis of Wright's landscape concept, we recommend Skipper (2004)]. Here, we shall understand the notion of landscape in a rigorous way as a mapping of genotypes onto nonnegative real numbers representing the fitness parameters, which enter the deterministic or stochastic dynamical systems describing the evolution of populations.

Evolution as an adaptive walk. Two basic elements define an adaptive walk: (i) a potential surface built upon genotype space and (ii) a move set being the collection of allowed changes of genotypes. Although Wright himself stresses multi-dimensionality of fitness landscapes as they are built upon genotype or sequence space,[2] which is a support of very high dimension, his landscapes, however, are always sketched on a continuous two-dimensional caricature of sequence space (Wright 1988, p. 117). Fisher (1941) challenges the usefulness of the two-dimensional metaphor by remarking correctly that the number of local optima decreases when the dimensionality of the support is raised, and in view of the enormously high dimensionality of genotype space, a single-peak landscape

[1]The expression *hypersurface* points at the fact that fitness landscapes are surfaces in high-dimensional space. Since we shall be dealing here almost exclusively with such high-dimensional objects, we drop the prefix 'hyper.'

[2]The genotype space in Wright's seminal paper (Wright 1932) is a space of genes, whereas we use virus genomes as elements of genotypes space. Accordingly, genotype space is identical with the space of DNA or RNA sequences of the chain length of virus genomes.

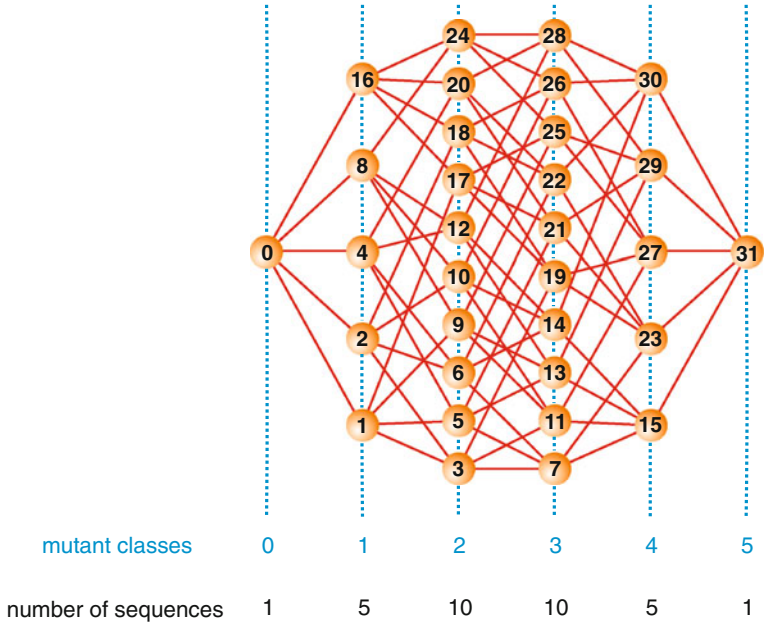

Fig. 1 Sketch of the binary sequence space with $l = 5$. The sequence space $\mathcal{Q}_5^{(2)}$ contains 32 sequences, which are indicated here by their equivalent decadic numbers and the assignments $0 \equiv \mathsf{C}$ and $1 \equiv \mathsf{G}$: $0 = \text{`}00000\text{'} \equiv \text{`}\mathsf{CCCCC}\text{'}$, $1 = \text{`}00001\text{'} \equiv \text{`}\mathsf{CCCCG}\text{'}$, $2 = \text{`}00010\text{'} \equiv \text{`}\mathsf{CCCGC}\text{'}, \ldots, 31 = \text{`}11111\text{'} \equiv \text{`}\mathsf{GGGGG}\text{'}$. Individual sequences are grouped in classes Γ_k that are defined by their Hamming distance to the reference sequence `CCCCC', $d_{j0}^{\mathrm{H}} = k$. The numbers of binary sequences in each Γ_k are given by the binomial distribution: $|\Gamma_k| = \binom{n}{k}$

will result that makes the sophisticated shifting balance process unnecessary since the summit can be reached by mutation and selection alone.

Sequence space (Fig. 1) is discrete, and local optima are simply defined by points that are higher in fitness than all their neighbors. Who the neighbors of a given genotype are is defined by the move set as the set of all sequences, which can be reached by a single move. Clearly, redefining the moves may turn local optima into saddle points or vice versa. An adaptive walk is a trajectory in sequence space that fulfills the condition of non-decreasing fitness $f_k = f(\mathsf{X}_k)$ in a time-ordered series of genotypes $\mathcal{X}(t) = \mathsf{X}_k$:

$$\begin{aligned} &(\mathcal{X}(t_1) = \mathsf{X}_1, \mathcal{X}(t_2) = \mathsf{X}_2, \ldots, \mathcal{X}(t_n) = \mathsf{X}_n) \quad \text{with} \\ &t_1 < t_2 < \ldots < t_n \quad \text{and} \quad f_1 \leq f_2 \leq \ldots < f_n, \end{aligned} \tag{1}$$

where we have implicitly assumed that the walk ends at a peak. The adaptive process is an illustration of evolutionary or natural selection in the sense of Darwin's *survival of the fittest*, although it is important to note that the adaptive

walk refers to a single trajectory, whereas evolution deals with optimization of mean fitness in a population. Equation (1) has an immediate consequence for adaptive walks: The same sequence cannot be visited twice or more times unless the instances are separated exclusively by sequences of identical fitness or, in the other words, loops can occur only if the trajectory is confined to a neutral subset of sequences called a *neutral network* (Reidys et al. 1997). Adaptation on fitness landscapes is a frequently analyzed topic, and a large number of original papers, reviews, and books are available. Representative for others we mention here Gavrilets (1997), Jain and Krug (2007), McGhee (2007), Walsh and Blows (2009).

Point mutations and sequence space. Here, we are interested in population dynamics of viruses and other asexually reproducing species, and accordingly, genotype space will be represented by sequence space $\mathcal{Q}$, which is an abstract space where every different sequence of nucleotides is represented by a point and the distance between pairs of sequences X_i and X_j is given by the Hamming distance d_{ij}^{H} (Hamming 1950, 1986). The simplest and most straightforward move set in sequence space $\mathcal{Q}$ is point mutations, leading to single nucleotide exchanges $d_{ij}^{\mathrm{H}} = 1$. Figure 1 sketches the sequence space of binary sequences—sequences over an alphabet with $\kappa = 2$ letters —of chain length $l = 5$ denoted by $\mathcal{Q}_5^{(2)}$ and shows a natural grouping of sequences with respect to a given reference sequence into classes: A class Γ_k is the set of all sequences at Hamming distance $d_{ij}^{\mathrm{H}} = d_{\mathrm{H}} = k$ from a reference sequence X_0:

$$\Gamma_k = \{\mathsf{X}_i | d_{i0}^{\mathrm{H}} = k\}. \tag{2}$$

Accordingly, $d_{\mathrm{H}} = 0$ defines the reference sequence $\mathsf{X}_0 \equiv \Gamma_0$, which is a class by itself, the class Γ_1 with $d_{\mathrm{H}} = 1$ contains all one-error mutants, class Γ_2 with $d_{\mathrm{H}} = 2$ all two-error mutants, etc., and eventually Γ_l with $d_{\mathrm{H}} = l$ is the class whose members have different nucleotides from the reference at all positions. In the binary alphabet, this is the (unique) complementary sequence of the reference, $|\Gamma_l| = 1$ (where we denote the cardinality of a class by the *absolute value* symbol) and we have $\mathsf{X}_{2^l-1} \equiv \Gamma_l$. In the four-letter alphabet, this class contains $|\Gamma_l| = (\kappa - 1)^l = 3^l$ different sequences where κ as said is the number of different nucleotides in the alphabet.

Simple fitness landscapes. In the early days of population genetics and later on before extensive computer work became accessible rather, drastic simplifications were necessary for any modeling of adaptive walks on fitness landscapes. For example, the same fitness is assigned to all sequences within a given mutant class. The fitness of the genotype of largest fitness, the *master genotype* X_0, is the reference value f_0 and, in addition, at least one second fitness value f_n is required that still needs to be specified. For simple landscapes, the most straightforward definition chooses f_n as the lowest fitness value found in the population and assumes that all genotypes in a given class have the same fitness. Two typical assumptions are as follows: (i) *additive fitness* and (ii) *multiplicative fitness* (Fig. 2). In the first case,

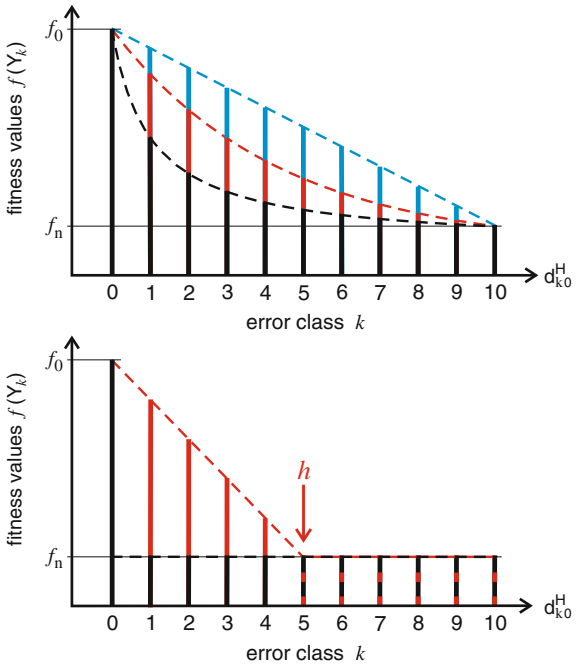

Fig. 2 Examples of simple fitness landscapes. The *upper sketch* shows three landscapes for which the fitness values of the different classes of sequences are given by continuous functions of the class index k: (i) the additive landscape (3a) in *blue*, (ii) the multiplicative landscape (3b) in *red*, and (iii) the hyperbolic fitness landscape (3c) in *black*. In the *lower drawing,* we present (iv) a single-peak landscape (3d) with a discontinuity in the derivative $\partial f/\partial k$ at $k = 0$ (*black*) and (v) the single-peak linear landscape (3e) where the discontinuity is located at $k = h$

every mutation decreases the fitness value of the master genotype by a constant amount $\Delta f/l$, and hence, the fitness of the genotypes in class Γ_k, $f_k = f(\Gamma_k)$ is

$$f_k = f_0 - \Delta f\frac{k}{l} \quad \text{with} \quad 0 < \Delta f = (f_0 - f_n) \leq f_0; k = 0, \ldots, l. \tag{3a}$$

The second case, multiplicative fitness, is characterized by

$$f_k = f_0 \cdot (\gamma_f)^{k/l} \quad \text{with} \quad 0 < \gamma_f = (f_n/f_0) < 1; k = 0, \ldots, l. \tag{3b}$$

Both cases are appropriate—if at all—for genes only and not for whole genotypes, since the basic argument for the usage of models (3a) or (3b) is the concept that species are located in local optima of fitness landscapes; hence, all mutations of reasonable probability are deleterious and reduce fitness. In addition, multiple mutations are assumed to have cumulative effects. As illustrated in Sect. 2, these requirements are not fulfilled by DNA of RNA sequences and point mutations as move set.

For the purpose of comparison, we mention a third landscape, the *hyperbolic fitness landscape*, which too has a continuous derivative $\partial f/\partial k$:

$$f_k = f_0 - \Delta f \frac{k}{l}\frac{l+1}{k+1} \quad \text{with} \quad 0 < \Delta f = (f_0 - f_n) < f_0;\ k = 0, \ldots, l. \tag{3c}$$

The hyperbolic landscape is special, because it shares some features with landscapes that exhibit discontinuities in the derivative.

Eventually, we consider fitness landscapes that are modeled by functions with discontinuities in the derivatives. The most popular representative of this type of landscapes is the *single-peak landscape*, which reminds of the mean field approximation often used in physics: The highest fitness value, f_0, is assigned to the master genotype, and all other genotypes are assumed to have identical fitness, f_n (Fig. 2).

$$f_k = \begin{cases} f_0 & \text{for } k = 0, \\ f_n & \text{for } k = 1, \ldots, l. \end{cases} \tag{3d}$$

A generalization of the single-peak landscape characterized as *single-peak linear landscape* combines features of linear and single-peak landscapes: Fitness decreases linearly in the range $0 \le k \le h$ and is constant for the rest of the domain, $h \le k \le l$:

$$f_k = \begin{cases} f_0 - \Delta f \frac{k}{h} & \text{for } k = 0, 1, \ldots, h-1, \\ f_n & \text{for } k = h, \ldots, l \end{cases} \qquad h = 1, \ldots, l. \tag{3e}$$

The landscapes (3a)–(3d) are completely described by the two parameters f_0 and f_n. Only the case (3e) requires a third parameter h defining the position of the discontinuity. We remark that single-peak linear landscapes with $h = 1$ are identical to single-peak landscapes and a landscape with $h = l$ is a linear landscape.

Fully resolved fitness landscapes. A fitness landscape is denoted as *fully resolved* when individual fitness values are determined for or assigned to different sequences and not only to classes as in case of simple fitness landscapes. The number of fitness values required is κ^l where κ denotes the number of different digits in the alphabet, e.g., $\kappa = 2$ for binary sequences and $\kappa = 4$ for natural nucleic acids. Within the last fifteen years, plenty of progress has been made in the determination of fitness values and trajectories of adaptive evolution of viruses (Betancourt and Bollback 2006; Elena and Sanjuán 2007) and successful attempts were made to measure distributions of fitness effects (Sanjuán et al. 2004). In general, exploration of fitness landscapes by site-directed mutagenesis is restricted to small neighborhoods—variants with Hamming distance $d_H = 1, 2, 3$—from the master sequence X_0 or, in other words, to local areas in sequence space. Global information on fully resolved fitness landscapes of real systems is still far out of reach because of high dimensionality and hyper-astronomical numbers of sequences. It is also important to stress that fitness values and landscapes depend strongly on environmental effects

and therefore, they can be determined efficiently only in approaches where a sufficiently large number of parameters can be kept constant, for example, in experimental evolution.

One of the earliest assays for experimental evolution was developed by Spiegelman and coworkers (Mills et al. 1967; Spiegelman 1971): RNA molecules from the bacteriophage Qβ were transfected into a stock solution containing excess of all materials required for replication—the four RNA building blocks, **ATP**, **UTP**, **GTP**, **CTP**, and the enzyme Qβ-replicase—under suitably controlled conditions such as pH, ionic strength, and $\mathbf{Mg}^{2\oplus}$. Spiegelman's test tube experiment is an extreme example of adaptive evolution by loss of function since the RNA in the test tube needs little more than a suitable binding site for the enzyme and accordingly, the chain length of the viral RNA is reduced from $l = 4217$ to a few hundred through fitness increasing deletions. Detailed investigations of RNA replication kinetics revealed the molecular mechanism of in vitro evolution (Biebricher 1983; Biebricher et al. 1983, 1984, 1985). The most striking result of these very elegant and systematic studies is the observation that the selection mechanism changes with an increasing concentration ratio of RNA to replicating enzyme because of a change in the rate-limiting step of the multi-step kinetics, which consists of binding the RNA to the enzyme, initiation and propagation of complementary step synthesis, and product release. For the landscape concept, this finding has the immediate consequence that extracellular RNA evolution takes place upon different landscapes depending on whether or not enzyme is supplied in excess.

One of the most extensive construction and analysis of a viral fitness landscape has been performed in clinical studies with the human immunodeficiency RNA retrovirus (HIV-1) (Kouyos et al. 2012). Fitness is measured as the in vitro reproductive capacity of HIV-derived amplicons that were prepared and inserted into a constant resistance test vector (Kouyos et al. 2011). The empirical basis of the study is $\sim$70,000 clinical HIV-1 isolates taken in the absence of drug treatment or in the presence of a single drug chosen from a collection of fifteen. The fitness landscape is derived from this data set by means of a statistical model predicting fitness from the amino acid sequences of entire HIV protease (99 aa)[3] and parts of HIV reverse transcriptase (a heterodimer consisting of p66 with 560 aa and p52 with 440 aa) with a total chain length of 460. Landscapes are constructed by fitting of parameters to data from 65,000 isolates as training set, and the remaining 5000 are used as test for the predictive power of parameter set. The landscape fitted to the fitness values of the drug-free isolates is taken as reference. Two features, which will be analyzed and discussed in Sect. 2, were found to be characteristic for the HIV fitness landscape: (i) *ruggedness* in the sense of containing many local fitness maxima and (ii) *neutrality* expressed as an appreciable fraction of sample points share the same fitness. In addition, but nor surprisingly from the molecular point of view, the results confirm that epistasis is highly important since the effect of a given

[3]Here, 'aa' stands for 'amino acid residue.'

point mutation depends strongly on the presence or absence of other mutations in the isolate.[4] Although the HIV study (Kouyos et al. 2011) is very extensive indeed and reaches the upper limit that can be achieved straightforwardly at present, a commentary (Weinreich 2011) correctly says that much more work in theory and experiment is needed in order to allow for clinically valuable predictions. As examples of bacterial landscapes, we mention a study of fitness landscape defined by gene expression levels in the core metabolism of *Methylobacterium extorquens* (Chou et al. 2014) and an extensive analysis of epistatic interactions in the fitness landscape of *Escherichia coli* (Beerenwinkel et al. 2007).

Tunable resolved fitness landscapes with random assignments. Despite the enormous progress in the empirical determination of fitness landscapes reported in the previous paragraph, models for assigning fitness value to genotypes are required. There are, for example, 8×10^{2538} different RNA sequences of the chain length of the Qβ-bacteriophage, and even if the vast majority of sequences are functionless as genotypes, the remainder would be beyond all technical bounds. Accordingly, model landscapes that allow for fast calculation of a large number of fitness values were invented. We mention here two of them: (i) the random Nk landscape (RNkL) proposed by Kauffman (Kauffman and Levin 1987; Kauffman and Weinberger 1989) and (ii) the realistic rugged landscape (RRL) and its variant the realistic neutral landscape (RNL) introduced by the author (Schuster 2012, 2013).

Random Nk fitness landscapes. The RNkL (Altenberg 1997) is a stochastic model that generates fitness values f_j for binary sequences of chain length $l = N$. In other words, we are dealing with a genotype consisting of N loci and two alleles at each locus: $\mathsf{X}_j = (x_1^{(j)}, x_2^{(j)}, \ldots, x_N^{(j)})$ with $x_i^{(j)} \in \{0, 1\} \forall i = 1, 2, \ldots, N$. The fitness of the genotype X_j is assumed to be the average of the fitness components $\phi_i^{(j)}$ contributed by the individual loci:

$$f_j = f(\mathsf{X}_j) = \frac{1}{N} \sum_{i=1}^{N} \phi_i^{(j)}(x_i^{(j)}; x_{i1}^{(j)}, x_{i2}^{(j)}, \ldots, x_{ik}^{(j)}) \quad \text{with} \quad x_{il}^{(j)} \in \{x_1^{(j)}, x_2^{(j)}, \ldots, x_N^{(j)}\}; \quad l \neq i, \text{all } l \text{ different.} \tag{4}$$

The fitness component of position i in sequence X_j, $\phi_i^{(j)}$ clearly depends on the allele at this position, $x_i^{(j)}$, and through epistatic interactions, it depends also on the alleles at k other positions denoted by $x_{il}^{(j)}$ with $l = 1, \ldots, k; l \neq i$. Two possibilities were considered by Kauffman: (i) *adjacent neighborhoods* and (ii) *random*

[4]Considering single nucleotides as sites in structural RNA elements requires complementarity of the nucleobase at another locus for the formation of a base pair, and accordingly, the two sites are strongly coupled epistasis (see Sect. 2).

neighborhoods. In the first case, the k genes lying closest to position i on the chromosome are chosen, whereas in the second case, the genes are chosen at random. Epistatic contributions are calculated by assuming a *house of cards* model of fitness effects as proposed by Kingman (1978); see also (Kingman 1980, p. 15): When an allele at one locus is changed, the fitness components of all alleles, which interact with this locus, are changed without correlations to their previous values. The metaphor illustrates the situation as follows: If a single card is pulled out of a house of cards, the house collapses and must be rebuilt from scratch.

The parameter k is designed as a tunable parameter for the ruggedness of the landscape: $k = 0$ implies a smooth, single-peak linear landscape often called *Mount Fuji landscape,* and the maximal value $k = n - 1$ gives rise to fully developed randomness. The Nk landscape for $k = 2$ was shown to be closely related to a spin glass Hamiltonian in the sense that the Nk model describes a special class of spin glasses (Kauffman 1993, p. 43) [for more details, see Reidys and Stadler (2001, 2002)]. The Nk landscape with two adjacent neighbors ($k = 2$), for example, can be derived from a linear chain of genes by closing it to a loop, and in the random model, of course, no such assumption is required.

Realistic random fitness landscapes. In order to introduce a random distribution of fitness values in the single-peak fitness landscape, we consider a band of fitness values for all sequences except the master sequence. The lack of detailed empirical data is supplemented by a random input and a tunable parameter d that determines the width of this band, and neglecting neutrality, the fitness values are calculated from the expression (Schuster 2013, p. 608):

$$f(\mathsf{X}_j) = f_j = \begin{cases} f_0 & \text{if } j = 0, \\ f_n + 2d\Delta f(\eta_j^{(s)} - 0.5) & \text{if } j = 1, \ldots, \kappa^l - 1. \end{cases} \tag{5a}$$

The parameters f_0 and f_n are defined as before, and $\eta_j(s)$ is the jth output of a pseudorandom number generator that has been started by using s as seed. In order to make the procedure fully determined, the method used in the generation of pseudorandom numbers has to be specified. In addition, we need to predefine the distribution of the pseudorandom numbers. Here, we use a uniform distribution on the unit interval, $0 \leq \eta_j^{(s)} \leq 1$.

Neutrality can be readily incorporated into RRLs by means of a tunable degree of neutrality, λ: The fitness value f_0 is assigned to the master sequence and to all sequences X_j with pseudorandom numbers $1 \leq \eta_j^{(s)} \leq 1 - \lambda$, and random scatter in the sense of Eq. (5a) is chosen for all other sequences:

$$f(\mathsf{X}_j) = \begin{cases} f_0 & \text{if } \; j = 0, \\ f_0 & \text{if } \; \eta_j^{(s)} \geq 1 - \lambda, \\ f_n + \frac{2d}{1-\lambda}\Delta f(\eta_j^{(s)} - 0.5) & \text{if } \; \eta_j^{(s)} < 1 - \lambda, \\ & j = 1, \ldots, \kappa^l - 1; j \neq m. \end{cases} \tag{5b}$$

As shown in Eq. (5b), the interval $0 \leq \eta_j^{(s)} < 1 - \lambda$ is stretched to the full bandwidth of d for the determination of the remaining f_j-values. Clearly, Eq. (5a) results from (5b) through setting $\lambda = 0$ which is tantamount to *no neutrality*. Accordingly, an RRL or RNL is fully characterized by:

$$\begin{aligned} \text{RNL} &: \mathcal{L} = \mathcal{L}(l, \kappa, f_0, f_n; \lambda, d, s) \quad \text{and} \\ \text{RRL} &: \mathcal{L} = \mathcal{L}(l, \kappa, f_0, f_n; 0.0, d, s). \end{aligned} \tag{6}$$

It is important to stress that the definition of realistic random landscapes according to (5a, 5b) does not allow for landscape design since the relation between the random seed s and the calculated fitness values is too complicated in order to allow for a reconstruction by an inverse method. This concept of landscapes can be rather understood as a mean for performing a kind of experiment in computational biology in three steps: (i) choose seeds for the random number generator, e.g., $s \in \{000, \ldots, 999\}$, (ii) compute landscape $\mathcal{L}(l, \kappa, f_0, f_n; \lambda, d, s)$ in the form of the fitness values $f(\mathsf{X}_j), j = 1, \ldots, \kappa^l - 1$, and (iii) compute and analyze the mutant distribution $\Upsilon(d, \lambda; p, t)$.

The two major questions that will be studied in the rest of this chapter are: (i) How does the quasispecies distribution change as a function of the mutation rate p; and (ii) do abrupt transitions at critical mutation rates, p_{cr}, exist, and if they exist, how do they depend on the extend of random scatter d? The answer to the second question is of particular importance because doubts have been raised whether or not the scenarios derived from single-peak landscapes are specific for this simple landscape, and accordingly might not be relevant for more general rugged landscapes [(Baake and Wagner 2001; Charlesworth 1990; Wiehe 1997); see Sect. 4].

2 Sequence Structure Mappings

In the previous section, we introduced several classes of fitness landscapes and mentioned the available empirical support for two general features of real landscapes: (i) ruggedness and (ii) neutrality. Here, we present additional arguments for this conjecture by considering the properties of known genotype–phenotype mappings. In experimental evolution with molecular systems (Biebricher 1983), the genotype is considered as a polynucleotide sequence, DNA or RNA, and the phenotype is the molecular structure. Predicting biopolymer structures from known sequences is still kind of a scientific art, but in case of simplified structures of RNA molecules, so-called *secondary structures*, it is possible to derive shapes by simultaneous consideration of free energies of substructures and some principles from combinatorics. Secondary structures of polynucleotides are graphically illustrated listings of nucleotide pairs where the graphs of structures are equivalent to representations by strings over a three-letter alphabet: (i) '(' opening of a base pair, (ii) ')' closing of a base pair, and (iii) '•' an unpaired nucleotide. The assignment of

opening parentheses to closing parentheses of base pairs follows mathematical rules, i.e., the first parenthesis opens a nucleotide pair and matches the parenthesis that encloses a complete set of closed parentheses. As an example, we show the string representation of the reference structure S_0 in Fig. 4

$$(((\cdot(((\cdot\cdot\cdot)))\cdot)))\,,$$

where the three left opening parentheses match the three rightmost closing parentheses and the three inner parentheses form the hairpin loop.

Landscapes are built from sequences by two consecutive mappings: (i) the map of biopolymer sequences into molecular structures [for a review of the RNA model, see, e.g., Schuster (2003, 2006)] and (ii) the map from structures into molecular properties. In a given and constant environment, replication parameters tantamount to fitness values are functions of molecular structures. The current paradigm of structural biology is based on the conjecture that structures can be derived from sequences, and molecular properties in the form of parameters in functions are derivable from structures:

$$\text{sequence} \quad \Rightarrow \quad \text{structure} \quad \Rightarrow \quad \text{function}.$$

Sequences, structures, and parameters in functions are objects of metric spaces (Fig. 3), and relations between them are defined by mappings. The Hamming

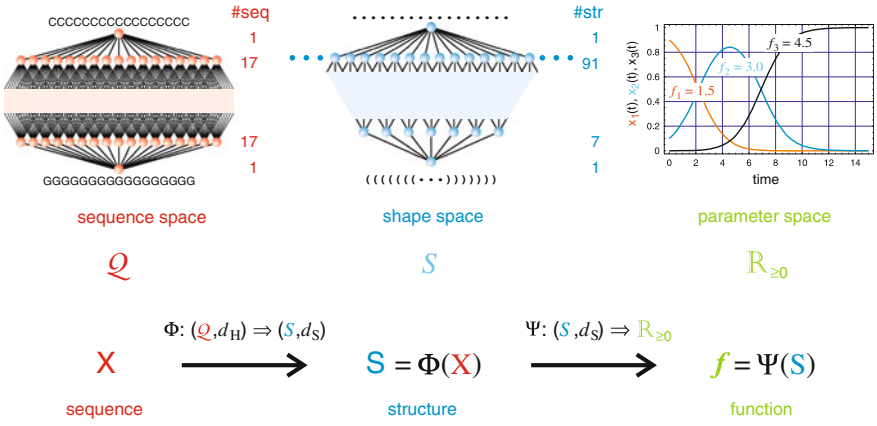

Fig. 3 The paradigm of structural biology. The relation between sequence, structure, and fitness is sketched as a sequence of two mappings from sequence space ($\mathcal{Q}_{17}^{(2)}$) into shape space ($\mathcal{S}_{17}^{(2)}$) and from shape space into nonnegative real numbers ($\mathbb{R}_{\geq 0}$). In order to facilitate drawing, sequences are assumed to chosen from a two-letter alphabet ($\mathbf{C}, \mathbf{G}$). For $l = 17$, sequence space contains $2^{17} = 131{,}072$ sequences, which form 530 different *acceptable RNA secondary structures* (Schuster 2006). These structures determine the fitness values f. Sequence space and shape space are metric spaces with the Hamming distance d_H and some structure distance d_s representing the metric. Parameter space is based on real numbers $\mathbb{R}$, and the absolute value of the difference, $|f_i - f_j| = d_{ij}$, is the metric

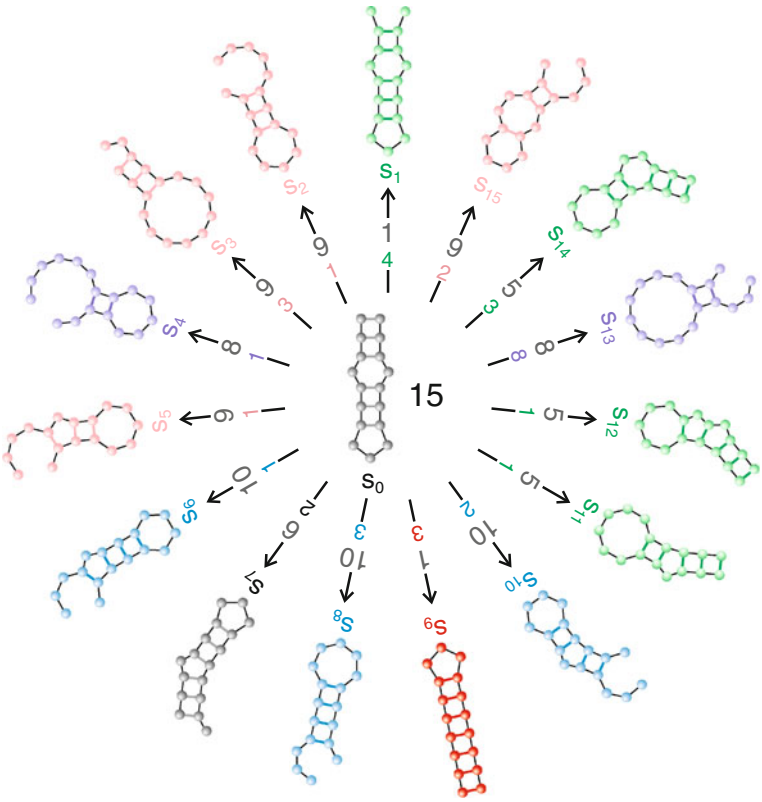

Fig. 4 Structures of the one-error mutant spectrum of a small RNA molecule. The figure presents the structures of all 51 single point mutations of sequence X_0. In total, 16 different structures S_k with $k = 0, 1, \ldots, 15$ were obtained. Structure S_0 in the *center* is the structure of the reference sequence X_0, and it is most frequent and occurs 15 times. The structures on the periphery are ordered according to their appearance in the series of consecutive mutations (Fig. 5). Inserted in the *arrows* pointing from S_0 to the individual structures S_k are (i) the numbers of occurrence (*color*) and (ii) the base pair distance $\mathrm{d}^{\mathrm{S}}_{0k}$ (larger numbers in *gray*). All drawings of structures begin at the 5′-end of the RNA, which is always the left end of the graph or string (in upright positioning), nucleotides are shown as beads, and base pairs are connected by a colored *thick line*. Colors encode number of base pairs: *red* 7, *black* 6, *green* 5, *blue* 4, *pink* 3, and *lavender* 2

distance d_{H} (Fig. 1) is the natural metric in sequence space for point mutations as the dominant changes in sequences. The base pair distance d_{H} can be chosen as a metric in *shape space* being the space of all RNA secondary structures that can be formed by all sequences of a given length l. It is defined as the number of base pairs in which two structures differ, for example, the base pair distance between the structures S_0 and S_7 (Fig. 4),

$$d_{07}^{\mathrm{S}} = \left\{ \begin{array}{l} (((\cdot(((\cdot\cdot\cdot)))\cdot))) \\ \cdot((((((\cdot\cdot\cdot)))\cdot))) \end{array} \right\} = 6.$$

The three inner base pairs of the hairpin loop (Fig. 4) remain the same, but the three outer base pairs are replaced by three other base pairs, and this leads to a structure distance of $d_{07}^{\mathrm{S}} = 3 + 3 = 6$, since three base pairs have to be removed first and then three base pairs are added.

At the current state of the art, a determination of kinetic parameters from structures is not possible without largely simplifying assumptions. In a previous evolution model, we estimated replication parameters either by the free melting energies of structures, $-\Delta G_0^T$ or more elaborately by cooperative melting of stacking regions (Fontana et al. 1989; Fontana and Schuster 1987) and assumed the degradation rates to be determined by the unpaired nucleotides in the structure. This model introduces complex behavior since optimization of fitness leads to frustration (Toulouse 1977, 1980) in the sense of spin glass theory (Edwards and Anderson 1975; Sherrington and Kirkpatrick 1975). The RNA-based model has been used to analyze replication and mutation-based evolution in silico in population of up to 10,000 RNA molecules (Fontana and Schuster 1998a, b). In particular, mean fitness in the population shows a stepwise approach toward the optimum value and transitions can be classified as minor changes in structure occurring at almost constant mean fitness and major changes, which are commonly accompanied by fitness increases.

The bizarre nature of sequence to structure and structure to fitness mappings is illustrated by means of a simple but nevertheless representative example consisting of a very small RNA molecule with chain length $l = 17$ and the sequence $\mathsf{X} = (\mathbf{AGCUUACUUAGUGCGCU})$. This chain length is just enough to form a maximum of seven base pairs, and all properties can be either counted or calculated, or seen by inspection. Despite its simplicity, the example reflects the most important features of sequence structure mappings. The minimum free energy structure S_0 is calculated[5] for X_0, and a free energy of folding $\Delta G_0^{(0^\circ\mathrm{C})} = \Delta G_0^0 = -6.39$ kcal/mole is obtained. Then, the same computations are performed for all 51 one-error mutants of X_0 and the numbers of occurrence for the individual structures are enumerated. The results are shown in Fig. 4: The most frequent structure is the structure of the reference sequence, S_0, and it is found 15 times, followed by structure S_{13}, which appears eight times, S_1 four times, S_3, S_8, S_9, and S_{14} three times each, S_7, S_{10} and S_{15} twice, and finally S_2, S_4, S_5, S_6, S_{11} and S_{12}, which occur only once. Thus, the local degree of neutrality in sequence space is $\lambda(\mathsf{X}_0) = 0.29$. Considering the free energy values of folding, ΔG_0^0 in Fig. 5 (upper plot), there is no relation between the frequency of occurrence and the folding energy: The most stable structure S_3 (red) appears three times, whereas the least stable structures S_2 and S_{13} occur

[5]Standard software packages are available for RNA secondary structure computation, for example, *mfold* (Zuker 1989) or the *Vienna RNA package* (Hofacker et al. 1994; Lorenz et al. 2011).

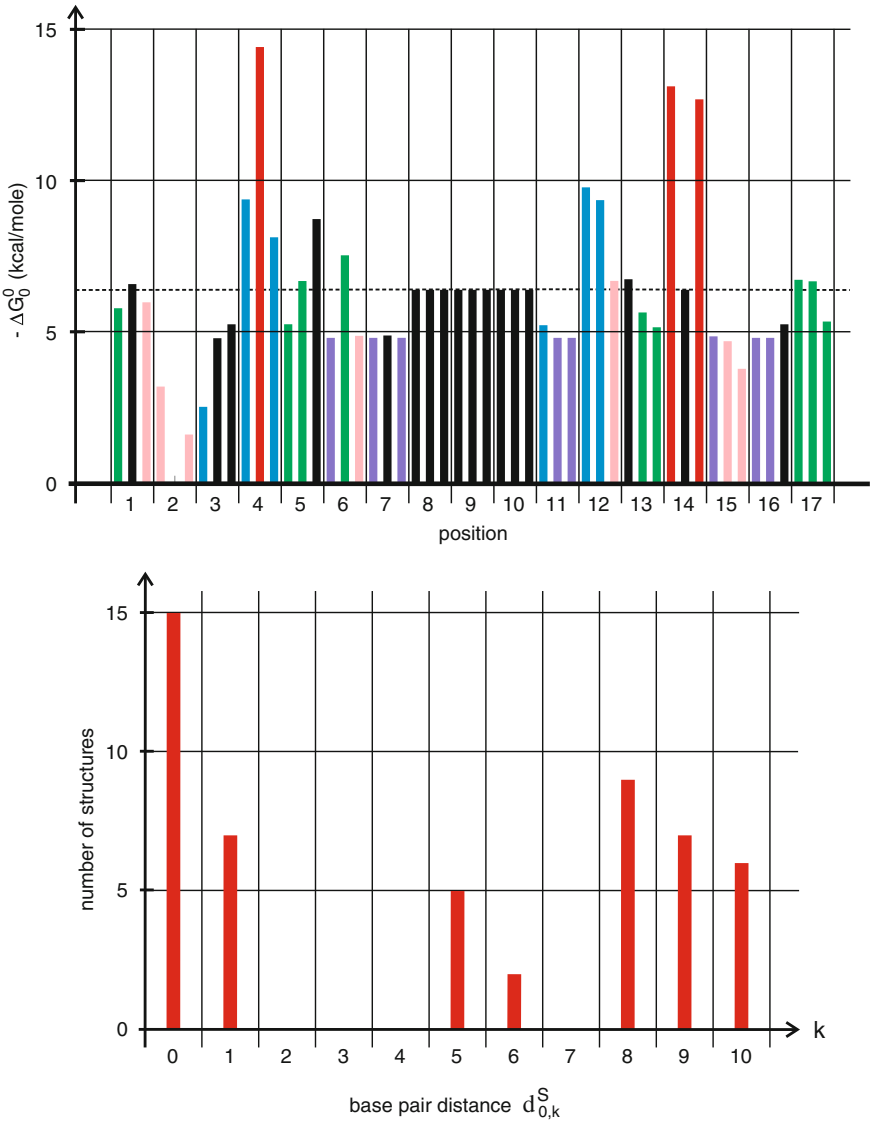

Fig. 5 Free energy of folding and base pair distances of one-error mutants. The *upper plot* shows the folding energies at 0 °C of the 51 one-error mutants of X_0. At each position 1–15, the sequence of mutants is $\mathbf{N} \rightarrow \mathbf{A}$, $\mathbf{N} \rightarrow \mathbf{U}, \mathbf{N} \rightarrow \mathbf{G}$, and $\mathbf{N} \rightarrow \mathbf{C}$, where the trivial replacement leaving the sequence unchanged is omitted ($\mathbf{N} = \{\mathbf{A}, \mathbf{U}, \mathbf{G}, \mathbf{C}\}$). The folding energy of the reference sequence is shown as *dotted line*, and the *color code* refers to the number of base pairs (see caption of Fig. 4). The lower histogram presents the numbers of structures in the mutant spectrum of X_0 at a given base pair distance d^{S}_{0k} from the reference structure $\mathsf{S}_0 = \Phi(\mathsf{X}_0)$

together nine times. As expected, there is appreciable scatter in folding energies between sequences, which form the same minimum free energy structures. Additional information on the ruggedness of the free energy landscape is provided by the correlation length of the folding energies, $\varrho(l)$ (Fontana et al. 1991, 1993): For a chain length $l = 17$ and the natural four-letter alphabet, a free energy correlation length of $\varrho(17) \approx 3.0$ is computed, which means that the energy values at Hamming distance $d_{\mathrm{H}} = 3$ have a correlation coefficient of $1/e = 0.37$ with the energy of the reference sequence X_0, at $d_{\mathrm{H}} = 10$, and this coefficient is only 0.036 implying that the neighborhood memory on X_0 has practically faded out and the statistics of the energy distribution is about the same as found at any randomly chosen point in sequence space. Eventually, we consider the relation between similarities between structures as expressed by the base pair distance d_{S} (Fig. 5, lower plot): The most frequently occurring distance is $d^{\mathrm{S}}_{0k} = 8(9\times)$, followed by $d^{\mathrm{S}}_{0k} = 1$ and $d^{\mathrm{S}}_{0k} = 9(7\times \text{ each})$, and $d^{\mathrm{S}}_{0k} = 10$, $d^{\mathrm{S}}_{0k} = 5$, and $d^{\mathrm{S}}_{0k} = 6(6, 5 \text{ and } 2\times, \text{respectively})$.

The experimental approach to determine fitness landscapes of small RNA molecules has been profiting substantially from the availability of deep sequencing and high-throughput methods (Pitt and Ferré-D'Amaré 2010). We mention here only recent work that succeeded to explore almost the entire sequence space of a small RNA molecule of chain length $l = 24$ (Athavale et al. 2014; Jiménez et al. 2013) and refer to Chap. 3 (this volume) for details.

A comparison of the landscape obtained from mapping structures into folding energies (Fig. 5) with the Nk model is tantamount to estimating the value of k for $N = l$, the chain length of the RNA sequence. In other words, we need to answer the question: 'Mutations at how many positions along the sequence change the free energy of folding?' Considering the upper plot in Fig. 5, we see that mutations in the unpaired nucleotides of the hairpin loop leave ΔG^0_0 unchanged, and in addition, we find seven more mutants exhibiting values close to the reference value. In total, we have 16 out of 51 mutations leaving 35 cases of change. Normalizing to sites gives a vague estimate of $k = 11$ suggesting that on average, 11 positions out of 17 exert influence of the energy of folding. As expected, a realistic landscape built from sequence-dependent biopolymer properties is very rugged but not completely uncorrelated as would be an Nk model with $k = l - 1 = 16$. The correlation although weak comes from the regularities of mapping structures into folding energies, and more base pairs yield higher energies in absolute value, for example.

3 Mutations and Population Dynamics

Before the seminal paper by Watson and Crick (1953), the concept of mutation was nebulous and it required molecular insight in order to conceive appropriate models for the replication process. After the proposal of the structure of, b-DNA was on the table; however, one could immediately guess how nucleic acids replicate and

mutate as the authors themselves stated: 'It has not escaped our notice that the specific pairing we have postulated suggests a copying mechanism for the genetic material.'

Mutation models. Two concepts are currently prevailing, which originate from different mutation mechanisms: (i) the quasispecies model introduced in 1971 by [Eigen (1971), Eigen and Schuster (1977)] and (ii) the selection–mutation model attributed to Crow and Kimura (1970, p. 265, Eq. 6.4.1), which is also know as *paramuse* (parallel mutation and selection) model (Baake et al. 1997). Mutation in the quasispecies model is attributed to the reproduction process, and correct replication and mutations are visualized as different reaction channels of the same replication step (Chap. 1, Fig. 1), whereas mutation in the paramuse model is due to some external process independent of reproduction [Fig. 6; for reviews, see Baake and Wagner (2001), Burger (1998)]. Nevertheless, the kinetic equations resulting from both models are closely related. The difference in the mutation mechanism has biological consequences: The number of mutations is proportional to the number of reproduction events or generations in the quasispecies model, whereas proportionality with respect to time is predicted by the paramuse model provided the external driving forces causing mutation are constant. Observations on organisms of largely different genome size from viroids to higher eukaryotes reveal roughly constant spontaneous mutation rates for classes of organisms. The mutation rates per genome and replication event range from 1 found with viroids, RNA viruses, and also with sexual reproduction of higher eukaryotes to 1/300 for microbes with DNA-based chromosomes (Drake et al. 1998; Gago et al. 2009). Proportionality with respect to real time is the basis of the molecular clock model (Ho and Duchêne 2014; Lanfear et al. 2010), which apart from still to be explained vagaries seems to be correct for vertebrates. Accordingly, it is a matter of the problem under consideration whether quasispecies or paramuse is the model of choice.

At this point, we would like to mention that substantial insight into quasispecies and error thresholds were gained by showing that the value matrix W of the quasispecies equation is equivalent to the row transfer matrix of a 2D Ising model of magnetism (Leuthäeusser 1986, 1987). In particular, the analogy to spin systems

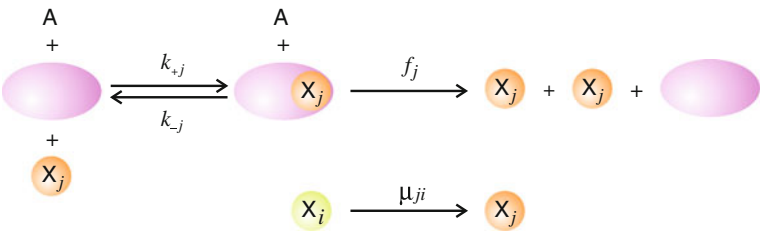

Fig. 6 The Crow–Kimura model of reproduction and mutation. The Crow–Kimura model combines error-free reproduction with replication-independent mutation. Although it leads to the same differential equation (7a) as the quasispecies replication–mutation model shown in Chap. 1 (Fig. 1), the interpretation of the parameters and the physical restrictions on them are different

allowed for the application of methods forms statistical physics and the generalization to spin glasses made it possible to show straightforwardly that the transitions on simple and more complex landscapes may fulfill the requirements of first-order phase transitions in the limit of infinite chain lengths l (Tarazona 1992). Similarly, it was shown that the paramuse model corresponds to the Hamiltonian of an Ising quantum chain (Baake et al. 1997; Baake and Wagner 2001) and methods from quantum statistical mechanics were successfully applied in the search for solutions of the replication–mutation problem [see Chap. 5 and, for example (Bratus et al. 2014; Galluccio 1997; Kang and Park 2008; Park et al. 2010; Saakian and Hu 2006; Saakian et al. 2004) as well as the review (Baake and Gabriel 1999)].

The kinetic differential equation of the quasispecies model [Chap. 1 (this volume), Eq. (3)], formulated in normalized variables $x_j = [\mathsf{X}_j]/\sum_{i=1}^{N}[\mathsf{X}_i]$ with $\sum_{i=1}^{N} x_i = 1$ can be easily written in matrix form,

$$\begin{aligned} \frac{\mathrm{d}x_j}{\mathrm{d}t} &= \sum_{i=1}^{N} Q_{ji} f_i x_i - x_j \bar{f}(t); \quad j = 1, \ldots, N \quad \text{or} \\ \frac{\mathrm{d}x}{\mathrm{d}t} &= (Q \cdot F - \bar{f}(t))x, \end{aligned} \tag{7a}$$

where $x = (x_1, \ldots, x_N)^t$ is the column vector of normalized concentrations $\sum_{i=1}^{N} x_i = 1, Q = \{Q_{ij}; i, j = 1, \ldots, N\}$, is the mutation matrix—with Q_{ij} being the frequency at which X_i is synthesized as a correct ($i = j$) or erroneous ($i \neq j$) copy of the template X_j—and the fitness values f_i are contained in the diagonal matrix $F = \{F_{ij} = f_i \delta_{i,j}; i, j = 1, \ldots, N\}$. The mean fitness of the population is denoted by $\bar{f}(t) = \sum_{i=1}^{N} f_i x_i(t)$. In case of the paramuse model, we obtain:

$$\frac{\mathrm{d}x_j}{\mathrm{d}t} = (f_j - \bar{f}(t))x_j + \sum_{j=1}^{N} \mu_{ji} x_j \quad \text{or} \quad \frac{\mathrm{d}x}{\mathrm{d}t} = (F + \boldsymbol{\mu} - \bar{f}(t))x. \tag{7b}$$

Herein, the mutation matrix is denoted by $\boldsymbol{\mu}$.

Both Eqs. (7a) and (7b) can be easily cast into identical form by introducing the value matrix W

$$\frac{\mathrm{d}x}{\mathrm{d}t} = (\mathrm{W} - \bar{f}(t))x \quad \text{with} \quad W = Q \cdot F \quad \text{or} \quad W = \boldsymbol{\mu} + F, \tag{7c}$$

respectively. The resulting Eq. (7a–7d) is mildly nonlinear and can be solved by means of an integrating factor transformation and the solution of the remaining eigenvalue problem (Eigen et al. 1988, 1989; Jones et al. 1976; Thompson and McBride 1974). The value matrix W has to be a primitive matrix in order to fulfill the conditions for the applicability of the Perron–Frobenius theorem (Seneta 1981,

pp. 3–11 and 22–23),[6] which guarantees that (i) the largest eigenvalue is real, positive, and non-degenerate; and (ii) the largest eigenvector has only strictly positive components. Exact solutions of Eq. (7c) are obtained through diagonalization of the value matrix: $H.W.B = \Lambda$ where the diagonal matrix $\Lambda = \{\Lambda_{ii} = \lambda_i; i = 1, \ldots, N\}$ embodies the eigenvalues λ_i. The matrices $H = \{h_{ij}\}$ and $B = \{b_{ij}\} = H^{-1}$ fulfill the eigenvalue equations $H.W = \Lambda.H$ and $W.B = B.\Lambda$ and contain the left-hand and right-hand eigenvectors of the value matrix W, which in explicit form are the row vectors $\mathbf{h}_k = (h_{ki}, i = 1, \ldots, N)$ and the column vectors $\mathbf{b}_j = (b_{ij}; i = 1, \ldots, N)^t$. The solutions can now be expressed by

$$\begin{aligned} x_j(t) &= \frac{\sum_{k=1}^{N} b_{jk} \sum_{l=1}^{N} h_{kl} x_l(0) \exp(\lambda_k t)}{\sum_{i=1}^{N} \sum_{k=1}^{N} b_{ik} \sum_{l=1}^{N} h_{kl} x_l(0) \exp(\lambda_k t)} \\ &= \frac{\sum_{k=1}^{N} b_{jk} \beta_k(0) \exp(\lambda_k t)}{\sum_{i=1}^{N} \sum_{k=1}^{N} b_{ik} \beta_k(0) \exp(\lambda_k t)} \quad \text{with} \quad \beta_k(0) = \sum_{l=1}^{N} h_{kl} x_l(0), \end{aligned} \tag{7d}$$

wherein the eigenvalues λ_k are the rate parameters and the coefficients $\beta_k(0)$ encapsulate the initial conditions.

The difference between the two mutation models cannot be seen from these mathematical results and boils down to two issues: (i) The quasispecies model treats replication and mutation as parallel reaction channels of one reaction step, and accordingly, the value matrix is a product of the mutation and the fitness matrix, whereas reproduction and mutation are independent reaction steps in the paramuse case and the two matrices are added; and (ii) the mutation matrix Q of the quasispecies is a stochastic matrix, $\sum_{i=1}^{N} Q_{ij} = 1$, because a replication has to be either correct or error-prone, whereas the condition $\sum_{i=1}^{N} \mu_{ij} = 0$ is used in the paramuse model. In addition, mutation is commonly restricted to single point mutations in the paramuse model. As said before, apart from these technical details, the mutation mechanisms shown in Fig. 1, Chap. 1 (this volume), and Fig. 6 are dealing with entirely different situations. In the quasispecies model, mutation occurs during the reproduction process and this is the situation that is relevant for viruses (see Chaps. 7, 9, 12, and 14, this volume).

Deterministic and stochastic autocatalysis. In order to set the stage for a discussion of the dynamics of quasispecies formation, we consider first the simple autocatalytic chemical reaction $\mathsf{A} + \mathsf{X} \rightarrow 2\mathsf{X}$ in the well-defined and controllable environment of a flow reactor (Schmidt 2004, p. 87ff). In order to relate to the quasispecies concept, we interpret simple autocatalysis as a replication–mutation system in which all individual sequences are lumped together in one species: $\mathsf{X} = \mathsf{X}_1 \oplus \mathsf{X}_2 \oplus \ldots \oplus \mathsf{X}_N$, and hence, the stochastic and deterministic variables take on the form $\mathcal{C} = \sum_{i=1}^{N} \mathcal{X}_i$ and $c = \sum_{i=1}^{N} x_i$, respectively. A solution containing the

[6] A matrix W is primitive if (i) all the elements of matrix W are nonnegative and (ii) some finite power W^m is a positive matrix, which means that all entries of W^m are strictly positive.

compound A in concentration a_0 flows into the reactor with a rate parameter r [vol $\times$ time^{-1}], and the inflow is compensated by an outflow of the volume of reactor solution, thus yielding the reaction equations

$$* \xrightarrow{a_0 \cdot r} \mathsf{A}; \tag{8a}$$

$$\mathsf{A} + \mathsf{X} \xrightarrow{f} 2\mathsf{X}, \tag{8b}$$

$$\mathsf{A} \xrightarrow{r} \text{ø}; \quad \text{and} \tag{8c}$$

$$\mathsf{X} \xrightarrow{r} \text{ø}. \tag{8d}$$

The rate parameter f is the analogue to fitness in the biological models and has the dimension [vol $\times$ mole^{-1} $\times$ time^{-1}].[7] The kinetic differential equations are obtained straightforwardly

$$\begin{aligned} \frac{\mathrm{d}a}{\mathrm{d}t} &= (a_0 - a)r - fac \quad \text{and} \\ \frac{\mathrm{d}c}{\mathrm{d}t} &= fac - cr = (fa - r)c, \end{aligned} \tag{8e}$$

The equation is also valid for the simplified system with the lumped concentrations $c(t) = \sum_{k=1}^{N} x_k$ if we replace the parameter f by the function $\bar{f}(t) = \sum_{k=1}^{N} f_k x_k(t) / \sum_{k=1}^{N} x_k(t)$, which represents the mean fitness of the population. Strictly speaking, the mean fitness is a function of time, and for common initial conditions, it is a non-decreasing function of time, and then, evolution is tantamount to fitness optimization. For the purpose of illustration, however, we shall assume a constant mean fitness corresponding to the rate parameter: $\hat{f} = f$. Then, it is straightforward to analyze the stationary states: $\mathrm{d}a/\mathrm{d}t = 0$ and $\mathrm{d}c/\mathrm{d}t = 0$ give rise to two solutions, S_1 and S_2,

$$\begin{aligned} &S_1 : \ \bar{a} = r \cdot \hat{f}^{-1}\bar{c}, \ = a_0 - r \cdot \hat{f}^{-1} && \text{asymp.stable for } a_0 > r \cdot \hat{f}^{-1}, \\ &S_2 : \ \bar{a} = a_0, \ \bar{c} = 0 && \text{asymp.stable for } a_0 < r \cdot \hat{f}^{-1}. \end{aligned} \tag{8f}$$

State S_1 corresponds to virus infection with a non-vanishing stationary virus concentration in the host, whereas S_2 models a situation where the virus dies out and the host recovers from the disease. With respect to stability, the two states are mutually exclusive: S_1, the state of infection, requires a minimum amount of susceptible material—cells or other forms of *nutrients*—and is asymptotically stable in the range $a_0 > r/\hat{f}$, whereas the state of extinction S_2 is asymptotically stable if

[7] We remark that autocatalytic steps play the key role in models of theoretical epidemiology. Features of the mechanism (8a–8g) for autocatalysis in the flow reactor remind, for example, of dynamical properties of models for infectious diseases (see, e.g., Mollison 1995).

$a_0 < r/\hat{f}$. At the inflow concentration $a_0 = r/\hat{f}$, the system exhibits a transcritical bifurcation [see, e.g., (Strogatz 1994, pp. 50–52)].

In order to analyze the influence of stochasticity on the reaction scheme (8a–8g), we formulate a bivariate master equation in the two random variables $\mathcal{A}$ and $\mathcal{C} = \sum_{k=1}^{N} \mathcal{X}_k$, where $\mathcal{X}_k$ is the random variable associated with X_k, with the probabilities $P_A = P(\mathcal{A}(t) = A)$ and $P_C = P(\mathcal{C}(t) = C)$, respectively. This master equation is the probabilistic analogue to Eq. (8e),

$$\begin{aligned}\frac{\mathrm{d}P_A(t)}{\mathrm{d}t} &= a_0 r P_{A-1}(t) + (\hat{f}A \cdot C - a_0 r - rA)P_A(t) \\ &\quad - (\hat{f}(A+1)(C-1) - r(A+1))P_{A+1}(t) \\ \frac{\mathrm{d}P_C(t)}{\mathrm{d}t} &= \hat{f}(A+1)(C-1)P_{C-1}(t) - (\hat{f}A \cdot C + rC)P_C(t) \\ &\quad + r(C+1)P_{C+1}(t),\end{aligned} \tag{8g}$$

which describes the probabilistic development of populations starting from initial probability distributions $P_A(0)$ and $P_C(0)$. For practical purposes, sharp initial distributions, $P_A(0) = \delta_{A,A_0}$ and $P_C(0) = \delta_{C,C_0}$, are almost always applied, because they are technically simpler to handle and they allow for direct comparison of the solutions derived from the ODE (8e) and from the master Eq. (8g). It is straightforward to show that the initial condition $C(0) = C_0 = 0$ implies $C(t) = 0$ for all $t > 0$. Whenever the number of autocatalytic units has reached the value zero, it remains there or in other words, the state $S_2(C = 0)$ is an absorbing state or boundary. This fact represents also the major difference between the deterministic and the stochastic model of autocatalysis: Since S_2 is the only absorbing state of the system, all trajectories have to converge to this state in the limit of infinite time, $\lim_{t\to\infty} C(t) = 0$. Under conditions at which the state S_1 is asymptotically stable in the deterministic system (8e), $a_0 > r/\hat{f}$, the master equations support a *quasistationary* state (Nåsell 2011): The concentration of the autocatalyst approaches a constant value, and for a sufficiently large initial number of autocatalytic units C, $C(0) = C_0 > C_{\mathrm{crit}}$, this value coincides with the value of c at $C(t) \approx \bar{c} = a_0 - r/\hat{f}$ and stays at this value for very long time, although the state S_2 will be reached with probability one at infinite time. For smaller values of C_0, the system converges to S_1 or goes extinct with a probability distribution depending on C_0. In Fig. 7, deterministic solution curves of (8e) are compared with the results of trajectory sampling for the master Eq. (8g).

There is one additional fundamental difference between the deterministic and the stochastic solution, which is also related to the fact that S_2 is absorbing. The deterministic equations are formulated in continuous variables, $a(t)$ and $x(t)$, which can become arbitrarily small without vanishing. This is not true for the stochastic variables, $\mathcal{A}(\mathrm{t})$ and $\mathcal{X}(t)$, which are integers by definition and take on only the values $0, 1, \ldots$. For sufficiently small values of $\mathcal{X}(0)$, the system may die out in the early phase with a certain probability, which decreases with increasing $\mathcal{X}(0)$. The problem

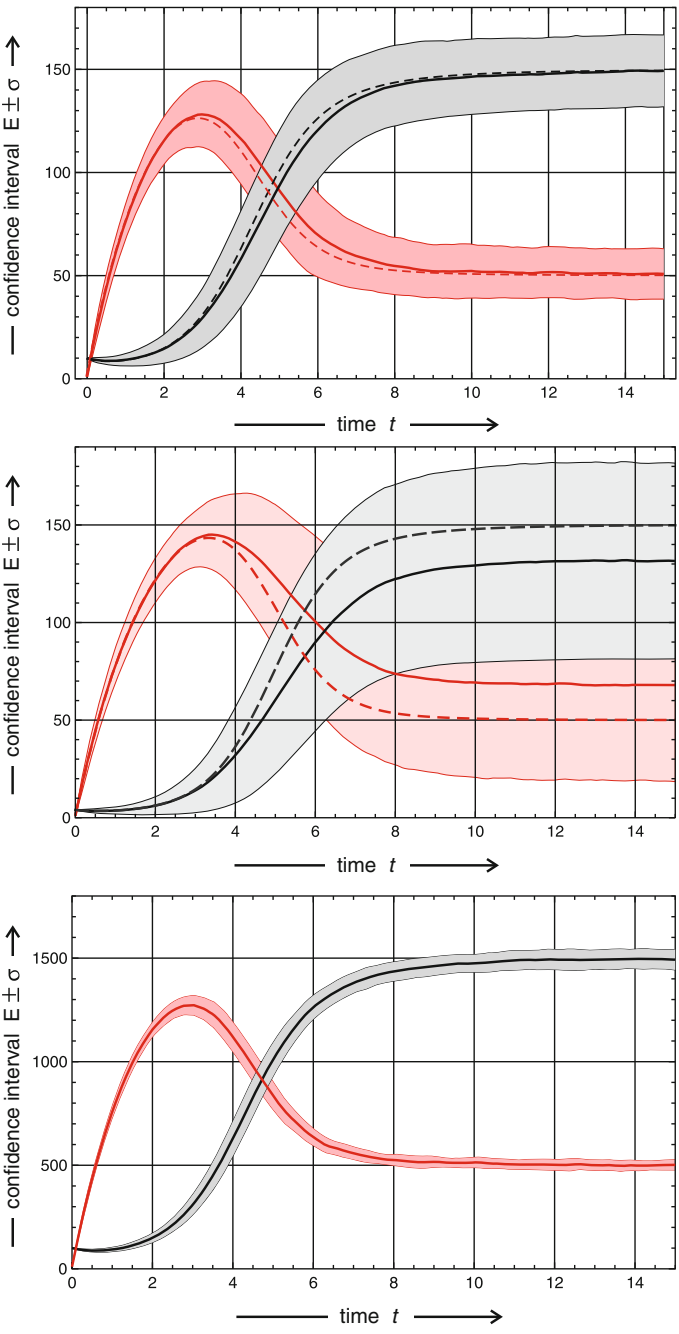
confidence interval E ± σ
150
100
50
0
0
2
4
6
8
10
12
14
time t
confidence interval E ± σ
150
100
50
0
0
2
4
6
8
10
12
14
time t
confidence interval E ± σ
1500
1000
500
0
0
2
4
6
8
10
12
14
time t

◀ **Fig. 7** Autocatalysis in the flow reactor. The figure illustrates two different sources of stochasticity in autocatalytic systems: (i) Random fluctuations become important at small particle numbers for every chemical reaction and (ii) the stochastic autocatalytic reaction has an absorbing boundary for zero autocatalytic units as this may lead to significant differences between the stochastic and the deterministic system. The topmost plot shows the expectation values of concentrations within the one standard deviation confidence interval, $E \pm \sigma$, for the input material A and the autocatalyst X calculated from a sample of 1000 trajectories calculated by means of an algorithm attributed to Daniel Gillespie (1977). The expectation values are compared with the deterministic solution integrated from the ODE (Eq. (8e); *dotted lines*; $x(0) = 10$). The plot in the middle shows the same system with a different initial condition ($x(0) = 4$). The change in the deterministic ODE integration concerns the initial phase, and both curves converge to identical stationary values, but the expectation value of the stochastic process leads to much smaller stationary amounts of autocatalyst when the initial value $x(0)$ was smaller. The plot at the bottom is dealing with the same reaction but with ten times larger particle numbers that give rise to smaller fluctuations relative to the expectation values. Shown are the expectation values within the one standard deviation confidence interval, $E \pm \sigma$ for the input material A and the autocatalyst X calculated from a sample of 100 trajectories. The deterministic solution curves coincide with the expectation value within the line width. Color code: $a(t)$ and $E(\mathcal{A}(t))$ *red*, and $x(t)$ and $E(\mathcal{X}(t))$ *black*. Choice of parameters for *upper* and *middle plot*: $a_0 = 200$, $r = 0.5$ and $f = 0.001$; initial conditions: $a(0) = 1$ and $x(0) = 4$ or $x(0) = 10$; choice of parameters for *lower plot*: $a_0 = 2000$, $r = 0.5$ and $f = 0.0001$; initial conditions: $a(0) = 10$ and $x(0) = 100$

is easily visualized by considering the probability densities $\mathrm{P}(\mathcal{A}(\mathrm{t}))$ and $\mathrm{P}(\mathcal{X}(\mathrm{t}))$, which are both bimodal for sufficiently long time and where the two modes correspond to the two states S_1 and S_2. Changing the initial condition, $\mathcal{X}(0)$ changes the relative weights of the two modes but not the (local) probability distributions around the modes themselves. In other words, for smaller initial numbers $\mathcal{X}(0)$, the probability to die out in the early phase is larger, more trajectories get absorbed in state S_2, and the expectation value $\mathrm{E}(\mathcal{X}(t))$ is diminished accordingly. This fact is nicely demonstrated by a comparison of the two plots at the top and in the middle of Fig. 7, which differ only in the initial condition $\mathcal{X}(0) = x(0)$ for which the values 10 or 4 were chosen. The deterministic solution curves converge to the same stationary values, whereas large differences in the stationary expectation values are observed. The phenomenon is important in virology and implies that initially small numbers of infectious units need not result in the development of disease.

Provided $\mathcal{X}(0)$ has been chosen large enough such that bifurcation in the early phase of the process plays no role, the stochastic expectation value follows the deterministic ODE solution except minor deviations, which disappear in the longtime limit when the (quasi-)stationary state is approached. Minor deviations between the stochastic expectation value and the deterministic solution are observed in full agreement with the analytic solution for the simple irreversible autocatalytic reaction $\mathsf{A} + \mathsf{X} \rightarrow 2\mathsf{X}$ (Arslan and Laurenzi 2008). Such small deviations have to be expected since the coincidence of the deterministic and the stochastic approach is true for linear systems only, in particular for first-order chemical reactions (van Kampen 2007, pp. 122–127). Autocatalysis in the flow reactor exhibits another feature: The fluctuations in the concentration of input material A meet the expectations for a conventional chemical systems and are near $\sqrt{N}$, whereas the

fluctuations around the expectation values of the concentration of the autocatalyst X are larger in agreement with the mentioned analytical results.

Deterministic and stochastic quasispecies dynamics. Although total virus populations are commonly large, the importance of stochastic effects cannot be ruled out for reasons that are related to the existence of an absorbing boundary S_2. As we outlined for the simple autocatalytic process in the previous paragraph, initial phases have no influence on the deterministic longtime results but may bias the stochastic expectation values.

In order to be able to compare deterministic and stochastic results, we choose again the controllable experimental setup of a flow reactor. The model simplifies the set of materials required for replication by the assumption of a virtual compound A that flows into the reactor with a rate parameter r in the form of a solution with concentration a_0. As before, the inflow is compensated by an outflow of the volume of reactor solution resulting in reaction equations that have been analyzed by Schuster and Sigmund (1985):

$$* \xrightarrow{a_0 \cdot r} \mathsf{A}; \tag{9a}$$

$$\mathsf{A} + \mathsf{X}_k \xrightarrow{w_{jk}} \mathsf{X}_j + \mathsf{X}_k,\ j,k = 1,\ldots,N; \tag{9b}$$

$$\mathsf{A} \xrightarrow{r} \text{ø}; \quad \text{and} \tag{9c}$$

$$\mathsf{X}_k \xrightarrow{r} \text{ø},\ k = 1,\ldots,N, \tag{9d}$$

where the parameters $w_{jk} = Q_{jk}f_k$ are the same as used in Eqs. (7a) and (7c). The kinetic differential equations are

$$\begin{aligned} \frac{\mathrm{d}a}{\mathrm{d}t} &= (a_0 - a)r - a\left(\sum\nolimits_{k=1}^{N} f_k x_k\right), \\ \frac{\mathrm{d}x_k}{\mathrm{d}t} &= a\left(\sum\nolimits_{j=1}^{N} Q_{kj} f_j x_j\right) - x_k r,\ k = 1,\ldots,N, \end{aligned} \tag{9e}$$

whereby we applied concentrations, $a = [\mathsf{A}]$ and $x_k = [\mathsf{X}_k](k = 1,\ldots,N)$, and made use of the condition $\sum_{i=1}^{N} Q_{ik} = 1$. Equation (9a–9e) can be modeled stochastically by means of a master equation that allows for numerical computation of trajectories by means of a simulation algorithm (see Fig. 8), which is attributed to Gillespie (1977, 2007).

The main issue of this section is a comparison of quasispecies formation according to (9a–9e) between the deterministic and the stochastic approach. Replication and mutation at constant total concentration, $c = \sum_{i=1}^{N} x_i(t) = \text{const}$, have been analyzed as a multi-type branching process (Demetrius et al. 1985), and the major result was that the longtime solutions of the ODE (7a) coincide with the stationary expectation values of the branching process. Since analytical results are available for the replication–mutation mechanism in exceptional cases only, the

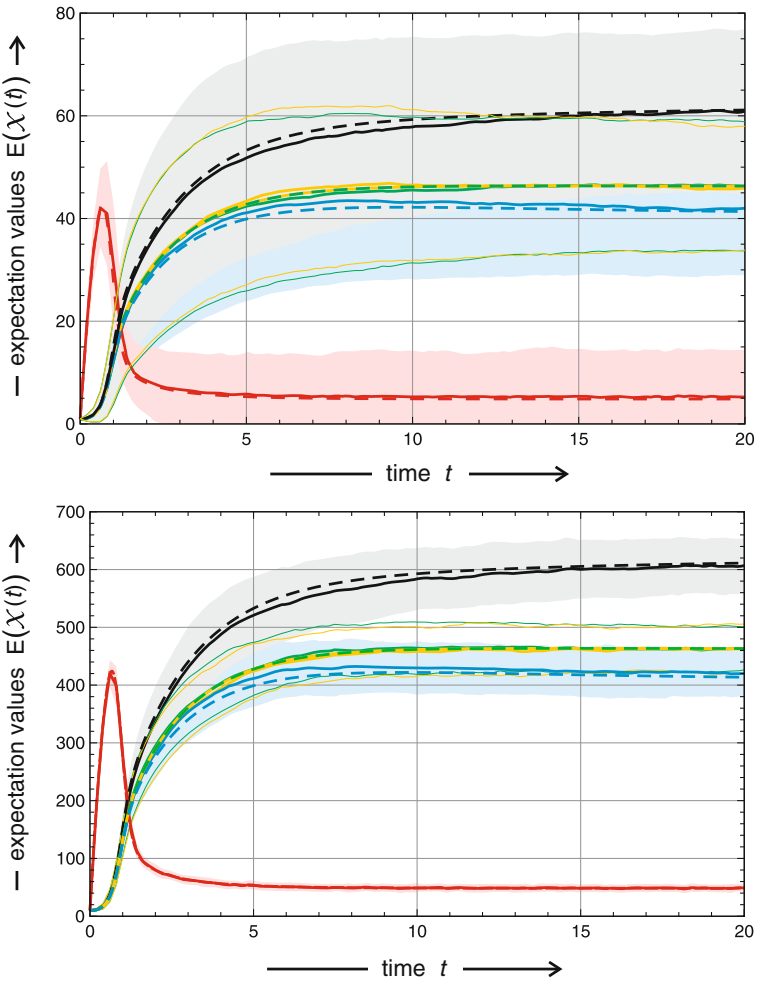

Fig. 8 Quasispecies formation in the flow reactor. The plots show the results of sampling 100 trajectories for the reaction mechanism (9a–9e) calculated by means of the Gillespie algorithm (Gillespie 1977). The smallest possible system was chosen: $l = 2$ with a master sequence X_1 (Γ_0) and three mutants X_2, X_3, and X_4, where X_2 and X_3 form the one-error class Γ_1 and yield identical deterministic solutions, and X_4 is the only sequence of the two-error class Γ_2. Shown are the expectation values within the one standard deviation confidence interval, $E \pm \sigma$, and the deterministic solutions obtained by integration of the ODE (9e) (*dashed lines*). Color code: $a(t)$ and $E(\mathcal{A}(t))$ *red* and *pink* confidence interval, $x_1(t)$ and $E(\mathcal{X}_1(t))$ *black* and *gray* confidence interval, $x_2(t)$ and $E(\mathcal{X}_2(t))$ *yellow* and confidence interval shown by *thin lines*, $x_3(t)$ and $E(\mathcal{X}_3(t))$ *green* and confidence interval shown by *thin lines*, and $x_4(t)$ and $E(\mathcal{X}_4(t))$ *blue* and *light blue* confidence interval. A single-peak landscape was used, and the uniform error rate model was applied. *Upper plot*, choice of parameters: $a_0 = 200$, $r = 0.5$, $f_m = 0.011$, $f = 0.010$ and $p = 0.1$ and initial conditions: $a(0) = x_1(0) = x_2(0) = x_3(0) = x_4(0) = 1$; *lower plot*, choice of parameters: $a_0 = 2000$, $r = 0.5$, $f_m = 0.0011$, $f = 0.0010$ and $p = 0.1$ and initial conditions: $a(0) = x_1(0) = x_2(0) = x_3(0) = x_4(0) = 10$

comparison of deterministic and stochastic quasispecies formation in the flow reactor is made here by means of numerical simulation. We choose two different initial conditions: (i) uniform distribution far away from the stationary distribution and (ii) the stationary distribution of the deterministic system. In the former case, the approach toward the stationary distribution is fast, and apart from some minor deviations, the expectation value obtained for the quasistationary distribution of the master equation is identical to the solution of the kinetic ODE (Fig. 8). The quasispecies in the flow reactor exhibits the same feature as autocatalysis: The fluctuations in the concentration of the input material A are near $\sqrt{N}$, whereas the fluctuations around the expectation values of concentrations for the members of the quasispecies, X_j, are larger, even larger than for autocatalysis. Again, minor deviation between the stochastic expectation value and the deterministic solution has to be expected and is observed indeed. Necessarily, the stochastic expectation and the deterministic result coincide at the stationary values.

A natural question to ask is whether or not the ranking of genotypes according to the frequency of occurrence in the population is changed through the action of fluctuations or, in other words, can the fittest genotype temporarily be outgrown by another sequence in the stochastic system. The answer is straightforward: The most important source of the fluctuations is self-enhancement of the replication process; the differences in the expectation values of the individual concentrations, $\mathrm{E}(\mathcal{X}_i(t))$, become smaller when the mutation rate increases; and thus, stochasticity may well interfere with the quasispecies structure in small populations or at high mutation rates. The two examples in Fig. 8 indicate two different scenarios: At the lower sample size $(a_0 = 200)$, the confidence intervals overlap and accordingly, we cannot expect that the most frequent sequence, which we isolate at some instant t_1, is the same as the most frequent sequence isolated at t_2, or in other words, the temporarily most frequent molecular species need not be fittest one. For the larger sample size $(a_0 = 2000)$, however, the confidence interval of the master sequence is well separated from the confidence intervals of the mutants and we can expect to find the master sequence almost always being present at the highest concentration irrespectively of fluctuations in the concentrations.

In summary, stochastic quasispecies formation meets all expectations from stochastic chemical kinetics. The most important difference to the deterministic approach concerns the fact that the quasispecies is quasistationary in the stochastic model, the only asymptotically stable state is the absorbing boundary, and every autocatalyst including mutant distributions such as quasispecies has to die out in the limit $t \to \infty$. In practice, this result is of academic interest only and has no consequences for real systems because the time to extinction is of hyper-astronomical length. A practical consequence, nevertheless, can arise from the bifurcation at short times: For small particle numbers, $C_0 = \sum_{k=1}^{N} \mathsf{X}_k(0) < 10$, the replication–mutation ensemble dies out with a non-negligible probability before it comes close to the quasistationary distribution. Apart from these specific effects, we obtained the general results that—not unexpectedly—concentration fluctuations are the more important and the higher the mutation rates, the smaller the population sizes are.

4 Quasispecies and Error Thresholds

Three kinds of studies on the dependence of quasispecies on mutation rates were performed: (i) analytical approximations using simple fitness landscapes and simplifications of the mutation matrix, for example, the *uniform error rate* model or the *zero mutational backflow* approximation; (ii) 'exact' numerical computations[8] on simple fitness landscapes with the full uniform error rate mutation matrix; and (iii) fully resolved fitness landscapes with the full uniform error rate mutation matrix. In general, we shall consider here stationary solutions of the replication–mutation ODE (7c) as functions of the error or mutation rate parameter per nucleotide site and replication denoted by p. In order to be able to handle the problem in a transparent way, we assume that the mutation rate is independent of the position on the sequence and characterize this simplifying assumption as the *uniform error rate model*. Then, the elements of the mutation matrix take on the simple form

$$Q_{ij}(p) = (1-p)^{l-\mathrm{d}_{ij}^H} p^{\mathrm{d}_{ij}^H} = (1-p)^l \varepsilon^{d_{ij}^{\mathrm{H}}} \quad \text{with} \quad \varepsilon = \frac{p}{1-p}, \tag{10}$$

wherein d_{ij}^H is the Hamming distance between the two sequences, X_i and X_j, and p is the mutation rate parameter. We shall assume further that we are dealing with binary sequences.[9] The concept of the error threshold is now introduced in three paragraphs reporting (i) 'exact' numerical results and two approximations, (ii) the zero mutational backflow assumption, and (iii) the phenomenological approach conceived by (Eigen 1971).

Solutions without approximation. 'Exact' solutions of the replication–mutation Eq. (7d) are obtained in terms of eigenvalues and eigenvectors of the value matrix W that, as said before, has to be a primitive matrix in order to fulfill Perron–Frobenius theorem (Seneta 1981, pp. 3–11 and 22–23). This theorem guarantees several important properties of the eigenvalues and eigenvectors of W. Two of them are of particular importance for the analysis of quasispecies and error thresholds: (i) The largest eigenvalue of W, λ_1 is non-degenerate, real and positive,

$$\lambda_1 > |\lambda_2| \geq |\lambda_3| \geq \ldots \geq |\lambda_N|, \ \lambda_1 = |\lambda_1| > 0,$$

and (ii) all components of the right-hand eigenvector $\mathbf{b}_1$ associated with λ_1 are strictly positive. Both properties are required for physically meaningful results of the replication–mutation problem. Uniqueness of the solution means that the stationary mutant distribution is completely determined by the fitness landscape,

[8] By the notion 'exact,' we mean here 'without approximations.' In order to make clear that numerical computations can never be exact in the strict sense, we put *exact* between apostrophes.

[9] The use of binary sequences ($\kappa = 2$) facilitates several operations and implies no loss of generality. Natural four-letter sequences ($\kappa = 4$) can be encoded by binary sequences of twice the chain length.

$\mathcal{L} = \{f_k; k = 1, \ldots, N\}$, and the matrix of mutation frequencies, Q. Exclusively positive components of the eigenvector $\mathbf{b}_1$ implies that all mutants are present in the mutant distribution and no mutant can vanish as a consequence of consecutive replication and mutation events. The second issue has been discussed already in Chap. 1 (this volume). It is necessary to distinguish between the deterministic approach, which allows small concentrations down to any fraction of single molecules, and the stochastic approach where random variables are restricted to positive integers, although probabilities and moments of distributions can be arbitrarily small. In reality, a mutant distribution will consist always of a core of mutants, which are permanently present, and a fluctuating periphery.

After sufficient long time, the solutions of the replication–mutation Eq. (7d) are dominated by the largest eigenvalue λ_1:

$$x_j(t) \approx \frac{b_{j1}\beta_1(0)\exp(\lambda_1 t)}{\sum_{i=1}^{N} b_{i1}\beta_1(0)\exp(\lambda_1 t)} = \frac{b_{j1}}{\sum_{i=1}^{N} b_{i1}} = \bar{x}_j \quad \text{for large } t.$$

The longtime solution is independent of time t and initial conditions $\beta_k(0)$. It is fully determined by the fitness landscape and the mutation matrix, and it represents the genetic reservoir of an asexually reproducing species and has been characterized as *quasispecies* (Eigen and Schuster 1977, pp. 541, 549 ff.): 'A quasispecies is defined as a given distribution of macromolecular species with closely interrelated sequences dominated by one or several (degenerate) master copies.' Here, we can make it more precise by saying that the concentration ratios of the individual components are given by the largest eigenvector $\mathbf{b}_1$ of the value matrix W. A quasispecies contains one fittest genotype X_m—or in case of neutrality, several fittest genotypes—surrounded by a cloud of closely related mutants. The dominant genotype X_m is characterized as *master sequence*. The relative stationary concentrations of individual mutants, $\bar{x}_j$, are determined by their own fitness f_j and by their Hamming distance from the master sequence, $d^H_{\mathsf{X}_j\mathsf{X}_m} = d^H_{jm}$.

The computation of 'exact' numerical solutions is facilitated enormously by using single-peak fitness landscapes (3d) and adopting the uniform error rate approximation. Then, all mutants in a given class are described by the same ODE and their concentrations can be lumped together into a *class concentration*: $y_k(t) = \sum_{i=1}^{N_k} x_i$ with $\mathsf{X}_i \in \Gamma_k$ and $N_k = \binom{l}{k}$ (Nowak and Schuster 1989; Swetina and Schuster 1982). Figure 9 shows the mutant distribution of a quasispecies expressed in class concentrations as a function of the mutation rate parameter p. Starting at $p = 0$, where the master sequence represents the selected genotype, the relative concentration of the master sequence in the quasispecies decreases gradually and mutants gain in relative amount. At some critical mutation rate, $p = p_{\text{tr}}$, the quasispecies distribution changes abruptly, and within a short interval Δp, the sequence distribution approaches the uniform distribution, $\mathcal{U} = \bar{x}_i = 1/l^2 \forall i = 1, \ldots, N$ (Swetina and Schuster 1982), which is the exact solution at $p = \frac{1}{2}$. The (approximate) uniform distribution then remains the stationary solution of the ODE (7a) in

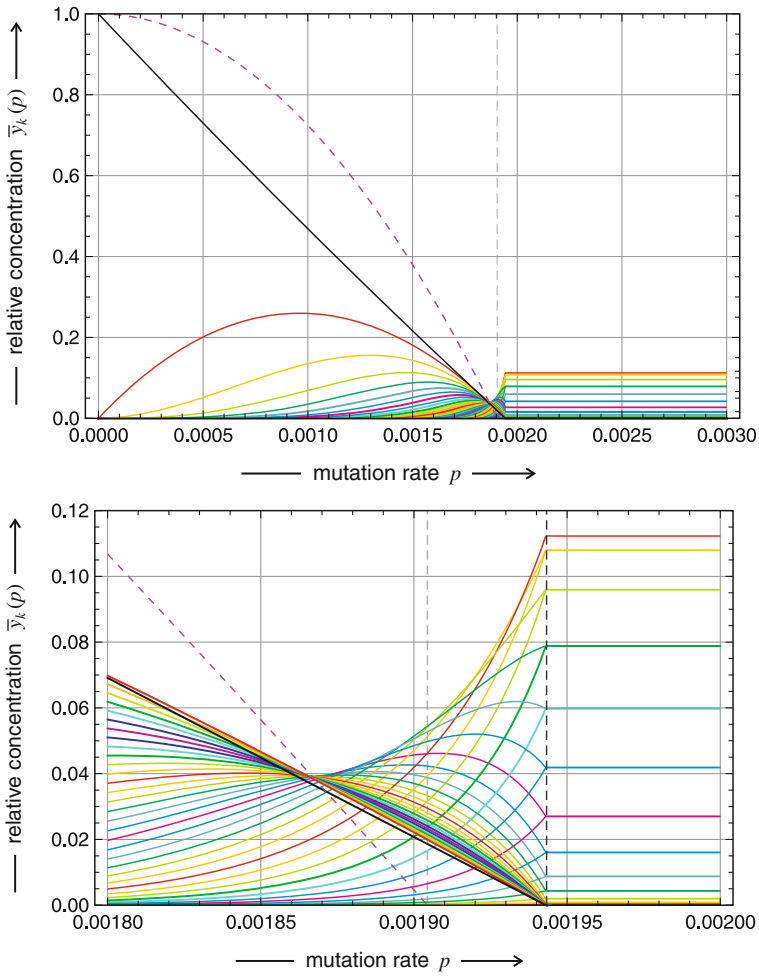

Fig. 9 Quasispecies as a function of the error rate. The *upper plot* shows numerically computed 'exact' curves. The *dashed gray line* indicates the error threshold at $p_{\mathrm{cr}} = 0.001904$ obtained by the phenomenological approach, and the *dashed violet curve* is the phenomenological total concentration $\hat{c}^{(0)}(p)$ obtained from (13). The *lower plot* is an enlargement and shows the error threshold derived from the mergence of the concentration curves for complementary classes, Γ_k and Γ_{l-k} (*dashed black line* at $p_{\mathrm{mg}}^{(\theta)} = 0.001943$). According to our knowledge, the work of (Swetina and Schuster 1982) was the first publication showing this shape of an error-induced transition in quasispecies. The positions of the error threshold calculated from level crossing are as follows: $p_{\mathrm{tr}}^{\vartheta} = 0.00192229, 0.00194101, 0.00194288, 0.00194307,$ and 0.00194308 for $\vartheta = 10^{-2}, 10^{-3}, 10^{-4}, 10^{-5}$, and 10^{-6}. Parameters: $l = 50, f_m = 1.1, \bar{f}_{-m} = f = 1.0$

the entire range $p_{\mathrm{tr}} \leq p \leq \frac{1}{2}$, and at $p = \frac{1}{2}\mathcal{U}$, it becomes the exact solution. The transition at $p = p_{\mathrm{tr}}$ increases in sharpness with increasing chain lengths l and reminds of cooperative transitions known in the theory of polymers (Lifson 1961;

Schwarz 1968; Zimm 1960). Exploiting the analogy of the quasispecies approach and equilibrium statistical mechanics of a two-dimensional spin lattice Tarazona (1992) was able to show that the error threshold on the single-peak fitness landscape corresponds to a first-order phase transition in the limit of infinite chain lengths l.

Two quantitative measures for the location of the error threshold are obtained by straightforward and simple numerical procedures:

(i) *Level crossing* determines the p-value at which the curve for the stationary concentration of the master sequence, $\bar{x}_m(p)$, crosses a predefined concentration level, $\bar{x}_m(p_{\text{tr}}^{(\vartheta)}) = \vartheta$ with ϑ being a threshold value that has to be chosen small enough for a given chain length l.[10] In the example shown in Fig. 9, the convergence of $p_{\text{tr}}^{(\vartheta)}$ with decreasing values of ϑ is very fast. Appropriately, the converged limit is taken as the position of the transition. We remark that we are dealing here with *semiconvergence* because the curve bends off to the at still lower ϑ-values in order to reach the point $\bar{x}_m(\frac{1}{2}) = 1/2^l$.

(ii) *Complementary class mergence* makes use of the fact that the uniform distribution implies coalescence of the concentrations, $\bar{y}_k = \sum_{i=1}^{N_k} \bar{x}_i$, $\mathsf{X}_i \in \Gamma_k$, for complementary classes (Γ_k, Γ_{l-k}), since $\binom{l}{k} = \binom{l}{l-k}$ and $\bar{y}_k = \bar{y}_{l-k} = \binom{l}{k}/2^l$. Accordingly, the p-values $p = (p_{\text{mg}}^{(\theta)})_k$ at which the difference $\Delta_k = |\bar{y}_k - \bar{y}_{l-k}|$ becomes as small as some predefined value $(\Delta_k)_{\text{cr}} = \theta$ can be taken as the kth coalescence error rate. Then, a measure for the sharpness of the transition is given by the width of the band spanned by the different locations of $(p_{\text{mg}}^{(\theta)})_k; k = 0, \ldots, \lfloor \frac{l}{2} \rfloor$, i.e., $\Delta p_{\text{mg}}^{(\theta)} = \max((p_{\text{mg}}^{(\theta)})_k) - \min((p_{\text{mg}}^{(\theta)}))_k$ with $k = 0, \ldots, \lfloor \frac{l}{2} \rfloor$. In the cases studied here, the values $(p\,\overline{\text{mg}}^{(\theta)})_k$ did not change monotonously with k but increased from $k = 0$ up to some maximum value but further on decreased until $k = \lfloor \frac{l}{2} \rfloor$ has been reached (examples for class mergence are presented in the paragraph *error thresholds on simple landscapes*). It is important to stress that both measures for the location of the transition, the converged value from level crossing as well as the value from complementary class mergence, yield very similar results for realistic chain lengths ($l \gg 50$) as shown in Fig. 9 for a single-peak landscape. Despite the fact that we have no analytical expression for p_{tr} and p_{mg}, the numerically calculated values are nicely confirming the existence of the error threshold as a transition phenomenon of the cooperative transition type.

[10]For sufficiently long sequences, the particular choice $\vartheta = 0.01$, 0.001 or 0.0001 is unimportant because the results for small values are very similar and converge to a limit (see Fig. 9), but for short chains, the concentration values of the uniform distribution $\mathcal{U}$ set a lower limit for $\bar{x}_m(p)$. For example, in case of $l = 10$, the value $\bar{x}_m(\frac{1}{2}) = 1/2^l = 1/1024$ is compatible only with the choice $\vartheta = 1/100$ because $\vartheta = 1/1000$ is too close to $\bar{x}_m(\frac{1}{2})$.

The zero mutational backflow approximation. The notion *mutational backflow* concerns mutations from the mutant cloud back to the master sequence:

$$\Phi_{\mathrm{x}_m \leftarrow \mathrm{x}_{(j)}} = \sum_{j=1, j\neq m}^{N} Q_{mj} f_j \bar{x}_j = \sum_{j=1, j\neq m}^{N} w_{mj} \bar{x}_j. \tag{11}$$

Zero mutational backflow and the consistent neglect of the mutational flow between mutants imply that all off-diagonal elements in the mutation matrix Q are zero except those describing the mutations from the master sequence to the mutant cloud. In other words, Q contains only the elements in the column of the master sequence, $Q_{jm}; j = 1, \ldots, N; j \neq m$, and the diagonal terms, Q_{ii}. The replication–mutation Eq. (7a) is modified and becomes much simpler:

$$\frac{\mathrm{d}x_m^{(0)}}{\mathrm{d}t} = (Q_{mm} f_m - \phi) x_m^{(0)}, \tag{12a}$$

$$\frac{\mathrm{d}x_j^{(0)}}{\mathrm{d}t} = (Q_{jj} f_j - \phi) x_j^{(0)} + Q_{jm} f_m x_m^{(0)}. \tag{12b}$$

The superscript '(0)' indicates the approximation. The flow by definition is adjusted to compensate for the net growth and accordingly takes on the form

$$\begin{aligned} \phi(\mathrm{x}^{(0)}(t)) &= \frac{1}{c^{(0)}} \left(\sum_{i=1}^{N} Q_{ii} f_i x_i^{(0)} + \sum_{j=1, j\neq m}^{N} Q_{jm} f_m x_m^{(0)} \right) \\ &= \frac{1}{c^{(0)}} \left(f_m x_m^{(0)} + Q f (c^{(0)} - x_m^{(0)}) \right), \end{aligned} \tag{12c}$$

where we applied a single-peak landscape with $\bar{f}_{-m} = f$ and the uniform error approximation $Q = (1-p)^l$. Stationary solutions of the ODE are readily calculated since Eqs. (12a) and (12c) contain only the variable $x_m^{(0)}$:

$$\bar{x}_m^{(0)} = \bar{c}^{(0)} \frac{Q(1-\sigma_m^{-1})}{1 - Q\sigma_m^{-1}} \quad \text{and} \quad \bar{x}_j^{(0)} = \bar{c}^{(0)} \frac{Q\varepsilon^{d_{jm}^{\mathrm{H}}}}{1 - Q\sigma_m^{-1}}. \tag{12d}$$

The input coming from the fitness landscape, $\sigma_m = f_m / \bar{f}_{-m}$, has been called the superiority of the master sequence, and it weights the fitness of the master sequence, f_m, against the mean fitness of all sequences except the master sequence: $\bar{f}_{-m} = \sum_{i=1, i\neq m}^{N} f_i x_i / (c - x_m)$. The assumption of zero mutational backflow is a fairly good approximation for small mutation rates (Swetina and Schuster 1982) and can be used as a reasonably accurate estimate of the stationary concentration of the master sequence, $\bar{x}_m(p)$, and the one-error class, $\bar{y}_1(p)$ (see Fig. 11), but fails to model quasispecies at larger mutation rates, in particular, near the error threshold.

The phenomenological approach. In the seminal paper on self-organization of macromolecules, Eigen (1971) introduced a variant of the zero mutational approximation that also allows for the derivation of analytical solutions for the stationary concentration. Eigen addressed his approach as *phenomenological theory of selection,* and therefore, we shall characterize it here as *phenomenological* as well. The approximation is only introduced into the growth term, and the change is not compensated in the flow ϕ. Accordingly, the condition of *constant organization* or constant population size of Eq. (7a) is violated, and hence, the total concentration, $\hat{c}^{(0)}$, will be a function of the mutation rate parameter p. The modified equations are identical with (12a) and (12b), but the flow term is different:

$$\phi(\mathrm{x}^{(0)}(t)) = \frac{1}{c^{(0)}}\sum_{i=1}^{N} f_i x_i^{(0)} = \frac{1}{c^{(0)}}\left(f_m x_m^{(0)} + \bar{f}_{-m}(c^{(0)} - x_m^{(0)})\right). \tag{12c}$$

Again, the problem is reduced to an ODE in a single variable and the stationary solution can be obtained straightforwardly[11]

$$\begin{aligned} &\hat{x}_m^{(0)} = \frac{Q - \sigma_m^{-1}}{1 - \sigma_m^{-1}},\ \hat{x}_j^{(0)} = \varepsilon d_{jm}^{\mathrm{H}}(Q - \sigma_m^{-1})(1 - \sigma_m^{-1})^2, \quad \text{and} \\ &\hat{c}^{(0)} = \frac{(1 - Q\sigma_m^{-1})(Q - \sigma_m^{-1})}{Q(1 - \sigma_m^{-1})^2}. \end{aligned} \tag{13}$$

The normalized concentrations of the phenomenological approach,

$$\frac{\hat{x}_m^{(0)}}{\hat{c}^{(0)}} = \frac{Q - \sigma_m^{-1}}{1 - \sigma_m^{-1}} \cdot \frac{Q(1 - \sigma_m^{-1})^2}{(1 - Q\sigma_m^{-1})(Q - \sigma_m^{-1})} = \frac{Q(1 - \sigma_m^{-1})}{1 - Q\sigma_m^{-1}} = \bar{x}_m^{(0)}$$

and $\hat{x}_j^{(0)}/\hat{c}^{(0)} = \bar{x}_j^{(0)}$ are identical to the solutions of the zero mutational backflow approximation. This is to be expected from a previously derived very general result, which states that normalized or relative concentrations are independent of the flow term $\phi(t)$ as long as the growth functions—here $\sum_{i=1}^{N} Q_{ji} f_i x_i$—are linear and the population size $c(t)$ does not vanish (Eigen and Schuster 1978, p. 13). The factor $Q - \sigma_m^{-1}$, which is common to all concentrations in the phenomenological approach, decreases with increasing mutation rate p and eventually becomes zero at the critical mutation rate $p = p_{\mathrm{cr}} = 1 - \sigma^{-1/l}$. At this point, the total concentration becomes zero and hence, the whole quasispecies vanishes. The key relation for survival of the quasispecies is the relation

$$Q \cdot \sigma_m \geq 1, \tag{14}$$

[11]The stationary concentrations of the phenomenological approach are denoted by the 'hat' symbol: $\hat{x}_m^{(0)}$, $\hat{x}_j^{(0)}$, $\hat{y}_k^{(0)}$, $\hat{c}^{(0)}$, etc.

which can be interpreted easily in qualitative terms: The loss of master copies due to error-prone replication, $Q = (1-p)^l$, has to be overcompensated by the higher fitness of the master as expressed by the superiority σ_m.

Beyond this error rate, $p > p_{\mathrm{cr}}$, genetic information cannot be transferred to future generations and therefore, the phenomenon has been characterized as *error threshold*. The equation for p_{cr} can be elegantly translated into a maximum error rate or a maximum chain length condition for successful transfer of genetic information to future generations. Simplified equations,

$$p_{\max} = p_{\mathrm{cr}} = 1 - \sigma^{-1/l} \approx \frac{\ln \sigma_m}{l} \quad \text{and} \quad l_{\max} \approx \frac{\ln \sigma_m}{p}, \tag{15}$$

were discussed in Chap. 1 (this volume) and are frequently applied to problems in virology, cancer research, and prebiotic evolution. In virology and cancer research, the key issue concerns the possibility to extinguish infections or stop proliferation by driving populations of viruses or cells into extinction by increasing the mutation rate. Two processes are fundamental for achieving this goal, either replication is pushed above the error threshold where the genetic information is lost or a large percentage of lethal variants is produced and the population becomes extinct (see Tejero et al. (2010) and Chap. 7, this volume). In prebiotic evolution, the phenomenological equation for the error threshold sets a limit to the chain l length of polynucleotides and thereby also to the information content, which can be faithfully transferred to future generation on the population level (see, e.g., Eigen and Schuster 1982).

The most remarkable property of the phenomenological approach is the quality of the results: As shown in Fig. 9 for a rather short chain length $l = 50$, the position of the transition to the uniform distribution, p_{tr}, is very close to the critical error rate p_{cr} where the quasispecies vanishes in the phenomenological approach, and the approximation becomes even better for increasing chain lengths. Here, we shall analyze the mathematical background of the approximations by considering the entire range of mutation rate parameters, $0 \le p \le \frac{1}{2}$. As shown in Fig. 11, the continuation of $\hat{x}_m^{(0)}(p)$ beyond the error threshold converges in the range of negative concentrations for $p \to \frac{1}{2}$ to the value

$$\hat{x}_m^{(0)}\left(\frac{1}{2}\right) = \frac{2^{-l} - \sigma_m^{-1}}{1 - \sigma_m^{-1}} \approx -\frac{1}{\sigma_m - 1}$$

(for binary sequences and $2^l \gg \sigma_m$). The curve $\hat{x}_m^{(0)}(p)$ is close to the exact curve $\bar{x}_m(p)$ up to the error threshold but then extends to negative values. The comparison with the consistent zero mutational backflow approximation $\bar{x}_m^{(0)}(p)$ shows three interesting features:

(i) Because the zero mutational backflow approximation fulfills the condition of constant population size, it reaches a positive value at $p = \frac{1}{2}$, which lies below the exact value of $\bar{x}_m = 2^{-l}$,

$$\bar{x}_m^{(0)}\left(\frac{1}{2}\right) = \frac{1-\sigma_m^{-1}}{2^l-\sigma_m^{-1}} \approx \frac{1-\sigma_m^{-1}}{2^l}.$$

Apart from very small mutation rates, the curve of the phenomenological approach $\hat{x}_m^{(0)}(p)$ lies closer to the exact curve $\bar{x}_m$ than the zero mutational backflow curve $\bar{x}_m^{(0)}(p)$ in the whole range $0 \le p \le \frac{1}{2}$.

(ii) Qualitatively, the downshift of the curve $\hat{x}_m^{(0)}(p)$ relative to the zero mutational backflow curve $\bar{x}_m^{(0)}(p)$ is easily explained: The flux ϕ is larger in the phenomenological approach than in the zero backflow approximation, and, other things being equal, this shifts the curve to lower values.

(iii) No only the relative stationary concentration $\hat{x}_m^{(0)}(p)$ is an excellent approximation for the master sequence but also the curve for the one-error mutants fits the exact curve very well, $\hat{y}_1^{(0)}(p) \approx \bar{y}_1(p)$, whereas the approach is very poor for all other sequences with two or more mutations (Fig. 11). This result is readily explained in terms of the mutation flow (Fig. 10): The sequences of the one-error class have the master sequence and $(l-1)$ sequences from the two-error class in their immediate neighborhood. The master sequence is described fairly correctly, and for small mutation rates, the sequences in the two-error class are present in very small concentrations only, and accordingly, also the absolute error in the stationary concentration is small. Sequences in the two-error class and in the higher error classes, however, receive mutational input in the zero backflow approximation only from the master sequence, and the larger inputs from the next lower error class are neglected.

All results calculated by the phenomenological approach are readily understood in qualitative terms, the high accuracy obtained in the approximation of the position of the error threshold, which makes the approach to an extremely useful and easy-to-handle tool, still waits for an explanation.

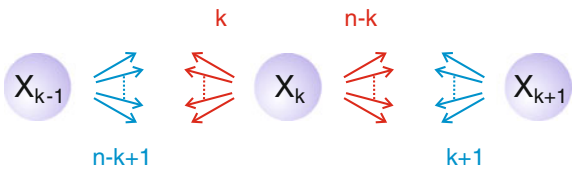

Fig. 10 Mutational flow in binary sequence space. The figure sketches the mutational flow on a hypercube. Every sequence has l Hamming distance one neighbors, k neighbors are situated in the class Γ_{k-1}, and $l-k$ neighbors in the class Γ_{k+1}. This implies that a sequence in Γ_k produces one-error mutants for k sequences in class Γ_{k-1} and for $l-k$ mutants in class Γ_{k+1}

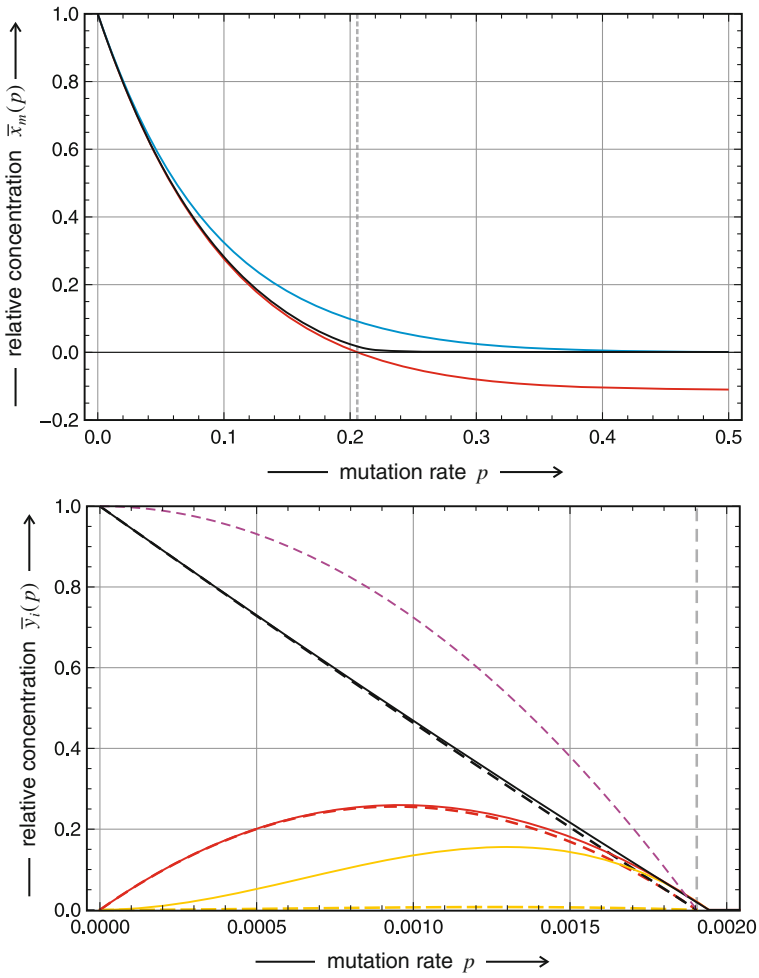

Fig. 11 The zero mutational backflow approximation and the phenomenological approach. In the *upper part* of the figure, the exact stationary concentration $\bar{x}_m(p)$ (*black*) is compared with the zero mutational backflow approximation $\bar{x}_m^{(0)}(p)$ (*blue*) and the phenomenological approach $\hat{x}_m^{(0)}(p)$ (*red*). Choice of parameters: $l = 10$, $f_m = 10.0$, $\bar{f}_{-m} = f = 1.0$, yielding an error threshold $p_{\text{cr}} = 0.2057$. The *lower plot* demonstrates the excellent agreement of the phenomenological approach (*dashed lines*) with the exact stationary concentrations of the master $\bar{x}_m(p) = \bar{y}_0(p)$ (*black*) and the one-error class $\bar{y}_1(p)$ (*red*). As outlined in the text, the agreement is poor as expected for the two-error class (*yellow*) and all other higher mutational classes (Note that the *dashed yellow curve* is hardly distinguishable from the abscissa axis). The error threshold is indicated by a gray dashed line and the total concentration of the phenomenological approach is shown in violet. Choice of parameters: $l = 50$, $f_m = 1.1$, $\bar{f}_{-m} = f = 1.0$, and $p_{\text{cr}} = 0.001904$

Error threshold on simple landscapes. Quasispecies on different simple fitness landscapes have been compared previously in several publications (see, e.g., Wiehe 1997; Schuster 2011). Here, we summarize only the most relevant findings. Some

smooth landscapes, for example, the linear (3a) and the multiplicative landscape (3b), do not exhibit a cooperative transition like abrupt change of the quasispecies distribution in the $(\bar{y}_k, p)$-plot $(k = 0, \ldots, l)$. In other words, the quasispecies changes smoothly from the selection of the master sequence, $\Upsilon(0) = (\bar{x}_m = 1, \bar{x}_j = 0; j = 1, \ldots, N, j \neq m)$, to the uniform distribution, $\Upsilon(\frac{1}{2}) = \mathcal{U}$. The error threshold on the single-peak landscape (3d) has been discussed in great detail in the preceding paragraphs: It supports an error threshold near the position $p_{\mathrm{cr}} = (Q - \sigma_m^{-1})/(1 - \sigma_m^{-1})$. The hyperbolic landscape (3c) shows a cooperative transition, but it looks different from the error threshold on the single-peak landscape since it does not directly lead to the uniform distribution $\mathcal{U}$. The single-peak linear landscape (3e) eventually shows an error threshold provided the position of the step, h, is located at a sufficiently low class number k. Interestingly, the error threshold occurs at a higher mutation rate p separated from the decline of the stationary concentration of the master sequence.

All simple landscapes can be readily classified by resolving the error threshold phenomenon into three features: (i) a decrease of the stationary concentration of the master sequence to very small values—still above the uniform concentration $(\bar{x}_m = 2^{-l})$, (ii) a sharp transition of the quasispecies from the characteristic fitness and Hamming distance determined distribution of mutants to a different distribution that is characteristic for high mutation rates, and (iii) the nature of the high mutation rate distribution that often but not always is the uniform distribution $\mathcal{U}$. Quantitative measures for the first two criteria have been given in the paragraph on approximation-free solutions. For feature (i), this is the p-value at which the curve for the stationary concentration of the master sequence crosses a predefined concentration level, $\bar{x}_m(p_{\mathrm{tr}}^{(\vartheta)}) = \vartheta$, and for features (ii) and (iii), we recall the mergence of the stationary concentrations of complementary classes, $|\bar{y}_k(p_{\mathrm{mg}}^{(\theta)}) - \bar{y}_{l-k}(p_{\mathrm{mg}}^{(\theta)})| = \theta$, where the spectrum of $\left(p_{\mathrm{mg}}^{(\theta)}\right)k$-values defines both the position and the width of the transition. It is worth remembering that for the examples presented in Fig. 9 and Table 1 $(h = 0)$, both quantitative measures give the same result, $p_{\mathrm{tr}}^{(\vartheta)} \approx p_{\mathrm{mg}}^{(\theta)}$ for $\vartheta = \theta$.[12]

The single-peak linear landscape (3e) with different h-values provides an excellent study case for the quantitative evaluation of error thresholds (Fig. 12). The width of the error threshold transition for sequences with $l = 10$ is compared for the single-peak landscape and the single-peak linear landscapes with $h = 2$, 3, and 4.[13]

[12]This agreement is not accidental as a simple consideration shows: The lowest mutation rate for merging two classes is $(p_{\mathrm{mg}}^{(\theta)})_0$, the p-value where $\Delta_0 = |\bar{y}_0 - \bar{y}_l| = |\bar{x}_m - \bar{x}_{-m}| = \theta$. Since the concentration of the complementary sequence of the master sequence with $\mathrm{d}^{\mathrm{H}}_{\mathsf{X}_m\mathsf{X}_{-m}} = l$ is commonly very small, $\bar{x}_{-m} \ll \bar{x}_m$, we find for $\vartheta = \theta$: $\Delta_0 \approx \bar{x}_m$ and $p_{\mathrm{tr}}^{(\vartheta)} \approx \min(p_{\mathrm{mg}}^{(\theta)})_k = (p_{\mathrm{mg}}^{(\theta)})_0$.

[13]The single-peak linear landscape with $h = 1$ is identical with the single peak fitness landscape. The error threshold for $h = 5$ extends almost to $p = \frac{1}{2}$, and landscapes with $h > 5$ do not support error thresholds at all.

Table 1 Concentration level crossing and complementary class mergence near the error threshold

h	Level crossing $p_{\text{tr}}^{(\vartheta)}$			Class mergence $p_{\text{mg}}^{(\theta)}$	
	$\vartheta = 1/100$	$\vartheta = 1/1000$	$\vartheta = 1/10000$	$\theta = 1/1000$	$\Delta p_{\text{mg}}^{(0.01)}$
0	0.1067	0.1103	0.1110	0.1103–0.1111	0.0008
2	0.1097	0.1227	0.1252	0.1227–0.1282	0.0055
3	0.0999	0.1342	0.1428	0.1342–0.1758	0.0416
4	0.0811	0.1365	0.1626	0.1365–0.3360	0.1995
5	0.0638	0.1244	0.1777	0.1244–0.4453	0.3209
6	0.0513	0.1053	0.1787	–	–
7	0.0426	0.0876	0.1650	–	–
8	0.0364	0.0737	0.1449	–	–

The decline of the master class, $\bar{y}_0 = \bar{x}_0$, at p-values near the error threshold p_{cr} is illustrated by means of the points $p_{\text{tr}}^{(\vartheta)}$ where the curves cross the level $\bar{x}_0(p) = \vartheta$. Complementary class mergence is characterized quantitatively by the band between the lowest and the highest $(p_{\text{tr}}^{(\vartheta)})_k$-value. The lowest value is always observed with $k = 0$ (see Fig. 12). Parameters: $l = 20$, $f_0 = 10.0$, and $f_n = 1.0$ yielding an error threshold at $p_{\text{cr}} = 0.1088$

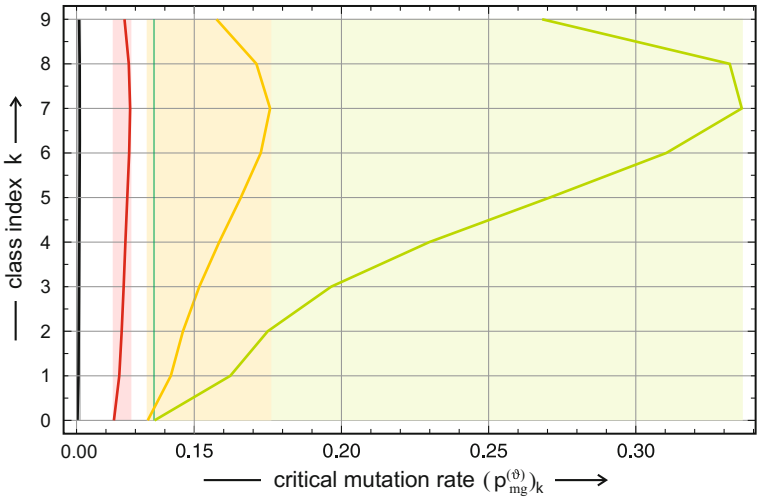

Fig. 12 The error threshold on single-peak linear landscapes. Shown are the critical mutation rates at which the curves for the stationary class concentrations approach each other up to a predefined difference, $(p_{mg}^{(\theta)})_k = |\bar{y}_k - \bar{y}_{l-k}| = \theta$ with $k = 0, 1, \ldots, \lfloor \frac{l}{2} \rfloor$. The areas in light colors represent the widths of the transitions. Parameter choice: $l = 20, f_0 = 10.0, f_n = 1.0$, $h = 0$ (*black*), $h = 2$ (*red*), $h = 3$ (*yellow*), and $h = 4$ (*chartreuse*)

Computed values for level crossing and complementary class mergence are shown in Table 1. The excellent agreement between the lower limit of the complementary class mergence values, $\left(p_{\text{mg}}^{(\theta)}\right)_0$, and the level crossing value for the same value, $p_{\text{tr}}^{(\vartheta)}$

Table 2 Complementary class mergence on single-peak and additive landscapes

$(p_{\mathrm{mg}}^{(0.01)})_k$	Additive landscape f_k (3a)		Single-peak landscape f_k (3d)	
k	$\nu = 10$	$\nu = 20$	$\nu = 10$	$\nu = 20$
0	0.01630	0.002552	0.01164	0.004969
1	0.06791	0.004363	0.01210	0.004977
2	0.17233	0.007967	0.01261	0.004983
3	0.24174	0.012590	0.01282	0.004990
4	0.22508	0.027993	0.01230	0.004997
5	–	0.064427	–	0.005005
6	–	0.113894	–	0.005011
7	–	0.153431	–	0.005013
8	–	0.162072	–	0.005009
9	–	0.120962	–	0.004990
$\Delta p_{\mathrm{mg}}^{(0.01)}$	0.22544	0.15952	0.00118	0.000045
$p_{\mathrm{tr}}^{(0.01)}$	0.01634	0.002552	0.01175	0.004969

Complementary class mergence characterized quantitatively by the bandwidth between the lowest and the highest $\left(p_{\mathrm{mg}}^{(\vartheta)}\right)_k$-value for $\vartheta = 0.01$ is compared for single-peak and linear landscapes with chain lengths $\nu = 10$ and $\nu = 20$. In all cases, the lowest value is always observed with $k = 0$ (see Fig. 12). In addition, the values for level crossing of the master class at $p_{\mathrm{tr}}^{(\theta)}$-values with $\theta = 0.01$ are given. Parameters: $\nu = 10$ and 20, $f_0 = 1.1$, and $f_n = 1.0$ for the single peak and $f_n = 0.9$ for the linear landscape yielding error thresholds on the single-peak landscape at $p_{\mathrm{cr}} = 0.00949$ and $p_{\mathrm{cr}} = 0.00475$, respectively

with $\theta = \vartheta$, is remarkable in all four cases (h = 0,2,3,4).[13] For h = 5, the band of complementary class mergence becomes so broad—$0.1244 \leq p_{\mathrm{mg}}^{(1/1000)} \leq 0.4453$ in the example shown in Table 1—that it extends almost to the limit $p = \frac{1}{2}$. For $h \geq 6$, no threshold is observed.

Equipped with the quantitative diagnostic tools for the detection of error thresholds, we return to the comparison of additive (3a) and single-peak landscapes (3d) in Table 2. The quantitative indicators reflect perfectly the visual inspection of the $\bar{y}_k(p)$-curves: For the chain length l = 10, the width of complementary class merging, $\Delta p_{\mathrm{mg}}^{(0.01)}$, for the additive landscape is 200 times as broad as for the single-peak landscape, and for l = 20, this factor is even 3500. Indeed, the error threshold has become very narrow already for short sequences of length l = 20 and shrinks further with increasing l. In addition, the relation between the two measures, $p_{\mathrm{tr}}^{(0.01)} \approx (p_{\mathrm{mg}}^{(0.01)})_0$, is already fulfilled up to 10^{-6} for sequences with l = 20.

In order to provide a hint on the prerequisites for the existence of an error threshold, we consider the derivative of the simple fitness landscapes with respect to the class index k (Fig. 13). All landscapes, which have a slope or derivative $|\partial f(k)/\partial k| > \alpha_{\mathrm{cr}}$, support error thresholds, whereas all less steep landscapes shown

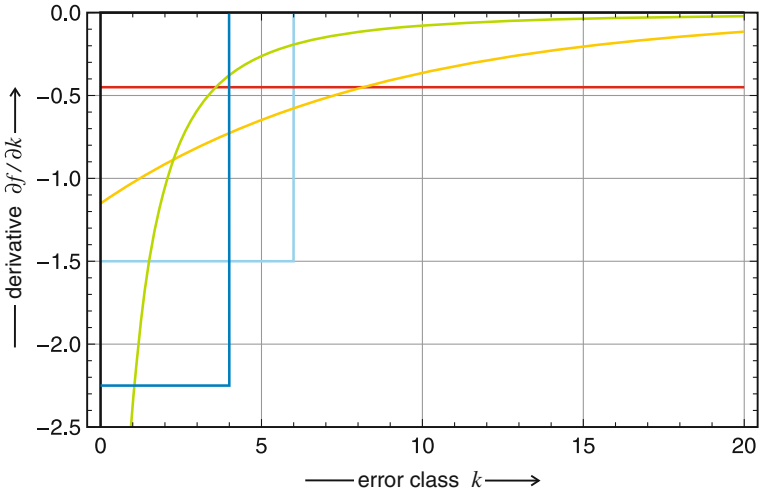

Fig. 13 The derivative of simple fitness landscapes. Shown are the derivatives, $\partial f/\partial k$, of the simple fitness landscapes (3a)–(3e). Choice of parameters: $l = 20$, $f_0 = 10.0$, and $f_n = 1.0$. *Color code* additive fitness (3a) in *red*, multiplicative fitness (3b) in *yellow*, hyperbolic fitness (3c) in *chartreuse*, single-peak step liner fitness (3e) $h = 6$ in *light blue* and $h = 4$ in *blue*, and the single-peak fitness (3d) in *black*. Error thresholds are found on the single peak, the single-peak linear with $h = 4$ and the hyperbolic fitness landscapes. On all other landscapes, smooth transitions from $p = 0$ to $p = \frac{1}{2}$ are observed

smooth transitions. For the examples given in the figure, this threshold values lie somewhere in the range $1.5 < \alpha_{cr} < 2.25$.

Out of all the simple landscapes analyzed here, only the single-peak landscape supports an error threshold that fulfills simultaneously the three conditions: (i) fast decrease of the concentration $\bar{x}_m$ slightly below p_{tr}, (ii) a sharp transition at $p_{tr}^{(\vartheta)}$ diagnosed by all $\left(p_{mg}^{(\theta=\vartheta)}\right)_k$-values lying in a narrow interval, and (iii) the uniform distribution being the high mutation rate distribution.

Error threshold on realistic landscapes. There are families of smooth landscapes in which no error thresholds occur and this raises the question what we can expect to happen on realistic landscapes. For this goal, quasispecies as functions of the mutation rate p were calculated on about twenty different random realistic landscapes (RRL, 5a) for sequences of chain length $l = 10$.[14] Two results are relevant for our purpose here: (i) Quasispecies on realistic random landscapes show error thresholds and (ii) the position of level crossing as a measure for the error threshold

[14]Numerical computations of eigenvalues and eigenvectors become highly demanding with respect to CPU time and memory above $l = 10$. For $l = 20$, the diagonalization of the W-matrix with about the size $10^6 \times 10^6$ requires certain tricks (Niederbrucker and Gansterer 2011), and for $l = 50$, the dimension of W is more than $10^{15} \times 10^{15}$ and diagonalization is far beyond current technical capacities.

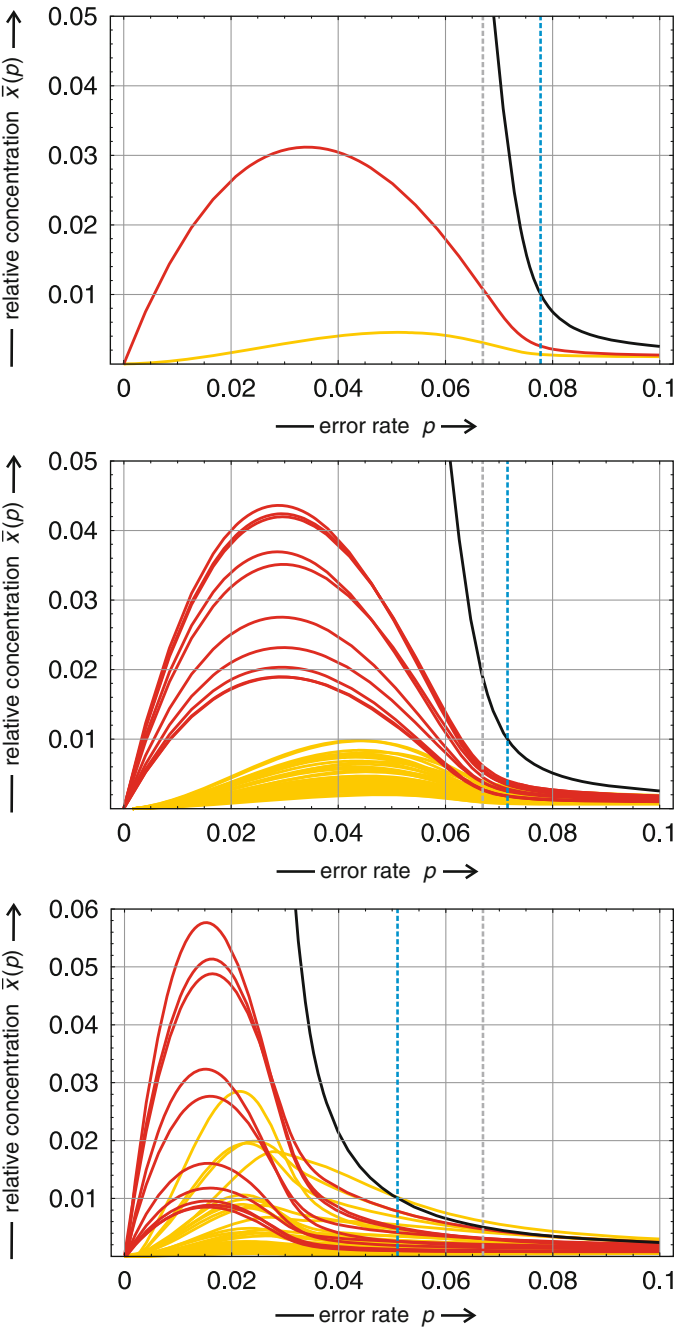
relative concentration $\bar{x}(p)$
0.05
0.04
0.03
0.02
0.01
0
0.02
0.04
0.06
0.08
0.1
error rate p
relative concentration $\bar{x}(p)$
0.05
0.04
0.03
0.02
0.01
0
0.02
0.04
0.06
0.08
0.1
error rate p
relative concentration $\bar{x}(p)$
0.06
0.05
0.04
0.03
0.02
0.01
0
0.02
0.04
0.06
0.08
0.1
error rate p

◀ **Fig. 14** Quasispecies on a realistic model landscape (RRL) with different random scatter d. Shown are the stationary concentrations $\bar{x}_j(p)$ on landscapes $\mathcal{L}(10, 2, 2.0, 1.0; 0.0, d, 491)$ for $d = 0$ (*upper plot*), $d = 0.5$ (*middle plot*), and $d = 0.9375$ (*lower plot*) for the classes Γ_0 (*black*), Γ_1 (*red*), and Γ_2 (*yellow*). In the topmost plot, the curves for all single point mutations $\mathsf{X}_j \in \Gamma_1$ and double point mutations $\mathsf{X}_j \in \Gamma_2$ coincide because of zero scatter, $d = 0$. The error threshold calculated by the phenomenological approach lies at $p_{\text{cr}} = 0.06697$ and is indicated by a *dashed gray line*, and the positions of the $p_{\text{tr}}^{(0.01)}$ values are 0.0778, 0.0716, and 0.0510 for $d = 0.0$, 0.5, and 0.9375, respectively (*dashed blue lines*)

moves to smaller mutation rates $p_{\text{tr}}^{(\vartheta)}(d)$ when the ruggedness of the landscape given by the parameter d is increased. An illustrative example is shown in Fig. 14 where we find $p_{\text{tr}}^{(0.01)}(0) = 0.0778$, $p_{\text{tr}}^{(0.01)}(0.5) = 0.0716$, and $p_{\text{tr}}^{(0.01)}(0.9375) = 0.0510$ for the cases shown in the plots. Figure 15 reports the movement of the position of $p_{tr}^{(m)}(d)$ toward lower mutation rate parameters with increasing scatter and illustrates the validity of the uniform distribution criterion independently of the extent of ruggedness as expressed by the parameter d: Despite the small chain length $l = 10$, convergence toward the uniform distribution at transition points far away from $p = \frac{1}{2}$ can be observed for all d-values and the $p_{\text{tr}}^{(0.01)}$-value computed from level crossing is a good indicator for the positions at which merging of the stationary concentrations for the complementary classes, $|\bar{y}_k(p_{\text{mg}}^{(\theta)}) - \bar{y}_{l-k}(p_{\text{mg}}^{(\theta)})| = \theta$, occurs. Based on the level crossing criterion for the location of the error threshold, we find that the transition migrates to smaller p-values for higher scatter of the fitness values. This observation is readily interpreted: An increase in scatter implies that the difference in fitness values between the master sequence and the sequence with the next highest fitness value becomes smaller, and a smaller difference in fitness other factors being unchanged causes the transition to occur at a smaller p-value.

Random scatter of fitness values introduces fitness differences among the sequences within a given mutant class Γ_k, and instead of a single curve as found for $d = 0$, we obtain a bundle of curves for the individual sequences $\mathsf{X}_{(k)}$ belonging to this class. For small d-values, corresponding to small scatter of fitness values and for p-values sufficiently lower than the error threshold, $p \ll p_{\text{cr}}$, the curves for the sequences belonging to given mutant classes form well-separated bands, which overlap at higher p- or higher d-values (Fig. 14). As seen in the class concentration plots (Fig. 15), the transition to the uniform distribution becomes somewhat irregular at high d-values. For example, in the bottom plot, the curves for ($k = 4$, $l - k = 6$) and for ($k = 3$, $l - k = 7$) cross first before they merge, which is due to the different spectra of f_j-values within the error classes. Nevertheless, also in these cases, the uniform distribution $\mathcal{U}$ is approached although at slightly higher p-values.

In proceeding toward the maximum scatter at the value $d = 1$, other transitions apart from the error thresholds are observed for the majority of RRLs (for exceptions, see next paragraph). These transitions, positioned at transition mutant rates, $p = (p_{\text{tr}}^{q})$, mark dramatic changes in the stationary mutant distributions, and the primary quasispecies Υ_m, which is the stable distribution from the selection state

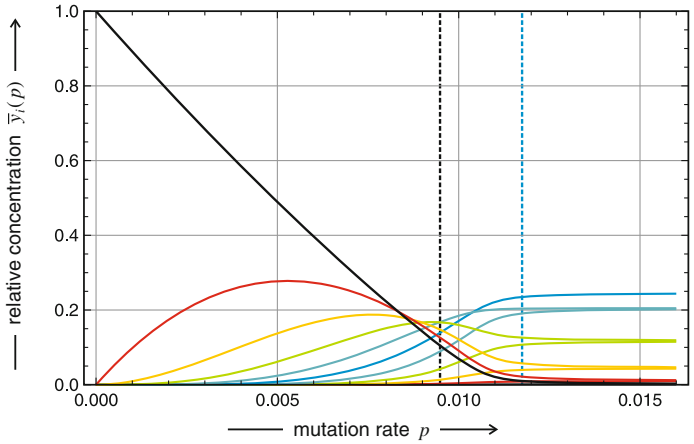
1.0
0.8
0.6
0.4
0.2
0.0
relative concentration $\overline{y}_i(p)$
0.000
0.005
0.010
0.015
mutation rate p

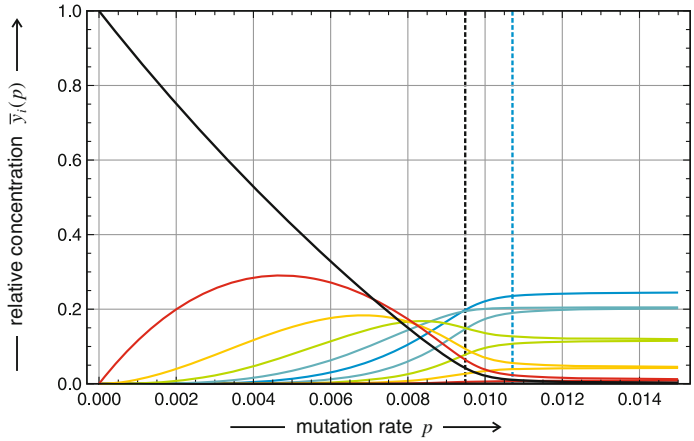
1.0
0.8
0.6
0.4
0.2
0.0
relative concentration $\overline{y}_i(p)$
0.000
0.002
0.004
0.006
0.008
0.010
0.012
0.014
mutation rate p

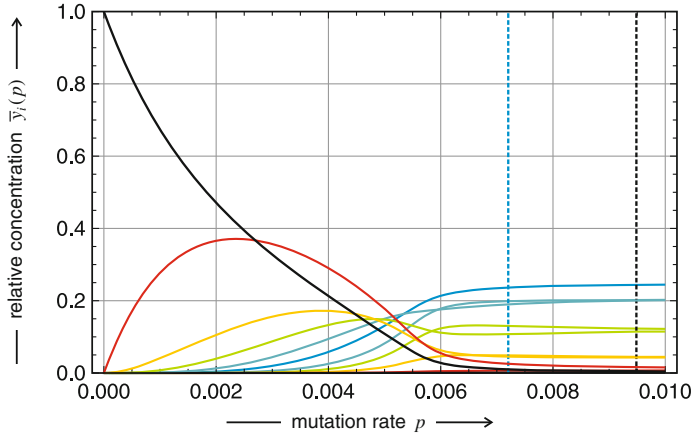
1.0
0.8
0.6
0.4
0.2
0.0
relative concentration $\overline{y}_i(p)$
0.000
0.002
0.004
0.006
0.008
0.010
mutation rate p

◀ **Fig. 15** Error thresholds on a *realistic* model landscape with different random scatter d. Shown are the stationary concentrations of classes $\bar{y}_j(p)$ on the landscapes $\mathcal{L}(10, 2, 1.1, 1.0; 0.0, d, 023)$ with $d = 0$ (*upper plot*), $d = 0.5$ (*middle plot*), and $d = 0.95$ (*lower plot*). The error threshold calculated by the phenomenological approach lies at $p_{\text{cr}} = 0.009486$ (*black dotted line*), and the positions for level crossing decrease with the width of random scatter d and are situated at $p_{\text{tr}}^{(0.01)} = 0.01175$, 0.01079, and 0.00720, respectively (*blue dotted lines*). For the analogous plots for fully developed randomness ($d = 1.0$), see Fig. 17

($p = 0$) onwards, is replaced at $p = (p_{\text{tr}}^{q})_{m,k}$ by another quasispecies Υ_k. The mechanism by which quasispecies replace each other has been worked out analytically (Schuster and Swetina 1988) and is easily interpreted:[15] The stationary mutational backflow stabilizes master sequences through adding a positive term to the production function

$$W(\mathsf{X}_m) = w_m = Q_{mm} f_m \bar{x}_m + \sum_{j=1, j\neq m}^{N} Q_{mj} f_j \bar{x}_j = Q_{mm} f_m \bar{x}_m + \Phi_{m\leftarrow(j)},$$

and likewise, we have for a potential master sequence X_k,

$$W(\mathsf{X}_k) = w_k = Q_{kk} f_k \bar{x}_k + \Phi_{k\leftarrow(j)}.$$

In general, the first term decreases and the second term increases with increasing p. The necessary—but not sufficient—condition for the existence of a transition is $\Delta\Phi = \Phi_{m\leftarrow(j)} - \Phi_{k\leftarrow(j)} < 0$. In other words, the mutational backflow to the original master sequence of Υ_0 has to be weaker than the backflow to the sequence X_k in Υ_k. Since the fitness value f_m is the largest by definition, we have $f_m > f_j \; \forall j = 1, \ldots, n$, and at sufficiently small mutation rates p, the differences in the selective values, $\Delta\Psi = Q_{mm} f_m - Q_{kk} f_k > 0$, will always outweigh the difference in the backflow, $\Delta\Phi > |\Delta\Psi|$, and the quasispecies Υ_m is stable. With increasing values of p, however, the replication accuracy and $\Delta\Phi$ will decrease because of the term $Q_{mm} = Q_{kk} \approx (1-p)^l$ in the uniform error approximation. At the same time, $\Delta\Psi$ will increase in absolute value and provided $\Delta\Psi < 0$ there might exist a mutation rate $p = p_{\text{tr}}^{(q)}$ smaller than the error threshold value $p_{\text{tr}}^{(q)} < p_{\text{cr}}$ at which the condition $\Delta\Phi + \Delta\Psi = 0$ is fulfilled and consequently, the quasispecies Υ_k is the stable stationary solution of equation at $p_{\text{tr}}^{(q)} < p < p_{\text{cr}}$ provided it is not replaced by another quasispecies in another transition.

The influence of a distribution of fitness values instead of the single value f of the single-peak landscapes can be predicted straightforwardly: Since f_m is independent of the fitness scatter d and f_k is increasing with increasing scatter, the difference

[15] Thirteen years after this publication, the phenomenon has been observed in quasispecies of digital organisms (Wilke et al. 2001) and was called *survival of the flattest*.

$f_m - f_k$ will decrease with increasing scatter d. Accordingly, the condition for a transition between quasispecies can be fulfilled at lower p-values and we expect to find one or more transitions below the error threshold p_{cr}. No transition can occur on the single-peak landscape, but as d increases the difference $\Delta\Phi$ becomes smaller, and it becomes more and more likely that the difference in backflow $\Delta\Psi$ becomes sufficiently strong for a replacement of Υ_m by Υ_k below p_{cr}.

As an example, we describe the development of quasispecies transitions on a typical RRL, $\mathcal{L}(10, 2, 1.1, 1.0; 0.0, d, 637)$, between the single-peak scenario ($d = 0$) and the full-band random landscape ($d = 1$). Starting form the unspecific error threshold scenario (Fig. 9), the error classes unfold into first separated and later overlapping bands until a scatter of $d = 0.85$ where the indication of a first $p_{\mathrm{tr}}^{(q)}$-transition appears near the error threshold. At $d = 0.925$, a transition $\Upsilon_0(\mathsf{X}_0) \rightarrow \Upsilon_1(\mathsf{X}_{247})$ can be identified, and this transition is the only transition at the d-values 0.95 and 0.975. Then, at $d = 0.995$, a second transition appears (see Fig. 16), and finally, we are dealing with three transitions at full randomness, $d = 1$. In addition to the quite common scenario of multiple transitions described here, we found also landscapes with a single transition at fully developed randomness (see Fig. 17) and landscapes sustaining no transition at all (see *strong quasispecies* in the next paragraph).

An important question is whether or not transitions between quasispecies have an influence on the convergence toward the uniform distribution $\mathcal{U}$ above threshold. Intuitively, we might suggest that this is not the case, but it is safer to consider a specific example. The RRL $\mathcal{L}(10, 2, 1.1, 1.0; 0.0, 1.0, 023)$ is chosen, because it exhibits a single transition, $\Upsilon_0(\mathsf{X}_0) \rightarrow \Upsilon_1(\mathsf{X}_{910})$, below the error threshold (Fig. 17). The middle plot shows the quasispecies Υ_1 centered around the master sequence X_{910} that is surrounded by three high-fitness sequences in the one-error class: X_{906}, X_{926}, and X_{942}, and one additional high-fitness sequence in the two-error class, X_{927}, which is directly attached to X_{926}. This example illustrates the role of mutational backflow Φ in stabilizing quasispecies above the transition. The lower plot shows the change of the class concentrations $\bar{y}_k(p)$ at the transition $\Upsilon_0(\mathsf{X}_0) \rightarrow \Upsilon_1(\mathsf{X}_{910})$ and at the error threshold, which leads to the uniform distribution $\mathcal{U}$. As expected, the fully developed random scatter smoothens the error threshold, shifts the lower boundary, $\min((p_{\mathrm{mg}}^{(\theta)})_k)$, of complementary class concentration merging to slightly smaller p-values but does not change the basic property of merging the concentrations of complementary classes (for a concrete quantitative example, see Table 3).

Finally, we remark that transitions between quasispecies provide a handicap for evolution because a small change in the mutation rate or in the fitness value may destabilize stationary mutant distributions, and we conjecture that natural systems will be driven toward landscapes with stable quasispecies in the sense that no transitions between quasispecies occur.

Strong quasispecies. A certain fraction of landscapes gives rise to scenarios for quasispecies as a function of the mutation rate p that are substantially different from the one discussed above: No transitions between quasispecies are observed not even

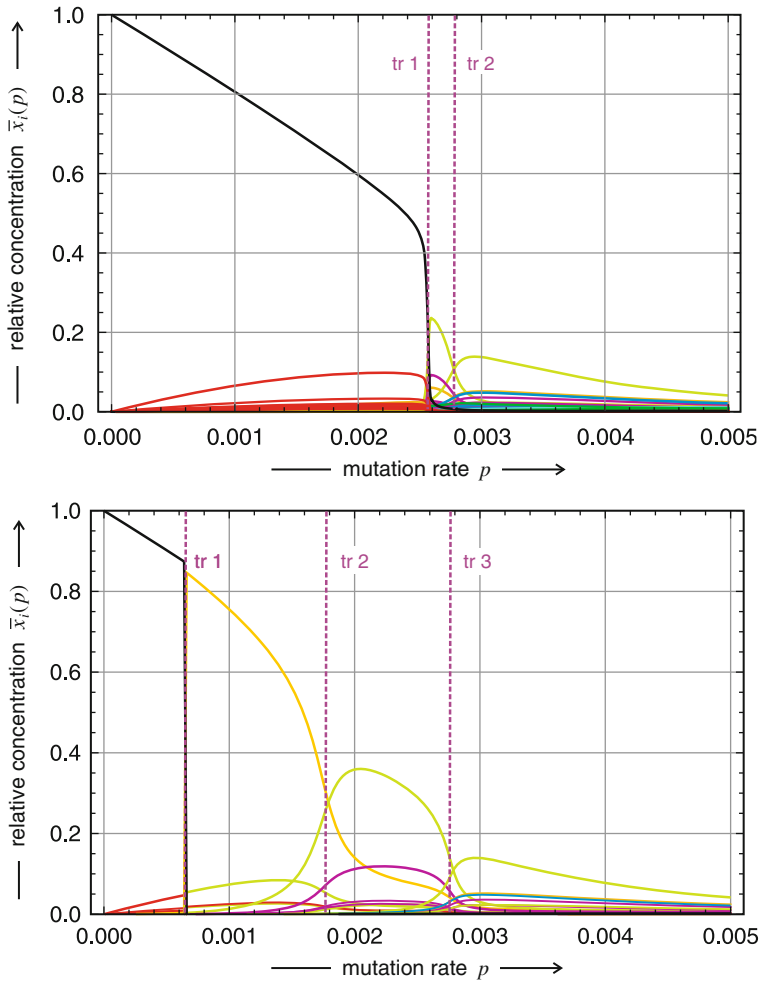

Fig. 16 A model landscape with multiple transitions between quasispecies. The plots present the stationary concentrations $\bar{x}_j(p)$ on landscapes $\mathcal{L}(10, 2, 1.1, 1.0; 0.0, d, 637)$ with $d = 0.995$ (*upper plot*) and with fully developed scatter $d = 1.0$ (*lower plot*). The following master sequences are involved in the transitions between quasispecies at $d = 1.0$: tr_1: $\Upsilon_0(\mathsf{X}_0) \rightarrow \Upsilon_1(\mathsf{X}_{1003})$; tr_2: $\Upsilon_1(\mathsf{X}_{1003}) \rightarrow \Upsilon_2(\mathsf{X}_{923})$; tr_3: $\Upsilon_2(\mathsf{X}_{923}) \rightarrow \Upsilon_3(\mathsf{X}_{247})$. The Hamming distances at the transitions are $d^{\text{H}}_{(0),}(1003) = 7$, $d^{\text{H}}_{(1003),(923)} = 3$, and $d^{\text{H}}_{(923),(247)} = 6$, respectively. For $d = 0.995$, the first transition does not exist; instead, we find $\Upsilon_0(\mathsf{X}_0) \rightarrow \Upsilon_1(\mathsf{X}_{923})$ and tr_3 becomes tr_2

at fully developed scatter d = 1.0 (Fig. 18). The most relevant feature of the quasispecies on these special landscapes concerns the classes to which the most frequent sequences belong. On the landscape defined by s = 919, these sequences are the master sequence (X_0; black curve), the one-error mutant (X_4; red curve), and

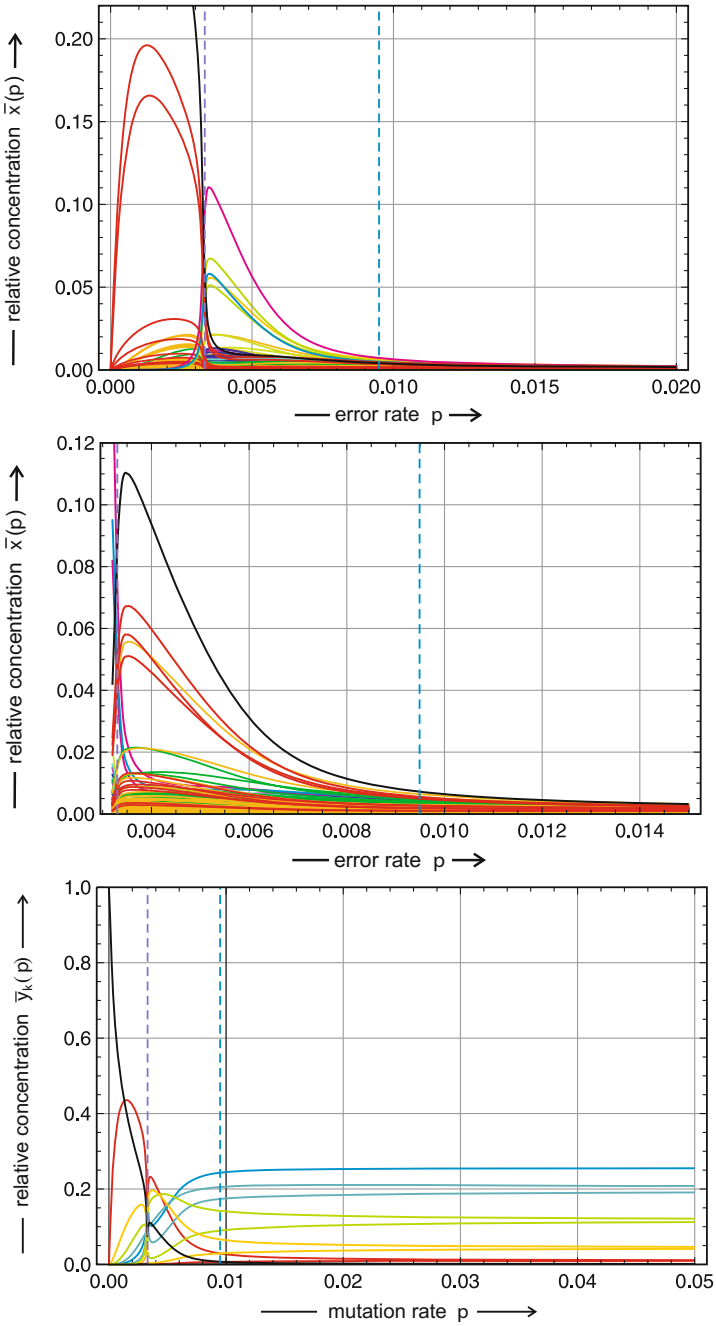
relative concentration $\bar{x}(p)$
0.20
0.15
0.10
0.05
0.00
0.000
0.005
0.010
0.015
0.020
error rate p
relative concentration $\bar{x}(p)$
0.12
0.10
0.08
0.06
0.04
0.02
0.00
0.004
0.006
0.008
0.010
0.012
0.014
error rate p
relative concentration $\bar{y}_k(p)$
1.0
0.8
0.6
0.4
0.2
0.0
0.00
0.01
0.02
0.03
0.04
0.05
mutation rate p

◀ **Fig. 17** Error threshold and transition between quasispecies. The landscape $\mathcal{L}(10, 2, 1.1, 1.0; 0.0, d, 023)$ supports a transition $\Upsilon_0(\mathsf{X}_0) \rightarrow \Upsilon_1(\mathsf{X}_{910})$ at $(p_{\text{tr}}^{q})_{0,910} \approx 0.00330$ (*violet dashed line*) and the error threshold computed from level crossing of X_{910} with $\vartheta = 0.01$ at $p_{\text{tr}}^{(0.01)} \approx 0.00837$. Above the error threshold, which lies at $p_{\text{cr}} = 0.00949$ (*blue dashed line*) in the corresponding single-peak landscape ($d = 0.0$), the quasispecies converges to the uniform distribution $\mathcal{U}$ as immediately seen from the mergence of complementary class concentration curves. The quasispecies above the transition at p_{tr}^{q} is centered around the sequence X_{910} corresponding to Υ_1. It is worth noticing that the one-error class Γ_1 (*red*) has a class concentration that exceeds the master sequence by a factor two. This is mainly due to three sequences of high fitness, X_{906}, X_{926}, and X_{942}

Table 3 Concentration level crossing and complementary class mergence on landscapes with random scatter of fitness values

$(p_{\text{mg}}^{(\theta)})_k$	Random scatter d						
k	0.0	0.5	0.7	0.9	0.95	0.975	1.0
0	0.01164	0.01097	0.01016	0.00884	0.00836	0.00809	0.00776
1	0.01210	0.01173	0.01123	0.01056	0.01039	0.01030	0.01022
2	0.01261	0.01292	0.01256	0.01161	0.01124	0.01103	0.01080
3	0.01282	0.01601	0.01768	0.01933	0.01972	0.01991	0.02009
4	0.01213	0.01283	0.01199	0.00962	0.00821	0.00757	0.00680
$p_{\text{tr}}^{(\vartheta)}$	0.01175	0.01108	0.01028	0.00895	0.00848	0.00820	0.00788
$\Delta p_{\text{mg}}^{(\theta)}$	0.00118	0.00504	0.00725	0.01049	0.01151*	0.01234*	0.01329*

Quantitative diagnostic tools are applied to the landscape $\mathcal{L}(10, 2, 1.1, 1.0; 0.0, d, 919)$. The decline of the master class, $\bar{y}_0 = \bar{x}_0$, at p-values near the error threshold $p_{\text{cr}} = 0.00948$ is illustrated by means of the points $p_{\text{tr}}^{(\vartheta)}$ where the curves cross the level $\bar{x}_0(p) = \vartheta = 0.01$. Complementary class mergence is characterized quantitatively by the band between the lowest and the highest $(p_{\text{mg}}^{(\theta)})_k$-value ($\theta = 0.01$). The lowest value is observed at $k = 0$ for $d = 0.0$, 0.5, 0.7, and 0.9. For the three highest random scatters, the lowest value is recorded for $k = 4$ (indicated by an asterisk '*')

the two-error mutant (X_{516}; yellow curve).[16] Coming from neighboring classes, the three special sequences are situated close-by in sequence space—Hamming distances $d^{\text{H}}_{(0),(4)} = d^{\text{H}}_{(4),(516)} = 1$ and $d^{\text{H}}_{(0),(516)} = 2$—and form a cluster, which is dynamically coupled by means of strong mutational flow (Fig. 19). As it turns out, such a quasispecies is not likely to be replaced in a transition by another one that is centered around a single master sequence and accordingly, we called such clusters *strong quasispecies*. The problem that ought to be solved now is the prediction of the occurrence of strong quasispecies from know fitness values.

A heuristic is mentioned that serves as an (almost perfect) diagnostic tool for detecting whether or not a given fitness landscape gives rise to a strong quasispecies: (i) For every mutant class, we identify the sequence with the highest fitness

[16]Naïvely, we would expect a band of one-error sequences at higher concentration than the two-error sequence.

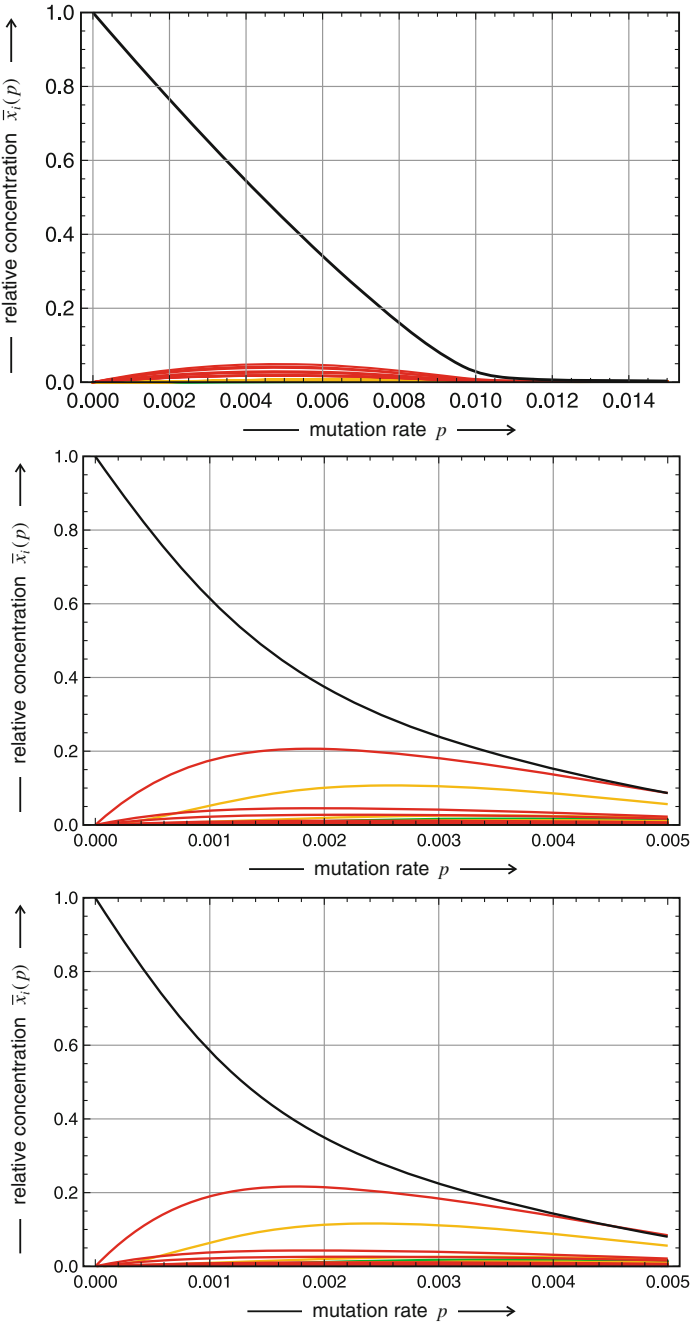

Fig. 18 Error thresholds on a model landscape with random scatter d and no transitions between quasispecies. The landscape $\mathcal{L}(10, 2, 1.1, 1.0; 0.0, d, 919)$ is computed and analyzed. Shown are the stationary concentrations $\bar{x}_j(p)$ for $d = 0.5$ (*upper plot*), for $d = 0.995$ (*middle plot*) and for fully developed random scatter $d = 1.0$ (*bottom plot*)

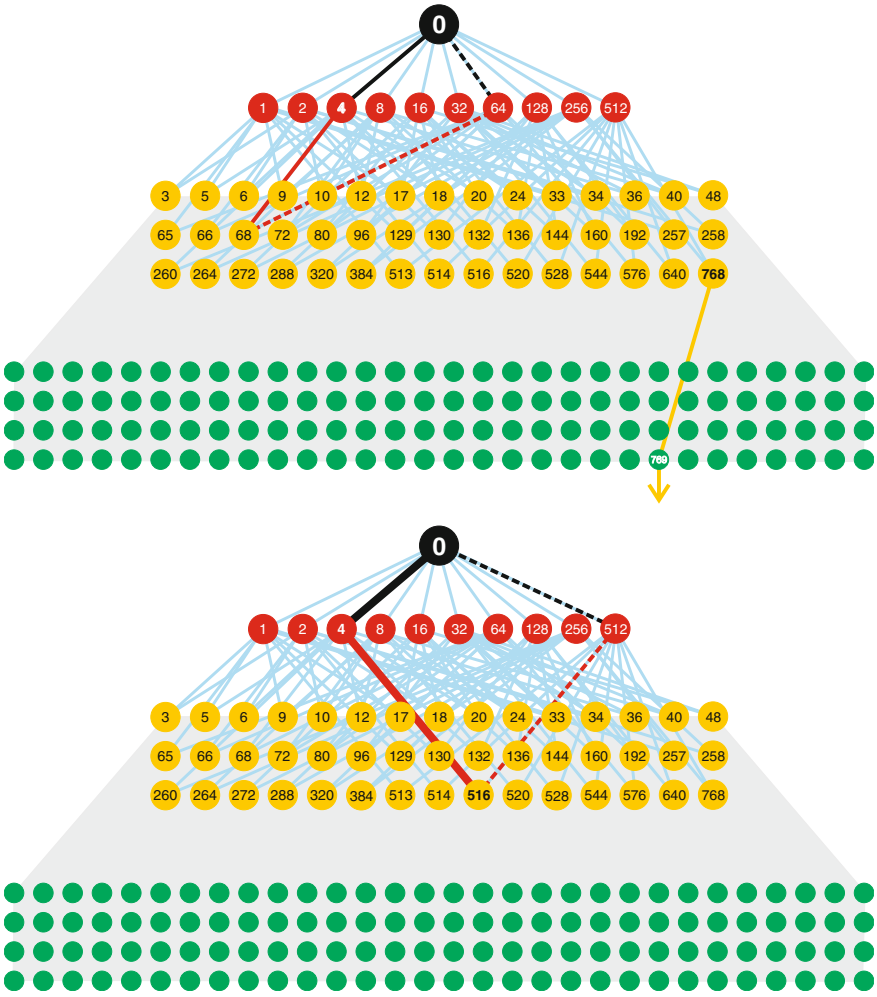

Fig. 19 Mutation flow in quasispecies. The sketch shows two typical situations in the distribution of fitness values in sequence space. In the *upper diagram* ($s = 637$), the fittest two-error mutant, X_{768}, has its fittest nearest neighbor, X_{769}, in the three-error class Γ_3. The fittest sequence in the one-error neighborhood of the fittest one-error mutant, X_4, is X_{68} and not $_{768}$, and hence, the mutational flow is not sufficiently strong for coupling the three sequences X_0, X_4, and X_{68} to a strong cluster, and transitions between different quasispecies are observed (Fig. 16). The lower diagram ($s = 919$) shows the typical fitness distribution for a strong quasispecies: The fittest two-error mutant, X_{516}, has its fittest nearest neighbor, X_4, in the one-error class Γ_1, and it coincides with the fittest one-error mutant. Here, the three sequences (X_0, X_4, and X_{516}) are strongly coupled by mutational flow, and a strong quasispecies is observed (Fig. 18)

value, f_m, $(f_{(1)})_{\max} = f(\mathbf{X}_{m(1)})$, $(f_{(2)})_{\max} = f(\mathbf{X}_{m(2)}), \ldots,$, and call them *class-fittest* sequences. Next, we determine the fittest sequences in the one-error neighborhood of the class-fittest sequences. Clearly, for the class k-fittest sequence $\mathbf{X}_{m(k)}$, this sequence lies either in class $k - 1$ or in class $k + 1$.[17] Simple combinatorics is favoring classes closer to the middle of sequence space because they have more members, $\binom{l}{k}$, in number. Any sequence in the two-error class, for example, has two nearest neighbors in the one-error class but $l - 2$ nearest neighbors in the three-error class (see Fig. 10). To be a candidate for a strong quasispecies requires that—against probabilities—the fittest sequence in the one-error neighborhood of $\mathbf{X}_{m(2)}$ lies in the one-error class: $(f_{(\mathbf{X}_{m(2)})_{m(1)}})_{\max}$ with $(\mathbf{X}_{m(2)})_{m(1)} \in \Gamma_1$ and preferentially, this is the fittest one-error sequence, $(\mathbf{X}_{m(2)})_{m(1)} \equiv \mathbf{X}_{m(1)}$. Since all mutation rates between nearest neighbor sequences in neighboring classes are the same —$(1-p)^{n-1}p$ within the uniform error model—the strength of mutational flow is dependent only on the fitness values, and the way in which the three sequences were determined guarantees optimality of the flow: If such a three-membered cluster was found, it is the one with the highest internal mutational flow for a given landscape. Figure 19 (lower picture, $s = 919$) shows an example where such three sequences form a strongly coupled cluster. There is always a fourth sequence—here $\mathbf{X}_{512}$—belonging to the cluster, but it may play no major role because of low fitness. The heuristic presented here was applied to all 21 fitness landscapes with different random scatter, and three strong quasispecies (s = 401, 577, and 919) were observed. How many would be expected by combinatorial arguments? The probability for a sequence in Γ_2 to have a neighbor in Γ_1 is 2/10 = 0.2, and, since the sequence $\mathbf{X}_{m(1)}$ is fittest in Γ_1 and hence also in the one-error neighborhood of $\mathbf{X}_{m(2)}$, this is also the probability for finding a strong quasispecies. The sample that has been investigated in this study comprised 21 landscapes, and hence, we expect to encounter 21/5 = 4.2 cases, which is—with respect to the small sample size—in full agreement with the three cases that we found. The suggestion put forward in the heuristic mentioned above—a cluster of sequences coupled by mutational flow that is stronger within the group than to the rest of sequence space because of frequent mutations and high-fitness values—has been analyzed and tested through the application of perturbation theory (Schuster 2012). We dispense here from details since we shall not make further use of the corresponding expressions.

In order to study the influence of random scatter on the numerical computation of the location of the error threshold, we apply the two criteria, level crossing and complementary class mergence to the strong quasispecies on the landscape $\mathcal{L}(10, 2, 1.1, 1.0; 0.0, d, 919)$. The results are shown in Table 3. As already shown for other RRLs, the position of the crossing of $\bar{x}_0$ migrates to smaller mutation rates $p_{\text{tr}}^{(\vartheta)}$ with increasing d. At the same time, the width of the transition increases by

[17]For class $k = 1$, we omit the master sequence $\mathbf{X}_m$, which trivially is the fittest sequence in the one-error neighborhood, and search only in class $k = 2$.

about one order of magnitude from $\Delta p_{\mathrm{tr}}^{(\theta)} = 0.0012-0.013$. Nevertheless, the quantitative diagnostic tools for the detection of the error threshold on complex landscapes works perfectly, and in contrast to doubts raised in the literature (Baake and Wagner 2001; Charlesworth 1990), even the landscapes with fully developed randomness (d = 1.0) sustain perfect error thresholds.

Selective neutrality. The second property of realistic fitness landscapes mentioned in Sect. 2 is *neutrality,* and in Eq. (5b), we made a proposal how neutrality can be implemented together with ruggedness. The resulting rugged and neutral fitness landscape (RNL) is characterized by two landscape specific parameters: (i) The random scatter is denoted by d as in the RRL landscape and (ii) a degree of neutrality λ. The value $\lambda = 0$ means absence of neutrality and $\lambda = 1$ describes the completely flat landscape in the sense of Kimura's *neutral evolution* (Kimura 1983). The result of the theory of neutral evolution that is most relevant here concerns *random selection*: Although fitness differences are absent, one randomly chosen sequence is selected by means of the autocatalytic replication mechanism, $\mathsf{X} \rightarrow 2\mathsf{X}$ and $\mathsf{X} \rightarrow \emptyset$. For most of the time, the randomly replicating population consists of a dominant genotype and a number of neutral variants at low concentration. An important issue of the landscape approach is the random positioning of neutral master sequences in sequence space, which is achieved by means of the same random number generator that is used to compute the random scatter of the other fitness values.

The RNL is the complete analogue to the rugged fitness landscape (RRL) under the condition that several master sequences exist, which have the same highest fitness values f_0. The fraction of neutral mutants is determined by the fraction of random numbers, which fall into the range $1 - \lambda < \eta \leq 1$, and apart from statistical fluctuations, this fraction is λ. At small values of the degree of neutrality λ, isolated peaks of highest fitness f_0 will appear in sequence space. Increasing λ will result in the formation of clusters of sequences of highest fitness. Connecting all fittest sequences of Hamming distance $d_{\mathrm{H}} = 1$ by an edge results in a graph that has been characterized as *neutral network* (Reidys et al. 1997; Reidys and Stadler 2002). Neutral networks were originally conceived as a tool to model, analyze, and understand the mapping of RNA sequences into secondary structures (Grüner et al. 1996a, b; Schuster et al. 1994). The neutral network in RNA sequence structure mappings is the preimage of a given structure in sequence space, and these networks can be approximated in zeroth order by random graphs (Erdős and Rényi 1959, 1960). Whereas neutral networks in RNA sequence structure mappings are characterized by a relatively high degree of neutrality around $\lambda \approx 0.3$ and sequence space percolation is an important phenomenon, we shall be dealing here with lower λ-values.

The two smallest clusters of mutationally coupled fittest sequences have Hamming distances $d_{\mathrm{H}} = 1$ and $d_{\mathrm{H}} = 2$ (Fig. 20). In the former case, we are dealing with the minimal neutral network of two neighboring sequences; in the latter case, the Hamming distance of two sequences are coupled through two intermediate sequences similarly as in the core of strong quasispecies. An exact

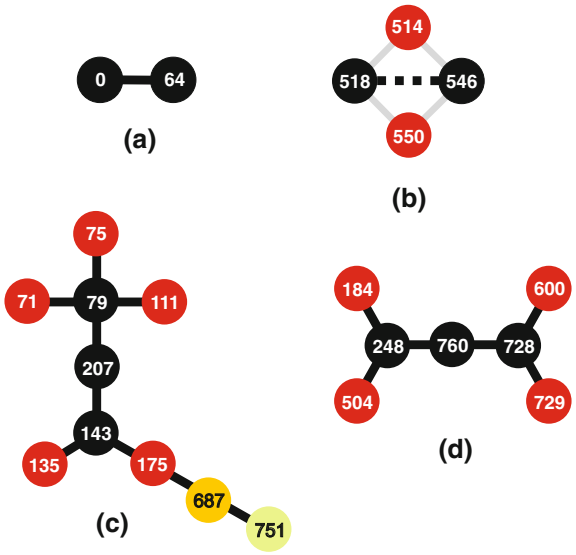

Fig. 20 Neutral networks in quasispecies. The sketch presents four special cases that were observed on rugged neutral landscapes defined in Eq. (5b). Part **a** shows the smallest possible network consisting of two sequences of Hamming distance $d_H = 1$ observed with $s = 367$ and $\lambda = 0.01$. Part **b** contains two sequences of Hamming distance $d_H = 2$, which are coupled through two $d_H = 1$ sequences; it was found with $s = 877$ and $\lambda = 0.01$. The neutral network in part **c** has a core of three sequences, surrounded by five one-error mutants, one of them having a chain of two further mutants attached to it; the parameters of the landscape are $s = 367$ and $\lambda = 0.1$. Part **d** eventually shows a symmetric network with three core sequences and four one-error mutants attached to it, observed with $s = 229$ and $\lambda = 0.1$. Choice of further parameters: $l = 10$, $f_0 = 1.1$, $f = 1.0$, and $d = 0.5$. Color code: core sequences in *black*, one-error mutants in *red*, two-error mutants in *yellow*, and three-error mutants in *green*

mathematical analysis is possible for both cases in the limit of vanishing mutation rates, $\lim p \to 0$ (Schuster and Swetina 1988). It yielded two results that are different from Kimura's neutral theory:

$$\lim_{p\to 0} \bar{x}_{\mathrm{I}} = \frac{1}{2}, \lim_{p\to 0} \bar{x}_{\mathrm{II}} = \frac{1}{2} \quad \text{for} \quad d^{\mathrm{H}}_{\mathsf{X}_{\mathrm{I}}\mathsf{X}_{\mathrm{II}}} = 1, \tag{16a}$$

$$\lim_{p\to 0} \bar{x}_{\mathrm{I}} = \frac{\alpha}{1+\alpha}, \lim_{p\to 0} \bar{x}_{\mathrm{II}} = \frac{1}{1+\alpha} \quad \text{for } d^{\mathrm{H}}_{\mathsf{X}_{\mathrm{I}}\mathsf{X}_{\mathrm{II}}} = 2, \tag{16b}$$

$$\begin{aligned} &\lim_{p\to 0} \bar{x}_{\mathrm{I}} = 1, \lim_{p\to 0} \bar{x}_{\mathrm{II}} = 0 \quad \text{or} \quad \lim_{p\to 0} \bar{x}_{\mathrm{I}} = 0, \lim_{p\to 0} \bar{x}_{\mathrm{II}} = 1, \\ &\text{for} \quad d^{\mathrm{H}}_{\mathsf{X}_{\mathrm{I}}\mathsf{X}_{\mathrm{II}}} \geq 3. \end{aligned} \tag{16c}$$

If the two neutral fittest sequences, X_{I} and X_{II}, are nearest neighbors in sequence space, $d^{\mathrm{H}}_{\mathsf{X}_{\mathrm{I}}\mathsf{X}_{\mathrm{II}}} = 1$, they are present at equal concentrations in the quasispecies in the

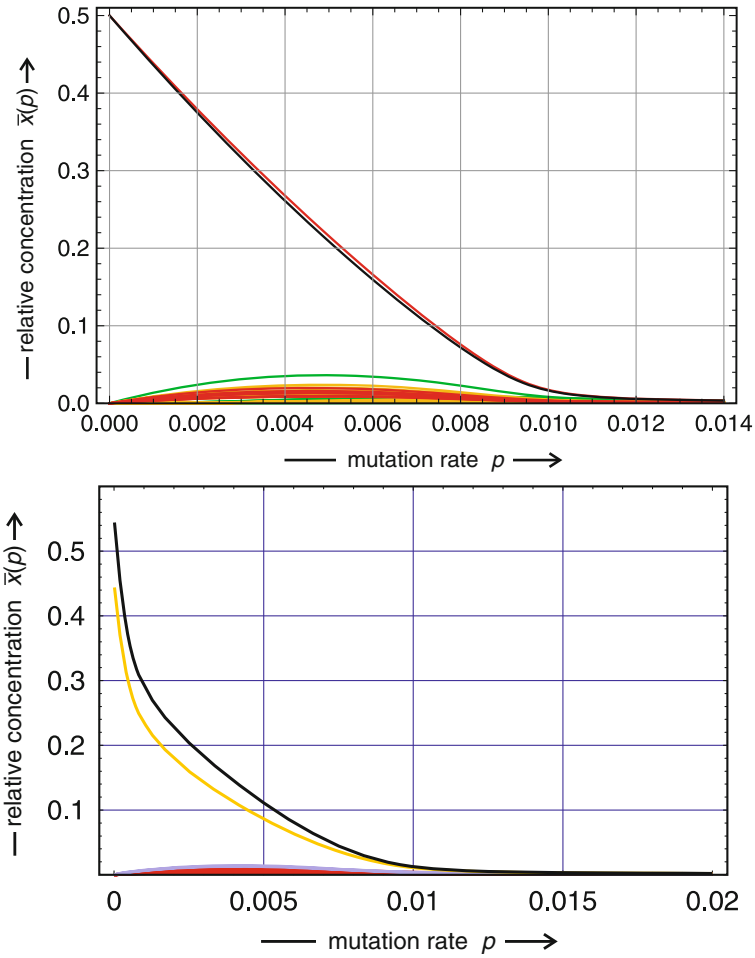

Fig. 21 Cluster on a weakly neutral rugged model landscapes. The plot at the *top* shows the quasispecies on the RNL $\mathcal{L}(10, 2, 1.1, 1.0; 0.1, 0.5, 637)$. The cluster in the core of the quasispecies is shown in Fig. 20a and consists of two Hamming distance $d_{\mathrm{H}} = 1$ master sequences, X_0 and X_{64}, which are present in equal concentrations from $p = 0$ to the error threshold. Further, we show their one-error neighborhoods, and the third fittest neutral sequence X_{324} at Hamming distance $d^{\mathrm{H}}_{(0),(324)} = 3$ (*green*). The *bottom plot* presents the quasispecies on the RNL $\mathcal{L}(10, 2, 1.1, 1.0; 0.1, 0.5, 877)$. The master pair X_{518} and X_{546} has Hamming distance $d_{\mathrm{H}} = 2$ and appears at roughly constant concentration ratio in the quasispecies over the entire range, $0 \leq p < p_{\mathrm{cr}}$

low mutation rate limit, and in case they are next nearest neighbors in sequence space, $d^{\mathrm{H}}_{\mathsf{X}_{\mathrm{I}}\mathsf{X}_{\mathrm{II}}} = 2$, they are observed at some ratio α, and in both cases, none of the two sequences vanishes. Only for Hamming distances $d^{\mathrm{H}}_{\mathsf{X}_{\mathrm{I}}\mathsf{X}_{\mathrm{II}}} \geq 3$, Kimura's scenario of random selection occurs. It is important to stress a difference between the two

scenarios, the deterministic ODE approach leading to clusters of neutral sequences and the random selection phenomenon of Kimura: In the quasispecies, we have strong mutational flow within the cluster of neutral sequences—which is not substantially different from the flow within the non-neutral clusters discussed in the previous paragraph—and this flow outweighs fluctuations. For Hamming distances d_{H} of three and more, the mutational flow is too weak to counteract random drift. In the random replication scenario, mutations do not occur and the only drive for change in particle numbers is random fluctuations.

In order to check the role of the predictions for the limit $p \longrightarrow 0$ in the case of nonzero mutation rates, we search for appropriate test cases by inspection of RNL landscapes according to (5b). For small degrees of neutrality, we found indeed suitable neutral clusters on the landscapes ($s = 637, \lambda = 0.01$ and $s = 877, \lambda = 0.01$ both shown in Fig. 21). In full agreement with the exact result, we find that two fittest sequences of Hamming distance $d_{\mathrm{H}} = 1$ are selected as a strongly coupled pair with equal frequency of both members and numerical results show that

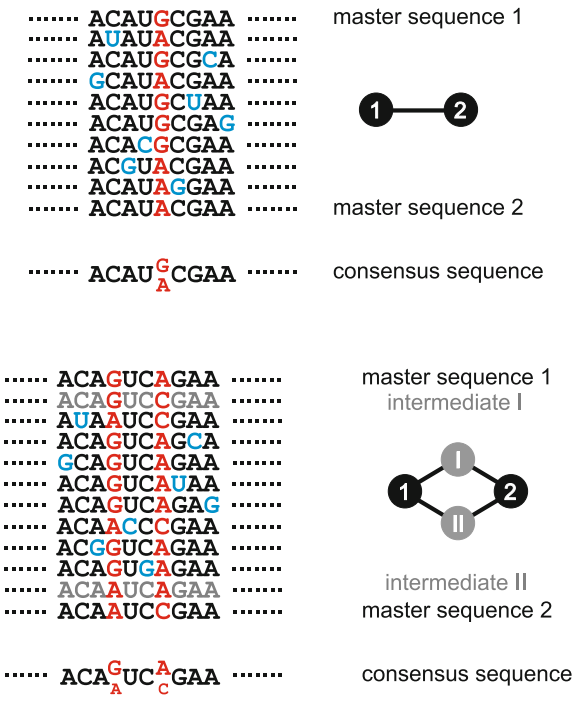

Fig. 22 Quasispecies and consensus sequences in case of neutrality. The *upper part* of the figure shows a sketch of sequences in the quasispecies of two fittest nearest neighbor sequences ($d_{\mathrm{H}} = 1$). The consensus sequence is not unique and differs in a single position where both nucleotides appear with equal frequency. In the *lower part,* the two master sequences have Hamming distance $d_H = 2$ and differ in two positions. The two sequences are present at some ratio α that is determined by the fitness values of other neighboring sequences, and the nucleobases corresponding to the differences in the two master sequences appear with the same ratio α

strong coupling does not occur only for small mutation rates but extends over the whole range of p-values from $p = 0$ up to the error threshold $p = p_{cr}$. Examples for the case $d_H = 2$ are also found on random neutral landscapes, and again, the exact result for vanishing mutation rate holds up to the error threshold. The existence of neutral nearest and next nearest neighbors manifests itself in the lack of unique consensus sequences of populations and has important consequences for the reconstruction of phylogenies (Fig. 22).

Neutral networks may comprise several sequences, and then, all neutral nearest neighbor sequences form a strongly coupled master cluster in reproduction. The distribution of individual members of the cluster in the limit $p \rightarrow 0$ is readily obtained by diagonalization of the adjacency matrix.[18] The components of the largest eigenvector are proportional to the concentrations of elements of the replication network. Increasing the degree of neutrality λ gives rise to the formation of larger neutral networks. Commonly, there is a *giant cluster* and many small clusters as predicted by random graph theory.

5 Conclusions and Perspectives

The landscape concept was shown to be applicable to asexually reproducing virus populations, although fully empirically determined examples are not achievable at the current state of the art. Realistic landscapes are characterized by two global features: (i) ruggedness and (ii) neutrality. At sufficiently low mutation rates, all these landscapes support stationary mutant distribution called quasispecies no matter how large the random scatter of the individual fitness values is. The frequencies of individual genotypes in quasispecies are determined by their fitness values and the distances to the master sequence. Contradicting previous conjectures, such realistic landscapes exhibit error thresholds in the sense that the mutant distributions change abruptly at a certain critical mutations rate, which can be fully characterized by quantitative criteria. Above threshold, the conventional deterministic description by means of kinetic differential equations yields the uniform distribution of sequences as stationary solution and hence cannot provide a correct picture of replication–mutation dynamics. Under these conditions, populations drift randomly through sequence space in the sense of Kimura's neutral theory of evolution.

Although the kinetic equations allow for the derivation of general solutions in terms of eigenvalue problems, they are limited in reality because numerical computations are facing unsurmountable difficulties even for relatively small sequence lengths ($l \approx 50$). A phenomenological approach originally proposed by Eigen

[18]The adjacency matrix of a graph, A, is a symmetric square matrix that has an entry $a_{jk} = a_{kj} = 1$ whenever the graph has an edge between the nodes for $\mathbf{X}_j$ and $\mathbf{X}_k$ and zero entries everywhere else.

introduces simplifications, which allow for straightforward handling of long genotypes. This approach cannot be deduced from the original equations in a consistent way but represents an enormously successful heuristic for the calculation of error thresholds in real-world situations, and fortunately, the results become more accurate for longer polynucleotide sequences.

A problem for future research concerns the classification of landscapes in view of the mutation–selection dynamics upon them. We have sketched here two examples where the quasispecies dynamics can be predicted from the distribution of fitness values: (i) landscapes supporting strong quasispecies and (ii) landscapes with a tunable degree of neutrality. These studies make several predictions, and the next natural step is to test them experimentally and to initiate thereby a dialogue between theorists and experimentalists. Precisely, this dialogue made physics so successful, but unfortunately, it is still underdeveloped in biology.

6 Color Code for Sequences and Classes

The individual curves in plots of quasispecies as functions of the mutation rate p are color coded in order to make them better distinguishable. Most plots refer to a chain length $l = 10$ and adopted the following color code. For concentrations of classes rather than individual sequences, we use a different color code in order to make merging of complementary classes better visible.

Class no.	Color	
	Sequences	Classes
0	Black	Black
1	Red	Red
2	Yellow	Yellow
3	Green	Green
4	Sea green	Sea green
5	Blue	Blue
6	Magenta	Sea green
7	Chartreuse	Green
8	Yellow	Yellow
8	Red	Red
10	Black	Black

Acknowledgements The calculations reported here were done with the package *Mathematica 9.0*. For the simulations based on Gillespie's algorithm, we made use of the open-source SSA-program within X-Cellerator package. We are grateful to Bruce Shapiro for making this software public.

The author wishes to acknowledge support by the University of Vienna, Austria, and the Santa Fe Institute, Santa Fe, USA. A number of colleagues have helped in discussions. I am particulary grateful to Reinhard Bürger, Esteban Domingo, Christoph Flamm, Leticia Gonzalez-Herrero, Ivo Hofacker, Markus Oppel, David Saakian, and Peter Stadler.

References

Altenberg L (1997) NK fitness landscapes. In: Bäck T, Fogel DB, Michalevicz Z (eds) Handbook of evlutionary computation, chapter B 2.7.2. Oxford University Press, Oxford, UK, pp 2.7.5–2.7.10

Arslan E, Laurenzi IJ (2008) Kinetics of autocatalysis in small systems. J Chem Phys 128:e015101

Athavale SS, Spicer B, Chen IA (2014) Experimental fitness landscapes to understand the molecular evolution of RNA-based life. Curr Opin Chem Biol 22:35–39

Baake E, Baake M, Wagner H (1997) Ising quantum chain is equivalent to a model of biological evolution. Phys Rev Lett 78:559–562

Baake E, Gabriel W (1999) Biological evolution through mutation, selection, and drift: an introductory review. In: Stauffer D (ed) Annual review of computational physics VII. World Scientific, Singapore, pp 203–264

Baake E, Wagner H (2001) Mutation-selection models solved exactly with methods of statistical mechanics. Genet Res Camb 78:93–117

Beerenwinkel N, Pachter L, Sturmfels B, Elena SF, Lenski RE (2007) Analysis of epistatic interactions and fitness landscapes using a new geometric approach. BMC Evol Biol 7:e60

Betancourt AJ, Bollback JP (2006) Fitness effects of beneficial mutations: the mutational landscape model in experimental evolution. Curr Opin Genet Dev 16:618–623

Biebricher CK (1983) Darwinian selection of self-replicating RNA molecules. In: Hecht MK, Wallace B, Prance GT (eds) Evolutionary biology, vol 16. Plenum Publishing Corporation, New York, pp 1–52

Biebricher CK, Eigen M, William C, Gardiner J (1983) Kinetics of RNA replication. Biochemistry 22:2544–2559

Biebricher CK, Eigen M, William C, Gardiner J (1984) Kinetics of RNA replication: plus-minus asymmetry and double-strand formation. Biochemistry 23:3186–3194

Biebricher CK, Eigen M, William C, Gardiner J (1985) Kinetics of RNA replication: competition and selection among self-replicating RNA species. Biochemistry 24:6550–6560

Bratus AS, Novozhilov AS, Semenov YS (2014) Linear algebra of the permutation invariant Crow-Kimura model of prebiotic evolution. Math Biosci 256:42–57

Bürger R (1998) Mathematical properties of mutation-selection models. Genetica 102(103):279–298

Charlesworth B (1990) Mutation-selection balance and the evolutionary advantage of sex and recombination. Genet Res Camb 55:199–221

Chou H-H, Delaney NF, Draghi JA, Marx CJ (2014) Mapping the fitness landscape of gene expression uncovers the cause of antagonism and sign epistasis between adaptive mutations. PLoS Genet 10:e1004149

Crow JF, Kimura M (1970) An introduction to population genetics theory. Harper & Row, New York (Reprinted at The Blackburn Press, Caldwell, NJ, 2009)

Demetrius L, Schuster P, Sigmund K (1985) Polynucleotide evolution and branching processes. Bull Math Biol 47:239–262

Drake JW, Charlesworth B, Charlesowrth D, Crow JF (1998) Rates of spontaneous mutation. Genetics 148:1667–1686

Edwards SF, Anderson PW (1975) Theory of spin glasses. J Phys F 5:965–974

Eigen M (1971) Selforganization of matter and the evolution of biological macromolecules. Naturwissenschaften 58:465–523
Eigen M, McCaskill J, Schuster P (1988) Molecular quasispecies. J Phys Chem 92:6881–6891
Eigen M, McCaskill J, Schuster P (1989) The molecular quasispecies. Adv Chem Phys 75:149–263
Eigen M, Schuster P (1977) The hypercycle. A principle of natural self-organization. Part A: emergence of the hypercycle. Naturwissenschaften 64:541–565
Eigen M, Schuster P (1978) The hypercycle. A principle of natural self-organization. Part B: the abstract hypercycle. Naturwissenschaften 65:7–41
Eigen M, Schuster P (1982) Stages of emerging life—five principles of early organization. J Mol Evol 19:47–61
Elena SF, Sanjuán R (2007) Virus evolution: insights from an experimental approach. Annu Rev Ecol Evol Syst 58:27–52
Erdös P, Rényi A (1959) On random graphs. I. Publ Math 6:290–295
Erdös P, Rényi A (1960) On the evolution of random graphs. Publ Math Inst Hung Acad Sci 5:17–61
Fisher RA (1941) Average excess and average effect of a gene substitution. Ann Eugenics 11:53–63
Fontana W, Griesmacher T, Schnabl W, Stadler PF, Schuster P (1991) Statistics of landscapes based od free energies, replication and degradation rate constants of RNA secondary structures. Mon Chem 122:795–819
Fontana W, Konings DAM, Stadler PF, Schuster P (1993) Statistics of RNA secondary structures. Biopolymers 33:1389–1404
Fontana W, Schnabl W, Schuster P (1989) Physical aspects of evolutionary optimization and adaptation. Phys Rev A 40:3301–3321
Fontana W, Schuster P (1987) A computer model of evolutionary optimization. Biophys Chem 26:123–147
Fontana W, Schuster P (1998a) Continuity in evolution. On the nature of transitions. Science 280:1451–1455
Fontana W, Schuster P (1998b) Shaping space. The possible and the attainable in RNA genotype-phenotype mapping. J Theor Biol 194:491–515
Gago S, Elena SF, Flores R, Sanjuan R (2009) Extremely high mutation rate of a hammerhead viroid. Science 323:1308
Galluccio S (1997) Exact solution of the quasispecies model in a sharply peaked fitness landscape. Phys Rev E 56:4526–4539
Gavrilets S (1997) Evolution and speciation on holey adaptive landscapes. Trends Ecol Evol 12:307–312
Gillespie DT (1977) Exact stochastic simulation of coupled chemical reactions. J Phys Chem 81:2340–2361
Gillespie DT (2007) Stochastic simulation of chemical kinetics. Annu Rev Phys Chem 58:35–55
Grüner W, Giegerich R, Strothmann D, Reidys C, Weber J, Hofacker IL, Schuster P (1996a) Analysis of RNA sequence structure maps by exhaustive enumeration. I. Neutral networks. Mon Chem 127:355–374
Grüner W, Giegerich R, Strothmann D, Reidys C, Weber J, Hofacker IL, Schuster P (1996b) Analysis of RNA sequence structure maps by exhaustive enumeration. II. Structures of neutral networks and shape space covering. Mon Chem 127:375–389
Hamming RW (1950) Error detecting and error correcting codes. Bell Syst Tech J 29:147–160
Hamming RW (1986) Coding and information theory, 2nd edn. Prentice-Hall, Englewood Cliffs, NJ
Ho SYW, Duchêne S (2014) Molecular-clock methods for estimating evolutionary rates and timescales. Mol Ecol 23:5947–5965
Hofacker IL, Fontana W, Stadler PF, Bonhoeffer LS, Tacker M, Schuster P (1994) Fast folding and comparison of RNA secondary structures. Mon Chem 125:167–188

Jain K, Krug J (2007) Adaptation in simple and complex fitness landscapes. In: Bastolla U, Porto M, Eduardo Roman H, Vendruscolo M (eds) Structural approaches to sequence evolution. Molecules, networks, populations, chapter 14. Springer, Berlin, pp 299–339

Janet A (1895) Considérations méchaniques sur l'évolution et le problème des espèces. In: Comptes Rendue des 3me Congrès International de Zoologie. 3me Congres International de Zoologie, Leyden, pp 136–145

Jiménez JI, Xulvi-Brunet R, Campbell GW, amd Irene A, Chen RT (2013) Comprehensive experimental fitness landscape and evolutionary network for small RNA. Proc Natl Acad Sci USA 110:14984–14989

Jones BL, Enns RH, Rangnekar SS (1976) On the theory of selection of coupled macromolecular systems. Bull Math Biol 38:15–28

Kang Y-G, Park J-M (2008) Survival probability of quasi-species model under environmental changes. J Korean Phys Soc 53:868–872

Kauffman S, Levin S (1987) Towards a general theory of adaptive walks on rugged landscapes. J Theor Biol 128:11–45

Kauffman SA (1993) The origins of order. Self-organization and selection in evolution. Oxford University Press, New York

Kauffman SA, Weinberger ED (1989) The N-k model of rugged fitness landscapes and its application to the maturation of the immune response. J Theor Biol 141:211–245

Kimura M (1983) The neutral theory of molecular evolution. Cambridge University Press, Cambridge

Kingman JFC (1978) A simple model for the balance between selection and mutation. J Appl Probab 15:1–12

Kingman JFC (1980) Mathematics of genetic diversity. Society for Industrial and Applied Mathematics, Philadelphia

Kouyos RD, Leventhal GE, Hinkley T, Haddad M, Whitcomb JM, Petropoulos CJ, Bonhoeffer S (2012) Exploring the complexity of the HIV-1 fitness landscape. PLoS Genet 8:e1002551

Kouyos RD, von Wyl V, Hinkley T, Petropoulos CJ, Haddad M, Whitcomb JM, Böni J, Yerly S, Cellerai C, Klimkait T, Günthard HF, Bonhoeffer S, The Swiss HIV Cohort Study (2011). Assessing predicted HIV-1 replicative capacity in a clinical setting. PLoS Pathog 7: e1002321

Lanfear R, Welch JJ, Bromham L (2010) Watching the clock: studying variation in rates of molecular evolution between species. TREE 25:495–503

Leuthäusser I (1986) An exact correspondence between Eigen's evolution model and a two-dimensional ising system. J Chem Phys 84:1884–1885

Leuthäusser I (1987) Statistical mechanics of Eigen's evolution model. J Stat Phys 48:343–360

Lifson S (1961) On the theory of helix-coil transitions in polypeptides. J Chem Phys 34:1963–1974

Lorenz R, Bernhart SH, Höner zu Siederdissen C, Tafer H, Flamm C, Stadler PF, Hofacker IL (2011) ViennaRNA package 2.0. Algorithms Mol Biol 6:e26

McCoy JW (1979) The origin of the "adaptive landscape" concept. Am Nat 113:610–613

McGhee GR Jr (2007) The geomerty of evolution: adaptive landscapes and theoretical morphospaces. Cambridge University Press, Cambridge

Mills DR, Peterson RL, Spiegelman S (1967) An extracellular Darwinian experiment with a self-duplicating nucleic acid molecule. Proc Natl Acad Sci USA 58:217–224

Mollison D (ed) (1995) Epidemis models: their structure and relation to data. Cambridge University Press, Cambridge

Nåsell I (2011) Extiction and quasi-stationarity in the stochastic logistic SIS model, vol 2022. Lecture Notes in Mathematics. Springer, Berlin

Niederbrucker G, Gansterer WN (2011) Efficient solution of evolution models for virus populations. Procedia Comput Sci 4:126–135

Nowak M, Schuster P (1989) Error thresholds of replication in finite populations. Mutation frequencies and the onset of Muller's ratchet. J Theor Biol 137:375–395

Park J-M, noz EM, Deem MW (2010) Quasispecies theory for finite populations. Phys Rev E 81: e011902

Pitt JN, Ferré-D'Amaré AR (2010) Rapid construction of empirical RNA fitness landscapes. Science 330:376–379
Provine WB (1986) Sewall wright and evolutionary biology. University of Chicago Press, Chicago
Reidys C, Stadler PF, Schuster P (1997) Generic properties of combinatory maps. Neutral networks of RNA secondary structure. Bull Math Biol 59:339–397
Reidys CM, Stadler PF (2001) Neutrality in fitness landscapes. Appl Math Comput 117:321–350
Reidys CM, Stadler PF (2002) Combinatorial landscapes. SIAM Rev 44:3–54
Ruse M (1996) Are pictures really necessary? The case of Sewall Wright's 'adaptive lanscapes'. In: Baigrie BS (ed) Picturing knowledge: historical and philosophical problems concerning the use of art in science. University of Toronto Press, Toronto, pp 303–337
Saakian DB, Hu C-K (2006) Exact solution of the Eigen model with general fitness functions and degradation rates. Proc Natl Acad Sci USA 113:4935–4939
Saakian DB, Hu C-K, Khachatryan H (2004) Solvable biological evolution models with general fitness functions and multiple mutations in parallel mutation-selection scheme. Phys Rev E 70: e041908
Sanjuán R, Moya A, Elena SF (2004) The distribution of fitness effects caused by single-nucleotide substitutions in an RNA virus. Proc Natl Acad Sci USA 101:8396–8401
Schmidt LD (2004) The engineering of chemical reactions, 2nd edn. Oxford University Press, New York
Schuster P (2003) Molecular insight into the evolution of phenotypes. In: Crutchfield JP, Schuster P (eds) Evolutionary dynamics—exploring the interplay of accident, selection, neutrality, and function. Oxford University Press, New York, pp 163–215
Schuster P (2006) Prediction of RNA secondary structures: from theory to models and real molecules. Rep Prog Phys 69:1419–1477
Schuster P (2011) Mathematical modeling of evolution. Solved and open problems. Theory Biosci 130:71–89
Schuster P (2012) Evolution on "realistic" fitness landscapes. Phase transitions, strong quasispecies, and neutrality. Working Paper 12-06-006, Santa Fe Institute, Santa Fe, NM
Schuster P (2013) Present day biology seen in the looking glass of physics of complexity. In: Rubio RG, Ryazantsev YS, Starov VM, Huang G, Chetverikov AP, Arena P, Nepomnyashchy AA, Ferrus A, Morozov EG (eds) Without bounds: a scientific canvas of nonlinearity and complex dynamics. Springer, Berlin, pp 589–622
Schuster P, Fontana W, Stadler PF, Hofacker IL (1994) From sequences to shapes and back: a case study in RNA secondary structures. Proc Roy Soc Lond B 255:279–284
Schuster P, Sigmund K (1985) Dynamics of evolutionary optimization. Ber Bunsenges Phys Chem 89:668–682
Schuster P, Swetina J (1988) Stationary mutant distribution and evolutionary optimization. Bull Math Biol 50:635–660
Schwarz G (1968) General theoretical approach to the thermodynamic and kinetic properties of cooperative intramolecular transformations of linear biopolymers. Biopolymers 6:873–897
Seneta E (1981) Non-negative matrices and Markov chains, 2nd edn. Springer, New York
Sherrington D, Kirkpatrick S (1975) Solvable model of spin glasses. Phys Rev Lett 35:1792–1796
Skipper RA Jr (2004) The heuristic role of Sewall Wright's 1932 adaptive landscape diagram. Philos Sci 71:1176–1188
Spiegelman S (1971) An approach to the experimental analysis of precellular evolution. Quart Rev Biophys 4:213–253
Strogatz SH (1994) Nonlinear dynamics and chaos. With applications to physics, biology, chemistry, and engineering. Westview Press at Perseus Books, Cambridge
Swetina J, Schuster P (1982) Self-replication with errors—a model for polynucleotide replication. Biophys Chem 16:329–345
Tarazona P (1992) Error thresholds for molecular quasispecies as phase transitions: from simple landscapes to spin glasses. Phys Rev A 45:6038–6050
Tejero H, Marín A, Moran F (2010) Effect of lethality on the extinction and on the error threshold of quasispecies. J Theor Biol 262:733–741

Thompson CJ, McBride JL (1974) On Eigen's theory of the self-organization of matter and the evolution of biological macromolecules. Math Biosci 21:127–142
Toulouse G (1977) Theory of frustration effect in spin-glasses. I. Commun Phys 2:115–119
Toulouse G (1980) The frustration model. In: Pękalski A, Przystawa JA (eds) Modern trends in the theory of condensed matter, vol 115., Lecture Notes in PhysicsBerlin, Springer, pp 195–203
van Kampen NG (2007) Stochastic processes in physics and chemistry, 3rd edn. Elsevier, Amsterdam
Walsh B, Blows MV (2009) Abundant variation + strong selection = multivariate genetic constraints: a geometric view of adaptation. Annu Rev Ecol Evol Syst 40:41–59
Watson JD, Crick FHC (1953) A structure for deoxyribose nucleic acid. Nature 171:737–738
Weinreich DM (2011) High-throughput identification of genetic interactions in HIV-1. Nat Genet 41:398–400
Wiehe T (1997) Model dependency of error thresholds: the role of fitness functions and contrasts between the finite and infinite sites models. Genet Res Camb 69:127–136
Wilke CO, Wang JL, Ofria C (2001) Evolution of digital organisms at high mutation rates leads to survival of the flattest. Nature 412:331–333
Wright S (1931) Evolution in Mendelian populations. Genetics 16:97–159
Wright S (1932) The roles of mutation, inbreeding, crossbreeding and selection in evolution. In: Jones DF (ed) International proceedings of the sixth international congress on genetics, vol 1. Brooklyn Botanic Garden, Ithaca, NY, pp 356–366
Wright S (1988) Surfaces of selective value revisited. American Naturalist 131:115–123
Zimm BH (1960) Theory of "melting" of the helical form in double chains of the DNA type. J Chem Phys 33:1349–1356
Zuker M (1989) On finding all suboptimal foldings of an RNA molecule. Science 244:48–52

Mathematical Models of Quasi-Species Theory and Exact Results for the Dynamics

David B. Saakian and Chin-Kun Hu

Abstract We formulate the Crow–Kimura, discrete-time Eigen model, and continuous-time Eigen model. These models are interrelated and we established an exact mapping between them. We consider the evolutionary dynamics for the single-peak fitness and symmetric smooth fitness. We applied the quantum mechanical methods to find the exact dynamics of the evolution model with a single-peak fitness. For the smooth symmetric fitness landscape, we map exactly the evolution equations into Hamilton–Jacobi equation (HJE). We apply the method to the Crow–Kimura (parallel) and Eigen models. We get simple formulas to calculate the dynamics of the maximum of distribution and the variance. We review the existing mathematical tools of quasi-species theory.

Contents

1 Introduction 122
2 The Definition of the Models 123
2.1 Eigen Model 123
2.2 The Discrete-Time Eigen Model 124
2.3 Crow–Kimura Model 124
2.4 The Solution of the Models 125
3 Relaxation on a Single-Peak Fitness Landscape 126
4 The Dynamics of Crow–Kimura Model with a Symmetric Fitness Landscape 127
4.1 HJE for the Crow–Kimura Model 128
4.2 The Solution of HJE by the Methods of Characteristics 130
4.3 The Flat Original Distribution 132

D.B. Saakian (✉)
A.I. Alikhanyan National Science Laboratory (Yerevan Physics Institute) Foundation, 2 Alikhanian Brothers St., Yerevan 375036, Armenia
e-mail: saakian@yerphi.am

C.-K. Hu
Institute of Physics, Academia Sinica, Nankang, Taipei 11529, Taiwan
e-mail: huck@phys.sinica.edu.tw

Current Topics in Microbiology and Immunology (2016) 392: 121–139
DOI 10.1007/82_2015_471

Published Online: 06 September 2015

5 The Dynamics of the Eigen Model 133
6 Discussion 135
References 138

1 Introduction

The quasi-species theory assumes an infinite virus population. The investigation of these evolution models (Eigen 1971; Eigen et al. 1989; Crow and Kimura 1970) is one of the fruitful applications of statistical mechanics (Leuthausser 1987; Schuster and Swetina 1982; Tarazona 1992; Woodcock and Higgs 1996; Peliti 1997; Franz and Peliti 1997; Baake et al. 1997; Alves and Fontanari 1998; Baake and Wagner 2001; Baake and Gabriel 2000; Drossel 2001; Hermisson et al. 2002; Saakian and Hu 2004a, b, 2006; Saakian et al. 2004; Saakian et al. 2006, 2008, 2009, 2011; Park and Deem 2006; Saakian 2007, 2008; Saakian and Fontanari 2009; Kirakossyan et al. 2010, 2011; Kirakossyan et al. 2012a, b; Galstyan and Saakian 2012). There is a direct connection of these models to the simple statistical models of spin chains, where the fitness is the analog of the energy (with a minus sign) and mean fitness is an analog of free energy. Another important two features of these models, allowing the application of the statistical physics, are the weakness of nonlinearity [the system of ordinary nonlinear equations is mapped exactly to the system of linear ordinary differential equations plus some nonlinear algebraic transformation (Thompson et al. 1974)], and there is a large number of degrees of freedom.

Continuous-time models with connected mutation–selection scheme (Eigen et al. 1989) and with parallel scheme (Crow and Kimura 1970; Baake et al. 1997) were considered as well as discrete-time models (Peliti 1997). In quasi-species models, one considers the infinite population limit and two evolution forces: selection and mutation. We assume a simple mutation scheme, when different nucleotides in the genome mutate independently. This is a simple, mean field-like process in the terminology of statistical physics, since there is no need for the concept of distance: The nucleotide mutates independently of the neighbors.

The real fitness landscapes based on the distribution of fitness for different genomes are highly complicated with both rugged and neutral features. Usually, one considers a simple version of selection, when fitness depends on a Hamming distance from some reference sequence, and there is a mutation which changes the sequence while keeping the length of genome constant. Such simplifications of fitness landscapes are popular in population genetics. In principle, it is possible to make further generalizations of the model, when the fitness is a function of Hamming distances from d reference sentences (Saakian et al. 2006). In an alternative version, one partitions the whole genome into d pieces, for every piece, we define a reference subsequence, and then, the fitness is modeled as a function of these d Hamming distances. Such fitness again corresponds to the mean fitness-like interaction. As both mutation and selection forces are mean field-like, solving such models exactly should be tractable. Indeed, it is possible to calculate the mean

fitness in the large genome length limit (Hermisson et al. 2002; Saakian et al. 2006; Kirakosyan et al. 2012a, b). It is intriguing that quasi-species models can be solved exactly using both the methods of quantum mechanics and the methods of classical Hamilton mechanics as represented by the Hamilton–Jacobi equation. The calculation of the mean fitness is equivalent to the search for the minimum of potentials in d-dimensional problem of classical mechanics: It is a solvable problem contrary to the exact solution of the motion of d particles. In this section, we show that it is possible to come up with exact dynamical solutions of the Hamilton–Jacobi equations for the models with one-dimensional symmetric fitness landscapes.

We first define different evolution models, review briefly the exact solution of the statics (mean fitness in the steady state), and later focus on the exact solutions of evolutionary dynamics. Here, two situations are considered: the case of single-peak fitness landscape and the case of smooth symmetric fitness landscape. Mapping the evolution model to Hamiltonian mechanics, we calculate exactly the dynamics of the maximum of distribution when the population is originally concentrated at a fixed distance from the reference sequence. The possibility of having analytical solutions, which give the dynamics in a closed form, is an important breakthrough in the theory of biological evolution. It allows the investigation of a plethora of evolutionary pathways within one consistent formalism. While we focus on the solution of the infinite population models, the HJE method could be applied successfully for the solution of finite population problems as well.

2 The Definition of the Models

We consider the simplified case when there are two nucleotides, and thus, genome could be described as a chain of two-value letters; therefore, there are 2^N different genomes for the genome length N (Swetina and Schuster 1982).

2.1 Eigen Model

In the case of Eigen model, we consider (Eigen et al. 1989)

$$\frac{\mathrm{d}P_i}{\mathrm{d}t} = \sum_j Q_{ij} r_j P_j - P_i \left(\sum_j r_j P_j \right), \tag{1}$$

where the matrix element Q_{ji} describes the transition probabilities from the type j to the type i. The elements of mutation matrix are $Q_{ij} = q^{N-d(j,i)}(1-q)^{d(j,i)}$; $d(j, i)$ is the Hamming distance between sequences j and i; q is the probability of errorless replication per nucleotide. The Hamming distance d_{ij} between configurations i and j is the number of point mutations between these configurations. The diagonal terms

of the mutation matrix are $Q_{ii} = q^N \equiv Q \equiv e^{-\gamma}$, where $\gamma = -N\ln(q) \approx N(1-q)$ is the parameter of mutation in the Eigen model and r_i is identified as a fitness of the sequence i. As index i is equivalent to the set of indices $s_1 \ldots s_N$, we can define r_i through the function f_0

$$r_i = f_0(s_1 \ldots s_N), \tag{2}$$

where $s_1 \ldots s_N$ correspond to the sequence i. We choose the 0th sequence with all up spins, $s_l = 1$. Here, P_i satisfy normalization condition $\sum_{i=0}^{M-1} P_i = 1$.

2.2 The Discrete-Time Eigen Model

Consider now the discrete-time Eigen model (Peliti 1997): The probabilities are defined at discrete-time moments n, and thus, we consider $P_i(n)$.

$$P_i(n+1) = \frac{\sum_j Q_{ij}\hat{r}_j P_j(n)}{\sum_j \hat{r}_j P_j(n)} \tag{3}$$

We again can define the lethal mutants as the sequences where $\hat{r}_j = 0$. We used notation $\hat{r}_j$ for the fitness of this model. We will connect them with the corresponding fitness r_j in Crow–Kimura model.

2.3 Crow–Kimura Model

The discrete-time Eigen model could be mapped into the continuous-time Crow–Kimura model (Baake et al. 1997) using the mapping

$$\begin{aligned} P_i(n\tau) &= P_i(n) \\ \gamma &= \tau\mu_0 \\ \hat{r}_i &= \exp(\tau r_i) \end{aligned} \tag{4}$$

where τ is a duration of elementary time step and μ_0 is a mutation rate per unit time period. We get the equations of Baake et al. (1997)

$$\frac{\mathrm{d}P_i}{\mathrm{d}t} = r_i P_i + \sum_j P_j \mu_{ij} - P_i\left(\sum_j r_j P_j\right) \tag{5}$$

μ_{ij} describes the mutation phenomenon: $\mu_{ii} = -\mu_0, \mu_{ij} = 1/N$ when the Hamming distance d_{ij} between two sequences is equal to 1 and $\mu_{ij} = 0$ for other case. There is a balance condition:

$$\sum_j \mu_{ij} = 0 \tag{6}$$

2.4 The Solution of the Models

Both the Crow–Kimura (parallel) and Eigen models are the systems of large number of differential equations, with a large parameter, the genome length N. We have chosen special scaling for the mutation rate and the fitness, to get a limiting solution at $N \to \infty$. To solve the system means to calculate:

1. The mean fitness;
2. The steady-state distribution;
3. The dynamics of the distribution.

The mean fitness of Crow–Kimura model has been calculated in Hermisson et al. (2002) using the algebraic methods, then in Saakian et al. (2004) using quantum statistical mechanics, including the multidimensional fitness landscape case (Saakian and Hu 2004a, 2006; Kirakosyan et al. 2012a), as well as using quantum field theory, first introduced in Saakian et al. (2004) and later applied in Saakian et al. (2006).

For the mean fitness, $R = \sum_i P_i r_i$ has been derived:

$$\begin{aligned} R &= \max[U(m)|_m \\ U(m) &= [f(m) + \mu(\sqrt{1-m^2} - 1)] \end{aligned} \tag{7}$$

where $-1 \le m \le 1$ is similar to magnetization, and it is assumed a symmetric fitness landscape.

For the Eigen model, the following equation has been derived (Saakian and Hu 2006):

$$R = \max[f(m)e^{\gamma(\sqrt{1-m^2}-1)}]|_m \tag{8}$$

The Crow–Kimura model gives the mean fitness of the Eigen model after the mapping:

$$\begin{aligned} R &\to e^R \\ f(m) &\to e^{f(m)} \\ \mu &\to \gamma \end{aligned} \tag{9}$$

The exact steady-state distribution has been calculated in Saakian (2007) and Sato and Kaneko (2007), and the exact dynamics has been calculated first for the single-peak fitness case (Saakian and Hu 2004a, b) later enlarged for the REM fitness (Saakian and Fontanari 2009). Much more powerful was the application of HJE to the dynamics (Saakian et al. 2008).

3 Relaxation on a Single-Peak Fitness Landscape

We follow Saakian and Hu (2004a, b).

The choice of different fitness corresponds to the choice of different functions $r_i = f(S_i)$. This choice of mutation matrix corresponds to the case of point mutations. Following Thompson and McBride (1974), we can drop the nonlinear term in Eq. (5), accompanied with nonlinear transformation

$$P_i \to \frac{P_i}{\sum_n P_n}$$

It has been observed (Baake et al. 1997) that the linear part of the system (5) with $r_i \equiv f(s_1^i \ldots s_N^i)$ evolves according to the Schrödinger equation with imaginary time

$$\frac{\mathrm{d}}{\mathrm{d}t}\sum_i p_i(t)|S\rangle = -H\sum_i p_i(t)|S\rangle \tag{10}$$

and the Hamiltonian:

$$-H = \gamma\sum_{i=1}^{N}(\sigma_i^x - 1) + f(\sigma_1^z \ldots \sigma_N^z) \tag{11}$$

Here, S means the spin configuration of the N spins $s_i = \pm 1$, and σ_x, σ_z are Pauli matrices. If one originally has some distribution of frequencies p_i^0, then after period of time t, the new distribution should be as follows:

$$\begin{aligned} p_j(t) &= \frac{\sum_i p_i^0 \langle S_j | e^{-Ht} | S_i \rangle}{Z} \\ Z &= \sum_{ij} p_i(0) Z_{ij}, Z_{ij} = \langle S_j | e^{-Ht} | S_i \rangle \end{aligned} \tag{12}$$

For the single-peak landscape case, we choose

$$\begin{aligned} f(S_1) &= J_0 N, S_1 \equiv +, +\ldots+, \\ f(S_i) &= 0, S_i \neq S_1. \end{aligned} \tag{13}$$

Let us briefly present the results of our work (Saakian and Hu 2004a) on the relaxation in a single-peak fitness landscape (13):

There are transverse terms (proportional to σ^x) and longitudinal terms (function of σ^z), as well as diagonal terms (constant terms) in the Hamiltonian. While calculating matrix elements of the evolution operator $\langle S_i|e^{-tH}|S_j\rangle$, one can miss either transverse or longitudinal terms. This is an exact result at the thermodynamical limit. Let us consider an evolution from some original configuration S_i, having an overlap Nm with the peak configuration: $\langle S_i|S_j\rangle = \sum_{k=1}^{N} S_i^k S_j^K = Nm$. First, there is a random diffusion phase till the moment t_0. After it, when $t > t_0$, one has

$$\begin{aligned}\langle S_j|\exp[-Ht]|S_i\rangle &\approx \langle S_j|\exp[-H_{\text{diff}}t]|S_i\rangle \\ &= \cosh(\beta)^{N(1+m)/2}\sinh(\beta)^{N(1-m)/2}\end{aligned} \tag{14}$$

where H_{diff} is our Hamiltonian with zero fitness. Equation (14) is a simple result of quantum mechanics.

For the peak configuration,

$$\langle S_1|\exp[-Ht]|S_i\rangle = \langle S_1|e^{-H_{\text{int}}(t-t_0)}|S_1\rangle\langle S_1|\exp[-H_{\text{diff}}t]|S_i\rangle, \tag{15}$$

where in $H_{\text{int}} = (J_0 - \gamma)|S_1\rangle\langle S_1|$, we missed the longitudinal part of Hamiltonian.

When the partition function of the peak configuration $\langle S_1|e^{-Ht}|S_i\rangle$ is becoming larger than the sum of partitions by other configurations $\sum_{j\neq 1}\langle S_i|e^{-Ht}|S_j\rangle$, the system relaxes to the steady-state configuration. One has an equation for the time t_0

$$\tanh[\gamma t_0] = \frac{1 - m_0}{k + \sqrt{k^2 - 1 + m_0^2}} \tag{16}$$

where $k = J_0/\gamma$. For the relaxation period t_1, we derive

$$t_1(J_0, \gamma, m) = \frac{[J_0 t_0 - \frac{1+m}{2}\ln\cosh(\gamma t_0) - \frac{1-m}{2}\ln\sinh(\gamma t_0)]}{J_0 - \gamma}. \tag{17}$$

4 The Dynamics of Crow–Kimura Model with a Symmetric Fitness Landscape

We follow Saakian et al. (2008). For the symmetric fitness function and permutation-invariant original distribution, one has a set of differential equations for the $N + 1$ relative probabilities $p_l, 0 \leq l \leq N$ (see Baake and Wagner 2001):

$$\frac{\mathrm{d}p_l}{\mathrm{d}t} = p_l\left[Nf\left(1-\frac{2l}{N}\right)-N\right] + (N-l+1)p_{l-1} + (l+1)p_{l+1}, \tag{18}$$

The probability of all configurations being at the Hamming distance l is $p_l/\sum_k p_k$ [this mapping of the system of nonlinear Eq. (5) to the system of linear Eq. (18) has been derived previously (Woodcock and Higgs 1996; Baake and Wagner 2001)]. In Eq. (18), we omit p_{-1} and p_{N+1} for $l = 0$ and $l = N$ and set $\gamma_0 = 1$.

In biological applications, a magnetization-like measure "surplus" or "surface magnetization" is considered, which is defined as follows:

$$x_m = \frac{\sum_l (1-2l/N)p_l}{\sum p_l} \tag{19}$$

The main goal of this work is to calculate the dynamics of x_m for the given initial distribution.

Having the value of x_c at the maximum point of Eq. (7), one can calculate x_m of the steady state from the equation (Baake and Wagner 2001)

$$f(x_m) = k \tag{20}$$

The different meanings of "bulk" magnetization x_c and "surface" magnetization x_m were analyzed thoroughly in Baake and Wagner (2001). We will solve the dynamics and determine the explicit role of x_c while considering different subphases in dynamics.

4.1 HJE for the Crow–Kimura Model

Following Saakian (2007), at a discrete $x = 1 - 2l/N$ we use the ansatz: $p_l(t) = \exp[Nu(x,t)], p_{l+1}(t) = \exp[Nu(x,t) - 2u'_x]$. Equation (18) can be written as a Hamilton–Jacobi equation for $u \equiv \ln p(x,t)/N$ [in Saakian (2007), we gave an equation for the sequence probabilities]

$$\frac{\partial u}{\partial t} + H(u', x) = 0, \tag{21}$$

where $u' = \partial u/\partial x$,

$$-H(u', x) = f(x) - 1 + \frac{1+x}{2}e^{2u'} + \frac{1-x}{2}e^{-2u'}, \tag{22}$$

the domain of x is $-1 \leq x \leq 1$ and the initial distribution is $u(x,0) = u_0(x)$. Equation (21) is for the class probabilities, while in Saakian (2007), we gave an equation for the sequence probabilities. Equation (21) has an asymptotic solution

$$u(x,t;k) = kt + u_k(x) \tag{23}$$

as $t \to \infty$ where $u_k(x)$ can be calculated from Eq. (21) (Saakian 2007) and $N \cdot k$ is the mean fitness. The function $U(x)$ from Eq. (7) has a simple physical interpretation: It is the potential (the minimum of $-H(u,v)$ in v at fixed x): $U(x) = \min_v[-H(v,x)]$. In mechanics, the motion is possible in the whole interval, when the energy is larger than the potential $U(x)$ inside the interval. In the maximum principle approach, the maximal eigenvalue is identified with the mean fitness k. Similarly, $-k$ is the maximal energy of the Hamiltonian $H(v,x)$ in Eq. (22). A very realistic hypothesis is that the asymptotic solution $u(x,t;k)$ is stable with respect to small perturbations only if k is calculated according to Eq. (7).

We can get more results, without solving the dynamics exactly: We know from physics that the motion in the potential with a single minimum is drastically different from the motion in the potential with two minima. Therefore, when $U(x)$ changes from a continuous line in Fig. 1 to the dashed line with two minima near $x = 0$ and two maxima, we can expect a phase transition in the dynamics.

Here, we focus on the fitness $f(x) = cx^2/2$ (solid curve in Fig. 1, $c = 2$). It results from Eq. (7) that in this case, $U(x)$ has two extrema located in $[-1;+1]$: the minimum at $x = 0$ and the maximum at $x = x_m$.

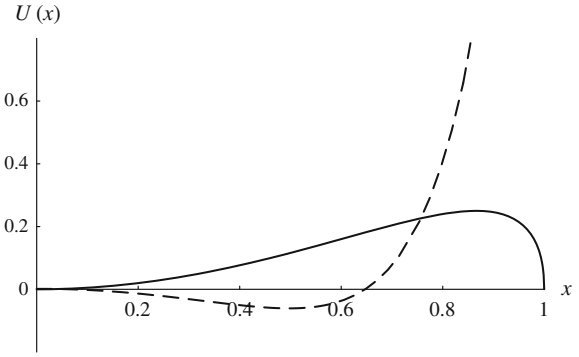

Fig. 1 Function $U(x) = f(x) + \sqrt{1-x^2} - 1$ for $f(x) = x^2$ (*solid curve*) and for $f(x) = 4\exp(-8+8x)$ (*dashed curve*). For the latter, there are two extrema where $U'(x) = 0$: the maximum at 0.9995 (it is too high and is not shown in the graphics) and the minimum at 0.497.

4.2 The Solution of HJE by the Methods of Characteristics

To solve Eq. (21) subject to initial data, we use a standard procedure, e.g., Melikyan (1998), allowing to reduce the partial differential equation to a system of ordinary differential equations. Namely, consider the equations

$$\begin{aligned}\dot{x} &= H_v(x,v) = -(1+x)^{2v} + (1-x)^{-2v},\\ \dot{v} &= -H_x(x,v) = f'(x) + (e^{2v} - e^{-2v})/2,\\ \dot{u} &= vH_v(x,v) - H(x,v) = v\dot{x} + q,\end{aligned} \tag{24}$$

subject to initial conditions: $x(0) = x_0, v(0) = v_0(x_0), u(0) = u_0(x_0)$. Here, $v := \partial u/\partial x, v_0(x) := u_0'(x), q := \partial u/\partial t$. The respective solution to Eq. (24) in $(x,\ t)$ space is called the *characteristic* of Eq. (21). Further, Eqs. (21) and (24) result in $\dot{q} = 0$. Along the characteristic $x = x(t)$, the variable q is constant, so q is selected to parameterize these curves. Using the equation $q = f(x) - 1 + (1+x)/2e^{2v} + (1-x)/2e^{-2v}$, we transform the first equation in (24) into

$$\dot{x} = \pm 2\sqrt{[q+1-f(x)]^2 + x^2 - 1}. \tag{25}$$

Having the solution of the characteristic system, Eq. (24), we can derive the solution of the original Eq. (21) (Melikyan 1998) by integrating the equation $\dot{u} = v\dot{x} + q$. In biology applications, it is important to know motions of the distributions maxima. Consider the following initial distribution:

$$u_0(x) = -a(x - x_0)^2. \tag{26}$$

It is easy to derive the relaxation formulas for the large value of parameter a. We can calculate it directly from Eq. (25), using the equation $q(x^*, t^*) = f(x^*)$ for the maximum point location x^*. The maximum of distribution moves along a branch of Eq. (25) that preserves the sign of x_0. Integrating Eq. (25) along the characteristic through the point (x^*, t^*) and assuming that $\dot{x}(t)$ does not change its sign, we get

$$t^* = \frac{1}{2}\int_{x^*}^{x_0} \frac{\mathrm{d}\xi}{\sqrt{(f(x^*)+1-f(\xi))^2 + \xi^2 - 1}}. \tag{27}$$

If at some point x_1 the characteristic $x(t)$ changes its direction, the x_1 can be determined from the condition

$$[f(x^*) + 1 - f(x_1)]^2 + x_1^2 - 1 = 0. \tag{28}$$

In this case, the integrals should be summed up over the intervals (x_0, x_1) and (x^*, x_1). The summation gives

$$t^* = \frac{1}{2}\left(\int_{x_0}^{x_1} \frac{\mathrm{d}\xi}{\sqrt{(f(x^*)+1-f(\xi))^2+\xi^2-1}} + \int_{x^*}^{x_1} \frac{\mathrm{d}\xi}{\sqrt{(f(x^*)+1-f(\xi))^2+\xi^2-1}}\right). \tag{29}$$

Let T_1 be such that for $t \le T_1$, Eq. (27) holds, and for $t > T_1$, Eq. (29) holds. At T_1, we have the condition

$$T_1 = \frac{1}{2}\int_{X_1}^{x_0} \frac{d\xi}{\sqrt{(f(X_1)+1-f(\xi))^2+\xi^2-1}}, \tag{30}$$

where X_1 is a root of $[f(X_1)+1-f(x_0)]^2 + x_0^2 - 1 = 0$.

For the quadratic fitness $f(x) = cx^2/2, c > 0$, the selective phase exists at $c > 1$, and then, $x_m = 1 - \frac{1}{c}$ and $x_c = \sqrt{1-c^{-2}}$. When $t \to \infty$, the maximum converges to $x = x_m$. To define the dynamics of the maximum at $-x_c \le x_0 \le x_c$, we use Eqs. (27) and (29), where

$$x_1 = x_0 \frac{\sqrt{c^2x^{*2} + 2(c-1) - 2[(c-1)^2 - c^2x^{*2}]^{1/2}}}{c}.$$

In the interval where $x_c \le |x_0| \le 1$, we use Eq. (27) and to find T_1 in accordance with Eq. (30). We use

$$X_1 = \sqrt{x_0^2 - \frac{2[1-(1-x_0^2)^{1/2}]}{c}}. \tag{31}$$

Figure 2 shows the evolution of the maximum for $c = 2$ and several values of x_0 ($x_0 = 0, 0.1, 0.3, 0.7, 0.95$). It demonstrates the excellent agreement of analytic solutions given by Eqs. (27) and (29) with the results of numerical integration of Eq. (5). Note that Fig. 2 shows that for $x_0 < x_m$, the maximum of the distribution initially moves away from the wild configuration and returns to its neighborhood later on. The minimal $x^*(t)$ is just X_1.

If $x^*(t)$ describes the position of maximum points, then $v(x^*(t), t) = \frac{dv(x^*(t),t)}{dt} = 0$ and Eq. (28) gives

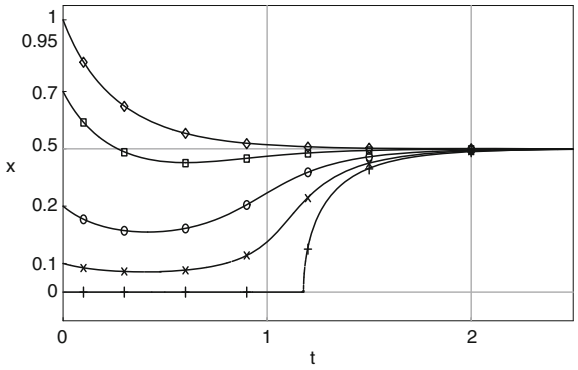

Fig. 2 The dynamics of the maximum point $x(t)$ for the Crow–Kimura model ($f(x) = x^2$) for different initial values x_0 in the distribution (26). The continuous curves are analytic results of Eqs. (27) and (29). The symbols are the results of numerical solutions of the Crow–Kimura model, where $N = 1000$. © with APS, 2008

$$\frac{dx^*(t)}{dt} = -2x^*(t) - \frac{f'(x^*(t))}{u_{xx}(x^*(t),t)}, \quad x(0) = x_0, \tag{32}$$

with $u_{xx}(x,t) = \partial v/\partial x$. The movement of the maximum of distribution either to the wild sequence or to the opposite side depends on the sign of $f'(x^*(t)) + 2x^*(t)u''(x^*(t),t)$.

4.3 The Flat Original Distribution

When any of 2^N configurations are uniformly populated, the initial condition for the class probability $\left(\frac{N!}{(N(1+x)/2)!}\right)\frac{1}{2^N}$ yields

$$u_0(x) = -\frac{1+x}{2}\ln\frac{1+x}{2} - \frac{1-x}{2}\ln\frac{1-x}{2}. \tag{33}$$

It has a peak at $x = 0$.

Let us calculate the threshold time T_2 such that for $t \le T_2$, the population's peak is in the class with $x = 0$. Assume that at the moment t^*, the maximum is at the point x^*. We consider Eq. (25) for the characteristics with the end point (x^*, t^*), thus taking $q = f(x^*)$.

The related characteristic curve starts at the point $x(0) = x^*$, passes through the point $(x_1, t^*/2)$ [x_1 is computed from Eq. (28)], turns, and finally reaches the point $(x*, t*)$. Thus, Eq. (28) gives

$$t^* = \int_{x^*}^{x_1} \frac{\mathrm{d}\xi}{\sqrt{(f(x^*) + 1 - f(\xi))^2 + \xi^2 - 1}}. \tag{34}$$

We proceed to the limit as $x^* \to 0$ and find the threshold time T_2. When $f(x) = cx^2/2$, $c > 1$, this time is

$$T_2 = \cos^{-1}(\sqrt{1 - 1/c})/\sqrt{c - 1}. \tag{35}$$

5 The Dynamics of the Eigen Model

We follow the treatment of the Eigen model by Saakian et al. (2008). We consider the symmetric distribution of $p_i = P_l$, where $l = d(i, 0)$ is the Hamming distance (HD) of the ith sequence from the master sequence, so that all sequences with the same HD from the master sequence have the same $p_i = P_l$. From such a sequence, one can generate a sequence S_j with HD n from S_i through n_1 up and n_2 down mutations and $n = n_1 - n_2$. The total number of such mutations is

$$\frac{l!}{n_1!(l - n_1)!}\frac{(L - l)!}{n_2!(L - l - n_2)!}. \tag{36}$$

Then, we derive the following equation for P_l:

$$\frac{\mathrm{d}P_l}{\mathrm{d}t} = \sum_{n_1=0}^{l}\sum_{n_2=0}^{L-l} \frac{l!}{n_1!(l - n_1)!}\frac{(L - l)!}{n_2!(L - l - n_2)!} Q_{n_1+n_2} P_{l-n} r_{l-n}, \tag{37}$$

where $n_1 - n_2 = n$.

We assume the following ansatz for the P_l

$$P_l = \exp[Lu(m, t)], \tag{38}$$

where $m = 1 - 2l/L$. Then, with $1/L$ accuracy, we replace in Eq. (36):

$$P_{l-n} \to P_l \exp[-2nu'(m)], r_{l-n} \to r_l \tag{39}$$

Then, using the formulas,

$$\begin{aligned} \frac{l!}{(l - n_1)!} \approx l^{n_1} &= \left(L\frac{1 - m}{2}\right)^{n_1} \\ \frac{(L - l)!}{(L - l - n_2)!} \approx (L - l)^{n_2} &= \left(L\frac{1 + m}{2}\right)^{n_2} \end{aligned} \tag{40}$$

we obtain

$$\frac{\mathrm{d}P_l}{\mathrm{d}t} = \sum_{n_1=0}^{l} \sum_{n_2=0}^{N-l} \frac{l^{n_1}}{n_1!} \frac{(L-l)^{n_2}}{n_2!} \bar{Q} \left(\frac{\gamma}{L}\right)^{(n_1+n_2)} e^{2(n_1-n_2)u'} P_l r_l \tag{41}$$

We consider the case $l \gg 1, N-l \gg 1$. Then, using an equality,

$$\sum_{n_1=0}^{\infty} \frac{a^{n_1}}{n_1!} \frac{b^{n_2}}{n_2!} = \sum_{n=0}^{\infty} \frac{(a+b)^n}{n!} \tag{42}$$

we obtain (Saakian et al. 2008; Kirakosyan et al. 2012b)

$$\frac{\partial u}{\partial t} = f(x) e^{\gamma[\mathrm{ch}(2u')+x\mathrm{sh}(2u')-1]}, \tag{43}$$

where $\tau = tN$. The asymptotic solutions $u(x,t;k) = kt + u_k(x)$ [k is a mean fitness (Saakian et al. 2006)] at $t \to \infty$ are

$$k = \max_{-1 \le x \le 1} U(x), \quad U(x) = f(x) \exp(\gamma[-1 + \sqrt{1-x^2}]), \tag{44}$$

where x_c and x_m are obtained from

$$U'(x_c) = 0, \quad f(x_m) = f(x_c) \exp(-\gamma[1 - \sqrt{1-x_c^2}]). \tag{45}$$

When $x_c < |x_0| < 1$, for the initial distribution given by Eq. (26) with $a \gg 1$, the position of the maximum $(t*, x*)$ is

$$t^* = 2 \int_{x^*}^{x_0} \frac{\mathrm{d}\xi}{f(x) \sqrt{\left(\ln \frac{f(x)}{f(\xi)} + \gamma\right)^2 - \gamma^2(1-\xi^2)}}. \tag{46}$$

Alternatively, the solution is

$$t^* = \frac{1}{2} \left(\int_{x_0}^{x_1} \frac{\mathrm{d}\xi}{f(x^*) \sqrt{\left(\ln \frac{f(x^*)}{f(\xi)} + \gamma\right)^2 - \gamma^2(1-\xi^2)}} + \int_{x^*}^{x_1} \frac{\mathrm{d}\xi}{f(x^*) \sqrt{\left(\ln \frac{f(x^*)}{f(\xi)} + \gamma\right)^2 - \gamma^2(1-\xi^2)}} \right), \tag{47}$$

where x_1 can be calculated from the condition:

$$\left(\ln\frac{f(x^*)}{f(x_1)}+\gamma\right)^2-\gamma^2(1-x_1^2)=0. \tag{48}$$

For the relaxation from the flat distribution, we get

$$t^*=\int_{x^*}^{x_1}\frac{\mathrm{d}\xi}{f(x^*)\sqrt{\left(\ln\frac{f(x^*)}{f(\xi)}+\gamma\right)^2-\gamma^2(1-\xi^2)}}, \tag{49}$$

6 Discussion

We defined different versions of quasi-species models and established the connection between them. The discrete-time Eigen model is equivalent to Crow–Kimura (parallel) model, and there is a connection between Eigen and Crow–Kimura models in the statics: The Eigen model with exponential fitness landscape has the same steady state as the Crow–Kimura model. Nevertheless, their dynamics is different. We investigated the dynamics of evolution models. First, we derived exact dynamics for the Crow–Kimura model with single-peak fitness (Saakian and Hu 2004a, b; Neves 2010; Anclif and Park 2010).

Later we derived an exact dynamics for the Crow–Kimura and Eigen models in the case of general 1D symmetric fitness landscape (Saakian et al. 2008). We considered the discrete error classes in a continuum approximation, replacing the system of equation of the molecular evolution model by a single partial nonlinear differential equation, the Hamilton–Jacobi equation and solve the latter to get the dynamics of our model. The method, used to derive Eq. (25), is qualitatively similar to the quasi-classical method in quantum mechanics. Equations (24) and (25) give an exact solution $u(x, t)$ of our HJE for the Crow–Kimura model and Eqs. (46)–(48) for the Eigen model. Our approach has an accuracy $1/N$, N is the genome length, and such accuracy is well confirmed by numerics. The evolution dynamics is a highly nontrivial phenomenon, and even for monotonic and smooth landscapes, it is possible to have (as we proved) discontinuous dynamics [like the punctuated evolution (Drossel 2001) or shock waves]. In our article, an analytical method is suggested to calculate the population distribution dynamics for the general fitness case. In Wagner et al. (1998), an analytic approximation (accurate for large c) has been suggested for the dynamics of Crow–Kimura model. We found discontinuous transitions even for smooth fitness landscapes as shown in Fig. 3. The transition points have been calculated in Saakian et al. (2014).

We considered HJE for the exact results in dynamics and Hamiltonian mechanics for the qualitative analysis of evolution models. Our results are valid for any analytic fitness function. The diffusion method described in the references

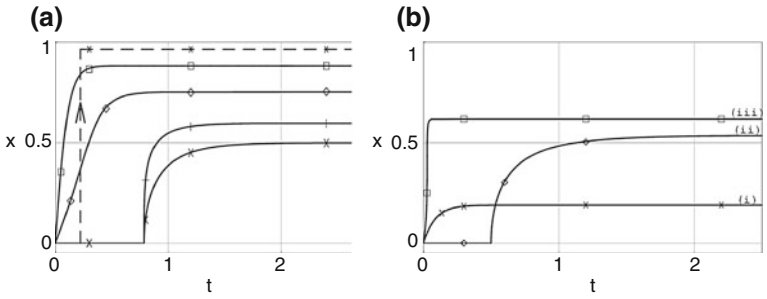

Fig. 3 The dynamics of maximum density points $x^*(t^*)$ for the flat initial distribution given by Eq. (33). **a** Crow–Kimura model where (i) $f(x) = 8x$, (ii) $f(x) = x^2$, (iii) $f(x) = x^2 + 0.2x^4$, (iv) $f(x) = 4\exp(x-1)$, and $f(x) = 4\exp(-8[1-x])$ (*dashed line*). **b** Eigen model where $\gamma = 2$ and (i) $f(x) = 2(x+1)$, (ii) $f_2(x) = x^2$, and (iii) $f(x) = \exp(4x)$. Continuous curves are the analytical results. The symbols are the solutions of numerical integration. © with APS, 2008

(Tsimring et al. 1996; Bagnoli and Bezzi 1997; Gerland and Hwa 2002; Peng et al. 2003) is valid only near the maximum of the distribution or with weak selection and yields inaccurate results when applied for long relaxation periods or for calculating mean fitness. The method yields an error greater than 50 % after $t = 0.2$ (see Sect. 4). The HJE approach is self-consistent, does not use the genome length (contrary to Tsimring et al. 1996; Bagnoli and Bezzi 1997; Gerland and Hwa 2002; Peng et al. 2003), and calculates the dynamics with an accuracy of $\sim 1/N$ (Figs. 4, 5).

We applied HJE for the exact solution of the evolution models which can be mapped into the system of linear equations. In Avetisyan and Saakian (2010), we solved exactly the dynamics of the recombination model with selection and with a single-peak fitness landscape.

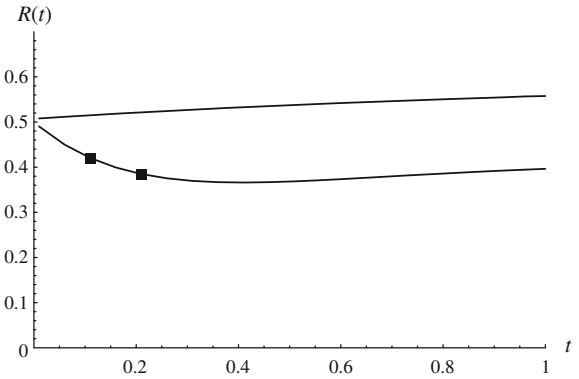

Fig. 4 The dynamics of the mean fitness $R(t)$ for the Crow–Kimura model ($f(x) = x$) for different initial values $x_0 = 0.5$ in the distribution (26). The symbols are the results of numerical solutions of the Crow–Kimura model given by Eq. (18), where $N = 1000$. The upper line is an approximate result by diffusion method, and the lower line is our exact result. © with APS, 2008

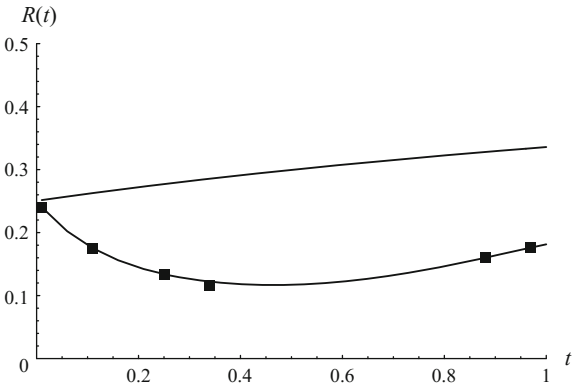

Fig. 5 The dynamics of the mean fitness $R(t)$ for the Crow–Kimura model ($f(x) = x^2$) for different initial values $x_0 = 0.5$ in the distribution (26). The symbols are the results of numerical solutions of the Crow–Kimura model given by Eq. (18), where $N = 1000$. The *upper line* is an approximate result by diffusion method, and the *lower line* is our exact result. © with APS, 2008

The HJE has been investigated first in Rouzin et al. (2003) (an approximate version of the linear fitness case) and later in Sato and Kaneko (2007), published independently of Saakian et al. (2008). Our results for the dynamics have been re-derived using the quantum field theoretical approach in Anclif and Park (2012).

Let us compare different mathematical methods in evolution research:

A. The maximum principle method of Baake and Wagner (2001) is especially useful in the case of four-value spins (it is easier to apply than the Suzuki–Trotter method) and in the case of the Eigen model (Suzuki–Trotter method could not be applied in a simple way). It is difficult to apply for the case of multipeak fitness landscapes or for the finite genome size corrections. I do not see any way to obtain exact results for this case.
B. The Suzuki–Trotter approach applied in references (Saakian and Hu 2004a, b; Saakian et al. 2004) is the simplest method in the case of two-value spins. It is the best to solve the case of multipeak fitness.
C. The high-temperature expansion method (Saakian and Hu 2006) works for the case of Eigen model, and the first exact solution of Eigen model has been derived by means of this method. The method could be applied for the case of multipeak fitness to give the mean fitness.
D. The functional integral method (Saakian et al. 2006; Park and Deem 2006) gives the solution of the Eigen model for the multipeak fitness case including the finite genome length corrections. It is especially useful for the case of disorder.
E. The exact dynamics method for the single-peak fitness is due to Saakian and Hu (2004a). It could be generalized for the case of the hierarchic random energy model like fitness landscapes, as well as for the nonlinear (diploid-like) evolution.

F. The Hamilton–Jacobi equation (HJE) method is especially efficient in the case of two-value spins. It gives finite genome size corrections to the mean fitness, exact steady state, variance as well as the dynamics for both Crow–Kimura and Eigen models. The HJE method could be applied for the genome growth model (Saakian 2008) and for several chains of equations (Galstyan and Saakian 2012). It gives the solution also for the evolution model with truncated selection (Saakian et al. 2009).

To be short, the most powerful and the simplest method is the HJE, the next one by efficiency is the method of Park and Deem (2006), while the latter is much more involved one. The maximum principle is also useful to calculate the mean fitness.

References

Alves D, Fontanari JF (1998) Error threshold in finite populations. Phys Rev E 57:7008
Ancliff M, Park JM (2012) Dynamics of quasi-species models with a complex spin coherent state representation. J Korean Phys Soc 61:1898
Ancliff M, Park JM (2010) Optimal mutation rates in dynamic environments: the Eigen model. Phys Rev E 82:021904
Avetisyan Zh, Saakian DB (2010) Recombination in one and two dimensional fitness landscapes. Phys Rev E 81:051916
Baake E, Baake M, Wagner H (1997) Ising quantum chain is equivalent a model of biological evolution. Phys Rev Lett 78:559
Baake E, Gabriel W (2000) Biological evolution through mutation, selection, and drift: an introductory review. In: Stauffer D (ed) Annual review of computational physics, vol VII. World Scientific, Singapore, pp 203–264
Baake E, Wagner H (2001) Mutation-selection models solved exactly with methods of statistical mechanics. Genet Res 78:93
Bagnoli F, Bezzi M (1997) Speciation as pattern formation by competition in a smooth fitness landscape. Phys Rev Lett 79:3302
Crow JF, Kimura M (1970) An introduction to population genetics theory. Harper Row, New York
Drossel B (2001) Biological evolution and statistical physics. Adv Phys 50:209
Eigen M (1971) Selforganization of matter and the evolution of biological macromolecules. Naturwissenschaften 58:465
Eigen M, McCaskill JS, Schuster P (1989) The molecular quasispecies. Adv Chem Phys 75:149
Franz S, Peliti L (1997) Error threshold in simple landscapes. J Phys A 30:4481
Galstyan V, Saakian DB (2012) Dynamics of the chemical master equation, a strip of chains of equations in d-dimensional space. Phys Rev E 86:011125
Gerland U, Hwa T (2002) On the selection and evolution of regulatory binding motifs. J Mol Evol 55:386
Hermisson J, Redner O, Wagner H, Baake E (2002) Mutation–selection balance: ancestry, load, and maximum principle. Theor Popul Biol 62:9
Kirakosyan Z, Saakian DB, Hu C-K (2010) Evolution models with lethal mutations on symmetric or random fitness landscapes. Phys Rev E 82:011904
Kirakosyan Z, Saakian DB, Hu C-K (2011) Finite genome length corrections for the mean fitness and gene probabilities in evolution models, vol 144, p 149
Kirakosyan Z, Saakian D, Hu C-K (2012a) Biological evolution in a multidimensional fitness landscape. Phys Rev E 86:031920

Kirakosyan Z, Saakian DB, Hu C-K (2012b) Eigen model with correlated multiple mutations and solution of error catastrophe paradox in the origin of life. J Phys soc Jpn 81:114801
Leuthausser I (1987) Statistical mechanics of Eigen's model. J Stat Phys 48:343
Melikyan A (1998) Generalized characteristics of first order PDEs. Birkhauser, Boston
Neves AGM (2010) Detailed analysis of an Eigen quasispecies model in a periodically moving sharp-peak landscape. Phys Rev E 82:031915
Park J-M, Deem MW (2006) Schwinger Boson formulation and solution of the Crow-Kimura and Eigen models of quasispecies theory. J Stat Phys 125:975–1015
Peliti L (1997) Introduction to the statistical theory of Darwinian evolution, cond-mat/9712027
Peng W, Gerland U, Hwa T, Levine H (2003) Dynamics of competitive evolution on a smooth landscape. Phys Rev Lett 90:088103
Rouzine IM, Wakeley J, Coffin JM (2003) The solitary wave of asexual evolution. Proc Natl Acad Sci USA 100:587
Saakian DB (2007) A new method for the solution of models of biological evolution: derivation of exact steady-state distributions. J Stat Phys 128:781
Saakian DB (2008) Evolution models with base substitutions, insertions, deletions and selection. Phys Rev E 78:061920
Saakian DB, Biebricher C, Hu C-K (2011) Lethal mutants and truncated selection together solve a paradox of the origin of life. Plos one 6:e21904
Saakian DB, Biebricher CK, Hu C-K (2009) Phase diagram for the Eigen quasispecies theory with the truncated fitness landscape. Phys Rev E 79:041905
Saakian DB, Fontanari JF (2009) Fontanari, evolutionary dynamics on rugged fitness landscapes: exact dynamics and information theoretical aspects. Phys Rev E 80:041903
Saakian DB, Gazaryan M, Hu C-K (2014) The shock waves and positive epistasis in evolution. Phys Rev E 90:022712
Saakian DB, Hu C-K (2004a) Eigen model as a quantum spin chain: exact dynamics. Phys Rev E 69:021913
Saakian DB, Hu C-K (2004b) Solvable biological evolution model with a parallel mutation-selection scheme. Phys Rev E 69:046121
Saakian DB, Hu C-K (2006) Exact solution of the Eigen model with general fitness functions and degradation rates. Proc Natl Acad Sci USA 103:4935
Saakian DB, Munoz E, Hu C-K, Deem MW (2006) Quasispecies theory for multiple-peak fitness landscapes. Phys Rev E 73:041913
Saakian DB, Hu C-K, Khachatryan H (2004) Solvable biological evolution models with general fitness functions and multiple mutations in parallel mutation-selection scheme. Phys Rev E 70:041908
Saakian DB, Rozanova O, Akmetzhanov A (2008) Exactly solvable dynamics of the Eigen and the Crow-Kimura model. Phys Rev E 78:041908
Sato K, Kaneko K (2007) Evolution equation of phenotype distribution: general formulation and application to error catastrophe. Phys Rev E 75:061909
Swetina J, Schuster P (1982) Self-replication with errors. A model for polynucleotide replication. Biophys Chem 16:329
Tarazona P (1992) Error threshold for molecular quasispecies as phase transitions: from simple landscapes to spin-glass models. Phys Rev A 45:6038
Thompson CJ, McBride JL (1974) On Eigen's theory of the self-organization of matter and the evolution of biological macromolecules. Math Biosci 21:127
Tsimring LS, Levine H, Kessler DA (1996) RNA virus evolution via a fitness-space model. Phys Rev Lett 76:4440
Wagner H, Baake E, Gerisch T (1998) J Stat Phys 92:1017
Woodcock H, Higgs PG (1996) Population evolution on a multiplicative single-peak fitness landscape. J Theor Biol 179:61

Theoretical Models of Generalized Quasispecies

Nathaniel Wagner, Yoav Atsmon-Raz and Gonen Ashkenasy

Abstract Theoretical modeling of quasispecies has progressed in several directions. In this chapter, we review the works of Emmanuel Tannenbaum, who, together with Eugene Shakhnovich at Harvard University and later with colleagues and students at Ben-Gurion University in Beersheva, implemented one of the more useful approaches, by progressively setting up various formulations for the quasispecies model and solving them analytically. Our review will focus on these papers that have explored new models, assumed the relevant mathematical approximations, and proceeded to analytically solve for the steady-state solutions and run stochastic simulations. When applicable, these models were related to real-life problems and situations, including changing environments, presence of chemical mutagens, evolution of cancer and tumor cells, mutations in *Escherichia coli*, stem cells, chromosomal instability (CIN), propagation of antibiotic drug resistance, dynamics of bacteria with plasmids, DNA proofreading mechanisms, and more.

Contents

References 157

This short review focuses on papers published by Tannenbaum and Shaknovich (2005) and beginning with the review. Many of these works have explored various extensions of semiconservative replication, while others have looked at genetic repair, dynamic landscapes, horizontal gene transfer (HGT), antibiotic drug resis-

In memory of Prof. Emmanuel David Tannenbaum (1978–2012).

N. Wagner · Y. Atsmon-Raz · G. Ashkenasy (✉)
Department of Chemistry, Ben-Gurion University of the Negev, Beer Sheva 84105, Israel
e-mail: gonenash@bgu.ac.il

Current Topics in Microbiology and Immunology (2016) 392: 141–159
DOI 10.1007/82_2015_456

Published Online: 16 September 2015

tance, repression, and derepression of plasmids within prokaryotes, sporulation, and chromosomal instability (CIN). Using a new approach, quasispecies theory was also applied to molecular catalytic networks. An additional series of papers has dealt with the evolution and selective advantages of sexual reproduction. As quasispecies theory may be viewed as a prototype model for all evolutionary dynamics in biological systems, other evolutionary themes have also been explored and mathematically solved, including those associated with division of labor, "junk" DNA and RNA networks, metabolism, associative learning, and cognition.

Briefly, Tannenbaum and Shakhnovich (2005) reviewed the recent advances at that time, primarily based on Tannenbaum et al. (2003, 2004a, b, 2005), Tannenbaum and Shakhnovich (2004a, b), and Brumer and Shakhnovich (2004a, 2005). The review begins with a basic overview of quasispecies theory and the derivation of the quasispecies equations:

$$\frac{\mathrm{d}x_\sigma}{\mathrm{d}t} = \sum_{\sigma'} \kappa_{\sigma'} p_\mathrm{m}(\sigma', \sigma) x_{\sigma'} - \bar{\kappa}(t) x_\sigma$$

where x_σ is the population fraction of a given genome σ, p_m (σ', σ) denotes the probability that genome σ' produces genome σ after replication, κ_σ is the fitness, i.e., the first-order growth rate constant of genome σ, and $\bar{\kappa}(t)$ is the time-dependent mean fitness of the population. It is then shown how steady-state analytical solutions may be found in the case of a single-fitness peak landscape in the limit of infinite sequence length, assuming negligible back mutations. Afterward, the semiconservative replication model is described and compared with conservative replication. The quasispecies equations for semiconservative replication are given by:

$$\begin{aligned}\frac{\mathrm{d}x_{\{\sigma,\bar{\sigma}\}}}{\mathrm{d}t} = &-\left(\kappa_{\{\sigma,\bar{\sigma}\}} + \bar{\kappa}(t)\right) x_{\{\sigma,\bar{\sigma}\}} \\ &+ \sum_{\{\sigma',\bar{\sigma}'\}} \kappa_{\{\sigma',\bar{\sigma}'\}} x_{\{\sigma',\bar{\sigma}'\}} \left[p(\sigma', \{\sigma,\bar{\sigma}\}) + p(\bar{\sigma}', \{\sigma,\bar{\sigma}\})\right]\end{aligned}$$

where $\bar{\sigma}$ is the complement of genome $\sigma, x_{\{\sigma,\bar{\sigma}\}}$ is the population fraction of the double strand $\{\sigma,\bar{\sigma}\}, p_\mathrm{m}(\sigma'\{\sigma,\bar{\sigma}\})$ denotes the probability that σ' becomes $\{\sigma,\bar{\sigma}\}$ after replication, $\kappa_{\{\sigma,\bar{\sigma}\}}$ is the fitness of $\{\sigma,\bar{\sigma}\}$, and $\bar{\kappa}(t)$ is the population mean fitness. Special emphasis was placed on semiconservative replication because it extends the quasispecies model, originally formulated as a system of ordinary differential equations particularly appropriate for modeling the evolutionary dynamics of replicating single-stranded RNA genomes, to include double-stranded semiconservative DNA replication, on which the genomes of actual living systems are based. The analytical results from solving these equations show that semiconservative replication is actually less robust, while conservative replication exhibits a selective advantage (Brumer and Shakhnovich 2005). This is because conservative replication preserves a copy of the original parent strand, so by replicating

sufficiently fast it is possible to "out-replicate" the *error catastrophe*, i.e., the mutation rate at which the quasispecies delocalizes can be made arbitrarily high. In semiconservative replication, however, there is an upper bound to this mutation rate, since the original parent genome is destroyed, and in order to avoid the error catastrophe, at least one viable genome must be produced, on average, per cycle. These results for semiconservative replication may help explain the effectiveness of chemical mutagens (i.e., chemotherapy) in treating cancer. The different mechanisms of conservative and semiconservative replication are compared in Fig. 1a, while Fig. 1b describes in more detail the three stages of semiconservative replication, assuming *perfect lesion repair*, i.e., mismatched base pairs among double-stranded genomes are not tolerated and are therefore immediately repaired, either by correcting the parent or the daughter.

Subsequently, Tannenbaum and Shakhnovich (2005) relaxed this assumption and looked at *imperfect lesion repair*, where the parameter λ gives the efficiency of the lesion repair, $0 \leq \lambda \leq 1$, and l expresses the cutoff length (in terms of Hamming distance) of the lesions, i.e., the genome can tolerate up to l lesions, $0 \leq l \leq \infty$. The analytical solutions and stochastic simulations show that at higher mutation rates it may become advantageous to suppress lesion repair, in order to avoid the risk of fixing a mutation in the parent strand, an effect which leads to a delay in the error catastrophe relative to the case of perfect lesion repair. Once lesions are assumed, *immortal strand co-segregation* (described below) is proposed as a mechanism by which stem cells protect the integrity of their genomes.

An additional model studied considers genes with explicit mechanisms for *mismatch repair*. Cells with such functional genes are called *repairers*, while cells with faulty copies of such genes are named *mutators*. Mutator strains of bacteria are believed to play an important role in the emergence of antibiotic drug resistance, while mutators may also serve as gateways for the emergence of cancer in multicellular organisms. Analytical solutions of this model lead to the *repair catastrophe*, similar to the error catastrophe, where a localization to delocalization transition occurs as the repair failure probability increases.

Finally, Tannenbaum and Shakhnovich (2005) looked at the dynamics of multiple-gened genomes, where each gene is itself a "single-fitness peak." This case enables the possibility of having not one error catastrophe, but a collection of localization to delocalization transitions known as an *error cascade*, where various genes in the genome lose their functionality as the mutation rate is increased. The error cascade is an example of a phenomenon known as "survival of the flattest" (Wilke 2005); while at low mutation rates the dominant population will be those replicating the fastest—"survival of the fittest," at high mutation rates the population may be dominated by more slowly replicating but mutationally more robust genomes.

In a subsequent paper on semiconservative replication, Tannenbaum et al. (2006) develop the semiconservative quasispecies equations for polysomic genomes, i.e., genomes consisting of not one, but several, chromosomes. Since the chromosomes are distinguishable, the genomes are effectively haploid. Assuming *imperfect lesion repair*, this work considers two possible mechanisms for separation and replication, as illustrated in Fig. 2. In *random segregation*, the chromosomes segregate and

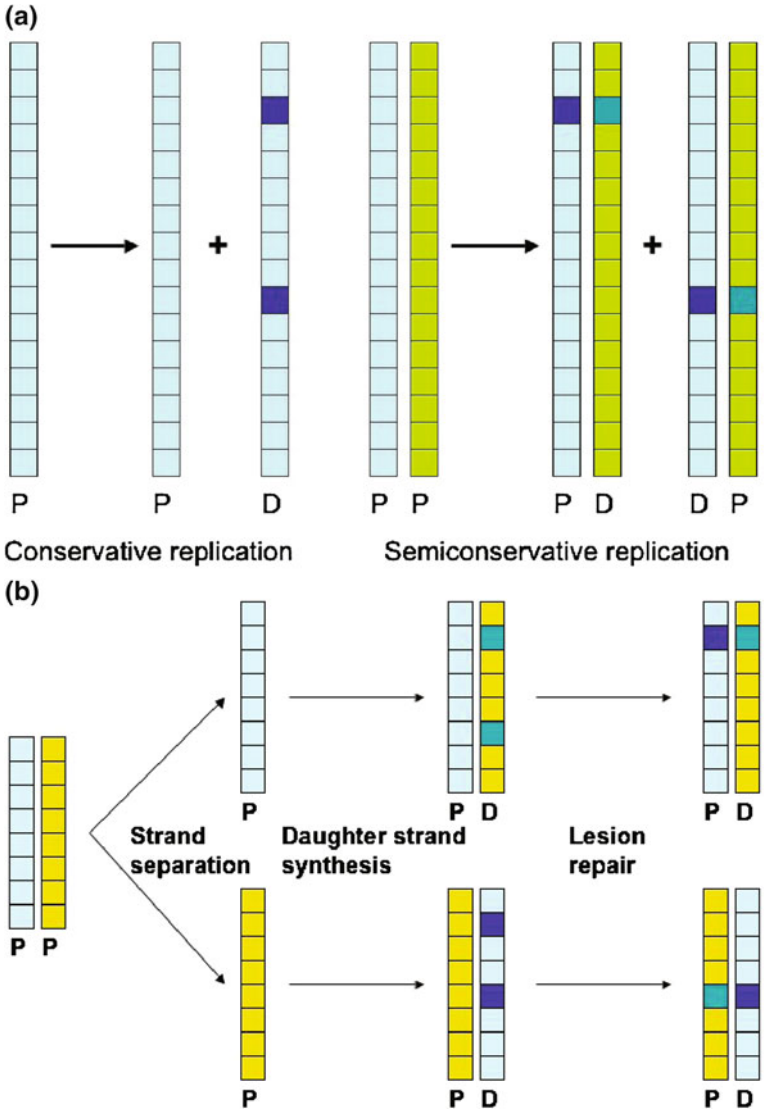

Fig. 1 **a** The different mechanisms of conservative and semiconservative replication. Both processes allow for random mutations. In conservative replication, the original strand is unaffected by the replication process. In semiconservative replication, each strand serves as a template for the synthesis of a complementary daughter strand, resulting in daughter genomes that may differ from the original parent. **b** The three stages of semiconservative replication, showing the effects of separation, replication, mutation, and repair. Due to the lack of parent–daughter discrimination, mismatches due to mutations may be repaired either by correcting the parent or the daughter. Reprinted, with permission, from Tannenbaum and Shakhnovich (2005)

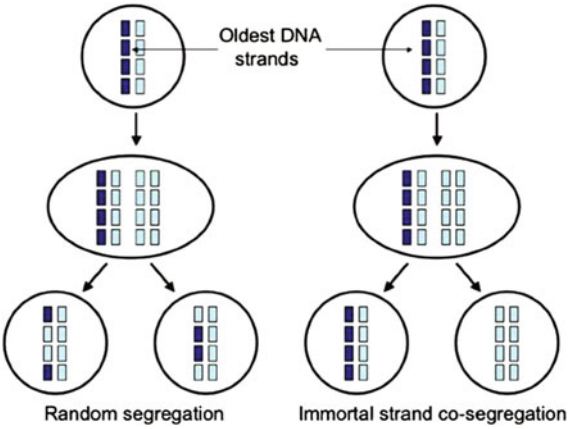

Fig. 2 Random segregation and immortal strand co-segregation mechanisms, where each genome consists of several chromosomes. The oldest DNA strands are colored *dark blue*, and the newly synthesized strands are *light blue*. During replication, the two strands of each chromosome separate, and each strand serves as the template for the synthesis of the complementary daughter strand. With random segregation, the chromosomes are segregated independently of each other into the daughter cells. With immortal strand co-segregation, one of the cells receives the chromosomes that contain the oldest DNA template strands. Reprinted, with permission, from Tannenbaum et al. (2006)

replicate independently; in *immortal strand co-segregation*, the segregation of the chromosomes is coordinated, so that one of the cells receives the chromosomes containing the oldest DNA template strands, which presumably contain less mutations. When solved analytically and simulated, immortal strand co-segregation leads to significantly improved preservation of the master genome than random segregation. Furthermore, when lesion repair is completely suppressed ($\lambda = 0$), immortal strand co-segregation allows the error threshold to reach arbitrarily high mutation rates, as this effectively corresponds to conservative replication. This result suggests that certain classes of tumor cells exhibit immortal strand co-segregation.

Brumer and Shakhnovich (2004a) and Brumer et al. (2006) have modeled cancerous tumors, which are characterized by genetical instability: Microsatellite instability (MIN) tumors have elevated point mutation rates, while CIN tumors have increased rates of losing or gaining chromosomes during cell division. Since MIN tumors replicate semiconservatively, yet display robust behavior at mutation rates higher than normal tissue cells, they concluded that the mechanisms of lesion repair must be suppressed, consistent with the above conclusion that semiconservative replication with suppressed lesion repair behaves like conservative replication, enabling viable replication at high mutation rates. Tannenbaum et al. (2006) have pointed out, however, that this holds only under the assumption of immortal strand co-segregation, and have therefore postulated that MIN tumors exhibit both suppressed lesion repair and immortal strand co-segregation. Brumer et al. (2006) have further noted that this is true only for MIN tumors, while CIN tumors show a

plateau in the maximum viable mutation rates for all values of repair efficiency, consistent with semiconservative replication using their model of chromosomal translocation.

The semiconservative polysomic quasispecies model was further extended by Itan and Tannenbaum (2010), who develop a more general formulation of the quasispecies equations applicable to diploid and even polyploid genomes. They also consider both random and immortal DNA strand chromosome segregation mechanisms. In contrast to the haploid case, they are unable to find a general analytical solution for the steady-state mean fitness in the polyploid case and accordingly solve the equations only for the restricted case of perfect lesion repair.

Two other papers have dealt with additional aspects of genetic repair. Gorodetsky and Tannenbaum (2008) studied the quasispecies dynamics of genetic mismatch repair (MMR) on a time-dependent fitness landscape, thus extending previous works that dealt with mutation and repair in static (Kessler and Levine 1998) or fluctuating environments (Palmer and Lipsitch 2006) or dynamic landscapes without repair (Nilsson and Snoad 2000). MMR is of particular interest to evolutionary biologists, because it is believed that mismatch-repair-deficient strains play a crucial role in the emergence of antibiotic drug resistance and may also act as gateway cells for the emergence of cancer. Their model, which they solve analytically, considers an asexual population of single-stranded, conservatively replicating genomes whose only source of genetic variation is due to copying errors during replication, under a time-dependent, single-fitness-peak landscape, where the master sequence changes by only a single point mutation at every time interval. The analytical solution agrees well with results from stochastic simulations.

In Kama and Tannenbaum (2010), a second class of genetic repair is considered. Whereas the first class, which includes MMR and DNA proofreading, consists of mechanisms that correct base mis-pairings during the replication cycle, the second classes, such as NER (Nucleotide Excision Repair) and the SOS response (a genomic repair mechanism that activates only when there is extensive damage to the cellular genome), repair mutated or damaged DNA during the growth phase of the cellular life cycle. This chapter develops a mathematical model that analyzes the selective advantage of the SOS response in unicellular organisms, by solving a quasispecies model that incorporates the SOS response, consisting of a unicellular, asexually replicating population of organisms whose genomes consist of a single, double-stranded DNA molecule, i.e., one chromosome. The model is set up using the quasispecies mathematical formalism of previous papers and solved for the steady-state behavior of the first-order rate equations, assuming a single-fitness peak landscape, in the limit of infinite sequence length. It is further assumed that repair of post-replication mismatched base pairs occurs with finite probability, but that the SOS response is triggered only when the total number of mismatched base pairs is greater than a pre-set threshold. The analytical results, also confirmed by stochastic simulation, indicate that the SOS response does indeed confer a fitness advantage to a population, provided that it is activated only when DNA damage is so extensive that a cell has “nothing to lose,” i.e., it will die if it does not attempt to repair its DNA, so is therefore willing to risk introducing deleterious mutations.

Genetic instability was revisited in an additional paper, Itan and Tannenbaum (2012), which develops a mathematical model describing the evolutionary dynamics of a unicellular, asexually replicating population exhibiting CIN, characterized by the gain or loss of entire chromosomes during cell division. Understanding the role of CIN is important, since it is applicable to the progression of cancer and is by far more prevalent than MIN. In their model, the cellular genome is assumed to consist of several homologous groups of chromosomes, and a single functional chromosome per homologous group is required for the cell to have the optimal fitness associated with the single-fitness peak approximation. Assuming fitness to be independent of the total number of chromosomes in the cell, the model has been analytically solved for steady-state behavior, yielding a mean fitness at mutation–selection balance identical to the mean fitness without CIN. On the other hand, when this assumption is relaxed and the total number of chromosomes is upper bounded, CIN leads to a reduction in mean fitness. This enables an understanding of some of the basic features of the mutation–selection balance associated with CIN.

Two papers by Raz and Tannenbaum have looked at another source of genetic variation, HGT, which is believed to play a major role in shaping bacterial genomes and disseminating new adaptive traits across bacterial strains (Knöppel et al. 2014) —such as antibiotic resistance, degradation of unusual substances, resistance to heavy metals, and translation of colicins (proteins produced by some strains of *Escherichia coli* that are potentially lethal for related strains) (Cascales et al. 2007). Despite its importance—HGT supposedly is primarily responsible for the rapid spread of Antibiotic drug resistance in bacterial populations—most studies on evolutionary dynamics have focused on point mutations as the main engine of genomic change. Raz and Tannenbaum (2010) therefore investigated conjugation-mediated HGT by developing a mathematical model where an F^+ bacterium, which contains an F-plasmid, fuses with an F^- bacterium, one lacking the F-plasmid, in the process turning the F^- into an F^+ (see Fig. 3), where in addition each genome is described by another two characteristics: if it is *viable*, i.e., having a fitness factor of 1, or *nonviable*, with a fitness factor of 0; and if it is resistant or not to antibiotics. The nonresistant genomes are assigned a first-order "death" rate constant. Assuming a mutation–selection balance is reached in the presence of a given concentration of antibiotic, to which the population must become resistant in order to survive, they find that HGT actually has a slightly deleterious effect on the mean fitness of a population in static environments. They conclude therefore that the evolutionary advantage of HGT must be in its ability to adapt faster in dynamic environments. This conclusion is consistent with observations that HGT is promoted when a population is under environmental stress.

This model was expanded with a more realistic model by Raz and Tannenbaum (2014), who introduced *repressed* and *de-repressed* states into the aforementioned system. A first-order rate constant was defined for the transition between the *repressed* F^- and *de-repressed* F^+ states, assigning first-order rate constants for the repression and de-repression transitions. Similarly, they also conclude that conjugation has a deleterious effect on the mean fitness of the population, suggesting that HGT provides no selective advantage in static environments and is useful only in

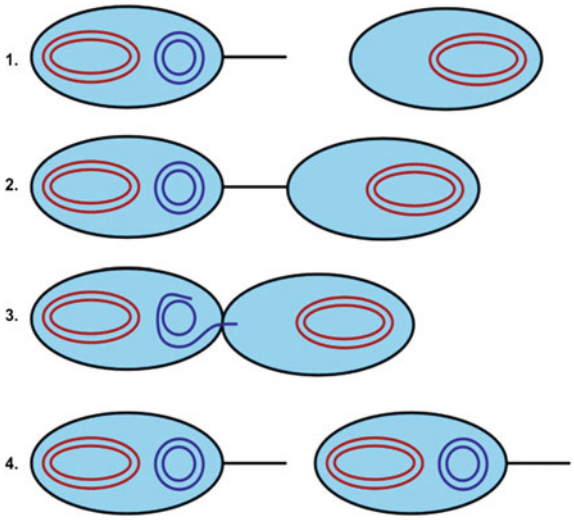

Fig. 3 Illustration of the process of bacterial conjugation used to model HGT. In steps 1 and 2, an F^+ bacterium containing the F-plasmid (*blue*) binds to an F^- bacterium lacking the plasmid. One of the template strands from the F-plasmid then moves into the F^- bacterium, as shown in step 3. In step 4, the complementary strands are synthesized to reform the complete F-plasmids in both bacteria. Both bacteria are now of the F^+ type. Reprinted, with permission, from Raz and Tannenbaum (2010)

adapting to new environments. However, they find that this effect can be lessened by repression, suggesting that while HGT is not necessarily advantageous in a static environment, its deleterious effects can be ameliorated by repression. This further suggests that the main evolutionary advantage of HGT is found in a dynamic landscape. Furthermore, their results demonstrate a delocalization effect of the population, similar to the error catastrophe observed in semiconservative replication that occurs as a result of an elevated level of HGT. Finally, they find that in the limiting case of vanishing spontaneous de-repression, the fraction of potential conjugators in the population, below a critical population density, goes to zero, thus displaying a phase transition. They note that their model bears similarities to previous models of infectious disease dynamics—e.g., the Susceptible-Infected-Susceptible (SIS) model—where the conjugators play the role of an *infected* class, and the non-conjugators play the role of a *susceptible* class.

Using a new approach from systems chemistry, quasispecies theory was also applied to molecular catalytic networks by Wagner et al. (2010b), who developed and solved a catalytic quasispecies model. Catalytic reaction networks (Dadon et al. 2008), operating both autocatalytically and cross-catalytically (Stadler et al. 1995, 2000), have been shown to be relevant to the origin of life and early molecular evolution (von Kiedrowski 1993). In the context of evolutionary dynamics (Chen and Nowak 2012), by looking at the catalytic interactions among genomes (Obermayer and Frey 2009, 2010), autocatalysis can be a mechanism for

self-replication and cross-catalysis may lead to mutation. In this study, it was shown, by solving the quasispecies equations for the steady-state solution, how second-order catalysis (Wagner and Ashkenasy 2009) yields a discontinuous phase transition in the population mean fitness, in contrast to first-order replication mechanisms, considered in the standard quasispecies model, that yield a continuous phase transition. These results may be applied toward understanding the nature of the error threshold in populations replicating with higher order mechanisms. For example, RNA viruses in highly mutating environments (e.g., HIV) could be expected to display sharp population discontinuities.

An entire series of papers have utilized the above quasispecies approach in order to understand the selective advantages of sexual reproduction (Tannenbaum 2006c, 2008a, c, 2009b; Tannenbaum and Fontanari 2008; Lee and Tannenbaum 2007; Kleiman and Tannenbaum 2009). Sexual reproduction combines genetic material from two distinct organisms (see illustration in Fig. 4). This incurs a cost, however, in the form of time and energy that each replicating organism must pay in order to find a genetic partner. Furthermore, in organisms with distinct sexes producing egg and sperm gametes, the potential rate of reproduction is half that of an asexually replicating population where each organism produces diploid eggs, known as the "twofold cost for sex." Despite these disadvantages, higher complex organisms reproduce sexually, indicating that sexual reproduction must confer an overall fitness advantage. A variety of theories have been proposed for the benefits of sex, which generally fall into two categories: (1) *Sex increases adaptability.* Sex evolved because it allows small populations to adapt more quickly to changing environments, i.e., by allowing for recombination among different organisms, sex potentially allows for isolated beneficial mutations to become incorporated into a single organism. The two most common theories are the "Vicar of Bray hypothesis" and the "Red Queen hypothesis." The Vicar of Bray hypothesis, whose name is derived from an English cleric who would change his political and religious views as necessary in order to remain office, simply assumes that sex allows for faster adaptation in dynamic environments. The Red Queen hypothesis, whose name is

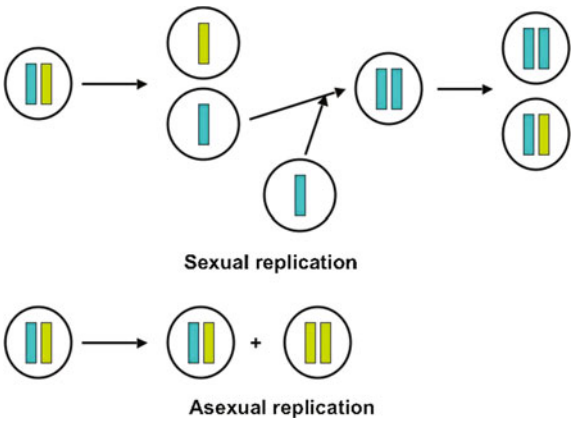

Fig. 4 Comparison of sexual and asexual replication pathways. Reprinted, with permission, from Tannenbaum (2006c)

derived from a character in Lewis Carroll's "Through the Looking Glass," is somewhat more complex, claiming that sex provides a fitness advantage as a result of a constant coevolutionary genetic "arms race" with fast replicating and evolving parasitic organisms. (2) *Sex prevents the accumulation of deleterious mutations.* Sex evolved because it allows organisms to discard defective genes in their own genomes and replace them with functional copies. Here the two most common theories are the genetic repair theory and Muller's ratchet theory. The genetic repair theory simply states that sex prevents the accumulation of deleterious mutations. Muller's ratchet theory argues that sex slows down a phenomenon in small populations known as Muller's ratchet, where deleterious mutations are irreversibly accumulated.

It should be noted that these various theories for sex are not necessarily contradictory or exclusive. Each of the above four theories, however, has certain difficulties making them incomplete. For example, the adaptability category of theories requires a dynamic environment for sex to confer a fitness advantage. However, a number of sexually replicating organisms, such as sharks and crocodiles, have remained apparently unevolved for tens of millions of years in what are seemingly fairly static environments. Similarly, Muller's ratchet theory suffers from its reliance on a small population. Besides being an ill-defined term, Muller's ratchet theory would then argue that the human population should eventually become asexual. This is then the background behind the motivation and usefulness in quasispecies modeling, for a variety of types of organisms, in order to understand the evolution and maintenance of sexual reproduction as a preferred replication strategy.

The first of these papers, Tannenbaum (2006c), has developed a simplified model for understanding the selective advantage of sexual reproduction within the quasispecies formalism. The model assumes a diploid genome consisting of two chromosomes, where the fitness is determined by the number of chromosomes that are identical to a given master sequence. It is also assumed that there is a cost to sexual reproduction, given by a characteristic time τ_{seek} during which haploid cells seek out a mate with which to recombine. If the mating strategy is such that only viable haploids can mate, then when $\tau_{\text{seek}} = 0$, it is possible to show that sexual reproduction will always outcompete asexual reproduction. However, as τ_{seek} increases, sexual reproduction only becomes advantageous at progressively higher mutation rates, and once the time cost for sex reaches a critical threshold, the selective advantage for sexual reproduction disappears entirely. The results here suggest that the selective advantage of sexual reproduction in small populations is found only in populations with low replication rates, where the cost for sex is sufficiently low so that the selective advantage obtained through recombination leads to the dominance of the strategy. In fact, sexual reproduction is selected for in high populations because of the reduced time spent finding a reproductive partner.

A following paper, Tannenbaum and Fontanari (2008), has developed a simplified model for the evolutionary dynamics of a population composed of competing obligate sexually and asexually reproducing unicellular organisms. The model assumes that the organisms have diploid genomes consisting of two

chromosomes, and that the sexual organisms replicate by first dividing into haploid intermediates which then combine with other haploids, followed by the normal mitotic division of the resulting diploid into two new daughter cells. It is assumed that the fitness landscape of the diploids is analogous to the single-fitness-peak approach often used in single-chromosome studies, i.e., it is assumed that a master chromosome becomes defective with just one point mutation. The diploid fitness then depends on whether the genome has zero, one, or two copies of the master chromosome. It is also assumed that only pairs of haploids with a master chromosome are capable of combining so as to produce sexual diploid cells, and that this process is described by second-order kinetics. The findings show, over a range of intermediate values of the replication fidelity, that sexually reproducing cells can outcompete the asexual ones, provided the initial abundance of sexual cells is above some threshold value. This range of values, where sexual reproduction outcompetes asexual reproduction, increases with decreasing replication rate and increasing population density. It is noted that this paper and the previous paper (Tannenbaum 2006c) reach the same general conclusions regarding the regimes where sexual and asexual strategies are, respectively, advantageous.

Another paper, Lee and Tannenbaum (2007), looks at replication via sporulation, which is the replication strategy used by yeast, fungi, algae, and protozoa. Here, diploid populations are considered that replicate via one of two possible sporulation mechanisms. (1) Asexual sporulation, where adult organisms produce single-celled diploid spores that grow into adults themselves. (2) Sexual sporulation, where adult organisms produce single-celled diploid spores that divide into haploid gametes. The haploid gametes enter a haploid "pool," where they may recombine with other haploids to form a diploid spore that then grows into an adult. In the simplified model presented here, the haploid fusion rate is given by second-order reaction kinetics, and the diploid genome consists of only two chromosomes, each of which may be rendered defective with a single point mutation of the wild-type. It is found, by solving for the steady-state mean fitness, that the asexual strategy is favored when the rate of spore production is high compared relative to the characteristic growth rate from a spore to a reproducing adult, while the sexual strategy is favored when the rate of spore production is relatively low. As the characteristic growth time increases, or as the population density increases, the critical ratio of spore production rate to organism growth rate—where the asexual strategy overtakes the sexual one—is pushed to higher values. Therefore, the results here suggest that, for complex multicellular organisms, sexual replication is favored at high population densities and low growth and sporulation rates.

Tannenbaum (2008a) has studied the mutation–selection balance for three simplified replication models: a population of organisms replicating via the production of asexual spores; a sexually replicating population that produces identical gametes; a sexually replicating population that produces distinct sperm and egg gametes. All of these models assume diploid organisms whose genomes consist of two chromosomes, each of which is taken to be viable if equivalent to the master sequence, and defective otherwise. In the asexual population, the asexual diploid spores develop directly into adult organisms. In the sexual populations, the haploid

gametes enter a haploid pool, where they may fuse with other haploids, and the resulting immature diploid organisms then proceed to develop into mature organisms. By solving for the steady-state of all three models, it is found that, as organism size increases, a sexually replicating population can only outcompete an asexually replicating population if the adult organisms produce distinct sperm and egg gametes. Additionally, a sexual replication strategy based on the production of large numbers of sperm cells, in order to fertilize a small number of eggs, is necessary in order to maintain a sufficiently low cost for sex and for this strategy to be selected for over a purely asexual strategy. The study of this model has provided valuable insight into understanding the evolution and maintenance of sexual replication as the preferred replication strategy in complex, multicellular organisms.

Tannenbaum (2008c) has developed simplified mathematical models for *Saccharomyces cerevisiae*, or Baker's yeast, which reproduces both asexually and sexually, describing the mutation–selection balance and based on the single-fitness-peak approximation in quasispecies theory. It is assumed that their diploid genomes consist of two chromosomes and that each chromosome is functional if and only if its base sequence is identical to some master sequence. The growth and replication of the yeast cells is modeled as a first-order process, with first-order growth rate constants that are determined by whether a given genome consists of zero, one, or two functional chromosomes. In the asexual pathway, it is assumed that a given diploid cell divides into two diploids. In the sexual pathway, it is assumed that a given diploid cell divides into two diploids, each of which then divide into two haploids, and the resulting four haploids enter a haploid pool where they grow and replicate until they meet another haploid. For sexual reproduction, two mating strategies are considered: (1) a selective strategy, where only haploids with functional chromosomes fuse with one another; (2) a random strategy, where haploids randomly fuse with one another. When the cost for sex is low, it is found that the selective mating strategy leads to the highest mean fitness of the population, but when the cost for sex is low, sexual replication with random mating also has a higher mean fitness than asexual replication. Moreover, at low replication fidelities, sexual replication with random mating has a higher mean fitness than asexual replication, as long as the cost for sex is low. If the fitness penalty for having a defective chromosome is sufficiently high and the cost for sex sufficiently low, then at low replication fidelities the random mating strategy has a mean fitness that is larger than the asexual mean fitness by a factor of $\sqrt{2}$. It is argued that the selective mating strategy is the one closest to reality for yeast, suggesting that sex may provide a selective advantage under considerably more relaxed conditions than previous research has indicated. The results of this paper also suggest that Baker's yeast switches from asexual to sexual replication when stressed, because stressful growth conditions provide an opportunity for the yeast to clear out deleterious mutations from their genomes.

In a similar direction, Tannenbaum (2009b) has developed simplified models describing asexual and sexual replication in unicellular diploid organisms. The models assume organisms whose genomes consist of two chromosomes, where each chromosome is assumed to be viable if equal to some master sequence and

non-functional otherwise. When the cost for sex is small, as measured by the ratio of the characteristic haploid fusion time to the characteristic growth time, it is found that sexual replication with random haploid fusion leads to a greater mean fitness than a purely asexual strategy. However, sexual replication with a selective mating strategy leads to a higher mean fitness than the random mating strategy, independent of the cost for sex. These results are consistent with previous studies suggesting that sex is favored at intermediate mutation rates, for slowly replicating organisms, and at high population densities. Additionally, the results provide a basis for understanding sex as a stress response in unicellular organisms such as Baker's yeast.

The final paper on the selective advantage of sexual reproduction is by Kleiman and Tannenbaum (2009), who developed mathematical models describing the evolutionary dynamics of both asexually and sexually reproducing populations of diploid unicellular organisms. As in previous papers, the asexual and sexual life cycles are based on the asexual and sexual life cycles of Baker's yeast, which normally reproduces by asexual budding, but switches to sexual reproduction when stressed. The mathematical models consider three reproduction pathways: (1) asexual reproduction; (2) self-fertilization; and (3) sexual reproduction. Two forms of genome organization are examined. In the first, the genome is assumed to consist of two multi-gene chromosomes, and in the second, the opposite extreme is assumed, i.e., each gene defines a separate chromosome and is called a multi-chromosome genome. These two cases are considered in order to explore the role that recombination has on the mutation–selection balance and the selective advantage of the various reproduction strategies. It is assumed that the purpose of diploidy is to provide redundancy, so that damage to a gene may be repaired using its other, presumably undamaged copy, a process known as homologous recombination repair. As a result, the fitness of the organism should only depend on the number of homologous gene pairs that contain at least one functional copy of a given gene. These models are solved for their steady-state mean fitness, and the sexual reproduction pathway for the multi-chromosomed genome is found to have a mean fitness exceeding those of all the other strategies. Furthermore, while other reproduction strategies experience a total loss of viability due to the steady accumulation of deleterious mutations, no such transition occurs in the sexual pathway. These results provide a basis for understanding the selective advantage of the specific pathways employed by sexually reproducing organisms and also suggest an explanation for why unicellular organisms such as Baker's yeast switch to a sexual mode of reproduction when stressed. While these models are based on mutation propagation in unicellular organisms, they nevertheless suggest that, in more complex organisms with significantly larger genomes, sex is necessary to prevent the loss of viability of a population due to genetic drift. Most importantly, the results of this article demonstrate a selective advantage for sexual reproduction under fewer and less restrictive assumptions than in previous studies.

Another series of papers has explored various evolutionary strategies based on the division of labor. Tannenbaum (2006a) has developed and investigated a two-cell quasispecies model with an optional survival strategy (Fig. 5), where pairs

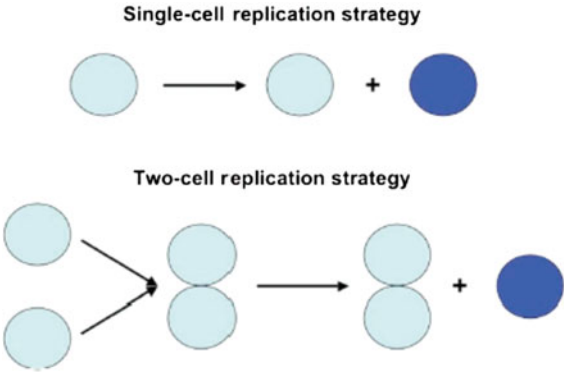

Fig. 5 Comparison of single-cell and two-cell replication strategies in the two-cell-differentiated quasispecies model. Reprinted, with permission, from Tannenbaum (2006a)

of cells join together and one of the cells sacrifices its own replicative ability for the sake of the other cell while devoting its metabolic efforts to sustaining the other cell. Such a survival strategy was inspired by the behavior of slime molds, which exist as a collection of single cells under favorable conditions, but under stressful conditions, such as resource depletion, respond by coalescing into a differentiated, multicellular organism. Solving this model yields two distinct regimes of behavior: At low concentrations of external resources, the two-cell strategy outcompetes the single-cell survival strategy, while at high resource concentrations, the single-cell survival strategy dominates. At low resource concentrations, the single-cell survival strategy becomes disadvantageous, because the energy costs of maintaining reproductive and metabolic pathways become prohibitively high, leaving little excess energy for replication. However, if the rate of energy production exceeds the energetic costs of maintaining metabolic pathways, then the excess energy, if shared among several cells, can pay for the reproductive costs of a single cell. The model also yields a localization to delocalization transition analogous to the error catastrophe in standard quasispecies models. The existence of such a transition indicates that multicellularity can emerge because natural selection does not act on specific cells, but rather on replicative strategies, consistent with the concept that natural selection does not act on individuals, but rather on populations.

Division of labor, as a general ubiquitous biological phenomenon enabling optimized system output, was further explored in Tannenbaum (2007b), who investigated two models: the compartment model, where a resource flows into a compartment of given volume and is processed by agents and converted into a product within this compartment; and the replication-metabolism model, where autoreplicating systems consist of replication and metabolic tasks that are divided among different agents. By mathematically solving for the steady-state behavior of these models, it was concluded that division of labor is favored only for intermediate values of the resource to agent ratio, with low intermediate products transport time cost. These results are consistent with the behavior of the cellular slime mold *Dictyostelium discodeum*, which switches from a single-celled to a multi-celled state when resources become limited, and also suggest an evolutionary basis for the

emergence of stem-cell-based tissue architecture in complex organisms. Additionally, this paper may help us understand how division of labor maximizes economic productivity at intermediate-size firms.

Subsequently, Tannenbaum (2008b) explored a specific division of labor strategy, namely temporal differentiation, whereby given tasks are broken up into several subtasks and the various subtasks are performed at different times. The idea is that a set of agents concentrates all its efforts on only one set of subtasks in a certain time interval, in order to increase the efficiency of each subtask and allow for faster completion of the overall task, in contrast to "standard" division of labor where all subtasks are performed simultaneously by different sets of agents. Examples of such a strategy include sleep and circadian rhythms, as well as household chores such as shopping and paying bills. This work therefore considers two simplified models that describe the processing of a resource into a final product. The first model describes the filling and emptying of a tank in the presence of a time-varying resource, and its optimal algorithm is proven to be where the tank is filled when a resource is available and emptied when a resource is not available. This simple model is then shown to be closely related to biological networks. The second model is an agent-based, three-step process, whereby some resource is converted into a final product in a series of three agent-mediated steps. Temporal differentiation is introduced by allowing the agents to oscillate between performing the first two steps and performing the third step. Solving for the steady-state solutions yields the result that temporal differentiation is more efficient at intermediate values of the number of agents, and when the intermediate processes have relatively long lifetimes. Overall, it is argued that in sufficiently complex biological systems, the amount of information and tasks that can be processed and completed is maximized when the system follows a strategy of temporal differentiation. The paper further speculates on temporal differentiation as an evolutionary basis for the emergence of sleep, distinct REM and non-REM sleep states, circadian rhythms, and oscillatory dynamics in complex systems.

Division of labor versus multitasking was again revisited in the context of metabolism and replication. Wagner et al. (2010a) investigated the selection advantage of metabolic replicators, presenting a kinetic analysis and simulation of the replication reactions of two competing replicators—one non-metabolic and the other metabolic. The analysis indicates that in a resource-rich environment the non-metabolic replicator is likely to be kinetically selected, while in a resource-poor environment it is the metabolic replicator that is kinetically more stable and thereby selected. This causal relationship suggests a mechanism for the emergence of metabolic systems and lends support for the "replication first" school of thought in the studies of the origin of life.

We conclude this review with a few more speculative papers on genomics and quasispecies and potential applications and implications. Tannenbaum (2006b) examined the evidence for vast sequences of genomes in higher eukaryotes —"junk" DNA, and has suggested that it is, in fact, a vast, RNA-based, genetic regulatory network that is responsible for the variety and complexity of terrestrial life. This network is therefore more properly viewed as an RNA "community,"

composed of a rich and largely unexplored biochemical web of RNA interactions. Moreover, it is hypothesized that this regulatory network can re-wire itself and employ various and evolvable mutational strategies in response to external pressures, suggesting that much evolutionary change is due to intracellular, RNA-mediated learning processes, which are then recorded into the DNA genome in a process termed *RNA-mediated DNA evolution*. Evidence and specific theorems are presented to test this framework. For example, this RNA community approach could reconcile actual timescales of macroevolutionary changes with observed point mutation and gene duplication rates. Furthermore, the RNA community viewpoint suggests that agent-based modeling techniques, used in mathematical economics, game theory, and neuroscience, may likely be useful in understanding the functioning of eukaryotic cells in the pathway-based approach of systems biology. The paper concludes by arguing that a sufficient amount of biological knowledge has been accumulated to initiate a systematic program of experimental and computational studies on the origins and macroevolution of terrestrial life.

Tannenbaum (2007a) takes a novel approach toward determining the importance of various genes to the viability of an organism, by treating a population of cells at various concentrations of chemical mutagens, and determining, as a function of the resulting spectrum of mutation rates, which genes lose functionality due to genetic drift. This was done by setting up a quasispecies formulation of asexual, single-chromosome organisms whose only source of variability is due to point mutations during replication. Since the genes that lose their functionality at higher mutation rates are generally those that are more essential for an organism's survival, and additionally, genes which lose or gain functionality together with other genes are most likely part of the same genetic network, this study may therefore lead to the elucidation of correlations among genes and the determination of redundant genetic pathways in the cell. Thus, data obtained from mutagen-based methods could be used to organize genes according to a hierarchy of increasing fitness and importance to the cell and also shed light on the evolutionary history of an organism.

Gandhi et al. (2007) followed the previous work of Tannenbaum (2006b) by looking at the RNA biochemical networks and observing that "animate" features, such as memory and associative learning, emerge naturally from their self-organization. By constructing and solving a simple kinetic model consisting of a chemostat, two species and their growth factors, associative learning emerges as a system "learns" to associate two stimuli with one another. For example, it is shown that when the chemostat is stimulated simultaneously by both growth factors for a certain amount of time, followed by a time gap without any stimulation, and then again by a period where the chemostat is stimulated by only one of the growth factors, then there will be a transient increase in the number of molecules activated by the other growth factor. Thus, the chemostat bears the imprint of the earlier stimulation from both growth factors, indicative of associative learning. The dynamics of the model are reminiscent of certain aspects of Pavlov's famous conditioning experiments in dogs. The paper further discusses how associative

learning can potentially emerge in vitro within RNA, DNA, or peptide networks, and how such this mechanism can be involved in genomic evolution and adaptation at the cellular level.

Finally, Tannenbaum (2009a) speculates on the emergence of self-awareness. It is argued that self-awareness emerges in organisms whose brains have a sufficiently integrated, complex ability for associative learning and memory, as continual sensory information inputs lead to the formation of organismal "self-image" associations. After suggesting a basic mechanism for the emergence of an organismal self-image, this paper lists a representative set of behaviors associated with self-awareness and shows how associative memory and learning, combined with an organismal self-image, lead to the emergence of these behaviors. This paper also discusses various tautologies that invariably emerge when discussing self-awareness, speculates on manipulating self-awareness, and discusses how concepts from set theory and mathematical logic may help understand the emergence of higher cognitive functions in complex organisms.

We have summarized here over thirty papers, works of Emmanuel Tannenbaum and colleagues that have dealt with theoretical models of quasispecies, demonstrating the power and applicability of the quasispecies model in understanding specific biological phenomena as well as more general evolutionary trends. In his life, Emmanuel made groundbreaking discoveries by continually expanding quasispecies theory and by applying its principles to a variety of biological topics, among them semiconservative replication, genetic instability and repair mechanisms, molecular replicators, evolution of antibiotic drug resistance, HGT, role of sex in organisms, origin of metabolism, division of labor, associative learning, and other "animate" features.

The field of theoretical biological modeling via quasispecies theory is by no means exhausted. Many biological challenges still remain, applicable yet mainly unexplored, such as stem cell dynamics, evolution and dynamics of mobile genetic elements (transposons) and viruses, host-parasite dynamics among prokaryotes/eukaryotes with plasmids, lipid superstructures, conformational landscapes of proteins, to name but a few. We can attempt to meet some of these challenges in the years ahead, aided and inspired by the theoretical models and mathematical methods summarized above.

References

Brumer Y, Shakhnovich EI (2004a) Host-parasite coevolution and optimal mutation rates for semiconservative quasispecies. Phys Rev E 69:061909

Brumer Y, Shakhnovich EI (2004b) Importance of DNA repair in tumor suppression. Phys Rev E 70:061912

Brumer Y, Shakhnovich EI (2005) Selective advantage for conservative viruses. Phys Rev E 71:031903

Brumer Y, Michor F, Shakhnovich EI (2006) Genetic instability and the quasispecies model. J Theor Biol 241:216–222

Cascales E, Buchanan SK, Duche D, Kleanthous C, Lloubes R, Postle K, Riley M, Slatin S, Cavard D (2007) Colicin biology. Microbiol Mol Biol Rev 71:158–229
Chen IA, Nowak MA (2012) From prelife to life: how chemical kinetics become evolutionary dynamics. Acc Chem Res 45:2088–2096
Dadon Z, Wagner N, Ashkenasy G (2008) The road to non-enzymatic molecular networks. Angew Chem Int Ed 47:6128–6136
Gandhi N, Ashkenasy G, Tannenbaum E (2007) Associative learning in biochemical networks. J Theor Biol 249:58–66
Gorodetsky P, Tannenbaum E (2008) Effect of mutators on adaptability in time-varying fitness landscapes. Phys Rev E 77:042901
Itan E, Tannenbaum E (2010) Semiconservative quasispecies equations for polysomic genomes: the general case. Phys Rev E 81:061915
Itan E, Tannenbaum E (2012) Effect of chromosomal instability on the mutation-selection balance in unicellular populations. PLoS ONE 7:e26513
Kama A, Tannenbaum E (2010) Effect of the SOS response on the mean fitness of unicellular populations: a quasispecies approach. PLoS ONE 5:e14113
Kessler D, Levine H (1998) Mutator dynamics on a smooth evolutionary landscape. Phys Rev Lett 80:2012–2015
Kleiman M, Tannenbaum E (2009) Diploidy and the selective advantage for sexual reproduction in unicellular organisms. Theor Biosci 128:249–285
Knöppel A, Lind PA, Lustig U, Näsvall J, Andersson DI (2014) Minor fitness costs in an experimental model of horizontal gene transfer in bacteria. Mol Biol Evol 31:1220–1227
Lee B, Tannenbaum E (2007) Asexual and sexual replication in sporulating organisms. Phys Rev E 76:021909
Nilsson M, Snoad N (2000) Error thresholds for quasispecies on dynamic fitness landscapes. Phys Rev Lett 84:191–194
Obermayer B, Frey E (2009) Escalation of error catastrophe for enzymatic self-replicators. Europhys Lett 88:48006
Obermayer B, Frey E (2010) Error thresholds for self- and cross-specific enzymatic replication. J Theor Biol 267:653–662
Palmer ME, Lipsitch M (2006) The influence of hitchhiking and deleterious mutation upon asexual mutation rates. Genetics 173:461–472
Raz Y, Tannenbaum E (2010) The influence of horizontal gene transfer on the mean fitness of unicellular populations in static environments. Genetics 185:327–337
Raz Y, Tannenbaum E (2014) Repression/Depression of conjugative plasmids and their influence on the mutation-selection balance in static environments. PLoS ONE 9:e96839
Stadler PF, Schnabl W, Forst CV, Schuster P (1995) Dynamics of small autocatalytic reaction networks—II. Replication, mutation and catalysis. Bull Math Biol 57:21–61
Stadler B, Stadler PF, Schuster P (2000) Dynamics of autocatalytic replicator networks based on higher-order ligation reactions. Bull Math Biol 62:1061–1086
Tannenbaum E (2006a) Selective advantage for multicellular replicative strategies: a two-cell example. Phys Rev E 73:010904
Tannenbaum E (2006b) An RNA-centered view of eukaryotic cells. Biosystems 84:217–224
Tannenbaum E (2006c) Selective advantage for sexual reproduction. Phys Rev E 73:061925
Tannenbaum E (2007a) Extracting viability landscapes from mutagen-response experiments. J Theor Biol 245:37–43
Tannenbaum E (2007b) When does division of labor lead to increased system output? J Theor Biol 247:413–425
Tannenbaum E (2008a) Comparison of three replication strategies in complex multicellular organisms: asexual replication, sexual replication with identical gametes, and sexual replication with distinct sperm and egg gametes. Phys Rev E 77:011915
Tannenbaum E (2008b) Temporal differentiation and the optimization of system output. Phys Rev E 77:011922

Tannenbaum E (2008c) A comparison of sexual and asexual replication strategies in a simplified model based on the yeast life cycle. Theor Biosci 127:323–333
Tannenbaum E (2009a) Speculations on the emergence of self-awareness in big-brained organisms: the roles of associative memory and learning, existential and religious questions, and the emergence of tautologies. Conscious Cogn 18:414–4427
Tannenbaum E (2009b) Selective advantage for sexual reproduction with random haploid fusion. Theor Biosci 128:85–96
Tannenbaum E, Fontanari JF (2008) A quasispecies approach to the evolution of sexual replication in unicellular organisms. Theor Biosci 127:53–65
Tannenbaum E, Shakhnovich EI (2004a) Error and repair catastrophes: a two-dimensional phase diagram in the quasispecies model. Phys Rev E 69:011902
Tannenbaum E, Shakhnovich EI (2004b) Solution of the quasispecies model for an arbitrary gene network. Phys Rev E 70:021903
Tannenbaum E, Shakhnovich EI (2005) Semiconservative replication, genetic repair, and many-gened genomes: extending the quasispecies paradigm to living systems. Phys Life Rev 2:290–317
Tannenbaum E, Deeds EJ, Shakhnovich EI (2003) Equilibrium distribution of mutators in the single fitness peak model. Phys Rev Lett 91:138105
Tannenbaum E, Deeds EJ, Shakhnovich EI (2004a) Semiconservative replication in the quasispecies model. Phys Rev E 69:061916
Tannenbaum E, Sherley JL, Shakhnovich EI (2004b) Imperfect DNA lesion repair in the semiconservative quasispecies model: derivation of the Hamming class equations and solution of the single-fitness-peak landscape. Phys Rev E 70:061915
Tannenbaum E, Sherley JL, Shakhnovich EI (2005) Evolutionary dynamics of adult stem cells: comparison of random and immortal strand segregation mechanisms. Phys Rev E 71:041914
Tannenbaum E, Sherley JL, Shakhnovich EI (2006) Semiconservative quasispecies equations for polysomic genomes: the haploid case. J Theor Biol 241:791–805
von Kiedrowski G (1993) Minimal replicator theory. I. Parabolic versus exponential growth. Bioorg Chem Front 3:113–146
Wagner N, Ashkenasy G (2009) Symmetry and order in systems chemistry. J Chem Phys 130:164907
Wagner N, Pross A, Tannenbaum E (2010a) Selection advantage of metabolic over non-metabolic replicators: a kinetic analysis. Biosystems 99:126–129
Wagner N, Tannenbaum E, Ashkenasy G (2010b) Second order catalytic quasispecies yields discontinuous mean fitness at error threshold. Phys Rev Lett 104:188101
Wilke O (2005) Quasispecies theory in the context of population genetics. BMC Evol Biol 5:44

Theories of Lethal Mutagenesis: From Error Catastrophe to Lethal Defection

Héctor Tejero, Francisco Montero and Juan Carlos Nuño

Abstract RNA viruses get extinct in a process called lethal mutagenesis when subjected to an increase in their mutation rate, for instance, by the action of mutagenic drugs. Several approaches have been proposed to understand this phenomenon. The extinction of RNA viruses by increased mutational pressure was inspired by the concept of the error threshold. The now classic quasispecies model predicts the existence of a limit to the mutation rate beyond which the genetic information of the wild type could not be efficiently transmitted to the next generation. This limit was called the error threshold, and for mutation rates larger than this threshold, the quasispecies was said to enter into error catastrophe. This transition has been assumed to foster the extinction of the whole population. Alternative explanations of lethal mutagenesis have been proposed recently. In the first place, a distinction is made between the error threshold and the extinction threshold, the mutation rate beyond which a population gets extinct. Extinction is explained from the effect the mutation rate has, throughout the mutational load, on the reproductive ability of the whole population. Secondly, lethal defection takes also into account the effect of interactions within mutant spectra, which have been shown to be determinant for the understanding the extinction of RNA virus due to an augmented mutational pressure. Nonetheless, some relevant issues concerning lethal mutagenesis are not completely understood yet, as so survival of the flattest, i.e. the development of resistance to lethal mutagenesis by evolving towards mutationally more robust regions of sequence space, or sublethal mutagenesis, i.e., the increase of the mutation rate below the extinction threshold which may boost the adaptability of RNA virus,

H. Tejero (✉) · F. Montero
Department of Biochemistry and Molecular Biology I, Universidad Complutense de Madrid, 28040 Madrid, Spain
e-mail: hector.tejero.81@gmail.com

J.C. Nuño
Department of Applied Mathematics, Universidad Politécnica de Madrid, 28040 Madrid, Spain

H. Tejero
Translational Bioinformatics Unit, Centro Nacional de Investigaciones Oncológicas, 28029 Madrid, Spain

Current Topics in Microbiology and Immunology (2016) 392: 161–179
DOI 10.1007/82_2015_463

Published Online: 26 July 2015

increasing their ability to develop resistance to drugs (including mutagens). A better design of antiviral therapies will still require an improvement of our knowledge about lethal mutagenesis.

Contents

1 Introduction 162
2 The Error Threshold and the Error Catastrophe 162
2.1 The Limits of the Error Catastrophe 163
3 Mutation–Selection-Based Models 165
3.1 Lethality, Extinction and Error Catastrophe 169
4 Lethal Defection 170
4.1 Stochastic Extinction Model 171
4.2 Interference, Complementation and Lethal Defection 172
5 Problems of Lethal Mutagenesis 173
5.1 Resistance and Survival of Flattest 173
5.2 Sublethal Mutagenesis 174
6 Concluding Remarks 175
References 176

1 Introduction

Lethal mutagenesis is taken to be the extinction of a micro-organism by accumulation of mutations due to the treatment with mutagenic drugs. This phenomenon has been verified empirically in a large number of RNA viruses (see Chap. 14), and consequently, its viability and potential application as an antiviral therapy is beyond doubt. However, in recent years, there has been a growing debate over how this phenomenon is produced, and which theoretical model can best explain it. The aim of this article is to review and compare the different models which have been put forward to explain this phenomenon.

2 The Error Threshold and the Error Catastrophe

In the classic quasispecies model, the error threshold is the mutation rate beyond which the master phenotype, which is the phenotype with the highest replicative capacity, is extinguished (Chap. 1). In this way, the population becomes exclusively composed of mutant phenotypes, i.e. all the phenotypes that differ from the master (Eigen 1971). Simultaneously to the disappearance of the master phenotype, the population delocalises over the sequence space which, in finite populations, can be interpreted as the quasispecies beginning to drift over the whole sequence space.

Given that this phenomenon takes place as a phase transition, with respect to the mutation rate, it is said that beyond the error threshold, the population enters into error catastrophe.

The definition and phenomenology of the error threshold and the entry into error catastrophe have not been free from controversy (Tejero et al. 2011). The problem largely arises from the nature of the models that were originally studied, mainly in a single-peak landscape in the absence of back mutations from the mutant phenotype to the master phenotype, factors on which it is extremely dependent (Hermisson et al. 2002; Schuster 2010). The differences that are observed for the phenomenology and definition of error catastrophe, and error threshold, can also be observed in the interpretation of both concepts (Tejero et al. 2011).

Both the loss of the master phenotype and the delocalisation of the quasispecies over the sequence space have been related to an information "crisis" or "loss", since the population is unable to maintain the information contained in the master phenotype (Biebricher and Eigen 2005; Eigen 2002; Eigen and Schuster 1979). Since the mutation rate from the master to the mutant phenotype is determined by the size of the sequences that compose them, the entry into error catastrophe establishes a maximum limit to the amount of information that a self-replicative system can maintain at a given mutation rate (Wilke 2005; Takeuchi et al. 2005; Obermayer and Frey 2010). After the RNA viruses have been conceptualised as quasispecies (Domingo et al. 1978), the possibility of pushing RNA viruses into error catastrophe by means of mutagenic drugs (Eigen 1993, 2002) was the origin of the first lethal mutagenesis experiments, as well as the first explanation for the extinction of the virus in these conditions (Cameron and Castro 2001; Holland et al. 1990; Loeb et al. 1999).

2.1 The Limits of the Error Catastrophe

Although the concept of error catastrophe was the first explanation for lethal mutagenesis, several objections were later raised to this explanation. In the classic quasispecies model, all the mutants have the capacity to reproduce themselves, that is to say there are no lethal mutants. Some papers have shown that if all the mutations were lethal, and therefore all the mutants were unable to reproduce themselves, error catastrophe could not happen (Summers and Litwin 2006; Bull et al. 2005). Earlier Wagner and Krall (1993) had shown, using a different model, that error catastrophe could not take place in the presence of lethal genotypes, a result which was confirmed by Wilke (2005). Subsequently, his results were justifiably criticised by Takeuchi and Hogeweg (2007), as they showed that the model used by Wagner and Krall contained a series of very limiting restrictions and that it was these restrictions which were responsible for the results obtained. To consider that all mutations are lethal, or to consider that they are all absent, are extreme, highly unlikely situations. When intermediate situations are studied, it can be seen that the presence of lethality does not prevent error catastrophe from taking place,

but it does cause it to happen at much higher mutation rates, that is to say it increases the error threshold (Sardanyes et al. 2014; Bonnaz and Koch 1998; Takeuchi and Hogeweg 2007; Tejero et al. 2010). This result appears to be independent of the distribution of lethality over the sequence space. Of course, from the point of view that entry into error catastrophe is the mechanism that underlies lethal mutagenesis, this result may appear to be counter-intuitive, since we would expect an increase in the proportion of lethal mutations to facilitate extinction caused by accumulation of mutations, and not the reverse. What was required was a clarification of the relation between the error threshold and the extinction threshold in quasispecies models since, strangely enough, this relation had not yet been defined, something which can be explained by the fact that the quasispecies models had been formulated under a constant population restriction.

Wilke was the first to correctly point out that most of the models for quasispecies and entry into error catastrophe considered constant population conditions which, consequently, by definition, ruled out the possibility of extinction (Wilke 2005). At around the same time, Bull et al. (2005) explicitly showed the need to differentiate between extinction, which involves the disappearance of the whole population, and entry into error catastrophe, in which it is the master phenotype that disappears. In other words, it is important to distinguish between the error threshold, namely the mutation rate at which the population enters into error catastrophe, and the extinction threshold, namely the mutation rate at which the population becomes extinct. Thus, both papers not only ruled out the possibility that lethal mutagenesis is caused by the entry of the quasispecies into error catastrophe, but they also suggested that the error catastrophe could in fact hinder or delay the extinction of a virus by lethal mutagenesis. The reason for this is that error catastrophe, ultimately, is caused by what is known as the "survival of the flattest" or, in other words, the dominance, at high mutation rates, of phenotypes with a lower replicative capacity but a higher tolerance to mutations (Cowperthwaite et al. 2008; Tejero et al. 2011; Bull et al. 2005, 2007). Specifically, Tejero et al. showed that the error threshold can be reformulated in terms of a selection coefficient that depends on the mutation rate and which is as follows:

$$s(Q_{\mathrm{m}}) = \frac{A_{\mathrm{k}}}{A_{\mathrm{m}} Q_{\mathrm{m}}} - 1 \tag{1}$$

where A_{k} and A_{m} are the replicative capacities of the mutant and master phenotypes, respectively, and Q_{m} is the quality factor, namely the probability that the master sequence is copied correctly. This reformulation shows that the error threshold is the value of the quality factor, Q_{m}, for which the selection coefficient, s, becomes zero. In other words, the selection coefficient is positive for mutation rates higher than the error threshold and, therefore, the mutant phenotype has a selective advantage over the master phenotype. To put it another way, before the error threshold natural selection favours the master phenotype, but beyond it natural selection favours the mutant phenotype.

The consideration that entry into error catastrophe is caused by the survival of the flattest phenotypes provides an explanation as to why lethality displaces the error threshold towards lower mutation rates. In the aforementioned papers, the introduction of lethality affected only the mutant phenotype, decreasing its mutational robustness. Because of this, the mutant phenotype becomes less competitive and, therefore, higher mutation rates are required in order to allow the mutant phenotype to dominate the master phenotype due to the survival of the flattest. Furthermore, the supposed absence of error catastrophe in the presence of lethality, together with the fact that it was considered to be a phenomenon different from extinction, led to the positing of new theoretical models which would be able to explain lethal mutagenesis.

3 Mutation–Selection-Based Models

The first model which tried to explain lethal mutagenesis in RNA viruses without explicitly taking error catastrophe into account was formulated by Bull et al. (2007). It explored in-depth the idea that it is necessary to differentiate between demographic processes, such as extinction, and genetic–evolutionary processes, such as error catastrophe. The mutation–selection equilibrium, which is the result of the interaction between the relative biological fitness of the alleles in the population and their mutation rates, determines composition and, more importantly in this case, average biological fitness at a stationary state. An increase in the mutation rate displaces the mutation–selection equilibrium towards a greater diversity in the population and, assuming that all the mutations are deleterious, towards a lower average biological fitness. Under a series of conditions, basically the absence of density or frequency-dependent selection, the population´s reproductive capacity can be taken to be the product of the absolute biological fitness of the master species expressed in Wrightian terms, R, and the average biological fitness, $\bar{w}(U)$. When this reproductive capacity falls below 1, the populations start to be extinguished. Consequently, the condition required in order for a population to become extinct can be described as:

$$R\bar{w}(U) < 1 \tag{2}$$

The extinction threshold would be the mutation rate at which this condition is complied with. In order to determine this threshold, it is necessary to know the dependence of the average biological fitness, $\bar{w}(U)$, with respect to the genomic mutation rate U, and to do this, it is necessary to define both the landscape of biological fitness in which the population evolves, and a series of assumptions about phenotypic mutation frequencies.

In Bull et al. (2007, 2008), a multiplicative fitness landscape was considered. As neither back mutations nor compensatory mutations were assumed, under these conditions, it was confirmed that the average biological fitness at a stationary state

is solely dependent on the genomic mutation rate U, according to $\bar{w} = e^{-U}$ (Kimura and Maruyama 1966). In this way, it is possible to determine an extinction threshold as follows:

$$U_{ex} = \log R \tag{3}$$

where U_{ex} is the extinction threshold, and R is the absolute Wrightian fitness.

It should be noted that, according to this model, the extinction threshold does not depend on the deleterious effects of the mutations. That is, ultimately, and without taking finite size effects into account, a virus in which all the mutations are lethal ($s = 1$) will have the same extinction threshold as a virus in which all the mutations are only slightly deleterious ($s \approx 0$). Despite this, although the extinction threshold does not depend on the deleterious effect of the mutations in this model, the time that the virus takes to reach the mutation–selection equilibrium does depend on it (Bull et al. 2013). Thus, the greater the deleterious effect of the mutations, the faster the average biological fitness of the population decreases, and the quicker it starts to become extinct. Naturally, as will be commented below, the fact that the extinction threshold isindependent of the deleterious effect of mutations comes from not con-sidering compensatory or back mutations. Shortly afterwards, Chen and Shaknovich (2009) studied a model in which the fitness landscape was based on an experimental distribution of the effect that mutations have on the thermal stability of proteins. It was subsequently verified that this fitness landscape is compatible with the distributions of the mutational effects obtained experimentally in RNA viruses (Wylie and Shakhnovich 2011). In this way, and as oppose to the multiplicative landscape in the absence of back mutations, this fitness landscape permits beneficial and compensatory mutations. The stability of a protein determines the percentage of time that the protein is folded. Ultimately, the biological fitness of a virus is the product of this value for a series of genes. Due to the complexity of the model used, it is not possible to obtain an explicit expression of the extinction threshold. However, under conditions of conservative replication, similar to those of RNA viruses, the error threshold obtained is approximately lineal (and not exponential) with respect to absolute fitness. Furthermore, in this paper, the differences between conservative and semiconservative replication are compared, showing that the critical mutation rate is less in the latter. The same phenomenon can be observed when considering semiconservative replication in a multiplicative model where there are only deleterious mutations (Bull and Wilke 2008). In this case, the extinction threshold is defined as:

$$U_d > \ln(2) - \ln\left(1 + \frac{1}{R}\right) \tag{4}$$

This, as it can be seen, establishes a maximum limit on the critical rate of deleterious mutations $U_d = \ln(2) \approx 0.69$. This dependence should also appear when studying other possible replicative modes, since it is known that these affect the mutational load (Sardanyés et al. 2009).

The same model was used to show that the lower the population size, the lower the mutational rate needed to extinguish the population (Wylie and Shakhnovich 2012), as was to be expected.

Lastly, Martin and Gandon (2010) used a fitness landscape based on a multivariate Gaussian function. Although this landscape represents a single optimum phenotype, genetically it is very rugged, and one in which epistasis and compensatory mutations occur. Finally, the idea that a given percentage of the mutations are lethal was considered. In this paper, the infective dynamic of the virus in the population using a SIR model was also examined (Nowak and May 2000). By doing this, the reproductive capacity depends on the demographic conditions: the lower the amount of virus, the higher the amount of susceptible cells and, therefore, the greater its reproductive capacity. However, this effect is probably offset by an increase in mutational meltdown phenomena due to finite populations. Furthermore, Wylie and Shaknovich have shown that, in their fitness landscape, the percentage of lethal mutations clearly increases when the population size decreases, which could help to offset the demographic effect. The chief finding of this paper is the derivation of a complex expression of the extinction threshold, which depends on the mutational effect and the growth rate of the optimum phenotype.

When the deleterious effect of the mutations is due, above all, to lethal mutations, the critical mutation rate depends lineally on the ratio between the Malthusian fitness (r_0) and the fraction of lethal mutants (p_L). This can be expressed as:

$$U_{ex} \approx \frac{r_0}{p_L} \tag{5}$$

Taking into account that the Malthusian fitness is the logarithm of the Wrightian fitness (Wu et al. 2013), the expression can be reduced to an equivalence of (3)

$$U_{ex} p_L \approx \log(R) \tag{6}$$

in which the product $U_{ex}p_L$ is the rate of lethal mutations by genome. However, when the deleterious mutations are chiefly non-lethal, the extinction threshold depends on the quotient of the square of the absolute biological fitness and a factor that is proportional to the deleterious effect of the mutations. These results confirm what has been discussed above: if the compensatory mutations are only of small importance (in this case due to the greater importance of the lethal mutations), the extinction threshold's dependence on the effect of the mutations is extremely low. Otherwise, the higher the deleterious effect of the mutations, the lower the mutation rate needed to extinguish the virus.

These three models are used to study different biological fitness landscapes, replication modes and infection dynamics. Figure 1 shows the effect of the different biological fitness landscapes on the extinction threshold. As has been commented, the extinction threshold obtained by Bull et al. (2007) is a lower limit due to the absence of compensatory mutations. The lower is the cost of mutations in Martin and Gandon (2010), the higher is the extinction threshold. Finally, the biophysical

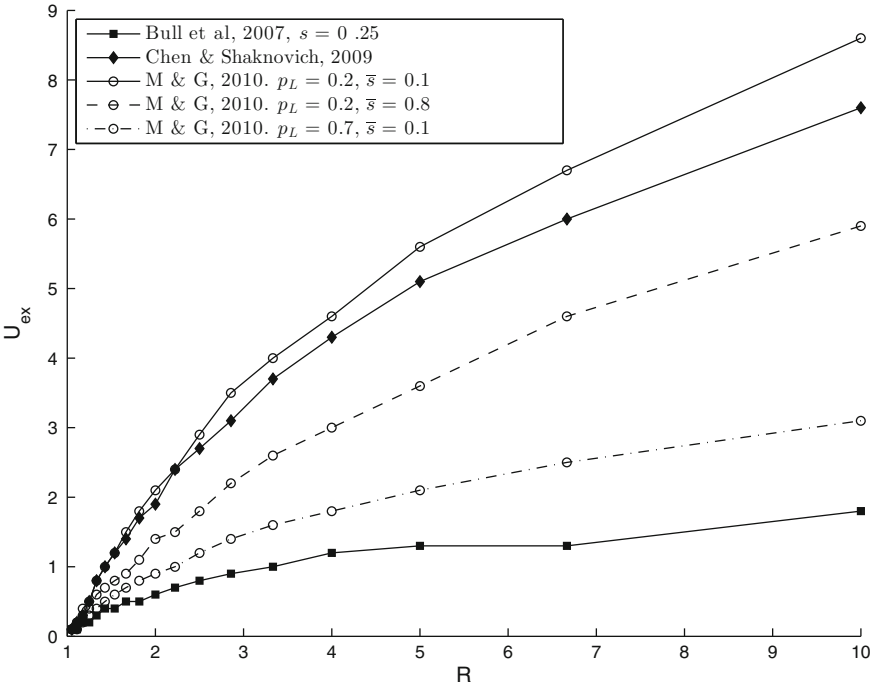

Fig. 1 Extinction threshold, U_{ex}, as a function of the Wrightian fitness, R. Results of simulating a simple stochastic model using a Gillespie algorithm (1977) with the three different fitness landscapes presented in the main text. *Symbols in the upper box* describe the three models used in the simulations; references are given in the text. Each point is obtained from 50 independent repetitions. The extinction threshold was taken as the mutation rate beyond which the populations got extinct in all simulations before a given final time. Therefore, this estimation must be considered an upper bound. The maximum population allowed in all the simulations was 1000 individuals. No cell infection dynamics was considered in Martin and Gandon (2010) model (M &G). In this model, p_L is the fraction of lethal mutations and $\overline{s}$ is the average selection coefficient of the mutations. In the (Bull et al. 2007) model, s is the selection coefficient. Simulations were carried out using Matlab®. Code is available at request

fitness landscape proposed by Chen and Shakhnovich (2009) determines an extinction threshold similar to that in which the average effect of mutations is not very high. Thus, despite these quantitative differences, the fundamental idea is the same in all the models: extinction by lethal mutagenesis is produced because an increase in the mutation rate displaces the mutation–selection equilibrium until the reproductive capacity of the population falls below a threshold beyond which it cannot maintain itself over time. Within this general framework, the differences between the three models, especially with respect to the biological fitness landscapes, give rise to three different predictions for the extinction threshold.

3.1 Lethality, Extinction and Error Catastrophe

According to some authors, an increase in the mutation rate can extinguish a population either by an excess of non-viable mutants or by an accumulation of errors "without limits" (Schuster 2011), in other words, by entry into error catastrophe. A similar idea had previously been proposed in Biebricher and Eigen (2006). Consequently, this leads to consider the relationship between entry into error catastrophe and extinction in the presence of lethality. When a quasispecies model is considered in a single-peak fitness landscape in the absence of lethality, extinction and entry into error catastrophe are mutually exclusive events (Bull et al. 2007, 2008). When the mutation rate increases, the population either becomes extinct or enters into error catastrophe, depending on whether or not the mutant phenotype is stable demographically, that is to say, whether it can self-maintain. Not only does this mean that entry into error catastrophe cannot explain population extinction due to an accumulation of mutations, but also that quite the reverse is true, in that only entry into error catastrophe can prevent the population from becoming extinct, as was mentioned earlier (Bull et al. 2007). The introduction of a fraction of lethal mutants $1 - p$, uniformly distributed over the sequence space, does not change this situation. The population either becomes extinct or enters into error catastrophe, depending on whether or not the mutant phenotype is stable demographically (Tejero et al. 2010) which, in this case, depends on the value of the fraction of lethal mutants.

This situation changes if we study a lethality distribution in which the self-replicative species has n "lethal positions", i.e. positions whose mutation generates lethal mutants. In this case, entry into error catastrophe and extinction are no longer mutually exclusive, since the lethality is not distributed uniformly. If the number of lethal positions in the sequence is low, the mutant phenotype can dominate the master phenotype when the mutation rate exceeds the error threshold. If the mutation rate continues to increase, the population—which would be in "error catastrophe"—will accumulate lethal mutants until its average productivity is less than zero and it becomes extinct. If, on the other hand, there are a high number of lethal positions, the population becomes extinct before entering error catastrophe (see Fig. 2). In this way, it is possible to define a "critical lethality", beyond which the error threshold disappears (Tejero et al. 2010). However, the mutation rate needed for the population to become extinct beyond the error threshold is always higher than the rate which occurs at high lethality rates. This means that the entry into "error catastrophe" hinders population extinction by lethal mutagenesis, as has been mentioned earlier (Bull et al. 2007) which, in turn, is a consequence of the fact that the dominance of the mutant phenotype over the master one is due to its greater mutational robustness. Lastly, it is important to highlight that, both before and after crossing the error threshold, extinction occurs because the average replicative capacity is lower than the degradation rate of the population. In this sense, we think that it is not possible to talk of two types of extinction, one associated with the entry into error catastrophe and the other independent of error catastrophe and, in fact,

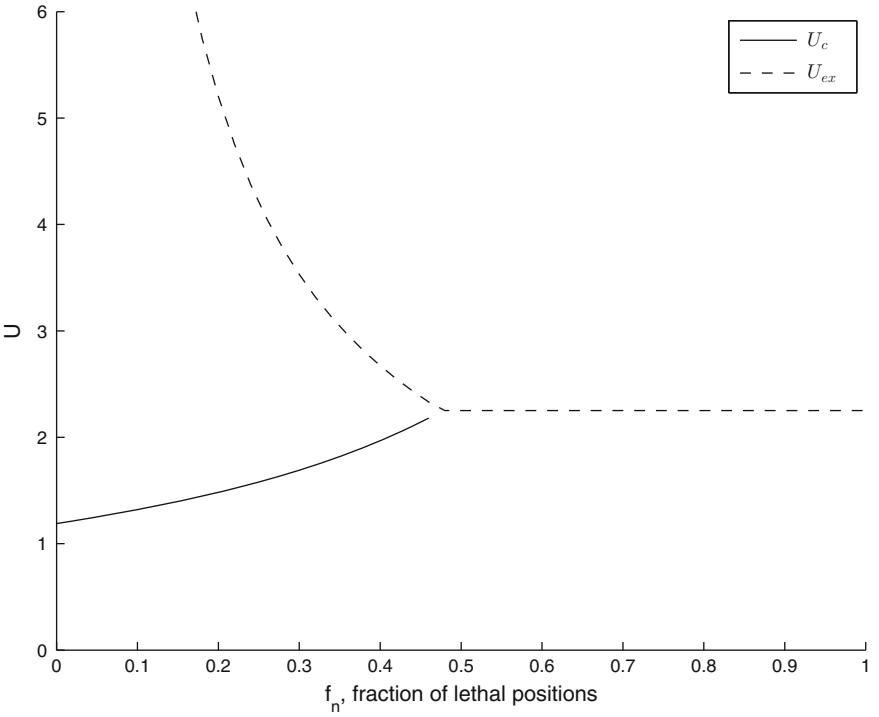

Fig. 2 Extinction and error thresholds as a function of the fraction of lethal mutations. U_c and U_{ex} are the error and extinction thresholds expressed in terms of the genomic mutation rate, $U = v(1 - q)$, where v is the genomic length and q the per digit quality factor. The Wrightian fitness of the master phenotype was $R_m = 10$ and that of the mutant phenotype was $R_k = 3$. The figure can be interpreted as a phase diagram. Below the error and the extinction thresholds, the population stays in a mutation–selection equilibrium. Above the extinction threshold, the population gets extinct. Above the error threshold, the population survives but enters into error catastrophe. In this case, critical lethality occurs at $f_n = 0.5$, so no error threshold appears for $f_n > 0.5$. See main text for further details

Fig. 2 shows a large region where the population is in a situation of error catastrophe but does not become extinct.

4 Lethal Defection

In conjunction with the models presented in the previous section, which are based solely on the effect of the mutation–selection equilibrium on the demographic behaviour of a quasispecies, there is also an alternative model in which the participation of a subpopulation of mutant viruses, known as defectors, is considered an essential factor in the extinction of a population. This section provides a brief

introduction to the experimental basis of this hypothesis and the theoretical model which explains it.

One of the characteristics of viral quasispecies is the suppression of variants with high biological fitness by the spectrum of mutants which accompany them (de la Torre and Holland 1990; Domingo et al. 2006, 2012). This phenomenon partly motivated the study of the interfering capacity of pre-extinction genomes in FMDV (Gonzalez-Lopez et al. 2004). Subsequent work with LCMV indicated that viral infectivity was lost much earlier than replicative capacity during the extinction by mutagenesis (Grande-Pérez et al. 2005) (see also Chap. 10). On the basis of these results, the hypothesis was made that the mutagenesis of a RNA virus would result in a subgroup of interfering mutant viruses, known as defectors, which would play a crucial role in the extinction of the virus. This hypothesis was called lethal defection (Grande-Pérez et al. 2005). Later experiments have confirmed the important role that defective and defector mutants play in the extinction of an RNA virus by increased mutation rate (see Chap. 14).

4.1 Stochastic Extinction Model

The origin of the lethal defection hypothesis is closely connected to the development of computational models and in silico studies (Grande-Pérez et al. 2005). The first model which was proposed to explain extinction by lethal defection was the stochastic extinction model (Iranzo and Manrubia 2009). Basically, the lethal defection model of Manrubia and Iranzo considered that viruses code two phenotypic traits: replicative capacity and infectivity, the latter being associated with the capacity to code the proteins needed for replication. The first trait acts solely in cis, while the second acts in trans. In virology, the terms interaction in cis or in trans are used to describe whether the action of a genetically coded element (a genomic sequence, secondary or tertiary RNA structure, protein, etc.) takes place with the genome that codes it, in which case it is called interaction in cis, or whether it takes place with other genomes, in which case it is an interaction in trans (see also Chap. 14). During replication, the viruses accumulate mutations that may affect both their replicative capacity and their infectivity. These mutations may be beneficial or deleterious. However, the effect of the mutations on both traits is coupled, since the model considers that the loss of infectivity by mutations means that the mutations simultaneously decrease their replicative capacity and vice versa, and the restoration of the infective capacity means that their replicative capacity increases. The viruses that code functional proteins are called viable, while those that have undergone mutations are called defective. In this way, the population's reproductive capacity is proportional to the number of viable viruses, and when these disappear, the population becomes extinct.

This model predicts that when a mutation rate is high enough, the population becomes extinct regardless of the presence of defectives in the population and at the same mutation rate value. This value is equivalent to the deterministic extinction

threshold. However, when the population size is small enough and the mutation rate is relatively low, the behaviour is qualitatively different: if there are no defectives, the population continues to exist over time, but if they are present, the population eventually becomes extinct, since the defective mutants displace the viable viruses (Grande-Pérez et al. 2005). This extinction is known as stochastic extinction (Iranzo and Manrubia 2009). Ultimately, what occurs is the fixation of the defective mutants as a consequence of the genetic drift effect and, therefore, the smaller the population size, the higher the likelihood of its occurrence.

Although the model of lethal defection by stochastic extinction can explain the extinction of a population by accumulation of defective viruses, it has several limitations. Firstly, the model is very dependent on the coupling of the effect of the mutations on the two phenotypic traits and the defective viruses not having a higher replicative capacity that the viable ones. If either of these assumptions are not complied with, the defectives will get fixed, extinguishing the population, at any mutation rate. Secondly, as the authors themselves acknowledge (Manrubia et al. 2010), this model does not explain the action of lethal defection in lytic infections, even though a large part of the experimental phenomenology on which the lethal defection hypothesis is based comes from lytic viruses (Gonzalez-Lopez et al. 2004; Perales et al. 2007). Furthermore, the model only explains extinction when the population sizes are relatively small (Iranzo and Manrubia 2009). In this regard, although the population sizes of RNA viruses can be extremely large in lytic and persistent infections, both inside and outside the cells, it is also true that not all viral genomes inside a cell are replicating, and this could significantly decrease the effective size of the population, thus facilitating stochastic extinction. (See also Chaps. 10 and 14 for discussion of the lethal defection model in connection with experimental results.)

4.2 Interference, Complementation and Lethal Defection

Interference and complementation interactions in RNA virus quasispecies are a phenomenon whose importance is increasingly recognised (Shirogane et al. 2013; Manrubia 2012; Perales et al. 2012) (Chap. 10). In this regard, the effect of defectors or defective mutants on lethal mutagenesis can also be explained by the complementation–interference interactions they establish with the rest of the virus. It must be recalled that, in most of the cases in which a high-fitness virus interacts in trans with a mutant virus with lower fitness, the fitness of the former decreases, whereas that of the mutant increases. The fitness loss of the higher fitness variant is called interference. Complementation is, on the other hand, the gain of fitness by the mutant virus. Thus, interference and complementation can be seen as two sides of the same interaction. In virology, complementation can also refer to the process by which two low-fitness viruses complement each other to increase their fitness. This case will not be considered here.

Several authors have studied, theoretically and computationally, the effect of complementation on the mutation–selection equilibrium of RNA viruses (Froissart et al.

2004; Wilke and Novella 2003; Gao and Feldman 2009; Novella et al. 2004). The main result of all these papers is that complementation displaces the mutation–selection equilibrium to higher frequencies of the mutant allele. Essentially, what happens is that complementation, by permitting the mutant allele to partially take advantage of the biological fitness of the wild-type allele, decreases the selective disadvantage of this allele with respect to the wild-type one, which in turn decreases the effect of natural selection. This also explains why, in a quasispecies, complementation makes error threshold occur at lower mutation rates (Sardanyés and Elena 2010).

In Moreno et al. (2012), a computational model based on interference–complementation interactions was developed to find out to what extent lethal defection can explain the effect of the initial MOI on lethal mutagenesis in certain viruses. Besides considering various phenotypic traits, the model was characterised by its consideration of a partial trans interaction and for coupling, in a nested way, the intra- and extracellular dynamics of RNA virus infections. This study also showed how the presence of trans interactions increases the percentage of inhibition of the virus titre, caused by an increase in the mutation rate. A simplified version of this model shows that the interfering action of the defective viruses causes the population to become extinct at lower mutation rates, and that this effect depends on the degree of trans interaction in the quasispecies (Tejero 2013).

The main criticism of a lethal defection model based on interference–complementation interactions is based on the fact that when population size decreases during the extinction process, interactions in the quasispecies become increasingly infrequent. Ultimately, this means that although the viral load may be lower in the presence of interference at intermediate mutation rates, the population's extinction threshold does not depend on lethal defection (Steinmeyer and Wilke 2009). However, this criticism does not take into account the fact that when the extracellular dynamic is considered, even when a single virus infects a cell, interference may be produced during the intracellular replication process among the progeny of the virus. The importance of this phenomenon will vary, depending on the replication mode of the virus (Sardanyés et al. 2009; Sardanyés and Elena 2011).

Despite its differences, and although the importance of lethal defection can depend on the biological characteristics of the virus and of the infection, the two models of lethal defection predict that it will always decrease both the extinction and the error threshold.

5 Problems of Lethal Mutagenesis

5.1 Resistance and Survival of Flattest

Like any other antiviral therapy, lethal mutagenesis will face the development of resistances. In this case, the resistances will be selected for their capacity to mitigate the effect of the mutations on the fitness of the virus. In addition to the classic

drug-resistant mutants, which can recognise and prevent the incorporation of a specific mutagen, and the fidelity mutants, i.e. viruses which have a lower mutation rate both in the presence and absence of mutagen drugs (see the Chap. 13 by Marco Vignuzzi in this book), RNA viruses may develop a resistance to lethal mutagenesis by evolving towards mutationally more robust regions of sequence space. As has been discussed in Sect. 2.1, when discussing the possibility that entry into error catastrophe hinders extinction by lethal mutagenesis, this mechanism is known as the *survival of the flattest*. Although this phenomenon has been observed experimentally (Codoñer et al. 2006; Sanjuán et al. 2007; Graci et al. 2011), it has not been proved that treatment with mutagens increases the mutational robustness of LCMV (Martín et al. 2008), nor has it been proved that a virus has escaped mutagenic treatments by increasing its robustness. Moreover, the only theoretical study that has addressed this point considers robustness unlikely to affect lethal mutagenesis, chiefly because of the difference in the timescales of acquisition of mutational robustness and increased mutagenesis (O'Dea et al. 2010).

5.2 Sublethal Mutagenesis

The second possible problem raised by mutagen therapies is "sublethal mutagenesis" or, to put it another way, an increase in the mutation rate which is not enough to extinguish the virus. Taking into account the role of mutations in evolution, some authors have suggested that sublethal doses of a mutagenic drug may increase the adaptability of a virus, which could be counterproductive clinically (Pillai et al. 2008), as it facilitates escape from the immune system or the appearance of mutants that are resistant to drugs, irrespective of whether they are mutagenic or non-mutagenic. This possibility has been demonstrated experimentally in the case of mutations that make the FMDV less sensitive to ribavirin. Thus, while it is possible to obtain a ribavirin-resistant mutant when it is subjected to serial passages in the presence of increasing concentrations of ribavirin (Sierra et al. 2007), when faced with high concentrations of ribavirin from the start, the virus does not dominate and the population becomes extinct (Perales et al. 2009). Another example of this effect is the change in the result with respect to interactions with other drugs, such as replication inhibitors (Iranzo et al. 2011). In this case, it can be seen that the combined action of certain dosages of mutagens and inhibitors is antagonistic—the mutagen diminishes the effect of the inhibitor—instead of synergistic due, mainly, to the increased probability that mutants resistant to the inhibitor will appear. (This point is treated in Chap. 14.)

Finally, sublethal mutagenesis can also occur due to the appearance of resistant mutants (either fidelity or drug-resistant ones) which convert lethal doses of mutagen into sublethal doses, with the risks mentioned above. Drug resistances are usually partial resistances which often allow the virus to gain biological fitness in the presence of the drug thanks to compensatory mutations. The consequence of a resistant or fidelity mutant appearing is that it will incorporate fewer mutations per

genome, which will displace the quasispecies to a region of sublethal mutagenesis, with the additional problem, at least in theory, that in this region an increase in adaptability will make the acquisition of compensatory mutations more likely.

6 Concluding Remarks

In this chapter, we have reviewed the main contributions of mathematical modelling to the theory of lethal mutagenesis produced in the last decades. Since the pioneer works of Manfred Eigen and Peter Schuster in the seventies of the twentieth century, the modelling of molecular evolution has achieved a period of great success that has allowed to disentangle reasonably the complex behaviour of populations of error-prone replicators (e.g. RNA viruses) in terms of the mutation rate and the fitness landscape. We find here one of the most appealing examples of how mathematical modelling has fostered new questions and concepts, and consequently, it has suggested new experiments. Besides, the mathematical formulation of these biological problems has attracted the attention of scientists from other fields, namely mathematics, physics and chemistry that have accelerated the progress of this theory more than ever before. This interdisciplinary interest has allowed the application of similar models to study the evolution of some kind of tumour lineages (Solé and Deisboeck 2004; Solé et al. 2014).

One of the central concepts of the quasispecies theory is the error threshold which, as it has been extensively described in the previous sections, quantifies the mutation rate below which the information codified in the master phenotype is surely maintained in the next generations (see also Chaps. 1 and 5). On the contrary, if the mutation rate is above this threshold, the presence of the wild phenotype in the population is no longer assured. This mathematical result was immediately borrowed by virologists as a possible therapy to drop the infectiveness of some RNA viruses by using mutagenic drugs. The strategy seems to be evident: to increase the mutation rate of the virus in order to cause the disappearance of the wild-type (more infective) copy. Implicitly, it was assumed that the extinction of the master was equivalent to the extinction of the whole population. Unfortunately, reality is more complex than mathematical models portray. As some experiments with mutagens presented the feasibility of lethal mutagenesis, the debate about the real meaning of the error catastrophe and its role as a therapy against virus infections was taken up again. To shed some light in the discussion, new mathematical models considered other factors that are essential for the extinction of the quasispecies, concretely the extinction threshold and the phenotype interactions within the quasispecies distribution. As this article has pointed out, a clear distinction between the error and extinction thresholds is required if we want to design an optimal therapy based on lethal mutagenesis. Furthermore, the existence of interactions among phenotypes can modify both thresholds and the relation between them and consequently the response of the whole population to a hypothetical

increase of the mutation rate. These, among others, are open questions that have to be answered necessarily by a close collaboration between theoretical and experimental groups.

Acknowledgments This paper has been supported in part by Grants no. BFU2012-39816-C02-02 from MINECO (Spain). Héctor Tejero was supported by AP2006-01044, from MEC (Spain) and Marie-Curie Career Integration Grant (CIG). CIG334361. Guillaume Martin and Sylvain Gandon kindly gave us the code necessary to simulate its model.

References

Biebricher C, Eigen M (2005) The error threshold. Virus Res 107(2):117–127

Biebricher C, Eigen M (2006) What is a quasispecies? Curr Top Microbiol Immunol 299:1–31

Bonnaz D, Koch AJ (1998) Stochastic model of evolving populations. J Phys A: Math Gen 31:417–429

Bull JJ, Wilke CO (2008) Lethal mutagenesis of bacteria. Genetics 180(2):1061–1070. doi:10.1534/genetics.108.091413

Bull JJ, Meyers LA, Lachmann M (2005) Quasispecies made simple. PLoS Comput Biol 1(6):e61

Bull JJ, Sanjuan R, Wilke CO (2007) Theory of lethal mutagenesis for viruses. J Virol 81(6):2930–2939

Bull JJ, Sanjuán R, Wilke CO (2008) Lethal mutagenesis. In: Domingo E, Parrish CR, Holland JJ (eds) Origin and evolution of viruses. Elsevier Academic Press, Amsterdam

Bull JJ, Joyce P, Gladstone E, Molineux IJ (2013) Empirical complexities in the genetic foundations of lethal mutagenesis. Genetics 195(2):541–552. doi:10.1534/genetics.113.154195

Cameron CE, Castro C (2001) The mechanism of action of ribavirin: lethal mutagenesis of RNA virus genomes mediated by the viral RNA-dependent RNA polymerase. Curr Opin Infect Dis 14(6):757–764

Chen P, Shakhnovich E (2009) Lethal mutagenesis in viruses and bacteria. Genetics 183(2):639–650. doi:10.1534/genetics.109.106492

Codoñer FM, Darós JA, Solé RV, Elena SF (2006) The fittest versus the flattest: experimental confirmation of the quasispecies effect with subviral pathogens. PLoS Pathog 2(12):e136. doi:10.1371/journal.ppat.0020136

Cowperthwaite MC, Economo EP, Harcombe WR, Miller EL, Meyers LA (2008) The ascent of the abundant: how mutational networks constrain evolution. PLoS Comput Biol 4(7):e1000110. doi:10.1371/journal.pcbi.1000110

de la Torre J, Holland J (1990) RNA virus quasispecies populations can suppress vastly superior mutant progeny. J Virol 64(12):6278–6281

Domingo E, Sabo D, Taniguchi T, Weissmann C (1978) Nucleotide sequence heterogeneity of an RNA phage population. Cell 13(4):735–744

Domingo E, Martin V, Perales C, Grande-Perez A, Garcia-Arriaza J, Arias A (2006) Viruses as quasispecies: biological implications. Curr Top Microbiol Immunol 299:51–82

Domingo E, Sheldon J, Perales C (2012) Viral quasispecies evolution. Microbiol Mol Biol Rev 76(2):159–216. doi:10.1128/mmbr.05023-11

Eigen M (1971) Self-organization of matter and the evolution of biological macromolecules. Naturwissenschaften 58(10):465–523

Eigen M (1993) The fifth Paul Ehrlich lecture. Virus strains as models of molecular evolution. Med Res Rev 13(4):385–398

Eigen M (2002) Error catastrophe and antiviral strategy. Proc Natl Acad Sci USA 99(21):13374–13376

Eigen M, Schuster P (1979) The hypercycle: a principle of natural self-organization. Springer, Berlin
Froissart R, Wilke CO, Montville R, Remold SK, Chao L, Turner PE (2004) Co-infection weakens selection against epistatic mutations in RNA viruses. Genetics 168(1):9–19. doi:10.1534/genetics.104.030205
Gao H, Feldman MW (2009) Complementation and epistasis in viral coinfection dynamics. Genetics 182(1):251–263. doi:10.1534/genetics.108.099796
Gillespie DT (1977) Exact stochastic simulation of coupled chemical reactions. J Phys Chem 81 (25):2340–2361
Gonzalez-Lopez C, Arias A, Pariente N, Gomez-Mariano G, Domingo E (2004) Preextinction viral RNA can interfere with infectivity. J Virol 78(7):3319–3324
Graci JD, Gnädig NF, Galarraga JE, Castro C, Vignuzzi M, Cameron CE (2011) Mutational robustness of an RNA virus influences sensitivity to lethal mutagenesis. J Virol. doi:10.1128/jvi.05712-11
Grande-Pérez A, Lázaro E, Lowenstein P, Domingo E, Manrubia S (2005) Suppression of viral infectivity through lethal defection. Proc Natl Acad Sci USA 102(12):4448–4452
Hermisson J, Redner O, Wagner H, Baake E (2002) Mutation-selection balance: ancestry, load, and maximum principle. Theor Popul Biol 62(1):9–46. doi:10.1006/tpbi.2002.1582
Holland JJ, Domingo E, de la Torre JC, Steinhauer DA (1990) Mutation frequencies at defined single codon sites in vesicular stomatitis virus and poliovirus can be increased only slightly by chemical mutagenesis. J Virol 64(8):3960–3962
Iranzo J, Manrubia S (2009) Stochastic extinction of viral infectivity through the action of defectors. EPL (Europhys Lett) 85(1):18001
Iranzo J, Perales C, Domingo E, Manrubia SC (2011) Tempo and mode of inhibitor–mutagen antiviral therapies: a multidisciplinary approach. Proc Natl Acad Sci. doi:10.1073/pnas.1110489108
Kimura M, Maruyama T (1966) The mutational load with epistatic gene interactions in fitness. Genetics 54(6):1337–1351
Loeb LA, Essigmann JM, Kazazi F, Zhang J, Rose KD, Mullins JI (1999) Lethal mutagenesis of HIV with mutagenic nucleoside analogs. Proc Natl Acad Sci USA 96(4):1492–1497
Manrubia SC (2012) Modelling viral evolution and adaptation: challenges and rewards. Curr Opin Virol 2(5):531–537. doi:10.1016/j.coviro.2012.06.006
Manrubia S, Domingo E, Lázaro E (2010) Pathways to extinction: beyond the error threshold. Philos Trans R Soc Lond B Biol Sci 365(1548):1943–1952. doi:10.1098/rstb.2010.0076
Martin G, Gandon S (2010) Lethal mutagenesis and evolutionary epidemiology. Philos Trans R Soc Lond B Biol Sci 365(1548):1953–1963. doi:10.1098/rstb.2010.0058
Martín V, Grande-Pérez A, Domingo E (2008) No evidence of selection for mutational robustness during lethal mutagenesis of lymphocytic choriomeningitis virus. Virology 378(1):185–192
Moreno H, Tejero H, de la Torre JC, Domingo E, Martín V (2012) Mutagenesis-mediated virus extinction: virus-dependent effect of viral load on sensitivity to lethal defection. PLoS ONE 7 (3):e32550. doi:10.1371/journal.pone.0032550
Novella IS, Reissig DD, Wilke CO (2004) Density-dependent selection in vesicular stomatitis virus. J Virol 78(11):5799–5804. doi:10.1128/jvi.78.11.5799-5804.2004
Nowak M, May R (2000) Virus dynamics. Mathematical principles of immunology and virology. Oxford University Press, Oxford
Obermayer B, Frey E (2010) Error thresholds for self- and cross-specific enzymatic replication. J Theor Biol. doi:10.1016/j.jtbi.2010.09.016
O'Dea EB, Keller TE, Wilke CO (2010) Does mutational robustness inhibit extinction by lethal mutagenesis in viral populations? PLoS Comput Biol 6(6):e1000811. doi:10.1371/journal.pcbi.1000811
Perales C, Mateo R, Mateu MG, Domingo E (2007) Insights into RNA virus mutant spectrum and lethal mutagenesis events: replicative interference and complementation by multiple point mutants. J Mol Biol 369(4):985–1000. doi:10.1016/j.jmb.2007.03.074

Perales C, Agudo R, Tejero H, Manrubia SC, Domingo E (2009) Potential benefits of sequential inhibitor-mutagen treatments of RNA virus infections. PLoS Pathog 5(11):e1000658. doi:10.1371/journal.ppat.1000658

Perales C, Iranzo J, Manrubia SC, Domingo E (2012) The impact of quasispecies dynamics on the use of therapeutics. Trends Microbiol 20(12):595–603. doi:10.1016/j.tim.2012.08.010

Pillai S, Wong J, Barbour J (2008) Turning up the volume on mutational pressure: Is more of a good thing always better? (A case study of HIV-1 Vif and APOBEC3). Retrovirology 5(1):26

Sanjuán R, Cuevas JM, Furió V, Holmes EC, Moya A (2007) Selection for robustness in mutagenized RNA viruses. PLoS Genet 3(6):e93

Sardanyés J, Elena SF (2010) Error threshold in RNA quasispecies models with complementation. J Theor Biol 265(3):278–286. doi:10.1016/j.jtbi.2010.05.018

Sardanyés J, Elena SF (2011) Quasispecies spatial models for RNA viruses with different replication modes and infection strategies. PLoS ONE 6(9):e24884. doi:10.1371/journal.pone.0024884

Sardanyes J, Simo C, Martinez R, Sole RV, Elena SF (2014) Variability in mutational fitness effects prevents full lethal transitions in large quasispecies populations. Sci Rep 4. doi:10.1038/srep04625. http://www.nature.com/srep/2014/140409/srep04625/abs/srep04625.html#supplementary-information

Sardanyés J, Solé R, Elena S (2009) Replication mode and landscape topology differentially affect RNA virus mutational load and robustness. J Virol 83(23):12579–12589. doi:10.1128/JVI.00767-09

Schuster P (2010) Mathematical modeling of evolution. Solved and open problems. Theory in biosciences. doi:10.1007/s12064-010-0110-z

Schuster P (2011) Lethal mutagenesis, error thresholds, and the fight against viruses: rigorous modeling is facilitated by a firm physical background. Complexity 17(2):5–9. doi:10.1002/cplx.20399

Shirogane Y, Watanabe S, Yanagi Y (2013) Cooperation: another mechanism of viral evolution. Trends Microbiol 21(7):320–324. doi:10.1016/j.tim.2013.05.004

Sierra M, Airaksinen A, Gonzalez-Lopez C, Agudo R, Arias A, Domingo E (2007) Foot-and-mouth disease virus mutant with decreased sensitivity to ribavirin: implications for error catastrophe. J Virol 81(4):2012–2024

Solé RV, Deisboeck TS (2004) An error catastrophe in cancer? J Theor Biol 228(1):47–54

Solé RV, Valverde S, Rodriguez-Caso C, Sardanyés J (2014) Can a minimal replicating construct be identified as the embodiment of cancer? BioEssays 36(5):503–512. doi:10.1002/bies.201300098

Steinmeyer S, Wilke C (2009) Lethal mutagenesis in a structured environment. J Theor Biol 261(1):67–73. doi:10.1016/j.jtbi.2009.07.014

Summers J, Litwin S (2006) Examining the theory of error catastrophe. J Virol 80(1):20–26. doi:10.1128/jvi.80.1.20-26.2006

Takeuchi N, Hogeweg P (2007) Error-threshold exists in fitness landscapes with lethal mutants. BMC Evol Biol 7(15)

Takeuchi N, Poorthuis P, Hogeweg P (2005) Phenotypic error threshold; additivity and epistasis in RNA evolution. BMC Evol Biol 5(1):9. doi:10.1186/1471-2148-5-9

Tejero H (2013) Mutación y extinción: de la catástrofe de error a la defección letal. Universidad Complutense de Madrid

Tejero H, Marín A, Montero F (2010) Effect of lethality on the extinction and on the error threshold of quasispecies. J Theor Biol 262(4):733–741. doi:10.1016/j.jtbi.2009.10.011

Tejero H, Marin A, Montero F (2011) The relationship between the error catastrophe, survival of the flattest, and natural selection. BMC Evol Biol 11(1):2

Wagner GP, Krall P (1993) What is the difference between models of error thresholds and Muller's ratchet? J Math Biol 32(1):33–44

Wilke CO (2005) Quasispecies theory in the context of population genetics. BMC Evol Biol 5(44)

Wilke C, Novella I (2003) Phenotypic mixing and hiding may contribute to memory in viral quasispecies. BMC Microbiol 3(1):11

Wu B, Gokhale CS, van Veelen M, Wang L, Traulsen A (2013) Interpretations arising from Wrightian and Malthusian fitness under strong frequency dependent selection. Ecol Evol 3 (5):1276–1280. doi:10.1002/ece3.500

Wylie CS, Shakhnovich EI (2011) A biophysical protein folding model accounts for most mutational fitness effects in viruses. Proc Natl Acad Sci 108(24):9916–9921. doi:10.1073/pnas.1017572108

Wylie CS, Shakhnovich EI (2012) Mutation induced extinction in finite populations: lethal mutagenesis and lethal isolation. PLoS Comput Biol 8(8):e1002609. doi:10.1371/journal.pcbi.1002609

Estimating Fitness of Viral Quasispecies from Next-Generation Sequencing Data

David Seifert and Niko Beerenwinkel

Abstract The quasispecies model is ubiquitous in the study of viruses. While having lead to a number of insights that have stood the test of time, the quasispecies model has mostly been discussed in a theoretical fashion with little support of data. With next-generation sequencing (NGS), this situation is changing and a wealth of data can now be produced in a time- and cost-efficient manner. NGS can, after removal of technical errors, yield an exceedingly detailed picture of the viral population structure. The widespread availability of cross-sectional data can be used to study fitness landscapes of viral populations in the quasispecies model. This chapter highlights methods that estimate the strength of selection in selective sweeps, assesses marginal fitness effects of quasispecies, and finally infers the fitness landscape of a viral quasispecies, all on the basis of NGS data.

Contents

1 Introduction 182
1.1 Viral Evolution 182
1.2 Fitness Landscapes 183
1.3 Next-Generation Sequencing 184
2 Methods for Determining Quasispecies Composition 186
2.1 Experimental Approaches to Haplotype Inference 186
2.2 Error Correction of Reads 187
2.3 Viral Haplotype Assembly 188
3 Methods for Estimating Viral Fitness 190

D. Seifert · N. Beerenwinkel (✉)
ETH Zurich, Basel, Switzerland
e-mail: niko.beerenwinkel@bsse.ethz.ch

D. Seifert
e-mail: david.seifert@bsse.ethz.ch

Current Topics in Microbiology and Immunology (2016) 392: 181–200
DOI 10.1007/82_2015_462

Published Online: 30 August 2015

3.1 Selective Sweeps After Recent Population Bottlenecks in Viral Populations 190
3.2 Determining Marginal Fitness Effects by Next-Generation Sequencing 192
3.3 Fitness Estimation from Equilibrium Quasispecies Distribution 194
4 Conclusions 198
References 199

1 Introduction

The quasispecies model is ubiquitous in evolutionary virology. Historically, viral populations could only be analyzed with molecular biology tools, such as gel electrophoresis, that provide only little insight into the genetic composition of viral populations. In this chapter, a number of methods aimed at analyzing viral mutant spectra and their fitness using modern next-generation sequencing (NGS) data are illustrated.

1.1 Viral Evolution

RNA viruses are at the lower end of the biological complexity spectrum. With their small genomes, RNA viruses usually possess a select few number of genes. This is exacerbated, for instance, as the lack of a proofreading mechanism in the RNA-dependent RNA polymerase of RNA viruses results in a high mutation rate. These dynamics lead to a rate of exploration of sequence space that is orders of magnitude larger than those known for even the most primitive prokaryotic organisms. All of these properties make viruses attractive model systems for studying evolution.

The aforementioned high mutation rate results in a system of RNA replicators or viruses that are coupled by mutation. This collection of closely coupled viruses has been termed a (viral) quasispecies. In the context of virology, single RNA sequences of a quasispecies have been termed haplotypes, genotypes, or viral strains. The central tenet governing the temporal evolution of a quasispecies consisting of m different haplotypes is the quasispecies equation

$$\frac{\mathrm{d}}{\mathrm{d}t}p_i(t) = \sum_{j=1}^{m} p_j(t) f_j q_{ji} - p_i(t) \sum_{j=1}^{m} p_j(t) f_j, \quad i \in \{1, \ldots, m\} \tag{1}$$

where t denotes time, $p_i(t)$ denotes the relative frequency of haplotype i at time t, f_i denotes the reproductive fitness of haplotype i, and q_{ij} denotes the probability of haplotype i mutating into haplotype j upon replication.

In quasispecies theory, due to the high mutation rate, selection will, in general, not select for a single highly fit haplotype. Instead, in quasispecies theory, the unit of selection is a group of highly similar haplotypes, contrary to classical Darwinian evolution. It has first been shown for digital organisms that for very high mutation

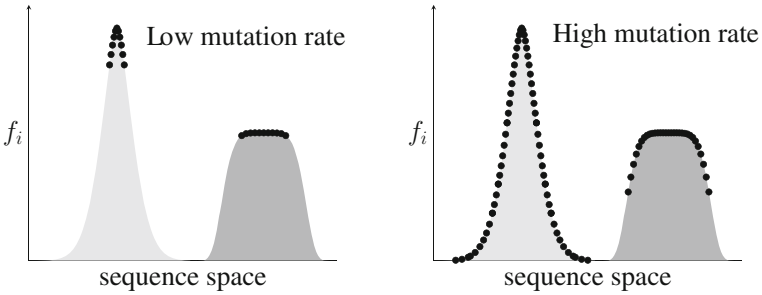

Fig. 1 Schematic representation of two different fitness landscapes on a continuous sequence space. In regimes with low mutations rates as depicted on the *left*, haplotypes with fitness landscapes possessing higher peaks will outcompete populations of haplotypes with fitness landscapes with lower maximum peaks, resembling the classical Darwinian survival-of-the-fittest effect. Under high mutation rates, however, the situation changes as illustrated on the *right*. Fitness landscapes where haplotypes possess more uniform fitness rates albeit lower than the maximum of other fitness landscapes can outcompete quasispecies with haplotypes possessing higher maximum fitness. This is due to improved coupling in the more uniform case, where newly produced haplotypes are less likely to be nonviable and participate in the growth of the population. [Adapted from Sanjuán et al. (2007)]

rates, a quasispecies with a lower maximum albeit higher average fitness can outcompete a quasispecies with a higher maximum fitness but lower overall average fitness (Wilke et al. 2001). This effect derives from the fact that quasispecies with more similar fitness values allow for faster overall growth of haplotypes than a quasispecies where most of the growth stems from very few haplotypes that cannot count on back mutation from their neighbors. This survival-of-the-flattest effect is illustrated in Fig. 1.

1.2 Fitness Landscapes

Studies of viral evolution are intrinsically linked to the studies of viral fitness landscapes. Wright (1932) defined a fitness landscape as the association of a positive real value, namely the replicative capacity, to each haplotype. More generally, viral fitness landscapes can be described as a function of the virus, the host, and their interactions. Fitness landscapes determine the course of evolution and are of interest in clinical practice, as they determine the evolution of drug resistance and hence clinical outcomes (Beerenwinkel et al. 2013). Selection acts on a population when haplotypes in the population differ in their fitness. Currently, little is known about intra-patient in vivo fitness landscapes, as fitness landscapes are a function of the host environment. Imitating such conditions in vitro in order to measure in vivo fitness landscapes is practically impossible.

We consider a binary genome consisting of L loci, where the allele at the ith locus is denoted by $x_i \in \{0, 1\}$. Each locus harbors either a wild-type 0 or mutant

allele 1. A fitness landscape on this genotype space is a mapping $f : \{0,1\}^L \to \mathbb{R}_+$, assigning to each genotype its growth rate. In the quasispecies Eq. (1), these growth rates are the fitness parameters $f_i,\ i \in \{1,\ldots,m\}$. For mathematical convenience, we prefer to write the fitness landscape as $f = \exp(w)$. The properties of the fitness landscape are equally captured by the log-fitness landscape $w : \{0,1\}^L \to \mathbb{R}$, which can be decomposed as:

$$w(x_1,\ldots,x_L) = \beta_{\text{wt}} + \sum_{i=1}^{L} \beta_i x_i + \sum_{i=1}^{L-1} \sum_{j=i+1}^{L} \beta_{ij} x_i x_j + \sum_{i=1}^{L-2} \sum_{j=i+1}^{L-1} \sum_{k=j+1}^{L} \beta_{ijk} x_i x_j x_k + \cdots \tag{2}$$

where β_{wt} denotes the wild-type fitness, β_i denotes the additive effects of the mutant alleles x_i, and β_{ij} is the pairwise effects of mutant alleles x_i and x_j acting in concert. Higher order nonlinear effects are denoted by terms involving more than two indices.

The higher order nonlinear effects contributing to fitness by the specific co-occurrence of two alleles at different loci are termed epistasis, an important feature of fitness landscapes (Wolf et al. 2000). The synergistic epistatic effect is, for instance, important in active sites of most enzymes, where only the simultaneous combination of specific alleles yields a functional molecule. Similarly, compensatory mutations in drug escape variants exist due to (positive) epistatic contributions to overall fitness (Fig. 2). In HIV, pairwise epistasis has been shown to be an important part of the fitness landscapes inferred from in vitro data (Hinkley et al. 2011). Beerenwinkel et al. (2007) have analyzed the combinatorial geometry of fitness landscapes. In HIV, they found evidence for both positive and negative pairwise epistasis depending on the genetic background, and they inferred the shape of a bi-allelic three-locus fitness landscape.

1.3 Next-Generation Sequencing

NGS is an umbrella term for a collection of technologies to infer the composition of DNA or RNA molecules in a highly parallel fashion. Previously, characterization of viral populations required cumbersome and laborious serial dilution assays with follow-up capillary sequencing. Nowadays, NGS provides more efficient ways of determining the genetic composition of an intra-host viral population.

In order to determine the genetic composition of a sample, all NGS technologies require fragmenting large DNA molecules into smaller fragments. A unifying feature of current NGS technologies is the massively parallel detection of these fragments. Historically, 454 was the first company to bring NGS to the market. The pyrosequencing technology championed by 454 has first been applied to HIV-1 by

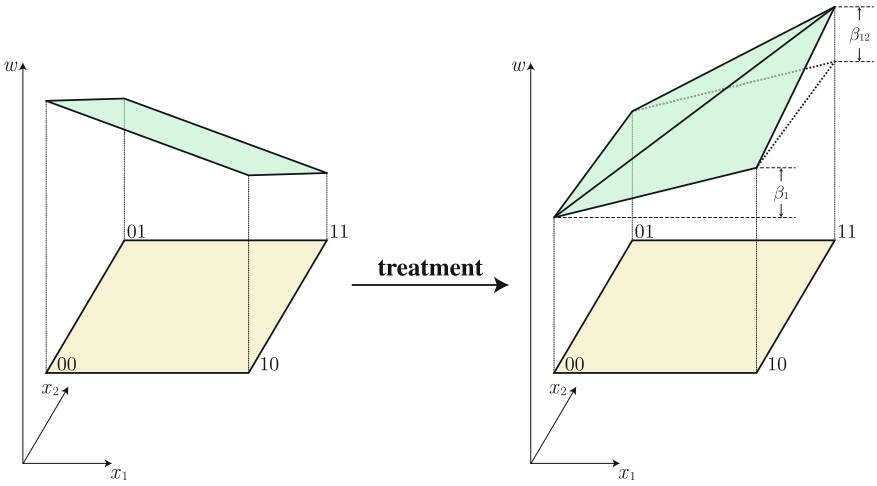

Fig. 2 Schematic of a bi-allelic two-locus fitness landscape. On the *left-hand side* is the depiction of a viral fitness landscape in a treatment-naive patient, where mutants only decrease the overall fitness with respect to the wild type and no epistasis is present. Under treatment, the fitness landscape drastically changes as shown on the *right*, where the wild-type haplotype 00 is the least fit. Here, x_1 represents the locus which confers resistance to the drug when mutated. Notice that the additive effect of mutant allele $x_2 = 1$ is $\beta_2 = 0$. By itself the second mutant allele does not add to overall fitness, but in concert with the drug resistance allele, it contributes a factor of β_{12} to restoring fitness to near pre-treatment levels. Thus, the second mutant allele represents an epistatic compensatory mutation

Wang et al. (2007), where the authors showed that NGS is capable of detection variants at far lower frequencies than with traditional Sanger sequencing.

NGS technologies can be divided into two classes. The first class can analyze a massive amount of fragments albeit of smaller size. This class is mainly driven by the technologies of Illumina and formerly 454. The second class has been pioneered by Pacific Biosciences and targets much longer but fewer reads. Both platforms have different strengths and see different practical applications. Ultra-deep sampling of populations is routinely performed with Illumina, while long haplotype phasing is performed with Pacific Biosciences.

Illumina performs sequencing by employing nucleotides with different fluorescent tags. For a prepared sequence, in every sequencing cycle, a mix of these fluorescent labeled nucleotides is added to the immobilized DNA sequence template container, where one nucleotide is incorporated per cycle. The fluorescence allows for detecting the incorporated base with a sensitive photodetector. Repeated wash-cycles with the reagents will deliver a series of colors captured and allow for inferring the DNA sequences in a massively parallel fashion. Pacific Biosciences also uses fluorescent nucleotides, yet uses circularized template DNA which is continuously duplicated by a modified polymerase. With this rolling-circle amplification, the template DNA is effectively transcribed multiple times.

Today, Illumina is the market leader and boasts a mature sequencing platform with a very high depth of coverage. It is the preferred sequencing platform not only for ultra-deep sequencing of low-frequent variants, but also because its error profile is well studied (Minoche et al. 2011). Pacific Biosciences is a newcomer, and its long-read technology allows for phasing of single-nucleotide variants (SNVs) due to its ability to capture long-range co-occurrences of SNVs, as shown for instance in HIV-1 (Di Giallonardo et al. 2014). Pacific Biosciences is known to have a high error rate, particularly prone to insertion–deletion (indel) errors. When dealing with viral populations that experience a high-level of biological indels, Pacific Biosciences' single-molecule, real-time technology will likely fail to detect low-frequent indel variants. On the other hand, Illumina's paired-end technology requires a delicate fragmentation of the biological material to yield a sample that has a mean average fragment length such that larger genomic regions can be properly phased. In practice, there is always a trade-off between depth of coverage and the average length of the reads (Zagordi et al. 2012).

2 Methods for Determining Quasispecies Composition

In order to determine the quasispecies population structure, a number of experimental and statistical methods have been devised. NGS data are marred with amplification and sequencing errors such that the raw data cannot be trusted at face value. Additionally, even with perfect error-free data, conclusions on long haplotypes could generally not be drawn easily, as NGS reads are very small in comparison with even the smallest viral genomes. In this section, we will summarize different methods for correcting the inherent technical errors and for phasing long-range haplotypes.

2.1 Experimental Approaches to Haplotype Inference

Determining the genetic composition of an intra-host quasispecies population can be performed at various levels: SNVs may be of interest, for example, to determine resistance to drugs that only require single amino acid substitutions. The next level of inference is concerned with determining the genetic composition of a genomic region of size on the order of the average read length. This might be of interest in determining resistance patterns that require more than one neighboring mutant allele. Finally, global inference deals with determining the population structure of a genomic region that is larger than the average read length.

Sample preparation protocols for NGS can be divided into two categories: Shotgun sequencing massively amplifies all viral genomes in the sample and fragments these for later sequencing. The second approach, termed targeted or amplicon sequencing, takes a more localized approach and designs PCR primers

such that only a small region, the amplicon, is amplified. In practice, mostly targeted sequencing is employed nowadays, due to the numerous difficulties encountered with the amplification required for shotgun sequencing.

2.2 Error Correction of Reads

While NGS allows for an unprecedented detailed picture of viral populations, due to the involved massive concurrent biochemical reactions, it has higher error rates than Sanger sequencing. As a result, NGS raw data cannot be used for making reliable inference of the viral quasispecies as it would vastly overestimate genetic diversity. Experimental as well as statistical methods have been developed to address this issue. Current experimental methods for error correction of reads are limited to correcting for base miscalls and indels, and they cannot determine the composition of genomic regions that are larger than the read length. For this purpose, combined error correction and phasing approaches with a statistical model is required and discussed in the next section; we will focus on experimental methods in this section.

An innovative approach to correcting for errors introduced in the PCR amplification of viral genomic material includes the use of primer identifiers (IDs). Jabara et al. (2011) have developed the Primer ID method, where each RNA molecule is tagged in the reverse transcription step with a primer that contains a random k-mer, termed the primer ID. If the diversity of the primer ID k-mers is substantially larger than the number of RNA molecules, a unique tagging of k-mers is guaranteed in practice. The usual downstream protocol of amplification of the cDNA with PCR and NGS sequencing is then performed. In the data analysis, assuming primer ID diversity requirements is met, all sequences with the same primer ID originate from the same reverse transcribed cDNA, and hence, all errors between such sequences are purely due to PCR or NGS errors. For correcting errors, simply calling the consensus sequence by majority vote for bases at each position is all that is required. A drawback of this method is its stringent requirement on practically unique primer IDs, without which collisions reduce its usability (Sheward et al. 2012). For instance, tagging 40,000 RNA sequences with random 10-mers will produce cDNA with a 1.9 % collision frequency.

Another method with the potential of error rates orders of magnitude below that of current sequencing technologies has been proposed by Lou et al. (2013). The circle sequencing protocol CirSeq the authors have developed circularizes single-stranded RNA and performs a rolling-circle reverse transcription, where the reverse transcriptase creates one single DNA molecule with multiple tandem copies of the original circular RNA. After sequencing, errors in the tandem copies within one read can be corrected as before by simply calling the consensus sequence. One advantage of the CirSeq approach lies in its ability to correct for reverse transcription errors, as RT errors show up in the pileup of the tandem copies of one original circular RNA. The previous PrimerID method only tags sample RNAs after reverse transcription and cannot correct for RT errors. While possessing the ability to greatly reduce the error rate, there exists an inherent trade-off with tandem length:

Given the inherent maximum read length limitation, every additional tandem copy in the read will lead to shorter tandem repeats, hence decreasing the effective read length. Another drawback of this method lies in its requirement of large amounts of sample DNA material. Due to the inefficient circularization step, a large fraction of the input sample material will not be reverse transcribed.

2.3 *Viral Haplotype Assembly*

While the previous experimental approaches require only simple data processing, they cannot give insights into the structure of genomic regions larger than the (effective) read length. In this case, computational approaches employing more sophisticated statistical methods are required. Roughly speaking, most computational approaches can be divided into two classes of methods, namely graph-based and probabilistic approaches. In addition, most tools have two phases of operation. The first phase is concerned with local (often SNV-level) error correction, where spurious, likely erroneous, low-frequency bases are removed with the help of some statistical model. In the second phase, supposedly correct reads are assembled into larger contiguous genomic regions with the help of phasing information (Fig. 3).

For (local) error correction, most computational methods resort to either (non-parametric) clustering algorithms or HMMs. *ShoRAH* by Zagordi et al. (2011) and *PredictHaplo* by Prabhakaran et al. (2014) employ a Bayesian clustering approach, where the (unknown) cluster centers represent true biological haplotypes and all deviations from the cluster centers are due to technical errors. A significant problem in such inference is determining the number of actual haplotypes present.

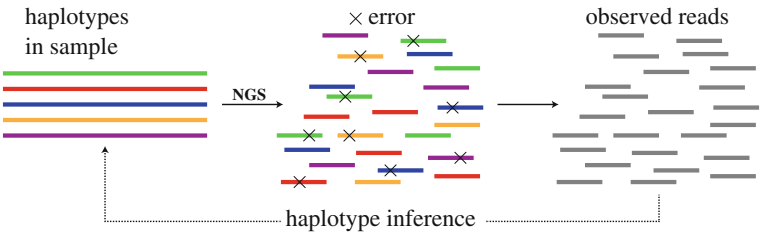

Fig. 3 Schematic overview of the steps involved in haplotype inference from NGS data. Starting with the original haplotypes in a patient sample on the *left*, viral RNA requires a multitude of steps of preparation that fragment and amplify the resulting cDNA to concentrations required for sequencing. In the process, the fragmented DNA includes errors from reverse transcription of RNA, PCR amplification, and sequencing errors, depicted in the *middle*. Ultimately though, the data present in the form of the observed reads on the *right*, where the number of haplotypes and the haplotype of origin of a read are not observable. The goal of haplotype inference lies in reconstructing the original haplotypes in the sample from these error-prone reads on the *right*

The Dirichlet process mixture is a nonparametric Bayesian approach that adapts to the amount of data and finds the optimum number of explanatory haplotypes due to its intrinsic regularization that strikes a balance between overfitting and underestimating viral diversity. In practice, a Gibbs sampler is employed to infer the posterior distribution of haplotypes and their frequencies.

QuRe by Prosperi and Salemi (2012) assumes a Poisson distribution of errors and uses this to remove SNVs that are likely to be errors. Importantly, in order to account for nonuniform technical error rates, *QuRe* assumes different Poisson distributions for homopolymeric stretches of DNA, which are known to have higher technical error rates, particularly for 454 data. Locally, the population structure is then modeled as a sample from a multinomial distribution.

After having corrected for errors, all of the aforementioned methods require an additional step to increase the analyzed region. *PredictHaplo* expands its region by constraining the emerging haplotypes to fulfill all window-wise local constraints. Most approaches to global inference have been inspired by ideas from graph theory. In order to phase large haplotypes, *ShoRAH* solves a minimal path cover problem to determine the minimum number of global haplotypes that explain the (error-corrected) reads. Another method for global inference, *ViSpA* by Astrovskaya et al. (2011), uses network flows on a transitively reduced read graph to infer the global haplotypes.

QuasiRecomb by Töpfer et al. (2013) approaches the inference problem from a different angle by employing a hidden Markov model (HMM). To this end, it models the reads as arising from recombinations of a select number of idealized "master" sequences and a locus-specific error process. Instead of using a Gibbs sampler as is common in the clustering approaches, *QuasiRecomb* learns its model parameters with an EM algorithm on a regularized likelihood function and provides a sample of the haplotype distribution encoded by the estimated model. By explicitly taking recombination into account, *QuasiRecomb* can infer population structures subject to recombination where the clustering approaches tend to disregard many haplotypes due to the inherent regularization. In addition, *QuasiRecomb* does away with the distinction of error correction and global assembly and performs all inference in one phase. Other clustering methods do not integrate paired-end information as naturally into their probabilistic formulation as *QuasiRecomb*.

An approach different from clustering approaches that employs methods from graph theory can be found in *HaploClique* by Töpfer et al. (2014) that also naturally integrates paired-end data. *HaploClique* builds a graph, where the nodes represent the reads and edges are drawn between reads when they are determined significantly similar by a suitable distance metric. In order to assess whether reads are significantly similar, the Phred scores are used to calculate the probability of pairs of sequences having arisen just by technical errors from one haplotype. To determine haplotypes, a max-clique enumeration algorithm is used, where haplotypes are represented by the maximal cliques, i.e., cliques that cannot be extended further. *HaploClique*'s advantages includes its robustness to indel errors, making it particularly useful in light of Pacific Biosciences' error profile, and its sensitivity for large genomic deletions, which remain hard to detect with probabilistic methods.

3 Methods for Estimating Viral Fitness

Historically, the genetic constellation of virus populations has been analyzed with laborious in vitro assays, such as limiting dilution assays followed by Sanger sequencing of the picked clones. NGS allows for gaining new insights into viral quasispecies by combining highly informative data with the wealth of knowledge developed in the field of population genetics and theoretical biology. In this section, we detail some of the approaches used to analyze quasispecies with the aid of deep sequencing data.

3.1 Selective Sweeps After Recent Population Bottlenecks in Viral Populations

During evolution, when new mutant alleles arise by mutation that have a high selective advantage over the wild-type allele, selective sweeps can occur. A selective sweep is characterized by the extinction of the wild-type allele and the fixation of the new mutant allele. The process, wherein neutral mutations occur on the sweeping haplotype and are amplified along, is referred to as genetic hitchhiking.

We consider a fitness landscape (2) with L loci, where only $\beta_1 > 0$ and $\beta_{i,(\cdot)} = 0$ for all $1 < i \leq L$ and $\beta_{\text{wt}} = 0$. For small values of β_1, the fitness landscape can be written as $f(x_1) = \exp(\beta_1 \cdot x_1) \approx 1 + s \cdot x_1$. Here s denotes the selection coefficient of the mutant allele at locus 1 under selective pressure. Messer and Neher (2012) have developed an estimator for s by deriving the frequency of hitchhiking variants of the adaptive allele as a function of the rank of the abundance. The model makes the infinite-sites assumption, where mutations will never occur more than once at the same locus. Once a newly seeded advantageous haplotype passes a critical threshold of $(2Ns)^{-1}$, where N denotes population size, selection trumps genetic drift and the haplotype will effectively grow in a deterministic, logistic fashion as $x(t) = \mathrm{e}^{st}/(\mathrm{e}^{st} + 2Ns)$. From this initial advantageous haplotype, selectively neutral mutants arise in an inhomogeneous Poisson process. The abundance of haplotypes is shown to follow a power-law distribution of the form

$$\frac{n_i}{n_0} \approx \left(\frac{u}{is}\right)^{1-u/s} \approx \frac{u}{is} \tag{3}$$

where n_i denotes the absolute count of haplotype with rank i, and u denotes the genome-wide mutation rate per generation. The second approximation comes from the fact that selection is assumed to be much stronger than the mutation rate $s \gg u$. This power-law dependency of haplotype frequency on rank is contrary to an exponential law that is expected from selectively neutral haplotypes. Plotting the rank-frequency spectrum on a log-log scale allows for determining whether a certain genomic region has recently experienced a selective sweep. Such data can

only be obtained by NGS, as a considerable number of haplotypes down to low-frequent variants need to be captured. Given an estimate for the mutation rate, the selection coefficient s can be estimated from the slope of this power-law abundance profile using (3) (Fig. 4).

In developing their model, Messer and Neher (2012) have been able to infer the selection coefficient in early HIV evolution purely from the rank-frequency spectrum of the viral quasispecies. This inference method does not require the use of time series data, which is rare in clinical practice. The estimated selection coefficient was close to estimates from validation time series data. As a second example, the selection coefficient of an 120 bp RT locus was estimated to be $s \approx 0.07$ which is indicative of moderate to strong selection.

The developed method is different from classical methods of estimating the strength of a selective sweep, which rely on the diversity signature around a candidate locus. In estimating the selective strength, such classical methods only take into account diversity introduced by recombination breaking up linkage with increasing distance from the locus under study. Thus, the (observed) rate of recombination strongly determines the variance of the selection estimate of classical methods. In the novel method by Messer and Neher (2012), the power-law nature of

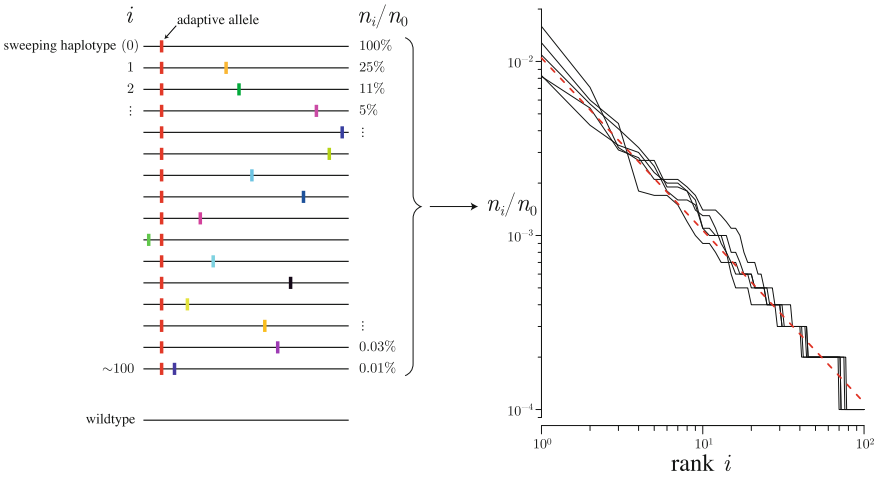

Fig. 4 Illustration of the Messer and Neher (2012) inference procedure for the selective advantage S of a mutant allele after a selective sweep. Shown on the *left* at the *top* is the sweeping haplotype which was produced by mutation from the wild-type haplotype at the *bottom*. The adaptive allele is depicted in *red*, whereas selectively neutral mutant alleles originating from the sweeping haplotype are depicted in different colors. Here, n_0 represents the counts in the population of the sweeping haplotype on which the initially adaptive mutation occurred, and n_i denotes the counts of the ith seeded haplotype. The ratio n_i/n_0 denotes the abundance of the ith seeded haplotype with respect to the sweeping haplotype. Messer and Neher (2012) have shown that under strong selection, the rank-frequency spectrum when plotted on a log-log scale as shown on the *right* follows a power law where the y-intercept is $\approx u/s$. Given an estimate of the mutation rate u by other means, the selection coefficient s can be estimated

the rank-frequency spectrum arises as an exponential growth process mediated by selection coupled to a random mutational attachment process. The resulting preferential attachment of mutations to the sweeping haplotype produces a rich haplotype spectrum of newly seeded mutants. Data required for determining the haplotype spectrum to such depth that sampling variance becomes minimal can only be obtained by ultra-deep sequencing.

3.2 *Determining Marginal Fitness Effects by Next-Generation Sequencing*

Measuring whole-genome fitness landscapes is practically impossible due to the exponentially in L growing number of parameters. Instead of determining all parameters of the whole-fitness landscape $w(x_1, \ldots, x_L)$, a more tractable approach to inference of fitness landscapes restricts itself? to the marginal effects. To illustrate how marginal effects are derived from the full 2^L fitness effects, we consider the bi-allelic two-locus genome and its log-fitness landscape $w : \{0,1\}^2 \to \mathbb{R}$

$$w(x_1, x_2) = \beta_{\text{wt}} + \beta_1 x_1 + \beta_2 x_2 + \beta_{12} x_1 x_2$$

Given an (infinite) population of haplotypes, we assume the marginal background probability or frequency of a mutant allele at locus 2 to be denoted by $P(x_2 = 1)$, then the marginal fitness of x_1 is as follows:

$$w(x_1) = \sum_{i \in \{0,1\}} P(x_2 = i) \cdot w(x_1, i)$$

Writing out this sum with additional algebraic manipulation yields

$$w(x_1) = \beta'_{\text{wt}} + \beta'_1 x_1$$

where the marginal effects are $\beta'_{\text{wt}} = \beta_{\text{wt}} + \rho\beta_2$, $\beta'_1 = \beta_1 + \rho\beta_{12}$, and $P(x_2 = 1) = \rho$ (Fig. 5). Generalizing to L loci, they only number linearly in L, drastically reducing the dimensionality of the parameter space from previously 2^L. This provides a route to determining properties of fitness landscapes without attempting to infer all parameters of the landscape at once.

Acevedo et al. (2014) have shown that NGS can be used to estimate marginal fitness effects at each locus of the polio genome. To this end, they employ the CirSeq protocol by Lou et al. (2013) for error correction, where the reverse transcriptase produces a cDNA with tandem copies of the same RNA in order to remove technical errors in downstream analysis. In order to estimate position-wise fitness, they subject the viral quasispecies to seven serial passages in a cell line. A sample of the viral population is taken after every passage and the cDNA library

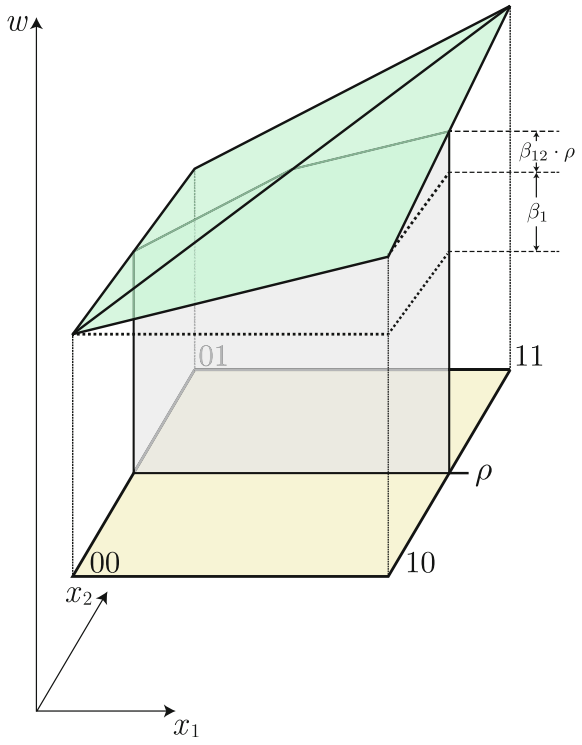

Fig. 5 Schematic of the same two-allelic two-locus fitness landscape as on the *right-hand side* of Fig. 2. Given some background frequency ρ of the mutant allele x_2, the fitness landscape as a function of just x_1 implicitly depends on the frequency of the other allele. The marginal additive effect β_1' depends on the strength of the epistatic effect and the additive effect. Given an estimate of the marginal effect β_1', the additive effect β_1 and the epistatic effect β_{12} cannot be determined uniquely. Here, the gray vertical plane is the fitness landscape as a function of x_1 given ρ

prepared according to the CirSeq protocol. Finally, the sample is sequenced in an ultra-deep fashion to infer the viral allele frequency spectrum.

In order to devise a simple model that can be used for estimating marginal fitness effects, a variant of quasispecies theory formulated for finite populations can be employed. Let A_t and a_t denote the counts of the wild-type, respectively, mutant allele at some position in the genome of the viral population after cell passage $t \in \mathbb{N}$. Furthermore, we assume the population size to be large and approximately constant. In order to determine the probability of the evolved population in the next passage, we calculate the probability $\psi(a_{t+1}|A_t, a_t)$ of the allele a_{t+1} in the next generation (Musso 2012)

$$\psi(a_{t+1}|A_t, a_t) = \frac{f_a' \cdot q_{aa} \cdot a_t + f_A' \cdot q_{Aa} \cdot A_t}{f_a' \cdot a_t + f_A' \cdot A_t} \tag{4}$$

where q_{ij} denotes the probability of i mutating to j upon replication, and $f'_A, f'_a \in \mathbb{R}_+$ denote the marginal reproductive fitnesses. Given that most mutants will be rare, we make the assumption $A_t \gg a_t$, such that $f'_a \cdot a_t + f'_A \cdot A_t \approx f'_A \cdot A_t$. Further assuming the degradation of the mutant allele by mutation to be negligible, i.e., $q_{aa} \approx 1$ and assuming the mutation rate $q_{Aa} = \mu$ to be the same for all loci, we obtain

$$\psi(a_{t+1}|A_t, a_t) \approx \frac{a_t}{A_t} \cdot \frac{f'_a}{f'_A} + \mu \tag{5}$$

The expected fraction of mutants in the next generation, $\mathbb{E}\left[\frac{a_{t+1}}{A_{t+1}}\right]$, is $\psi(a_{t+1}|A_t, a_t)$ and hence substituting for f'_A and f'_a

$$\mathbb{E}\left[\frac{a_{t+1}}{A_{t+1}}\right] \approx \frac{a_t}{A_t} \cdot \mathrm{e}^{\beta'_1} + \mu \tag{6}$$

The recursive relation in (6) resembles an autoregressive model. Acevedo et al. (2014) have used this formulation in a maximum-likelihood setting with a Poisson distributed number of mutant alleles between generations to estimate the ratio of marginal fitnesses $f'_a/f'_A = \mathrm{e}^{\beta'_1}$. The counts a_t and A_t after each transfection generation t were determined by ultra-deep sequencing. With their derived estimators, the authors could show that 2 % of synonymous mutations were marginally highly beneficial and 10 % lethal.

3.3 *Fitness Estimation from Equilibrium Quasispecies Distribution*

As the simplest model of viral evolution that captures the effects of selection and mutation, quasispecies theory lends itself as a simple evolutionary model to capture the change of an intra-host virus population. In the aforementioned sections, it has been shown how some properties of the fitness landscape can be inferred. If we are willing to make stronger assumptions, the entire fitness landscape can be inferred. In order for cross-sectional data to be useful in such an estimation scheme, we show that a number of reasonable assumptions need to hold or approximately hold.

While quasispecies theory has seen little experimental evidence supporting it beside circumstantial evidence of the existence of an error threshold, most experiments have not contradicted its postulates. One of the general conclusions of quasispecies theory is convergence of the viral population to a mutation–selection equilibrium, which is determined by the timescale of the evolutionary process. Importantly, the timescale depends on the mean replication time of the virus. If the timescale of replication is much smaller than the time span since infection, quasispecies theory predicts a population equilibrium, the quasispecies, where the average fitness of the population is maximized.

In one of the earliest studies of equilibrium, Domingo et al. (1978) analyzed the quasispecies spectrum of a multiply passaged Qβ-phage population, starting with different initial clones. After 10–20 cell passages, the diversified phage population showed the same polyacrylamide gel pattern as the wild-type population, lending credence to the existence of a dynamic equilibrium. In the same vein, Steinhauer et al. (1989) have shown a dynamic equilibrium of vesicular stomatitis virus when passaged multiply. The quasispecies concept has been extended to bacteria, where Covacci and Rappuoli (1998) have shown a supposed dynamic equilibrium in chronic Helicobacter pylori infections. Finally, Herrmann et al. (2003) have demonstrated how chronic hepatitis C infection exists as a dynamic equilibrium of viral production and degradation.

3.3.1 The Quasispecies Equation and Mutation–Selection Equilibrium

Seifert et al. (2015) have devised a model based on the equilibrium quasispecies population. The quasispecies Eq. (1) assumes the limit of an infinitely large population size, a regime in which genetic drift is negligible. The mutation matrix $\boldsymbol{Q} = \left(q_{ij}\right)$ is determined by the mutation rate μ of the reverse transcriptase

$$q_{ij} = \mu^{d(i,j)} \cdot (1-\mu)^{L-d(i,j)} \tag{7}$$

where $d(i,j)$ denotes the Hamming distance of haplotype i to haplotype j, i.e., the number of loci at which i and j differ. As $d(i,j) = d(j,i)$, the mutation matrix $\boldsymbol{Q}$ is symmetric. For practical purposes, we assume the mutation rate μ to be known, as the mutation matrix $\boldsymbol{Q}$ and the fitness landscape are jointly nonidentifiable (Falugi and Giarré 2009). Rewriting the quasispecies Eq. (1) in matrix notation

$$\frac{\mathrm{d}}{\mathrm{d}t}\boldsymbol{p}(t) = \boldsymbol{Q}^{\mathrm{T}}\mathrm{diag}(\boldsymbol{f})\boldsymbol{p}(t) - \phi(\boldsymbol{p}(t), \boldsymbol{f})\boldsymbol{p}(t) \tag{8}$$

where $\boldsymbol{f}$ is the fitness landscape, and $\phi(\boldsymbol{p}(t),\boldsymbol{f}) = \sum_{j=1}^{m} p_j(t) f_j$ denotes the average fitness of the population. In the limit as $t \to \infty$, the population approaches its single global equilibrium distribution, which is independent of the initial population. In order to determine the equilibrium distribution, we set $\frac{\mathrm{d}}{\mathrm{d}t}\boldsymbol{p}(t) = 0$ to obtain

$$\phi\boldsymbol{p} = \boldsymbol{Q}^{\mathrm{T}}\mathrm{diag}(\boldsymbol{f})\boldsymbol{p} \tag{9}$$

The matrix $\boldsymbol{Q}$ is a positive matrix, and as such, the Perron–Frobenius theorem guarantees the existence of a unique global equilibrium distribution as the eigenvector $\boldsymbol{p}$ corresponding to the largest eigenvalue ϕ.

An important property of the quasispecies equation is that no haplotype can go extinct, due to the constant mutational flux between haplotypes. On the other hand,

the frequency also has an upper bound which is determined in part by the replication fidelity. Thus, $\boldsymbol{p}$ can be constrained further to lie within a subset $\mathcal{Q}^{m-1} \subsetneqq \Delta^{m-1}$, the quasispecies space, that is, the set of all equilibrium distributions that can arise from the quasispecies equation in equilibrium for some fitness landscape $\boldsymbol{f} \in \mathbb{R}_+^m$.

Given a fitness landscape $\boldsymbol{f}$, we can now ask the inverse question, namely which fitness landscape has led to some particular quasispecies $\boldsymbol{p}$? We find

$$\boldsymbol{f} \in \ker\left(\boldsymbol{Q}^{\mathrm{T}}\mathrm{diag}(\boldsymbol{p}) - \boldsymbol{p}\boldsymbol{p}^{\mathrm{T}}\right) \tag{10}$$

Thus, given an equilibrium distribution, the fitness landscape is scale invariant. This inherently unknowable scale is the timescale of the evolutionary trajectory which determines the convergence of the population to its mutation–selection equilibrium. We can hence only make statements about relative but not absolute fitness from equilibrium data.

With the previously highlighted possibility of a dynamic equilibrium, we assume the timescale of evolution to be smaller than the time span under observation, for which the population will then be close to its equilibrium distribution. In order to be able to determine (relative) fitness values from frequencies, we make assumptions on the timescale by fixing $\phi = 1$. With this, (9) simplifies to

$$\boldsymbol{f} = \mathrm{diag}(\boldsymbol{p})^{-1}\boldsymbol{Q}^{-\mathrm{T}}\boldsymbol{p} \tag{11}$$

By introducing the eigenvalue constraint $\phi = 1$, we effectively reduce full fitness space $\mathbb{R}_+^m$ by one degree of freedom to the nonlinear space $\mathcal{F}^{m-1} = \{\boldsymbol{f} \in \mathbb{R}_+^m : \phi = \boldsymbol{p} \cdot \boldsymbol{f} = 1\}$, which we refer to as fitness space.

As most haplotype sets inferred from NGS data will not show the complete picture due to incomplete sampling of all haplotypes in practice, a number of unobserved haplotypes need to be included. Haplotypes are included such that the graph of haplotypes forms one connected component, where edges between haplotypes are drawn if their Hamming distance is equal to one. In order for $\boldsymbol{Q}$ to still be a transition matrix, we calculate its off-diagonal elements as in (7) and simply set its diagonal entries to $q_{ii} = 1 - \sum_{j \in \{1,\ldots,n\} \setminus \{i\}} q_{ij}$. This retains the desirable symmetric property of a stochastic matrix.

3.3.2 Bayesian Inference of Fitness Landscapes

NGS data yield a sample $\boldsymbol{X} \in \mathbb{N}^n$ of counts for all n haplotypes with a total of $N = \sum_{i=1}^n X_i$ reads, where X_i denotes the count of reads representing haplotype i in the sample. In order to estimate p, a multinomial likelihood $\mathrm{Mult}(\boldsymbol{X}|p, N)$ for the finite NGS sample is employed. This likelihood implicitly depends on the fitness landscape $\boldsymbol{f}$ through the relation (11).

The problem of estimating the fitness landscape f is solved in a Bayesian fashion. Given that most higher order coefficients in (2) will be zero, realistic fitness landscapes will always include a degree of correlation between fitnesses of closely related haplotypes. In order to make inference more amenable to Markov Chain Monte Carlo methods, a transformation $t : \mathbb{R}^{n-1} \to \mathcal{F}^{n-1}$ is introduced. Working on the full Euclidean space allows for a rich set of proposal distributions that can capture the aforementioned correlation inherent in practical fitness landscapes.

With a multivariate Gaussian distribution as a proposal on the Euclidean space $\mathbb{R}^{n-1}$, the correlation of the fitness landscapes is automatically learned by employing a highly parallelizable globally adaptive MCMC scheme called differential evolution (DE) MCMC. This scheme, in nature similar to parallel tempering in physics, estimates the posterior distribution of fitnesses by taking the difference between random members of the currently active candidates. This difference captures the covariance of the target distribution well (Fig. 6). The DE MCMC scheme is of the Metropolis variant, due to the inherent symmetry of choosing the other two proposal members without replacement, and thus, the acceptance probability only depends on the functional form of the posterior distribution

$$\log p(\mathbf{y}|\mathbf{X}) = \log d(\mathbf{y}) + \sum_{i=1}^{n} X_i \log p_i + \text{const.} \quad \mathbf{y} \in \mathbb{R}^{n-1} \tag{12}$$

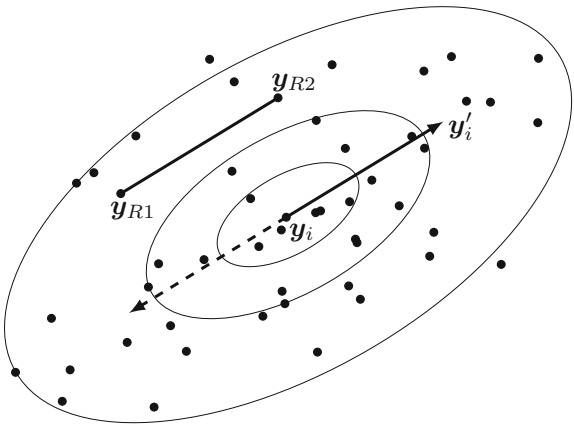

Fig. 6 Depicted here is an idealized correlated Gaussian in $\mathbb{R}^2$ where the *ellipses* represent the contours of the distribution. In DE MCMC, the sampler is run with some population of candidate realizations, represented by the *dots*, that capture the current state of the Markov chain. In each generation, the algorithm cycles through all members of the population $\mathbf{y}_i$ and generates a new proposal sample $\mathbf{y}'_i$ by taking the difference of two other members of the current population $\mathbf{y}_{R1}$ and $\mathbf{y}_{R2}$ and adding it to the current sample $\mathbf{y}_i$. The difference $\mathbf{y}_{R2} - \mathbf{y}_{R1}$ depicted by the *arrow* $\mathbf{y}'_i$ optimally captures the direction of the ellipses and thus allows for inference of correlated target distributions where the covariance structure is initially unknown. The *dashed arrow* indicates the symmetry of this Metropolis-type scheme, as the probability of having generated the difference $\mathbf{y}_{R2} - \mathbf{y}_{R1}$ is equal to the probability of having picked $\mathbf{y}_{R1} - \mathbf{y}_{R2}$

where $\log d(\mathbf{y})$ captures the nonlinear transformation of probability densities from $\mathcal{F}^{n-1}$ to $\mathbb{R}^{n-1}$.

Once the posterior has been determined, a number of properties of the fitness landscape can be assessed. The fitness landscape (2) can be written in matrix form as follows:

$$\log \boldsymbol{f} = \boldsymbol{w} = \boldsymbol{A} \cdot \boldsymbol{\beta} \tag{13}$$

where the logarithm is applied component-wise to $\boldsymbol{f}$ and the matrix $\boldsymbol{A}$ encodes the decomposition (2) of the log-fitness landscape. For example, for the standard bi-allelic two-locus genome $\mathcal{A} = \{0,1\}$ and $L = 2$, we have

$$\begin{pmatrix} w_{00} \\ w_{10} \\ w_{01} \\ w_{11} \end{pmatrix} = \begin{pmatrix} \beta_{\text{wt}} & & & \\ \beta_{\text{wt}} & +\beta_1 & & \\ \beta_{\text{wt}} & & +\beta_2 & \\ \beta_{\text{wt}} & +\beta_1 & +\beta_2 & +\beta_{12} \end{pmatrix} = \begin{pmatrix} 1 & 0 & 0 & 0 \\ 1 & 1 & 0 & 0 \\ 1 & 0 & 1 & 0 \\ 1 & 1 & 1 & 1 \end{pmatrix} \cdot \begin{pmatrix} \beta_{\text{wt}} \\ \beta_1 \\ \beta_2 \\ \beta_{12} \end{pmatrix} \tag{14}$$

Inverting the relationship (13) allows for determining whether each of these effects is credible. A significant benefit of this method is that it can go beyond marginal effects as in Acevedo et al. (2014) and elucidate the structure of interaction effects. In this example, β_{12} denotes the interaction effect between the two loci. This is a feature that normally requires extensive testing for linkage disequilibrium, whereas the illustrated model can address this statistical question on the basis of the quasispecies model and NGS data.

4 Conclusions

With NGS the study of fitness landscapes has been significantly advanced due to the ease of tracking populations and inferring parameters from such evolutionary dynamics. On a whole-genome scale, inference of marginal fitness effects of viral quasispecies seems possible and provides a first handle for disentangling observed fitness differences to yield a clearer picture of the underlying fitness landscape (2).

In many cases, cell passage experiments cannot be conducted to assess the evolutionary dynamics of viruses. In most clinical settings, time series data cannot be collected for a number of practical, biological, or ethical reasons. In such cases, the rank-frequency spectrum contains the selective advantage of an adaptive allele. From a single cross-sectional experiment, insights can be gained into the strength of selection. Finally, when the population is believed to be in sufficient mutation–selection equilibrium, the quasispecies model provides a way to infer the complete fitness landscape from cross-sectional data.

References

Acevedo A, Brodsky L, Andino R (2014) Mutational and fitness landscapes of an RNA virus revealed through population sequencing. Nature 505(7485):686–690

Astrovskaya I, Tork B, Mangul S, Westbrooks K, Măndoiu I, Balfe P, Zelikovsky A (2011) Inferring viral quasispecies spectra from 454 pyrosequencing reads. BMC Bioinformatics 12 (Suppl 6):S1

Beerenwinkel N, Pachter L, Sturmfels B (2007) Epistasis and shapes of fitness landscapes. Statistica Sinica 17:1317–1342

Beerenwinkel N, Montazeri H, Schuhmacher H, Knupfer P, von Wyl V, Furrer H, Battegay M, Hirschel B, Cavassini M, Vernazza P et al (2013) The individualized genetic barrier predicts treatment response in a large cohort of HIV-1 infected patients. PLOS Comput Biol 9(8): e1003203

Covacci A, Rappuoli R (1998) Helicobacter pylori: molecular evolution of a bacterial quasi-species. Curr Opin Microbiol 1(1):96–102

Di Giallonardo F, Töpfer A, Rey M, Prabhakaran S, Duport Y, Leemann C, Schmutz S, Campbell NK, Joos B, Lecca MR et al (2014) Full-length haplotype reconstruction to infer the structure of heterogeneous virus populations. Nucleic Acids Res 42(14):e115

Domingo E, Sabo D, Taniguchi T, Weissmann C (1978) Nucleotide sequence heterogeneity of an RNA phage population. Cell 13(4):735–744

Falugi P, Giarré L (2009) Identification and validation of quasispecies models for biological systems. Syst Control Lett 58(7):529–539

Herrmann E, Lee JH, Marinos G, Modi M, Zeuzem S (2003) Effect of ribavirin on hepatitis C viral kinetics in patients treated with pegylated interferon. Hepatology 37(6):1351–1358

Hinkley T, Martins J, Chappey C, Haddad M, Stawiski E, Whitcomb JM, Petropoulos CJ, Bonhoeffer S (2011) A systems analysis of mutational effects in HIV-1 protease and reverse transcriptase. Nat Genet 43(5):487–489

Jabara CB, Jones CD, Roach J, Anderson JA, Swanstrom R (2011) Accurate sampling and deep sequencing of the HIV-1 protease gene using a primer ID. Proc Natl Acad Sci 108 (50):20166–20171

Lou DI, Hussmann JA, McBee RM, Acevedo A, Andino R, Press WH, Sawyer SL (2013) High-throughput DNA sequencing errors are reduced by orders of magnitude using circle sequencing. Proc Natl Acad Sci 110(49):19872–19877

Messer PW, Neher RA (2012) Estimating the strength of selective sweeps from deep population diversity data. Genetics 191(2):593–605

Minoche AE, Dohm JC, Himmelbauer H et al (2011) Evaluation of genomic high-throughput sequencing data generated on Illumina HiSeq and genome analyzer systems. Genome Biol 12 (11):R112

Musso F (2012) On the relation between the Eigen model and the asexual Wright-Fisher model. Bull Math Biol 74(1):103–115

Prabhakaran S, Rey M, Zagordi O, Beerenwinkel N, Roth V (2014) HIV Haplotype inference using a propagating Dirichlet process mixture model. IEEE/ACM Trans Comput Biol Bioinform 11:182

Prosperi MC, Salemi M (2012) QuRe: software for viral quasispecies reconstruction from next-generation sequencing data. Bioinformatics 28(1):132–133

Sanjuán R, Cuevas JM, Furió V, Holmes EC, Moya A (2007) Selection for robustness in mutagenized RNA viruses. PLoS Genet 3(6):e93

Seifert D, Di Giallonardo F, Metzner KJ, Günthard HF, Beerenwinkel N (2015) A framework for inferring fitness landscapes of patient-derived viruses using quasispecies theory. Genetics 199 (1):191–203

Sheward DJ, Murrell B, Williamson C (2012) Degenerate primer IDs and the birthday problem. Proc Natl Acad Sci 109(21):E1330

Steinhauer D, de la Torre JC, Meier E, Holland J (1989) Extreme heterogeneity in populations of vesicular stomatitis virus. J Virol 63(5):2072–2080

Töpfer A, Zagordi O, Prabhakaran S, Roth V, Halperin E, Beerenwinkel N (2013) Probabilistic inference of viral quasispecies subject to recombination. J Comput Biol 20(2):113–123

Töpfer A, Marschall T, Bull RA, Luciani F, Schönhuth A, Beerenwinkel N (2014) Viral Quasispecies assembly via maximal clique enumeration. PLOS Comput Biol 10(3):e1003515

Wang C, Mitsuya Y, Gharizadeh B, Ronaghi M, Shafer RW (2007) Characterization of mutation spectra with ultra-deep pyrosequencing: application to HIV-1 drug resistance. Genome Res 17(8):1195–1201

Wilke CO, Wang JL, Ofria C, Lenski RE, Adami C (2001) Evolution of digital organisms at high mutation rates leads to survival of the flattest. Nature 412(6844):331–333

Wolf JB, Brodie ED, Wade MJ (2000) Epistasis and the evolutionary process. Oxford University Press, Oxford

Wright S (1932) The roles of mutation, inbreeding, crossbreeding and selection in evolution. In: Proceedings of the sixth international congress on genetics, vol 1, pp 356–366

Zagordi O, Bhattacharya A, Eriksson N, Beerenwinkel N (2011) ShoRAH: estimating the genetic diversity of a mixed sample from next-generation sequencing data. BMC Bioinformatics 12(1):119

Zagordi O, Däumer M, Beisel C, Beerenwinkel N (2012) Read length versus depth of coverage for viral quasispecies reconstruction. PLOS ONE 7(10):e47046

Getting to Know Viral Evolutionary Strategies: Towards the Next Generation of Quasispecies Models

Susanna Manrubia and Ester Lázaro

Abstract Viral populations are formed by complex ensembles of genomes with broad phenotypic diversity. The adaptive strategies deployed by these ensembles are multiple and often cannot be predicted a priori. Our understanding of viral dynamics is mostly based on two kinds of empirical approaches: one directed towards characterizing molecular changes underlying fitness changes and another focused on population-level responses. Simultaneously, theoretical efforts are directed towards developing a formal picture of viral evolution by means of more realistic fitness landscapes and reliable population dynamics models. New technologies, chiefly the use of next-generation sequencing and related tools, are opening avenues connecting the molecular and the population levels. In the near future, we hope to be witnesses of an integration of these still decoupled approaches, leading into more accurate and realistic quasispecies models able to capture robust generalities and endowed with a satisfactory predictive power.

Contents

1 Introduction 202
2 The Complex Response of RNA Viruses to Increases in the Mutation Rate 204
3 The Effect of Mutations on Fitness 207
4 Fitness Landscapes 209
5 Discussion and Prospects 211
References 212

S. Manrubia (✉)
Centro Nacional de Biotecnología (CSIC), c/Darwin 3, 28049 Madrid, Spain
e-mail: smanrubia@cnb.csic.es

S. Manrubia · E. Lázaro
Grupo Interdisciplinar de Sistemas Complejos (GISC), Madrid, Spain

E. Lázaro
Centro de Astrobiología (INTA-CSIC), Ctra. de Ajalvir km. 4, 28850 Torrejón de Ardoz
Madrid, Spain
e-mail: lazarole@cab.inta-csic.es

Current Topics in Microbiology and Immunology (2016) 392: 201–217
DOI 10.1007/82_2015_457

Published Online: 14 August 2015

1 Introduction

Our intuition on the origin and mechanisms of adaptation often fails when confronted with the products of evolution. We tend to depict the adaptation of populations, and the strategies that permit it, in the way an engineer would do. But natural selection, relying on an apparently simple trial-and-error principle, prospers through the deployment of a large number of unforeseeable solutions for the survival of organisms. Viruses, in their quality of fast evolving entities, count among the most creative adapters on Earth. And they are as well excellent examples of how our educated guesses do not succeed at predicting the outcome of evolutionary experiments or the strategies used in adaptation.

Very often, we resort to three features of viruses that underlie their enormous plasticity (large population numbers, high mutation rates—especially in RNA viruses—and short generation time) to "explain" their adaptive success. But these are just the very plain ingredients of the receipt. Viral populations are diverse not only because they contain a variety of self-sustained genotypes, but especially because several different phenotypes might coexist in the same quasispecies. In this sense, the idea of a fittest genome (often known as the "master sequence"), and of its preeminence above all other mutants, loses meaning. Perhaps concepts borrowed from ecology, where organisms with different roles are necessary to sustain the system in a dynamic equilibrium, would offer a better picture of the complex relationships established among the genomes that integrate a single viral population. In the context of a viral ecology, it would be easier to integrate cheaters, defectors or altruistic cooperators as different phenotypes that simultaneously thrive in quasispecies. Understanding the strengths of a heterogeneous ensemble of mutants is a step forward towards understanding the diversity of strategies that viruses might use to ensure their survival.

There are abundant examples of viral adaptation that challenge classical theories and a priori expectations of viral behaviour. Let us illustrate this statement with three examples. Our first example regards the origin of fitness gain in bipartite viruses. Multipartite viruses have fragmented genomes encapsidated in different particles and represent about 50 % of all viruses infecting plants (Hull 2013). To complete an infection cycle, at least one representative of each of the fragments must be present inside the cell, a condition that usually requires a very high multiplicity of infection (MOI). The success of multipartite viruses in front of non-fragmented counterparts requires that the cost of high MOI be compensated by an advantage originating from the fragmentation and separated encapsidation of the genome. Classical theories suggested that an increase either in the speed of replication or in higher copying fidelity due to shortened genomes might compensate for the disadvantage of mandatory coinfection (Nee 1987; Chao 1991). However, a series of experiments where a complete, wild-type genome of foot-and-mouth disease virus (FMDV) was displaced at high MOI by a cognate, bipartite form evolved in vitro (García-Arriaza et al. 2004) failed to detect any of those putative advantages. After several years of efforts, the advantageous mechanism could be

eventually identified. Viral particles in the bipartite form of FMDV enjoy a higher stability, likely due to a decreased pressure exerted in the capsid by genomes of smaller size (Ojosnegros et al. 2011). Higher stability translates into longer average lifetime, sufficient to displace the wild type at an MOI that permits frequent coinfection. Subsequent studies have shown, however, that the initial transition towards genome segmentation was favoured by the accumulation of mutations during the evolution of the standard genome and that those mutations conferred higher replicative fitness to the segmented genome version than to the standard genome (Moreno et al. 2014). The relative stability of the wild-type versus the bipartite form is related in a specific functional manner to the MOI, setting limits to the emergence of multipartite viruses from complete cognate wild types (Iranzo and Manrubia 2012). Several questions on the adaptive strategies of multipartite viruses remain open, since the mechanism leading to the fixation of bipartite forms described in the previous studies (segment deletion followed by competition with a non-fragmented counterpart) cannot explain the success of multipartite viruses with more than three fragments or the recently identified imbalance in the frequencies of genomic fragments of Alfalfa mosaic virus (Sánchez-Navarro et al. 2013) and Faba bean necrotic stunt virus (Sicard et al. 2013).

Our second example regards a potentially lethal role played by defective viral genomes in the population. Replication of RNA viable viral genomes steadily generates defective mutants able to replicate through the use in *trans* of essential resources provided by complementary genomes. A puzzling observation arose in an experiment with persistent infections of lymphocytic choriomeningitis virus (LCMV) under the action of mild doses of a mutagenic drug: while the intracellular levels of RNA seemed unaffected by the mutagen, the ability of the virus to infect new cells systematically declined until extinction (Grande-Pérez et al. 2005). There were some important elements in those experiments that caused the final output. First, a persistent infection permits the accumulation of defective, replicatively competent forms that may lose the ability to infect, since this latter trait is not actively selected in that scenario. Second, there is a competition within the quasi-species for replicative resources, used by all genomes but produced only by the "altruists" that survive. Third, since the number of genomes inside a cell is finite, and the replicative process is by nature affected by severe fluctuations in the numbers of defectors versus wild-type genomes, there is a nonzero probability that defectors take over and, subsequently, the population goes extinct due to the absence of basic resources (Iranzo and Manrubia 2009). In the experiment with LCMV, the collective dynamics of the population, together with the particular environment, is essential to determine the final outcome, which would be much alleviated in the case of a lytic infection or if the system would be described through a model with an infinitely large population—as assumed in many mathematical models of viral evolution. There are other formal scenarios where intraspecific competition might lead to potential threats to the survivability of viral populations, e.g. when there is a limitation in the number of susceptible cells for infection, which may cause decreases in diversity (Aguirre and Manrubia 2008) and eventually the extinction of the population if resistant cells appear (Cuesta et al. 2011). In many

cases, the consideration of a limited number of viral particles, and even of extreme population bottlenecks, becomes essential to our understanding of the dynamics and fate of viral populations in many realistic situations (Lázaro et al. 2006; Manrubia and Lázaro 2006).

Our third example has to do with how compensatory mutations act to balance the accumulation of deleterious mutations (and thus to avoid sustained degradation) in small populations. Muller's ratchet theory (Muller 1964) posits that small asexual populations must accumulate mutations in an irreversible way. Assuming that the least mutated genomes are the fittest ones, an irreversible process of fitness loss might be triggered by the systematic application of extreme bottlenecks. With this proviso, an experiment was designed to force the accumulation of mutations in FMDV with the aim of quantifying the process of extinction (Escarmís et al. 2002). Unexpectedly, after several passages, the virus stopped losing fitness and entered a regime with a well-defined average population size subjected to strong fluctuations (Lázaro et al. 2003), the sustained accumulation of mutations notwithstanding. The only explanation for this behaviour is that, contrary to expectations, not all mutations fixed have a deleterious effect in fitness, as assumed by theory. Actually, the fraction of compensatory, even beneficial, mutations increases as the average fitness of the population decreases. Eventually, a balance between the size of the bottlenecks and the degree of optimization of the population is established (Lázaro et al. 2002).

The previous examples illustrate the complex behaviour of viruses at the population level and the many factors that may contribute to the collective organization and response of those populations to different selection pressures. There is, however, a number of underlying molecular mechanisms, also with unexpected effects at the level of phenotypes, that make possible and at the same time condition population dynamics. Most empirical efforts have been devoted to the description and understanding of the effect of specific mutations in particular genomes, as reviewed in the first sections of this contribution. Only a deeper understanding of the quality and quantity of interactions between mutations, of the genotypic and phenotypic diversity of quasispecies, of the effect of different mutational mechanisms and also of the interactions between coexisting viral phenotypes can lead to a reliable theory of viral evolution and adaptation, eventually endowed with the ability to predict the responses of viral populations to changing environments. A new generation of quasispecies models should emerge from the integration of molecular information with population behaviour (Manrubia 2012).

2 The Complex Response of RNA Viruses to Increases in the Mutation Rate

Early quasispecies theory predicted the existence of a maximum error rate—the error threshold, compatible with the maintenance of genetic information (Eigen 1971; Biebricher and Eigen 2005). Above that threshold, the population is displaced towards regions of the sequence space occupied by similar, low-fitness

genomes. At that point, selection is no longer efficient and genetic information cannot be maintained (Eigen 2002). The predicted value of the error threshold depends strongly on the specific features considered, among others the length of genomes, the roughness of the fitness landscape, the abundance of lethal mutants or the molecular degradation rate (Saakian and Hu 2006; Saakian et al. 2006; Takeuchi and Hogeweg 2007). Theoretical expectations motivated empirical studies aimed at evaluating the likelihood that artificial increases in the error rate could cause the extinction of viral populations (Eigen 2002). In vitro experiments to test this so-called lethal mutagenesis hypothesis have achieved remarkable success (Agudo et al. 2009; Crotty et al. 2001; Dapp et al. 2009; Grande-Pérez et al. 2002; Holland et al. 1990; Loeb et al. 1999; Severson et al. 2003; Sierra et al. 2000), demonstrating that viral extinction can indeed be caused by sufficiently large increases in the mutation rate (reviewed in Perales et al. 2011b; Domingo et al. 2012). This success nonetheless, there is as yet no convincing proof that the observed extinctions are the consequence of crossing an informational error threshold of the kind described in Eigen's quasispecies theory (Bull et al. 2007; Manrubia et al. 2010; see also Chaps. 13 and 14).

In general, well-adapted viral populations propagated in constant environments under the action of high concentration of mutagens are extinguished or reduce their infectivity (Moreno et al. 2012; Perales et al. 2011a; Arias et al. 2013; Arribas et al. 2011). However, when the viral population is allowed to adapt to gradual increases in mutagen concentration, variants that better resist the drug can be selected, and the population may escape extinction (Arias et al. 2008; Arribas et al. 2011; Agudo et al. 2010; Pfeiffer and Kirkegaard 2003). In addition to raising concerns on the efficacy of antiviral therapies based on lethal mutagenesis (Iranzo et al. 2011; Perales et al. 2012), these mutants have shown that the high error rates of RNA viruses are a necessary condition for efficient adaptation to complex selective pressures (Pfeiffer and Kirkegaard 2005; Vignuzzi et al. 2006). There could even be circumstances in which increases in the error rate might occasionally enhance virus performance. For instance, a study carried out with an RNA bacteriophage showed that the lytic plaques developed from a low-fitness mutant in the presence of a mutagenic nucleoside analogue had higher titres than those developed from the same virus at standard error rate (Cases-González et al. 2008). Those results suggest a positive effect of the increase of the error rate in low-fitness viruses, more prone to experience beneficial mutations. A similar effect might be observed when mutagenic treatments are applied in changing environments. At the first stages of an adaptation process, there is a larger availability of beneficial mutations, again potentially implying a beneficial action of an increased error rate. Some viruses that replicate in alternating hosts experience higher mutation rates in one of them (Coffey et al. 2011; Vasilakis et al. 2009), maybe responding to the need of generating a larger genetic diversity to permit adaptation. The effects of mutagens might be confounded due to their capacity to simultaneously inhibit virus replication (Pariente et al. 2003). For example, a study carried out with VSV subjected to a mutagenic treatment showed decreased fitness and adaptability (Lee et al. 1997), two typical outcomes of inhibited viral replication.

Mutation rates vary across viruses and even within the same virus when growing in different environments and are dependent on the genetic background. These dependencies draw a complex picture where the response to additional increases in the error rate may differ largely between populations. The estimated error rate for RNA viruses ranges from 10^{-5} to 10^{-3} errors per nucleotide per cell infection (Drake and Holland 1999; Gago et al. 2009; Holland et al. 1982; Sanjuán et al. 2010). The host cell may induce variations of the viral error rate depending on factors such as nucleotide composition (Julias and Pathak 1998), presence of mutagenic reactive oxygen species derived from the metabolism of the cell (Seronello et al. 2011) or expression of genes such as APOBEC3 or ADAR, which cause hypermutability in several viruses (Holtz and Mansky 2013; Harris et al. 2003). Differences in the viral mutation rates have also been observed across hosts or cell type infected (Pita et al. 2007). Actually, lethal mutagenesis studies yield many examples of the variety of responses elicited from RNA viruses subjected to artificial increases in the error rate: fitness decreases and extinction (Perales et al. 2011a; Domingo et al. 2012), genomic shifts in sequence space (Perales et al. 2011c), alterations of the network of interactions within the mutant spectrum (Grande-Pérez et al. 2005) or selection of resistant mutants (Arias et al. 2008; Arribas et al. 2011; Agudo et al. 2010; Pfeiffer and Kirkegaard 2003; Iranzo et al. 2011). The evolutionary history of a viral population eventually determines the region of the sequence space it occupies (its genomic diversity), a fact that affects genetic robustness, viral plasticity and the effect of new mutations (Sanjuán et al. 2007; Graci et al. 2012).

Augmenting the error rate also disturbs current interactions within the mutant spectrum, as shown in the case of lethal defective particles (Grande-Pérez et al. 2005; Iranzo and Manrubia 2009). The role of defective interfering genomes was further demonstrated also in FMDV and other viruses (Perales et al. 2007). The transition from the mainly cooperative interactions that occur in optimized virus quasispecies to the defective interactions in preextinction quasispecies can be understood as a continuum driven by the error rate (Domingo et al. 2005). High multiplicities of infection may favour interactions among mutants and thus require higher error rates to achieve extinction. In this sense, population bottlenecks could be very effective to clean viable genomes from the poisoning effect of hypermutated mutant spectra (Manrubia et al. 2010; Lázaro et al. 2006). Mutagenic treatments enlarge the region of sequence space explored by a virus (Ojosnegros et al. 2008) due to an increase in the diversity of the population. Examination of the FMDV mutant spectrum in the presence of ribavirin showed an increase in the frequency of A/G and C/U transitions, causing a displacement towards regions of sequence space where the virus was more prone to experience deleterious mutations (Perales et al. 2011c). A ribavirin-resistant mutant isolated in that same virus restored the normal transition pattern without affecting the average mutation frequency or the incorporation of ribavirin by the replicase (Agudo et al. 2010). This kind of displacements could be very effective at moving populations to unexplored regions of the sequence space and could have unexpected evolutionary consequences, particularly if the increase of the error rate is transitory and the hypermutated variants have the

opportunity to recover fitness through compensatory mutations that stabilize the population in the new genomic region. These are excellent examples of the complex interplay between molecular changes and population dynamics, and a step forward towards connecting these two levels.

3 The Effect of Mutations on Fitness

The development of useful theories of viral evolution and adaptation depends on our knowledge of the effects of mutations on phenotype. The examples of the previous section illustrate a non-trivial collective response of viral populations when the mutation rate increases, including enhanced adaptability. Natural mutation rates suffice in most cases to guarantee the latter, often not only through point mutations, but also through other mutational mechanisms that cause segment deletions, genome recombination or genome fragment shuffling. In this section, we review the empirical efforts addressed at quantitatively characterizing the effect of point mutations in fitness, and their dependence on the genetic background and on the current environment.

Studies carried out with site-directed randomly chosen single mutants of vesicular stomatitis virus (VSV) (Sanjuán et al. 2004a), bacteriophage Qβ (Domingo-Calap et al. 2009) and tobacco etch virus (TEV) (Carrasco et al. 2007) show that a high fraction—from 0.20 to 0.41—of the mutations that arise in the genome is lethal. Focusing on viable mutations, deleterious mutations are much more frequent than beneficial, and mutations of mild effect are more likely than those of large effect (Sanjuán 2010). The high amount of deleterious and lethal mutations might be partly due to the small size of most RNA virus genomes, which imposes a high degree of compaction of the genetic information in overlapping reading frames and coding sequences that simultaneously hold structural functions (Holmes 2003). Despite this apparently low tolerance to mutations, RNA viruses maintain high heterogeneity and adaptability, due to the multifactorial and context-dependent effect of mutations. In particular, interactions between mutations modulate their value, such that the fitness of a viral genome is continuously redefined along evolution.

Mutations that occur in genomes differing in more than a single substitution permit the appearance of interactions among mutations, or epistasis (Phillips 2008). Epistatic interactions show up when the combined effect of different mutations in the same genome does not equal the sum of the effects of each independent mutation. Several classes of epistasis arise depending on whether the mutations that interact are beneficial or deleterious, and on whether the sum of effects is higher or lower than expected by simple addition of their individual effects (case of no epistasis). Particular cases are synergistic (antagonistic) epistasis, where the total effect of two mutations increasing fitness is larger (smaller) than the sum of the individual effects, sign epistasis (a deleterious mutation reverts its negative effect in the context of a positive mutation) and reciprocal sign epistasis (two deleterious

mutations have a positive effect when they co-occur). Epistasis has been detected in many RNA viruses such as bacteriophage Φ6 (Burch and Chao 2004), TEV (Lalić and Elena 2012), FMDV (Elena 1999), Chikungunya virus (Tsetsarkin et al. 2009), VSV (Sanjuán et al. 2004b) and Human immunodeficiency virus (HIV) (Martínez et al. 2011; Bonhoeffer et al. 2004; Kouyos et al. 2012). Compensatory mutations are a case of reciprocal sign epistasis that likely plays an essential role in evolution and adaptation (Covert et al. 2013). Fitness changes monitored in several clones of FMDV transmitted through successive population bottlenecks, where the fixation of mutations proceeded independently of their selective value, were interpreted on the basis of a higher availability of compensatory mutations in low-fitness genomes (Lázaro et al. 2002; 2003). Compensatory mutations also balance the fitness cost of drug-resistant mutants, causing the permanence of the resistant phenotype in the absence of the drug (Buckheit 2004). The dynamics of adaptation to new selective pressures, showing the largest fitness gains at the beginning of the process, has been ascribed, at least partially, to a diminished effect of beneficial mutations as fitness increases, which is also a form of epistasis (Bull et al. 2000; Rokyta et al. 2011).

The sign and the magnitude of the effect of mutations are also strongly influenced by the environment and in the particular case of viruses by the host they infect. Often, adaptation to a host has a cost that translates into worsened performance in alternative hosts (Turner and Elena 2000; Weaber et al. 1999; Lalić et al. 2011). In other cases, however, evolution in a particular host does not entail a cost in others (Núñez et al. 2007) and can even result in fitness gains (Remold et al. 2008; Coffey and Vignuzzi 2011). A cost of fitness across environments has been also observed in drug-resistant mutants, which usually pay a fitness cost when the drug is absent (Armstrong et al. 2011). In the case of escape mutants, genomic changes carried by resistant phenotypes typically target critical virus functions and are accompanied by fitness decreases (Das et al. 2011). This kind of fitness trade-offs can be due to antagonistic pleiotropy, that is to mutations beneficial in the selected environment but deleterious elsewhere, or to the accumulation of mutations neutral in one environment but disadvantageous in others. Whereas these studies clearly demonstrate that a particular combination of mutations does not perform equally in different environments, they usually do not identify the contribution of individual mutations to the overall effect. This question was addressed by Elena and co-workers in a study where they characterized a collection of twenty single-nucleotide substitution mutants of TEV across a set of eight host environments, five of which were natural hosts for the virus (Lalić et al. 2011). They found that the fraction of lethal, deleterious, neutral and beneficial mutations depended on the specific host, and this dependence varied with the phylogenetic distance among hosts. In the same way that the fitness effects of mutations change with the environment, there is no reason to expect that epistatic interactions are independent of the environment or of the overall genomic context. Another study carried out with TEV virus compared the effect of pairs of mutations in different hosts, showing that epistasis was indeed affected by the degree of genetic divergence between the primary and the alternative hosts (Lalić and Elena 2013).

4 Fitness Landscapes

A fitness landscape is a mapping from the genomic, multidimensional space, to a real value that represents fitness (Wright 1931; see also Chap. 4). The empirical observations described up to now offer glimpses of the local structure of viral fitness landscapes and of the short-term consequences of their structure. Often, only mutants differing in one or few sequence positions have been studied, and even landscapes as small as that in Fig. 1b have not been fully described. Further, the dependence of fitness on the endogenous environment and on current selective pressures extraordinarily complicates the picture. At this point, there are two different approaches one can take in order to advance in the understanding of viral evolution. First, one can target particular model systems and the value of precise mutations. These studies are relevant to understand the effect of specific mutations in the studied context and may have predictive power regarding the system under study. On the negative side, these models are difficult to generalize. Second, one can take a statistical point of view, where emphasis is put on the average effects of mutations in fitness and the typical structure of fitness landscapes in order to derive expectations on the dynamics of populations. In this second case, the ability to perform specific predictions diminishes, but the results might be applicable, as a first approximation, to a larger number of systems and evolutionary contexts. It is likely that new techniques soon yield quantitative information on much larger regions of the sequence space, working towards a convergence of those currently separated approaches.

There have been abundant formal attempts to derive a functional relationship between the mutations acquired by a genome and its fitness, which represents a first step towards characterizing the structure of fitness landscapes. Early on, simple dependencies led to assuming that evolution was occurring on a smooth, Fujiyama-like landscape (Kimura and Maruyama 1966), where epistasis was absent. Populations would steadily accumulate beneficial mutations until the unique, global fitness maximum would be reached. At the other extreme, there was the assumption of a random landscape, which ignored correlations between the phenotype yielded by a genome and that of its mutational neighbours, and predicted an exponential shape for the distribution of beneficial effects (Orr 2003). The study of the functional form of the effect of mutations in fitness is actually a complementary way to probe the structure of a fitness landscape. In highly correlated landscapes (e.g. Fujiyama-like), most mutations have a small effect on fitness and yield similar phenotypes; mutations with a large effect are exponentially rare, implying that they are not to be detected in practice. In random landscapes, the effect of a mutation cannot be predicted, in the sense that any change in fitness is possible. As it could have been guessed, a realistic fitness landscape lies somewhere in between those extremes: most mutations have a small effect in fitness (Orr 1998; Lourenço et al. 2011), but the probability to have a mutation with a medium-to-large effect is non-negligible (Lalić et al. 2011). Significant advances in this direction might arrive soon in the light of recent achievements regarding the

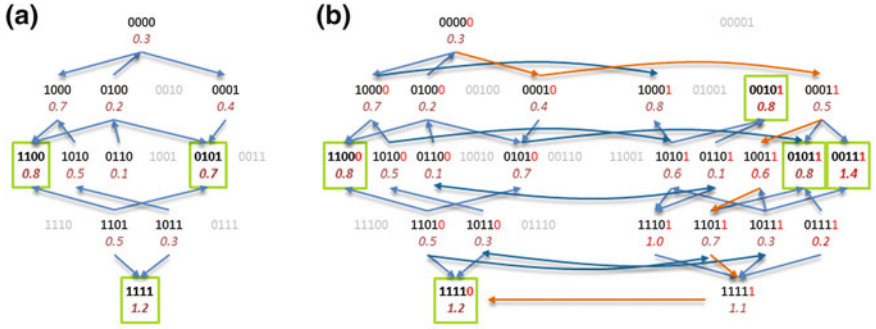

Fig. 1 Epistasis and roughness of fitness landscapes. Fitness is indicated below each of the sequences. Sequences of zero fitness are represented in *pale grey*. *Arrows* point towards increases in fitness. Local maxima appear in *bold face* within a *green square*. **a** Example of fitness landscape for a genome of length 4. This landscape has three maxima, two local and one global. The latter (1111) cannot be reached through point mutations from most other sequences (1101 and 1011 are the exceptions). There are several cases of epistasis, which make the landscape rough. An example of negative sign epistasis is the group {0000,1000,0100,1100} and one of reverse sign epistasis {1100,0100,0101,1101}. **b** When longer sequences are considered, new pathways for adaptation appear, and the position of global and local maxima might change. Now, the former global maximum 11110 can be attained through point mutations from 00000, as indicated by *orange arrows*, and from several other sequences. However, it has become a local maximum, and it is likely that the population either attains the new global maximum 00111 or gets trapped at the local maximum 01011. Sequences {00101,10101,01101,11101} form an example of reverse sign epistasis and {00010,00011,01010,01011} of no epistasis (thus not affecting landscape roughness). There are also two neutral mutations, between pairs {01100,01101} and {10110,10111}. Note that those same mutations change value when the genomic context varies

overall structure of viral fitness landscapes (Kouyos et al. 2012; Acevedo et al. 2014). A precise description of the shape of the distribution of fitness effects (Good et al. 2012), and by extension of the structure of fitness landscapes, is essential to understand the evolution and adaptation of viral populations. Quantitative information on the local and global structure of fitness landscapes will probably experience a boost in the near future thanks to the extended use of next-generation sequencing technologies (Beerenwinkel and Zagordi 2011; Radford et al. 2012).

Epistasis and roughness of fitness landscapes are two sides of the same coin. Depending on the type of epistasis dominant in natural populations, fitness landscapes can rank from smooth (no epistasis or magnitude epistasis) to rough, with multiple adaptive peaks. Meta-analyses of empirically characterized fitness landscapes point to the existence of certain general properties in landscapes described to date that make them compatible with a rough, Fujiyama-like structure (Szendro et al. 2013). In the case of RNA viruses, the abundance of sign and reverse sign epistasis speaks for rugged fitness landscapes, with many peaks and valleys a few mutational steps away (Withlock et al. 1995; Poelwijk et al. 2011). Epistatic interactions are also responsible for the appearance of ridges in the fitness landscape, that is sets of genomes of similar fitness that permit an easy exploration of

the space of genotypes. In the limit where genomes have equal fitness and are mutually accessible through mutations, it has been shown that populations tend to select the most connected regions of this neutral network, where they attain maximal robustness (de Visser et al. 2003; Huynen et al. 1996). Robustness may be a property only observable in large populations that have evolved for a sufficiently long time at high error rate (Lauring et al. 2013). Though rarely observed, this collective behaviour has been detected in micro-RNAs (Borenstein and Ruppin 2006), viroids (Codoñer et al. 2006) and RNA viruses (Sanjuán et al. 2007).

5 Discussion and Prospects

The adaptive potential of RNA viruses depends on the interplay among many factors, such as high mutation rates, epistasis (dependence of mutations on the genomic context), robustness (or tolerance to mutations) or interactions within the mutant spectrum. Adaptation depends on environmental conditions, which determine the number and strength of selective pressures applied to viruses and promote the appearance of specific solutions (of which resistance to drugs is a particular case). A complete theory with predictive power seems a formidable task at the moment, though empirical knowledge and steady improvements in quasispecies models (be they applied to specific experimental scenarios or aimed at capturing general features of viral evolution) are widening our view of the problem and, hopefully, offering a broadening and increasingly complete picture (see Chaps. 1, 3, and 4).

The properties of the fitness landscape determine the nature of the evolutionary trajectories available to populations (Poelwijk et al. 2007). Our current picture is that of a correlated (relatively smooth) landscape at the local scale, crossing over to a rougher and eventually random landscape at large genomic distances (Kouyos et al. 2012). Local correlations, that is the presence of mutations that affect little or do not affect fitness, might construct long pathways that, as proposed by Maynard Smith decades ago, should permit the almost costless navigation of the genome space (Maynard Smith 1970). Regions of high robustness to mutations support a larger diversity of the population and consequently grant access to a larger number of evolutionary innovations (novel phenotypes), eventually promoting adaptation (Wagner 2012). There is indirect evidence that the number of different genotypes yielding an almost invariable phenotype is a large set that under very general conditions might span most of the genome space (Wagner 2011). If this is so, most phenotypes might be a few mutational steps away. At present, we have a handful of examples where evolution consisting in periods of drift along quasineutral networks of genotypes, followed by the identification and fixation of a phenotype of higher fitness, has been described (Koelle et al. 2006; Woo and Reifman 2012), but the way towards characterization of this behaviour in other systems is paved.

As it occurs in most of the empirical and theoretical analysis performed to date, we have mostly reviewed the effect of point mutations in evolution and adaptation

—with the exception of the few examples on the role of large genomic deletions in population dynamics. If we assume single mutations as the mechanism that drives movement on genotype spaces, only contiguous genotypes can be accessed. However, other mechanisms as recombination modify the accessibility of different genotypes and the simple image of diffusive movement on a landscape. The final states of the population are significantly modified when recombination comes into play: mutation–selection equilibrium is no longer unique and depends on the evolutionary history of the population. Other mutational mechanisms and sources of variability, and their effects when coupled to a particular genomic, populational or environmental context, should be included in future conceptual and formal approaches to viral evolution.

Our hope for a meaningful theory of viral quasispecies relies in the existence of generic mechanisms or, at least, in a reduced number of evolutionary classes. The identification of universal patterns in the fitness landscape of viruses and other evolutionary systems (as proteins or whole genomes) should prove a tremendous advance in the development of evolutionary theories of broad applicability. The first steps in that direction are encouraging and promise very exciting challenges and advances in the near future.

Acknowledgments The authors acknowledge support of the Spanish MINECO through projects BFU2013-41329, FIS2011-27569, and FIS2014-57686.

References

Acevedo A, Brodsky L, Andino R (2014) Mutational and fitness landscapes of an RNA virus revealed through population sequencing. Nature 505:686–690

Agudo R, Arias A, Domingo E (2009) 5-fluorouracil in lethal mutagenesis of foot-and-mouth disease virus. Future Med Chem 1:529–539

Agudo R, Ferrer-Orta C, Arias A, de la Higuera I, Perales C, Pérez-Luque R, Verdaguer N, Domingo E (2010) A multi-step process of viral adaptation to a mutagenic nucleoside analogue by modulation of transition types leads to extinction-escape. PLoS Pathog 6:e1001072

Aguirre J, Manrubia SC (2008) Effects of spatial competition on the diversity of a quasispecies. Phys Rev Lett 100:038106

Arias A, Arnold JJ, Sierra M, Smidansky ED, Domingo E, Cameron CE (2008) Determinants of RNA-dependent RNA polymerase (in)fidelity revealed by kinetic analysis of the polymerase encoded by a foot-and-mouth disease virus mutant with reduced sensitivity to ribavirin. J Virol 82:12346–12355

Arias A, Isabel de Ávila A, Sanz-Ramos M, Agudo R, Escarmís C, Domingo E (2013) Molecular dissection of a viral quasispecies under mutagenic treatment: positive correlation between fitness loss and mutational load. J Gen Virol 94:817–830

Armstrong KL, Lee TH, Essex M (2011) Replicative fitness costs of nonnucleoside reverse transcriptase inhibitor drug resistance mutations on HIV subtype C. Antimicrob Agents Chemother 55:2146–2153

Arribas M, Cabanillas L, Lázaro E (2011) Identification of mutations conferring 5-azacytidine resistance in bacteriophage Qβ. Virology 417:343–352

Beerenwinkel N, Zagordi O (2011) Ultra-deep sequencing for the analysis of viral populations. Curr Opin Virol 1:1–6

Biebricher CK, Eigen M (2005) The error threshold. Virus Res 107:117-127
Bonhoeffer S, Chappey C, Parkin NT, Whitcomb JM, Petropoulos CJ (2004) Evidence for positive epistasis in HIV-1. Science 306:1547–1550
Borenstein E, Ruppin E (2006) Direct evolution of genetic robustness in microRNA. Proc Natl Acad Sci USA 103:6593–6598
Buckheit RW Jr (2004) Understanding HIV resistance, fitness, replication capacity and compensation: targeting viral fitness as a therapeutic strategy. Expert Opin Investig Drugs 13:933–958
Bull JJ, Badgett MR, Wichman HA (2000) Big-benefit mutations in a bacteriophage inhibited with heat. Mol Biol Evol 17:942–950
Bull JJ, Sanjuán R, Wilke CO (2007) Theory of lethal mutagenesis for viruses. J Virol 81:2930–2939
Burch CL, Chao L (2004) Epistasis and its relationship to canalization in the RNA virus phi 6. Genetics 167:559–567
Carrasco P, de la Iglesia F, Elena SF (2007) Distribution of fitness and virulence effects caused by single-nucleotide substitutions in Tobacco Etch virus. J Virol 81:12979–12984
Cases-González C, Arribas M, Domingo E, Lázaro E (2008) Beneficial effects of population bottlenecks in an RNA virus evolving at increased error rate. J Mol Biol 384:1119–1120
Chao L (1991) Levels of selection, evolution of sex in RNA viruses, and the origin of life. J Theor Biol 153:229–246
Codoñer FM, Darós JA, Solé RV, Elena SF (2006) The fittest versus the flattest: experimental confirmation of the quasispecies effect with subviral pathogens. PLoS Pathog 2:e136
Coffey LL, Beeharry Y, Bordería AV, Blanc H, Vignuzzi M (2011) Arbovirus high fidelity variant loses fitness in mosquitoes and mice. Proc Natl Acad Sci USA 108:16038–16043
Coffey LL, Vignuzzi M (2011) Host alternation of chikungunya virus increases fitness while restricting population diversity and adaptability to novel selective pressures. J Virol 85:1025–1035
Covert AW, Lenski RE, Wilke CO, Ofria C (2013) Experiments on the role of deleterious mutations as stepping stones in adaptive evolution. Proc Natl Acad Sci USA 110:E3171–E3178
Crotty S, Cameron CE, Andino R (2001) RNA virus error catastrophe: direct molecular test by using ribavirin. Proc Natl Acad Sci (USA) 98:6895–6900
Cuesta JA, Aguirre J, Capitán JA, Manrubia SC (2011) Struggle for space: viral extinction through competition for cells. Phys Rev Lett 106:028104
Dapp MJ, Clouser CL, Patterson S, Mansky LM (2009) 5-Azacytidine can induce lethal mutagenesis in human immunodeficiency virus type 1. J Virol 83:11950–11958
Das SR, Hensley SE, David A et al (2011) Fitness costs limit influenza A virus hemagglutinin glycosylation as an immune evasion strategy. Proc Natl Acad Sci (USA) 108:E1417–E1422
de Visser JAGM, Hermisson J, Wagner GP, Meyers LA, Bagheri HC, Blanchard JL, Chao L, Cheverud JM, Elena SF, Fontana W, Gibson G, Hansen TF, Krakauer D, Lewontin RC, Ofria C, Rice SH, von Dassow G, Wagner A, Whitlock MC (2003) Evolution and detection of genetic robustness. Evolution 57:1959–1972
Domingo E, Sheldon J, Perales C (2012) Viral quasispecies evolution. Microbiol Mol Biol Rev 76:159–216
Domingo E, González-Lopez C, Pariente N, Airaksinen A, Escarmís C (2005) Population dynamics of RNA viruses: the essential contribution of mutant spectra. In: Peters CJ, Calisher CH (eds) Infectious diseases from nature: mechanisms of viral emergence and persistence, pp 59–71
Domingo-Calap P, Cuevas JM, Sanjuán R (2009) The fitness effects of random mutations in single-stranded DNA and RNA bacteriophages. PLoS Genet 5:e1000742
Drake JW, Holland JJ (1999) Mutation rates among RNA viruses. Proc Natl Acad Sci (USA) 96:13910–13913
Eigen M (1971) Selforganization of matter and the evolution of biological macromolecules. Naturwissenschaften 58:465–523

Eigen M (2002) Error catastrophe and antiviral strategy. Proc Natl Acad Sci U S A 99:13374–13376

Elena SF (1999) Little evidence for synergism among deleterious mutations in a nonsegmented RNA virus. J Mol Evol 49:703–707

Escarmís C, Gómez-Mariano G, Dávila M, Lázaro E, Domingo E (2002) Resistance to extinction of low fitness virus subjected to plaque-to-plaque transfers: diversification by mutation clustering. J Mol Biol 315:647–661

Gago S, Elena SF, Flores R, Sanjuán R (2009) Extremely high mutation rate of a hammerhead viroid. Science 323:1308

García-Arriaza J, Manrubia SC, Toja M, Domingo E, Escarmís C (2004) Evolutionary transition toward defective RNAs that are infectious by complementation. J Virol 78:11678–11685

Good BH, Rouzine IM, Balick DJ, Hallatschek O, Desai MM (2012) Distribution of fixed beneficial mutations and the rate of adaptation in asexual populations. Proc Natl Acad Sci USA 109:4950–4955

Graci JD, Gnädig NF, Galarraga JE, Castro C, Vignuzzi M, Cameron CE (2012) Mutational robustness of an RNA virus influences sensitivity to lethal mutagenesis. J Virol 86:2869–2873

Grande-Pérez A, Sierra S, Castro MG, Domingo E, Lowenstein PR (2002) Molecular indetermination in the transition to error catastrophe: systematic elimination of lymphocytic choriomeningitis virus through mutagenesis does not correlate linearly with large increases in mutant spectrum complexity. Proc Natl Acad Sci (USA) 99:12938–12943

Grande-Pérez A, Lázaro E, Lowenstein P, Domingo E, Manrubia SC (2005) Suppression of viral infectivity through lethal defection. Proc Natl Acad Sci U S A 102:4448–4452

Harris RS, Bishop KN, Sheehy AM, Craig HM, Petersen-Mahrt SK et al (2003) DNA deamination mediates innate immunity to retroviral infection. Cell 113:803–809

Holland J, Spindler K, Horodyski F, Grabau E, Nichol S, VandePol S (1982) Rapid evolution of RNA genomes. Science 215:1577–1585

Holland JJ, Domingo E, de la Torre JC, Steinhauer DA (1990) Mutation frequencies at defined single codon sites in vesicular stomatitis virus can be increased only slightly by chemical mutagenesis. J Virol 64:3960–3962

Holmes EC (2003) Error thresholds and the constraints to RNA virus evolution. Trends Microbiol 11:543–546

Holtz CM, Mansky LM (2013) Variation of HIV-1 mutation spectra among cell types. J Virol 87:5296–5299

Hull R (2013) Plant virology. Academic Press, p 1120

Huynen MA, Stadler PF, Fontana W (1996) Smoothness within ruggedness: The role of neutrality in adaptation. Proc Natl Acad Sci USA 93:397–401

Iranzo J, Manrubia SC (2009) Stochastic extinction of viral infectivity through the action of defectors. Europhys Lett 85:18001

Iranzo J, Manrubia SC (2012) Evolutionary dynamics of genome segmentation in multipartite viruses. Proc R Soc Lond B 279:3812–3819

Iranzo J, Perales C, Domingo E, Manrubia S (2011) Tempo and mode of inhibitor-mutagen antiviral therapies: A multidisciplinary approach. Proc Natl Acad Sci USA 108:16008–16013

Julias JG, Pathak VK (1998) Deoxyribonucleoside triphosphate pool imbalances in vivo are associated with an increased retroviral mutation rate. J Virol 72:7941–7949

Kimura M, Maruyama T (1966) The mutational load with epistatic interactions in fitness. Genetics 54:1337–1351

Koelle K, Cobey S, Grenfell B, Pascual M (2006) Epochal evolution shapes the phylodynamics of interpandemic influenza A (H3N2) in humans. Science 314:1898–1903

Kouyos RD, Leventhal GE, Hinkley T, Haddad M, Whitcomb JM, Petropoulos CJ, Bonhoeffer S (2012) Exploring the complexity of the HIV-1 fitness landscape. PLoS Genet 8:e1002551

Lalić J, Cuevas JM, Elena SF (2011) Effect of host species on the distribution of mutational fitness effects for an RNA virus. PLoS Genet 7:e1002378

Lalić J, Elena SF (2012) Magnitude and sign epistasis among deleterious mutations in a positive-sense plant RNA virus. Heredity 109:71–77

Lalić J, Elena SF (2013) Epistasis between mutations is host-dependent for an RNA virus. Biol Lett 9:20120396

Lauring AS1, Frydman J, Andino R (2013) The role of mutational robustness in RNA virus evolution. Nat Rev Microbiol 11:327–336

Lázaro E, Escarmís C, Domingo E, Manrubia SC (2002) Modeling viral genome fitness evolution associated with serial bottleneck events: evidence of stationary states of fitness. J Virol 76:8675–8681

Lázaro E, Escarmís C, Pérez-Mercader J, Manrubia SC, Domingo E (2003) Resistance of virus to extinction on bottleneck passages: study of a decaying and fluctuating pattern of fitness loss. Proc Natl Acad Sci USA 100:10830–10835

Lázaro E, Escarmís C, Manrubia SC (2006) Population bottlenecks in quasispecies dynamics. Curr Top Microbiol Immunol 299:141–170

Lee CH, Gilbertson DL, Novella IS, Huerta R, Domingo E, Holland JJ (1997) Negative effects of chemical mutagenesis on the adaptive behavior of vesicular stomatitis virus. J Virol 71: 3636–3640

Loeb LA, Essigmann JM, Kazazi F, Zhang J, Rose KD, Mullins JI (1999) Lethal mutagenesis of HIV with mutagenic nucleoside analogs. Proc Natl Acad Sci USA 96:1492–1497

Lourenço J, Galtier N, Glémin S (2011) Complexity, pleiotropy, and the fitness effect of mutations. Evolution 65:1559–1571

Manrubia SC, Domingo E, Lázaro E (2010) Pathways to extinction: Beyond the error threshold. Phil Trans R Soc London B 365:1943–1952

Manrubia SC, Lázaro E (2006) Viral evolution. Phys Life Revs 3:65–92

Manrubia SC (2012) Modelling viral evolution and adaptation: challenges and rewards. Curr Opin Virol 2:531–537

Martínez JP, Bocharov G, Ignatovich A, Reiter J, Dittmar MT, Wain-Hobson S, Meyerhans A (2011) Fitness ranking of individual mutants drives patterns of epistatic interactions in HIV-1. PLoS ONE 6:e18375

Maynard Smith J (1970) Natural Selection and the concept of a protein space. Nature 225:563–564

Moreno H, Tejero H, de la Torre JC, Domingo E, Martín V (2012) Mutagenesis-mediated virus extinction: virus-dependent effect of viral load on sensitivity to lethal defection. PLoS ONE 7: e32550

Moreno E, Ojosnegros S, García-Arriaza J, Escarmís C, Domingo E, Perales C (2014) Exploration of sequence space as the basis of viral RNA genome segmentation. Proc Natl Acad Sci USA 111:6678–6683

Muller HJ (1964) The relation of recombination to mutational advance. Mutat Res 1:2–9

Nee S (1987) The evolution of multicompartmental genomes in viruses. J Mol Evol 25:277–281

Núñez JI, Molina N, Baranowski E, Domingo E, Clark S, Burman A, Berryman S, Jackson T, Sobrino F (2007) Guinea pig-adapted foot-and-mouth disease virus with altered receptor recognition can productively infect a natural host. J Virol 81:8497–8506

Ojosnegros S, Agudo R, Sierra M, Briones C, Sierra S, González-López C, Domingo E, Cristina J (2008) Topology of evolving, mutagenized viral populations: quasispecies expansion, compression, and operation of negative selection. BMC Evol Biol 8:207

Ojosnegros S, García-Arriaza J, Escarmís C, Manrubia SC, Perales C, Arias A, García Mateu M, Domingo E (2011) Viral genome segmentation can result from a trade-off between genetic content and particle stability. PLoS Genet 7:e1001344

Orr HA (1998) The population genetics of adaptation: the distribution of factors fixed during adaptive evolution. Evolution 52:935–949

Orr HA (2003) The distribution of fitness effects among beneficial mutations. Genetics 163: 1519–1526

Pariente N, Airaksinen A, Domingo E (2003) Mutagenesis versus inhibition in the efficiency of extinction of foot-and-mouth disease virus. J Virol 77:7131–7138

Perales C, Mateo R, Mateu MG, Domingo E (2007) Insights into RNA virus mutant spectrum and lethal mutagenesis events: replicative interference and complementation by multiple point mutants. J Mol Biol 369:985–1000

Perales C, Agudo R, Manrubia SC, Domingo E (2011a) Influence of mutagenesis and viral load on the sustained low-level replication of an RNA virus. J Mol Biol 407:60–78
Perales C, Martín V, Domingo E (2011b) Lethal mutagenesis of viruses. Curr Opin Virol 1: 419–422
Perales C, Henry M, Domingo E, Wain-Hobson S, Vartanian JP (2011c) Lethal mutagenesis of foot-and-mouth disease virus involves shifts in sequence space. J Virol 85:12227–12240
Perales C, Iranzo J, Manrubia SC, Domingo E (2012) The impact of quasispecies dynamics on the use of therapeutics. Trends Microbiol 20:595–603
Pfeiffer JK, Kierkegaard K (2003) A single mutation in poliovirus RNA-dependent RNA polymerase confers resistance to mutagenic nucleotide analogs via increased fidelity. Proc Natl Acad Sci USA 100:7289–7294
Pfeiffer JK, Kierkegaard K (2005) Increased fidelity reduces poliovirus fitness and virulence under selective pressure in mice. PLoS Pathog 1:e11
Phillips PC (2008) Epistasis—the essential role of gene interactions in the structure and evolution of genetic systems. Nat Rev Genet 9:855–867
Pita JS, de Miranda JR, Schneider WL, Roossinck MJ (2007) Environment determines fidelity for an RNA virus replicase. J Virol 81:9072–9077
Poelwijk FJ, Kiviet DJ, Weinreich DM, Tans SJ (2007) Empirical fitness landscapes reveal accessible evolutionary paths. Nature 445:383–386
Poelwijk FJ, Tănase-Nicola S, Kiviet DJ, Tans SJ (2011) Reciprocal sign epistasis is a necessary condition for multi-peaked fitness landscapes. J Theor Biol 272:141–144
Radford AD, Chapman D, Dixon L, Chantrey J, Darby AC, Hall N (2012) Application of next-generation sequencing technologies in virology. J Gen Virol 93:1853–1868
Remold SK, Rambaut A, Turner PE (2008) Evolutionary genomics of host adaptation in vesicular stomatitis virus. Mol Biol Evol 25:1138–1147
Rokyta DR, Joyce P, Caudle SB, Miller C, Beisel CJ, Wichman HA (2011) Epistasis between beneficial mutations and the phenotype-to-fitness map for a ssDNA virus. PLoS Genet 7(6): e1002075
Saakian DB, Hu C-K (2006) Exact solution of the Eigen model with general fitness functions and degradation rates. Proc Natl Acad Sci USA 103:4935–4939
Saakian DB, Muñoz E, Hu C-K, Deem MW (2006) Quasispecies theory for multiple-peak fitness landscapes. Phys Rev E 73:041913
Sierra S, Dávila M, Lowenstein PR, Domingo E (2000) Response of foot-and-mouth disease virus to increased mutagenesis: influence of viral load and fitness in loss of infectivity. J Virol 74:8316–8323
Sánchez-Navarro JA, Zwart MP, Elena SF (2013) Effects of the number of genome segments on primary and systemic infections with a multipartite plant RNA virus. J Virol 87:10805–10815
Sanjuán R, Moya A, Elena SF (2004a) The distribution of fitness effects caused by single-nucleotide substitutions in an RNA virus. Proc Natl Acad Sci USA 101:8396–8401
Sanjuán R, Moya A, Elena SF (2004b) The contribution of epistasis to the architecture of fitness in an RNA virus. Proc Natl Acad Sci USA 101:15376–15379
Sanjuán R, Cuevas JM, Furió V, Holmes EC, Moya A (2007) Selection for robustness in mutagenized RNA viruses. PLoS Genet 3:e93
Sanjuán R (2010) Mutational fitness effects in RNA and single-stranded DNA viruses: common patterns revealed by site-directed mutagenesis studies. Phil Trans R Soc Lond B 365: 1975–1982
Sanjuán R, Nebot MR, Chirico N, Mansky LM, Belshaw R (2010) Viral mutation rates. J Virol 84:9733–9748
Seronello S, Montanez J, Presleigh K, Barlow M, Park SB et al (2011) Ethanol and reactive species increase basal sequence heterogeneity of hepatitis C virus and produce variants with reduced susceptibility to antivirals. PLoS ONE 6:e27436
Severson WE, Schmaljohn CS, Javadian A, Jonsson CB (2003) Ribavirin causes error catastrophe during Hantaan virus replication. J Virol 77:481–488

Sicard A, Yvon M, Timchenko T, Gronenborn B, Michalakis Y et al (2013) Gene copy number is differentially regulated in a multipartite virus. Nat Commun 4:2248
Szendro IG, Schenk MF, Franke J, Krug J, de Visser AGM (2013) Quantitative analyses of empirical fitness landscapes. J Stat Mech P01005
Takeuchi N, Hogeweg P (2007) Error-threshold exists in fitness landscapes with lethal mutants. BMC Evol Biol 7:15
Tsetsarkin KA, McGee CE, Volk SM, Vanlandingham DL, Weaver SC, Higgs S (2009) Epistatic roles of E2 glycoprotein mutations in adaption of chikungunya virus to Aedes albopictus and Ae. aegypti mosquitoes. PLoS ONE 4:e6835
Turner PE, Elena SF (2000) Cost of host radiation in an RNA virus. Genetics 156:1465–1470
Vasilakis N, Deardorff ER, Kenney JL, Rossi SL, Hanley KA, Weaver SC (2009) Mosquitoes put the brake on arbovirus evolution: experimental evolution reveals slower mutation accumulation in mosquito than vertebrate cells. PLoS Pathog 5:e1000467
Vignuzzi M, Stone JK, Arnold JJ, Cameron CE, Andino R (2006) Quasispecies diversity determines pathogenesis through cooperative interactions in a viral population. Nature 39: 344–348
Wagner A (2011) The origins of evolutionary innovations. Oxford University Press, Oxford
Wagner A (2012) The role of robustness in phenotypic adaptation and innovation. Proc R Soc Lond B 279:1249–1258
Weaver SC, Brault AC, Kang W, Holland JJ (1999) Genetic and fitness changes accompanying adaptation of an arbovirus to vertebrate and invertebrate cells. J Virol 73:4316–4326
Withlock MC, Phillips PC, Moore FBG, Tonsor SJ (1995) Multiple fitness peaks and epistasis. Annu Rev Ecol Evol Syst 26:601–629
Woo HJ, Reifman J (2012) A quantitative quasispecies theory-based model of virus escape mutation under immune selection. Proc Natl Acad Sci USA 109:12980–12985
Wright S (1931) Evolution in mendelian populations. Genetics 16:97–159

Cooperative Interaction Within RNA Virus Mutant Spectra

Yuta Shirogane, Shumpei Watanabe and Yusuke Yanagi

Abstract RNA viruses usually consist of mutant spectra because of high error rates of viral RNA polymerases. Growth competition occurs among different viral variants, and the fittest clones predominate under given conditions. Individual variants, however, may not be entirely independent of each other, and internal interactions within mutant spectra can occur. Examples of cooperative and interfering interactions that exert enhancing and suppressing effects on replication of the wild-type virus, respectively, have been described, but their underlying mechanisms have not been well defined. It was recently found that the cooperation between wild-type and variant measles virus genomes produces a new phenotype through the heterooligomer formation of a viral protein. This observation provides a molecular mechanism underlying cooperative interactions within mutant spectra. Careful attention to individual sequences, in addition to consensus sequences, may disclose further examples of internal interactions within mutant spectra.

Contents

1 Introduction 220
2 Cooperation Within Mutant Spectra 220
3 Cooperation Through the Heterooligomer Formation of a Viral Protein 221
3.1 Measles Virus Membrane Fusion and Entry 221
3.2 A New Phenotype Produced Through the Cooperative Interaction Between Subunits of the Measles Virus F Protein 223
3.3 New Property Exhibited by the Measles Virus Carrying Mixed Genomes 226
3.4 Conditions Under Which the Cooperation Through the Heterooligomer Formation Can Occur 227
4 Conclusions 228
References 228

Y. Shirogane · S. Watanabe · Y. Yanagi (✉)
Department of Virology, Faculty of Medicine, Kyushu University, Fukuoka 812-8582, Japan
e-mail: yyanagi@virology.med.kyushu-u.ac.jp

Current Topics in Microbiology and Immunology (2016) 392: 219–229
DOI 10.1007/82_2015_461

Published Online: 11 July 2015

1 Introduction

Although the genome of an RNA virus is usually expressed as a consensus sequence, the viral population indeed consists of various clones having slightly different genomes (mutant spectra, also called quasispecies), because of the high error rate of the viral RNA polymerase (Holland et al. 1982; Eigen 1993; Duffy et al. 2008; Lauring and Andino 2010; Domingo et al. 2012; Perales et al. 2012). This feature is thought to contribute to the rapidly evolving nature of RNA viruses, allowing them to adapt to the environment in which they grow (Domingo et al. 2012). Thus, RNA viruses may expand their cell tropism and host range, and develop resistance to host immune responses and antiviral agents. These evolutionary changes presumably occur because the fittest clones among preexisting variants are selected under given conditions.

Studies, however, have revealed that individual variants are not entirely independent of each other and that internal interactions may exist within mutant spectra (Vignuzzi et al. 2006; Ciota et al. 2007, 2012; Arbiza et al. 2010; Nonacs and Kapheim 2012; Shirogane et al. 2012, 2013; Villarreal and Witzany 2013). Thus, even when two RNA virus populations have the same consensus sequence, they may have different fitness values and phenotypes, depending on their composition of mutant spectra.

A well-known example of the internal interactions is complementation, a phenomenon by which a genome expressing a functional protein can support replication of another closely related genome whose corresponding protein is defective or suboptimal (Domingo et al. 2012). The long-term transmission of a defective RNA genome possessing a non-sense mutation in the surface envelope protein gene was reported in patients infected with dengue virus (Aaskov et al. 2006). Complementation by the functional virus was proposed to explain this finding.

Internal interactions within a quasispecies population may be categorically classified into three types: cooperation, interference, and complementation. In this article, cooperative interactions are defined as those that produce a new and/or advantageous phenotype as compared with the wild-type virus, while interfering interactions are as those that exert suppressing effects on replication of the wild-type virus. Complementation usually does not influence fitness values and thus is not under positive or negative selection pressures (that is "neutral"), with regard to the wild-type virus. However, certain types of complementation can be considered as cooperative (see Sect. 2). Examples of cooperative and interfering interactions within RNA virus mutant spectra have been reported (Vignuzzi et al. 2006; Ciota et al. 2007, 2012; Perales et al. 2007; Domingo et al. 2012; Nonacs and Kapheim 2012), but their molecular mechanisms have not been well characterized.

2 Cooperation Within Mutant Spectra

There are several documented cooperative interactions within mutant spectra. A poliovirus carrying an RNA polymerase with high fidelity was found to lose its neuropathogenicity, and the virus regained the pathogenicity when its genome

diversity was expanded by chemical mutagenesis prior to infection (Vignuzzi et al. 2006). The change in viral tropism was probably caused by a narrow mutant spectrum and the resultant lack of cooperative interactions within the virus population. Increases in the replicative ability of West Nile virus in mosquito cells were found to correlate with increases in the size of the mutant spectrum, rather than changes in the consensus sequence (Ciota et al. 2007). Furthermore, it was shown that complementation operates on mutant spectra of West Nile virus, which acts to maintain phenotypic and genotypic diversity, and that the resulting cooperative interactions may lead to the average fitness level that exceeds the fitness level of any individual genotype (Ciota et al. 2012). Nonacs and Kapheim (2012) reported a model based on group-level selection acting on genetically complementary mutant spectra (social genome model), which was shown to nicely simulate the observed evolution of HIV.

As these examples convincingly indicate, cooperation occurs within viral mutant spectra, but its detailed molecular mechanisms remain to be clarified. In the next section, one of the molecular mechanisms accounting for it will be presented.

3 Cooperation Through the Heterooligomer Formation of a Viral Protein

3.1 Measles Virus Membrane Fusion and Entry

Measles virus, a member of the genus *Morbillivirus* in the family *Paramyxoviridae*, is an enveloped virus with a nonsegmented negative-sense RNA genome (Fig. 1). It has two envelope glycoproteins, the hemagglutinin (H) and fusion (F) protein (Lamb and Parks 2007). The H protein forms tetramers, whereas the F protein acts as trimers. Measles virus enters a cell by pH-independent membrane fusion at the cell surface. Attachment of the H protein to a cell surface receptor is thought to induce the conformational change of the H protein tetramer, which in turn triggers the adjacently located F protein trimer (prefusion form) for the large-scale conformational change, leading to the fusion of the viral envelope with the host cell membrane (Fig. 1) (Lamb and Parks 2007; Hashiguchi et al. 2011; Nakashima et al. 2013; Plattet and Plemper 2013). Upon infection of susceptible cells (receptor-expressing cells), measles virus usually induces cell–cell fusion, producing syncytia. Susceptible cells also develop syncytia when they are transfected with expression plasmids encoding the H and F proteins. The matrix (M) protein that associates with the inner surface of the envelope interacts with the cytoplasmic tails of the H and F proteins, thereby affecting membrane fusion (Lamb and Parks 2007). Two distinct types of cellular receptors for measles virus are known, the signaling lymphocyte activation molecule (SLAM) (also called CD150) on immune cells and nectin 4 (also called poliovirus-receptor-like-4) on epithelial cells (Tatsuo et al. 2000; Mühlebach et al. 2011; Noyce et al. 2011).

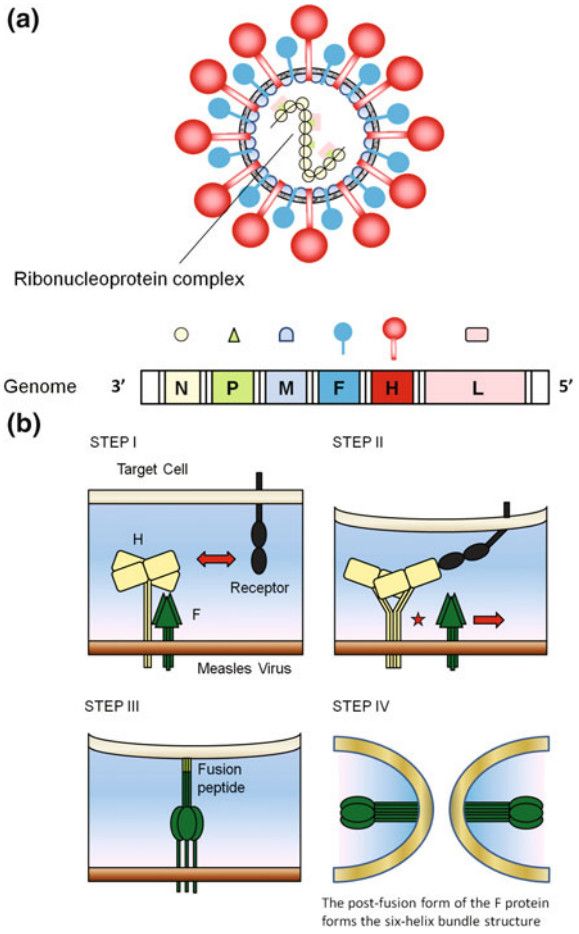

Fig. 1 Measles virus and membrane fusion. **a** Schematic diagrams of a measles virus particle and the genome structure. The RNA genome encapsidated by the nucleocapsid (N) protein forms the ribonucleoprotein complex with the viral RNA polymerase comprised of the phospho- (P) and large (L) proteins. Viral genes are indicated by the same colors as their corresponding proteins. **b** A model of measles virus membrane fusion (Hashiguchi et al. 2011). *STEP 1* The H protein tetramers associate with the F protein trimers (prefusion form), and the head domain of the F protein is in contact with the stalk of the H protein. The head domain of the H protein binds to its cell surface receptor. *STEP II* The binding of the H protein to a receptor in a twisted head-to-head orientation likely leads to the reduction of the distance between the viral envelope and the cell membrane, leading to the subsequent conformational shift of the H protein tetramer (dimer-of-dimers). Accordingly, the structure of the H protein stalk domain is affected, which in turn facilitates the dissociation of the F protein from the preassembled H/F complex. *STEP III* The destabilized and liberated F trimers subsequently undergo irreversible structural rearrangement, forming the prehairpin intermediate structure. During the conformational rearrangement, the fusion peptide of the F protein is exposed on its surface and inserted into the target cell membrane. *STEP IV* The F protein trimers refold into the stable postfusion conformation with the six-helix bundle structure, and membrane merger and fusion pore formation are completed

3.2 A New Phenotype Produced Through the Cooperative Interaction Between Subunits of the Measles Virus F Protein

It was uncovered by the following experiments that the "cooperation" between subunits of an oligomeric protein can produce a new phenotype (Shirogane et al. 2012, 2013). The recombinant measles virus that has the H protein fused with the FLAG-TEV-MYC tag at its C terminus (H-tag) was found not to cause syncytia in SLAM-expressing cells, unlike the virus possessing the wild-type H protein (Fig. 2). Presumably, the added tag sequence adversely affected the interaction of the H protein with the receptor and/or the F protein, thereby preventing membrane fusion from occurring. However, the recombinant virus started to cause cell-to-cell fusion after a few blind passages. Viruses that regained the ability to cause syncytia were plaque-purified, and their H, F, and M genes were subjected to sequence analysis. All of eight such viruses examined had one or two amino acid substitutions in the F protein, but none in the H (H-tag) protein. There was also no substitution in the M protein.

SLAM-expressing cells did not form syncytia when they were transfected with plasmids encoding H-tag and wild-type F proteins, but they formed syncytia when transfected with those encoding H-tag and mutant F proteins (Fig. 3). An exception was the F(G264R) protein in which glycine at amino acid position 264 was changed to arginine. No syncytia were detected in cells transfected with plasmids encoding H-tag and F(G264R) proteins (Fig. 3), inconsistent with the observation with the recombinant virus possessing this mutant F protein.

Rechecking the sequence data revealed that there were two overlapped signal peaks corresponding to the position 264 encoded in the F gene of this virus. The major and minor peaks were predicted to encode arginine and glycine (the residue present in the wild-type F protein), respectively, suggesting that this virus contained two types of genomes differing in the F gene. This is possible because paramyxoviruses usually include several genomes in one viral particle, the property called polyploidy (Hosaka et al. 1966; Dahlberg and Simon 1969; Rager et al. 2002). Consistent with this interpretation, SLAM-expressing cells formed syncytia when they were transfected with plasmids encoding H-tag, wild-type F, and F(G264R) proteins (Fig. 3). The result indicated that wild-type F and F(G264R) proteins together, but not individually, can mediate membrane fusion in conjunction with the H-tag protein.

The F protein of paramyxoviruses, including measles virus, is known to form trimers (Lamb and Parks 2007). In fact, a coimmunoprecipitation assay revealed the complex formation between wild-type F and F(G264R) proteins (Fig. 4), suggesting that heterotrimers comprised of wild-type F and F(G264R) proteins exhibited a new phenotype distinct from that of homotrimers of either the wild-type F or F(G264R) protein. Interestingly, copresence of the wild-type F and F(G264R) proteins was found to induce larger syncytia in SLAM-expressing cells, in conjunction with the wild-type H protein, as compared with the wild-type F protein alone (Table 1).

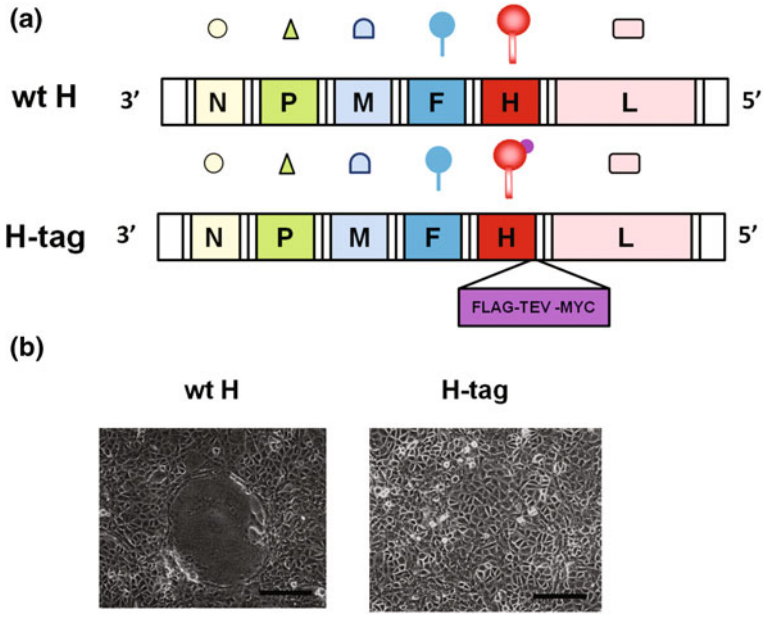

Fig. 2 The addition of a tag to the H protein interfered with fusion activity of measles virus. **a** Genome structures of recombinant measles viruses encoding the wild-type (wt) H protein and that fused to the FLAG-TEV-MYC tag (H-tag), respectively. **b** Wild-type measles virus caused syncytia in Vero cells expressing the SLAM receptor, while the virus expressing the H-tag protein did not. Scale bars, 200 μm. From Shirogane et al. (2012)

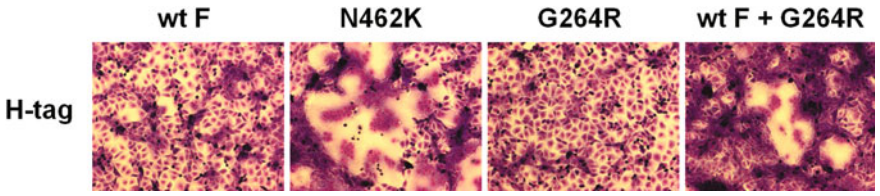

Fig. 3 Fusion assay based on plasmid-mediated expression of measles virus H and F proteins. SLAM-expressing Vero cells were transfected with expression plasmids encoding H-tag and wt F, F(N462 K), F(G264R) or wt F plus F(G264R). The mutant F(N462 K) protein caused syncytia in conjunction with the H-tag protein. From Shirogane et al. (2012)

More importantly, heterotrimers of wild-type F and F(G264R) proteins could induce cell–cell fusion even in cells expressing neither SLAM nor nectin 4 (Table 1).

At 30 °C, syncytia were observed in SLAM-expressing cells transfected with plasmids encoding H-tag and F(G264R) proteins, but not in those transfected with plasmids encoding H-tag and wild-type F proteins (Table 1). By contrast, syncytia were formed in cells transfected with plasmids encoding H-tag and wild-type F

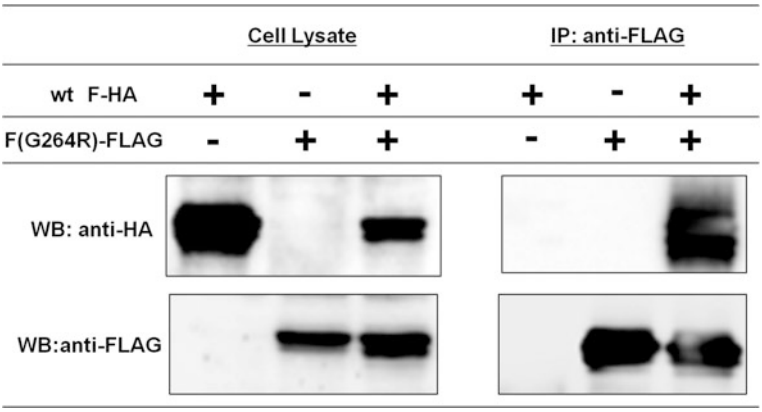

Fig. 4 Heterooligomer formation between wt F and F(G264R) proteins. HEK293T cells were cotransfected with expression plasmids encoding the HA-tagged wt F protein and/or FLAG-tagged F(G264R) protein, and the complex formation between these proteins was examined by coimmunoprecipitation and Western blot analysis. *IP* immunoprecipitation. *WB* Western blot. From Shirogane et al. (2012)

Table 1 Summary of the plasmid-mediated fusion assay

H	F	$SLAM^+$ cells			$SLAM^-$ nectin 4^- cells
		50 °C	37 °C	30 °C	37 °C
H-tag	wt F	+	−	−	ND
	G264R	−	−	+	ND
	wt F + G264R	ND	+	+	ND
wt H	wt F	ND	+	ND	−
	G264R	ND	−	ND	−
	wt F + G264R	ND	++	ND	+

ND, not done. From Shirogane et al. (2012)

proteins after 10 min of incubation at 50 °C. These results suggested that the prefusion form of the wild-type F protein, in conjunction with the H-tag protein, is too stable to be triggered for conformational change at 37 °C (triggering requires higher temperatures), whereas that of the F(G264R) protein is unstable at 37 °C, also precluding its proper triggering. Heterotrimers of the wild-type F and F (G264R) proteins presumably have the intermediate stability between wild-type F and F (G264R) proteins, so that they can be triggered at 37 °C after the binding of the H-tag protein to an appropriate receptor.

Furthermore, heterotrimers of the wild-type F and F(G264R) proteins appear to have enhanced fusion activity in conjunction with the wild-type H protein, as compared with homotrimers of the wild-type F protein. Thus, when expressed together with the wild-type H protein, the heterotrimers produce larger syncytia in SLAM- or nectin 4-expressing cells and induce cell–cell fusion even in SLAM- and

nectin 4-negative cells. It is likely that heterotrimers of the wild-type F and F (G264R) proteins, but not homotrimers of the wild-type F protein, are triggered for conformational change upon the binding of the wild-type H protein to a nonauthentic receptor molecule (its identity is currently unknown).

Among the eight recombinant viruses that regained the ability to induce cell–cell fusion, two viruses, including the one described above, possessed two types of the F protein, the combination of which was required for membrane fusion (Shirogane et al. 2012).

3.3 *New Property Exhibited by the Measles Virus Carrying Mixed Genomes*

The recombinant measles virus containing the two types of genomes was generated by using one full-length genome plasmid carrying the wild-type F gene and red fluorescent DsRed gene, and the other carrying the F(G264R) gene and enhanced green fluorescent protein gene (Shirogane et al. 2012). This virus recapitulated the findings obtained with plasmid-mediated expressions of the H and F proteins. Furthermore, the data indicated that most individual virus particles contained both types of genomes (due to polyploidy).

The recombinant virus containing the wild-type H and wild-type F genes did not spread in the brain of 7-day-old hamsters inoculated intracerebrally, presumably because hamsters do not have efficient receptors for measles virus. However, the virus containing mixed genomes (one carrying the wild-type H and wild-type F genes, and the other carrying the wild-type H and F(G264R) genes) did spread extensively (Fig. 5). Viruses recovered from the brain inoculated with the mixed genome virus still had both types of genomes. Thus, the “cooperation” of two

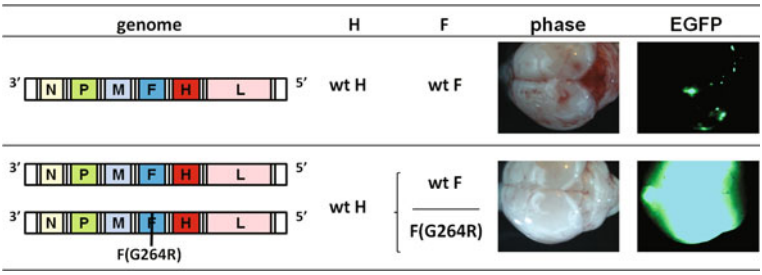

Fig. 5 Measles virus containing the mixed genomes spread in hamster brains. The virus having the two types of genomes encoding the wt H and wt F proteins and wt H and F(G264R) proteins, respectively, spreads in hamster brain tissues efficiently. The recombinant viruses also contain the gene encoding the enhanced green fluorescent protein (*EGFP*) (not shown in the genomic map). From Shirogane et al. (2012)

different genomes could provide the virus with the ability to propagate in nonhost, receptor-negative tissues, in which the wild-type virus does not propagate.

3.4 Conditions Under Which the Cooperation Through the Heterooligomer Formation Can Occur

In complementation, a genome encoding a functional protein allows replication of another closely related genome whose corresponding protein is defective. In the "cooperation" described above, neither of two genomes complements the defects of the other to exhibit the normal (wild-type) phenotype, but two genomes produce a new phenotype through an interaction between variant proteins. Thus, this study establishes that the heterooligomer formation between variant viral proteins can act as a molecular mechanism for the cooperation within mutant spectra, by producing a new or better phenotype as compared with the wild-type virus.

Apparently, polyploidy contributed to the "cooperation" between different measles virus genomes. Polyploidy is found in enveloped paramyxoviruses (Hosaka et al. 1966; Dahlberg and Simon 1969; Rager et al. 2002) and nonenveloped birnaviruses (Luque et al. 2009), but most other viruses contain only a single copy of each gene (haploid). Yet, the "cooperation" could occur in any viruses, when a single cell is coinfected with more than one virion containing different genomes or when mutations allowing the "cooperation" arise during genome replication within a single infected cell. Thus, the cooperation can occur in various types of viruses, and we should keep the possibility of the cooperation in mind, when we study virus populations.

Boulay et al. (1988) reported that different influenza virus hemagglutinins expressed in the same cells could form mixed heterotrimers, which exhibited the intermediate property regarding the acid-induced conformational change. This is an another example of the cooperation through the heterooligomer formation. Since the pH within the endosomes is different depending on species, mixed heterotrimers exhibiting different optimal pH for the acid-induced conformational change may efficiently induce membrane fusion in nonhost species, potentially affecting the host range of the influenza virus.

The long-term transmission of defective dengue virus genomes described above is thought to be caused by complementation (Aaskov et al. 2006). However, cotransmission of defective and functional dengue viruses has been shown to have a higher transmission potential than transmission of functional viruses alone (Ke et al. 2013), inconsistent with simple complementation. It is possible that the cooperation between the defective and functional viral genomes occurs through the heterooligomer formation or other unknown mechanisms, providing coinfecting defective and functional viruses with growth/transmission advantage over functional viruses alone. Some of the examples described in the Sect. 2 may also be mediated through the heterooligomer formation between variant proteins.

4 Conclusions

Viruses having defects in different genes may complement one another. In this case, the average fitness of an uncloned virus population may be higher than that of any clone within the population. Thus, complementation can serve as one of the mechanisms for cooperative interactions within mutant spectra. The heterooligomer formation between variant proteins described in this article may be another mechanism. Importantly, the heterooligomer formation between variant proteins can also explain interference within mutant spectra, by producing nonfunctional (or functionally suboptimal) viral proteins.

Because cooperation through the heterooligomer formation provides viral proteins with new properties, it may allow viruses to adapt to new environments, expanding their tissue tropisms and host ranges. Cooperation has also been proposed to play a role in the emergence of segmented viral genomes and evolution of heteromultimeric molecules such as hemoglobins (Shirogane et al. 2013).

The importance of individual variants (sequences) within mutant spectra cannot be emphasized too strongly. By relying only on genetic information based on consensus sequences, one may be easily misled into wrong interpretations of experimental data. The next-generation sequencing technology, combined with reverse genetics, may reveal not only the diversity of individual genome sequences within RNA virus populations, but also their intricate interactions relevant to virus biology and pathogenicity.

References

Aaskov J, Buzacott K, Thu HM et al (2006) Long-term transmission of defective RNA viruses in humans and Aedes mosquitoes. Science 311:236–238

Arbiza J, Mirazo S, Fort H (2010) Viral quasispecies profiles as the result of the interplay of competition and cooperation. BMC Evol Biol 10:137

Boulay F, Doms RW, Webster RG et al (1988) Posttranslational oligomerization and cooperative acid activation of mixed influenza hemagglutinin trimers. J Cell Biol 106:629–639

Ciota AT, Ehrbar DJ, Van Slyke GA et al (2012) Cooperative interactions in the West Nile virus mutant swarm. BMC Evol Biol 12:58

Ciota AT, Ngo KA, Lovelace AO et al (2007) Role of the mutant spectrum in adaptation and replication of West Nile virus. J Gen Virol 88:865–874

Dahlberg JE, Simon EH (1969) Physical and genetic studies of Newcastle disease virus: evidence for multiploid particles. Virology 38:666–678

Domingo E, Sheldon J, Perales C (2012) Viral quasispecies evolution. Microbiol Mol Biol Rev 76:159–216

Duffy S, Shackelton LA, Holmes EC (2008) Rates of evolutionary change in viruses: patterns and determinants. Nat Rev Genet 9:267–276

Eigen M (1993) Viral quasispecies. Sci Am 269:42–49

Hashiguchi T, Ose T, Kubota M et al (2011) Structure of the measles virus hemagglutinin bound to its cellular receptor SLAM. Nat Struct Mol Biol 18:135–141

Holland J, Spindler K, Horodyski F et al (1982) Rapid evolution of RNA genomes. Science 215:1577–1585

Hosaka Y, Kitano H, Ikeguchi S (1966) Studies on the pleomorphism of HVJ virions. Virology 29:205–221

Ke R, Aaskov J, Holmes EC et al (2013) Phylodynamic analysis of the emergence and epidemiological impact of transmissible defective dengue viruses. PLoS Pathog 9:e1003193

Lamb RA, Parks GD (2007) Paramyxoviridae: the viruses and their replication. In: Knipe DM, Howley PM, Griffin DE, Lamb RA, Martin MA, Roizman B, Straus SE (eds) Fields Virology, 5th edn. Lippincott Williams & Wilkins, Philadelphia, pp 1449–1496

Lauring AS, Andino R (2010) Quasispecies theory and the behavior of RNA viruses. PLoS Pathog 6:e1001005

Luque D, Rivas G, Alfonso C et al (2009) Infectious bursal disease virus is an icosahedral polyploid dsRNA virus. Proc Nat Acad Sci USA 106:2148–2152

Mühlebach MD, Mateo M, Sinn PL et al (2011) Adherens junction protein nectin-4 is the epithelial receptor for measles virus. Nature 480:530–533

Nakashima M, Shirogane Y, Hashiguchi T et al (2013) Mutations in the putative dimer-dimer interfaces of the measles virus hemagglutinin head domain affect membrane fusion triggering. J Biol Chem 288:8085–8091

Nonacs P, Kapheim KM (2012) Modeling disease evolution with multilevel selection: HIV as a quasispecies social genome. J Evol Med 1:235553

Noyce RS, Bondre DG, Ha MN et al (2011) Tumor cell marker PVRL4 (nectin 4) is an epithelial cell receptor for measles virus. PLoS Pathog 7:e1002240

Perales C, Iranzo J, Manrubia SC et al (2012) The impact of quasispecies dynamics on the use of therapeutics. Trends Microbiol 20:595–603

Perales C, Mateo R, Mateu MG et al (2007) Insights into RNA virus mutant spectrum and lethal mutagenesis events: replicative interference and complementation by multiple point mutants. J Mol Biol 369:985–1000

Plattet P, Plemper RK (2013) Envelope protein dynamics in paramyxovirus entry. MBio 4: e00413-13

Rager M, Vongpunsawad S, Duprex WP et al (2002) Polyploid measles virus with hexameric genome length. EMBO J 21:2364–2372

Shirogane Y, Watanabe S, Yanagi Y (2012) Cooperation between different RNA virus genomes produces a new phenotype. Nat Commun 3:1235

Shirogane Y, Watanabe S, Yanagi Y (2013) Cooperation: another mechanism of viral evolution. Trends Microbiol 21:320–324

Tatsuo H, Ono N, Tanaka K et al (2000) SLAM (CDw150) is a cellular receptor for measles virus. Nature 406:893–897

Vignuzzi M, Stone JK, Arnold JJ et al (2006) Quasispecies diversity determines pathogenesis through cooperative interactions in a viral population. Nature 439:344–348

Villarreal LP, Witzany G (2013) Rethinking quasispecies theory: From fittest type to cooperative consoria. World J Biol Chem 4:79–90

Arenavirus Quasispecies and Their Biological Implications

Ana Grande-Pérez, Veronica Martin, Hector Moreno and Juan C. de la Torre

Abstract The family *Arenaviridae* currently comprises over 20 viral species, each of them associated with a main rodent species as the natural reservoir and in one case possibly phyllostomid bats. Moreover, recent findings have documented a divergent group of arenaviruses in captive alethinophidian snakes. Human infections occur through mucosal exposure to aerosols or by direct contact of abraded skin with infectious materials. Arenaviruses merit interest both as highly tractable experimental model systems to study acute and persistent infections and as clinically important human pathogens including Lassa (LASV) and Junin (JUNV) viruses, the causative agents of Lassa and Argentine hemorrhagic fevers (AHFs), respectively, for which there are no FDA-licensed vaccines, and current therapy is limited to an off-label use of ribavirin (Rib) that has significant limitations. Arenaviruses are enveloped viruses with a bi-segmented negative strand (NS) RNA genome. Each genome segment, L (ca 7.3 kb) and S (ca 3.5 kb), uses an ambisense coding strategy to direct the synthesis of two polypeptides in opposite orientation, separated by a noncoding intergenic region (IGR). The S genomic RNA encodes the virus nucleoprotein (NP) and the precursor (GPC) of the virus surface glycoprotein that mediates virus receptor recognition and cell entry via endocytosis. The L genome RNA encodes the viral RNA-dependent RNA polymerase (RdRp, or L polymerase) and the small (ca 11 kDa) RING finger protein Z that has functions of a bona fide matrix protein including directing virus budding. Arenaviruses were thought to be relatively stable genetically with intra- and interspecies amino acid sequence identities of 90–95 % and 44–63 %, respectively. However, recent evidence has documented extensive arenavirus genetic variability in the field. Moreover, dramatic phenotypic differences have been documented among closely related LCMV isolates. These data provide strong evidence of viral quasispecies

A. Grande-Pérez · V. Martin · H. Moreno · J.C. de la Torre (✉)
Department of Immunology and Microbial Science, The Scripps Research Institute, La Jolla, CA, USA
e-mail: juanct@scripps.edu

Current Topics in Microbiology and Immunology (2016) 392: 231–275
DOI 10.1007/82_2015_468

Published Online: 16 October 2015

involvement in arenavirus adaptability and pathogenesis. Here, we will review several aspects of the molecular biology of arenaviruses, phylogeny and evolution, and quasispecies dynamics of arenavirus populations for a better understanding of arenavirus pathogenesis, as well as for the development of novel antiviral strategies to combat arenavirus infections.

Contents

1 Arenaviruses as Both Important Human Pathogens and Highly Tractable Experimental Systems for the Investigation of Virus–Host Interactions 232
1.1 Arenaviruses and Their Impact in Human Health 232
1.2 LCMV Infection of the Mouse as the Rosetta Stone of Virus–Host Interaction 234
2 Molecular and Cell Biology of Arenaviruses 234
2.1 Arenavirus Genome Organization 234
2.2 Arenavirus Life Cycle 235
2.3 Arenavirus Reverse Genetics 238
3 Genetic Variability of Arenaviruses 241
3.1 Organization and Phylogenetic Relationships of the Arenaviridae Family 241
3.2 Mechanisms of Arenavirus Genetic Diversity 243
3.3 Arenavirus Hypermutation 245
4 Contribution of Genetic Variability to Arenavirus–Host Interactions and Associated Disease 247
4.1 Coevolution of Arenaviruses and Their Natural Reservoirs: Intra- versus Inter-host Genetic Variation of Arenaviruses 247
4.2 Contribution of Viral Quasispecies to Arenavirus Pathogenesis 249
5 Implications of Arenavirus Genetic Variability for the Development of Antiviral Drugs and Vaccines to Combat Human Pathogenic Arenaviruses 252
5.1 Lethal Mutagenesis as a Novel Antiviral Strategy to Combat Arenavirus Infections 252
5.2 Advantages of Combination Versus Single Drug Therapy to Inhibit Arenavirus Multiplication 255
5.3 Arenavirus Genetic Variation and Development of Broad-Spectrum Vaccines 258
References 259

1 Arenaviruses as Both Important Human Pathogens and Highly Tractable Experimental Systems for the Investigation of Virus–Host Interactions

1.1 Arenaviruses and Their Impact in Human Health

Arenaviruses cause chronic infections of rodents across the world, and human infections occur through mucosal exposure to aerosols or by direct contact of abraded skin with infectious materials (Buchmeier et al. 2007). Both viral and host

factors contribute to a variable outcome of arenavirus infection, ranging from virus control and clearance by the host defenses to chronic infection in the absence of clinical symptoms to severe disease. Several arenaviruses cause hemorrhagic fever (HF) disease in humans and pose a serious public health problem in their endemic regions. Thus, the Old World (OW) arenavirus, Lassa virus (LASV), infects several hundred thousand individuals yearly in West Africa resulting in a high number of Lassa fever (LF) cases associated with high morbidity and mortality (Bray 2005; Geisbert and Jahrling 2004). The current LF endemic areas cover approximately 80 % of Sierra Leone and Liberia; 50 % of Guinea; 40 % of Nigeria; 30 % of each of Côte d'Ivoire, Togo, and Benin; and 10 % of Ghana (Fichet-Calvet and Rogers 2009), and recent studies have found evidence for expansion of LASV endemic regions into Mali, Senegal, and the Democratic Republic of Congo (Sogoba et al. 2012). Thus, it is quite likely that population at risk of LF includes most of West Africa and can be as high as 200 million people (Richmond and Baglole 2003); hence, with dengue fever exception, the estimated global burden of LF is the highest among viral HF (Falzarano and Feldmann 2013). Notably, increased traveling to and from endemic regions has led to the importation of LF cases into non-endemic metropolitan areas around the globe (Freedman and Woodall 1999; Isaacson 2001). Likewise, the New World (NW) arenavirus, Junin virus (JUNV), causes Argentine HF (AHF), a disease endemic to the Argentinean Pampas with hemorrhagic and neurological manifestations and a case fatality of 15–30 % (Peters 2002). In addition, evidence indicates that the worldwide-distributed prototypic arenavirus, lymphocytic choriomeningitis virus (LCMV), is a neglected human pathogen of clinical significance (Jahrling and Peters 1992; Mets et al. 2000; Palacios et al. 2008; Peters 2006).

Public health concerns about arenavirus infections are exacerbated because of the lack of FDA-approved vaccines against HF arenaviral diseases and current therapy to combat arenavirus infections being limited to an off-label use of the nucleoside analogue ribavirin (Rib) (Huggins 1989; Kilgore et al. 1995, 1997; McCormick et al. 1986; McKee et al. 1988). However, Rib is only partially effective, and its use has several limitations including the need of intravenous (iv) and early administration for optimal efficacy, and significant side effects (Damonte and Coto 2002). Although the live-attenuated Candid1 strain of JUNV has been shown to be an effective vaccine against AHF (Enria and Barrera Oro 2002), outside Argentina Candid1 has only investigational new drug (IND) status and it does not protect against LF. Despite efforts dedicated to the development and testing of LASV vaccines, not a single LASV vaccine candidate has entered a clinical trial although several vaccine platforms, including the MOPV/LASV reassortant ML29 and recombinant VSV and vaccinia virus expressing viral antigens, have been successfully tested in non-human primates (Falzarano and Feldmann 2013; Lukashevich 2012).

1.2 LCMV Infection of the Mouse as the Rosetta Stone of Virus–Host Interaction

Studies using LCMV infection of its natural host, the mouse, have led to major advances in virology and immunology that apply universally to other microbial infections and viral infections of humans including virus-induced immunopathological disease, MHC restriction, T cell-mediated killing, and effectiveness of adoptive immune T cell therapy in clearing viral infection (Zinkernagel 2002; Oldstone 2002). Likewise, the initial description of the contribution to viral persistence of negative immune regulators such as PDL-1 was made first with LCMV in mice (Barber et al. 2006). The outcome of LCMV infection of its natural host, the mouse, varies dramatically depending on the age, immunocompetence and genetic background of the host, as well as the route of infection, and the strain and dose of infecting virus (Oldstone 2002; Zinkernagel 2002; Buchmeier et al. 2007). Thus, iv inoculation of adult immunocompetent mice with LCMV Armstrong (ARM) strain results in an acute infection that induces a protective immune response that mediates virus clearance in 10–14 days, a process predominantly mediated by virus-specific CD8+ cytotoxic T lymphocytes (CTL). In contrast, iv inoculation with a high ($\geq 2 \times 10^6$ PFU) dose of the immunosuppressive LCMV clone 13 (Cl-13) strain, which differs from ARM only at three amino acid positions, causes persistent infection associated with generalized immune suppression (Ahmed and Oldstone 1988; Ahmed et al. 1984, 1988). These dramatic phenotypic differences between genetically very closely related viruses provide investigators with a superb experimental system to examine both host immune mechanisms of virus control and viral counteracting strategies.

2 Molecular and Cell Biology of Arenaviruses

2.1 Arenavirus Genome Organization

Arenaviruses are enveloped viruses with a bi-segmented negative-stranded (NS) RNA genome and a life cycle restricted to the cell cytoplasm (Buchmeier et al. 2007). Virions appear pleomorphic when examined by cryoelectron microscopy, ranging in size from 40 to more than 200 nm in diameter. Each genomic viral RNA segment, L (ca 7.3 kb) and S (ca 3.5 kb), uses an ambisense coding strategy to direct the synthesis of two polypeptides in opposite orientation, separated by a noncoding IGR that has been shown to act as a bona fide transcription termination signal (Fig. 1). There are significant differences in sequence and predicted folded structure between the S and L IGR, but among strains of the same arenavirus species, the S and L IGR sequences are highly conserved. The S RNA encodes the viral NP and the glycoprotein precursor (GPC) that is posttranslationally cleaved by the cellular site 1 protease (S1P) to yield the two mature virion glycoproteins GP1 and GP2 that form the spikes that decorate the virus surface

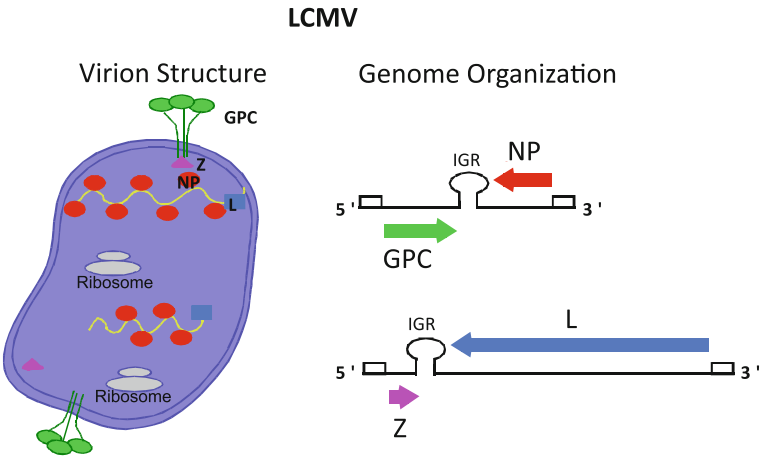

Fig. 1 Arenavirus genome organization and virion structure. Arenaviruses are enveloped viruses with a bi-segmented NS RNA genome. Each genome segment uses an ambisense coding strategy to direct the synthesis of two viral polypeptides. The small (S, ca 3.5 kb) segment encodes for the glycoprotein precursor (*GPC*) and nucleoprotein (*NP*). Posttranslational processing of GPC by the cellular protease S1P results in the production of GP1 and GP2. The large (L, ca 7.3 kb) segment encodes for the virus RNA-dependent RNA polymerase (*L*) and a small RING finger protein (*Z*) that has the properties of the bona fide matrix proteins (*M*) found in many enveloped NS RNA viruses

(Beyer et al. 2003; Lenz et al. 2001; Pinschewer et al. 2003). GP1 mediates virus receptor recognition and cell entry via endocytosis, whereas GP2 mediates the pH-dependent fusion event required to release the virus ribonucleoprotein (RNP) core into the cytoplasm of infected cells (Buchmeier et al. 2007). The L RNA encodes the viral RNA-dependent RNA polymerase (RdRp, or L polymerase) and the small RING finger protein Z that has functions of a bona fide matrix protein including directing virus budding (Perez et al. 2003; Strecker et al. 2003).

Arenaviruses exhibit high degree of sequence conservation at the genome 3′-termini (17 out of 19 nt are identical), and, as with other NS RNA viruses, arenavirus genome termini exhibit terminal complementarity with the 5′- and 3′-ends of both L and S genome segments predicted to form panhandle structures (Buchmeier et al. 2007). This prediction is supported by electron microscopy (EM) data showing the presence within the virion particles of circular RNP complexes (Young and Howard 1983). It has been proposed, based on EM studies, that host ribosomes can be also incorporated into virions, but the biological significance of this remains to be determined (Muller et al. 1983).

2.2 *Arenavirus Life Cycle*

Cell entry Arenavirus cell entry occurs via receptor-mediated endocytosis, which involves a pH-dependent fusion event between viral and cellular membranes within

the acidic environment of the endosome (Rojek and Kunz 2008; Rojek et al. 2008a, b). The widely expressed cell surface receptor for extracellular matrix proteins (ECM), alpha-dystroglycan (αDG), has been identified as a main receptor for LCMV, LASV, and several other arenaviruses (Kunz et al. 2002, 2004). To function as an arenavirus receptor, αDG needs to undergo several posttranslational modifications including a critical like-acetylglucosaminyltransferase (LARGE)-dependent glycosylation (Kunz et al. 2005). Intriguingly, recent genome-wide studies have uncovered evidence of positive selection of specific LARGE alleles within the Yoruba people living in regions of West Africa where LASV is endemic (Sabeti et al. 2007). Endocytic vesicles of the OW arenavirus LCMV were found to be non-coated, and LCMV cell entry process was reported to be cholesterol-dependent but clathrin-, dynamin-, caveolin-, ARF6-, flotillin-, and actin-independent (Rojek et al. 2008b). OW arenavirus cell entry follows an endocytic pathway that bypasses classical Rab5/EEA-1 positive early endosomes, but merges into the classical endocytotic pathway at the level of the multivesicular body (MVB) and is then delivered to the late endosome in an endosomal sorting complex required for transport (ESCRT)-dependent process (Pasqual et al. 2011). The unusual endocytotic pathway followed by LCMV and LASV may reflect the natural cellular trafficking of their receptor αDG. Nevertheless, it cannot be ruled out that binding of GP to αDG could trigger a novel route of entry for αDG that is tailored specifically to benefit virus cell entry as previously documented for other pathogens. Differently to OW arenaviruses, many NW arenaviruses, including the HFA JUNV, use the human transferrin receptor to initiate cell entry via clathrin-mediated endocytosis (Rojek et al. 2008b).

Expression and replication of the viral genome The fusion between viral and cellular membranes within the late endosome compartment releases the viral RNP into the cytoplasm where both RNA replication and gene transcription of the genome take place (Buchmeier et al. 2007). The NP and L coding regions are transcribed into a genomic complementary mRNA, whereas the GPC and Z coding regions are not translated directly from genomic RNA, but rather from genomic sense mRNAs that are transcribed using as templates the corresponding antigenome RNA species, which also function as replicative intermediates. Arenavirus mRNAs are non-polyadenylate and contain at their 5′-ends a short (4- to 5-nucleotide) non-templated sequence and a cap structure that are likely obtained from cellular mRNAs via a cap-snatching mechanism whose details remain to be determined, but the endonuclease activity associated with the arenavirus L polymerase likely contributes to this process (Morin et al. 2010). Transcription termination of viral mRNAs was mapped to multiple sites within the distal side of the IGR (Meyer et al. 2002; Meyer and Southern 1994; Tortorici et al. 2001), suggesting that the IGR acts as a bona fide transcription termination signal for the virus polymerase, which has been confirmed using cell-based minireplicon systems (Pinschewer et al. 2005).

NP and L are the only viral trans-acting factors required for efficient arenavirus RNA synthesis, whereas Z has been shown to exert a dose-dependent inhibitory effect on the RNA biosynthetic activities of the arenavirus polymerase complex

(Cornu and de la Torre 2001, 2002). The arenavirus L protein has the characteristic sequence motifs conserved among the RdRp (L proteins) of NS RNA viruses (Poch et al. 1989). Bioinformatic analysis and functional assays have provided evidence that LASV L protein is organized into three distinct structural domains and that the N- and C-parts of L are able to functionally trans-complement each other (Brunotte et al. 2011). Notably, the recent EM characterization of a functional MACV L protein has revealed a core ring domain decorated by appendages, which may reflect a modular organization of the arenavirus polymerase (Kranzusch and Whelan 2011). The NP is the main structural element of the viral RNP that directs viral RNA synthesis. NP exhibits also a type I interferon (IFN-I) counteracting activity that was mapped to its C-terminus (Martinez-Sobrido et al. 2006, 2007, 2009). Two recently determined crystal structures of LASV NP at 1.80 Å (Qi et al. 2010) and 1.5 Å (Hastie et al. 2011) resolution identified distinct N- and C-terminal domains connected by a flexible linker. The N-terminal domain was proposed to contain a potential cap-binding site that could provide the host-derived primers to initiate transcription by the virus polymerase (Qi et al. 2010). However, analysis of the structure of the N-terminal domain of LASV NP in complex with ssRNA suggests that this originally proposed cap-binding site likely corresponds to a binding site for the viral genome (Hastie et al. 2011). The C-terminal of NP has a folding that mimics that of the DEDDH family of 3′–5′ exoribonucleases (Hastie et al. 2011; Qi et al. 2010). Functional studies confirmed the 3′–5′ exoribonuclease activity of LASV NP, which was proposed to be critical for the anti-IFN activity of NP but dispensable for the role of NP on replication and transcription of the viral genome (Hastie et al. 2011; Qi et al. 2010). However, LCMV with a mutant NP lacking the 3′–5′ exoribonuclease had a large decrease in fitness during its replication in IFN-deficient Vero cells (Martinez-Sobrido et al. 2009).

Assembly and budding Assembly and cell release of infectious arenavirus progeny require both Z and correct processing of GPC into GP1 and GP2 by the cellular site 1 protease (S1P) (Kunz et al. 2003b; Perez et al. 2003; Pinschewer et al. 2003; Strecker et al. 2003; Urata et al. 2006). GP1 and GP2 together with a stable 58 amino acid long signal peptide (SSP) form the functional GP complex. SSP has been implicated in different aspects of the trafficking and function of the viral envelope glycoproteins (Saunders et al. 2007; York and Nunberg 2006, 2007; York et al. 2004). GP1 located at the top of the spike and held in place by ionic interactions with the N-terminus of the transmembrane GP-2 mediates virus interaction with host cell surface receptors, whereas GP2 exhibits similarities with fusion-active domains of other viral envelope proteins. The arenavirus RING finger protein Z is a structural component of the virion that has no homologue among other known NS RNA viruses. In LCMV-infected cells, Z has been shown to interact with several cellular proteins including the promyelocytic leukemia (PML) protein and the eukaryote translation initiation factor 4E (eIF4E), which have been proposed to contribute to the non-cytolytic nature of LCMV infection and repression of cap-dependent translation, respectively (Borden et al. 1998; Campbell Dwyer et al. 2000; Djavani et al. 2001; Volpon et al. 2010). For most

enveloped viruses, a matrix (M) protein is involved in organizing the virion components prior to assembly. Interestingly, arenaviruses do not have an obvious counterpart of M. However, structural and functional studies indicated that Z was the arenavirus counterpart of the M protein found in many other enveloped NS RNA viruses that play a critical role in assembly and cell release of mature infectious virions (Perez et al. 2003; Strecker et al. 2003; Urata et al. 2006). Accordingly, Z has been shown to be the main driving force of arenavirus budding, a process mediated by the Z late (L) domain motifs: PTAP and PPPY similar to those known to control budding of several other viruses including HIV and Ebola virus, via interaction with specific host cell proteins (Perez et al. 2003; Strecker et al. 2003; Urata et al. 2006). Consistent with this observation, Z exhibited features characteristic of bona fide budding proteins: (1) ability to bud from cells by itself and (2) substituted efficiently for other L domain. Targeting of Z to the plasma membrane, the location of arenavirus budding, strictly required its myristoylation (Perez et al. 2004; Strecker et al. 2006). Results derived from cryoelectron microscopy of arenavirus particles (Neuman et al. 2005) were also consistent with the role of Z as a functional M protein.

2.3 Arenavirus Reverse Genetics

In contrast to positive-stranded RNA viruses, deproteinized genomic and antigenomic RNAs of NS RNA viruses, such as LCMV, cannot function as mRNAs and are not infectious. This reflects the fact that the template of the polymerases of NS RNA viruses is exclusively a nucleocapsid consisting of the genomic RNA tightly encapsidated by the NP, which associated with the virus polymerase proteins forms a RNP complex. Thus, generation of biologically active synthetic NS viruses from cDNA requires trans-complementation by all viral proteins involved in virus replication and transcription. These considerations hindered the application of recombinant DNA technology to the genetic analysis of these viruses. However, significant progress has been made in this area, and for members of all families of NS RNA viruses, it has become possible to develop cell-based minireplicon systems and to rescue infectious virus from cloned cDNAs (Neumann and Kawaoka 2004). The use of reverse genetics approaches has revolutionized the analysis of cis-acting sequences and trans-acting proteins required for virus replication, transcription, maturation, and budding. In addition, the possibility to generate predetermined specific mutations within the virus genome and analyze their phenotypic expression in vivo in the context of the virus natural infection is contributing very significantly to the elucidation of the molecular mechanisms underlying virus–host interactions at the cellular and molecular levels, which has provided investigators with novel and powerful approaches for the investigation of viral pathogenesis. In addition, these developments have also paved the way for engineering these viruses for vaccine and gene therapy purposes (Subbarao and Katz 2004; von Messling and Cattaneo 2004).

Arenavirus minireplicon (MR) systems Cell-based minireplicon (MR) systems have been developed for a variety of arenaviruses (Emonet et al. 2011a), and their use provided conclusive evidence that NP and L are the minimal viral trans-acting factors required for efficient RNA synthesis mediated by the arenavirus polymerase complex (Hass et al. 2004; Lee et al. 2000; Lopez et al. 2001). Moreover, LCMV MR assays uncovered that oligomerization of L was required for the activity of the LCMV polymerase (Sanchez and de la Torre 2005). Consistent with this finding, LASV L protein was shown to contain both N- and C-termini domains that mediate L–L interaction (Brunotte et al. 2011). MR-based assays facilitated mutation-function studies that identified residues within the N-terminus of L that played a critical role in synthesis of viral mRNA but not in RNA replication (Lelke et al. 2010). Moreover, MR-based assays together with structural data uncovered within the N-terminus of LASV L protein, an endonuclease functional domain that was critically required for arenavirus transcription (Morin et al. 2010). Mutation-function analysis of the genome 5′- and 3′-termini using LCMV and LASV MR-based assays demonstrated that the activity of the arenavirus genomic promoter requires both sequence specificity within the highly conserved 3′-terminal 19 nt of arenavirus genomes and the integrity of the predicted panhandle structure formed between the 5′- and 3′-termini of viral genome RNAs (Hass et al. 2006; Perez and de la Torre 2002). Likewise, MR-based assays provided direct experimental confirmation that the IGR is a bona fide transcription termination signal (Pinschewer et al. 2005). These studies also uncovered that Z exhibited a dose-dependent inhibitory effect on both RNA replication and gene transcription by the arenavirus polymerase complex (Cornu and de la Torre 2001, 2002; Cornu et al. 2004; Hass et al. 2004; Lopez et al. 2001).

Generation of infectious recombinant arenaviruses Generation of infectious virus from cloned cDNAs has been reported for LCMV (Flatz et al. 2006; Sanchez and de la Torre 2006), PICV (Lan et al. 2009), JUNV (Albarino et al. 2009; Emonet et al. 2011b), and LASV (Albarino et al. 2011). Both RNA polymerase I and T7 RNA polymerase (T7RP)-based systems haven been successfully used, and with similar efficiencies, to direct intracellular synthesis of L and S genome RNA species required for the rescue of infectious recombinant arenaviruses (Emonet et al. 2011a). Intriguingly, the rescue of PICV and JUNV using the T7RP-based system did not require plasmid-supplied viral NP and L proteins, indicating that T7RP-mediated RNA synthesis produced both viral antigenome RNA species that were substrate for encapsidation and replication, and mRNAs that serve as template to produce levels of NP and L sufficiently high to facilitate virus rescue. This phenomenon has been reported for several other negative-sense RNA viruses (Emonet et al. 2011a). Reverse genetics approaches similar to those used to rescue infectious LCMV, PICV, JUNV, and LASV from cloned cDNAs should be now applicable to other arenaviruses. The ability to generate recombinant arenaviruses with predetermined specific mutations and analyze their phenotypic expression in the context of the natural course of infection has opened new opportunities to investigate arenavirus–host interactions that influence a variable infection outcome,

ranging from virus control and clearance by the host defenses to long-term chronic infection associated with subclinical disease, and severe acute disease including HF. Thus, the use of rLCMV/VSVG uncovered the arenavirus GP as a viral Achilles' heal and provided the foundations for a novel strategy to develop safe and effective live-attenuated arenavirus vaccines (Pinschewer et al. 2003). Likewise, rLCMV/VSVG was very instrumental in facilitating studies aimed at understanding the regulation of CD8+ T cell function within the infected brain (Pinschewer et al. 2010), as well as how viruses can induce organ-specific immune disease in the absence of molecular mimicry and without disruption of self-tolerance (Merkler et al. 2006). Other engineered rLCM viruses have been used to study LASV cell entry pathway (Rojek et al. 2008b) and the role of NP in the inhibition of induction of IFN-I by LCMV (Martinez-Sobrido et al. 2009). Similarly, studies aimed at examining the critical role played by the S1P-mediated processing of arenavirus GPC in the virus life cycle were aided by the use of recombinant viruses where the S1P cleavage site within GPC was replaced by a canonical furin cleavage site (Albarino et al. 2009; Rojek et al. 2010; Urata et al. 2011). The rescue of attenuated and virulent forms of PICV (Lan et al. 2009; Liang et al. 2009) or the Docile and Aggressive strains of LCMV (Chen et al. 2008) has allowed for the identification of specific genetic determinants of virus virulence. Moreover, it has been possible to generate single-cycle infectious, reporter-expressing, recombinant LCMV in which the GPC open reading frame (ORF) was replaced by GFP (rLCMVDGP/GFP) (Rodrigo et al. 2011). Genetic complementation with plasmids or stable cell lines expressing arenavirus GPCs of interest produces the corresponding GPC-pseudotyped rLCMVΔGP/GFP that can be used to evaluate antibody responses to HF arenaviruses using a Biosafety Level 2 (BSL2) platform.

Despite recombinant arenaviruses could be generated very efficiently, the ability to rescue arenaviruses expressing additional genes of interest posed unexpected difficulties. This problem was overcome by the generation of tri-segmented rLCMV (r3LCMV) containing 1L and 2S segments. Each of the two S segments was altered to replace one of the two viral ORF, GPC, or NP, by a gene of interest (GOI) (Emonet et al. 2009b). The rationale behind this approach was that the physical separation of GP and NP into two different S segments would represent a strong selective pressure to select and maintain a virus capable of packaging 1L and 2S segments. A variety of r3LCMV has been rescued that express one or two additional GOI. Depending on the GOI expressed (protein function, size of the gene), these r3LCMV showed little or no attenuation in cultured cells and they exhibited long-term genetic stability as reflected by unaltered expression levels during serial virus passages of the GOI incorporated into the S segment. The use of r3LCMV expressing appropriate reporter genes should facilitate the development of chemical screens to identify antiviral drugs, as well as siRNA-based genetic screens to identify host cell genes contributing to the different steps of the arenavirus life cycle. However, the use of r3LCMV to study virus–host interactions in mice has

encountered some limitations due to the observation that r3LCMV with WT growth properties in cultured cells usually exhibits attenuation in mice due to reasons that remain to be determined.

3 Genetic Variability of Arenaviruses

3.1 Organization and Phylogenetic Relationships of the Arenaviridae Family

Until recently, the family *Arenaviridae* has consisted of a single genus, *Arenavirus,* that includes 25 recognized species. Based on their antigenic properties, arenaviruses are divided into two distinct groups: The OW arenaviruses (Lassa–lymphocytic choriomeningitis serocomplex) include viruses indigenous to Africa and the ubiquitous LCMV, and the NW arenaviruses (Tacaribe serocomplex) include viruses indigenous to the Americas. Subsequent genetic analyses based on sequencing data supported very well the previously defined antigenic grouping (Bowen et al. 1997). The monogeneric phylogenetic view of arenaviruses has recently shifted dramatically with the discovery of a divergent group of arenaviruses in captive alethinophidian snakes (Bodewes et al. 2013; Hetzel et al. 2013; Stenglein et al. 2012). Preliminary phylogenetic studies indicate that these reptilian arenaviruses constitute a sister clade to mammalian arenaviruses, and have been proposed to represent a new genus within the family Arenaviridae.

OW arenaviruses form one monophyletic group that is deeply rooted to the three identified NW arenavirus phylogenetic groups, clades A, B, and C. Clade B contains the human pathogenic viruses Chapare (CHPV), Guanarito (GTOV), JUNV, Machupo (MACV), and Sabiá (SABV), as well as several nonpathogenic including Tacaribe virus (TCRV) (Fig. 2). Among OW arenaviruses, LASV, Mobala virus (MOBV), and Mopeia virus (MOPV) are monophyletic, while Ippy virus (IPPYV) and LCMV are more distantly related. The recently discovered Lujo virus (LUJV), endemic in Zambia, is most closely related to OW arenaviruses, but its GPC contains elements of NW arenavirus sequences. Both OW and NW arenaviruses have been evolved from a common ancestor, developing a wide range of antigenic specificity, host species range, pathogenicity, and virulence (Zapata and Salvato 2013).

As with other RNA viruses, arenavirus replication is mediated by an error-prone polymerase complex, which together with reassortment events of its segmented genome generates the genetic variability that provides arenavirus with the potential for rapid evolution and high capability of adaptation to new environments. The contribution of recombination to arenavirus genetic variability has not been explored at length, but similarly to other NS RNA viruses, recombination events among arenavirus genomes appear to be extremely rare. Nevertheless, both reassortment and recombination events need to be taken into account to understand the evolution and population dynamics of arenaviruses (Albarino et al. 1998; Archer and Rico-Hesse 2002; Charrel and de Lamballerie 2003; Charrel et al. 2001, 2003).

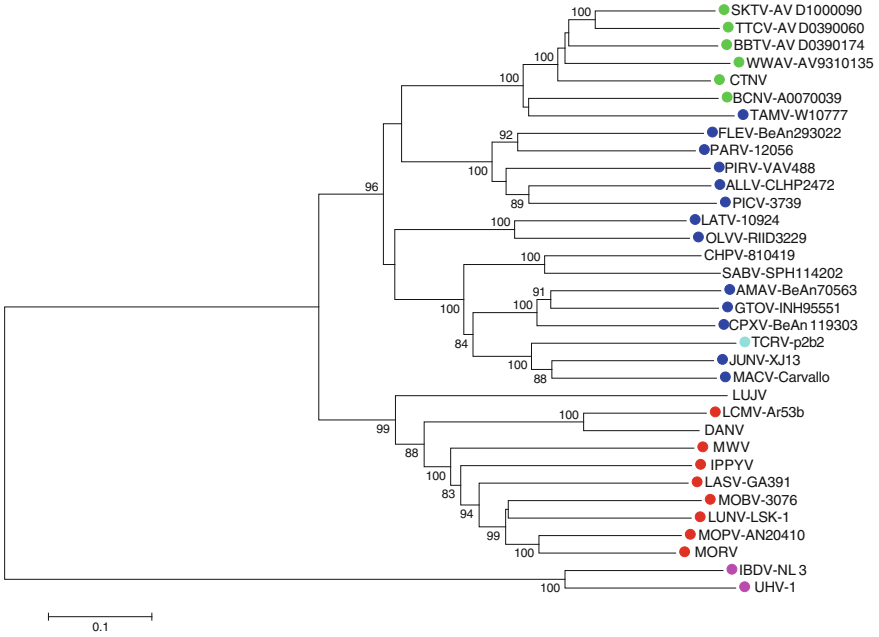

Fig. 2 Rooted tree of arenavirus S segment. Phylogeny reconstruction by neighbor joining with 10,000 bootstrap replications under maximum composite likelihood substitution model was done with Mega 6 (Tamura et al. 2013). Bootstrap values below 80 % are hidden. A similar tree was obtained for the L segment. GenBank accession numbers of S segment (all complete sequences) used to generate the tree, as well as species names of rodent reservoirs were obtained from previously published data (King et al. 2012), with the following exceptions: *Skinner tank virus* (SKTV, EU123328.1) from *Neotoma mexicana* (USA); *Tonto creek virus* (TTCV, EF619034.1) from *Neotoma albigula*; *Big brushy tank virus* (BBTV, EF619035.1) from *Neotoma albigula,* Arizona (USA); *Catarina virus* (CTNV, DQ865244) from *Neotoma micropus* (Cajimat et al. 2013); *and* Luna virus (LUNV-LSK-1, AB693148.1) from *Mastomys natalensis*, Zambia (Ishii et al. 2012). *Colored dots next virus isolates* indicate reservoir species: *green*, *neotominae* subfamily; *blue*, *sigmodontinae* subfamily; *red*, *murinae* subfamily; *cian*, the bat *Artibeus* spp, proposed reservoir of *Tacaribe virus* (TCRV-p2b2); and *magenta*, the *Boa constrictor* snake, reservoir of the recently reported putative arenaviruses *University of Helsinki virus* (UHV-1) and *inclusion body disease virus* (IBDV-NL3) (Bodewes et al. 2013; Hetzel et al. 2013). *Absence of colored dot* indicates unknown reservoir

It is worth noting that arenaviruses exhibit a superinfection inhibition feature that diminishes the possibilities for recombination and reassortment events since both are dependent on two different arenaviruses infecting the same cell (Ellenberg et al. 2004, 2007; Moreno et al. 2012b). The mechanisms underlying virus superinfection inhibition vary among different viruses (Geleziunas et al. 1994; Horga et al. 2000; Huang et al. 2008; Morrison and McGinnes 1989). In the case of arenaviruses, high levels of Z protein inhibit de novo formation of a functional polymerase complex thus leading to inhibition of viral RNA synthesis (Cornu and de la Torre 2001, 2002; Cornu et al. 2004; Kranzusch and Whelan 2011; Loureiro et al. 2011).

Hence, infected cells may express levels of Z that do not permit synthesis of RNA by the polymerase complex of a second infecting arenavirus (Ellenberg et al. 2004, 2007; Moreno et al. 2012b).

3.2 *Mechanisms of Arenavirus Genetic Diversity*

3.2.1 Arenavirus Mutation Frequencies

RNA viruses have high mutation rates, in the range of 10^{-3} to 10^{-5} (Drake and Holland 1999) due to the error-prone nature of their viral RdRp (Domingo 2007). Accordingly, early studies already suggested high genetic variability of arenavirus populations based on the observation that CTL escape mutants could be readily selected both in vivo (Pircher et al. 1990) and in cell culture (Aebischer et al. 1991; Lewicki et al. 1995). Likewise, emergence of neutralization-resistant LCMV mutants in persistently infected mice was found to be a rather frequent event associated with single point mutations (Ciurea et al. 2000, 2001). More recent studies have examined the mutation frequencies (the number of nucleotide substitutions and indels per nucleotide sequenced) in LCMV populations recovered after one or several passages in BHK-21 cells. These studies involved sequencing of multiple clones of several regions of the GP, NP, and L genes and found mutation frequencies in the range of 1.0×10^{-4} to 2.7×10^{-4} and 1.0×10^{-4} to 5.7×10^{-4} for populations after one and nine, respectively, cell culture passages (Grande-Perez et al. 2002). The highest mutation frequency detected corresponded to the NP region and the lowest to the L region. These values correlated with the corresponding values of Shannon entropy, parameter that measures the genetic heterogeneity of the viral population (Domingo 2006). Other studies have documented mutation frequencies for arenaviruses in the range of 2.6×10^{-4} to 5.5×10^{-4} mutations per nucleotide during serial passages in cell culture (Ruiz-Jarabo et al. 2003). In addition, mutation frequencies in the range of 1.2×10^{-4} to 3.5×10^{-4} substitutions per nucleotide were estimated for both the intracellular and released viral populations during LCMV persistence in BHK-21 cells (Grande-Perez et al. 2005b). These figures are consistent with a large body of literature documenting the genetic variability of both negative- and positive-stranded RNA viruses (Domingo 2007) and support the view that arenavirus populations are ensembles of genetically closely related mutant genomes, called quasispecies, subjected to natural selection and genetic drift (Sevilla and de la Torre 2006).

3.2.2 RNA Recombination in Arenaviruses

Discrepancies between NP- and GPC-based phylogenetic trees observed between clades A and B arenaviruses and North American (lineage A/Rec) arenaviruses

including White Water Arroyo virus (WWAV) and the two newly discovered North America arenaviruses, Catarina and Skinner Tank viruses, led to hypothesize that a recombination event between members of clades A and B led to the emergence of lineage A/Rec (Archer and Rico-Hesse 2002; Charrel et al. 2001, 2002, 2003; Fulhorst et al. 2001). Additional recombination events have been suggested to explain the evolutionary relationships between Oliveros (OLIV) and Pichinde (PICV) viruses with OW arenaviruses (Albarino et al. 1998). However, the generation of recombinant arenaviruses requires cells to be simultaneously infected by two different arenaviruses, and although coinfection with two different arenaviruses has been reported in cultured cells (Ellenberg et al. 2004, 2007; Lukashevich et al. 2005; Moreno et al. 2012b; Riviere et al. 1986), in nature it may be less likely and further restricted by the superinfection exclusion feature associated with arenavirus infection (Ellenberg et al. 2004, 2007; Lukashevich et al. 2005; Moreno et al. 2012b; Riviere et al. 1986). Some arenaviruses share a common geographic localization, such as Guanarito and Pirital (PIRV) viruses in Venezuela (Fulhorst et al. 1999; Weaver et al. 2000); Junin and Oliveros viruses in Argentina (Mills et al. 1996); and Machupo, Latino, and Chapare viruses in Bolivia (Delgado et al. 2008). Likewise, different arenaviruses can some times infect the same rodent species, such as Guanarito and Pirital viruses, which were isolated both in cotton rats *Sigmodon alstoni* and in cane mice *Zygodontomys brevicauda* (Weaver et al. 2000). However, despite an extensive genetic characterization, the existence of a GTOV-PIRV recombinant virus has never been demonstrated (Cajimat and Fulhorst 2004; Fulhorst et al. 2008), which might be explained by superinfection exclusion among arenaviruses (Damonte et al. 1983; Ellenberg et al. 2004, 2007). Since no A/Rec arenavirus has been isolated in South America and neither clade A nor clade B arenavirus has been isolated in North America, it is difficult to explain how the recombination occurred. It is plausible that the two parental arenaviruses were originally present in North America but disappeared, either by natural extinction, migration or by being outcompeted by the recombinant arenavirus. The migration to North America of a recombinant arenavirus generated in South America seems improbable because South America arenaviruses most likely descend from an ancestral arenavirus located in North America (Cajimat et al. 2007). Moreover, North America arenaviruses have a long-term coevolutionary relationship with rodents from *Neotominae* subfamily, which are almost exclusively found in North America (Cajimat et al. 2007). It should be noted that clade C arenaviruses also exhibit a shift between GPC- and NP-based trees (Charrel et al. 2008), and it seems unlikely that such a rare event would be the origin of two different lineages. It seems more plausible that the phylogenetic information derived from arenavirus GPC is influenced by specific selection pressures (Cajimat et al. 2007). The reasons why GPC would be under a selection pressure different from the other arenavirus genes need to be determined. Likewise, the statistical significance of the recombination event found in North America and clade C arenaviruses using recombination detection softwares should be validated using an up-to-date arenavirus genetic database.

The recently discovered arenaviruses associated with cases of inclusion body disease (IBD) in snakes (Bodewes et al. 2013; Hetzel et al. 2013; Stenglein et al. 2012) might represent a very special case of heterologous recombination between an arenavirus and a filovirus within a coinfected host (snake). Phylogenetic analysis showed that snake-related arenaviruses constitute a monophyletic lineage separated from NW and OW arenaviruses (Bodewes et al. 2013; Stenglein et al. 2012). Intriguingly, the GPC of snake-related arenaviruses was more closely related to the GPC of filoviruses than to arenaviruses, but the natural history of events favoring this potential recombination event between filo- and arenaviruses remains to be elucidated.

3.2.3 Arenavirus Genomic Reassortments

Reassortment events require, like recombination, a coinfection event that can be readily recreated in cultured cells (Ellenberg et al. 2004, 2007; Lukashevich 1992; Lukashevich et al. 2005; Moreno et al. 2012b; Moshkoff et al. 2007; Riviere et al. 1986; Riviere and Oldstone 1986). However, in nature, there is only one documented case of an arenavirus reassortant event (Palacios et al. 2008). Extensive phylogenetic analysis of NW and OW arenaviruses revealed no proof of detectable genomic reassortment events during their evolution (Charrel et al. 2003), with the exception of an arenavirus isolated from three fatal cases of LCMV infection in transplantation patients who received organs from a single donor (Palacios et al. 2008). Phylogenetic analysis revealed a new arenavirus, in which L and S segments were related to LE and M1-M2 LCMV strains, respectively, suggesting that likely a reassortment event was involved in the generation of this arenavirus. The lower reassortant frequency in arenaviruses may be due to the superinfection exclusion exhibited by the members of this family (Ellenberg et al. 2004, 2007; Moreno et al. 2012b).

Since reassortment of arenaviruses in nature seems to be restricted to some specific combinations of L and S segments (Lukashevich 1992; Riviere et al. 1986), and recombination in arenaviruses is extremely infrequent (Archer and Rico-Hesse 2002; Charrel et al. 2002), mutations during genome replication by an error-prone polymerase arenaviruses are thought to be the main contributing factor to arenavirus genetic variability.

3.3 Arenavirus Hypermutation

Interferon-inducible adenosine deaminase that acts on double-stranded RNA (ADAR1) has been suggested to play a role in the innate immune response against LCMV (Zahn et al. 2007). ADARs are a family of dsRNA-binding enzymes present in animals that deaminate adenosine to inosine, and are involved in the regulation of a variety of posttranscriptional processes as well as in an antiviral response (Nishikura 2010). Since inosine and adenosine have different base-pairing properties, editing can

alter protein-coding transcripts and noncoding targets including microRNA, small interfering RNA viral transcripts, and repeat elements (Hundley and Bass 2010; Mallela and Nishikura 2012). Upon LCMV infection of murine L929 cells, both expression and activity of ADAR1-L were upregulated and its editing activity was not inhibited by viral replication (Zahn et al. 2007). An adenosine-to-guanosine (A-to-G) transition bias was found in cDNA clones of the GPC gene derived from LCMV RNA isolated from L929 cells at seven days post-infection. Likewise, an A-to-G/U-to-C transition bias was observed in clones of LCMV genomic RNA species derived from RNA isolated from spleen of LCMV-infected C57BL/6 mice at four days post-infection, whereas no G-to-A/C-to-U transition was observed. Moreover, two of 54 analyzed clones showed an A-to-G or U-to-C hypermutation pattern in a very short stretch of the GP where 38 % of all adenosines or 14 % of uracils were mutated. In LCMV clones isolated from mice, no hypermutated LCMV clones were found. Approximately 50 % of the clones with an amino acid mutation were non-functional, suggesting that ADAR1-L-induced mutations in LCMV RNA reduce viral infectivity and protein function, thus supporting a contribution of ADAR1-L to the innate antiviral immune response. Nevertheless, multiplication of LCMV was not increased in mouse embryonic fibroblasts derived from ADAR1−/− mice, which raises some questions about a direct role of ADAR1 in restricting LCMV multiplication (Ward et al. 2011).

Hypermutation has been related to posttranscriptional editing by host adenosine deaminases of viral genomes from persistent infections of other RNA viruses such as measles virus (Cattaneo and Billeter 1992), human parainfluenza virus (Murphy et al. 1991; Rima et al. 2014), and respiratory syncytial viruses (Rueda et al. 1994). In these studies, the estimated mutation frequencies of U → C or A → G transitions were in the range of 3.3×10^{-2} to 1.0×10^{-1} mutations per nucleotide. The existence of hypermutated genomes had been hypothesized as proof of the genetic melting that occurs when the error catastrophe threshold is crossed as a result of chemical mutagenesis (Grande-Perez et al. 2002). However, evidence of hypermutated viral genomes has not been found in preextinction populations. In particular, hypermutated sequences of LCMV from 5-fluorouracil (FU) mutagenized populations were not amplified despite using a battery of oligonucleotide primers with different degrees of degeneracy targeting LCMV genomic RNA (Grande-Perez et al. 2005a). In this study, only one sequence was found that harbored nine mutations, six U → C transitions and the other three A → G, C → A, and G → A in an amplicon of 558 nucleotides (excluding primers), which renders a mutation frequency (relative to the consensus sequence of the sample from which it was obtained) of 1.6×10^{-2} mutations per nucleotide sequenced. No further analyses were conducted to find out whether this hypermutated molecule was the result of chemical mutagenesis or host adenosine deaminase. However, in a subsequent study (Martin et al. 2010), the participation of ADAR-like enzymes in the 5-FU-mediated increase of A → G transitions of LCMV genome was ruled out because the context in the immediate neighborhood of the observed A → G transitions was not preferred by the dsRNA adenosine deaminase (Polson and Bass 1994).

4 Contribution of Genetic Variability to Arenavirus–Host Interactions and Associated Disease

4.1 Coevolution of Arenaviruses and Their Natural Reservoirs: Intra- versus Inter-host Genetic Variation of Arenaviruses

Arenaviruses establish long-life persistent infections in their natural reservoirs in the absence of noticeable clinical symptoms (Childs and Peters 1993). Arenavirus natural reservoirs include rodent species from the family *Muridae* (Salazar-Bravo et al. 2002), but a notable exception is Tacaribe virus whose natural host is thought to be the fruit-eating bat *Artibeus* sp. (Downs et al. 1963). Coevolution of the arenaviruses with their natural hosts has likely been a major driving evolutionary force that has generated the currently existing arenavirus–host associations (Bowen et al. 1997), with groups of genetically closely related arenaviruses infecting closely related rodent species. Thus, OW arenaviruses are found in rodents from the subfamily *Murinae*, whereas NW arenavirus reservoirs belong to rodents from subfamilies *Sigmodontinae* and *Neotominae* (Fig. 2). Furthermore, inside the OW arenaviruses, the LASV complex (LASV, MOBV, MOPV, and IPPYV) is associated with *Praomys* rodents, while LCMV and Kodoko virus are found in rodents from the genus *Mus* (Lecompte et al. 2007). Likewise, within NW arenaviruses, the reservoirs of most North American arenaviruses are mainly rodents from the subfamily *Neotominae,* whereas the reservoirs of the South American arenaviruses belong to the subfamily *Sigmodontinae* (Emonet et al. 2009a). However, this coevolution hypothesis, which assumes also occasional host switching, could not be tested empirically due to the lack of detailed knowledge about rodent phylogeny. Studies trying to reconciliate the viral and host phylogenies for both OW (Hugot et al. 2001; Coulibaly-N'Golo et al. 2011) and NW (Jackson and Charleston 2004) arenaviruses did not find evidence of congruence between both phylogenies. Recent evidence has suggested that for OW arenaviruses, coevolutionary associations may have been concealed by the occurrence of multiple host switching and extinction events (Coulibaly-N'Golo et al. 2011). In addition, studies based on the recent availability of molecular data from both NW arenaviruses and their rodent reservoirs found evidence of arenavirus evolution via host switching, rather than codivergence between these arenaviruses and their hosts (Irwin et al. 2012).

Studies on the interaction between the surface glycoprotein GP1 of several NW arenaviruses and their cell entry receptor, the transferring receptor 1 (TfR1) (Abraham et al. 2009; Choe et al. 2011; Demogines et al. 2013; Flanagan et al. 2008; Radoshitzky et al. 2007, 2008), have suggested that arenaviruses might have exerted some degree of positive selection in their rodent reservoirs. These studies suggest that the dynamic of GP1–TfR1 interaction has had a direct impact in sequences of these viral and host genes. Interestingly, identified rapidly evolving positions within TfR1 were located within the TfR1 region that mediates interaction with the virus GP1. Mutations at these TfR1 residues altered the interaction with the viral GP1 without affecting TfR1 expression or function. As a consequence of the

introduction of genetic divergence, this rodent receptor locus might have the potential to act as a species barrier to viral transmission limiting both the cross-species and zoonotic transmission of these viruses. Nevertheless, there is evidence that JUNV can enter cells very efficiently in a TfR1-independent manner, raising some questions about the true impact of the TfR1 gene as a key determinant of JUNV host range. NW arenaviruses, Junin virus, Machupo virus, and Guanarito virus, have acquired the ability to bind human TfR1 and are currently emerging in South America as zoonosis (Choe et al. 2011; Flanagan et al. 2008) associated with severe morbidity (Peters 2002). Intriguingly, a mutation within TfR1 predicted to affect infection by NW arenaviruses that use this receptor for cell entry was identified in Asian population (Demogines et al. 2013).

Genomic analysis of full-length genome sequences of 29 strains of LCMV collected from a variety of geographic regions at different times showed these viruses to be genetically highly diverse (Albarino et al. 2010). Several distinct lineages of LCMV could be identified, but there was little correlation with time or place of isolation. Bayesian analysis enabled estimation of the rate of evolution of the S and L genome segments of LCMV and Kodoko virus sequences and found them to be similar to other negative-stranded RNA viruses. The molecular evolutionary rate was estimated to be 3.3×10^{-4} and 3.7×10^{-4} substitutions per nucleotide and year for the S and L segments, respectively. The Bayesian analysis also indicated that the most recent common ancestor for LCMV S- and L genome RNA segments was estimated to be 1235 and 5142 years ago, respectively. These data indicate that LCMV is quite ancient, and the extensive diversity of the virus has accumulated over the past 1000–5000 years. Also, despite similar rates of evolution, the evolutionary history of the L segment appears to be more complex and can be traced back substantially longer than that for the S segment.

Arenaviruses coevolve with their natural hosts, but animal species other than the corresponding reservoir can be infected (Dalldorf 1939; Greenwood and Sanchez 2002; Salazar-Bravo et al. 2002). Information about possible arenavirus pathogenicity in their natural reservoir is rather limited, but data from LCMV infection of the mouse have shown that the same virus can behave differently depending on the host. For instance, C3H/st, BALB/WEHI, and SWR/J mice infected at birth with LCMV Armstrong, E-350, or Pasteur strains develop persistent infection, but only C3H/st mice develop growth hormone deficiency syndrome. In contrast, LCMV strains Traub and WE did not cause disease in those animals (Oldstone et al. 1984, 1985). Differential host-specific selection may be the reason why quasispecies diversity of Guanarito virus isolates from rodents in Venezuela had higher sequence variation than human isolates. One rodent isolate included a mixture of two phylogenetically distinct genotypes, suggesting a dual infection (Weaver et al. 2000). Likewise, the characterization by pyro-sequencing of the genetic stability and complexity of the Lassa vaccine candidate ML29 in vaccinated rhesus monkeys, marmosets, and mice (Zapata and Salvato 2013) revealed accumulation over time of some host-specific mutations. Protein prediction analysis showed that those mutations, at the amino acid level, induced potential structural changes in GPC and NP.

4.2 Contribution of Viral Quasispecies to Arenavirus Pathogenesis

RNA viruses within hosts exist as complex distribution of genetically closely related mutants, termed quasispecies, subjected to a process of genetic variation, competition, and selection (Domingo 1992; Domingo et al. 2001). Foremost, this swarm of mutants is possible because of the low copy-fidelity of viral RdRp. Studies in cultured cells found mutation frequencies of 1×10^{-4} to 5.7×10^{-4} substitutions per nucleotide for the Z, NP, GP, and L regions analyzed of LCMV (Grande-Perez et al. 2002, 2005a; Martin et al. 2010; Moreno et al. 2011), which are consistent with previous findings on genetic heterogeneity of LCMV (Sevilla et al. 2002) and other arenaviruses (Bowen et al. 1996, 1997; Bowen et al. 2000; Charrel and de Lamballerie 2003; Fulhorst et al. 2001; Garcia et al. 2000; Weaver et al. 2000, 2001) and also within the range commonly observed for riboviruses (10^{-3} to 10^{-5} substitutions per nucleotide) (Domingo et al. 1988; Drake and Holland 1999) (see Sect. 3.2.1).

Error-prone replication might contribute to spatial and temporal heterogeneities in RNA genome populations, favoring their rapid evolution and adaptation to different environments. The entire virus cloud contributes to the characteristics of the virus strain and will be the target of selection instead of individual variants (Perales et al. 2005). Cooperation and complementation events between variants of the quasispecies that permit the mutants carrying lethal mutations can be maintained within the population and even compete and interfere with fitter variants (de la Torre and Holland 1990; Gonzalez-Lopez et al. 2004; Martin et al. 2010; Mas et al. 2010; Perales et al. 2007; Zapata and Salvato 2013).

In addition to an error-prone polymerase, RNA recombination (Charrel et al. 2001; Fulhorst et al. 1996) and genome reassortment (Riviere 1987; Riviere et al. 1986; Riviere and Oldstone 1986) can also contribute to arenavirus genetic diversity. However, both recombination and reassortment events appear to be extremely rare in nature and only between phylogenetically closely related strains (Archer and Rico-Hesse 2002; Charrel et al. 2002; Emonet et al. 2006; Jay et al. 2005). The ability of the arenavirus to infect a wide variety of hosts could also contribute to their genetic variability (Zapata and Salvato 2013). The genetic diversity within and between arenavirus groups suggests that the spatial heterogeneity may be reflected in host range and pathogenicity (Blasdell et al. 2008). Biological functions of RNA virus distributions remain poorly understood, but evidence suggests that different arenavirus strains may exhibit different biological properties and pathogenesis attributable to differences in their quasispecies (Sevilla et al. 2002). Moreover, the genetic complexity of a quasispecies structure provides RNA viruses, including arenaviruses, with a great capacity to adapt to changing host environments (Novella et al. 1995). The quasispecies plasticity may facilitate that arenaviruses can overcome barriers to its spread, both within the host and between species (Oldstone and Campbell 2010; Sevilla et al. 2002). Viral variants, initially present at low frequency in the quasispecies, that become dominant under a

selective pressure have been documented for different RNA viruses including rabies (Morimoto et al. 1998), coxsackie viruses (Beaucourt et al. 2011; Domingo et al. 2008), poliovirus (PV) (Pfeiffer and Kirkegaard 2005; Vignuzzi et al. 2006), foot-and-mouth disease virus (FMDV) (Haydon et al. 2001; Martin and Domingo 2008), and human parainfluenza virus (Prince et al. 2001). Arenaviruses are no exception, and selection of organ-specific LCMV variants with different pathogenic properties has been documented (Ahmed and Oldstone 1988; Ahmed et al. 1984). Likewise, as with other RNA viruses (Hotchin 1973; Hotchin et al. 1971; Hotchin and Sikora 1973), serial passages in cultured cells can yield LCMV variants that differ in pathogenicity with respect to the original isolate (Hotchin and Sikora 1973; Lukashevich 1992; Pulkkinen and Pfau 1970), further emphasizing the contribution of the quasispecies' plasticity to arenavirus pathogenesis. These studies in cell culture provide strong support for the view that specific environmental conditions can influence virus–host interactions and promote selection of specific RNA species with distinct phenotypic features within the genetically complex quasispecies. The application of New Generation Sequencing to the field of virology is allowing scientists to start getting a detailed view of the genetic complexity and dynamic of RNA viral quasispecies of how they impact virus–host interactions and associated disease.

4.2.1 Selection of Immunosuppressive Variants During LCMV Persistence

Chronic infections provide investigators with an excellent experimental system for studying the contribution of virus quasispecies dynamics to virus–host interactions and associated disease as sustained virus multiplication in the persistently infected host facilitates virus evolution and adaptation resulting in selection of novel viral phenotypes that could influence the outcome of infection. Persistent infections can favor selection of viral variants with tissue-specific growth advantages that could be associated with different phenotypes and disease manifestations (Ahmed et al. 1984). Studies examining viral populations replicating in different tissues and organs of the same infected host have uncovered intra-host viral variability and selection of tissue-specific virus populations due to differences in selective pressures exerted by the different environments associated with these compartmentalized areas of the infected host (Ahmed and Oldstone 1988; Brown et al. 2011; Cabot et al. 2000; Cheng-Mayer et al. 1989; Deforges et al. 2004; Hall et al. 2001; Jelcic et al. 2004; Jridi et al. 2006; Sanjuan et al. 2004; Trivedi et al. 1994; Wright et al. 2011). LCMV can cause acute or persistent infections in mice, its natural host, and has been used as a model to study viral population dynamics in vivo (Ahmed et al. 1988; Evans et al. 1994). The age, genetics, and immune status of the host, as well as the composition of the viral quasispecies, route of infection, and dose of infecting virus, contribute to the outcome of the infection. Mice infected with LCMV within 24 h of birth do not develop an effective antiviral CTL response and become persistently infected (Matloubian et al. 1990; Salvato et al. 1991). On the

other hand, iv inoculation of adult immunocompetent mice with a high ($\geq 2 \times 10^6$ PFU) dose of Armstrong (ARM) strain of LCMV causes an acute infection that induces a protective immune response, which culminates in CD8+ CTL-mediated virus clearance. In contrast, a similar infection with the immunosuppressive clone 13 (Cl-13) strain of LCMV causes a persistent infection associated with generalized immune suppression (Ahmed et al. 1984, 1991; Ahmed and Oldstone 1988; Baranowski et al. 2000; Evans et al. 1994; Tishon et al. 1993; Wu-Hsieh et al. 1988). At early times, post-infection ARM exhibits tropism for macrophages of the red pulp of the spleen, while Cl-13 targets preferentially dendritic cells (DCs) of the spleen's white pulp (Borrow et al. 1995; Sevilla et al. 2000). Notably, ARM and Cl-13 differ only at five nucleotide positions that involve three amino acid changes, two within GP1 [N(ARM)-176-D(Cl-13) and F(Arm)-260-L(Cl-13)] and one in the L polymerase [K(Arm)-1079-Q(C13)] (Matloubian et al. 1990, 1993; Salvato and Shimomaye 1989; Sevilla et al. 2000). Mutation F260L was found to be responsible for the strong binding affinity of Cl-13 to its receptor αDG that is expressed in DCs and facilitates over time high levels of DC infection by Cl-13 (Cao et al. 1998; Kunz et al. 2002), which is associated with Cl-13 persistence. However, at early stages of infection, ARM and Cl-13 infect similar numbers of DCs and macrophages indicating that differences between Cl-13 and ARM regarding early and yet-unknown interactions with host cell factors may determine whether LCMV persists (Cl-13) or is cleared ARM. Interestingly, mutation K1076Q in the L polymerase was found to play a critical role in the persisting phenotype of Cl-13 (Bergthaler et al. 2010; Sullivan et al. 2011).

4.2.2 Contribution of Viral Variants to LCMV-Induced Growth Hormone Deficiency Syndrome

Neonatal infection of C3He mice with certain strains of LCMV results in the development of a growth hormone disease syndrome (GHDS) characterized by growth retardation and severe hypoglycemia that result in death of the infected mice within 15–20 days of infection (Oldstone 2002; Oldstone et al. 1984, 1985). LCMV-induced GHSD was associated with decreasing levels of growth hormone (GH) mRNA that results in decreased GH protein synthesis in the anterior pituitary (Klavinskis and Oldstone 1989; Valsamakis et al. 1987). Virus-induced GHDS strictly correlated with the virus's ability to replicate at high levels in the GH-producing cells in the anterior pituitary. Studies using reassortant viruses between strains of LCMV, which do (ARM) or do not (WE) cause GHSD, mapped the ability to cause this disorder to the S RNA (Riviere 1987). Notably, clonal analysis of the parental GHDS-nil WE population showed, as expected, that the majority (58/61) of the clones examined behaved as the parental WE clonal population and did not cause GHDS, but three clones isolated from the WE parental population did cause the characteristic GHDS (Buesa-Gomez et al. 1996). These results provided evidence that variants with the ability to cause GHDS (GHDS+) may be present within a GHDS-nil replicating WE parental population. Clonal

isolates from the same parental virus population are genetically closely related. Accordingly, characterization of WEc54 (GHDS+) and WEc2.5 (GHDS−) clonal populations derived from the WE parental population identified a single amino acid at position 153 in GP1 as a critical viral genetic determinant required for induction of GHDS, illustrating how minor changes in the virus genome may have great impact in the biology of the infected host (Buesa-Gomez et al. 1996; Teng et al. 1996).

5 Implications of Arenavirus Genetic Variability for the Development of Antiviral Drugs and Vaccines to Combat Human Pathogenic Arenaviruses

5.1 Lethal Mutagenesis as a Novel Antiviral Strategy to Combat Arenavirus Infections

RNA viruses owe their potential for rapid evolution and adaptation to their genetic structure of quasispecies that is determined mainly by their low-fidelity replication machineries. Quasispecies is defined as the spectrum of closely related but non-identical genomes (see Chaps. 1, 3, and 5). Within replicating viral quasispecies, many individual species may have the potential to exhibit distinct phenotypes including drug-resistant mutants that pose a main obstacle to the success of antiviral therapy. The high polymerase mutation rates responsible for the genetic heterogeneity displayed by RNA viruses are close to a limit, know as error threshold, beyond which the quasispecies theory predicts that biologically meaningful genetic information cannot be maintained. In the case of RNA viruses, violation of this limit is predicted to lead viral extinction, a process termed entry into error catastrophe (Eigen 2002). This model would predict that treatment of ribovirus-infected cells with mutagenic agents that increase the virus polymerase mutation rate could exert an antiviral effect by promoting viral entry into error catastrophe. Initial experimental evidence in support of this was obtained by Holland and colleagues when investigating the effect of mutagens on VSV and PV multiplication (Holland et al. 1990; Lee et al. 1997), and subsequently, the term "lethal mutagenesis" was coined by Loeb and colleagues to describe the antiviral effect of the mutagen 5-hydrodeoxycytidine in HIV-1 infections (Loeb et al. 1999).

Because of the quasispecies genetic structure of RNA viruses, the interaction, either positive or negative, among all members of the quasispecies strongly influences the behavior of the viral population. Thereby, it is the quasispecies, rather than single independent genome species, that is subjected to selective pressures and evolution. Notably, low dose of a mutagenic agent can increase the number of mutations per genome (m) without reaching the error threshold (m_c), which could result in the generation of defective-interfering genomes (DIG) that can interfere virus multiplication and production of infectious progeny, a process that has been

termed "lethal defection." This model is supported by experimental results and in silico predictions (Ahmed et al. 1984, 1991; Ahmed and Oldstone 1988; Baranowski et al. 2000; Evans et al. 1994; Gonzalez-Lopez et al. 2004; Grande-Perez et al. 2005b; Manrubia et al. 2010; Moreno et al. 2012a; Perales et al. 2007; Tishon et al. 1993; Wu-Hsieh et al. 1988). Lethal defection can explain why viral populations subjected to lethal mutagenesis can be extinguished in the absence of the loss of the master sequence, the sequence present at the highest frequency within the quasispecies, and randomization of the virus genome sequence both predicted by the quasispecies theory (Grande-Perez et al. 2005a). Disappearance of the master sequence and melting of the genetic information of the population would be observed only in situations where m increases beyond m_c (Fig. 3), a situation that is highly unlikely to be observed in viral populations as the inhibitory effects exerted by DIG together with the loss of essential viral functions due to single mutations within the genome can result in viral extinction without changes in the consensus sequence of the viral population.

Experimental evidences of lethal mutagenesis in cell culture have been achieved in several viral systems such as HIV-1 (Dapp et al. 2009, 2012; Harris et al. 2005), PV (Graci et al. 2007), or HCV (Ortega-Prieto et al. 2013). In coronavirus, the Nsp14 contains an 3′–5′ exonuclease domain that is responsible of the first

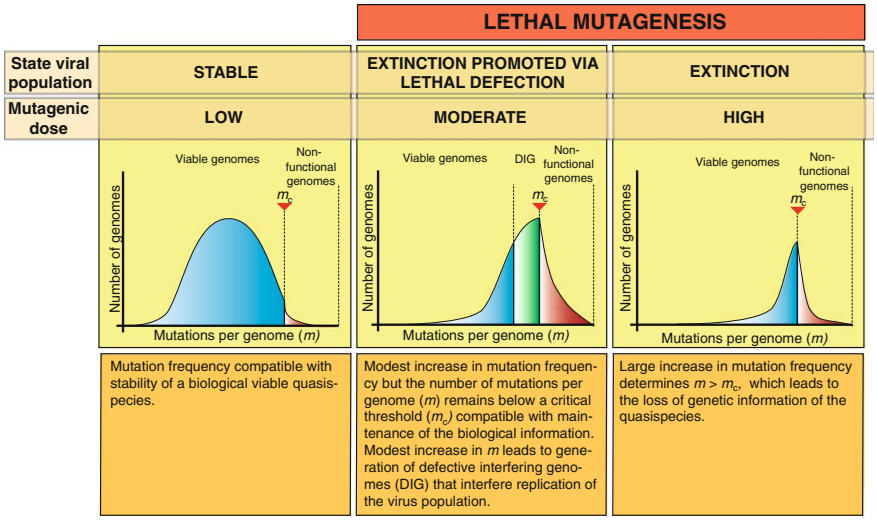

Fig. 3 Lethal mutagenesis. The lethal mutagenesis concept predicts that increasing the dose of a mutagenic agent will result in an increasing number of mutations per genome (m) in the virus population. When m crosses an error threshold ($m > m_c$), the virus population will enter into error catastrophe that is associated with the melting of the genetic information and viral extinction. The lethal defection model considers that under a moderate mutagenic dose, compatible with maintenance of the biological information, defective-interfering genomes (*DIG*) are generated and they interfere with the multiplication of the virus population, which could result in virus extinction in the absence of the sequence signatures of error catastrophe

described proofreading activity in riboviruses (Denison et al. 2011). Accordingly, viral mutants lacking this activity exhibit increased sensitivity to lethal mutagenesis (Smith et al. 2013). In arenaviruses, loss of infectivity and virus extinction through lethal mutagenesis have been achieved under laboratory conditions (Grande-Perez et al. 2005b; Martin et al. 2010; Moreno et al. 2011, 2012b; Ruiz-Jarabo et al. 2003) supporting the feasibility of entry into error catastrophe as a new antiviral strategy to combat arenavirus infections, a view that has been further reinforced by results from in vivo experiments (Ruiz-Jarabo et al. 2003; Sanz-Ramos et al. 2012).

Mutagenesis of LCMV with 100 μg/ml 5-FU achieved dose-dependent decreases in infectivity and systematic extinction after 48 h in one or two passages when BHK-21 cell cultures were inoculated with a moi of 0.01. However, nucleoside analogue 5-azacytidine (AZC) at 5 or 10 μg/ml was not able to eliminate LCMV after 13 passages in BHK-21 cells, not even when viral load was decreased tenfold (Grande-Perez et al. 2002). Increments in mutation frequencies in the L region reached 16.8-fold, whereas in the GP region, it was just 2.6-fold and 4.1-fold in the NP region in populations treated with a low dose (20 μg/ml) of 5-FU. However, in a preextinction population treated with 100 μg/ml of 5-FU, the mutation frequency of the polymerase increased 3.4-fold compared with the 1.6-fold found for the GP and NP regions (Grande-Perez et al. 2002). Notably, the largest increments in mutation frequencies did not correlate linearly with the lowest infectivity values (Grande-Perez et al. 2002). The type of mutations found differed between the two analogues being predominant the transitions U → C and A → G, followed by C → U in 5-FU-treated populations, whereas in AZC-treated populations, transversions C → G were the most frequent followed by C → A, G → C, and G → U. Despite the high diversity of LCMV mutagenized preextinction populations, their consensus genomic nucleotide sequences remained unaltered (Grande-Perez et al. 2005a). Furthermore, alternate virus passages in the presence and absence of 5-FU led to profound differences in fitness (measured as the capacity of LCMV to produce progeny), without modification of the consensus genomic sequence. LCMV viral populations in their way to extinction were enriched with mutants harboring a limited number of mutations called defectors (Grande-Perez et al. 2005a, b) (Fig. 3). Detailed analysis of the molecular scenario of LCMV persistent infections treated with 100 μg/ml of 5-FU showed an infectivity decrease that was paralleled by a significant increase of intracellular viral genomic L RNA. Preextinction populations recovered at different times post-infection showed specific infectivities (measured as plaque-forming units per genomic RNA molecule) lower than control populations. These experimental results together with silico simulations led to the lethal defection model of lethal mutagenesis that suggests the participation of defective-interfering genomes to explain virus extinction in cell culture when low-level mutagenesis is exerted by a mutagenic nucleoside analogue (Grande-Perez et al. 2005b). Interference caused by defectors is different to the LCMV natural defective-interfering particles, and it is produced as a consequence of 5-FU treatment (Martin et al. 2010). Supernatants of 5-FU-treated monolayers displayed interference capacity specific for LCMV, sensitive to UV irradiation and dose- and time-dependent (Martin et al. 2010). Interference did not involve

significant increases of mutant spectrum complexity, as predicted by the lethal defection model (see also Chaps. 13 and 14).

Moreover, LCMV populations subjected to lethal mutagenesis exhibited a negative correlation between viral load and extinction, and infection at low moi in the presence of 5-FU was accompanied by a higher increase of mutant spectrum complexity and a higher antiviral effect than infection at high moi (Moreno et al. 2012b). This behavior was shared by VSV, another negative-stranded RNA virus, whereas the opposite was observed for the positive-stranded RNA viruses FMDV and EMCV. Increased mutagenesis caused by 5-FU treatment promoted the generation of DIG that inhibited viral RNA synthesis, which resulted in increased protection of the virus population against the mutagenic effect of 5-FU. This finding illustrates the biological consequences associated with the generation and activity of DIG. Nucleoside analogues are actively being pursued as candidate antiviral drugs that could exhibit a broad-spectrum mutagenic activity against a variety of riboviruses (Bonnac et al. 2013). The discovery of new nucleotide analogues that increase the viral mutation frequency while minimizing cell toxicity will represent a major advance for our understanding of lethal mutagenesis and its application as a novel antiviral strategy (Graci et al. 2008; Harki et al. 2002; Harris et al. 2005; Hicks et al. 2013).

5.2 *Advantages of Combination Versus Single Drug Therapy to Inhibit Arenavirus Multiplication*

Current antiviral drug therapy against arenavirus infections is limited to an off-label use of the nucleoside analogue ribavirin that has a limited prophylactic efficacy. In vitro and in vivo studies have documented the prophylactic and therapeutic value of RIb against several arenaviruses (Damonte and Coto 2002). Importantly, Rib reduced both morbidity and mortality in humans associated with LASV infection and experimentally in Machupo and Junin infections, if given early in the course of clinical disease (Damonte and Coto 2002). Despite its validated clinical benefits, the use of Rib has the limitations of its frequent and significant side effects, including anemia and congenital disorders, and the need of an early and intravenous administration for optimal efficacy. Several inhibitors of IMPDH (Andrei and De Clercq 1993), the S-adenosylhomocysteine (SAH) hydrolase and a variety of sulfated polysaccharides (Andrei and De Clercq 1990), phenotiazines compounds (Candurra et al. 1996), brassinosteroids (Wachsman et al. 2000), myristic acid (Cordo et al. 1999), and valproic acid (Vazquez-Calvo et al. 2013) have been reported to have antiarenaviral activity. However, most of these compounds displayed only modest and rather nonspecific effects associated with significant toxicity. Therefore, there is a pressing need for novel effective antiarenaviral drugs. In this regard, a recent high-throughput screening (HTS) using a virus-induced cytopathic effect (CPE)-based assay identified a potent small molecule inhibitor of Tacaribe virus and several other NW arenaviruses (Bolken et al. 2005). Likewise,

cell-based HTS identified several small molecule inhibitors of virus cell entry mediated by LASV GP (Lee et al. 2008). These findings illustrate how complex chemical libraries used in the context of appropriate screening assays can be harnessed into a powerful tool to identify candidate antiviral drugs with highly specific activities.

Rib has been documented to be a broad-spectrum antiviral drug active against a variety of RNA viruses (Sidwell et al. 1974; Streeter et al. 1973). Several mechanisms of action have been proposed for the antiviral activity of Rib including direct incorporation into the RNA during replication, alteration of dNTP pools through IMPDH inhibition, direct inhibition of RNA synthesis, RNA capping inhibition, and immunomodulation (Graci and Cameron 2006). In LCMV-infected cells, treatment with high (100–400 μm) concentration of Rib did not increase mutation frequency values but inhibited dramatically both viral RNA synthesis and production of infectious progeny (Ruiz-Jarabo et al. 2003). However, treatment with low (20 μm) concentration of Rib increased 2.3-fold the mutation frequency of LCMV (Moreno et al. 2011), a finding that revealed a dose-dependent dual inhibitory and mutagenic activity of ribavirin for LCMV. The antiviral activity of Rib in LCMV-infected cells could be either totally or partially prevented by adding guanosine to the culture medium (Moreno et al. 2011). Inhibition of IMPDH by mycophenolic acid, which decreases intracellular GTP levels, did not increase but rather decreased LCMV mutation frequencies, thus raising some questions about whether targeting of IMPDH by Rib contributes to Rib-mediated inhibition of arenavirus multiplication. An alternative explanation for the protective effect of guanosine would be the dilution of Rib into the intracellular nucleotide pools, suggesting that Rib may be a competitive inhibitor (Moreno et al. 2011). The use of 5-FU as mutagenic agent and Rib either as inhibitor or as mutagen revealed that a treatment protocol based on a sequential inhibitor–mutagen administration exhibited the most potent antiviral activity compared to other combinations (Moreno et al. 2012a).

Rib-resistant escape mutants have been reported for several RNA viruses including PV, HCV, and FMDV (Pfeiffer and Kirkegaard 2003, 2005; Scheidel et al. 1987; Young et al. 2003) but are in general difficult to emerge. This likely reflects that Rib exerts its antiviral effect through different, mutually non-exclusive, mechanisms and thereby, a mutation conferring a virus with resistance to one mechanism may not allow viral escape from the overall antiviral activity of Rib. The observation that antiviral drugs exert their actions as a result of several mechanisms of action is not uncommon. Thus, 5-FU exerts its antiviral activity against FMDV through both its mutagenic activity and as inhibitor of initiation of viral RNA replication (Agudo et al. 2008). In coronavirus, the lack of the 3′–5′ exonuclease activity responsible of Nsp14 protein proofreading activity increases virus sensitivity to Rib and 5-FU mutagenesis, but evidence indicates that additional mechanisms of action associated with Rib treatment contribute to the overall observed reduction in virus infectivity (Smith et al. 2013). In the case of arenaviruses, Rib has been shown to exhibit a dose-dependent dual inhibitory and mutagenic activity (Moreno et al. 2011). At low concentrations (20 μm), Rib has

been reported to increase the mutation frequency and mutant spectrum complexity of the population, whereas at higher concentrations (100 μm), Rib inhibited arenavirus replication without affecting the virus quasispecies complexity. The lack of a mutagenic effect of Rib when used at high concentration is not unexpected, because the corresponding strong inhibition of virus replication would limit the incorporation of Rib into the template RNA, which is required to exert its mutagenic effect.

The use of monotherapy-based treatments usually facilitates the selection of drug escape-resistant mutant within the population and subsequent virus rebound and therapy failure (Domingo 1989; Nijhuis et al. 2009; Young et al. 2003). Thus, inhibitor escape mutants have been isolated from virtually any virus for which a specific inhibitor has been developed, which poses a general problem in antimicrobial therapy (Domingo 2006). Combination therapy has proven effective to minimize and delay the selection of escape mutants (Pariente et al. 2003; Tapia et al. 2005). However, the emergence of variants resistant to more than one antiviral drug is not uncommon. A novel concept of combination therapy that is based on combining antiviral drugs targeting specific steps of the virus life cycle and lethal mutagenesis could contribute to overcome this problem. Importantly, recent evidence indicates that combination therapy of inhibitors of virus multiplication together with lethal mutagenesis can be dramatically more effective, while exhibiting much less toxicity, in controlling and clearing RNA virus infections than classic combination therapy (Perales et al. 2012). Moreover, evidence indicates that mutagen-mediated increase in virus mutation rate promotes the accumulation of non-functional viral gene products that often exhibit a strong dominant negative phenotype that further contributes to inhibition of virus multiplication, which has been referred to as lethal defection model of virus extinction (Grande-Perez et al. 2005b). Therefore, modest mutagenic intensities may be sufficient to help driving a virus to extinction, which further supports a combination antiviral therapy that incorporates lethal mutagenesis.

The interactions (neutral, positive, or negative) between drugs used in combination therapy are determined by the mechanism of action and pharmacokinetics of each drug, and thereby, the implementation of combination therapy requires a detailed understanding of the mechanisms of action of each drug. It is important noting that the mutagenic effect exerted by a drug could be masked or reduced by a replication inhibitor when used in combination, whereas the sequential administration of both drugs can result in a stronger antiviral effect than the sum of both drug effects (Moreno et al. 2012a; Perales et al. 2009). Therefore, combination therapy involving the use of a mutagenic agent should employ protocols involving the sequential administration of the drugs. In this regard, theoretical predictions (Eigen 1971, 2002) support the idea that reduced viral load promotes mutagen-induced viral extinction. Studies with FMDV provided the first experimental evidence for this prediction (Perales et al. 2009; Sierra et al. 2000). Likewise, studies with LCMV showed that administration of Rib at concentrations that favored its replication inhibition activity followed (sequential treatment) by administration of the mutagen 5-FU resulted in a stronger antiviral effect than when

drugs were administered simultaneously or individually (Moreno et al. 2012a). This antiviral effect correlated with a low viral progeny production, low viral RNA synthesis, and a noticeable increase in quasispecies mutant spectrum complexity. The inhibition of viral replication by Rib potentiated the mutagenic effect of the subsequently added 5-FU, promoting the generation of DIG that contributed to the loss of infectivity. None of these effects were observed when mutagenic doses of Rib were used either in combination or sequentially with 5-FU. The lesser antiviral effect observed when inhibitory concentrations of Rib were administered together with the mutagen 5-FU could be explained due to a negative interaction between mutagen and replication inhibitor (Moreno et al. 2012a). The implications of these findings for the design of protocols to treat arenavirus infections in vivo remain to be investigated.

5.3 *Arenavirus Genetic Variation and Development of Broad-Spectrum Vaccines*

There are not FDA-approved vaccines against HF arenaviral diseases. The JUNV live-attenuated Candid1 strain has been shown to be an effective vaccine against Argentine hemorrhagic fever (AHF) disease (Enria and Barrera Oro 2002; Enria et al. 2008). However, outside Argentina, Candid1 has only IND status and studies addressing long-term immunity and safety have not been conducted. Moreover, Candid1 does not protect against LASV. Despite significant efforts dedicated to the development of LASV vaccines, not a single LASV vaccine candidate has entered a clinical trial although the MOPV/LASV reassortant ML29, as well as recombinant VSV and vaccinia virus expressing specific LASV antigens, has shown promising results (Falzarano and Feldmann 2013). Specifically, ML29 exhibited good safety and efficacy profiles in animal models of LASV infection. However, the high prevalence of HIV within LASV endemic regions raises safety concerns about the use of VSV- or vaccinia-based platforms.

Control of LASV infection seems to be mediated mainly by cellular immune responses, and significant titers of LASV neutralizing antibodies (NAbs) are usually observed only in patients who have clinically recovered (Jahrling and Peters 1984). However, passive antibody transfer has been shown to induce protection in animal models of LF (Jahrling 1983) and in limited human studies (Monath and Casals 1975) suggesting that an ideal vaccine should induce the right combination of cellular and humoral responses.

Sequence comparison of all proteins of seven pathogenic arenaviruses revealed a high degree of genetic variation among different geographical and temporal isolates of the same virus species (Bowen et al. 2000; Fulhorst et al. 2001; Garcia et al. 2000; Weaver et al. 2000). Overall, strain variation among 54 LASV strains was found to be as high as 27 and 15 % at the nucleotide and amino acid levels, respectively (Bowen et al. 2000). The high degree of LASV genetic diversity likely

contributes to underestimating its prevalence and poses also a great challenge for vaccine development. In some endemic areas, up to 32 % of anti-LASV-positive samples would not have been detected, if the IFA had only been run with LASV-Josiah (Jos) strain, which is historically used as antigen in IFA or ELISA (Emmerich et al. 2008). This underscores the need for a multivalent or "universal" LASV vaccine able to protect against infections by the related isolates of the four lineages currently identified for LASV. The rML29/Jos expresses NP and GP antigens of Josiah strain, the prototype of LASV lineage IV, the largest sublineage, containing strains isolated in Guinea, Liberia, and Sierra Leone (Bowen et al. 2000). A single dose of ML29 vaccine effectively protected guinea pigs against challenge with homologous (lineage IV) or heterologous (lineage II) strains (Carrion et al. 2012). Lineage III and IV had a sister relationship, and the protection elicited by ML29 against LASV strains from lineage II strongly suggests that ML29 will also protect against members of lineage III. In contrast, sequence differences between LP (I) and Jos (IV) are 23.6 and 20.8 % for NP and GPC genes, respectively, and only one of the three recently predicted HL2-A2-restricted CTL epitopes was conserved in GP sequences of both viruses (Botten et al. 2006). This potential problem could be overcome by the use of arenavirus reverse genetics to generate rML29 expressing NP and GP antigens from lineages I and IV to generate a blended vaccine able to provide cross-protection against members of all LASV lineages. Despite the very promising features of the rML29 platform for the development of pan-LASV vaccine, it should be noted that the mechanisms of ML29 attenuation remain poorly understood and additional mutations, including reversions, in ML29 or reassortants between ML29 and circulating virulent LASV strains, could result in viruses with enhanced virulence.

References

Abraham J, Kwong JA, Albarino CG, Lu JG, Radoshitzky SR, Salazar-Bravo J, Farzan M, Spiropoulou CF, Choe H (2009) Host-species transferrin receptor 1 orthologs are cellular receptors for nonpathogenic New World clade B arenaviruses. PLoS Pathog 5(4):e1000358. doi:10.1371/journal.ppat.1000358

Aebischer T, Moskophidis D, Rohrer UH, Zinkernagel RM, Hengartner H (1991) In vitro selection of lymphocytic choriomeningitis virus escape mutants by cytotoxic T lymphocytes. Proc Natl Acad Sci USA 88(24):11047–11051

Agudo R, Arias A, Pariente N, Perales C, Escarmis C, Jorge A, Marina A, Domingo E (2008) Molecular characterization of a dual inhibitory and mutagenic activity of 5-fluorouridine triphosphate on viral RNA synthesis: implications for lethal mutagenesis. J Mol Biol 382 (3):652–666. doi:10.1016/j.jmb.2008.07.033

Ahmed R, Oldstone MB (1988) Organ-specific selection of viral variants during chronic infection. J Exp Med 167(5):1719–1724

Ahmed R, Salmi A, Butler LD, Chiller JM, Oldstone MB (1984) Selection of genetic variants of lymphocytic choriomeningitis virus in spleens of persistently infected mice: role in suppression of cytotoxic T lymphocyte response and viral persistence. J Exp Med 160(2):521–540

Ahmed R, Simon RS, Matloubian M, Kolhekar SR, Southern PJ, Freedman DM (1988) Genetic analysis of in vivo-selected viral variants causing chronic infection: importance of mutation in the L RNA segment of lymphocytic choriomeningitis virus. J Virol 62(9):3301–3308

Ahmed R, Hahn CS, Somasundaram T, Villarete L, Matloubian M, Strauss JH (1991) Molecular basis of organ-specific selection of viral variants during chronic infection. J Virol 65(8):4242–4247

Albarino CG, Posik DM, Ghiringhelli PD, Lozano ME, Romanowski V (1998) Arenavirus phylogeny: a new insight. Virus Genes 16(1):39–46

Albarino CG, Bergeron E, Erickson BR, Khristova ML, Rollin PE, Nichol ST (2009) Efficient reverse genetics generation of infectious junin viruses differing in glycoprotein processing. J Virol 83(11):5606–5614. doi:10.1128/JVI.00276-09

Albarino CG, Palacios G, Khristova ML, Erickson BR, Carroll SA, Comer JA, Hui J, Briese T, St George K, Ksiazek TG, Lipkin WI, Nichol ST (2010) High diversity and ancient common ancestry of lymphocytic choriomeningitis virus. Emerg Infect Dis 16(7):1093–1100. doi:10.3201/eid1607.091902

Albarino CG, Bird BH, Chakrabarti AK, Dodd KA, Erickson BR, Nichol ST (2011) Efficient rescue of recombinant Lassa virus reveals the influence of S segment noncoding regions on virus replication and virulence. J Virol 85(8):4020–4024. doi:10.1128/JVI.02556-10

Andrei G, De Clercq E (1990) Inhibitory effect of selected antiviral compounds on arenavirus replication in vitro. Antiviral Res 14(4–5):287–299

Andrei G, De Clercq E (1993) Molecular approaches for the treatment of hemorrhagic fever virus infections. Antiviral Res 22(1):45–75

Archer AM, Rico-Hesse R (2002) High genetic divergence and recombination in Arenaviruses from the Americas. Virology 304(2):274–281

Baranowski E, Ruiz-Jarabo CM, Sevilla N, Andreu D, Beck E, Domingo E (2000) Cell recognition by foot-and-mouth disease virus that lacks the RGD integrin-binding motif: flexibility in aphthovirus receptor usage. J Virol 74(4):1641–1647

Barber DL, Wherry EJ, Masopust D, Zhu B, Allison JP, Sharpe AH, Freeman GJ, Ahmed R (2006) Restoring function in exhausted CD8 T cells during chronic viral infection. Nature 439(7077):682–687

Beaucourt S, Borderia AV, Coffey LL, Gnadig NF, Sanz-Ramos M, Beeharry Y, Vignuzzi M (2011) Isolation of fidelity variants of RNA viruses and characterization of virus mutation frequency. J Vis Exp 52:2953–2982. doi:10.3791/2953

Bergthaler A, Flatz L, Hegazy AN, Johnson S, Horvath E, Lohning M, Pinschewer DD (2010) Viral replicative capacity is the primary determinant of lymphocytic choriomeningitis virus persistence and immunosuppression. Proc Natl Acad Sci USA 107(50):21641–21646. doi:10.1073/pnas.1011998107

Beyer WR, Popplau D, Garten W, von Laer D, Lenz O (2003) Endoproteolytic processing of the lymphocytic choriomeningitis virus glycoprotein by the subtilase SKI-1/S1P. J Virol 77(5):2866–2872

Blasdell KR, Becker SD, Hurst J, Begon M, Bennett M (2008) Host range and genetic diversity of arenaviruses in rodents United Kingdom. Emerg Infect Dis 14(9):1455–1458. doi:10.3201/eid1409.080209

Bodewes R, Kik MJ, Raj VS, Schapendonk CM, Haagmans BL, Smits SL, Osterhaus AD (2013) Detection of novel divergent arenaviruses in boid snakes with inclusion body disease in The Netherlands. J Gen Virol 94(Pt 6):1206–1210. doi:10.1099/vir.0.051995-0

Bolken TC, Laquerre S, Zhang Y, Bailey TR, Pevear DC, Kickner SS, Sperzel LE, Jones KF, Warren TK, Amanda Lund S, Kirkwood-Watts DL, King DS, Shurtleff AC, Guttieri MC, Deng Y, Bleam M, Hruby DE (2005) Identification and characterization of potent small molecule inhibitor of hemorrhagic fever New World arenaviruses. Antiviral Res

Bonnac LF, Mansky LM, Patterson SE (2013) Structure-activity relationships and design of viral mutagens and application to lethal mutagenesis. J Med Chem 56(23):9403–9414. doi:10.1021/jm400653j

Borden KL, Campbell Dwyer EJ, Salvato MS (1998) An arenavirus RING (zinc-binding) protein binds the oncoprotein promyelocyte leukemia protein (PML) and relocates PML nuclear bodies to the cytoplasm. J Virol 72(1):758–766

Borrow P, Evans CF, Oldstone MB (1995) Virus-induced immunosuppression: immune system-mediated destruction of virus-infected dendritic cells results in generalized immune suppression. J Virol 69(2):1059–1070

Botten J, Alexander J, Pasquetto V, Sidney J, Barrowman P, Ting J, Peters B, Southwood S, Stewart B, Rodriguez-Carreno MP, Mothe B, Whitton JL, Sette A, Buchmeier MJ (2006) Identification of protective Lassa virus epitopes that are restricted by HLA-A2. J Virol 80 (17):8351–8361. doi:10.1128/JVI.00896-06 ([pii] 80/17/8351)

Bowen MD, Peters CJ, Nichol ST (1996) The phylogeny of New World (Tacaribe complex) arenaviruses. Virology 219(1):285–290. doi:10.1006/viro.1996.0248

Bowen MD, Peters CJ, Nichol ST (1997) Phylogenetic analysis of the arenaviridae: patterns of virus evolution and evidence for cospeciation between arenaviruses and their rodent hosts. Mol Phylogenet Evol 8(3):301–316

Bowen MD, Rollin PE, Ksiazek TG, Hustad HL, Bausch DG, Demby AH, Bajani MD, Peters CJ, Nichol ST (2000) Genetic diversity among Lassa virus strains. J Virol 74(15):6992–7004

Bray M (2005) Pathogenesis of viral hemorrhagic fever. Curr Opin Immunol 17(4):399–403

Brown RJ, Peters PJ, Caron C, Gonzalez-Perez MP, Stones L, Ankghuambom C, Pondei K, McClure CP, Alemnji G, Taylor S, Sharp PM, Clapham PR, Ball JK (2011) Intercompartmental recombination of HIV-1 contributes to env intrahost diversity and modulates viral tropism and sensitivity to entry inhibitors. J Virol 85(12):6024–6037. doi:10.1128/JVI.00131-11

Brunotte L, Lelke M, Hass M, Kleinsteuber K, Becker-Ziaja B, Gunther S (2011) Domain structure of Lassa virus L protein. J Virol 85(1):324–333. doi:10.1128/JVI.00721-10

Buchmeier MJ, Peters CJ, de la Torre JC (2007) Arenaviridae: the viruses and their replication. In: Knipe DM, Holey PM (eds) Fields virology, 5th edn, vol 2, pp 1792–1827

Buesa-Gomez J, Teng MN, Oldstone CE, Oldstone MB, de la Torre JC (1996) Variants able to cause growth hormone deficiency syndrome are present within the disease-nil WE strain of lymphocytic choriomeningitis virus. J Virol 70(12):8988–8992

Cabot B, Martell M, Esteban JI, Sauleda S, Otero T, Esteban R, Guardia J, Gomez J (2000) Nucleotide and amino acid complexity of hepatitis C virus quasispecies in serum and liver. J Virol 74(2):805–811

Cajimat MN, Fulhorst CF (2004) Phylogeny of the venezuelan arenaviruses. Virus Res 102 (2):199–206. doi:10.1016/j.virusres.2004.01.032 ([pii] S0168170204000735)

Cajimat MN, Milazzo ML, Hess BD, Rood MP, Fulhorst CF (2007) Principal host relationships and evolutionary history of the North American arenaviruses. Virology 367(2):235–243. doi:10.1016/j.virol.2007.05.031 ([pii] S0042-6822(07)00399-6)

Cajimat MN, Milazzo ML, Mauldin MR, Bradley RD, Fulhorst CF (2013) Diversity among Tacaribe serocomplex viruses (family arenaviridae) associated with the southern plains woodrat (Neotoma micropus). Virus Res 178(2):486–494. doi:10.1016/j.virusres.2013.10.004 ([pii] S0168-1702(13)00351-1)

Campbell Dwyer EJ, Lai H, MacDonald RC, Salvato MS, Borden KL (2000) The lymphocytic choriomeningitis virus RING protein Z associates with eukaryotic initiation factor 4E and selectively represses translation in a RING-dependent manner. J Virol 74(7):3293–3300

Candurra NA, Maskin L, Damonte EB (1996) Inhibition of arenavirus multiplication in vitro by phenotiazines. Antiviral Res 31(3):149–158

Cao W, Henry MD, Borrow P, Yamada H, Elder JH, Ravkov EV, Nichol ST, Compans RW, Campbell KP, Oldstone MB (1998) Identification of alpha-dystroglycan as a receptor for lymphocytic choriomeningitis virus and Lassa fever virus. Science 282(5396):2079–2081 (see comments)

Carrion R Jr, Bredenbeek P, Jiang X, Tretyakova I, Pushko P, Lukashevich IS (2012) Vaccine platforms to control arenaviral hemorrhagic fevers. J Vaccines Vaccin 3(7). doi:10.4172/2157-7560.1000160

Cattaneo R, Billeter MA (1992) Mutations and A/I hypermutations in measles virus persistent infections. Curr Top Microbiol Immunol 176:63–74

Charrel RN, de Lamballerie X (2003) Arenaviruses other than Lassa virus. Antiviral Res 57(1–2):89–100

Charrel RN, de Lamballerie X, Fulhorst CF (2001) The whitewater Arroyo virus: natural evidence for genetic recombination among Tacaribe serocomplex viruses (family arenaviridae). Virology 283(2):161–166. doi:10.1006/viro.2001.0874

Charrel RN, Feldmann H, Fulhorst CF, Khelifa R, de Chesse R, de Lamballerie X (2002) Phylogeny of New World arenaviruses based on the complete coding sequences of the small genomic segment identified an evolutionary lineage produced by intrasegmental recombination. Biochem Biophys Res Commun 296(5):1118–1124

Charrel RN, Lemasson JJ, Garbutt M, Khelifa R, De Micco P, Feldmann H, de Lamballerie X (2003) New insights into the evolutionary relationships between arenaviruses provided by comparative analysis of small and large segment sequences. Virology 317(2):191–196

Charrel RN, de Lamballerie X, Emonet S (2008) Phylogeny of the genus arenavirus. Curr Opin Microbiol 11(4):362–368. doi:10.1016/j.mib.2008.06.001 ([pii] S1369-5274(08)00073-8)

Chen M, Lan S, Ou R, Price GE, Jiang H, de la Torre JC, Moskophidis D (2008) Genomic and biological characterization of aggressive and docile strains of lymphocytic choriomeningitis virus rescued from a plasmid-based reverse-genetics system. J Gen Virol 89(Pt 6):1421–1433. doi:10.1099/vir.0.83464-0 ([pii] 89/6/1421)

Cheng-Mayer C, Weiss C, Seto D, Levy JA (1989) Isolates of human immunodeficiency virus type 1 from the brain may constitute a special group of the AIDS virus. Proc Natl Acad Sci USA 86(21):8575–8579

Childs JE, Peters CJ (1993) Ecology and epidemiology of arenaviruses and their hosts. In: Salvato M (ed) The arenaviridae. Plenum Press, New York, pp 331–384

Choe H, Jemielity S, Abraham J, Radoshitzky SR, Farzan M (2011) Transferrin receptor 1 in the zoonosis and pathogenesis of New World hemorrhagic fever arenaviruses. Curr Opin Microbiol 14(4):476–482. doi:10.1016/j.mib.2011.07.014 ([pii] S1369-5274(11)00098-1)

Ciurea A, Klenerman P, Hunziker L, Horvath E, Senn BM, Ochsenbein AF, Hengartner H, Zinkernagel RM (2000) Viral persistence in vivo through selection of neutralizing antibody-escape variants. Proc Natl Acad Sci USA 97(6):2749–2754. doi:10.1073/pnas.040558797

Ciurea A, Hunziker L, Zinkernagel RM, Hengartner H (2001) Viral escape from the neutralizing antibody response: the lymphocytic choriomeningitis virus model. Immunogenetics 53(3):185–189

Cordo SM, Candurra NA, Damonte EB (1999) Myristic acid analogs are inhibitors of Junin virus replication. Microbes Infect 1(8):609–614

Cornu TI, de la Torre JC (2001) RING finger Z protein of lymphocytic choriomeningitis virus (LCMV) inhibits transcription and RNA replication of an LCMV S-segment minigenome. J Virol 75(19):9415–9426

Cornu TI, de la Torre JC (2002) Characterization of the arenavirus RING finger Z protein regions required for Z-mediated inhibition of viral RNA synthesis. J Virol 76(13):6678–6688

Cornu TI, Feldmann H, de la Torre JC (2004) Cells expressing the RING finger Z protein are resistant to arenavirus infection. J Virol 78(6):2979–2983

Coulibaly-N'Golo D, Allali B, Kouassi SK, Fichet-Calvet E, Becker-Ziaja B, Rieger T, Olschlager S, Dosso H, Denys C, Ter Meulen J, Akoua-Koffi C, Gunther S (2011) Novel arenavirus sequences in Hylomyscus sp. and Mus (Nannomys) setulosus from Cote d'Ivoire: implications for evolution of arenaviruses in Africa. PLoS ONE 6(6):e20893. doi:10.1371/journal.pone.0020893 ([pii] PONE-D-11-02828)

Dalldorf G (1939) The simultaneous occurrence of the viruses of canine distemper and lymphocytic choriomeningitis : a correction of "canine distemper in the rhesus monkey". J Exp Med 70(1):19–27

Damonte EB, Coto CE (2002) Treatment of arenavirus infections: from basic studies to the challenge of antiviral therapy. Adv Virus Res 58:125–155

Damonte EB, Mersich SE, Coto CE (1983) Response of cells persistently infected with arenaviruses to superinfection with homotypic and heterotypic viruses. Virology 129 (2):474–478

Dapp MJ, Clouser CL, Patterson S, Mansky LM (2009) 5-Azacytidine can induce lethal mutagenesis in human immunodeficiency virus type 1. J Virol 83(22):11950–11958. doi:10.1128/JVI.01406-09

Dapp MJ, Holtz CM, Mansky LM (2012) Concomitant lethal mutagenesis of human immunodeficiency virus type 1. J Mol Biol 419(3–4):158–170. doi:10.1016/j.jmb.2012.03.003

de la Torre JC, Holland JJ (1990) RNA virus quasispecies populations can suppress vastly superior mutant progeny. J Virol 64(12):6278–6281

Deforges S, Evlashev A, Perret M, Sodoyer M, Pouzol S, Scoazec JY, Bonnaud B, Diaz O, Paranhos-Baccala G, Lotteau V, Andre P (2004) Expression of hepatitis C virus proteins in epithelial intestinal cells in vivo. J Gen Virol 85(Pt 9):2515–2523. doi:10.1099/vir.0.80071-0 ([pii] 85/9/2515)

Delgado S, Erickson BR, Agudo R, Blair PJ, Vallejo E, Albarino CG, Vargas J, Comer JA, Rollin PE, Ksiazek TG, Olson JG, Nichol ST (2008) Chapare virus, a newly discovered arenavirus isolated from a fatal hemorrhagic fever case in Bolivia. PLoS Pathog 4(4): e1000047. doi:10.1371/journal.ppat.1000047

Demogines A, Abraham J, Choe H, Farzan M, Sawyer SL (2013) Dual host-virus arms races shape an essential housekeeping protein. PLoS Biol 11(5):e1001571. doi:10.1371/journal.pbio.1001571 ([pii] PBIOLOGY-D-12-04902)

Denison MR, Graham RL, Donaldson EF, Eckerle LD, Baric RS (2011) Coronaviruses: an RNA proofreading machine regulates replication fidelity and diversity. RNA Biol 8(2):270–279

Djavani M, Rodas J, Lukashevich IS, Horejsh D, Pandolfi PP, Borden KL, Salvato MS (2001) Role of the promyelocytic leukemia protein PML in the interferon sensitivity of lymphocytic choriomeningitis virus. J Virol 75(13):6204–6208

Domingo E (1989) RNA virus evolution and the control of viral disease. Prog Drug Res Fortschritte der Arzneimittelforschung Progres des recherches pharmaceutiques 33:93–133

Domingo E (1992) Genetic variation and quasi-species. Curr Opin Genet Dev 2(1):61–63

Domingo E (2006) Quasispecies: concepts and implications for virology, vol 299., Current topics in microbiology and immunologySpringer, Berlin

Domingo E (2007) Virus evolution. In: Knipe DM, Holey PM (eds) Fields virology, 5th edn

Domingo E, Holland JJ, Ahlquist P (1988) RNA Genetics, vol I, II, III. CRC Press, Boca Ratón

Domingo E, Mas A, Yuste E, Pariente N, Sierra S, Gutierrez-Riva M, Menendez-Arias L (2001) Virus population dynamics, fitness variations and the control of viral disease: an update. Prog Drug Res 57:77–115

Domingo E, Martin V, Perales C, Escarmis C (2008) Coxsackieviruses and quasispecies theory: evolution of enteroviruses. Curr Top Microbiol Immunol 323:3–32

Downs WG, Anderson CR, Spence L, Aitken TH, Greenhall AH (1963) Tacaribe virus, a new agent isolated from artibeus bats and mosquitoes in Trinidad, West Indies. Am J Trop Med Hyg 12:640–646

Drake JW, Holland JJ (1999) Mutation rates among RNA viruses. Proc Natl Acad Sci USA 96 (24):13910–13913

Eigen M (1971) Selforganization of matter and the evolution of biological macromolecules. Die Naturwissenschaften 58(10):465–523

Eigen M (2002) Error catastrophe and antiviral strategy. Proc Natl Acad Sci USA 99(21):13374–13376. doi:10.1073/pnas.212514799

Ellenberg P, Edreira M, Scolaro L (2004) Resistance to superinfection of Vero cells persistently infected with Junin virus. Arch Virol 149(3):507–522. doi:10.1007/s00705-003-0227-1

Ellenberg P, Linero FN, Scolaro LA (2007) Superinfection exclusion in BHK-21 cells persistently infected with Junin virus. J Gen Virol 88(Pt 10):2730–2739. doi:10.1099/vir.0.83041-0

Emmerich P, Gunther S, Schmitz H (2008) Strain-specific antibody response to Lassa virus in the local population of west Africa. J Clin Virol 42(1):40–44. doi:10.1016/j.jcv.2007.11.019 ([pii] S1386-6532(07)00437-4)

Emonet S, Lemasson JJ, Gonzalez JP, de Lamballerie X, Charrel RN (2006) Phylogeny and evolution of old world arenaviruses. Virology 350(2):251–257. doi:10.1016/j.virol.2006.01.026

Emonet SF, de la Torre JC, Domingo E, Sevilla N (2009a) Arenavirus genetic diversity and its biological implications. Infect Genet Evol J Mol Epidemiol Evol Genet Infect Dis 9(4):417–429. doi:10.1016/j.meegid.2009.03.005

Emonet SF, Garidou L, McGavern DB, de la Torre JC (2009b) Generation of recombinant lymphocytic choriomeningitis viruses with trisegmented genomes stably expressing two additional genes of interest. Proc Natl Acad Sci USA 106(9):3473–3478. doi:10.1073/pnas.0900088106

Emonet SE, Urata S, de la Torre JC (2011a) Arenavirus reverse genetics: new approaches for the investigation of arenavirus biology and development of antiviral strategies. Virology 411(2):416–425. doi:10.1016/j.virol.2011.01.013 ([pii] S0042-6822(11)00018-3)

Emonet SF, Seregin AV, Yun NE, Poussard AL, Walker AG, de la Torre JC, Paessler S (2011b) Rescue from cloned cDNAs and in vivo characterization of recombinant pathogenic Romero and live-attenuated Candid #1 strains of Junin virus, the causative agent of argentine hemorrhagic fever disease. J Virol 85(4):1473–1483. doi:10.1128/JVI.02102-10

Enria DA, Barrera Oro JG (2002) Junin virus vaccines. Curr Top Microbiol Immunol 263:239–261

Enria DA, Briggiler AM, Sanchez Z (2008) Treatment of argentine hemorrhagic fever. Antiviral Res 78(1):132–139. doi:10.1016/j.antiviral.2007.10.010 ([pii] S0166-3542(07)00433-0)

Evans CF, Borrow P, de la Torre JC, Oldstone MB (1994) Virus-induced immunosuppression: kinetic analysis of the selection of a mutation associated with viral persistence. J Virol 68(11):7367–7373

Falzarano D, Feldmann H (2013) Vaccines for viral hemorrhagic fevers–progress and short comings. Curr Opin Virol 3(3):343–351. doi:10.1016/j.coviro.2013.04.007 ([pii] S1879-6257(13)00062-X)

Fichet-Calvet E, Rogers DJ (2009) Risk maps of Lassa fever in West Africa. PLoS Negl Trop Dis 3(3):e388. doi:10.1371/journal.pntd.0000388

Flanagan ML, Oldenburg J, Reignier T, Holt N, Hamilton GA, Martin VK, Cannon PM (2008) New world clade B arenaviruses can use transferrin receptor 1 (TfR1)-dependent and -independent entry pathways, and glycoproteins from human pathogenic strains are associated with the use of TfR1. J Virol 82(2):938–948. doi:10.1128/JVI.01397-07

Flatz L, Bergthaler A, de la Torre JC, Pinschewer DD (2006) Recovery of an arenavirus entirely from RNA polymerase I/II-driven cDNA. Proc Natl Acad Sci USA 103(12):4663–4668

Freedman DO, Woodall J (1999) Emerging infectious diseases and risk to the traveler. Med Clin North Am 83(4):865–883

Fulhorst CF, Bowen MD, Ksiazek TG, Rollin PE, Nichol ST, Kosoy MY, Peters CJ (1996) Isolation and characterization of whitewater Arroyo virus, a novel North American arenavirus. Virology 224(1):114–120. doi:10.1006/viro.1996.0512

Fulhorst CF, Bowen MD, Salas RA, Duno G, Utrera A, Ksiazek TG, De Manzione NM, De Miller E, Vasquez C, Peters CJ, Tesh RB (1999) Natural rodent host associations of Guanarito and pirital viruses (family arenaviridae) in central Venezuela. Am J Trop Med Hyg 61(2):325–330

Fulhorst CF, Charrel RN, Weaver SC, Ksiazek TG, Bradley RD, Milazzo ML, Tesh RB, Bowen MD (2001) Geographic distribution and genetic diversity of whitewater Arroyo virus in the southwestern United States. Emerg Infect Dis 7(3):403–407. doi:10.3201/eid0703.010306

Fulhorst CF, Cajimat MN, Milazzo ML, Paredes H, de Manzione NM, Salas RA, Rollin PE, Ksiazek TG (2008) Genetic diversity between and within the arenavirus species indigenous to western Venezuela. Virology 378(2):205–213. doi:10.1016/j.virol.2008.05.014 ([pii] S0042-6822(08)00341-3)

Garcia JB, Morzunov SP, Levis S, Rowe J, Calderon G, Enria D, Sabattini M, Buchmeier MJ, Bowen MD, St Jeor SC (2000) Genetic diversity of the Junin virus in Argentina: geographic and temporal patterns. Virology 272(1):127–136. doi:10.1006/viro.2000.0345 ([pii] S0042682200903453)

Geisbert TW, Jahrling PB (2004) Exotic emerging viral diseases: progress and challenges. Nat Med 10(12 Suppl):S110–S121

Geleziunas R, Bour S, Wainberg MA (1994) Cell surface down-modulation of CD4 after infection by HIV-1. FASEB J 8(9):593–600

Gonzalez-Lopez C, Arias A, Pariente N, Gomez-Mariano G, Domingo E (2004) Preextinction viral RNA can interfere with infectivity. J Virol 78(7):3319–3324

Graci JD, Cameron CE (2006) Mechanisms of action of ribavirin against distinct viruses. Rev Med Virol 16(1):37–48. doi:10.1002/rmv.483

Graci JD, Harki DA, Korneeva VS, Edathil JP, Too K, Franco D, Smidansky ED, Paul AV, Peterson BR, Brown DM, Loakes D, Cameron CE (2007) Lethal mutagenesis of poliovirus mediated by a mutagenic pyrimidine analogue. J Virol 81(20):11256–11266. doi:10.1128/JVI.01028-07

Graci JD, Too K, Smidansky ED, Edathil JP, Barr EW, Harki DA, Galarraga JE, Bollinger JM Jr, Peterson BR, Loakes D, Brown DM, Cameron CE (2008) Lethal mutagenesis of picornaviruses with N-6-modified purine nucleoside analogues. Antimicrob Agents Chemother 52(3):971–979. doi:10.1128/AAC.01056-07

Grande-Perez A, Sierra S, Castro MG, Domingo E, Lowenstein PR (2002) Molecular indetermination in the transition to error catastrophe: systematic elimination of lymphocytic choriomeningitis virus through mutagenesis does not correlate linearly with large increases in mutant spectrum complexity. Proc Natl Acad Sci USA 99(20):12938–12943. doi:10.1073/pnas.182426999

Grande-Perez A, Gomez-Mariano G, Lowenstein PR, Domingo E (2005a) Mutagenesis-induced, large fitness variations with an invariant arenavirus consensus genomic nucleotide sequence. J Virol 79(16):10451–10459. doi:10.1128/JVI.79.16.10451-10459.2005

Grande-Perez A, Lazaro E, Lowenstein P, Domingo E, Manrubia SC (2005b) Suppression of viral infectivity through lethal defection. Proc Natl Acad Sci USA 102(12):4448–4452

Greenwood AG, Sanchez S (2002) Serological evidence of murine pathogens in wild grey squirrels (Sciurus carolinensis) in North Wales. Vet Rec 150(17):543–546

Hall JS, French R, Hein GL, Morris TJ, Stenger DC (2001) Three distinct mechanisms facilitate genetic isolation of sympatric wheat streak mosaic virus lineages. Virology 282(2):230–236. doi:10.1006/viro.2001.0841 ([pii] S0042-6822(01)90841-4)

Harki DA, Graci JD, Korneeva VS, Ghosh SK, Hong Z, Cameron CE, Peterson BR (2002) Synthesis and antiviral evaluation of a mutagenic and non-hydrogen bonding ribonucleoside analogue: 1-beta-D-Ribofuranosyl-3-nitropyrrole. Biochemistry 41(29):9026–9033

Harris KS, Brabant W, Styrchak S, Gall A, Daifuku R (2005) KP-1212/1461, a nucleoside designed for the treatment of HIV by viral mutagenesis. Antiviral Res 67(1):1–9. doi:10.1016/j.antiviral.2005.03.004

Hass M, Golnitz U, Muller S, Becker-Ziaja B, Gunther S (2004) Replicon system for Lassa virus. J Virol 78(24):13793–13803

Hass M, Westerkofsky M, Muller S, Becker-Ziaja B, Busch C, Gunther S (2006) Mutational analysis of the lassa virus promoter. J Virol 80(24):12414–12419

Hastie KM, Kimberlin CR, Zandonatti MA, MacRae IJ, Saphire EO (2011) Structure of the Lassa virus nucleoprotein reveals a dsRNA-specific 3′ to 5′ exonuclease activity essential for immune suppression. Proc Natl Acad Sci USA 108(6):2396–2401. doi:10.1073/pnas.1016404108

Haydon DT, Bastos AD, Knowles NJ, Samuel AR (2001) Evidence for positive selection in foot-and-mouth disease virus capsid genes from field isolates. Genetics 157(1):7–15

Hetzel U, Sironen T, Laurinmaki P, Liljeroos L, Patjas A, Henttonen H, Vaheri A, Artelt A, Kipar A, Butcher SJ, Vapalahti O, Hepojoki J (2013) Isolation, identification, and characterization of novel arenaviruses, the etiological agents of boid inclusion body disease. J Virol 87(20):10918–10935. doi:10.1128/JVI.01123-13

Hicks C, Clay P, Redfield R, Lalezari J, Liporace R, Schneider S, Sension M, McRae M, Laurent JP (2013) Safety, tolerability, and efficacy of KP-1461 as monotherapy for 124 days in antiretroviral-experienced, HIV type 1-infected subjects. AIDS Res Hum Retroviruses 29(2):250–255. doi:10.1089/AID.2012.0093

Holland JJ, Domingo E, de la Torre JC, Steinhauer DA (1990) Mutation frequencies at defined single codon sites in vesicular stomatitis virus and poliovirus can be increased only slightly by chemical mutagenesis. J Virol 64(8):3960–3962

Horga MA, Gusella GL, Greengard O, Poltoratskaia N, Porotto M, Moscona A (2000) Mechanism of interference mediated by human parainfluenza virus type 3 infection. J Virol 74(24):11792–11799

Hotchin J (1973) Transient virus infection: spontaneous recovery mechanism of lymphocytic choriomeningitis virrus-infected cells. Nat New Biol 241(113):270–272

Hotchin J, Sikora E (1973) Low-pathogenicity variant of lymphocytic choriomeningitis virus. Infect Immun 7(5):825–826

Hotchin J, Kinch W, Benson L (1971) Lytic and turbid plaque-type mutants of lymphocytic choriomeningitis virus as a cause of neurological disease or persistent infection. Infect Immun 4(3):281–286

Huang IC, Li W, Sui J, Marasco W, Choe H, Farzan M (2008) Influenza A virus neuraminidase limits viral superinfection. J Virol 82(10):4834–4843. doi:10.1128/JVI.00079-08

Huggins JW (1989) Prospects for treatment of viral hemorrhagic fevers with ribavirin, a broad-spectrum antiviral drug. Rev Infect Dis 11(Suppl 4):S750–S761

Hugot JP, Gonzalez JP, Denys C (2001) Evolution of the Old World arenaviridae and their rodent hosts: generalized host-transfer or association by descent? Infect Genet Evol J Mol Epidemiol Evol Genet Infect Dis 1(1):13–20 ([pii] S156713480100003X)

Hundley HA, Bass BL (2010) ADAR editing in double-stranded UTRs and other noncoding RNA sequences. Trends Biochem Sci 35(7):377–383. doi:10.1016/j.tibs.2010.02.008 ([pii] S0968-0004(10)00029-0)

Irwin NR, Bayerlova M, Missa O, Martinkova N (2012) Complex patterns of host switching in New World arenaviruses. Mol Ecol 21(16):4137–4150. doi:10.1111/j.1365-294X.2012.05663.x

Isaacson M (2001) Viral hemorrhagic fever hazards for travelers in Africa. Clin Infect Dis 33 (10):1707–1712

Ishii A, Thomas Y, Moonga L, Nakamura I, Ohnuma A, Hang'ombe BM, Takada A, Mweene AS, Sawa H (2012) Molecular surveillance and phylogenetic analysis of Old World arenaviruses in Zambia. J Gen Virol 93(Pt 10):2247–2251. doi:10.1099/vir.0.044099-0

Jackson AP, Charleston MA (2004) A cophylogenetic perspective of RNA-virus evolution. Mol Biol Evol 21(1):45–57. doi:10.1093/molbev/msg232

Jahrling PB (1983) Protection of Lassa virus-infected guinea pigs with Lassa-immune plasma of guinea pig, primate, and human origin. J Med Virol 12(2):93–102

Jahrling PB, Peters CJ (1984) Passive antibody therapy of Lassa fever in cynomolgus monkeys: importance of neutralizing antibody and Lassa virus strain. Infect Immun 44(2):528–533

Jahrling PB, Peters CJ (1992) Lymphocytic choriomeningitis virus A neglected pathogen of man. Arch Pathol Lab Med 116(5):486–488

Jay MT, Glaser C, Fulhorst CF (2005) The arenaviruses. J Am Vet Med Assoc 227(6):904–915

Jelcic I, Hotz-Wagenblatt A, Hunziker A, Zur Hausen H, de Villiers EM (2004) Isolation of multiple TT virus genotypes from spleen biopsy tissue from a Hodgkin's disease patient: genome reorganization and diversity in the hypervariable region. J Virol 78(14):7498–7507. doi:10.1128/JVI.78.14.7498-7507.2004 ([pii] 78/14/7498)

Jridi C, Martin JF, Marie-Jeanne V, Labonne G, Blanc S (2006) Distinct viral populations differentiate and evolve independently in a single perennial host plant. J Virol 80(5):2349–2357. doi:10.1128/JVI.80.5.2349-2357.2006 ([pii] 80/5/2349)

Kilgore PE, Peters CJ, Mills JN, Rollin PE, Armstrong L, Khan AS, Ksiazek TG (1995) Prospects for the control of Bolivian hemorrhagic fever. Emerg Infect Dis 1(3):97–100

Kilgore PE, Ksiazek TG, Rollin PE, Mills JN, Villagra MR, Montenegro MJ, Costales MA, Paredes LC, Peters CJ (1997) Treatment of Bolivian hemorrhagic fever with intravenous ribavirin. Clin Infect Dis 24(4):718–722

King AMQ, Adams MJ, Carstens EB, Lefkowitz EJ (2012) Ninth report of the international committee on taxonomy of viruses. In: King AMQ, Adams MJ, Carstens EB, Lefkowitz EJ (eds) Virus taxonomy: classification and nomenclature of viruses. Elsevier, San Diego

Klavinskis LS, Oldstone MB (1989) Lymphocytic choriomeningitis virus selectively alters differentiated but not housekeeping functions: block in expression of growth hormone gene is at the level of transcriptional initiation. Virology 168(2):232–235

Kranzusch PJ, Whelan SP (2011) Arenavirus Z protein controls viral RNA synthesis by locking a polymerase-promoter complex. Proc Natl Acad Sci USA 108(49):19743–19748. doi:10.1073/pnas.1112742108

Kunz S, Borrow P, Oldstone MB (2002) Receptor structure, binding, and cell entry of arenaviruses. Curr Top Microbiol Immunol 262:111–137

Kunz S, Edelmann KH, de la Torre J-C, Gorney R, Oldstone MBA (2003a) Mechanisms for lymphocytic choriomeningitis virus glycoprotein cleavage, transport, and incorporation into virions. Virology (in press)

Kunz S, Edelmann KH, de la Torre JC, Gorney R, Oldstone MB (2003b) Mechanisms for lymphocytic choriomeningitis virus glycoprotein cleavage, transport, and incorporation into virions. Virology 314(1):168–178 ([pii] S0042682203004215)

Kunz S, Sevilla N, Rojek JM, Oldstone MB (2004) Use of alternative receptors different than alpha-dystroglycan by selected isolates of lymphocytic choriomeningitis virus. Virology 325 (2):432–445

Kunz S, Rojek JM, Kanagawa M, Spiropoulou CF, Barresi R, Campbell KP, Oldstone MB (2005) Posttranslational modification of alpha-dystroglycan, the cellular receptor for arenaviruses, by the glycosyltransferase LARGE is critical for virus binding. J Virol 79(22):14282–14296. doi:10.1128/JVI.79.22.14282-14296.2005 ([pii] 79/22/14282)

Lan S, McLay Schelde L, Wang J, Kumar N, Ly H, Liang Y (2009) Development of infectious clones for virulent and avirulent pichinde viruses: a model virus to study arenavirus-induced hemorrhagic fevers. J Virol 83(13):6357–6362. doi:10.1128/JVI.00019-09

Lecompte E, ter Meulen J, Emonet S, Daffis S, Charrel RN (2007) Genetic identification of Kodoko virus, a novel arenavirus of the African pigmy mouse (Mus Nannomys minutoides) in West Africa. Virology 364(1):178–183. doi:10.1016/j.virol.2007.02.008 ([pii] S0042-6822(07)00118-3)

Lee CH, Gilbertson DL, Novella IS, Huerta R, Domingo E, Holland JJ (1997) Negative effects of chemical mutagenesis on the adaptive behavior of vesicular stomatitis virus. J Virol 71 (5):3636–3640

Lee KJ, Novella IS, Teng MN, Oldstone MB, de La Torre JC (2000) NP and L proteins of lymphocytic choriomeningitis virus (LCMV) are sufficient for efficient transcription and replication of LCMV genomic RNA analogs. J Virol 74(8):3470–3477

Lee AM, Rojek JM, Spiropoulou CF, Gundersen AT, Jin W, Shaginian A, York J, Nunberg JH, Boger DL, Oldstone MB, Kunz S (2008) Unique small molecule entry inhibitors of hemorrhagic fever arenaviruses. J Biol Chem 283(27):18734–18742. doi:10.1074/jbc.M802089200

Lelke M, Brunotte L, Busch C, Gunther S (2010) An N-terminal region of Lassa virus L protein plays a critical role in transcription but not replication of the virus genome. J Virol 84(4):1934–1944. doi:10.1128/JVI.01657-09

Lenz O, ter Meulen J, Klenk HD, Seidah NG, Garten W (2001) The Lassa virus glycoprotein precursor GP-C is proteolytically processed by subtilase SKI-1/S1P. Proc Natl Acad Sci USA 98(22):12701–12705. doi:10.1073/pnas.221447598

Lewicki H, Tishon A, Borrow P, Evans CF, Gairin JE, Hahn KM, Jewell DA, Wilson IA, Oldstone MB (1995) CTL escape viral variants I: generation and molecular characterization. Virology 210(1):29–40. doi:10.1006/viro.1995.1314 ([pii] S0042-6822(85)71314-1)

Liang Y, Lan S, Ly H (2009) Molecular determinants of Pichinde virus infection of guinea pigs–a small animal model system for arenaviral hemorrhagic fevers. Ann N Y Acad Sci 1171(Suppl 1):E65–E74. doi:10.1111/j.1749-6632.2009.05051.x ([pii] NYAS5051)

Loeb LA, Essigmann JM, Kazazi F, Zhang J, Rose KD, Mullins JI (1999) Lethal mutagenesis of HIV with mutagenic nucleoside analogs. Proc Natl Acad Sci USA 96(4):1492–1497

Lopez N, Jacamo R, Franze-Fernandez MT (2001) Transcription and RNA replication of tacaribe virus genome and antigenome analogs require N and L proteins: z protein is an inhibitor of these processes. J Virol 75(24):12241–12251

Loureiro ME, Wilda M, Levingston Macleod JM, D'Antuono A, Foscaldi S, Marino Buslje C, Lopez N (2011) Molecular determinants of arenavirus Z protein homo-oligomerization and L polymerase binding. J Virol 85(23):12304–12314. doi:10.1128/JVI.05691-11

Lukashevich IS (1992) Generation of reassortants between African arenaviruses. Virology 188 (2):600–605

Lukashevich IS (2012) Advanced vaccine candidates for Lassa fever. Viruses 4(11):2514–2557. doi:10.3390/v4112514

Lukashevich IS, Patterson J, Carrion R, Moshkoff D, Ticer A, Zapata J, Brasky K, Geiger R, Hubbard GB, Bryant J, Salvato MS (2005) A live attenuated vaccine for Lassa fever made by reassortment of Lassa and Mopeia viruses. J Virol 79(22):13934–13942. doi:10.1128/JVI.79.22.13934-13942.2005

Mallela A, Nishikura K (2012) A-to-I editing of protein coding and noncoding RNAs. Crit Rev Biochem Mol Biol 47(6):493–501. doi:10.3109/10409238.2012.714350

Manrubia SC, Domingo E, Lazaro E (2010) Pathways to extinction: beyond the error threshold. Philos Trans R Soc Lond B Biol Sci 365(1548):1943–1952. doi:10.1098/rstb.2010.0076

Martin V, Domingo E (2008) Influence of the mutant spectrum in viral evolution: focused selection of antigenic variants in a reconstructed viral quasispecies. Mol Biol Evol 25(8):1544–1554. doi:10.1093/molbev/msn099

Martin V, Abia D, Domingo E, Grande-Perez A (2010) An interfering activity against lymphocytic choriomeningitis virus replication associated with enhanced mutagenesis. J Gen Virol 91(Pt 4):990–1003. doi:10.1099/vir.0.017053-0

Martinez-Sobrido L, Zuniga EI, Rosario D, Garcia-Sastre A, de la Torre JC (2006) Inhibition of the type I interferon response by the nucleoprotein of the prototypic arenavirus lymphocytic choriomeningitis virus. J Virol 80(18):9192–9199

Martinez-Sobrido L, Giannakas P, Cubitt B, Garcia-Sastre A, de la Torre JC (2007) Differential inhibition of type I interferon induction by arenavirus nucleoproteins. J Virol 81(22):12696–12703

Martinez-Sobrido L, Emonet S, Giannakas P, Cubitt B, Garcia-Sastre A, de la Torre JC (2009) Identification of amino acid residues critical for the anti-interferon activity of the nucleoprotein of the prototypic arenavirus lymphocytic choriomeningitis virus. J Virol 83(21):11330–11340. doi:10.1128/JVI.00763-09

Mas A, Lopez-Galindez C, Cacho I, Gomez J, Martinez MA (2010) Unfinished stories on viral quasispecies and Darwinian views of evolution. J Mol Biol 397(4):865–877. doi:10.1016/j.jmb.2010.02.005 ([pii] S0022-2836(10)00155-5)

Matloubian M, Somasundaram T, Kolhekar SR, Selvakumar R, Ahmed R (1990) Genetic basis of viral persistence: single amino acid change in the viral glycoprotein affects ability of lymphocytic choriomeningitis virus to persist in adult mice. J Exp Med 172(4):1043–1048

Matloubian M, Kolhekar SR, Somasundaram T, Ahmed R (1993) Molecular determinants of macrophage tropism and viral persistence: importance of single amino acid changes in the polymerase and glycoprotein of lymphocytic choriomeningitis virus. J Virol 67(12):7340–7349

McCormick JB, King IJ, Webb PA, Scribner CL, Craven RB, Johnson KM, Elliott LH, Belmont-Williams R (1986) Lassa fever: effective therapy with ribavirin. N Engl J Med 314 (1):20–26

McKee KT Jr, Huggins JW, Trahan CJ, Mahlandt BG (1988) Ribavirin prophylaxis and therapy for experimental argentine hemorrhagic fever. Antimicrob Agents Chemother 32(9):1304–1309

Merkler D, Horvath E, Bruck W, Zinkernagel RM, Del la Torre JC, Pinschewer DD (2006) "Viral deja vu" elicits organ-specific immune disease independent of reactivity to self. J Clin Invest 116(5):1254–1263

Mets MB, Barton LL, Khan AS, Ksiazek TG (2000) Lymphocytic choriomeningitis virus: an underdiagnosed cause of congenital chorioretinitis. Am J Ophthalmol 130(2):209–215

Meyer BJ, Southern PJ (1994) Sequence heterogeneity in the termini of lymphocytic choriomeningitis virus genomic and antigenomic RNAs. J Virol 68(11):7659–7664
Meyer BJ, de la Torre JC, Southern PJ (2002) Arenaviruses: genomic RNAs, transcription, and replication. Curr Top Microbiol Immunol 262:139–149
Mills JN, Barrera Oro JG, Bressler DS, Childs JE, Tesh RB, Smith JF, Enria DA, Geisbert TW, McKee KT Jr, Bowen MD, Peters CJ, Jahrling PB (1996) Characterization of Oliveros virus, a new member of the Tacaribe complex (arenaviridae: arenavirus). Am J Trop Med Hyg 54 (4):399–404
Monath TP, Casals J (1975) Diagnosis of Lassa fever and the isolation and management of patients. Bull World Health Organ 52(4–6):707–715
Moreno H, Gallego I, Sevilla N, de la Torre JC, Domingo E, Martin V (2011) Ribavirin can be mutagenic for arenaviruses. J Virol 85(14):7246–7255. doi:10.1128/JVI.00614-11
Moreno H, Grande-Perez A, Domingo E, Martin V (2012a) Arenaviruses and lethal mutagenesis: prospects for new ribavirin-based interventions. Viruses 4(11):2786–2805. doi:10.3390/v4112786
Moreno H, Tejero H, de la Torre JC, Domingo E, Martin V (2012b) Mutagenesis-mediated virus extinction: virus-dependent effect of viral load on sensitivity to lethal defection. PLoS ONE 7 (3):e32550. doi:10.1371/journal.pone.0032550
Morimoto K, Hooper DC, Carbaugh H, Fu ZF, Koprowski H, Dietzschold B (1998) Rabies virus quasispecies: implications for pathogenesis. Proc Natl Acad Sci USA 95(6):3152–3156
Morin B, Coutard B, Lelke M, Ferron F, Kerber R, Jamal S, Frangeul A, Baronti C, Charrel R, de Lamballerie X, Vonrhein C, Lescar J, Bricogne G, Gunther S, Canard B (2010) The N-terminal domain of the arenavirus L protein is an RNA endonuclease essential in mRNA transcription. PLoS Pathog 6(9):e1001038. doi:10.1371/journal.ppat.1001038
Morrison TG, McGinnes LW (1989) Avian cells expressing the Newcastle disease virus hemagglutinin-neuraminidase protein are resistant to Newcastle disease virus infection. Virology 171(1):10–17
Moshkoff DA, Salvato MS, Lukashevich IS (2007) Molecular characterization of a reassortant virus derived from Lassa and Mopeia viruses. Virus Genes 34(2):169–176. doi:10.1007/s11262-006-0050-3
Muller G, Bruns M, Martinez Peralta L, Lehmann-Grube F (1983) Lymphocytic choriomeningitis virus. IV. Electron microscopic investigation of the virion. Arch Virol 75(4):229–242
Murphy DG, Dimock K, Kang CY (1991) Numerous transitions in human parainfluenza virus 3 RNA recovered from persistently infected cells. Virology 181(2):760–763
Neuman BW, Adair BD, Burns JW, Milligan RA, Buchmeier MJ, Yeager M (2005) Complementarity in the supramolecular design of arenaviruses and retroviruses revealed by electron cryomicroscopy and image analysis. J Virol 79(6):3822–3830
Neumann G, Kawaoka Y (2004) Reverse genetics systems for the generation of segmented negative-sense RNA viruses entirely from cloned cDNA. Curr Top Microbiol Immunol 283:43–60
Nijhuis M, van Maarseveen NM, Boucher CA (2009) Antiviral resistance and impact on viral replication capacity: evolution of viruses under antiviral pressure occurs in three phases. Handb Exp Pharmacol 189:299–320. doi:10.1007/978-3-540-79086-0_11
Nishikura K (2010) Functions and regulation of RNA editing by ADAR deaminases. Annu Rev Biochem 79:321–349. doi:10.1146/annurev-biochem-060208-105251
Novella IS, Duarte EA, Elena SF, Moya A, Domingo E, Holland JJ (1995) Exponential increases of RNA virus fitness during large population transmissions. Proc Natl Acad Sci USA 92 (13):5841–5844
Oldstone MB (2002) Biology and pathogenesis of lymphocytic choriomeningitis virus infection. In: Oldstone MB (ed) Arenaviruses, vol 263, pp 83–118
Oldstone MB, Campbell KP (2010) Decoding arenavirus pathogenesis: essential roles for alpha-dystroglycan-virus interactions and the immune response. Virology 411(2):170–179. doi:10.1016/j.virol.2010.11.023 ([pii] S0042-6822(10)00741-5)

Oldstone MB, Rodriguez M, Daughaday WH, Lampert PW (1984) Viral perturbation of endocrine function: disordered cell function leads to disturbed homeostasis and disease. Nature 307 (5948):278–281

Oldstone MB, Ahmed R, Buchmeier MJ, Blount P, Tishon A (1985) Perturbation of differentiated functions during viral infection in vivo I: relationship of lymphocytic choriomeningitis virus and host strains to growth hormone deficiency. Virology 142(1):158–174

Ortega-Prieto AM, Sheldon J, Grande-Perez A, Tejero H, Gregori J, Quer J, Esteban JI, Domingo E, Perales C (2013) Extinction of hepatitis C virus by ribavirin in hepatoma cells involves lethal mutagenesis. PLoS ONE 8(8):e71039. doi:10.1371/journal.pone.0071039

Palacios G, Druce J, Du L, Tran T, Birch C, Briese T, Conlan S, Quan PL, Hui J, Marshall J, Simons JF, Egholm M, Paddock CD, Shieh WJ, Goldsmith CS, Zaki SR, Catton M, Lipkin WI (2008) A new arenavirus in a cluster of fatal transplant-associated diseases. N Engl J Med 358 (10):991–998

Pariente N, Airaksinen A, Domingo E (2003) Mutagenesis versus inhibition in the efficiency of extinction of foot-and-mouth disease virus. J Virol 77(12):7131–7138

Pasqual G, Rojek JM, Masin M, Chatton JY, Kunz S (2011) Old world arenaviruses enter the host cell via the multivesicular body and depend on the endosomal sorting complex required for transport. PLoS Pathog 7(9):e1002232. doi:10.1371/journal.ppat.1002232 ([pii] 10-PLPA-RA-4139)

Perales C, Martin V, Ruiz-Jarabo CM, Domingo E (2005) Monitoring sequence space as a test for the target of selection in viruses. J Mol Biol 345(3):451–459. doi:10.1016/j.jmb.2004.10.066 ([pii] S0022-2836(04)01372-5)

Perales C, Mateo R, Mateu MG, Domingo E (2007) Insights into RNA virus mutant spectrum and lethal mutagenesis events: replicative interference and complementation by multiple point mutants. J Mol Biol 369(4):985–1000. doi:10.1016/j.jmb.2007.03.074

Perales C, Agudo R, Tejero H, Manrubia SC, Domingo E (2009) Potential benefits of sequential inhibitor-mutagen treatments of RNA virus infections. PLoS Pathog 5(11):e1000658. doi:10.1371/journal.ppat.1000658

Perales C, Iranzo J, Manrubia SC, Domingo E (2012) The impact of quasispecies dynamics on the use of therapeutics. Trends Microbiol 20(12):595–603. doi:10.1016/j.tim.2012.08.010 ([pii] S0966-842X(12)00155-2)

Perez M, de la Torre JC (2002) Characterization of the genomic promoter of the prototypic arenavirus lymphocytic choriomeningitis virus (LCMV). J Virol (in Press)

Perez M, Craven RC, de la Torre JC (2003) The small RING finger protein Z drives arenavirus budding: implications for antiviral strategies. Proc Natl Acad Sci USA 100(22):12978–12983

Perez M, Greenwald DL, de la Torre JC (2004) Myristoylation of the RING finger Z protein is essential for arenavirus budding. J Virol 78(20):11443–11448

Peters CJ (2002) Human Infection with Arenaviruses in the Americas. In: Oldstone MB (ed) Arenaviruses i, vol 262., Current topics in microbiology and immunologySpringer, Berlin, pp 65–74

Peters CJ (2006) Lymphocytic choriomeningitis virus—an old enemy up to new tricks. N Engl J Med 354(21):2208–2211

Pfeiffer JK, Kirkegaard K (2003) A single mutation in poliovirus RNA-dependent RNA polymerase confers resistance to mutagenic nucleotide analogs via increased fidelity. Proc Natl Acad Sci USA 100(12):7289–7294. doi:10.1073/pnas.1232294100

Pfeiffer JK, Kirkegaard K (2005) Increased fidelity reduces poliovirus fitness and virulence under selective pressure in mice. PLoS Pathog 1(2):e11. doi:10.1371/journal.ppat.0010011

Pinschewer DD, Perez M, Sanchez AB, de la Torre JC (2003) Recombinant lymphocytic choriomeningitis virus expressing vesicular stomatitis virus glycoprotein. Proc Natl Acad Sci USA 100(13):7895–7900

Pinschewer DD, Perez M, de la Torre JC (2005) Dual role of the lymphocytic choriomeningitis virus intergenic region in transcription termination and virus propagation. J Virol 79 (7):4519–4526

Pinschewer DD, Flatz L, Steinborn R, Horvath E, Fernandez M, Lutz H, Suter M, Bergthaler A (2010) Innate and adaptive immune control of genetically engineered live-attenuated arenavirus vaccine prototypes. Int Immunol 22(9):749–756. doi:10.1093/intimm/dxq061

Pircher H, Moskophidis D, Rohrer U, Burki K, Hengartner H, Zinkernagel RM (1990) Viral escape by selection of cytotoxic T cell-resistant virus variants in vivo. Nature 346(6285):629–633. doi:10.1038/346629a0

Poch O, Sauvaget I, Delarue M, Tordo N (1989) Identification of four conserved motifs among the RNA-dependent polymerase encoding elements. EMBO J 8(12):3867–3874

Polson AG, Bass BL (1994) Preferential selection of adenosines for modification by double-stranded RNA adenosine deaminase. EMBO J 13(23):5701–5711

Prince GA, Ottolini MG, Moscona A (2001) Contribution of the human parainfluenza virus type 3 HN-receptor interaction to pathogenesis in vivo. J Virol 75(24):12446–12451. doi:10.1128/JVI.75.24.12446-12451.2001

Pulkkinen AJ, Pfau CJ (1970) Plaque size heterogeneity: a genetic trait of lymphocytic choriomeningitis virus. Appl Microbiol 20(1):123–128

Qi X, Lan S, Wang W, Schelde LM, Dong H, Wallat GD, Ly H, Liang Y, Dong C (2010) Cap binding and immune evasion revealed by Lassa nucleoprotein structure. Nature 468 (7325):779–783. doi:10.1038/nature09605

Radoshitzky SR, Abraham J, Spiropoulou CF, Kuhn JH, Nguyen D, Li W, Nagel J, Schmidt PJ, Nunberg JH, Andrews NC, Farzan M, Choe H (2007) Transferrin receptor 1 is a cellular receptor for New World haemorrhagic fever arenaviruses. Nature 446(7131):92–96 (Epub 2007 Feb 2007)

Radoshitzky SR, Kuhn JH, Spiropoulou CF, Albarino CG, Nguyen DP, Salazar-Bravo J, Dorfman T, Lee AS, Wang E, Ross SR, Choe H, Farzan M (2008) Receptor determinants of zoonotic transmission of New World hemorrhagic fever arenaviruses. Proc Natl Acad Sci USA 105(7):2664–2669. doi:10.1073/pnas.0709254105

Richmond JK, Baglole DJ (2003) Lassa fever: epidemiology, clinical features, and social consequences. BMJ 327(7426):1271–1275. doi:10.1136/bmj.327.7426.1271

Rima BK, Gatherer D, Young DF, Norsted H, Randall RE, Davison AJ (2014) Stability of the parainfluenza virus 5 genome revealed by deep sequencing of strains isolated from different hosts and following passage in cell culture. J Virol. doi:10.1128/JVI.03351-13

Riviere Y (1987) Mapping arenavirus genes causing virulence. Curr Top Microbiol Immunol 133:59–65

Riviere Y, Oldstone MB (1986) Genetic reassortants of lymphocytic choriomeningitis virus: unexpected disease and mechanism of pathogenesis. J Virol 59(2):363–368

Riviere Y, Ahmed R, Oldstone MB (1986) The use of lymphocytic choriomeningitis virus reassortants to map viral genes causing virulence. Med Microbiol Immunol 175(2–3):191–192

Rodrigo WW, de la Torre JC, Martinez-Sobrido L (2011) Use of single-cycle infectious lymphocytic choriomeningitis virus to study hemorrhagic fever arenaviruses. J Virol 85 (4):1684–1695. doi:10.1128/JVI.02229-10

Rojek JM, Kunz S (2008) Cell entry by human pathogenic arenaviruses. Cell Microbiol 10 (4):828–835

Rojek JM, Perez M, Kunz S (2008a) Cellular entry of lymphocytic choriomeningitis virus. J Virol 82(3):1505–1517

Rojek JM, Sanchez AB, Thao NN, de la Torre JC, Kunz S (2008b) Different mechanisms of cell entry by human pathogenic Old World and New World arenaviruses. J Virol

Rojek JM, Pasqual G, Sanchez AB, Nguyen NT, de la Torre JC, Kunz S (2010) Targeting the proteolytic processing of the viral glycoprotein precursor is a promising novel antiviral strategy against arenaviruses. J Virol 84(1):573–584. doi:10.1128/JVI.01697-09

Rueda P, Garcia-Barreno B, Melero JA (1994) Loss of conserved cysteine residues in the attachment (G) glycoprotein of two human respiratory syncytial virus escape mutants that contain multiple A-G substitutions (hypermutations). Virology 198(2):653–662 ([pii] S0042682284710774)

Ruiz-Jarabo CM, Ly C, Domingo E, de la Torre JC (2003) Lethal mutagenesis of the prototypic arenavirus lymphocytic choriomeningitis virus (LCMV). Virology 308(1):37–47

Sabeti PC, Varilly P, Fry B, Lohmueller J, Hostetter E, Cotsapas C, Xie X, Byrne EH, McCarroll SA, Gaudet R, Schaffner SF, Lander ES, Frazer KA, Ballinger DG, Cox DR, Hinds DA, Stuve LL, Gibbs RA, Belmont JW, Boudreau A, Hardenbol P, Leal SM, Pasternak S, Wheeler DA, Willis TD, Yu F, Yang H, Zeng C, Gao Y, Hu H, Hu W, Li C, Lin W, Liu S, Pan H, Tang X, Wang J, Wang W, Yu J, Zhang B, Zhang Q, Zhao H, Zhou J, Gabriel SB, Barry R, Blumenstiel B, Camargo A, Defelice M, Faggart M, Goyette M, Gupta S, Moore J, Nguyen H, Onofrio RC, Parkin M, Roy J, Stahl E, Winchester E, Ziaugra L, Altshuler D, Shen Y, Yao Z, Huang W, Chu X, He Y, Jin L, Liu Y, Sun W, Wang H, Wang Y, Xiong X, Xu L, Waye MM, Tsui SK, Xue H, Wong JT, Galver LM, Fan JB, Gunderson K, Murray SS, Oliphant AR, Chee MS, Montpetit A, Chagnon F, Ferretti V, Leboeuf M, Olivier JF, Phillips MS, Roumy S, Sallee C, Verner A, Hudson TJ, Kwok PY, Cai D, Koboldt DC, Miller RD, Pawlikowska L, Taillon-Miller P, Xiao M, Tsui LC, Mak W, Song YQ, Tam PK, Nakamura Y, Kawaguchi T, Kitamoto T, Morizono T, Nagashima A, Ohnishi Y, Sekine A, Tanaka T, Tsunoda T, Deloukas P, Bird CP, Delgado M, Dermitzakis ET, Gwilliam R, Hunt S, Morrison J, Powell D, Stranger BE, Whittaker P, Bentley DR, Daly MJ, de Bakker PI, Barrett J, Chretien YR, Maller J, McCarroll S, Patterson N, Pe'er I, Price A, Purcell S, Richter DJ, Sabeti P, Saxena R, Sham PC, Stein LD, Krishnan L, Smith AV, Tello-Ruiz MK, Thorisson GA, Chakravarti A, Chen PE, Cutler DJ, Kashuk CS, Lin S, Abecasis GR, Guan W, Li Y, Munro HM, Qin ZS, Thomas DJ, McVean G, Auton A, Bottolo L, Cardin N, Eyheramendy S, Freeman C, Marchini J, Myers S, Spencer C, Stephens M, Donnelly P, Cardon LR, Clarke G, Evans DM, Morris AP, Weir BS, Johnson TA, Mullikin JC, Sherry ST, Feolo M, Skol A, Zhang H, Matsuda I, Fukushima Y, Macer DR, Suda E, Rotimi CN, Adebamowo CA, Ajayi I, Aniagwu T, Marshall PA, Nkwodimmah C, Royal CD, Leppert MF, Dixon M, Peiffer A, Qiu R, Kent A, Kato K, Niikawa N, Adewole IF, Knoppers BM, Foster MW, Clayton EW, Watkin J, Muzny D, Nazareth L, Sodergren E, Weinstock GM, Yakub I, Birren BW, Wilson RK, Fulton LL, Rogers J, Burton J, Carter NP, Clee CM, Griffiths M, Jones MC, McLay K, Plumb RW, Ross MT, Sims SK, Willey DL, Chen Z, Han H, Kang L, Godbout M, Wallenburg JC, L'Archeveque P, Bellemare G, Saeki K, An D, Fu H, Li Q, Wang Z, Wang R, Holden AL, Brooks LD, McEwen JE, Guyer MS, Wang VO, Peterson JL, Shi M, Spiegel J, Sung LM, Zacharia LF, Collins FS, Kennedy K, Jamieson R, Stewart J (2007) Genome-wide detection and characterization of positive selection in human populations. Nature 449(7164):913–918. doi:10.1038/nature06250

Salazar-Bravo J, Ruedas LA, Yates TL (2002) Mammalian reservoirs of arenaviruses. In: Oldstone MBA (ed) Arenaviruses I: the epidemiology, molecular and cell biology of arenaviruses, vol 262., Current topics in microbiology and immunologySpringer, Berlin, pp 25–63

Salvato MS, Shimomaye EM (1989) The completed sequence of lymphocytic choriomeningitis virus reveals a unique RNA structure and a gene for a zinc finger protein. Virology 173(1):1–10

Salvato M, Borrow P, Shimomaye E, Oldstone MB (1991) Molecular basis of viral persistence: a single amino acid change in the glycoprotein of lymphocytic choriomeningitis virus is associated with suppression of the antiviral cytotoxic T-lymphocyte response and establishment of persistence. J Virol 65(4):1863–1869

Sanchez AB, de la Torre JC (2005) Genetic and biochemical evidence for an oligomeric structure of the functional L polymerase of the prototypic arenavirus lymphocytic choriomeningitis virus. J Virol 79(11):7262–7268

Sanchez AB, de la Torre JC (2006) Rescue of the prototypic Arenavirus LCMV entirely from plasmid. Virology 350(2):370–380

Sanjuan R, Codoner FM, Moya A, Elena SF (2004) Natural selection and the organ-specific differentiation of HIV-1 V3 hypervariable region. Evolution 58(6):1185–1194

Sanz-Ramos M, Rodriguez-Calvo T, Sevilla N (2012) Mutagenesis-mediated decrease of pathogenicity as a feature of the mutant spectrum of a viral population. PLoS ONE 7(6): e39941. doi:10.1371/journal.pone.0039941

Saunders AA, Ting JP, Meisner J, Neuman BW, Perez M, de la Torre JC, Buchmeier MJ (2007) Mapping the landscape of the lymphocytic choriomeningitis virus stable signal peptide reveals novel functional domains. J Virol 81(11):5649–5657. doi:10.1128/JVI.02759-06

Scheidel LM, Durbin RK, Stollar V (1987) Sindbis virus mutants resistant to mycophenolic acid and ribavirin. Virology 158(1):1–7

Sevilla N, de la Torre JC (2006) Arenavirus diversity and evolution: quasispecies in vivo. In: Domingo E (ed) Quasispecies: concepts and implications for virology, current topics in microbiology and immunology, vol 299, pp 315–335

Sevilla N, Kunz S, Holz A, Lewicki H, Homann D, Yamada H, Campbell KP, de La Torre JC, Oldstone MB (2000) Immunosuppression and resultant viral persistence by specific viral targeting of dendritic cells. J Exp Med 192(9):1249–1260

Sevilla N, Domingo E, de la Torre JC (2002) Contribution of LCMV towards deciphering biology of quasispecies in vivo. Curr Top Microbiol Immunol 263:197–220

Sidwell RW, Huffman JH, Allen LB, Meyer RB Jr, Shuman DA, Simon LN, Robins RK (1974) In vitro antiviral activity of 6-substituted 9-beta-D-ribofuranosylpurine 3′, 5′-cyclic phosphates. Antimicrob Agents Chemother 5(6):652–657

Sierra S, Davila M, Lowenstein PR, Domingo E (2000) Response of foot-and-mouth disease virus to increased mutagenesis: influence of viral load and fitness in loss of infectivity. J Virol 74 (18):8316–8323

Smith EC, Blanc H, Vignuzzi M, Denison MR (2013) Coronaviruses lacking exoribonuclease activity are susceptible to lethal mutagenesis: evidence for proofreading and potential therapeutics. PLoS Pathog 9(8):e1003565. doi:10.1371/journal.ppat.1003565

Sogoba N, Feldmann H, Safronetz D (2012) Lassa fever in West Africa: evidence for an expanded region of endemicity. Zoonoses Public Health 59(Suppl 2):43–47. doi:10.1111/j.1863-2378.2012.01469.x

Stenglein MD, Sanders C, Kistler AL, Ruby JG, Franco JY, Reavill DR, Dunker F, Derisi JL (2012) Identification, characterization, and in vitro culture of highly divergent arenaviruses from boa constrictors and annulated tree boas: candidate etiological agents for snake inclusion body disease. MBio 3(4):e00180–e00112. doi:10.1128/mBio.00180-12

Strecker T, Eichler R, Meulen J, Weissenhorn W, Dieter Klenk H, Garten W, Lenz O (2003) Lassa virus Z protein is a matrix protein and sufficient for the release of virus-like particles. J Virol 77 (19):10700–10705 (corrected)

Strecker T, Maisa A, Daffis S, Eichler R, Lenz O, Garten W (2006) The role of myristoylation in the membrane association of the Lassa virus matrix protein Z. Virol J 3:93. doi:10.1186/1743-422X-3-93

Streeter DG, Witkowski JT, Khare GP, Sidwell RW, Bauer RJ, Robins RK, Simon LN (1973) Mechanism of action of 1-D-ribofuranosyl-1,2,4-triazole-3-carboxamide (Virazole), a new broad-spectrum antiviral agent. Proc Natl Acad Sci USA 70(4):1174–1178

Subbarao K, Katz JM (2004) Influenza vaccines generated by reverse genetics. Curr Top Microbiol Immunol 283:313–342

Sullivan BM, Emonet SF, Welch MJ, Lee AM, Campbell KP, de la Torre JC, Oldstone MB (2011) Point mutation in the glycoprotein of lymphocytic choriomeningitis virus is necessary for receptor binding, dendritic cell infection, and long-term persistence. Proc Natl Acad Sci USA 108(7):2969–2974. doi:10.1073/pnas.1019304108

Tamura K, Stecher G, Peterson D, Filipski A, Kumar S (2013) MEGA6: molecular evolutionary genetics analysis version 6.0. Mol Biol Evol 30(12):2725–2729. doi:10.1093/molbev/mst197

Tapia N, Fernandez G, Parera M, Gomez-Mariano G, Clotet B, Quinones-Mateu M, Domingo E, Martinez MA (2005) Combination of a mutagenic agent with a reverse transcriptase inhibitor results in systematic inhibition of HIV-1 infection. Virology 338(1):1–8. doi:10.1016/j.virol.2005.05.008

Teng MN, Borrow P, Oldstone MB, de la Torre JC (1996) A single amino acid change in the glycoprotein of lymphocytic choriomeningitis virus is associated with the ability to cause growth hormone deficiency syndrome. J Virol 70(12):8438–8443

Tishon A, Eddleston M, de la Torre JC, Oldstone MB (1993) Cytotoxic T lymphocytes cleanse viral gene products from individually infected neurons and lymphocytes in mice persistently infected with lymphocytic choriomeningitis virus. Virology 197(1):463–467 ([pii] S0042682283716132)

Tortorici MA, Albarino CG, Posik DM, Ghiringhelli PD, Lozano ME, Rivera Pomar R, Romanowski V (2001) Arenavirus nucleocapsid protein displays a transcriptional antitermination activity in vivo. Virus Res 73(1):41–55 ([pii] S0168-1702(00)00222-7)

Trivedi P, Meyer KK, Streblow DN, Preuninger BL, Schultz KT, Pauza CD (1994) Selective amplification of simian immunodeficiency virus genotypes after intrarectal inoculation of rhesus monkeys. J Virol 68(11):7649–7653

Urata S, Noda T, Kawaoka Y, Yokosawa H, Yasuda J (2006) Cellular factors required for Lassa virus budding. J Virol 80(8):4191–4195

Urata S, Yun N, Pasquato A, Paessler S, Kunz S, de la Torre JC (2011) Antiviral activity of a small-molecule inhibitor of arenavirus glycoprotein processing by the cellular site 1 protease. J Virol 85(2):795–803. doi:10.1128/JVI.02019-10

Valsamakis A, Riviere Y, Oldstone MB (1987) Perturbation of differentiated functions in vivo during persistent viral infection III: decreased growth hormone mRNA. Virology 156(2):214–220

Vazquez-Calvo A, Martin-Acebes MA, Saiz JC, Ngo N, Sobrino F, de la Torre JC (2013) Inhibition of multiplication of the prototypic arenavirus LCMV by valproic acid. Antiviral Res 99(2):172–179. doi:10.1016/j.antiviral.2013.05.012

Vignuzzi M, Stone JK, Arnold JJ, Cameron CE, Andino R (2006) Quasispecies diversity determines pathogenesis through cooperative interactions in a viral population. Nature 439 (7074):344–348. doi:10.1038/nature04388

Volpon L, Osborne MJ, Capul AA, de la Torre JC, Borden KL (2010) Structural characterization of the Z RING-eIF4E complex reveals a distinct mode of control for eIF4E. Proc Natl Acad Sci USA 107(12):5441–5446. doi:10.1073/pnas.0909877107

von Messling V, Cattaneo R (2004) Toward novel vaccines and therapies based on negative-strand RNA viruses. Curr Top Microbiol Immunol 283:281–312

Wachsman MB, Lopez EM, Ramirez JA, Galagovsky LR, Coto CE (2000) Antiviral effect of brassinosteroids against herpes virus and arenaviruses. Antivir Chem Chemother 11(1):71–77

Ward SV, George CX, Welch MJ, Liou LY, Hahm B, Lewicki H, de la Torre JC, Samuel CE, Oldstone MB (2011) RNA editing enzyme adenosine deaminase is a restriction factor for controlling measles virus replication that also is required for embryogenesis. Proc Natl Acad Sci USA 108(1):331–336. doi:10.1073/pnas.1017241108

Weaver SC, Salas RA, de Manzione N, Fulhorst CF, Duno G, Utrera A, Mills JN, Ksiazek TG, Tovar D, Tesh RB (2000) Guanarito virus (arenaviridae) isolates from endemic and outlying localities in Venezuela: sequence comparisons among and within strains isolated from Venezuelan hemorrhagic fever patients and rodents. Virology 266(1):189–195. doi:10.1006/viro.1999.0067 ([pii] S0042-6822(99)90067-3)

Weaver SC, Salas RA, de Manzione N, Fulhorst CF, Travasos da Rosa AP, Duno G, Utrera A, Mills JN, Ksiazek TG, Tovar D, Guzman H, Kang W, Tesh RB (2001) Extreme genetic diversity among Pirital virus (Arenaviridae) isolates from western Venezuela. Virology 285 (1):110–118. doi:10.1006/viro.2001.0954 ([pii] S0042-6822(01)90954-7)

Wright CF, Morelli MJ, Thebaud G, Knowles NJ, Herzyk P, Paton DJ, Haydon DT, King DP (2011) Beyond the consensus: dissecting within-host viral population diversity of foot-and-mouth disease virus by using next-generation genome sequencing. J Virol 85 (5):2266–2275. doi:10.1128/JVI.01396-10

Wu-Hsieh B, Howard DH, Ahmed R (1988) Virus-induced immunosuppression: a murine model of susceptibility to opportunistic infection. J Infect Dis 158(1):232–235

York J, Nunberg JH (2006) Role of the stable signal peptide of Junin arenavirus envelope glycoprotein in pH-dependent membrane fusion. J Virol 80(15):7775–7780. doi:10.1128/JVI.00642-06 ([pii] 80/15/7775)

York J, Nunberg JH (2007) Distinct requirements for signal peptidase processing and function in the stable signal peptide subunit of the Junin virus envelope glycoprotein. Virology 359(1):72–81. doi:10.1016/j.virol.2006.08.048 ([pii] S0042-6822(06)00620-9)

York J, Romanowski V, Lu M, Nunberg JH (2004) The signal peptide of the Junin arenavirus envelope glycoprotein is myristoylated and forms an essential subunit of the mature G1-G2 complex. J Virol 78(19):10783–10792. doi:10.1128/JVI.78.19.10783-10792.2004 ([pii] 78/19/10783)

Young PR, Howard CR (1983) Fine structure analysis of Pichinde virus nucleocapsids. J Gen Virol 64(Pt 4):833–842

Young KC, Lindsay KL, Lee KJ, Liu WC, He JW, Milstein SL, Lai MM (2003) Identification of a ribavirin-resistant NS5B mutation of hepatitis C virus during ribavirin monotherapy. Hepatology 38(4):869–878. doi:10.1053/jhep.2003.50445

Zahn RC, Schelp I, Utermohlen O, von Laer D (2007) A-to-G hypermutation in the genome of lymphocytic choriomeningitis virus. J Virol 81(2):457–464. doi:10.1128/JVI.00067-06

Zapata JC, Salvato MS (2013) Arenavirus variations due to host-specific adaptation. Viruses 5 (1):241–278. doi:10.3390/v5010241

Zinkernagel RM (2002) Lymphocytic choriomeningitis virus and immunology. Curr Top Microbiol Immunol 263:1–5

Models of Viral Population Dynamics

Pranesh Padmanabhan and Narendra M. Dixit

Abstract Models of viral population dynamics have contributed enormously to our understanding of the pathogenesis and transmission of several infectious diseases, the coevolutionary dynamics of viruses and their hosts, the mechanisms of action of drugs, and the effectiveness of interventions. In this chapter, we review major advances in the modeling of the population dynamics of the human immunodeficiency virus (HIV) and briefly discuss adaptations to other viruses.

Contents

1 Overview 278
2 Basic Model of Viral Dynamics 279
3 Drug Resistance 282
3.1 Preexistence of Drug Resistance 283
3.2 Emergence of Drug Resistance During Treatment 285
4 Drug Pharmacokinetics 286
5 The Quasispecies Theory and HIV 288
6 Viral Dynamics and Immune Response 289
7 Models for Other Viruses 291
7.1 Hepatitis C Virus 291
7.2 Influenza A Virus 294
8 Concluding Remarks 295
References 295

P. Padmanabhan · N.M. Dixit (✉)
Department of Chemical Engineering, Indian Institute of Science, Bangalore 560012, Karnataka, India
e-mail: narendra@chemeng.iisc.ernet.in

Current Topics in Microbiology and Immunology (2016) 392: 277–302
DOI 10.1007/82_2015_458

Published Online: 15 July 2015

1 Overview

Models of viral population dynamics have yielded key insights into the progression of several infectious diseases and guided strategies of intervention. In this chapter, we focus on models of human immunodeficiency virus (HIV) infection, which have occupied the center stage in the field, highlight the insights gained, and briefly discuss models of other viral infections. We begin with the basic model of HIV dynamics, which successfully described short-term changes in plasma viraemia following the onset of antiretroviral therapy and presented the first estimates of viral and infected cell life spans, establishing the rationale for highly active antiretroviral therapy that has saved millions of lives. The need for lifelong therapy for HIV infection, the associated difficulty of adhering to recommended treatment protocols, and the propensity of the virus to develop drug resistance drove the integration of the basic model of viral dynamics with models of drug pharmacokinetics and viral evolution that could present a framework for rational treatment optimization. Models of viral evolution, inspired by the quasispecies theory, have presented new insights into the limits on viral evolvability, the feasibility of mutagenesis as an intervention strategy, and the coevolution of viruses and their hosts. Simultaneously, models of viral dynamics and evolution together with those of the immune response allowed description of the progression of the disease to AIDS and suggested guidelines for vaccine design. Recognizing that viral evolution typically occurs during viral replication within infected cells, models describing the intracellular events of the viral life cycle have been constructed. Such multiscale models have served to elucidate the mechanisms of action of new drugs against hepatitis C and could potentially be employed to identify vulnerabilities in the viral life cycle. At the same time, models that integrate within-host viral dynamics with inter-host transmission may help identify fundamental differences between pathogenic and nonpathogenic viruses, guide vaccine and immunogen design, and present a rational framework for the comparative analysis of alternative healthcare policies.

The outline of this chapter is as follows. In Sect. 2, we discuss insights gained into HIV disease progression and treatment response from the basic model of viral dynamics. In Sect. 3, we present our current understanding of treatment failure due to drug resistance. In Sect. 4, we explore the effects of drug pharmacokinetics on HIV treatment outcomes. In Sect. 5, we discuss the application of the quasispecies theory to HIV and the potential of mutagenesis as a novel strategy against HIV. In Sect. 6, we present models of HIV dynamics that explicitly consider host immune responses. In Sect. 7, we discuss models of the population dynamics of other viruses, with focus on hepatitis C and influenza. We present concluding remarks in Sect. 8.

2 Basic Model of Viral Dynamics

The basic model of the within-host dynamics of HIV infection (Fig. 1a) describes disease progression as the result of the interactions between populations of uninfected cells, T, infected cells, I, and free virions, V (Nowak and May 2000; Perelson 2002). Uninfected cells are assumed to be produced at the rate λ and die at the rate $d_T T$. Uninfected cells become productively infected by free virions at the rate βVT. These infected cells then produce new virions at the rate pI and die at an enhanced rate δI due to virus-induced cytopathicity and immune-mediated killing. Free virions are cleared at the rate cV.

This basic model, without explicit consideration of the immune response, has been able to quantitatively describe viral load changes in the early acute phase and the steady state in the subsequent chronic phase of HIV infection in the absence of intervention (Phillips 1996; Stafford et al. 2000) (Fig. 2a). Importantly, analysis of the acute phase has yielded estimates of the basic reproductive ratio, R_0, that quantifies the potential of the virus to establish infection in an individual (Little et al. 1999; Phillips 1996; Ribeiro et al. 2010; Stafford et al. 2000). R_0 is defined as the number of productively infected cells produced from a single productively infected cell at the start of the infection (Nowak and May 2000). When $R_0 < 1$, the number of infected cells gradually decreases and leads to viral clearance, whereas when $R_0 > 1$, infected cells rise and lead to viral persistence. According to the basic model, $R_0 = \frac{\beta p \lambda}{\delta c d_T}$ (Nowak and May 2000). The most recent estimate of R_0 of HIV-1 is ~ 8 (Ribeiro et al. 2010), which implies that following transmission to a new host, infection rapidly grows and becomes persistent.

The viral load following transmission eventually attains a quasi steady state, also known as the set-point viral load (SPVL) (Fig. 2a). The basic model describes this set point as a balance between viral production and clearance as well as between the production and the loss of infected cells. The viral load remains at the set point for years despite the continuous and rapid turnover of virus and infected cells. Indeed, estimation of the latter turnover rates from analysis of viral load changes following the onset of antiretroviral therapy is a key success of the basic model.

Intervention with antiretroviral drugs during the chronic phase of infection perturbs the balance between viral production and clearance that establishes the set point. The viral load consequently declines following the onset of therapy (Fig. 2b). The basic model has been modified to account for drug action in order to analyze the latter decline (Fig. 1b) and estimate key parameters associated with HIV infection, viz. the half-lives of infected cells and free virions (Ho et al. 1995; Perelson et al. 1996; Wei et al. 1995). The model, assuming a constant target cell population over short durations under treatment, predicts that the viral load declines exponentially following the start of treatment at a rate determined by the loss rate of infected cells, the virion clearance rate, and the efficacy of treatment. Early studies, assuming perfect treatment efficacy, analyzed this first-phase viral decline, which lasts up to two weeks, and estimated the HIV virion half-life to be ~ 6 h, the life span of infected cells to be ~ 2.2 days, and the HIV production rate to be $\sim 10^{10}$

(a)

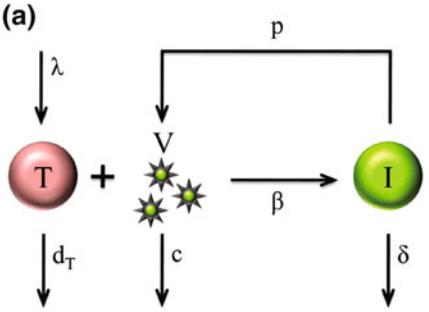

$$\frac{dT}{dt} = \lambda - d_T T - \beta TV$$

$$\frac{dI}{dt} = \beta TV - \delta I$$

$$\frac{dV}{dt} = pI - cV$$

(b)

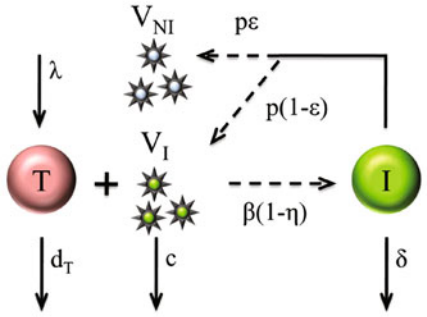

$$\frac{dT}{dt} = \lambda - d_T T - \beta(1-\eta)TV$$

$$\frac{dI}{dt} = \beta(1-\eta)TV - \delta I$$

$$\frac{dV_I}{dt} = p(1-\varepsilon)I - cV_I$$

$$\frac{dV_{NI}}{dt} = p\varepsilon I - cV_{NI}$$

(c)

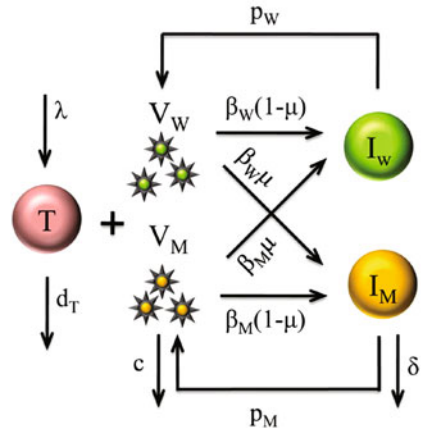

$$\frac{dT}{dt} = \lambda - d_T T - \beta_W TV_W - \beta_M TV_M$$

$$\frac{dI_W}{dt} = \beta_W(1-\mu)TV_W + \beta_M \mu TV_M - \delta I_W$$

$$\frac{dI_M}{dt} = \beta_W \mu TV_W + \beta_M(1-\mu)TV_M - \delta I_M$$

$$\frac{dV_W}{dt} = p_W I_W - cV_W$$

$$\frac{dV_M}{dt} = p_M I_M - cV_M$$

◀ **Fig. 1** Schematic of models of viral dynamics and corresponding model equations. **a** The basic model of viral dynamics assumes that uninfected cells, T, are produced at the rate λ and die at the rate $d_T T$. Productively infected cells, I, are produced due to infection at the rate βVT and die at the rate δI. New virions are produced at the rate pI and are cleared at the rate cV. **b** During treatment, drugs such as reverse transcriptase inhibitors, integrase inhibitors, entry inhibitors, and fusion inhibitors prevent new infections and are modeled as lowering the de novo infection rate with efficacy η. Protease inhibitors render newly produced virions non-infectious with efficacy ε. Accordingly, infectious virions, V_{I}, and non-infectious virions, V_{NI}, are produced at rates $p(1-\varepsilon)I$ and $p\varepsilon I$, respectively. **c** A two-strain model of drug resistance considers two subpopulations, wild type (subscript W) and drug resistant (subscript M), to describe the evolution of drug-resistant strains during treatment, with μ the effective mutation rate at which the wild type converts to a drug-resistant strain and vice versa. In **a**–**c**, the corresponding model equations are presented in the respective panels to the *right*

virions per day (Perelson et al. 1996). Subsequent studies, combining independent modeling and experiments, have refined these estimates, with the half-lives of HIV virions and productively infected cells being $\sim$0.5–2 h (Ramratnam et al. 1999) and $\sim$1 day (Markowitz et al. 2003), respectively, and established the notion of rapid viral turnover at the set point. The consequent realization of the enormous potential for viral evolution and the associated development of drug resistance (see Sect. 3) led to the introduction of combination therapy with three drugs—highly active antiretroviral therapy—which has since become the standard-of-care and drastically reduced HIV-related deaths.

The first-phase decline is typically followed by a slower second-phase decline during combination treatment (Fig. 2b). The basic model has been expanded to include other types of infected cells to analyze the second-phase viral decline (Perelson et al. 1997). The analysis revealed that long-lived infected cells with a half-life of about 1–4 weeks were the major contributors to the second phase and that eliminating this compartment would require 3–4 years of treatment. Recent studies have identified third and fourth phases of viral decline with the viral level remaining nearly constant in the fourth phase (Maldarelli et al. 2007; Palmer et al. 2008) (Fig. 2b inset), suggesting that HIV infection cannot be eradicated and lifelong treatment is required to control the infection.

Indeed, long-term treatment has been found to keep the infection under control, transforming the once deadly infection to a manageable condition in settings with affordable and accessible health care. With long-term treatment, however, arise other complications, managing which is an ongoing effort (Deeks et al. 2013; Volberding and Deeks 2010). In particular, adherence to treatment is expected to drop as treatment durations rise. With poor adherence, temporary reduction in treatment efficacy may provide just the window of opportunity for HIV to replicate, evolve, and acquire drug resistance. Resistance mutations for all the available antiretroviral drugs have been documented (Clavel and Hance 2004; Johnson et al. 2013). It is of interest, therefore, to identify the drug combination that offers the greatest barrier to resistance. Models of viral population dynamics have been coupled with evolutionary theory to describe the development of drug resistance during HIV treatment. We discuss these models next.

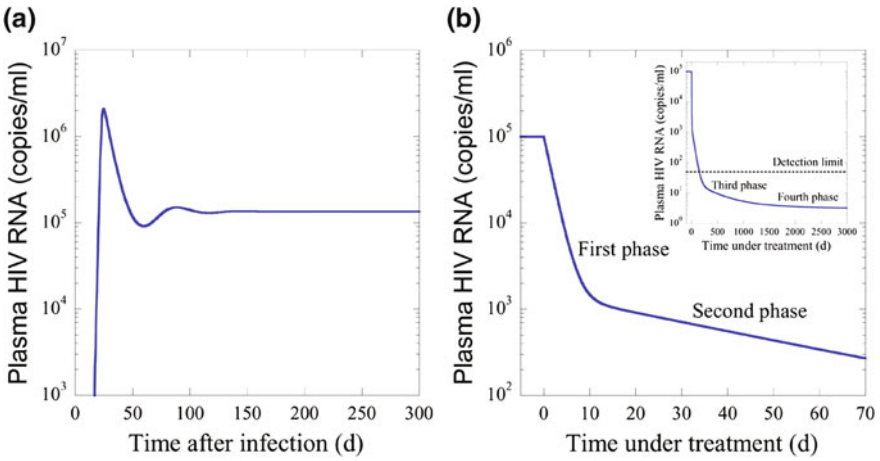

Fig. 2 Viral dynamics after infection and during treatment. **a** The basic model of viral dynamics describes the early acute phase and the subsequent set point of the chronic phase of HIV infection. The prediction is obtained by solving model equations in Fig. 1a using the following parameter values: $\lambda = 85\ \text{ml}^{-1}\,\text{day}^{-1}$; $d_T = 8.5 \times 10^{-3}\,\text{day}^{-1}$; $\beta = 6.6 \times 10^{-7}\ \text{ml}\,(\text{virion day})^{-1}$; $\delta = 0.17\ \text{day}^{-1}$; $p = 830\ \text{virion day}^{-1}$; and $c = 3\,\text{day}^{-1}$. The profile is typical of predictions that captured patient data in Stafford et al. (2000). **b** HIV viral load declines in a multiphasic manner during treatment, with the first two phases of viral decline occurring in days and the last two phases in months to years (*inset*)

3 Drug Resistance

HIV replication is a highly erroneous process with an average mutation rate of 1.4–4.6×10^{-5} per base per generation (Abram et al. 2010; Mansky and Temin 1995; Schlub et al. 2014) driving the rapid emergence of drug-resistant strains and treatment failure. Describing the development of drug resistance requires explicit consideration of viral subpopulations with different combinations of potential drug resistance mutations. Models of drug resistance thus increase in complexity compared to the basic model. A two-strain model that considers two subpopulations—wild type and drug resistant—has been used extensively to describe the evolution and growth of resistant strains during treatment (Bonhoeffer et al. 1997) (Fig. 1c). The outcome of treatment is determined by the basic reproductive ratios of the two strains in the presence of drugs. In the model equations (Fig. 1c), I_W and I_M represent cells infected by the wild-type strain, V_W, and the drug-resistant mutant strain, V_M, respectively. p_W, p_M, β_W, and β_M are the respective strain-specific virion production and de novo infection rate constants during treatment. μ is the effective mutation rate between the wild-type and the drug-resistant strain (Alexander and Bonhoeffer 2013). The basic reproductive ratio of the wild-type strain, $R_W = \frac{\beta_W p_W \lambda}{\delta c d_T}$, and the mutant strain, $R_M = \frac{\beta_M p_M \lambda}{\delta c d_T}$, can be related as $R_M = R_W(1 - s)$, where s is the selective disadvantage due to mutations. During treatment, the basic

reproductive ratios of the wild-type and mutant strains reduce to $R'_W = R_W(1 - \varepsilon_W)$ and $R'_M = R_M(1 - \varepsilon_M)$, respectively, with ε_W and $\varepsilon_M (< \varepsilon_W)$ the efficacies of the treatment against the two strains. When the treatment efficacy is very low, both R'_W and R'_M are greater than unity. Treatment fails with either the wild-type or the mutant strain dominating depending on which has the higher basic reproductive ratio. When the treatment is potent against the wild type alone, such that $R'_M > 1 > R'_W$, the wild type declines under treatment and viral breakthrough happens due to the growth of the mutant strain. When the treatment is potent against both the strains, so that both R'_W and R'_M are less than unity, the treatment is successful and HIV persists at a very low level due to latent reservoirs and sanctuary sites for HIV replication (Hoetelmans 1998; Siliciano and Greene 2011).

When $R'_M > 1 > R'_W$, i.e., when the resistant strain is predicted to dominate, treatment can fail in two ways. First, resistant strains can preexist due to viral diversification following infection prior to the start of the treatment and grow after the start of the treatment. Second, when such strains do not preexist, viral evolution can lead to their emergence during treatment causing treatment failure. Models of viral population dynamics have been constructed to assess the relative probabilities of either mode of treatment failure, and, where appropriate, to estimate the frequency of preexistence of resistant strains or to time their emergence during treatment. Below, we discuss the insights gained from these modeling approaches.

3.1 Preexistence of Drug Resistance

Mutation–selection balance The two-strain model of drug resistance is best-suited to describe resistance due to a single point mutation. When multiple point mutations are required for drug resistance, typically the case with combination treatment, the complexity of the models is increased dramatically for the following reasons. First, the number of strains, or viral subpopulations, that must be considered grows exponentially with the number of drug resistance loci involved. Second, recombination, which can alter the association of mutations, begins to play a role. (Note that recombination is inconsequential in the two-strain model.) Third, mutations at different loci interact in complex ways to determine the relative fitness of strains. Fourth, given that mutations are intrinsically rare, stochastic effects tend to dominate the dynamics of strains carrying multiple mutations. Neglecting stochastic effects and recombination, models inspired by the molecular quasispecies theory (Eigen 1971; Eigen et al. 1989) have been developed to describe scenarios where multiple mutations are required to confer resistance (Ribeiro and Bonhoeffer 2000; Ribeiro et al. 1998). Using a multiplicative fitness landscape, where each mutation independently incurs a fitness penalty s, Ribeiro et al. (1998) predicted the equilibrium frequency, or the relative prevalence, of mutant strains to be approximately $n!\left(\frac{\mu}{s}\right)^n$, where $n \in \{1, 2, 3 \ldots\}$ denotes the number of substitutions away from the wild type. With about 10^8 infected cells in a chronically infected patient (Chun et al. 1997) and an average mutation rate of 3×10^{-5} per base per generation, Ribeiro

et al. (1998) predicted that all possible single and double mutants with $s < 0.4$, triple mutants with $s < 0.03$, and quadruple mutants with $s < 0.007$ would exist at the start of treatment. These estimates serve to identify the minimum genetic barrier, or the number of mutations required for resistance, that treatment must offer to avert failure due to preexistent resistant strains. Subsequent studies have refined these estimates by incorporating the other evolutionary forces driving HIV diversification mentioned above, namely recombination, multiple infections of cells, epistatic interactions, and random genetic drift.

Influence of evolutionary forces on the preexistence of resistant strains During the reverse transcription of viral RNA to proviral DNA, the enzyme reverse transcriptase shuttles between the two RNA strands of an infecting virion, producing a mosaic genome in a process called recombination. HIV recombines at a very high rate, $0.8–1.5 \times 10^{-3}$ per site per reverse transcription (Levy et al. 2004; Schlub et al. 2014; Suryavanshi and Dixit 2007). Infections by heterozygous virions allow recombination to bring together or drive apart mutations, affecting viral diversity. Multiple infections of cells are a prerequisite for the production of heterozygous virions and determine the extent of the effect of recombination on viral diversity. While an early study reported a very high frequency ($\sim$100 %) of multiple infections (Jung et al. 2002), recent observations suggest much lower frequencies (<10 %) (Josefsson et al. 2011, 2013), hence a much weaker influence of recombination (Batorsky et al. 2011; Neher and Leitner 2010).

The strength of stochastic effects is thought to depend on the within-host effective population size, N_e, defined in the population genetics literature as the size of an idealized population that has the same population genetic properties as that of the natural population (Hartl and Clark 2007). Intriguingly, the effect of recombination on viral diversity is also predicted to depend on N_e. With large N_e, recombination decreases viral diversity (Boerlijst et al. 1996; Bretscher et al. 2004; Gheorghiu-Svirschevski et al. 2007; Rouzine and Coffin 2005; Vijay et al. 2008), whereas, with small N_e, recombination increases viral diversity (Bocharov et al. 2005; Vijay et al. 2008). This non-monotonic dependence of the effect of recombination on viral diversity is due to the subtle interplay of epistasis, selection, and genetic drift that has diverse outcomes at different N_e (Vijay et al. 2008).

Estimates of N_e for HIV are widely varying. Studies assuming neutral evolution estimated N_e to be $10^2–10^5$ (Brown 1997; Nijhuis et al. 1998; Rodrigo et al. 1999; Seo et al. 2002), while a two-loci two-allele model with selection estimated N_e to be $>10^5$ (Rouzine and Coffin 1999). Multiple-loci models with selection and recombination estimated the effective population size to be $10^2–10^4$ (Balagam et al. 2011; Vijay et al. 2008). A recent study estimated N_e to be 1.5×10^5 by analyzing the frequencies of hard and soft selective sweeps (Pennings et al. 2014). These disparate estimates of N_e confound our understanding of the effects of stochastic forces and recombination on viral evolution and diversity (Kouyos et al. 2006).

Notwithstanding, in a recent study, Gadhamsetty and Dixit (2010) employed both continuum viral dynamics, where N_e is infinitely large, and a population

genetics-based framework, where N_e is finite and small, and incorporating all the above evolutionary factors estimated the preexistence of resistant strains against the drug nevirapine. The study found that single mutants are likely to exist but at frequencies close to or below assay detection limits. The existence of double mutants is subject to strong stochastic fluctuations. Triple and higher mutants are expected not to be present at the start of the treatment. Pennings (2012), using a population dynamics and population genetics model, showed that resistance evolved from preexisting mutations in 39 % of patients under nevirapine monotherapy and in 6 % of patients under standard triple combination therapy, suggesting that there is a need to improve treatments further to prevent failure due to preexistence of drug-resistant mutations.

3.2 *Emergence of Drug Resistance During Treatment*

Models suggest that treatment failure is more likely to be due to the preexistence of drug-resistant strains than due to the emergence of resistant strains during therapy (Bonhoeffer and Nowak 1997; Ribeiro and Bonhoeffer 2000). Yet, when therapy presents a large enough genetic barrier that resistant strains may not preexist, treatment failure would have to happen if at all by the emergence of resistance during treatment. This emergence again depends on the multiple evolutionary forces mentioned above and additionally on drug efficacy against the different intermediate strains. Models have been developed to elucidate the roles of these evolutionary forces and time the emergence of drug resistance.

These models have typically employed two metrics to quantify the development of resistance, namely the waiting time, defined as the time required for the mutant of interest to first emerge, and the fixation time, defined as the time required for the mutant to grow to a certain frequency (say 90 %). Again, of enormous interest has been the influence of recombination on these metrics. While studies have found recombination to reduce the waiting time (Arora and Dixit 2009; Christiansen et al. 1998), its effect on the fixation time appears more complex and has been suggested to depend on the interplay between recombination, selection, and drift, with the latter two factors often characterized by epistasis and the effective population size, respectively (Althaus and Bonhoeffer 2005; Arora and Dixit 2009; Bretscher et al. 2004; Carvajal-Rodriguez et al. 2007; Fraser 2005; Kouyos et al. 2009; Suryavanshi and Dixit 2007).

Because mutations are intrinsically rare and because viral levels drop during treatment, the emergence of resistant strains becomes highly stochastic. Further, with potent therapy, timing the emergence of strains that overcome the large barrier offered requires description of the competitive dynamics of a large number of strains with intermediate levels of resistance, carrying different combinations of mutations, and their evolution. In a recent study, Arora and Dixit (2009) developed a model that considers this competitive evolutionary dynamics. The model assumes that strains emerge at their expected waiting times, thus accounting in an

approximate way for underlying stochastic effects while keeping the model deterministic. The model was able to describe quantitatively the emergence of resistance to tipranavir, an HIV protease inhibitor with a large genetic barrier, in in vitro serial passage experiments (Doyon et al. 2005). The model also explains the diverse observations of the influence of recombination on the waiting and fixation times.

The ability to describe the emergence of resistance to a drug with a large genetic barrier quantitatively suggests that the model accurately captures the roles of the underlying evolutionary forces in vitro. Extension of this model to describe multidrug resistance in vivo will present a quantitative framework for treatment optimization. Two factors not present in vitro but critical in vivo render such an extension a challenge: First, the immune system tilts the fitness landscape in vivo in ways that remain to be fully understood. Second, whereas drug concentrations are precisely controlled in vitro, they vary significantly in vivo due to pharmacokinetic properties, inter-patient variations, and imperfect adherence. Indeed, several studies have attempted integrating drug pharmacokinetics and immune responses with models of viral dynamics. In the sections below, we discuss some of these studies.

4 Drug Pharmacokinetics

A basic model of pharmacokinetics to describe drug concentration profiles in the plasma following oral administration is as follows (Fig. 3a). The model assumes that the concentration in the gut, C_g, increases instantaneously following oral dosage and then drops as the drug gets absorbed into the blood. The drug concentration in the plasma, C_b, increases due to absorption from the gut and decreases due to elimination (Austin et al. 1998; Dixit and Perelson 2004). This model can be solved analytically, and model parameters can be obtained by comparisons of model predictions (Fig. 3b) with experimental observations characterizing the time course of the drug concentration in patients (Dixit and Perelson 2005). The instantaneous efficacy of a drug, $\varepsilon(t)$, can be related to the plasma concentration as $\varepsilon(t) = \frac{\varepsilon_{\max}[C_b(t)]^m}{[IC_{50}]^m + [C_b(t)]^m}$. Here, IC_{50} is the concentration at which the efficacy is 50 % of the maximum efficacy, $\varepsilon_{\max}$, and m is the slope of the dose–response curve. IC_{50} and m are typically estimated from in vitro experiments. $\varepsilon_{\max}$ is usually assumed to be equal to one. Further, the efficacy term is modified as $\varepsilon(t+\tau) = \frac{\varepsilon_{\max}[C_b(t)]^m}{[IC_{50}]^m + [C_b(t)]^m}$, where τ accounts for pharmacological and intracellular delays (Dixit and Perelson 2004; Herz et al. 1996). More complex models that explicitly consider intracellular pharmacokinetics (Dixit and Perelson 2004) or additional compartments (Mohanty and Dixit 2008) have also been constructed. These models along with the model of viral dynamics have provided insights into the relationship between drug pharmacokinetics, adherence, and the emergence of resistance and treatment failure (Gilmore et al. 2013; Rosenbloom et al. 2013; Sedaghat et al. 2008; Smith 2006; Wahl and Nowak 2000; Wu et al. 2005).

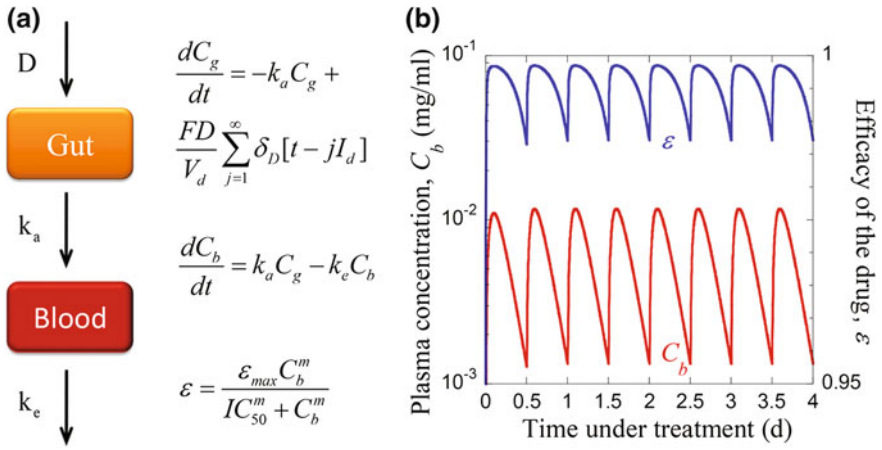

Fig. 3 Basic model of pharmacokinetics. **a** Schematic of the basic model of drug pharmacokinetics assumes that the drug concentration in the gut, C_g, and in the plasma, C_b, change due to oral drug dosage, absorption of the drug from the gut into the blood, and elimination of the drug from the blood. Here, D is the mass of the drug administered in a dose; k_a and k_e are the rate constants of absorption and elimination, respectively; I_d is the dosing interval; ε is the drug efficacy; m is the slope parameter; and IC_{50} is the plasma drug concentration for 50 % of the maximum efficacy, ε_{max}. **b** Model predictions of C_b and ε during treatment obtained using the following parameter values: $F = 1$; $D = 600\,\text{mg}$; $V_d = 28,000\,\text{ml}$; $k_a = 14.64\,\text{day}^{-1}$; $k_e = 6.86\,\text{day}^{-1}$; $I_d = 0.5\,\text{day}$; $IC_{50} = 1.75 \times 10^{-5}\,\text{mg ml}^{-1}$; and $m = 1$

Earlier studies ignored the importance of the slope parameter, m, and often assumed it equal to one. Interestingly, Shen et al. (2008) observed that m was drug class-specific. For instance, integrase inhibitors and nucleoside reverse transcriptase inhibitors had $m = 1$, non-nucleoside reverse transcriptase inhibitors (NNRTIs) and fusion inhibitors had $m \sim 1.7$, and protease inhibitors (PIs) had m between 1.8 and 4.5. Further, Shen et al. (2008) developed a new metric called the instantaneous inhibitory potential (IIP) that combines IC_{50}, m, and drug concentrations. IIP provides an estimate of the log reduction in single round infectivity due to the drug. The NNRTIs and PIs had very high IIP, explaining their high effectiveness in vivo. Sampah et al. (2011) found that resistant strains had a modified m value, again underscoring the importance of m. m is analogous to the Hill coefficient, with $m > 1$ indicating positive co-operativity in a multivalent ligand–receptor interaction (Weiss 1997). PIs and NNRTIs, however, bind to a single site on their target proteins, and co-operativity is not expected. Shen et al. (2011) postulated that a critical number of enzyme molecules are required at each step of the HIV life cycle and explained $m > 1$ based on the resulting inter-molecular cooperativity. Alternatively, Rabi et al. (2013) suggested that the involvement of the HIV protease in multiple steps of the HIV life cycle could underlie its high m. Irrespective of the mechanism, higher m yields higher treatment effectiveness at clinical drug concentrations and must be considered while evaluating different treatment regimens. Shen et al. (2008) obtained IIP values for individual drugs. Current treatment involves combinations of drugs,

and IIP values of combinations will be required to identify effective treatment regimens. Jilek et al. (2012) developed a new metric called the degree of independence (DI) to calculate IIP of combination regimen. Importantly, they found that their estimates of IIP of combinations of drugs correlated with clinical outcome. They also suggested a minimum IIP value of 5–8 for successful control of HIV infection. Recently, Rosenbloom et al. (2013) developed a model of viral dynamics incorporating pharmacokinetic properties, fitness interactions, mutation, and adherence to address the varied adherence–resistance relationship observed for different drugs. The model predicts that drugs with sharp dose–response curves and short half-lives will allow short durations for the selection of resistant strains and are therefore more susceptible to virological failure due to the growth of the wild type, explaining the observed pattern of treatment failure with PIs. Building on these promising advances, future research seems poised to identify treatment regimens that are least likely to fail, minimize drug exposure, and tolerate longer or more frequent drug holidays improving significantly the quality of life of HIV patients.

5 The Quasispecies Theory and HIV

Recognizing that combination treatment is a lifelong process, tremendous efforts are underway to develop alternative treatment strategies to cure HIV infection. Treatments aimed at reversing latency are under investigation (Siliciano and Greene 2011). Gene therapies that render target cells resistant to infections have met some clinical success (Tebas et al. 2014). A promising strategy to drive HIV past its mutational error threshold, based on predictions of the quasispecies theory, is also being explored (Eigen 2002). We discuss models examining the latter strategy here.

The quasispecies theory predicts the existence of a critical mutation rate, called the error threshold, beyond which the viral quasispecies disperses in sequence space and the viability of the viral population is compromised (Eigen 1971; Eigen et al. 1989; Nowak and Schuster 1989). Based on this concept, mutagenic drugs are being designed to drive the HIV mutation rate beyond its error threshold (Dapp et al. 2009; Harris et al. 2005; Loeb et al. 1999; Mullins et al. 2011). This strategy is a double-edged sword because a suboptimal increase in the mutation rate may counterproductively increase viral diversity and improve viral adaptation. Several studies have identified conditions under which a well-defined threshold may or may not exist (Saakian and Hu 2006; Summers and Litwin 2006; Wilke 2005) leaving unclear the existence of an error threshold for HIV and raising questions about the feasibility of mutagenic strategies targeting HIV.

Key limitations in applying the quasispecies theory to HIV arise from several assumptions in the theory that do not hold for HIV in vivo. The theory considers the asexual reproduction of an infinitely large population of haploid organisms, whereas HIV is diploid, undergoes recombination, and is thought to have a small effective population size. Population genetics-based frameworks have been constructed that overcome these limitations for HIV-1 and capture patient data of viral diversification

quantitatively (Balagam et al. 2011; Vijay et al. 2008). Using such a framework, in a recent study, Tripathi et al. (2012) predicted that HIV-1 does experience a sharp transition to error catastrophe and estimated the error threshold to be ~twofold to sixfold higher than the natural mutation rate. This estimate suggests the feasibility of and presents a quantitative target for HIV mutagens in development (Dapp et al. 2009; Harris et al. 2005; Loeb et al. 1999; Mullins et al. 2011).

Mutagenic activity is also attributed to APOBEC3G (A3G), a host protein, in its role in controlling HIV-1 infection (Malim 2009; Smith 2011). A3G induces hyper-mutations in HIV and compromises HIV infectivity. Vif, an HIV protein, targets A3G for proteasomal degradation, suppressing A3G action and allowing persistent infection. The A3G–Vif interaction is thus a promising target of intervention (Cen et al. 2010; Dapp et al. 2009; Ejima et al. 2011; Nathans et al. 2008). The implications of such intervention, however, remain unclear. Whether A3G can drive HIV past its error threshold is not known. An alternative mode of A3G activity is to induce premature stop codons in the HIV genome leading to unproductive infection, which could render infection unsustainable, effectively driving R_0 below unity. In a recent study, Thangavelu et al. (2014) using both population genetics-based and viral population dynamics-based models predicted that A3G acts by driving HIV past an extinction threshold ($R_0 < 1$) when about 80 % of progeny virions incorporate A3G. The study thus elucidates the predominant mode of action of A3G, presents quantitative guidelines for intervention, and also marks a point of convergence between population genetics-based and viral dynamics-based approaches [see Wilke (2005) for a discussion of this issue; also see Dixit et al. (2012)].

6 Viral Dynamics and Immune Response

The basic model of viral dynamics describes the early phases of HIV infection but fails to describe the natural progression of infection to AIDS. Several hypothesis-driven models have been proposed to describe the progression to AIDS. Here, we discuss models based on the quasispecies theory (see Alizon and Magnus (2012) for a comprehensive review of all prevailing hypotheses).

Nowak and colleagues developed a model of the HIV quasispecies interacting with immune cells to describe disease progression to AIDS (Nowak et al. 1990, 1995; Nowak and McLean 1991; Regoes et al. 1998). In this model, HIV impairs the immune system by infecting and killing immune cells in a nonspecific manner, whereas immune cells control HIV in a strain-specific manner. Further, HIV diversifies owing to its high mutation rate and develops immune escape variants. Beyond a certain diversity threshold, the immune system cannot suppress HIV replication, marking progression to AIDS. While this model qualitatively captures the progression to AIDS, quantitative comparison with patient data has been a challenge. Recent studies have focused on estimating the rates of emergence of escape variants (for example, see Asquith et al. 2006; Ganusov and De Boer 2006; Ganusov et al. 2011; Mostowy et al. 2011; also reviewed in Perelson and Ribeiro 2013), estimating the rates

of lymphocyte-mediated killing of HIV-infected cells (e.g., see Elemans et al. 2014; Gadhamsetty et al. 2014; Yates et al. 2007; also reviewed in Regoes et al. 2007) and quantifying turnover rates of lymphocytes (reviewed in De Boer and Perelson 2013) to quantitatively describe disease progression.

Key insights into disease progression are emerging from studies of a small fraction of HIV-infected individuals, called elite controllers, in whom HIV infection remains suppressed and does not progress to AIDS. Host factors such as HLA molecules and the lack of functional CCR5 molecules (called CCR5-Δ32 variants) that contribute to the control of infection have been recently indentified (Ballana and Esté 2012; Deeks and Walker 2007). Kosmrlj et al. (2010) carried out in silico thymic selection experiments and found that self-peptide binding properties of the HLA molecules dictate the cross-reactivity of T cells and control of HIV infection. HLA molecules such as HLA-B*57 bind to fewer self-peptides during thymic selection resulting in a T cell repertoire with receptors that bind to only a few sites on the peptides presented by the corresponding HLA for T cell recognition. In contrast, HLA molecules such as HLA-B*8 bind to a larger number of self-peptides during thymic selection resulting in a T cell repertoire with receptors that bind to a larger number of sites on presented peptides. Mutations of the non-binding sites on viral peptides do not affect T cell recognition. Consequently, the HLA-B*57-restricted T cell repertoires are more cross-reactive. Further, Kosmrlj et al. (2010), using a framework of virus and immune dynamics, showed that individuals with high T cell cross-reactivity were better controllers of HIV infection.

Controllers have lower set-point viral loads (SPVL), which also renders them poorer transmitters of infection to other individuals. The SPVL is strongly correlated with the virulence and the duration of disease progression (Bonhoeffer et al. 2003; Fraser et al. 2007, 2014). Fraser et al. (2007) suggested that HIV might have evolved to an optimal SPVL to maximize transmission events. If SPVL is high, the probability of transmission per contact is high, but the time duration for transmission will be low, whereas if SPVL is low, the probability of transmission per contact is low, but the time duration for transmission will be high. Fraser et al. (2007) found that, in two untreated HIV patients, the SVPL centered on the value that maximized the transmission potential. While host factors have been shown to be important in determining the SPVL and the course of infection, they only explain 9 % of the variability in SPVL observed (Fellay et al. 2009). Fraser et al. (2014) found that viral factors contributed to 33 % of the variability in SPVL, suggesting that HIV might have employed its virulence factors to maximize transmission fitness at the population level. Identifying these viral factors will provide guidelines for interventions to prevent the spread of the disease and control the epidemic.

Developing vaccines to prevent HIV infection is a great challenge. Both antibody-based and cytotoxic T cell (CTL)-based vaccines are being explored (Stephenson and Barouch 2013). Future models will focus on understanding the role of the immune response in elite controllers (Deeks and Walker 2007), individuals with strong CTL responses against HIV, and elite neutralizers (Simek et al. 2009), individuals who have strong antibody responses against HIV, to provide guidelines for vaccine design.

7 Models for Other Viruses

Following the success of models of HIV population dynamics, similar models have been developed to understand the pathogenesis and disease progression following infection with several other viruses, namely hepatitis B virus (HBV) (Nowak et al. 1996; Perelson and Ribeiro 2004), hepatitis C virus (HCV) (Chatterjee et al. 2013; Dixit et al. 2004; Neumann et al. 1998), influenza A virus (IAV) (Murillo et al. 2013; Smith et al. 2011), simian immunodeficiency virus (SIV) (Mohri et al. 1998; Vaidya et al. 2010), cytomegalovirus (CMV) (Emery et al. 1999, 2002), and Theiler's murine encephalomyelitis virus (TMEV) (Zhang et al. 2013). Below, we briefly discuss models of hepatitis C and influenza A virus dynamics.

7.1 Hepatitis C Virus

Interferon-α (IFNα) has been the backbone of the treatment for HCV infection for about 25 years. IFNα monotherapy is successful in only about 10–25 % of patients treated (Heim 2013a). The viral load typically declines in a biphasic manner following the start of treatment with the first phase lasting up to two days during IFNα treatment. Analysis of the viral decay with the basic viral dynamics model (Fig. 1a) suggested that IFNα primarily acts by lowering the viral production or release rate from infected cells (Neumann et al. 1998). According to the model, the slope of the first-phase decline is the product of the virion clearance rate and treatment effectiveness and the slope of the second-phase decline is the product of the loss rate of infected cells and treatment effectiveness. Comparison of model predictions with patient data estimated the average half-life of the HCV virion to be 2.7 h and the average infected cell death rate to be 0.14 day^{-1} (Neumann et al. 1998). Combination treatment (PR) with pegylated IFNα and ribavirin (RBV) improved treatment response to about 50 % of the patients treated (Ghany et al. 2011). RBV appears to increase the second-phase slope of viral decline and improve treatment response. Modeling the viral decay during PR treatment suggested that RBV acts by rendering virions non-infectious, presumably by mutagenesis (Dixit et al. 2004). The predominant mechanism(s) by which RBV renders the virus non-infectious remain to be established (Thomas et al. 2012). Dahari et al. (2007a) advanced the model of Dixit et al. (2004) and attributed the triphasic decline observed in some patients to the proliferation of hepatocytes due to liver homeostasis. The latter model predicts a critical effectiveness of treatment below which viral breakthrough occurs. The cause of variations in the effectiveness across patients and treatment failure, however, remained elusive.

Recent experiments and clinical observations have shed light on the mechanisms of action of IFNα against HCV. IFNα interacts with cell surface receptors to trigger the JAK–STAT signaling pathway and induce several hundred genes known as interferon-stimulated genes (ISGs) (Heim 2013b). These ISGs induce an antiviral

state in cells and control HCV infection. Counterintuitively, the pretreatment ISG expression was higher in the livers of non-responders than responders to PR treatment and did not increase further in the non-responders during treatment (Heim 2013b). For years, how HCV persists despite strong endogenous IFN activation in some patients and why the response to IFNα treatment is poor in these patients has remained unclear. Padmanabhan et al. (2014) developed a mathematical model of the IFN signaling network in the presence of HCV and found that HCV induces bistability in the network, with one state where HCV persists and the other where it is cleared by IFNα. Cells that admit only the former steady state are refractory to IFNα treatment. Using a viral dynamics model that explicitly considered cell subpopulations with these distinct interferon response phenotypes (Fig. 4), they showed that the treatment failed when the fraction of IFN-refractory cells exceeds a critical value. According to their framework, patients with high endogenous IFN

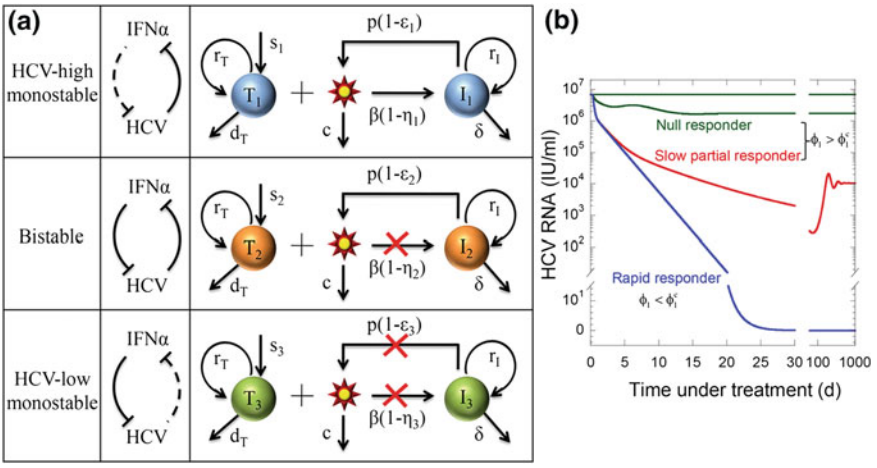

Fig. 4 HCV viral kinetics following IFNα treatment. **a** Schematic of viral kinetics incorporating distinct cellular responses to IFNα. HCV interferes with the intracellular signaling by IFNα, whereas IFNα controls HCV infection within a cell (*left*). This double-negative feedback can lead to bistability, with one state where HCV persists and the other state where HCV is cleared. *Top* Cells that have poor IFNα control of HCV (*left*) admit the state where HCV always persists, and these cells are refractory to IFNα (*right*). *Middle* Cells that have intermediate IFNα control of HCV and vice versa (*left*) admit both the states and thus continue viral production when infected but are protected from new infections by IFNα (*right*). *Bottom* Cells that have strong IFNα control of HCV (*left*) always clear HCV and are sensitive to IFNα (*right*). Target cells in the three subpopulations, T_i, where $i = 1, 2$ and 3, are produced at the rates s_i, proliferate with the rate constant r_T, die with the rate constant d_T, and are lost due to de novo infection with the rate constant β. The corresponding infected cells I_i proliferate with the rate constant r_I and die with the rate constant δ. Free virions are produced by infected cells with the rate constant p and are cleared with the rate constant c. The de novo infection rate and virion production rate were assumed to be blocked with efficacies η_i and ε_i in the respective subpopulations due to IFNα treatment. **b** Model predictions of different viral response patterns following IFN treatment for different distributions of cells in the three IFN response phenotypes. Patients with pretreatment frequency of IFNα-refractory cells, ϕ_1, less than a critical value, ϕ_1^c, clear infection during treatment. This figure is reproduced from Padmanabhan et al. (2014)

production and compromised IFN effector function represent non-responders to treatment. These patients predominantly contain IFN-refractory cells, and HCV infection is established despite high ISG expression. Further, addition of exogenous IFN does not aid in controlling the infection. This model presents an alternative interpretation of viral load decay during IFNα treatment. The slope and the extent of the first-phase decline are determined by the virion clearance rate and the pre-treatment frequency of cells sensitive to IFNα. The slope of the second phase is determined by the loss rate of infected cells and the fraction of IFN-refractory cells. The critical effectiveness predicted by the standard models is equivalent to the level of IFNα activity necessary to render the fraction of IFN-refractory cells below the critical value.

Several drugs targeting HCV proteins called direct acting antivirals (DAAs) are in clinical trials and some are in clinical use (Pawlotsky 2014). Although monotherapy with the PIs telaprevir and boceprevir failed in all patients, in conjunction with PR, they improved treatment response to over 70 % of patients treated (Ghany et al. 2011). Padmanabhan et al. (2014) showed that DAAs can eliminate HCV-induced bistability in the IFN signaling network and presented a mechanism by which DAAs synergize with IFNα.

Recent clinical trials without interferon have been stunningly successful, and HCV treatment is heading toward IFN-free regimen with a combination of DAAs. Modeling HCV viral kinetics has given insights into the mechanisms of action of several DAAs. Guedj et al. (2012) found that silibinin acts by blocking both viral production and de novo infection. Guedj et al. (2013) developed a multiscale model integrating viral dynamics with intracellular replication and suggested that daclatasvir, an HCV NS5A inhibitor, acts by blocking viral replication and release. The model of Guedj et al. (2013) employs a simplistic description of intracellular events. More detailed models of HCV intracellular replication (Binder et al. 2013; Dahari et al. 2007b) are being developed to understand the HCV replication process and to identify potential therapeutic targets. Further, models of protein–protein interactions preceding HCV entry coupled with viral dynamics models have provided key insights into the HCV entry process (Padmanabhan and Dixit 2011, 2012). Future modeling efforts will focus on identifying synergistic combinations of drugs based on the HCV life cycle.

One major roadblock in treatments with DAAs is drug resistance. Modeling viral kinetics during monotherapy with PIs suggested that treatment failure could be due to the preexistence of the drug-resistant strains (Rong et al. 2010). Quasispecies models of HCV dynamics are now employed to describe the evolution of drug-resistant strains during treatment with DAAs (Adiwijaya et al. 2010; Rong et al. 2012). While these models paint a qualitative picture of viral evolution during treatment, they have limitations in describing the evolution quantitatively. Models integrating both the intracellular and the extracellular dynamics (Ribeiro et al. 2012) will be required to describe viral evolution during treatment. Unlike HIV, cure is possible with HCV. With several new classes of drugs in clinical trials, a quantitative framework that describes the evolution of drug resistance would pave the way for rational treatment optimization.

7.2 *Influenza A Virus*

In the past decade, several viral population dynamics models have been developed to describe infection by influenza A virus (IAV). IAV infection is an acute respiratory infection and is cleared within 10 days following infection (Taubenberger and Morens 2008). The basic viral dynamics model has been modified to account for the delay in the production of new virions by infected cells to describe the infection dynamics (Baccam et al. 2006; Beauchemin et al. 2008) (Fig. 5). The model allowed estimation of viral kinetic parameters and presented a way to compare the virulence of different influenza strains (Smith et al. 2011). Quantification of innate and adaptive immune responses during influenza virus infection in animal models has allowed the development of models of viral dynamics coupled with the immune response (Chang and Young 2007; Hancioglu et al. 2007; Miao et al. 2010; Pawelek et al. 2012; Saenz et al. 2010). These models provide key insights into the contributions of interferons, antibodies, and T cells in controlling IAV infection. Currently, two classes of drugs, namely the adamantanes and the neuraminidase inhibitors, are available for the treatment of influenza infection (Jefferson et al. 2006). Comparison of model predictions with patient data allowed estimation of treatment efficacies (Baccam et al. 2006; Beauchemin et al.

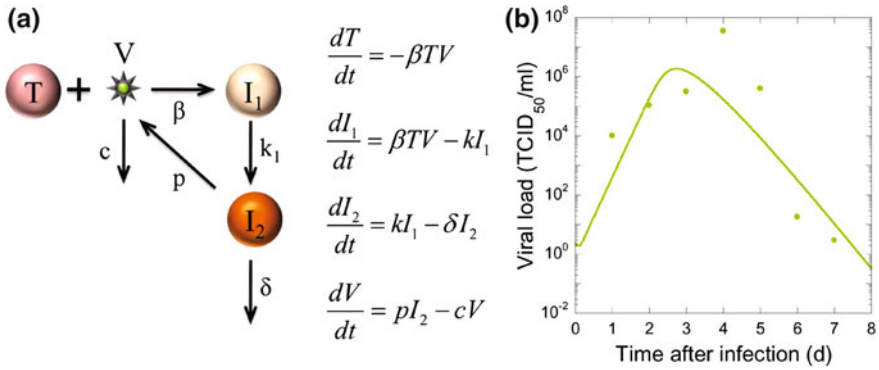

Fig. 5 Basic model of influenza A viral dynamics. **a** Schematic and model equations of the basic model of influenza A viral dynamics. This model differs from the basic model of viral dynamics in two ways. First, the model assumes that uninfected cells, T, are limiting during infection and ignores production and death of uninfected cells. Second, the model accounts for the eclipse phase during infection by considering two compartments of infected cells: non-productively infected cells, I_1, and productively infected cells, I_2. Target cells get infected at the rate βVT to produce non-productively infected cells. The non-productively infected cells transition to productively infected cells at the rate kI_1. **b** The model predictions (*line*) quantitatively describe the viral dynamics following infection observed in an infected individual (*symbols*). Experimental data have been digitized from Baccam et al. (2006) and model predictions have been obtained using the following parameter values: $\beta = 8.4 \times 10^{-6}\,\text{ml}\,(\text{TCID}_{50}\,\text{day})^{-1}$; $k = 4.4\,\text{day}^{-1}$; $\delta = 5.2\,\text{day}^{-1}$; $p = 7.1 \times 10^{-2}\,\text{TCID}_{50}\,(\text{ml day})^{-1}$; and $c = 3.7\,\text{day}^{-1}$. TCID_{50} stands for 50 % tissue culture infective dose

2008). A two-strain model of viral dynamics, similar to the one used for HIV, has been employed to describe the development of resistance to these drugs, and these models recommend early treatment start (less than 48 h post-infection) for effective treatment (Baccam et al. 2006; Holder et al. 2011). Recently, a multiscale model integrating both intracellular and extracellular dynamics has been developed to understand influenza virus infection and to identify novel therapeutic targets (Heldt et al. 2013). Future models will focus on integrating the models of within-host dynamics with epidemic models of inter-host dynamics to guide intervention strategies (Coombs et al. 2007; Murillo et al. 2013).

8 Concluding Remarks

Models of viral population dynamics have provided several insights into HIV pathogenesis and treatment response. With an eye to preventing treatment failure, these models have been expanded to consider viral evolution and drug resistance as well as the influence of drug pharmacokinetics. Future studies will focus on constructing a comprehensive framework that integrates these components along with a description of the underlying immune response to predict treatment outcomes, assess the efficacy of novel intervention strategies, and rationally identify optimal treatment protocols. Such a framework may also have implications for other viral infections. With the limited success of current T cell- and antibody-based vaccines for HIV, it is becoming increasingly clear that strategies for future vaccine design will involve stimulation of multiple arms of the immune system. Models that incorporate these different arms of the immune response against HIV will be required to describe the complex coevolutionary dynamics of the virus and the immune system and pave the way to designing and evaluating potent vaccines against HIV. Finally, multiscale models that combine within-host and inter-host dynamics will facilitate the establishment of guidelines for mass intervention and healthcare policies.

Acknowledgments This work was supported by the Department of Science and Technology, Government of India.

References

Abram ME, Ferris AL, Shao W et al (2010) Nature, position, and frequency of mutations made in a single cycle of HIV-1 replication. J Virol 84:9864–9878

Adiwijaya BS, Herrmann E, Hare B et al (2010) A multi-variant, viral dynamic model of genotype 1 HCV to assess the in vivo evolution of protease-inhibitor resistant variants. PLoS Comput Biol 6:e1000745

Alexander HK, Bonhoeffer S (2013) Pre-existence and emergence of drug resistance in a generalized model of intra-host viral dynamics. Epidemics 4:187–202

Alizon S, Magnus C (2012) Modelling the course of an HIV infection: insights from ecology and evolution. Viruses 4:1984–2013

Althaus CL, Bonhoeffer S (2005) Stochastic interplay between mutation and recombination during the acquisition of drug resistance mutations in human immunodeficiency virus type 1. J Virol 79:13572–13578

Arora P, Dixit NM (2009) Timing the emergence of resistance to anti-HIV drugs with large genetic barriers. PLoS Comput Biol 5:e1000305

Asquith B, Edwards CT, Lipsitch M et al (2006) Inefficient cytotoxic T lymphocyte-mediated killing of HIV-1-infected cells in vivo. PLoS Biol 4:e90

Austin DJ, White NJ, Anderson RM (1998) The dynamics of drug action on the within-host population growth of infectious agents: melding pharmacokinetics with pathogen population dynamics. J Theor Biol 194:313–339

Baccam P, Beauchemin C, Macken CA et al (2006) Kinetics of influenza A virus infection in humans. J Virol 80:7590–7599

Balagam R, Singh V, Sagi AR et al (2011) Taking multiple infections of cells and recombination into account leads to small within-host effective-population-size estimates of HIV-1. PLoS ONE 6:e14531

Ballana E, Esté J (2012) HIV-1 infection and CCR5Δ32 homozygosis. Future Virol 7:653–658

Batorsky R, Kearney MF, Palmer SE et al (2011) Estimate of effective recombination rate and average selection coefficient for HIV in chronic infection. Proc Natl Acad Sci USA 108: 5661–5666

Beauchemin CA, McSharry JJ, Drusano GL et al (2008) Modeling amantadine treatment of influenza A virus in vitro. J Theor Biol 254:439–451

Binder M, Sulaimanov N, Clausznitzer D et al (2013) Replication vesicles are load- and choke-points in the hepatitis C virus lifecycle. PLoS Pathog 9:e1003561

Bocharov G, Ford NJ, Edwards J et al (2005) A genetic-algorithm approach to simulating human immunodeficiency virus evolution reveals the strong impact of multiply infected cells and recombination. J Gen Virol 86:3109–3118

Boerlijst MC, Bonhoeffer S, Nowak MA (1996) Viral quasi-species and recombination. Proc R Soc Lond B 263:1577–1584

Bonhoeffer S, Nowak MA (1997) Pre-existence and emergence of drug resistance in HIV-1 infection. Proc Biol Sci 264:631–637

Bonhoeffer S, May RM, Shaw GM et al (1997) Virus dynamics and drug therapy. Proc Natl Acad Sci USA 94:6971–6976

Bonhoeffer S, Funk GA, Gunthard HF et al (2003) Glancing behind virus load variation in HIV-1 infection. Trends Microbiol 11:499–504

Bretscher MT, Althaus CL, Muller V et al (2004) Recombination in HIV and the evolution of drug resistance: for better or for worse? BioEssays 26:180–188

Brown AJ (1997) Analysis of HIV-1 env gene sequences reveals evidence for a low effective number in the viral population. Proc Natl Acad Sci USA 94:1862–1865

Carvajal-Rodriguez A, Crandall KA, Posada D (2007) Recombination favors the evolution of drug resistance in HIV-1 during antiretroviral therapy. Infect Genet Evol 7:476–483

Cen S, Peng ZG, Li XY et al (2010) Small molecular compounds inhibit HIV-1 replication through specifically stabilizing APOBEC3G. J Biol Chem 285:16546–16552

Chang DB, Young CS (2007) Simple scaling laws for influenza A rise time, duration, and severity. J Theor Biol 246:621–635

Chatterjee A, Smith PF, Perelson AS (2013) Hepatitis C viral kinetics: the past, present, and future. Clin Liver Dis 17:13–26

Christiansen FB, Otto SP, Bergman A et al (1998) Waiting with and without recombination: the time to production of a double mutant. Theor Popul Biol 53:199–215

Chun TW, Carruth L, Finzi D et al (1997) Quantification of latent tissue reservoirs and total body viral load in HIV-1 infection. Nature 387:183–188

Clavel F, Hance AJ (2004) HIV drug resistance. N Engl J Med 350:1023–1035

Coombs D, Gilchrist MA, Ball CL (2007) Evaluating the importance of within- and between-host selection pressures on the evolution of chronic pathogens. Theor Popul Biol 72:576–591
Dahari H, Ribeiro RM, Perelson AS (2007a) Triphasic decline of hepatitis C virus RNA during antiviral therapy. Hepatology 46:16–21
Dahari H, Ribeiro RM, Rice CM et al (2007b) Mathematical modeling of subgenomic hepatitis C virus replication in Huh-7 cells. J Virol 81:750–760
Dapp MJ, Clouser CL, Patterson S et al (2009) 5-Azacytidine can induce lethal mutagenesis in human immunodeficiency virus type 1. J Virol 83:11950–11958
De Boer RJ, Perelson AS (2013) Quantifying T lymphocyte turnover. J Theor Biol 327:45–87
Deeks SG, Walker BD (2007) Human immunodeficiency virus controllers: mechanisms of durable virus control in the absence of antiretroviral therapy. Immunity 27:406–416
Deeks SG, Lewin SR, Havlir DV (2013) The end of AIDS: HIV infection as a chronic disease. Lancet 382:1525–1533
Dixit NM, Perelson AS (2004) Complex patterns of viral load decay under antiretroviral therapy: influence of pharmacokinetics and intracellular delay. J Theor Biol 226:95–109
Dixit NM, Perelson AS (2005) Influence of drug pharmacokinetics on HIV pathogenesis and therapy. In: Wu H, Tan WY (eds) Deterministic and stochastic models on AIDS and HIV with intervention. World Scientific Press, Singapore, pp 287–311
Dixit NM, Layden-Almer JE, Layden TJ et al (2004) Modelling how ribavirin improves interferon response rates in hepatitis C virus infection. Nature 432:922–924
Dixit NM, Srivastava P, Vishnoi NK (2012) A finite population model of molecular evolution: theory and computation. J Comput Biol 19:1176–1202
Doyon L, Tremblay S, Bourgon L et al (2005) Selection and characterization of HIV-1 showing reduced susceptibility to the non-peptidic protease inhibitor tipranavir. Antiviral Res 68:27–35
Eigen M (1971) Selforganization of matter and the evolution of biological macromolecules. Naturwissenschaften 58:465–523
Eigen M (2002) Error catastrophe and antiviral strategy. Proc Natl Acad Sci USA 99: 13374–13376
Eigen M, McCaskill J, Schuster P (1989) The molecular quasi-species. Adv Chem Phys 75: 149–263
Ejima T, Hirota M, Mizukami T et al (2011) An anti-HIV-1 compound that increases steady-state expression of apolipoprotein B mRNA-editing enzyme-catalytic polypeptide-like 3G. Int J Mol Med 28:613–616
Elemans M, Florins A, Willems L et al (2014) Rates of CTL killing in persistent viral infection in vivo. PLoS Comput Biol 10:e1003534
Emery VC, Cope AV, Bowen EF et al (1999) The dynamics of human cytomegalovirus replication in vivo. J Exp Med 190:177–182
Emery VC, Hassan-Walker AF, Burroughs AK et al (2002) Human cytomegalovirus (HCMV) replication dynamics in HCMV-naive and -experienced immunocompromised hosts. J Infect Dis 185:1723–1728
Fellay J, Ge D, Shianna KV et al (2009) Common genetic variation and the control of HIV-1 in humans. PLoS Genet 5:e1000791
Fraser C (2005) HIV recombination: what is the impact on antiretroviral therapy? J R Soc Interface 2:489–503
Fraser C, Hollingsworth TD, Chapman R et al (2007) Variation in HIV-1 set-point viral load: epidemiological analysis and an evolutionary hypothesis. Proc Natl Acad Sci USA 104: 17441–17446
Fraser C, Lythgoe K, Leventhal GE et al (2014) Virulence and pathogenesis of HIV-1 infection: an evolutionary perspective. Science 343:1243727
Gadhamsetty S, Dixit NM (2010) Estimating frequencies of minority nevirapine-resistant strains in chronically HIV-1-infected individuals naive to nevirapine by using stochastic simulations and a mathematical model. J Virol 84:10230–10240
Gadhamsetty S, Maree AF, Beltman JB et al (2014) A general functional response of cytotoxic T lymphocyte-mediated killing of target cells. Biophys J 106:1780–1791

Ganusov VV, De Boer RJ (2006) Estimating costs and benefits of CTL escape mutations in SIV/HIV infection. PLoS Comput Biol 2:e24

Ganusov VV, Goonetilleke N, Liu MK et al (2011) Fitness costs and diversity of the cytotoxic T lymphocyte (CTL) response determine the rate of CTL escape during acute and chronic phases of HIV infection. J Virol 85:10518–10528

Ghany MG, Nelson DR, Strader DB et al (2011) An update on treatment of genotype 1 chronic hepatitis C virus infection: 2011 practice guideline by the American Association for the Study of Liver Diseases. Hepatology 54:1433–1444

Gheorghiu-Svirschevski S, Rouzine IM, Coffin JM (2007) Increasing sequence correlation limits the efficiency of recombination in a multisite evolution model. Mol Biol Evol 24:574–586

Gilmore JB, Kelleher AD, Cooper DA et al (2013) Explaining the determinants of first phase HIV decay dynamics through the effects of stage-dependent drug action. PLoS Comput Biol 9: e1002971

Guedj J, Dahari H, Pohl RT et al (2012) Understanding silibinin's modes of action against HCV using viral kinetic modeling. J Hepatol 56:1019–1024

Guedj J, Dahari H, Rong L et al (2013) Modeling shows that the NS5A inhibitor daclatasvir has two modes of action and yields a shorter estimate of the hepatitis C virus half-life. Proc Natl Acad Sci USA 110:3991–3996

Hancioglu B, Swigon D, Clermont G (2007) A dynamical model of human immune response to influenza A virus infection. J Theor Biol 246:70–86

Harris KS, Brabant W, Styrchak S et al (2005) KP-1212/1461, a nucleoside designed for the treatment of HIV by viral mutagenesis. Antiviral Res 67:1–9

Hartl DL, Clark AG (2007) Principles of Population Genetics. Sinauer Associates Inc., Sunderland

Heim MH (2013a) 25 years of interferon-based treatment of chronic hepatitis C: an epoch coming to an end. Nat Rev Immunol 13:535–542

Heim MH (2013b) Innate immunity and HCV. J Hepatol 58:564–574

Heldt FS, Frensing T, Pflugmacher A et al (2013) Multiscale modeling of influenza A virus infection supports the development of direct-acting antivirals. PLoS Comput Biol 9:e1003372

Herz AV, Bonhoeffer S, Anderson RM et al (1996) Viral dynamics in vivo: limitations on estimates of intracellular delay and virus decay. Proc Natl Acad Sci USA 93:7247–7251

Ho DD, Neumann AU, Perelson AS et al (1995) Rapid turnover of plasma virions and CD4 lymphocytes in HIV-1 infection. Nature 373:123–126

Hoetelmans RM (1998) Sanctuary sites in HIV-1 infection. Antivir Ther 3(Suppl 4):13–17

Holder BP, Simon P, Liao LE et al (2011) Assessing the in vitro fitness of an oseltamivir-resistant seasonal A/H1N1 influenza strain using a mathematical model. PLoS ONE 6:e14767

Jefferson T, Demicheli V, Rivetti D et al (2006) Antivirals for influenza in healthy adults: systematic review. Lancet 367:303–313

Jilek BL, Zarr M, Sampah ME et al (2012) A quantitative basis for antiretroviral therapy for HIV-1 infection. Nat Med 18:446–451

Johnson VA, Calvez V, Gunthard HF et al (2013) Update of the drug resistance mutations in HIV-1: March 2013. Top Antivir Med 21:6–14

Josefsson L, King MS, Makitalo B et al (2011) Majority of $CD4^+$ T cells from peripheral blood of HIV-1-infected individuals contain only one HIV DNA molecule. Proc Natl Acad Sci USA 108:11199–11204

Josefsson L, Palmer S, Faria NR et al (2013) Single cell analysis of lymph node tissue from HIV-1 infected patients reveals that the majority of $CD4^+$ T-cells contain one HIV-1 DNA molecule. PLoS Pathog 9:e1003432

Jung A, Maier R, Vartanian JP et al (2002) Recombination: multiply infected spleen cells in HIV patients. Nature 418:144

Kosmrlj A, Read EL, Qi Y et al (2010) Effects of thymic selection of the T-cell repertoire on HLA class I-associated control of HIV infection. Nature 465:350–354

Kouyos RD, Althaus CL, Bonhoeffer S (2006) Stochastic or deterministic: what is the effective population size of HIV-1? Trends Microbiol 14:507–511

Kouyos RD, Fouchet D, Bonhoeffer S (2009) Recombination and drug resistance in HIV: population dynamics and stochasticity. Epidemics 1:58–69
Levy DN, Aldrovandi GM, Kutsch O et al (2004) Dynamics of HIV-1 recombination in its natural target cells. Proc Natl Acad Sci USA 101:4204–4209
Little SJ, McLean AR, Spina CA et al (1999) Viral dynamics of acute HIV-1 infection. J Exp Med 190:841–850
Loeb LA, Essigmann JM, Kazazi F et al (1999) Lethal mutagenesis of HIV with mutagenic nucleoside analogs. Proc Natl Acad Sci USA 96:1492–1497
Maldarelli F, Palmer S, King MS et al (2007) ART suppresses plasma HIV-1 RNA to a stable set point predicted by pretherapy viremia. PLoS Pathog 3:e46
Malim MH (2009) APOBEC proteins and intrinsic resistance to HIV-1 infection. Philos Trans R Soc Lond B Biol Sci 364:675–687
Mansky LM, Temin HM (1995) Lower in vivo mutation rate of human immunodeficiency virus type 1 than that predicted from the fidelity of purified reverse transcriptase. J Virol 69: 5087–5094
Markowitz M, Louie M, Hurley A et al (2003) A novel antiviral intervention results in more accurate assessment of human immunodeficiency virus type 1 replication dynamics and T-cell decay in vivo. J Virol 77:5037–5038
Miao H, Hollenbaugh JA, Zand MS et al (2010) Quantifying the early immune response and adaptive immune response kinetics in mice infected with influenza A virus. J Virol 84: 6687–6698
Mohanty U, Dixit NM (2008) Mechanism-based model of the pharmacokinetics of enfuvirtide, an HIV fusion inhibitor. J Theor Biol 251:541–551
Mohri H, Bonhoeffer S, Monard S et al (1998) Rapid turnover of T lymphocytes in SIV-infected rhesus macaques. Science 279:1223–1227
Mostowy R, Kouyos RD, Fouchet D et al (2011) The role of recombination for the coevolutionary dynamics of HIV and the immune response. PLoS ONE 6:e16052
Mullins JI, Heath L, Hughes JP et al (2011) Mutation of HIV-1 genomes in a clinical population treated with the mutagenic nucleoside KP1461. PLoS ONE 6:e15135
Murillo LN, Murillo MS, Perelson AS (2013) Towards multiscale modeling of influenza infection. J Theor Biol 332:267–290
Nathans R, Cao H, Sharova N et al (2008) Small-molecule inhibition of HIV-1 Vif. Nat Biotechnol 26:1187–1192
Neher RA, Leitner T (2010) Recombination rate and selection strength in HIV intra-patient evolution. PLoS Comput Biol 6:e1000660
Neumann AU, Lam NP, Dahari H et al (1998) Hepatitis C viral dynamics in vivo and the antiviral efficacy of interferon-alpha therapy. Science 282:103–107
Nijhuis M, Boucher CA, Schipper P et al (1998) Stochastic processes strongly influence HIV-1 evolution during suboptimal protease-inhibitor therapy. Proc Natl Acad Sci USA 95: 14441–14446
Nowak MA, May RM (2000) Virus dynamics: mathematical principles of immunology and virology. Oxford University Press, New York
Nowak MA, McLean AR (1991) A mathematical model of vaccination against HIV to prevent the development of AIDS. Proc Biol Sci 246:141–146
Nowak M, Schuster P (1989) Error thresholds of replication in finite populations mutation frequencies and the onset of Muller's ratchet. J Theor Biol 137:375–395
Nowak MA, May RM, Anderson RM (1990) The evolutionary dynamics of HIV-1 quasispecies and the development of immunodeficiency disease. Aids 4:1095–1103
Nowak MA, May RM, Phillips RE et al (1995) Antigenic oscillations and shifting immunodominance in HIV-1 infections. Nature 375:606–611
Nowak MA, Bonhoeffer S, Hill AM et al (1996) Viral dynamics in hepatitis B virus infection. Proc Natl Acad Sci USA 93:4398–4402

Padmanabhan P, Dixit NM (2011) Mathematical model of viral kinetics in vitro estimates the number of E2-CD81 complexes necessary for hepatitis C virus entry. PLoS Comput Biol 7: e1002307
Padmanabhan P, Dixit NM (2012) Viral kinetics suggests a reconciliation of the disparate observations of the modulation of Claudin-1 expression on cells exposed to hepatitis C virus. PLoS ONE 7:e36107
Padmanabhan P, Garaigorta U, Dixit NM (2014) Emergent properties of the interferon signaling network may underlie the success of hepatitis C treatment. Nat Commun. doi:10.1038/ncomms4872
Palmer S, Maldarelli F, Wiegand A et al (2008) Low-level viremia persists for at least 7 years in patients on suppressive antiretroviral therapy. Proc Natl Acad Sci USA 105:3879–3884
Pawelek KA, Huynh GT, Quinlivan M et al (2012) Modeling within-host dynamics of influenza virus infection including immune responses. PLoS Comput Biol 8:e1002588
Pawlotsky JM (2014) New hepatitis C therapies: the toolbox, strategies, and challenges. Gastroenterology. doi:10.1053/j.gastro.2014.03.003
Pennings PS (2012) Standing genetic variation and the evolution of drug resistance in HIV. PLoS Comput Biol 8:e1002527
Pennings PS, Kryazhimskiy S, Wakeley J (2014) Loss and recovery of genetic diversity in adapting populations of HIV. PLoS Genet 10:e1004000
Perelson AS (2002) Modelling viral and immune system dynamics. Nat Rev Immunol 2:28–36
Perelson AS, Ribeiro RM (2004) Hepatitis B virus kinetics and mathematical modeling. Semin Liver Dis 24(Suppl 1):11–16
Perelson AS, Ribeiro RM (2013) Modeling the within-host dynamics of HIV infection. BMC Biol 11:96
Perelson AS, Neumann AU, Markowitz M et al (1996) HIV-1 dynamics in vivo: virion clearance rate, infected cell life-span, and viral generation time. Science 271:1582–1586
Perelson AS, Essunger P, Cao Y et al (1997) Decay characteristics of HIV-1-infected compartments during combination therapy. Nature 387:188–191
Phillips AN (1996) Reduction of HIV concentration during acute infection: independence from a specific immune response. Science 271:497–499
Rabi SA, Laird GM, Durand CM et al (2013) Multi-step inhibition explains HIV-1 protease inhibitor pharmacodynamics and resistance. J Clin Invest 123:3848–3860
Ramratnam B, Bonhoeffer S, Binley J et al (1999) Rapid production and clearance of HIV-1 and hepatitis C virus assessed by large volume plasma apheresis. Lancet 354:1782–1785
Regoes RR, Wodarz D, Nowak MA (1998) Virus dynamics: the effect of target cell limitation and immune responses on virus evolution. J Theor Biol 191:451–462
Regoes RR, Yates A, Antia R (2007) Mathematical models of cytotoxic T-lymphocyte killing. Immunol Cell Biol 85:274–279
Ribeiro RM, Bonhoeffer S (2000) Production of resistant HIV mutants during antiretroviral therapy. Proc Natl Acad Sci USA 97:7681–7686
Ribeiro RM, Bonhoeffer S, Nowak MA (1998) The frequency of resistant mutant virus before antiviral therapy. AIDS 12:461–465
Ribeiro RM, Qin L, Chavez LL et al (2010) Estimation of the initial viral growth rate and basic reproductive number during acute HIV-1 infection. J Virol 84:6096–6102
Ribeiro RM, Li H, Wang S et al (2012) Quantifying the diversification of hepatitis C virus (HCV) during primary infection: estimates of the in vivo mutation rate. PLoS Pathog 8: e1002881
Rodrigo AG, Shpaer EG, Delwart EL et al (1999) Coalescent estimates of HIV-1 generation time in vivo. Proc Natl Acad Sci USA 96:2187–2191
Rong L, Dahari H, Ribeiro RM et al (2010) Rapid emergence of protease inhibitor resistance in hepatitis C virus. Sci Transl Med 2:30ra32
Rong L, Ribeiro RM, Perelson AS (2012) Modeling quasispecies and drug resistance in hepatitis C patients treated with a protease inhibitor. Bull Math Biol 74:1789–1817

Rosenbloom DI, Hill AL, Rabi SA et al (2013) Antiretroviral dynamics determines HIV evolution and predicts therapy outcome. Nat Med 18:1378–1385
Rouzine IM, Coffin JM (1999) Linkage disequilibrium test implies a large effective population number for HIV in vivo. Proc Natl Acad Sci USA 96:10758–10763
Rouzine IM, Coffin JM (2005) Evolution of human immunodeficiency virus under selection and weak recombination. Genetics 170:7–18
Saakian DB, Hu CK (2006) Exact solution of the Eigen model with general fitness functions and degradation rates. Proc Natl Acad Sci USA 103:4935–4939
Saenz RA, Quinlivan M, Elton D et al (2010) Dynamics of influenza virus infection and pathology. J Virol 84:3974–3983
Sampah ME, Shen L, Jilek BL et al (2011) Dose-response curve slope is a missing dimension in the analysis of HIV-1 drug resistance. Proc Natl Acad Sci USA 108:7613–7618
Schlub TE, Grimm AJ, Smyth RP et al (2014) Fifteen to twenty percent of HIV substitution mutations are associated with recombination. J Virol 88:3837–3849
Sedaghat AR, Dinoso JB, Shen L et al (2008) Decay dynamics of HIV-1 depend on the inhibited stages of the viral life cycle. Proc Natl Acad Sci USA 105:4832–4837
Seo TK, Thorne JL, Hasegawa M et al (2002) Estimation of effective population size of HIV-1 within a host: a pseudomaximum-likelihood approach. Genetics 160:1283–1293
Shen L, Peterson S, Sedaghat AR et al (2008) Dose-response curve slope sets class-specific limits on inhibitory potential of anti-HIV drugs. Nat Med 14:762–766
Shen L, Rabi SA, Sedaghat AR et al. (2011) A critical subset model provides a conceptual basis for the high antiviral activity of major HIV drugs. Sci Transl Med 3:91ra63
Siliciano RF, Greene WC (2011) HIV latency. Cold Spring Harb Perspect Med 1:a007096
Simek MD, Rida W, Priddy FH et al (2009) Human immunodeficiency virus type 1 elite neutralizers: individuals with broad and potent neutralizing activity identified by using a high-throughput neutralization assay together with an analytical selection algorithm. J Virol 83:7337–7348
Smith RJ (2006) Adherence to antiretroviral HIV drugs: how many doses can you miss before resistance emerges? Proc Biol Sci 273:617–624
Smith HC (2011) APOBEC3G: a double agent in defense. Trends Biochem Sci 36:239–244
Smith AM, Adler FR, McAuley JL et al (2011) Effect of 1918 PB1-F2 expression on influenza A virus infection kinetics. PLoS Comput Biol 7:e1001081
Stafford MA, Corey L, Cao Y et al (2000) Modeling plasma virus concentration during primary HIV infection. J Theor Biol 203:285–301
Stephenson KE, Barouch DH (2013) A global approach to HIV-1 vaccine development. Immunol Rev 254:295–304
Summers J, Litwin S (2006) Examining the theory of error catastrophe. J Virol 80:20–26
Suryavanshi GW, Dixit NM (2007) Emergence of recombinant forms of HIV: dynamics and scaling. PLoS Comput Biol 3:2003–2018
Taubenberger JK, Morens DM (2008) The pathology of influenza virus infections. Annu Rev Pathol 3:499–522
Tebas P, Stein D, Tang WW et al (2014) Gene editing of CCR5 in autologous CD4 T cells of persons infected with HIV. N Engl J Med 370:901–910
Thangavelu PU, Gupta V, Dixit NM (2014) Estimating the fraction of progeny virions that must incorporate APOBEC3G for suppression of productive HIV-1 infection. Virology 449: 224–228
Thomas E, Ghany MG, Liang TJ (2012) The application and mechanism of action of ribavirin in therapy of hepatitis C. Antivir Chem Chemother 23:1–12
Tripathi K, Balagam R, Vishnoi NK et al (2012) Stochastic simulations suggest that HIV-1 survives close to its error threshold. PLoS Comput Biol 8:e1002684
Vaidya NK, Ribeiro RM, Miller CJ et al (2010) Viral dynamics during primary simian immunodeficiency virus infection: effect of time-dependent virus infectivity. J Virol 84: 4302–4310

Vijay NN, Vasantika Ajmani R et al (2008) Recombination increases human immunodeficiency virus fitness, but not necessarily diversity. J Gen Virol 89:1467–1477
Volberding PA, Deeks SG (2010) Antiretroviral therapy and management of HIV infection. Lancet 376:49–62
Wahl LM, Nowak MA (2000) Adherence and drug resistance: predictions for therapy outcome. Proc Biol Sci 267:835–843
Wei X, Ghosh SK, Taylor ME et al (1995) Viral dynamics in human immunodeficiency virus type 1 infection. Nature 373:117–122
Weiss JN (1997) The Hill equation revisited: uses and misuses. Faseb J 11:835–841
Wilke CO (2005) Quasispecies theory in the context of population genetics. BMC Evol Biol 5:44
Wu H, Huang Y, Acosta EP et al (2005) Modeling long-term HIV dynamics and antiretroviral response: effects of drug potency, pharmacokinetics, adherence, and drug resistance. J Acquir Immune Defic Syndr 39:272–283
Yates A, Graw F, Barber DL et al (2007) Revisiting estimates of CTL killing rates in vivo. PLoS ONE 2:e1301
Zhang J, Lipton HL, Perelson AS et al (2013) Modeling the acute and chronic phases of Theiler murine encephalomyelitis virus infection. J Virol 87:4052–4059

Fidelity Variants and RNA Quasispecies

Antonio V. Bordería, Kathryn Rozen-Gagnon and Marco Vignuzzi

Abstract By now, it is well established that the error rate of the RNA-dependent RNA polymerase (RdRp) that replicates RNA virus genomes is a primary driver of the mutation frequencies observed in RNA virus populations—the basis for the RNA quasispecies. Over the last 10 years, a considerable amount of work has uncovered the molecular determinants of replication fidelity in this enzyme. The isolation of high- and low-fidelity variants for several RNA viruses, in an expanding number of viral families, provides evidence that nature has optimized the fidelity to facilitate genetic diversity and adaptation, while maintaining genetic integrity and infectivity. This chapter will provide an overview of what fidelity variants tell us about RNA virus biology and how they may be used in antiviral approaches.

Contents

1 RNA Virus Mutation Rates and Mutators/Antimutators in the Microbial World 304
2 RNA Virus High-Fidelity Variants/Antimutators 305
3 RNA Virus Low-Fidelity Variants/Mutators 306
4 Is There a Natural Range in RdRp Fidelity? 308
5 RdRp Structure 308
6 Structural and Kinetic Basis of Fidelity 310
7 In Vitro Trends of Fidelity Variants 311
8 In Vivo Trends of Fidelity Variants 312
9 Fidelity Variants as Vaccine Candidates 315
10 Fidelity Variants and Lethal Mutagenesis 316
References 317

Antonio Borderia and Kathryn Rozen-Gagnon have contributed equally to this work.

A.V. Bordería · K. Rozen-Gagnon · M. Vignuzzi (✉)
Institut Pasteur, 28 rue du Dr Roux, 75724 Paris cedex 15, France
e-mail: marco.vignuzzi@pasteur.fr

Current Topics in Microbiology and Immunology (2016) 392: 303–322
DOI 10.1007/82_2015_483

Published Online: 25 October 2015

1 RNA Virus Mutation Rates and Mutators/Antimutators in the Microbial World

RNA viruses possess the highest mutation rates in nature. As calculated by Drake et al. (1998), Drake and Holland (1999), even the comparatively modest retroviruses, generating 0.1 mutations per genome per replication cycle, lead to enormous variation in viral progeny. RNA virus mutation rates are therefore magnitudes higher than DNA organisms, such as *Escherichia coli* (0.0025) or *Saccharomyces cerevisiae* (0.0027). This is in large part due to the lack of proofreading mechanisms in their RNA-dependent RNA polymerases (RdRps).

Are mutation rates fixed for a given organism? High- and low-fidelity variants in *E. coli* and yeast were already described as early as the 1970s (Flury et al. 1976; Gillin and Nossal 1976). Three principal mechanisms contribute to fidelity in *E. coli*: intrinsic polymerase fidelity (how many correct versus incorrect nucleotides are incorporated), exonuclease proofreading activity, and DNA mismatch repair (Schaaper 1993). These mechanisms can be altered to obtain variants with altered replication fidelity. Interestingly, work in *E. coli* also suggested that mutation rates in a given organism are not fixed, but are dynamic. For instance, at least one percent of natural isolates are mutator variants (Jyssum 1960; Gross and Siegel 1981; LeClerc et al. 1996). Remarkably, by passaging *E. coli* for 10,000 generations in a limited glucose environment, Sniegowski et al. (1997) showed that some bacterial populations develop mutation rates one- or twofold higher than wild type, suggesting that in fluctuating environments mutator alleles are potentially beneficial (Taddei et al. 1997).

Following work in bacteria, studies in T4 bacteriophage and herpes simplex virus demonstrated that these observations could be extended to DNA viruses (Muzyczka et al. 1972; Hall et al. 1984). In some cases, these strains were missing essential proofreading functions, and in other cases, point mutations in the polymerase led to altered correct nucleotide incorporation rates (Muzyczka et al. 1972; Reha-Krantz et al. 1991). For retroviruses, some base analog-resistant HIV strains were reported with reverse transcriptase mutations (e.g., M184V) that altered the fidelity of this RNA-dependent DNA polymerase. However, the measurement of the fidelities of these strains was controversial and not clearly established until recently (Wainberg et al. 1996; Bakhanashvili et al. 1996; Dapp et al. 2013; Keulen et al. 1999; Mansky et al. 2000). The most recent discoveries that intrinsic RdRp fidelity can be altered allowed researchers to examine how restricting (high-fidelity/antimutator) or expanding (low-fidelity/mutator) viral population diversity impacts viral pathogenesis, adaptability, and evolution.

2 RNA Virus High-Fidelity Variants/Antimutators

The first *bona fide* high-fidelity variant of an RNA virus was isolated independently by two laboratories (Pfeiffer and Kirkegaard 2003; Vignuzzi et al. 2006), by serially passaging poliovirus in the presence of ribavirin to select for resistant variants. The incorporation of ribavirin directly into nascent genomes during poliovirus replication results in transition mutations, principally A → G, G → A or C → U, with detrimental effects to the virus. Sequencing of the polymerase gene of the ribavirin-resistant population revealed one amino acid change, G64S. It was hypothesized that resistance was due to (a) a more active polymerase, simply generating more progeny genomes permitting better survival; (b) a polymerase that no longer recognized ribavirin as a base analog; or (c) an overall increase in polymerase fidelity and selection of the correct nucleotide. Several observations supported this last mechanism: G64S exhibited the same replication as wild-type virus in single-cycle infections; G64S generated fewer escape mutants to antiviral compounds; and G64S was also resistant to base analogs of different structure (Pfeiffer and Kirkegaard 2003; Vignuzzi et al. 2006). In parallel, a biochemical study confirmed that G64S was a high-fidelity enzyme by directly demonstrating that the rate of incorrect nucleotide incorporation was fourfold lower than wild type (Arnold et al. 2005), and direct sequencing of genomes revealed that the mutation frequency was sixfold lower in the G64S population (Vignuzzi et al. 2006). Additionally, introducing the amino acids A, T, V, or L at position 64 also generated high-fidelity variants (Vignuzzi et al. 2008).

Following these studies in poliovirus, performing passages in mutagens to generate resistant variants became a general strategy for isolating high-fidelity/antimutator variants (Beaucourt et al. 2011). Coxsackie virus B3, also from the *Picornaviridae* family, was treated with moderate concentrations of ribavirin or 5-azacytidine (5-AZC, another RNA mutagen). Within 10–20 passages, a new mutation, A372V, arose in the RdRp. This mutation alone conferred resistance to the effects of three RNA mutagens at high concentrations, and its increased fidelity was confirmed by sequencing and biochemical assays (Levi et al. 2010). Guided by the high-fidelity poliovirus studies, Sadeghipour et al. (2013) identified G64R and G64T as ribavirin-resistant variants of human enterovirus 71 (HEV71). Although altered growth kinetics make results more difficult to interpret, at least one variant, G64R, was a *bona fide* antimutator. In addition, serial passaging of HEV71 in ribavirin led to another mutation in the RdRp, S264L, that conferred resistance and increased fidelity (Sadeghipour et al. 2013). Recently, another group found a mutation in the HEV71 RdRp, L123F, that increased fidelity (Meng and Kwang 2014). Finally, a high-fidelity polymerase variant was found for foot-and-mouth disease virus (FMDV, also in the *Picornaviridae* family), selected by serial passage in the RNA mutagen, 5-fluorouracil (5-FU). The resistance phenotype correlated with the appearance of mutation R84H in the RdRp. This mutation also conferred cross-resistance to ribavirin and 5-AZC, and mutation frequencies were significantly lower than wild-type virus (Zeng et al. 2013).

The same group later isolated a quadruple polymerase mutant (D5N:A38V:M194I:M296V or DAMM) that exhibited a twofold decrease in replication errors, yet was not cross-resistant to other mutagens (Zeng et al. 2014), which raises questions as to whether DAMM is truly high-fidelity.

More recently, a number of high-fidelity RdRp variants have been described outside of the picornavirus family. A high-fidelity chikungunya virus C483Y was obtained during serial passage in ribavirin and 5-FU (Coffey et al. 2011). As with picornavirus high-fidelity variants, this variant was resistant to multiple RNA mutagens and generated populations with more restricted genetic diversity than wild-type virus. A mutagen-resistant influenza A virus variant, PB1-V43I, was also shown to increase fidelity (Cheung et al. 2014). Two mutations in the West Nile virus NS5 RdRp were also shown to confer mutagen resistance and fidelity increases (Van Slyke et al. 2015). Thus, mutagen resistance has proven to be a useful strategy for isolating variants with high-fidelity polymerases.

3 RNA Virus Low-Fidelity Variants/Mutators

The first RdRp variant that was confirmed to have lower fidelity was the FMDV M296I mutant, which, unexpectedly, was isolated in a screen for resistance to ribavirin. Interestingly, the mutant spectrum generated by this variant did not contain the bias toward transition mutations expected after exposure to ribavirin, and the complexity of the mutant spectrum was similar to the wild-type virus in the absence of ribavirin (Sierra et al. 2007). Further passage of M296I in ribavirin resulted in selection of a triple mutant, M296I:P44S:P169S, that was resistant to ribavirin without acquiring resistance to other mutagens such as 5-FU (Agudo et al. 2010). Collectively, these data support the hypothesis that these variants specifically resist ribavirin incorporation during RNA synthesis. Indeed, biochemical studies showed that while the M296I polymerase incorporated twofold less RTP than wild-type enzyme, it generated twofold more A → G transitions. This explains both the lack of mutagenesis in the presence of ribavirin as well as the lack of lower mutant frequencies.

Although informative, this FMDV M296I variant appears to be an exception to the rule. Generally, one would expect mutagen sensitivity, rather than resistance, to be a hallmark of low fidelity. However, selection for mutagen-sensitive variants is more challenging, so how to generate low-fidelity variants? In one case, influenza viruses with mutator phenotypes were isolated by selecting for escape variants by single plaque transfers during sequential treatment with monoclonal antibodies (Suárez et al. 1992). This work preceded other studies of RdRp fidelity by over a decade and did not go further to confirm whether the mutator status mapped to the polymerase genes. For the most part, low-fidelity RdRp variants have been identified by performing site-directed mutagenesis on targeted residues near the catalytic site. This approach was proven successful with both HIV and poliovirus polymerases (Martin-Hernandez et al. 1996; Korneeva and Cameron 2007).

Additionally, poliovirus fidelity was lowered by introducing an amino acid change (T362I) near the catalytic site of the poliovirus RdRp (Liu et al. 2013). An initial study on mutagens of Coxsackie virus B3 uncovered a low-fidelity RdRp variant, S299T (Levi et al. 2010). A more recent study targeted residues in Coxsackie virus B3 based on their implication in the closely related poliovirus fidelity network and on predicted polymerase structure during catalysis (Arnold et al. 2005; Gong and Peersen 2010). Nine lower fidelity variants were isolated that presented elevated mutation frequencies (Gnädig et al. 2012) (Fig. 1a). For FMDV, 5 low-fidelity variants were recently shown to increase mutation frequencies and render the variants more susceptible to mutagenesis (Xie et al. 2014). In order to obtain low-fidelity variants for chikungunya virus, all possible amino acids were swapped into polymerase position 483, which was previously shown to result in a high-fidelity enzyme (C483Y) (Rozen-Gagnon et al. 2014) (Fig. 1b). Three variants proved to be low-fidelity: C483A, C483G, and C483W. Since the cysteine in position 483 is highly conserved among the alphaviruses, similar mutations in Sindbis virus at the analogous position 482 also generated two mutators, C482A and C482G. For West Nile virus, a T248I mutation in the methyl transferase domain of the NS5 protein was shown to decrease replication fidelity, likely

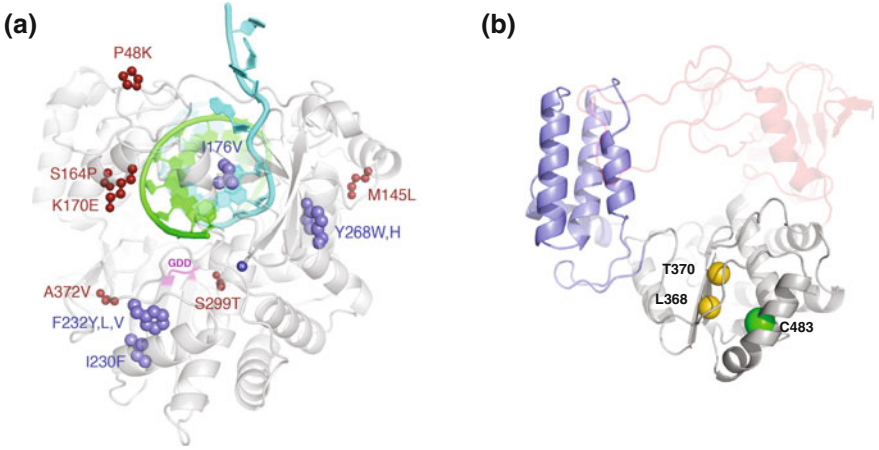

Fig. 1 Viral polymerase structures. **a** Coxsackie virus B3 structure depicting the positions of all viable low-fidelity mutants (*blue*) likely to favor or alter different conformational states of the polymerase active site. The locations of compensatory mutations are shown in *red*. Adapted from (Liu et al. 2013). **b** Structural homology model of the CHIK nsp4 core polymerase showing the predicted locations of C483 (*green sphere*) and two nearby residues (L368 and T370, shown as *gold spheres*) that are the structural equivalents of known fidelity-altering sites in Coxsackie virus polymerase (positions I230 and F232, respectively, panel a) (Liu et al. 2013). Adapted from (Gnädig et al. 2012). Three domains are depicted in this figure: (1) the polymerase palm domain (*gray*), where the fidelity-altering mutations are located, is modeled with fairly high confidence because of the large number of conserved polymerase sequence motifs (motifs A–D); (2) the thumb domain (*purple*); (3) the fingers (*red*). Domains where the modeling is weak are shown as semitransparent

through an interaction with the NS5 RdRp (Van Slyke et al. 2015). Finally, Eckerle and colleagues mutagenized the active sites needed for coronavirus 3-5′ exonuclease activity. Ablating coronavirus (CoV) proofreading activity resulted in 15-fold (murine hepatitis virus; MHV-CoV) (Eckerle et al. 2007) or a 21-fold (severe acute respiratory syndrome; SARS-CoV) (Eckerle et al. 2010) increases in mutation frequencies.

4 Is There a Natural Range in RdRp Fidelity?

The majority of viral fidelity variants identified have been significantly attenuated in vivo; as a consequence, fidelity variants are rarely observed in natural isolates. However, the phenotypic and genotypic assays used to discriminate between these fidelity changes may not be sensitive enough to detect subtle differences among natural isolates. Furthermore, given the quasispecies nature of RNA virus populations, it is not known whether fidelity variants exist at low frequencies within the mutant spectrum and whether they would modulate overall population fidelity. For instance, Coxsackie virus B3 mutator strains that presented mutation frequencies nearer to wild-type values did not display attenuated phenotypes (Gnädig et al. 2012). This raises the possibility that slightly elevated mutation rates could be advantageous in conditions that require more rapid adaptation. Interestingly, the A372V and S299T Coxsackie virus variants, respectively, presenting moderately higher and lower fidelities, exist as natural isolates. Threonine at position 299 is found in 5 % of the isolates, while valine at position 372 is found in 86 % (Harrison et al. 2008). It is thus possible that at any given time, a RNA virus quasispecies contains a subpopulation of mutators and antimutators, whose frequencies may fluctuate when environmental pressures require more rapid evolution or better maintenance of genetic integrity. Importantly, the study of fidelity variants in tissue culture has been nearly exclusively performed in highly permissible, immortalized cell lines during only a few replication cycles. Recent studies show that the mutation rates and frequencies of viruses can dramatically change depending on cell type (Rozen-Gagnon et al. 2014; Combe and Sanjuan 2014). Therefore, under more stringent selective pressures, the fidelity of RNA viruses may be adjusted. Indeed, evolution of mutation rates has been observed in bacteria during colonization in vivo or in conditions of starvation (Sniegowski et al. 1997). A similar phenomenon may occur for RNA viruses, but this remains to be demonstrated.

5 RdRp Structure

The error-prone viral RdRp is a primary source of the diversity we observe in RNA virus populations. Indeed, most RNA virus fidelity variants isolated have contained mutations in the RdRp (the only exceptions thus far have been the mutator

coronaviruses lacking exonuclease activity) (Eckerle et al. 2007, 2010). The RdRp has a structure conserved across virus families. RdRp structures have been solved for members of the *Flaviviridae*, including hepatitis C virus, bovine viral diarrhea virus, Japanese encephalitis virus, West Nile virus, and dengue virus (Lu and Gong 2013; Yap et al. 2007; Malet et al. 2007; Choi et al. 2004; Bressanelli et al. 1999; Lesburg et al. 1999); the *Calciviridaie*, including rabbit hemorrhagic disease virus, Norwalk virus, sapovirus, reovirus λ3, and bacteriophage ϕ6 (Ng et al. 2002, 2004; Fullerton et al. 2007; Butcher et al. 2001; Salgado et al. 2004; Tao et al. 2002); the *Picornaviridae*, including Coxsackie virus B3, poliovirus, FMDV, HEV71, human rhinovirus, and encephalomyocarditis virus (Chen et al. 2013; Gruez et al. 2008; Love et al. 2004; Ferrer-Orta 2004; Appleby et al. 2005; Thompson and Peersen 2004; Hansen et al. 1997; Vives-Adrian et al. 2014); the *Birnaviridae,* including infectious bursal disease virus (Pan et al. 2007); and the *Orthomyxoviridae*, including influenza A virus (He et al. 2008). All these polymerases have a "right-handed" architecture, which is comprised of finger, palm, and thumb domains. The RdRps exist in a closed hand formation, accomplished by connections between the finger and thumb domains [for review see (Ferrer-Orta et al. 2006; Ng et al. 2008)]. Loops extending from the fingers (fingertips) surround the active site and create the entrance to the template channel, where template recognition occurs (Butcher et al. 2001; Ferrer-Orta 2004; O'Farrell et al. 2003). The template channel itself connects the fingers to the active site, located in the palm. The palm is made up of a three-stranded β-sheet and 3 α-helices and is a highly conserved feature. This catalytic domain contains 7 conserved motifs (A–G) present in all RdRps thus far, which catalyze the nucleotidyl transfer reaction.

The enzymatic function relies on a *two-metal-ion* mechanism proposed for all polymerases. This mechanism was first shown for RdRps using the poliovirus RdRp (Ng et al. 2008; Steitz 1998; Arnold et al. 1999). The incoming nucleotide enters the active site with metal ion B, which orients the NTP in the active site using the β- and γ-phosphates of the NTP and a conserved aspartic acid (Asp) in motif A. Following this, metal ion A binds the α-phosphate group of the NTP, the Asp of motif A, and another conserved Asp in motif C. In addition, metal ion A binds the 3′-OH of the nascent RNA strand, lowering the 3′-OH affinity for the H to allow nucleophilic attach of the NTP α-phosphate (Ng et al. 2008; Steitz 1998). Therefore, two protons are transferred during this reaction (Castro et al. 2007): one from the nascent RNA 3′-OH to an unknown acceptor and one to the pyrophosphate (PPi) leaving group from a general acid, usually a lysine, in Motif D (Castro et al. 2009; Cameron et al. 2009). The presence of this general acid greatly enhances the efficiency of catalysis (Castro et al. 2009) (Fig. 1a, b).

6 Structural and Kinetic Basis of Fidelity

The structures of wild-type and RdRp fidelity variants are essentially identical, having only one or few amino acid changes, indicating that structural dynamics of nucleotide addition are more likely to alter fidelity than large-scale structural changes (Cameron et al. 2009; Marcotte et al. 2007). The isolation of the high-fidelity variant G64S and the design of novel substrates for biochemical studies uncovered the mechanisms of nucleotide addition. This novel symmetrical substrate, called sym/sub, was a self-complementary 10-nucleotide heteropolymeric RNA primer. Regardless of the orientation of enzyme binding, both 3′-OHs permit extension of the substrate (Arnold and Cameron 2000). Using sym/sub, five kinetic steps are observed during the incorporation of a single nucleotide to a nascent RNA, called the single-nucleotide addition cycle. This cycle, which is most likely conserved for all RdRps, begins with (1) NTP binding to the enzyme-template complex (ER_nNTP), followed by a conformational change (2), which allows the complex becomes catalytically active ($*ER_nNTP$). (3) Phosphodiester bonds are then formed between the incoming nucleotide and the nascent strand ($*ER_{n+1}PP_i$), leading to a second conformational change (4) ($ER_{n+1}PP_i$), followed by (5) pyrophosphate release (ER_{n+1})(Arnold and Cameron 2004; Arnold et al. 2004)(Fig. 2).

It has been shown that steps 2 (first conformational change) and 3 (phosphoryl transfer) are partially rate-limiting in the single-nucleotide addition cycle and therefore likely to influence fidelity. Step 2 involves reorientation of the triphosphate of the NTP to be available for phosphoryl transfer, and interactions with residues in the ribose-binding pocket. These interactions should be altered for an incorrect bound nucleotide, reducing the stability of complex with the bound nucleotide and the rate of the following phosphoryl transfer (Arnold and Cameron 2004; Arnold et al. 2004; Gohara et al. 2000). Therefore, residues in the binding pocket should be crucial for determining if the correct nucleotide is present (Gohara et al. 2004). Indeed, several conserved residues play major roles in orienting and stabilizing the incoming NTP (Gohara et al. 2000, 2004). Once the triphosphate is properly oriented, it is stabilized by a hydrogen bond network within residues of the binding pocket, mostly located in motif A. Additionally, in motif A, Asp-238 interacts with the 3′OH, and in motif B, Asn-297 interacts with the 2'OH to tightly hold the incoming triphosphate in the proper orientation. Asn-238 was also shown to be crucial for NTP orientation in the FMDV RdRp (Ferrer-Orta et al. 2007). Furthermore, Asp-238 and motif A are conserved in all animal virus RdRps

Fig. 2 The five kinetic steps in the single-nucleotide addition cycle. ER, enzyme-template complex. *ER, active enzyme-template complex. PP, phosphodiester bond. Adapted from (Arnold and Cameron 2000, 2004)

(Koonin 1991). Based on this work, it was proposed that the binding pocket can be divided into a universal portion (motif A) and an adapted portion (motif B). These motifs intersect in the nucleotide-binding pocket, where motif A carries out the universal enzymatic functions and motif B is involved with nucleotide selection. Motif A residue Asp-238 presumably links the rate of phosphoryl transfer to the selection of the nucleotide, reducing the transfer efficiency when the incorrect nucleotide is bound (Gohara et al. 2004). Both the hydrogen bond network and interactions between the triphosphate and these specific binding pocket residues determine the stability of the active complex and the rate of the following phosphoryl transfer.

Recent work also links motif D to the efficiency and fidelity of newly incorporated nucleotides. A conserved lysine (L359 in poliovirus) was shown to act as a general acid to protonate the PP_i (Castro et al. 2009). New results indicate that this motif D lysine might interact with the β-phosphate of the NTP to achieve an active (closed) enzyme conformation. Furthermore, binding of the incorrect NTP shifts the RdRp conformation away from the active state, and the motif D lysine must be protonated in order to achieve the RdRp active state (Yang et al. 2012). This may explain why poliovirus mutants in motif D have altered fidelity phenotypes (Liu et al. 2013; Castro et al. 2009; Yang et al. 2012). The dynamic changes of motif D (shown by nuclear magnetic resonance) (Cameron et al. 2009) were previously masked in crystal structures of RdRps in elongation complexes (Gong and Peersen 2010; Ferrer-Orta et al. 2007).

Although residue 64 is remote from the active site (in the fingers domain), G64S polymerase was shown to have a lower equilibrium constant for the conformational change that orients and stabilizes the incoming NTP (step 2). In fact, this residue is indirectly connected to motif A via hydrogen bonds; substitution of an S in this position ablates hydrogen bonding, explaining the reduced equilibrium constant for step 2 (Arnold et al. 2005). Although it is unclear how G64S could be connected to motif D, a conformational change was found to occur in motif D for G64S when the incorrect nucleotide is bound that does not occur for the wild-type polymerase. This decreases G64S′ ability to switch to the catalytically active form when the incorrect nucleotide is bound, leading to a higher fidelity polymerase (Arnold et al. 2005; Yang et al. 2010, 2012). Similar mechanisms were shown to be involved for the equivalent mutation in FMDV (G62S) (Ferrer-Orta et al. 2010).

7 In Vitro Trends of Fidelity Variants

It is somewhat difficult to make generalizations from biochemical experiments examining fidelity, which are only available for poliovirus, FMDV, and Coxsackie virus B3. Although there are some exceptions (Arias et al. 2008), it seems that higher fidelity polymerases tend to be kinetically slower, and low-fidelity polymerases tend to be faster. Notably, this was shown to be the case for high-fidelity

poliovirus G64S and FMDV G62S (Arnold et al. 2005; Yang et al. 2010; Ferrer-Orta et al. 2010), and low-fidelity poliovirus and CVB3 strains (Liu et al. 2013; Gnädig et al. 2012). The kinetic proofreading hypothesis predicts that there is most likely a trade-off between fast or faithful replication (Coffey et al. 2011; Hopfield 1974). Without proofreading mechanisms (which is the case for the majority of RNA viruses), increased accuracy may only be achieved by reducing the rate of polymerization. This allows decreased stability of incorrect nucleotides and higher dissociation constants, resulting in a preference for the correct nucleotide. This phenomenon is well supported from structural and biochemical studies with poliovirus (Arnold et al. 2005; Castro et al. 2009; Yang et al. 2010, 2012). It has also been shown that biochemical fidelity assays correlate well with in vitro tissue culture measurements of mutation frequencies (Gnädig et al. 2012).

However, there are discrepancies between relative rates of nucleotide incorporation in biochemical assays using RdRp enzymes versus overall virus growth in tissue culture. For example, even though biochemical data suggested that G46S poliovirus had a 2.5-fold reduced yield from assembled elongation complexes, it grew identically to wild type in one-step growth curves. This is not necessarily surprising; given that a single-nucleotide incorporation cycle is cell-free solution is not equivalent to a complete viral life cycle within infected cells (including binding, entry, replication, packaging, and egress). Interestingly, growing G64S in competition with wild type did reveal a reduced relative fitness (Arnold et al. 2005). This in vitro growth pattern has since developed as a recurring trend. Most RdRp fidelity variants (high and low) grow similarly to wild type in isolation, but in competition with wild type suffer replicative fitness costs (Zeng et al. 2014; Coffey et al. 2011; Gnädig et al. 2012; Furió et al. 2005; Levi et al. 2010). Some studies with reverse transcriptase anti/mutators show that the further the mutation frequency from wild type, the lower the relative fitness in competition assays (Dapp et al. 2013; Furió et al. 2007). Important exceptions to this general rule are the MHV and SARS coronavirus mutators lacking 5-3′ exonuclease activity. These variants exhibited clear and stable defects (up to one log) in replication compared to the wild type (Eckerle et al. 2007, 2010; Graham et al. 2012).

8 In Vivo Trends of Fidelity Variants

Fidelity variants generate more or fewer mutations than wild-type viruses without presenting altered consensus sequences with respect to their parental strains. Therefore, they have proven to be invaluable tools to address the role of the mutant spectrum in virus fitness and the behavior of quasispecies in vivo. Although major growth defects are generally not observed in vitro, in vivo attenuation seems to be the general rule for fidelity variants (Fig. 3). The precedent for in vivo attenuation was set with the G64S poliovirus high-fidelity variant. Pfeiffer and Kirkegaard

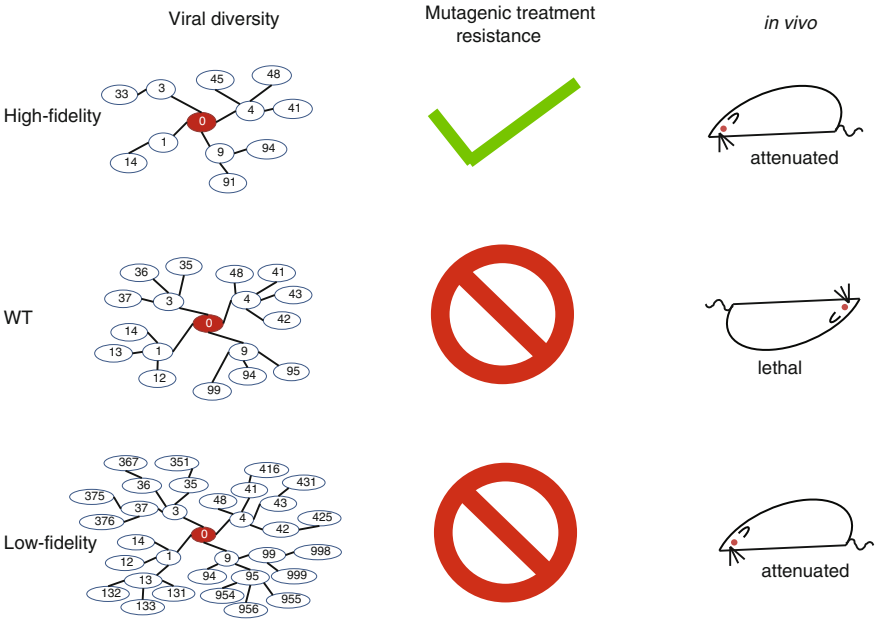

Fig. 3 Schematic depicting the effects of viral diversity, due to viral polymerase fidelity changes, on mutagenic drug resistance and attenuation in vivo. The numbers in the viral diversity schematic are arbitrary illustrations meant to represent genetically inter-connected progeny genomes, comprising populations with low, normal, and high degrees of diversity

(2005) demonstrated that G64S was less pathogenic than wild-type virus in mice, despite not finding significant replication differences in vitro. Vignuzzi et al. (2006) also demonstrated an attenuated phenotype for G64S, where the 50 % lethal dose (LD_{50}) in mice was 300-fold higher than in wild type. Furthermore, while both virus populations could colonize and infect spleens, kidneys, muscles, and intestines when a systemic inoculation was performed, G64S was unable to disseminate more distally to infect the CNS or to be shed in feces. Sequencing of individual genomes from the high-fidelity population in vivo confirmed its restricted genetic diversity. In this study, the restricted quasispecies of G64S was artificially expanded by mutagen treatment to present the same number of mutations as wild type. Importantly, the expanded G64S population ($G64S^{eQS}$) recovered the ability to infect and colonize the spinal cord and brain and had a similar lethal dose compared to wild type. Furthermore, coinfections of a restricted G64S population with either wild type or $G64S^{eQS}$ allowed the genetically restricted G64S population to invade the spinal cord and brain. This seminal work provided strong evidence that not only consensus changes impact virulence and pathogenesis, but that mutant spectrum complexity can also be critical to pathogenesis and/or virus survival in vivo (although this is not always the case). This study also provided

indirect evidence that cooperative interactions within the quasispecies may play a role in virus infection and disease progression. Since this first report, altering mutation frequency has been linked to attenuation in animal models for several variants. A recent study with FMDV also demonstrated that the higher their fidelity, the greater the attenuation in a newborn mouse model (Zeng et al. 2014). For HEV71, the higher fidelity G64R and S264L variants alone or in combination were attenuated in mice (Sadeghipour and McMinn 2013). More recently, another HEV71 antimutator, L123F, also exhibited reduced virulence and delayed symptoms in the AG129 mouse model (Meng and Kwang 2014). Finally, the chikungunya virus, high-fidelity variant, C483Y, was more quickly cleared in the newborn mouse model and was moderately attenuated in mosquitoes (Coffey et al. 2011). Significant attenuation was also observed in colonized and field mosquitoes infected with West Nile virus high-fidelity variants (Van Slyke et al. 2015). While the high-fidelity influenza A virus replicated to wild-type-like titers in the lungs of infected mice, lethality and neurotropism were reduced ten-fold (Cheung et al. 2014).

Similar trends have been observed with low-fidelity/mutator variants. Mice inoculated with the SARS-CoV strain lacking exonuclease activity (ExoN) exhibited reduced symptoms and more rapid clearance of virus from the lungs. Furthermore, the ExoN mutant retained elevated mutation frequencies in vivo (Graham et al. 2012). Coxsackie virus B3 mutator strains exhibited reduced titers in several target organs in the mouse model and were unable to establish persistent infection. Generally, the degree of attenuation correlated with the extremity of the mutator phenotype (Gnädig et al. 2012). A recent study demonstrated higher survival in mice inoculated with a low-fidelity poliovirus (Liu et al. 2013). For the alphaviruses, the low-fidelity variants of chikungunya virus showed reduced titers in all tissues tested in mice, including the primary target tissue (muscle). Similarly, a Sindbis virus mutator was attenuated in mice, presenting fewer neurological symptoms (such as limb paralysis) and was also attenuated in the fruit fly model, *Drosophila melanogaster* (Rozen-Gagnon et al. 2014) (Fig. 3). The low-fidelity NS5 methyl transferase variant of West Nile virus was also shown to be compromised in the mosquito host (Van Slyke et al. 2015).

Some exceptions to this rule do exist: In FMDV, the high-fidelity R84H presented a 1.4-fold increase in mutation frequency that did not result attenuation in mice (Zeng et al. 2013). A possible explanation for this lack of mutation is that these variants manifest only moderate differences in mutation frequencies (under twofold), compared to the attenuated variants described for FMDV. Therefore, there may be a threshold for mutation frequency, below which no attenuation is observed. In support of this threshold, a recent study demonstrated that for a range of low-fidelity FMDV RdRp variants, the more extreme mutators were attenuated in vivo, while those presenting twofold increases in mutation frequency retained virulence (Xie et al. 2014). Similar data were found in Coxsackie virus B3 (Gnädig et al. 2012), and only mutators with the highest mutation frequencies were

attenuated. Consequently, this threshold should be different depending on the virus and its ability to cope with increased mutational load (Graci et al. 2012).

9 Fidelity Variants as Vaccine Candidates

Based on the nearly universal attenuation of fidelity variants in vivo, such strains are being explored as live attenuated vaccines (LAVs). Very few groups have used fidelity variants to elicit protection, but these studies have been promising. A first study examined immunogenicity and protection of the original high-fidelity G64S poliovirus, as well as high-fidelity strains G64A/V/T/L, in mice. The authors observed reduced viral shedding and high neutralizing antibody titers (indeed, higher than those induced by inoculation with the Sabin vaccine strain). Importantly, immunization conferred long-term protection; 6 months after a single immunization with fidelity variants, the majority of mice survived lethal challenge with wild-type poliovirus (Vignuzzi et al. 2008). A second study evaluated the SARS-CoV ExoN mutator as a vaccine candidate and showed that the mutator remains attenuated even in immunocompromised or aged mice (groups of concern during routine immunizations). In addition, immunization with the mutator strain elicited antibody responses and conferred resistance against lethal challenge; no virus was detectable in the lungs of immunized mice (Graham et al. 2012). LAVs have proven more efficacious than subunit vaccine counterparts, but pose safety concerns [for review see (Lauring et al. 2010)]. One principal concern in LAVs is reversion to virulence, which has been observed for a number of LAVs, including the Sabin strains of poliovirus (Cann et al. 1984). While mutator strains raise the question of safety and stability as LAVs because they generate more mutations than wild-type viruses, the SARS-CoV ExoN mutator was shown to remain stable in mouse models. Likewise, when the ExoN mutator was allowed to establish a persistent infection in SCID mice for up to 30 days, no reversion was detected at inactivated exonuclease sites. Interestingly, one of the attenuating mutations present in the RdRp of the Sabin strain of poliovirus was shown to decrease fidelity. This raises the possibility that in currently used vaccines, attenuation is already achieved in part by altering the natural fidelity of an RNA virus (although whether the strain including all attenuating mutations retains this lower fidelity has not been shown) (Liu et al. 2013). In addition, the high-fidelity G64S/A/V/T/L polioviruses passaged in mice did not revert at position 64 and remained attenuated. For LAV development high-fidelity variants may be of particular interest, since lowered mutation frequencies make mutations conferring virulence less likely to occur. Indeed, under selective pressure to revert in vivo, high-fidelity variants were less able to do so, whereas the wild-type virus quickly reverted at a significantly higher number of sites (Vignuzzi et al. 2008). Since fidelity-altering mutations map to single or few residues, combining these with other conventional attenuating mutations may be a good strategy to further reduce reversion to virulence.

10 Fidelity Variants and Lethal Mutagenesis

Viruses appear to have fine-tuned their mutation rate in order to maximize adaptation, while at the same time maintaining genomic integrity. Deviation from these optimized mutation rates have been shown to be attenuating. The proposed explanation for the observed attenuation is mutational meltdown, losing the ability to maintain genetic information due to the extrinsic increase in mutation rates (Eigen 1971; Domingo et al. 2005). Importantly, a consequence of the study of lethal mutagenesis as an antiviral approach was the discovery of the high-fidelity variants, which generally were more resistant to mutation-inducing drugs. This discovery further boosted interest in determining how viral mutation rates could be modulated intrinsically, leading to the isolation of more fidelity variants. Large panels of high- and low-fidelity variants are now available to feedback into the research on lethal mutagenesis as an antiviral approach: Due to their altered sensitivity to such compounds, they are excellent tools to investigate the mutagenic activities of known compounds or identify new mutagenic compounds. Indeed, the first high- and low-fidelity variants of Coxsackie virus B3 were key in identifying a previously unknown mutagenic activity for amiloride compounds (Levi et al. 2010). Similar screens using compound libraries may thus identify other classes of antivirals with mutagenic effects (Table 1).

Table 1 List of published high- and low-fidelity polymerase variants

Virus	Position RdRp	Phenotype	Reference
Poliovirus	G64S	High-fidelity	Pfeiffer and Kirkegaard (2003), Vignuzzi et al. (2006)
CVB3	A372V	High-fidelity	Levi et al, plos pathogens
	I176V	Low-fidelity	Gnädig et al. (2012)
	L241I	Low-fidelity	Gnädig et al. (2012)
	S164P	Low-fidelity	Gnädig et al. (2012)
	P48K	Low-fidelity	Gnädig et al. (2012)
	A239G	Low-fidelity	Gnädig et al. (2012)
	Y268W	Low-fidelity	Gnädig et al. (2012)
	Y268H	Low-fidelity	Gnädig et al. (2012)
	F232Y	Low-fidelity	Gnädig et al. (2012)
	I230F	Low-fidelity	Gnädig et al. (2012)
HEV71	G64R	High-fidelity	Sadeghipour et al. (2013)
	S264L	High-fidelity	Sadeghipour et al. (2013)
	L123F	High-fidelity	Meng and Kwang (2014)
FMDV	R84H	High-fidelity	Zeng et al. (2013)
	D5N/A38V/M194I/M296V	High-fidelity	Zeng et al. (2014)
	M296I	Low-fidelity	Arias et al. (2008)

(continued)

Table 1 (continued)

Virus	Position RdRp	Phenotype	Reference
	M296I/P44S/P169S	Low-fidelity	Arias et al. (2008)
	D165E	Low-fidelity	Xie et al. (2014)
	K172R	Low-fidelity	Xie et al. (2014)
	K177R	Low-fidelity	Xie et al. (2014)
	G361S	Low-fidelity	Xie et al. (2014)
	Y241F	Low-fidelity	Xie et al. (2014)
FLU	unknown	Low-fidelity	Suárez et al. (1992)
	PB1-V43I	High-fidelity	Cheung et al. (2014)
CHIKV	C483Y	High-fidelity	Coffey et al. (2011)
	C483A	Low-fidelity	Rozen-Gagnon et al. (2014)
	C483G	Low-fidelity	Rozen-Gagnon et al. (2014)
	C483W	Low-fidelity	Rozen-Gagnon et al. (2014)
SINV	C482A	Low-fidelity	Rozen-Gagnon et al. (2014)
	C482G	Low-fidelity	Rozen-Gagnon et al. (2014)
WNV	T248I	Low-fidelity	Van Slyke et al. (2015)
	V793I	High-fidelity	Van Slyke et al. (2015)
	G806R	High-fidelity	Van Slyke et al. (2015)
MHV-CoV	3-5′ exonuclease (ExoN)	Low-fidelity	Eckerle et al. (2007)
SARS-CoV	3-5′ exonuclease (ExoN)	Low-fidelity	Eckerle et al. (2010)

References

Agudo R, Ferrer-Orta C, Arias A, la Higuera de I, Perales C, Pérez-Luque R, Verdaguer N, Domingo E (2010) A multi-step process of viral adaptation to a mutagenic nucleoside analogue by modulation of transition types leads to extinction-escape. Plos Pathogens 6:e1001072

Appleby TC, Luecke H, Shim JH, Wu JZ, Cheney IW, Zhong W, Vogeley L, Hong Z, Yao N (2005) Crystal structure of complete rhinovirus RNA polymerase suggests front loading of protein primer. J Virol 79:277–288

Arias A, Arnold JJ, Sierra M, Smidansky ED, Domingo E, Cameron CE (2008) Determinants of RNA-dependent RNA polymerase (in) fidelity revealed by kinetic analysis of the polymerase encoded by a foot-and-mouth disease virus mutant with reduced sensitivity to ribavirin. J Virol 82:12346–12355

Arnold JJ, Cameron CE (2000) Poliovirus RNA-dependent RNA polymerase (3D(pol)). Assembly of stable, elongation-competent complexes by using a symmetrical primer-template substrate (sym/sub). J Biol Chem 275:5329–5336

Arnold JJ, Cameron CE (2004) Poliovirus RNA-dependent RNA polymerase (3D pol): pre-steady-state kinetic analysis of ribonucleotide incorporation in the presence of Mg^{2+}. Biochemistry 43:5126–5137

Arnold JJ, Ghosh SKB, Cameron CE (1999) Poliovirus RNA-dependent RNA Polymerase (3Dpol) divalent cation modulation of primer, template, and nucleotide selection. J Biol Chem 274:37060–37069

Arnold JJ, Gohara DW, Cameron CE (2004) Poliovirus RNA-dependent RNA polymerase (3D pol): pre-steady-state kinetic analysis of ribonucleotide incorporation in the presence of Mn^{2+}. Biochemistry 43:5138–5148

Arnold JJ, Vignuzzi M, Stone JK, Andino R, Cameron CE (2005) Remote site control of an active site fidelity checkpoint in a viral RNA-dependent RNA polymerase. J Biol Chem 280:25706–25716

Bakhanashvili M, Avidan O, Hizi A (1996) Mutational studies of human immunodeficiency virus type 1 reverse transcriptase: the involvement of residues 183 and 184 in the fidelity of DNA synthesis. FEBS Lett 391:257–262

Beaucourt S2P, Border 237 AAV, Coffey LL, Gn 228 Dig NF, Sanz-Ramos M, Beeharry Y, Vignuzzi M (2011) Isolation of fidelity variants of RNA viruses and characterization of virus mutation frequency. J Vis Exp 52

Bressanelli S, Tomei L, Roussel A, Incitti I, Vitale RL, Mathieu M, De Francesco R, Rey FA (1999) Crystal structure of the RNA-dependent RNA polymerase of hepatitis C virus. Proc Natl Acad Sci 96:13034–13039

Butcher SJ, Grimes JM, Makeyev EV, Bamford DH, Stuart DI (2001) A mechanism for initiating RNA-dependent RNA polymerization. Nature 410:235–240

Cameron CE, Moustafa IM, Arnold JJ (2009) Dynamics: the missing link between structure and function of the viral RNA-dependent RNA polymerase? Curr Opin Struct Biol 19:768–774

Cann AJ, Stanway G, Hughes PJ, Minor PD, Evans DMA, Schild GT, Almond JW (1984) Reversion to neurovirulence of the live-attenuated Sabin type 3 oral poliovirus vaccine. Nucleic Acids Res 12:7787–7792

Castro C, Smidansky E, Maksimchuk KR, Arnold JJ, Korneeva VS, Götte M, Konigsberg W, Cameron CE (2007) Two proton transfers in the transition state for nucleotidyl transfer catalyzed by RNA- and DNA-dependent RNA and DNA polymerases. Proc Natl Acad Sci 104:4267–4272

Castro C, Smidansky ED, Arnold JJ, Maksimchuk KR, Moustafa I, Uchida A, Götte M, Konigsberg W, Cameron CE (2009) Nucleic acid polymerases use a general acid for nucleotidyl transfer. Nat Struct Mol Biol 16:212–218

Chen C, Wang Y, Shan C, Sun Y, Xu P, Zhou H, Yang C, Shi P-Y, Rao Z, Zhang B et al (2013) Crystal structure of enterovirus 71 RNA-dependent RNA polymerase complexed with its protein primer VPg: implication for a trans mechanism of VPg uridylylation. J Virol 87:5755–5768

Cheung PPH, Watson SJ, Choy K-T, Fun Sia S, Wong DDY, Poon LLM, Kellam P, Guan Y, Malik Peiris JS, Yen H-L (2014) Generation and characterization of influenza A viruses with altered polymerase fidelity. Nat Commun 5:4794

Choi KH, Groarke JM, Young DC, Kuhn RJ, Smith JL, Pevear DC, Rossmann MG (2004) The structure of the RNA-dependent RNA polymerase from bovine viral diarrhea virus establishes the role of GTP in de novo initiation. Proc Nat Acad Sci USA 101:4425–4430

Coffey LL, Beeharry Y, Bordería AV, Blanc H, Vignuzzi M (2011) Arbovirus high fidelity variant loses fitness in mosquitoes and mice. Proc Natl Acad Sci USA 108:16038–16043

Combe M, Sanjuan R (2014) Variation in RNA virus mutation rates across host cells. PLoS Pathog 10:e1003855

Dapp MJ, Heineman RH, Mansky LM (2013) Interrelationship between HIV-1 fitness and mutation rate. J Mol Biol 425:41–53

Domingo E, Escarmís C, Lázaro E, Manrubia SC (2005) Quasispecies dynamics and RNA virus extinction. Virus Res 107:129–139

Drake JW, Holland JJ (1999) Mutation rates among RNA viruses. Proc Natl Acad Sci 96:13910–13913

Drake JW, Charlesworth B, Charlesworth D, Crow JF (1998) Rates of spontaneous mutation. Genetics 148:1667–1686

Eckerle LD, Lu X, Sperry SM, Choi L, Denison MR (2007) High fidelity of murine hepatitis virus replication is decreased in nsp14 exoribonuclease mutants. J Virol 81:12135–12144

Eckerle LD, Becker MM, Halpin RA, Li K, Venter E, Lu X, Scherbakova S, Graham RL, Baric RS, Stockwell T et al (2010) Infidelity of SARS-CoV Nsp14-exonuclease mutant virus replication is revealed by complete genome sequencing. PLoS Pathog 6:e1000896

Eigen M (1971) Selforganization of matter and the evolution of biological macromolecules. Naturwissenschaften 58:465–523
Ferrer-Orta C (2004) Structure of foot-and-mouth disease virus RNA-dependent RNA polymerase and its complex with a template-primer RNA. J Biol Chem 279:47212–47221
Ferrer-Orta C, Arias A, Escarmis C, Verdaguer N (2006) A comparison of viral RNA-dependent RNA polymerases. Curr Opin Struct Biol 16:27–34
Ferrer-Orta C, Arias A, Pérez-Luque R, Escarmís C, Domingo E, Verdaguer N (2007) Sequential structures provide insights into the fidelity of RNA replication. Proc Nat Acad Sci 104:9463–9468
Ferrer-Orta C, Sierra M, Agudo R, la Higuera de I, Arias A, Perez-Luque R, Escarmis C, Domingo E, Verdaguer N (2010) Structure of foot-and-mouth disease virus mutant polymerases with reduced sensitivity to ribavirin. J Virol 84:6188–6199
Flury F, Von Borstel RC, Williamson DH (1976) Mutator activity of petite strains of Saccharomyces cerevisiae. Genetics 83:645–653
Fullerton SWB, Blaschke M, Coutard B, Gebhardt J, Gorbalenya A, Canard B, Tucker PA, Rohayem J (2007) Structural and functional characterization of sapovirus RNA-dependent RNA polymerase. J Virol 81:1858–1871
Furió V, Moya A, Sanjuán R (2005) The cost of replication fidelity in an RNA virus. Proc Natl Acad Sci 102:10233–10237
Furió V, Moya A, Sanjuán R (2007) The cost of replication fidelity in human immunodeficiency virus type 1. Proc Biol Sci 274:225–230
Gillin FD, Nossal NG (1976) Control of mutation frequency by bacteriophage T4 DNA polymerase. I. The CB120 antimutator DNA polymerase is defective in strand displacement. J Biol Chem 251:5219–5224
Gnädig NF, Beaucourt S, Campagnola G, Bordería AV, Sanz-Ramos M, Gong P, Blanc H, Peersen OB, Vignuzzi M (2012) Coxsackievirus B3 mutator strains are attenuated in vivo. Proc Natl Acad Sci USA 109:E2294–E2303
Gohara DW, Crotty S, Arnold JJ, Yoder JD, Andino R, Cameron CE (2000) Poliovirus RNA-dependent RNA polymerase (3Dpol): structural, biochemical, and biological analysis of conserved structural motifs A and B. J Biol Chem 275:25523–25532
Gohara DW, Arnold JJ, Cameron CE (2004) Poliovirus RNA-dependent RNA polymerase (3D pol): kinetic, thermodynamic, and structural analysis of ribonucleotide selection. Biochemistry 43:5149–5158
Gong P, Peersen OB (2010) Structural basis for active site closure by the poliovirus RNA-dependent RNA polymerase. Proc Natl Acad Sci 107:22505–22510
Graci JD, Gnädig NF, Galarraga JE, Castro C, Vignuzzi M, Cameron CE (2012) Mutational robustness of an RNA virus influences sensitivity to lethal mutagenesis. J Virol 86:2869–2873
Graham RL, Becker MM, Eckerle LD, Bolles M, Denison MR, Baric RS (2012) A live, impaired-fidelity coronavirus vaccine protects in an aged, immunocompromised mouse model of lethal disease. Nat Med 18:1820–1826
Gross MD, Siegel EC (1981) Incidence of mutator strains in *Escherichia coli* and coliforms in nature. Mutat Res Lett 91:107–110
Gruez A, Selisko B, Roberts M, Bricogne G, Bussetta C, Jabafi I, Coutard B, De Palma AM, Neyts J, Canard B (2008) The crystal structure of coxsackievirus B3 RNA-dependent rna polymerase in complex with its protein primer VPg confirms the existence of a second VPg binding site on picornaviridae polymerases. J Virol 82:9577–9590
Hall JD, Coen DM, Fisher BL, Weisslitz M, Randall S, Almy RE, Gelep PT, Schaffer PA (1984) Generation of genetic diversity in herpes simplex virus: an antimutator phenotype maps to the DNA polymerase locus. Virology 132:26–37
Hansen JL, Long AM, Schultz SC (1997) Structure of the RNA-dependent RNA polymerase of poliovirus. Structure 5:1109–1122
Harrison DN, Gazina EV, Purcell DF, Anderson DA, Petrou S (2008) Amiloride derivatives inhibit coxsackievirus B3 RNA replication. J Virol 82:1465–1473

He X, Zhou J, Bartlam M, Zhang R, Ma J, Lou Z, Li X, Li J, Joachimiak A, Zeng Z et al (2008) Crystal structure of the polymerase PA(C)-PB1(N) complex from an avian influenza H5N1 virus. Nature 454:1123–1126

Hopfield JJ (1974) Kinetic proofreading: a new mechanism for reducing errors in biosynthetic processes requiring high specificity. Proc Nat Acad Sci 71:4135–4139

Jyssum K (1960) Observations on two types of genetic instability in *Escherichia coli*. Acta Pathologica Microbiol Scand 48:113–120

Keulen W, van Wijk A, Schuurman R, Berkhout B, Boucher Charles AB (1999) Increased polymerase fidelity of lamivudine-resistant HIV-1 variants does not limit their evolutionary potential. Aids 13:1343–1349

Koonin EV (1991) The phylogeny of RNA-dependent RNA polymerases of positive-strand RNA viruses. J Gen Virol 72(Pt 9):2197–2206

Korneeva VS, Cameron CE (2007) Structure-function relationships of the viral RNA-dependent RNA polymerase: fidelity, replication speed, and initiation mechanism determined by a residue in the ribose-binding pocket. J Biol Chem 282:16135–16145

Lauring AS, Jones JO, Andino R (2010) Rationalizing the development of live attenuated virus vaccines. Nat Biotechnol 28:573–579

LeClerc JE, Li B, Payne WL, Cebula TA (1996) High mutation frequencies among *Escherichia coli* and Salmonella pathogens. Science 274:1208–1211

Lesburg CA, Cable MB, Ferrari E, Hong Z, Mannarino AF, Weber PC (1999) Crystal structure of the RNA-dependent RNA polymerase from hepatitis C virus reveals a fully encircled active site. Nat Struct Biol 6:937–943

Levi LI, Gnädig NF, Beaucourt S, McPherson MJ, Baron B, Arnold JJ, Vignuzzi M (2010) Fidelity Variants of RNA Dependent RNA Polymerases Uncover an Indirect, Mutagenic Activity of Amiloride Compounds 6:e1001163

Levi LI, Gnädig NF, Beaucourt S, McPherson MJ, Baron B, Arnold JJ, Vignuzzi M (2010b) Fidelity variants of RNA dependent RNA polymerases uncover an indirect, mutagenic activity of amiloride compounds. PLoS Pathog 6:e1001163

Liu X, Yang X, Lee CA, Moustafa IM, Smidansky ED, Lum D, Arnold JJ, Cameron CE, Boehr DD (2013) Vaccine-derived mutation in motif D of poliovirus RNA-dependent RNA polymerase lowers nucleotide incorporation fidelity. J Biol Chem 288:32753–32765

Love RA, Maegley KA, Yu X, Ferre RA, Lingardo LK, Diehl W, Parge HE, Dragovich PS, Fuhrman SA (2004) The crystal structure of the RNA-dependent RNA polymerase from human rhinovirus. Structure 12:1533–1544

Lu G, Gong P (2013) Crystal structure of the full-length Japanese encephalitis virus NS5 reveals a conserved methyltransferase-polymerase interface. PLoS Pathog 9:e1003549

Malet H, Egloff MP, Selisko B, Butcher RE, Wright PJ, Roberts M, Gruez A, Sulzenbacher G, Vonrhein C, Bricogne G et al (2007) Crystal structure of the RNA polymerase domain of the West Nile virus non-structural protein 5. J Biol Chem 282:10678–10689

Mansky LM, Bernard LC (2000) 3′-Azido-3′-deoxythymidine (AZT) and AZT-resistant reverse transcriptase can increase the in vivo mutation rate of human immunodeficiency virus type 1. J Virol 74:9532–9539

Marcotte LL, Wass AB, Gohara DW, Pathak HB, Arnold JJ, Filman DJ, Cameron CE, Hogle JM (2007) Crystal structure of poliovirus 3CD protein: virally encoded protease and precursor to the RNA-dependent RNA polymerase. J Virol 81:3583–3596

Martin-Hernandez AM, Domingo E, Menendez-Arias L (1996) Human immunodeficiency virus type 1 reverse transcriptase: role of Tyr115 in deoxynucleotide binding and misinsertion fidelity of DNA synthesis. EMBO J 15:4434–4442

Meng T, Kwang J (2014) Attenuation of human enterovirus 71 high-replication-fidelity variants in AG129 mice. J Virol 88:5803–5815

Muzyczka N, Poland RL, Bessman MJ (1972) Studies on the biochemical basis of spontaneous mutation. I. A comparison of the deoxyribonucleic acid polymerases of mutator, antimutator, and wild type strains of bacteriophage T4. J Biol Chem 247:7116–7122

Ng K, Cherney MM, Vázquez AL (2002) Crystal structures of active and inactive conformations of a caliciviral RNA-dependent RNA polymerase. J Biol Chem 277:1381–1387
Ng K, Pendás-Franco N, Rojo J, Boga JA (2004) Crystal structure of Norwalk virus polymerase reveals the carboxyl terminus in the active site cleft. J Biol Chem 279:16638–16645
Ng KKS, Arnold JJ, Cameron CE (2008) Structure-function relationships among RNA-dependent RNA polymerases. Curr Top Microbiol Immunol 320:137–156
O'Farrell D, Trowbridge R, Rowlands D, Jäger J (2003) Substrate complexes of hepatitis C virus RNA polymerase (HC-J4): structural evidence for nucleotide import and de-novo initiation. J Mol Biol 326:1025–1035
Pan J, Vakharia VN, Tao YJ (2007) The structure of a birnavirus polymerase reveals a distinct active site topology. Proc Nat Acad Sci 104:7385–7390
Pfeiffer JK, Kirkegaard K (2003) A single mutation in poliovirus RNA-dependent RNA polymerase confers resistance to mutagenic nucleotide analogs via increased fidelity. Proc Natl Acad Sci USA 100:7289–7294
Pfeiffer JK, Kirkegaard K (2005) Increased fidelity reduces poliovirus fitness and virulence under selective pressure in mice. PLoS Pathog 1:e11
Reha-Krantz LJ, Stocki S, Nonay RL, Dimayuga E, Goodrich LD, Konigsberg WH, Spicer EK (1991) DNA polymerization in the absence of exonucleolytic proofreading: in vivo and in vitro studies. Proc Natl Acad Sci 88:2417–2421
Rozen-Gagnon K, Stapleford KA, Mongelli V, Blanc H, Failloux A-B, Saleh M-C, Vignuzzi M (2014) Alphavirus mutator variants present host-specific defects and attenuation in mammalian and insect models. PLoS Pathog 10:e1003877
Sadeghipour S, McMinn PC (2013) A study of the virulence in mice of high copying fidelity variants of human enterovirus 71. Virus Res 176:265–272
Sadeghipour S, Bek EJ, McMinn PC (2013) Ribavirin-resistant mutants of human enterovirus 71 express a high replication fidelity phenotype during growth in cell culture. J Virol 87:1759–1769
Salgado PS, Makeyev EV, Butcher SJ, Bamford DH, Stuart DI, Grimes JM (2004) The structural basis for RNA specificity and Ca2+ inhibition of an RNA-dependent RNA polymerase. Structure 12:307–316
Schaaper RM (1993) Base selection, proofreading, and mismatch repair during DNA replication in *Escherichia coli*. J Biol Chem 268:23762–23765
Sierra M, Airaksinen A, Gonzalez-Lopez C, Agudo R, Arias A, Domingo E (2007) Foot-and-mouth disease virus mutant with decreased sensitivity to ribavirin: implications for error catastrophe. J Virol 81:2012–2024
Sniegowski PD, Gerrish PJ, Lenski RE (1997) Evolution of high mutation rates in experimental populations of *E. coli*. Nature 387:703–705
Steitz TA (1998) Structural biology: a mechanism for all polymerases. Nature 391:231–232
Suárez P, Valcárcel J, Ortín J (1992) Heterogeneity of the mutation rates of influenza A viruses: isolation of mutator mutants. J Virol 66:2491–2494
Taddei F, Radman M, Maynard-Smith J, Toupance B, Gouyon PH, Godelle B (1997) Role of mutator alleles in adaptive evolution. Nature 387:700–702
Tao Y, Farsetta DL, Nibert ML, Harrison SC (2002) RNA synthesis in a cage–structural studies of reovirus polymerase lambda3. Cell 111:733–745
Thompson AA, Peersen OB (2004) Structural basis for proteolysis-dependent activation of the poliovirus RNA-dependent RNA polymerase. EMBO J 23:3462–3471
Van Slyke GA, Arnold JJ, Lugo AJ, Griesemer SB, Moustafa IM, Kramer LD, Cameron CE, Ciota AT (2015) Sequence-specific fidelity alterations associated with west nile virus attenuation in mosquitoes. PLoS Pathog 11:e1005009
Vignuzzi M, Stone JK, Arnold JJ, Cameron CE, Andino R (2006) Quasispecies diversity determines pathogenesis through cooperative interactions in a viral population. Nature 439:344–348
Vignuzzi M, Wendt E, Andino R (2008) Engineering attenuated virus vaccines by controlling replication fidelity. Nat Med 14:154–161

Vives-Adrian L, Lujan C, Oliva B, van der Linden L, Selisko B, Coutard B, Canard B, van Kuppeveld FJM, Ferrer-Orta C, Verdaguer N (2014) The crystal structure of a cardiovirus RNA-dependent RNA polymerase reveals an unusual conformation of the polymerase active site. J Virol 88:5595–5607

Wainberg MA, Drosopoulos WC, Salomon H, Hsu M, Borkow G, Parniak MA, Gu Z, Song Q, Manne J, Islam S et al (1996) Enhanced fidelity of 3TC-selected mutant HIV-1 reverse transcriptase. Science 271:1282–1285

Xie X, Wang H, Zeng J, Li C, Zhou G, Yang D, Yu L (2014) Foot-and-mouth disease virus low-fidelity polymerase mutants are attenuated. Arch Virol 159:2641–2650

Yang X, Welch JL, Arnold JJ, Boehr DD (2010) Long-range interaction networks in the function and fidelity of poliovirus RNA-dependent RNA polymerase studied by nuclear magnetic resonance. Biochemistry 49:9361–9371

Yang X, Smidansky ED, Maksimchuk KR, Lum D, Welch JL, Arnold JJ, Cameron CE, Boehr DD (2012) Motif D of viral RNA-dependent RNA polymerases determines efficiency and fidelity of nucleotide addition. Structure 20:1519–1527

Yap TL, Xu T, Chen Y-L, Malet H, Egloff M-P, Canard B, Vasudevan SG, Lescar J (2007) Crystal structure of the dengue virus RNA-dependent RNA polymerase catalytic domain at 1.85-angstrom resolution. J Virol 81:4753–4765

Zeng J, Wang H, Xie X, Yang D, Zhou G, Yu L (2013) An increased replication fidelity mutant of foot-and-mouth disease virus retains fitness in vitro and virulence in vivo. Antiviral Res 100:1–7

Zeng J, Wang H, Xie X, Li C, Zhou G, Yang D, Yu L (2014) Ribavirin-resistant variants of foot-and-mouth disease virus: the effect of restricted quasispecies diversity on viral virulence. J Virol 88:4008–4020

Antiviral Strategies Based on Lethal Mutagenesis and Error Threshold

Celia Perales and Esteban Domingo

Abstract The concept of error threshold derived from quasispecies theory is at the basis of lethal mutagenesis, a new antiviral strategy based on the increase of virus mutation rate above an extinction threshold. Research on this strategy is justified by several inhibitor-escape routes that viruses utilize to ensure their survival. Successive steps in the transition from an organized viral quasispecies into loss of biologically meaningful genomic sequences are dissected. The possible connections between theoretical models and experimental observations on lethal mutagenesis are reviewed. The possibility of using combination of virus-specific mutagenic nucleotide analogues and broad-spectrum, non-mutagenic inhibitors is evaluated. We emphasize the power that quasispecies theory has had to stimulate exploration of new means to combat pathogenic viruses.

Contents

1 Introduction. Quasispecies Dynamics as an Obstacle for Virus Disease Control 324
2 Mechanisms of Antiviral Resistance 325
3 Error Catastrophe, Lethal Defection, and Lethal Mutagenesis: Deleterious Effects of Mutations in Theoretical Replicons and Viruses 328
4 Quasispecies Dynamics and New Lethal Mutagenesis-Based Antiviral Designs 333

C. Perales · E. Domingo (✉)
Centro de Biología Molecular "Severo Ochoa" (CSIC-UAM), Consejo Superior de Investigaciones Científicas (CSIC), Campus de Cantoblanco, 28049 Madrid, Spain
e-mail: edomingo@cbm.csic.es

C. Perales
e-mail: cperales@cbm.csic.es

C. Perales · E. Domingo
Centro de Investigación Biomédica En Red de Enfermedades Hepáticas y Digestivas (CIBERehd), Barcelona, Spain

C. Perales
Liver Unit, Internal Medicine, Laboratori of Malalties Hepàtiques, Vall d'Hebron Institut de Recerca-Hospital Universitari Vall d'Hebron, Universitat Autonoma de Barcelona, 08035, Barcelona, Spain

Current Topics in Microbiology and Immunology (2016) 392: 323–339
DOI 10.1007/82_2015_459

Published Online: 21 August 2015

5 Potential of Sequential Treatments 335
6 Summary and Prospects 336
References 337

1 Introduction. Quasispecies Dynamics as an Obstacle for Virus Disease Control

High mutation rates and quasispecies dynamics of viruses have as one of their main consequences the continuous supply of variant genomes whose frequency in the population depends on their fitness in each environment. Under natural conditions, the biological environment in which viruses replicate is changing continuously in such a manner that the fitness landscapes should be depicted as extremely rugged and variable, like waves with peaks and valleys in a stormy ocean. Even the "flattest" in its position of advantage (Schuster 2016) pales in the middle of the storm. Rugged fitness landscapes (meaning fitness variations as a function of position in sequence space or the environment) are a consequence of fitness effects of single mutations in viral genomes. Ruggedness does not exclude that different genomes display equal fitness in the same environment or that the same genome displays the same fitness in two different environments.Fitness landscapes in connection with quasispecies theory are studied by Schuster (2016). Rough fitness landscapes are further promoted by the mutant spectrum being itself part of the environment, and its composition being affected by the stochastic nature of mutant generation (see Sect. 3 for evidence of the influence of mutant spectra). An experimental proof of the complex nature of fitness landscape during virus replication is the great number of hidden and transient selective pathways undertaken by viral populations in response to inhibitory activities, as revealed by next-generation sequencing (NGS) (Cale et al. 2011; Fischer et al. 2010; Tsibris et al. 2009). The challenge for theoretical biology to grasp such a level of complexity is enormous, but excitingly, important progress in this direction has been accomplished in recent years, as documented in previous chapters. Thanks to the persistence of some, the gap between theory and experimentation is gradually being bridged. A salient merit of quasispecies theory for virology has been the realization of the implications of successions of dynamic mutant spectra for virus adaptation and survival in the face of selective pressures intended to limit their multiplication. How quasispecies dynamics can inspire new antiviral strategies is the subject of the present chapter.

Important difficulties for the control of viral disease stem from the fact that among the virus variants generated, there are many that can overcome an immune response or replicate in the presence of antiviral inhibitors [reviewed in (Domingo and Schuster 2016; Domingo et al. 2012; Nijhuis et al. 2009; Padmanabhan and Dixit 2016; Perales et al. 2015; Richman 1996)]. Replicating RNA viruses are "moving targets" regarding antiviral interventions. We term inhibitor-escape mutants those that are present or arise in viral populations and that increase in

frequency when the inhibitor is present during replication. A priori, there is no reason for the genomic sites that encode residues that affect sensitivity to inhibitors to be more mutable than the average genomic site in a virus. Inhibitor resistance determinants are generally in protein-coding regions, and there is no evidence that their surrounding nucleotides are in structures predictive of a hot spot for variation (mutation rates above average). Consistently, when viruses have diversified in nature and their populations are large and heterogeneous, mutations related to inhibitor resistance can be present even without prior replication of the virus in the presence of the inhibitor. This fact which by itself constitutes a specific example of the adaptive value of mutant spectra was first documented with natural populations of HIV-1 at a time in which the use of several antiretroviral agents was still limited (Nájera et al. 1995). Many additional cases have been reported for pathogenic viruses that display error-prone replication (reviewed in Domingo et al. 2012). From all evidence, many selective pressures to which viruses are subjected during their replication cycles remain undefined, such is the complexity of the virus–host interactions, no matter the level at which we examine them. Fortunately, in the case of viral inhibitors, the selective pressure is well defined and quantifiable: it is adequate for scientific scrutiny and for preclinical explorations.

2 Mechanisms of Antiviral Resistance

The frequency of mutations that confer resistance to one or several inhibitors depends on two parameters: the genotypic barrier to resistance and the phenotypic barrier to resistance. The two parameters are linked to two key concepts of quasispecies: transitions in sequence space and fitness (Domingo and Schuster 2016; Schuster 2016). The genetic barrier is determined by the number and types of mutations required to go from a drug-sensitive virus into a resistant one. A low genetic barrier means that only one step (one mutation) in sequence space is sufficient for the phenotypic transition toward resistance, and for most viral polymerases, transition mutations (those that occur among purines or pyrimidines) are more frequent than transversion mutations (those that occur between purines and pyrimidines). The shorter the distance in sequence space and the easier to produce the needed mutations, the lower the genetic barrier to drug resistance.

The phenotypic barrier to resistance is more difficult to specify in molecular terms since it is given by the fitness cost that the virus has to endure as a consequence of acquisition of the mutations needed for resistance. In this case, the type of mutation is not a relevant determinant, since even a frequent transition can produce a deleterious amino acid change or a perturbation in a regulatory region (through a change in secondary or higher order structure in the viral genome). Fitness cost may be due to effects at the RNA or protein level, or both. Since the frequency of individual genomes tends to be ranked according to fitness (compare again with Domingo and Schuster 2016), the higher the fitness cost of a mutation, the lower the frequency of the genome harboring the mutation will be in the mutant spectrum. As a consequence,

the less likely will be the dominance of the resistant mutant in the event that the viral population size undergoes random fluctuations. The reason for fitness cost inflicted by an inhibitor resistance mutation may lie in involvement of the protein targetted by the inhibitor in any of the steps of a virus life cycle. Since most viral proteins are multifunctional, the assignment of fitness decrease to a specific viral function is challenging. The dynamics of mutant testing is such that even mutations that imply a high fitness cost may be present transiently, since compensatory mutations may increase fitness without reversion of the resistance mutations. Such compensatory mutations that do not confer *bona fide* resistance but mediate the survival of inhibitor-resistant mutants have been described for many viruses, and the reader is referred to relevant database compilations.

One of the aims of current therapies is to produce a sharp fitness decrease without allowing time and replicative capacity to the virus to find compensatory mutations and pathways for fitness recovery. That is, the aim is to render fitness loss an irreversible transition. We documented that when a population of foot-and-mouth disease virus (FMDV) is small enough, it can continue replicating minimally without the virus acquiring resistance to an inhibitor present during replication (Perales et al. 2011a). Therefore, a sustained low viral load that may give an opportunity to the host immune system to clear a virus may be also considered a valuable antiviral strategy. The impact of quasispecies dynamics on the survival of virus in the face of administration of inhibitors has been extensively recognized and reviewed from theoretical, experimental, and clinical points of view (Padmanabhan and Dixit 2016). We have previously reviewed several observations and models, with emphasis on hepatitis B virus (HBV), hepatitis C virus (HCV), and human immunodeficiency virus type 1 (HIV-1), that can serve the reader to appreciate the complexity of the problem and to complement the information given in the present book (Domingo et al. 2012). The data banks that compile inhibitor resistance mutations identified in infected patients serve to alert of a possible failure of treatments that include the inhibitor. Unfortunately, the traditional sequence data banks ignore mutant spectra of viral genomes, and relevant biological information is not available when the genetic identity of viruses is limited to consensus sequences (Domingo et al. 2006).

The presence of specific amino acid substitutions that decrease the sensitivity to inhibitors is not the only molecular pathway for a virus to achieve drug resistance. A recently discovered mechanism for HCV is the association of high replicative fitness with multidrug resistance (Sheldon et al. 2014). This finding was possible thanks to the recent implementation of a cell culture system for HCV (Lindenbach et al. 2005; Wakita et al. 2005; Zhong et al. 2005). The system allows the productive infection of human hepatoma cells by a specific chimeric genotype 2a HCV, under controlled laboratory conditions, with prospects of extension to other HCV genotypes (Gerold and Pietschmann 2014; Li et al. 2015). The new cell culture system for HCV allows robust viral production over hundreds of passages, rendering the classic virus passage experiments (Domingo and Schuster 2016) feasible for HCV. The initial virus is the progeny of a transcript from a plasmid introduced into the cells. Therefore, the parental genome has a precise nucleotide sequence to which subsequent genomic variations can be compared. Using this

system, we showed that HCV that had been subjected to 100 passages in human hepatoma cells increased its replicative fitness, and acquired resistance to multiple inhibitors used in anti-HCV therapy, some directed to viral targets and others directed to cellular targets. The fitness increase was accompanied of a broadening of the mutant spectrum, in the sense that the average number of genomes with multiple mutations increased. This raised the question of whether the multidrug resistancemultidrug resistance was due to the broadening of the mutant spectrum that might entail an increase of the frequency of resistance mutations or to the fitness increase. The observed drug resistance was not due to inhibitor resistance mutations, as established by independent experimental tests. One was the absence of known HCV inhibitor mutations in mutant spectra of resistant HCV populations examined by standard molecular cloning and Sanger sequencing, as well as by NGS. In addition, the virus displayed a parallel kinetics of viral production in the absence and presence of inhibitors over a 1000-fold range of the initial multiplicity of infection (MOI, or the number of infecting particles per cell); the parallel kinetics at different MOIs is incompatible with the drug resistance being due to the presence of resistance mutations in a minority of the components of the mutant spectrum. Finally, individual biological clones isolated from the parental, resistant population did not manifest any decrease in resistance, again incompatible with the presence of standard resistance mutations in a minority of mutant spectrum components (Sheldon et al. 2014). Thus, the results have established high fitness (or a trait associated with high fitness) as a new mechanism of multidrug resistance in HCV, and it would not be surprising if the same conclusion proved valid for other viruses.

Therefore, quasispecies dynamics may facilitate resistance to antiviral agents by at least two different mechanisms that may, however, be interconnected: by increase of the complexity of mutant spectra that will display a high proportion of specific resistance mutations and by a fitness increase itself prompted by continued replication in the same environment. Interestingly, fitness, viral load, and population heterogeneity have been previously recognized as related parameters linked to the survival and pathogenic potential of viruses (Domingo et al. 2012). A possible molecular mechanism to explain why fitness is a drug-resistant determinant has been proposed based on the likely competition between the number of replicating viral genomes per cell in the HCV replication complexes (modified cellular membrane sites where the viral polymerase and other viral and cellular proteins colocalize to perform viral RNA synthesis) and the number of inhibitor molecules that can potentially reach their target (Sheldon et al. 2014). Some aspects of this competition model, at present merely tentative, are under investigation in our laboratory. These observations underline that quasispecies features of viral populations encompass multifaced complications for therapeutic interventions. Not surprisingly, it has been amply recognized that new paradigms are necessary to deal with the control of diseases associated with heterogeneous, rapidly evolving pathogens [not only viruses but also bacteria, cellular parasites, and cancer cells, as well as prions and other protein conformation-associated neurological diseases (further justification in Domingo and Schuster 2016)]. Next, we address some strategies to confront the challenge.

3 Error Catastrophe, Lethal Defection, and Lethal Mutagenesis: Deleterious Effects of Mutations in Theoretical Replicons and Viruses

The term "error catastrophe" was first used by Leslie Orgel to describe a cascade of events affecting cellular information that implicated deterioration of both nucleic acid and protein function in connection with the process of aging (Orgel 1963, 1973). Then, the same words were used in quasispecies theory to refer to loss of stability of a mutant distribution when it ceases to be dominated by a master sequence. The concepts behind the cascade of events in aging and loss of viral quasispecies stability are closely related in that modification of key biological macromolecules leads to functional deterioration. Quasispecies stability necessitates that the ratio between fitness of the master genome and fitness of the rest of genomes be above a certain value. The critical ratio depends on the average mutation rate per nucleotide and the complexity of the encoded genetic information that usually can be equated with genome length. For a given genomic complexity, the mutation rate above which the information cannot be maintained is termed the error threshold, expressed as the error threshold relationship. The theoretical origins of the error catastrophe and error threshold concepts are presented in Domingo and Schuster (2016) and Schuster (2016).

The challenge of translating the error threshold concept into experimental evidence was undertaken for the first time by John J. Holland and his colleagues who demonstrated that error frequencies at specific genomic sites of poliovirus (PV) and vesicular stomatitis virus (VSV) could be increased minimally by chemical mutagenesis, therefore proving that mutagenic treatments adversely affected virus infectivity (Holland et al. 1990). This first experimental study was followed by another by Larry Loeb, Jim Mullins, and colleagues who showed that replication of HIV-1 in the presence of the pyrimidine nucleoside analogue 5-hydroxydeoxycytidine (5-OH-dC) as mutagenic agent led to increases in the frequency of G to A transitions, predicted from the misincorporation of 5-OH-dC during reverse transcription, together with loss of HIV-1 replicative potential (Loeb et al. 1999). This mutagenic analogue was at the origin of related compounds, and one of them was later administered in the first mutagen-based clinical trial with AIDS patients [(Mullins et al. 2011); see Sect. 6 in this chapter]. Loeb and colleagues coined the term "lethal mutagenesis" to refer to mutagen-driven lethality. These initial studies were followed by many others that have used purine and pyrimidine analogues licensed for human use to investigate mutagenesis as a means to extinguish viruses that employ different replication strategies (single stranded segmented or unsegmented, positive and negative strand RNA viruses, and retroviruses). The conclusion of these studies has been that viruses do not tolerate substantial increases in mutation rate and that an excess of induced mutations can lead to viral extinction [references for most specific studies can be found in the reviews by (Anderson et al. 2004; Dapp et al. 2013; Domingo 2005; Domingo et al. 2012; Graci and Cameron 2008)], in confirmation of the predictions of quasispecies theory. It should be noted that despite

the generally deleterious effects that mutations have in viruses well adapted to an environment, the results of sensitivity of viruses to increased mutation rates were not necessarily to be expected. Some complex DNA viruses and bacteria not only tolerate increases of mutation rate, but actually their adaptive potential can be enhanced by the incorporation of mutations in the genome. An example is provided by mutator bacteria that benefit of increases in mutation rate of 10^2- to 10^3- fold over basal levels that operate in standard bacteria. Also, in contrast to the early results of Holland and colleagues, the reversion induced by chemical mutagenesis of several mutations of the *Escherichia coli* Lac Z gene tolerated increases in frequency of 10^2- to 10^3-fold, with good survival rates (Cupples and Miller 1989). These observations suggest that the key point is not whether mutations are deleterious or not, but whether a biological system has evolved to replicate near or far from an error (or extinction) threshold that determines its tolerability to mutations. The mutation rates of RNA viruses are poised near a maximum compatible with survival, while they are still effective for adaptation (Domingo 2000; Drake and Holland 1999).

Several theoretical models have been proposed to explain lethal mutagenesis of viruses as well as the relationship between the error threshold of quasispecies theory and lethal mutagenesis; they are discussed in (Tejero et al. 2016). The models range from straightforward arguments such as that extinction is associated with insufficient virus progeny production for the virus to be propagated, to models that conclude that the transition into error catastrophe as defined by quasispecies theory would preclude virus extinction. We will not evaluate such proposals except to state that some of them have failed to incorporate information provided by experimental results, and as stated by Manfred Eigen, "pure theory" can become "poor theory" (Eigen 2013). Here, we will summarize a view that has been based on an increased understanding of how mutagenic agents affect viral genomes at the molecular level, and how the alterations translate into loss of infectivity. The major observations that led to our current understanding of mutagenesis-driven RNA virus extinction are expressed in Fig. 1. The flow of experimental evidence went as follows. The initial studies established an association of mutagenic activity with decreases of infectivity but did not exclude that the effects of mutagenic agents could be unrelated to the mutations introduced in the viral genomes (Loeb et al. 1999; Sierra et al. 2000). A subsequent study on the mutagenic activity of ribavirin on PV documented a decrease of specific infectivity (the ratio between infectivity and amount of viral RNA) concomitantly with an increase in mutant frequency of the viral population, thus reinforcing the conclusion that most antiviral activity of ribavirin was exerted through mutagenesis of the viral genome (Crotty et al. 2001). The critical experiments that led to our current view of the molecular events that underlie mutagenesis-driven extinction were performed by Ana Grande-Perez and colleagues working with the arenavirus lymphocytic choriomeningitis virus (LCMV) (see also Grande-Perez et al. 2016). The key point was the analysis of the kinetics of decrease of infectivity and viral RNA in persistently infected cell cultures treated and untreated with the mutagenic base analogue 5-fluorouracil (FU). The decay of infectivity preceded the decay of viral RNA, suggesting that non-infectious but replication-competent viral RNA was generated during the transition

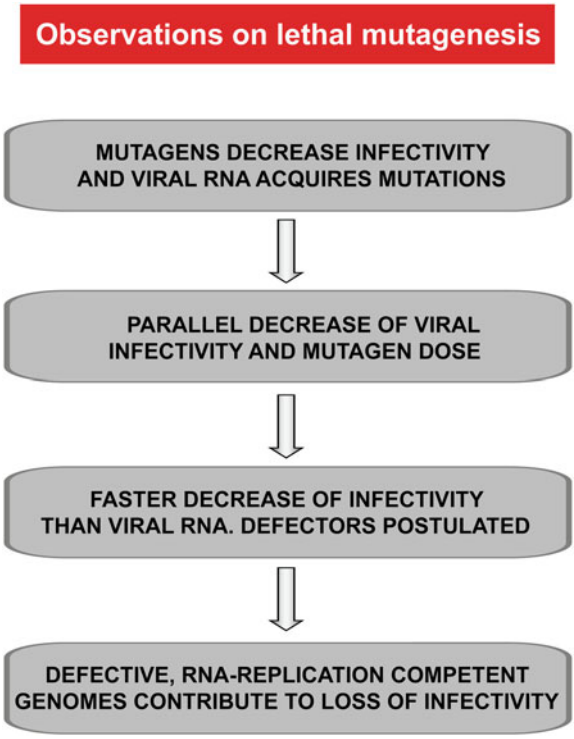

Fig. 1 Flow of the main findings that have converted the concept of error threshold into a viable antiviral strategy. The main experimental and theoretical observations with relevant references are described in the text

toward extinction; the experimental results were supported by a theoretical model developed by Susanna Manrubia that predicted the requirement of a class of defective genomes, termed defectors, in LCMV extinction (Grande-Pérez et al. 2005b).

Two pathways for viral extinction were distinguished: one at low mutagenic intensities that allow viral replication to proceed and generate interfering, defector mutants that jeopardize replication of standard virus and contribute to decrease of infectivity. This pathway was termed lethal defection, and it is now known as the lethal defection model of viral extinction. The second pathway occurs with higher mutagen doses and leads to extinction because the viral quasispecies fails to replicate and to infect (Grande-Pérez et al. 2005b). The final step in Fig. 1 recapitulates experiments with specific foot-and-mouth disease virus capsid and polymerase mutant RNAs that exerted an inhibitory activity on standard, infectious foot-and-mouth disease virus (FMDV) RNA co-electroporated in the same cells (Perales et al. 2007). The inhibitory effect of specific mutants reinforces the lethal defection model of viral extinction which is also in agreement with previous results on the inhibition of FMDV RNA replication by mutagenized pre-extinction FMDV populations (González-López et al. 2004). More recent results with FMDV have documented that infectious clones retrieved from the complex population in which lethal defection takes place display up to 100-fold fitness decreases relative to

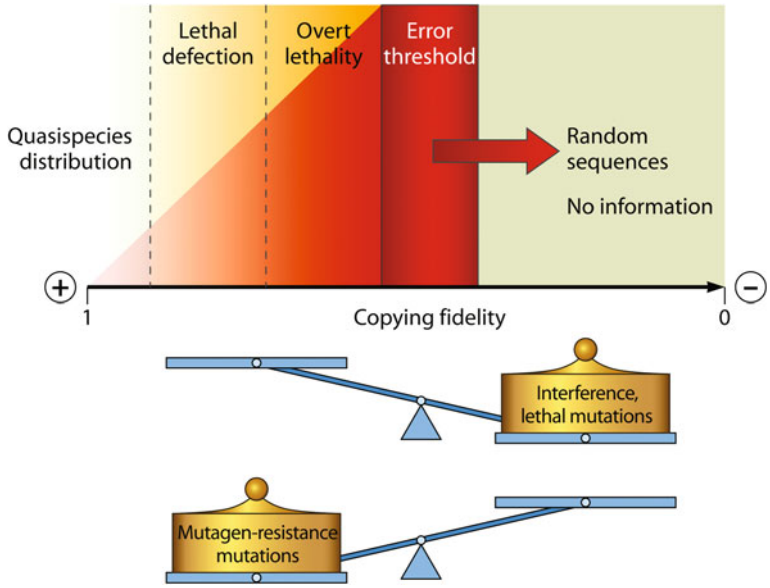

Fig. 2 Scheme that relates the error threshold concept of quasispecies theory with virus extinction by lethal mutagenesis. The profound influence of copying fidelity (horizontal axis) is illustrated by five successive domains corresponding to decreasing fidelity values (increase in error rate). The first domain of quasispecies stability is followed by one of lethal defection (due to generation of interfering genomes) that precedes overt lethality due to accumulation of mutations that drives the system beyond an error threshold, translated into an extinction threshold in the case of viruses. On the right, once the threshold has been crossed, the resulting entity has lost any biological meaning, and it can be thought of as being composed of random sequences devoid of information. Below the diagram, some influences that favor virus extinction and others that favor virus survival are depicted, as justified in the text. The figure is reproduced from Domingo et al. (2012), with permission from the American Society for Microbiology, Washington DC, USA

clones from control populations (Arias et al. 2013). This result suggests an overlap between the lethal defection and overt lethality steps as depicted in Fig. 2 that summarizes our current understanding of lethal mutagenesis. Interestingly, the mechanism of lethal mutagenesis of viruses derived from experimental results fits well the early descriptions of Leslie Orgel in that fitness deterioration was due to collapse of interdependent nucleic acids and protein *trans*-networks (Orgel 1963). The studies of Celia Perales and colleagues with specific defector mutants suggest a molecular mechanism of interference consisting in the production of altered proteins that cannot form functional complexes needed to complete the viral infectious cycle. According to this model, such "defective" complexes can decrease the functionality of the partner that includes unaltered proteins, as visualized in Fig. 3 (Perales et al. 2007). There is yet no direct evidence of the presence of such inactive homopolymeric or heteropolymeric complexes in virus-infected cells subjected to mutagenesis, but the model is consistent with several experimental observations made with different RNA viruses.

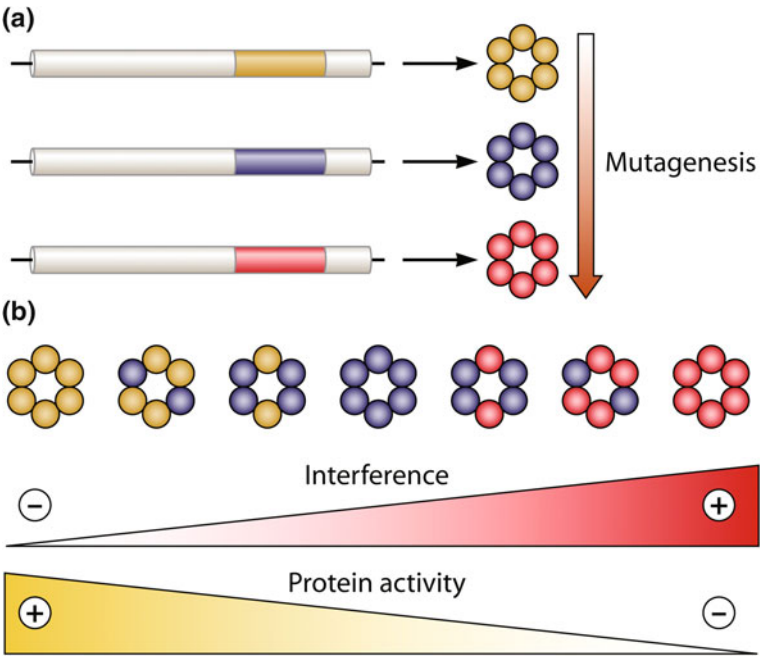

Fig. 3 A model of lethal defection mediated by trans-acting viral gene products. Increased mutagenesis of viral genomes (*vertical arrow*) results in a protein that is active as an hexameric complex, with increasing number of deleterious amino acid substitutions (*yellow*, *blue* and *red*). In a replicating quasispecies, depending on the mutational load, the hexameric protein can display a range of interfering and protein activities, as given by the subunit composition of the hexamer. It is worth noting that the blue subunit may rescue some activity when the red protein is the majority, but may decrease the activity when the yellow protein is the majority. This model assumes that the protein acts in *trans* and that the activity of the hexamer is modulated by the subunit composition. References that justify the model are given in the text. The figure is reproduced from Domingo et al. (2012), with permission from the American Society for Microbiology, Washington DC, USA

The negative effects of increased mutation rates in viruses have to be interpreted not only in terms of proximity to an error threshold as in quasispecies theory, but also in view of the several steps that separate the occurrence of mutations from their functional consequences. Specifically, the effects of mutations have to do with the complex programs of gene expression evolved by viruses which are perfectly exemplified in the present volume by the intricacies of arenavirus–host interactions described by Juan Carlos de la Torre and colleagues (Grande-Perez et al. 2016). Mutations may perturb viral replication in at least two different ways. One is the detrimental effect of any individual mutation on the genome harboring it, due to loss of function. Since many viral are multifunctional (again, among multitude of examples in the literature, Grande-Perez et al. 2016 describe the specific case of arenavirus nucleoprotein), amino acid replacements in a viral protein can have a multiplicative effect that depends on the array of functions in which the protein is involved. A second

mechanism is a consequence of the *trans*-acting activity of many viral , as mentioned in the molecular bases of lethal defection (Fig. 3). When viral proteins are defective due to amino acid substitutions, they can jeopardize replication of other genomes despite the latter expressing a functional protein because many proteins function in association with other proteins in oligomeric or multimeric complexes (Perales et al. 2007) (Fig. 3). The accumulation of mutations, with the resulting amino acid substitutions, triggers an amplification effect in deleteriousness due to the very nature of viral replication cycles.

It may seem that the mechanisms that underlie the violation of an error threshold for stability of genetic information in viruses may be irreconcilably far from the simple mathematical basis proposed by quasispecies theory (loss of superiority of the master sequence). Consideration of the error threshold and events preceding virus extinction from the point of view of the occupation of sequence space suggests that the two events are conceptually closely related. Indeed, loss of superiority of the master sequence can be equated with drift of any mutant sequence in sequence space (Tejero et al. 2016). Random drift in sequence space would lead to viral genomes soon hitting a region incompatible with function, and this possibility is actually supported experimentally. Studies with several mutagens have shown that the effect of a mutagen is to displace viral clouds toward regions of sequence space that are unfavorable for survival. Direct evidence was provided by experiments of selective amplification of A, U-rich subpopulations of FMDV genomes on their way to extinction by ribavirin mutagenesis (Perales et al. 2011b). Movements toward unfavorable regions of sequence space are also suggested by mutant spectrum analyses of other viruses subjected to nucleotide analogue mutagenesis (Agudo et al. 2008; Ortega-Prieto et al. 2013). Thus, in practical terms, loss of virus infectivity is a consequence of delocalization of genomic sequences in sequence space. How such a drift can be applied to antiviral strategies is addressed next.

4 Quasispecies Dynamics and New Lethal Mutagenesis-Based Antiviral Designs

For the crossing of the error threshold value to lead to the elimination of a virus during a natural infection, several conditions must be fulfilled. If the effect of a mutagen is not sufficient to eliminate all viable genomes, and the concentration of mutagenic agent ceases to be effective with time, the virus will rapidly regain its replicative capacity and may re-invade susceptible cells and tissues. The capacity to regain fitness was documented with LCMV in cell culture by quantifying the recovery of infections progeny production after serial rounds of heavy mutagenesis by 5-fluorouracil (a dose that evoked a 10^5- to 10^8-fold decrease in virus titer in infections at a MOI of 0.01 infectious units per cell) followed by recovery passages in the absence of 5-fluorouracil. In the absence of mutagen, viral fitness was transiently impaired, but by passage 2 or 3, progeny production reached normal

levels (Grande-Pérez et al. 2005a). Recovery of viral infectivity upon removal of a mutagenic activity prior to virus extinction was also supported by a theoretical model of virus dynamics in the presence of mutagens and inhibitors that was developed by Susanna Manrubia (Perales et al. 2009).

An important aspect of lethal mutagenesis in vivo is viral compartmentalization into different tissues and organs, a situation that was treated in a theoretical model by Steinmeyer and Wilke (Steinmeyer and Wilke 2009). The model addressed virus sanctuaries or refugia, as well as virus migration among refugia. In clinical practice, in the absence of quantification of inter-compartment migration, it will be desirable to ensure the access of the mutagenic agent to all sites where the virus replicates. This is actually a condition that should be fulfilled in any antiviral intervention, and one of the reasons of resistance to lethal mutagenesis treatments of retroviruses that establish latency mediated by provirus integration.

Despite these limitations, considerable evidence suggests that lethal mutagenesis using base or nucleoside analogues that are licensed for human use or under advanced clinical trials can effectively inhibit viral infections in vivo (Arias et al. 2014; Ruiz-Jarabo et al. 2003). Of particular interest is the introduction of a new nucleoside analogue termed favipiravir or T-705 which is a broad-spectrum antiviral agent, active against many viruses, including viruses of emerging infections with pandemic potential such as Ebola hemorrhagic disease virus (De Clercq 2015; Oestereich et al. 2014; Smither et al. 2014). In many cases, the mechanism of action of favipiravir has not been elucidated, but at least in two virus–host systems, human influenza virus in cell culture and murine norovirus in vivo, this analogue exerts its activity at least partly through lethal mutagenesis (Arias et al. 2014; Baranovich et al. 2013).

The events that allow diagnosing an antiviral activity as being a consequence of lethal mutagenesis are as follows: (i) irreversible loss of viral infectivity and absence of viral RNA in the cells or organism following treatment. (ii) Transient occurrence of the specific types of mutations expected from the base pairing properties of the analogue, prior to virus extinction. Preferred mutation types observed with several viruses are A → G, U → C in the case of 5-fluorouracil and favipiravir, and G → A, C → U in the case of ribavirin. (iii) Decrease of specific infectivity, which is given by the ratio between the amount of infectivity and the amount of viral RNA at a given time point in the course of lethal mutagenesis. This is probably due to the increase in frequency of defective viral genomes that, irrespective of their capacity to replicate genomic RNA, cannot produce infectious particles, at least measured by established experimental methods. The progressive load of defective genomes is consistent with the decrease of infectivity preceding the decrease of viral RNA in the course of treatment, observed with several virus–host systems. In fact, the lack of synchronization of decrease of infectivity and viral RNA was one of the early signs that led to the formulation of the lethal defection model of viral extinction (Grande-Pérez et al. 2005b) (Sect. 3). (iv) Invariance of the consensus sequence during the transition toward extinction (González-López et al. 2005; Grande-Pérez et al. 2005a; Ortega-Prieto et al. 2013). This is expected from the fact that no selection of specific mutants occurs during the transition to

extinction, except in the case in which a mutagen-resistant mutant is selected during treatment, an unlikely occurrence (see Sect. 6). An invariance of consensus sequence is consistent with uncontrolled drift of genomic sequences underlying loss of infectivity, in agreement with some theoretical models (Sect. 3 and Chap. 7). The invariance of consensus sequence in a process that results in virus elimination illustrates how relevant it is to monitor modification of mutant spectra, and how limited is the information provided exclusively by the consensus sequence.

5 Potential of Sequential Treatments

The use of combination therapies, with two or ideally more antiviral agents administered simultaneously, has been successful for the control viral infections because it is a means to greatly increase the genetic barrier to resistance [review in (Domingo et al. 2012); see also Chap. 12]. Our initial experiments using a single mutagenic agent documented also that treatment efficacy was significantly increased by administering a standard, non-mutagenic inhibitor together with the mutagenic agent, particularly to achieve extinction of high-fitness viruses (Pariente et al. 2001, 2003; Tapia et al. 2005). Yet, subsequent experiments, supported by a theoretical model that took into consideration the interplay between a mutagenic and an inhibitory activity during viral replication, indicated that a sequential inhibitor–mutagen administration could be more effective than either the corresponding combination or the converse order of administration (mutagen–inhibitor) (Iranzo et al. 2011, Moreno et al. 2012; Perales et al. 2009, 2012). The advantage of the sequential inhibitor–mutagen administration has two main reasons: (i) the interplay between mutagens and inhibitors; when both are present during viral replication, the mutagen may increase the frequency of inhibitor-resistant mutants thus delaying or preventing extinction; and (ii) the need of defector mutants to replicate their RNA to exert their lethal defection activity. When the inhibitor is present together with the mutagen which is responsible of generating defectors, the inhibitor prevents defector activity (Perales et al. 2007, 2012). Extension of sequential protocols to treat infections in animal models is needed to evaluate their potential as a new antiviral design.

The advantage of a sequential inhibitor–mutagen administration is probably not universal. This suggestion is based upon the fact that the theoretical model of interplay between mutagens and inhibitors predicts a different range of mutagenic and inhibitory activities for which the sequential or combined administration is preferred (Iranzo et al. 2011; Perales et al. 2012). This range has to be defined, both theoretically with replicative parameters and experimentally for each virus–host system. There is no universal predictive diagram. In the experiments carried out with FMDV, we observed that the advantage of the sequential treatment was more accentuated with high concentrations of inhibitor (Perales et al. 2009, 2012). This implies that if the virus to be extinguished displays an intrinsically high inhibitor resistance (as a consequence of any of the resistance mechanisms described in

Sect. 2), the advantage of the sequential treatment may require high inhibitor concentrations that might not be attainable. This is an important point which is now under investigation in our laboratory.

6 Summary and Prospects

The progress that has taken place between the time at which it was discovered that quasispecies dynamics applied to RNA viruses and the time at which we are realistically approaching new antiviral strategies based on the error threshold concept is impressive. The practical influence that quasispecies theory has had in virology is without antecedent. Until the series of observations sketched in Fig. 1 were initiated, it was necessary to dispel the incredulity of the scientific community regarding the high mutation rates that distinguished RNA viruses from cellular genomes. It was also necessary to calculate mutant spectrum complexities to ascertain that the population heterogeneities that render RNA virus mutant clouds were real and portrayed an unprecedented level of intrapopulation diversity. Finally, it was necessary to argue that there was no conceptual barrier for quasispecies to be an adequate framework to explain virus evolution and pathogenesis (Domingo and Schuster 2016). Many authors have contributed to solve the points listed above, but here, we like to stress the contribution of the late John J. Holland in this endeavor. In the outstanding review written in 1982 by Holland et al. (1982), a number of disease implications of rapid RNA genome evolution were proposed, and many of them have been confirmed. It is expected that parallel progress in quasispecies theory and experimental studies (as exemplified in different chapters of this book) will continue to provide new insights in the understanding of RNA viruses and ways to combat them.

Regarding antiviral treatments, some recent developments, not only those related to lethal mutagenesis that we have summarized, offer great promise. Some inhibitors that target cellular functions required for virus replication may be effective and provide a high barrier to resistance. In this line, some inhibitors of nucleotide metabolism have proven to display antiviral activity, not only because they deprive the cell of nucleotide substrates that are needed in large concentrations in the virus replication complexes, but also because they induce in the cells some components of the innate immune response that are active to inhibit virus replication [among several studies, see (Lucas-Hourani et al. 2013; Ortiz-Riano et al. 2014) and references therein]. This class of compounds displays a broad-spectrum antiviral activity, meaning that they can inhibit a considerable number of viruses under different host context. This is expected if the mechanism of action is to evoke a general immune response since the virus must produce a constellation of mutations to overcome it (Perales et al. 2013, 2014). Interestingly, some of the lethal mutagens in use or under investigation are also broad-spectrum antiviral agents, probably due to structural similarities among viral polymerases that render likely the incorporation of nucleotide analogues. It cannot be excluded, however, that the

broad-spectrum antiviral nature of mutagens may be favored by independent mechanisms of activity, as has been well studied in the case of ribavirin. Thus, it may be possible to develop new sequential or combination treatments in which inhibition and mutagenesis, the two legs of the design, produce a broad-spectrum antiviral activity that offers a high genetic and phenotypic barrier to resistance. Quasispecies research is an example of how basic science can lead to unanticipated practical applications.

Acknowledgments We are indebted to many colleagues in our laboratory for their contributions to quasispecies investigation, as reflected in the reference list. Work supported by grants BFU2011-23604 and SAF2014-52400-R from Spanish Ministries, and S2013/ABI-2906 (PLATESA) from Comunidad Autónoma de Madrid and Fundación Ramón Areces. CIBERehd (Centro de Investigación Biomédica en Red de Enfermedades Hepáticas y Digestivas) is funded by Instituto de Salud Carlos III. C.P. is supported by the Miguel Servet program of the Instituto de Salud Carlos III (CP14/00121).

References

Agudo R, Arias A, Pariente N et al (2008) Molecular characterization of a dual inhibitory and mutagenic activity of 5-fluorouridine triphosphate on viral RNA synthesis. Implications for lethal mutagenesis. J Mol Biol 382:652–666

Anderson JP, Daifuku R, Loeb LA (2004) Viral error catastrophe by mutagenic nucleosides. Annu Rev Microbiol 58:183–205

Arias A, Isabel de Avila A, Sanz-Ramos M et al (2013) Molecular dissection of a viral quasispecies under mutagenic treatment: positive correlation between fitness loss and mutational load. J Gen Virol 94:817–830

Arias A, Thorne L, Goodfellow I (2014) Favipiravir elicits antiviral mutagenesis during virus replication in vivo. eLife 3:e03679

Baranovich T, Wong SS, Armstrong J et al (2013) T-705 (favipiravir) induces lethal mutagenesis in influenza A H1N1 viruses in vitro. J Virol 87:3741–3751

Cale EM, Hraber P, Giorgi EE et al (2011) Epitope-specific CD8 + T lymphocytes cross-recognize mutant simian immunodeficiency virus (SIV) sequences but fail to contain very early evolution and eventual fixation of epitope escape mutations during SIV infection. J Virol 85:3746–3757

Crotty S, Cameron CE, Andino R (2001) RNA virus error catastrophe: direct molecular test by using ribavirin. Proc Natl Acad Sci USA 98:6895–6900

Cupples CG, Miller JH (1989) A set of lacZ mutations in Escherichia coli that allow rapid detection of each of the six base substitutions. Proc Natl Acad Sci USA 86:5345–5349

Dapp MJ, Patterson SE, Mansky LM (2013) Back to the future: revisiting HIV-1 lethal mutagenesis. Trends Microbiol 21:56–62

De Clercq E (2015) Ebola virus (EBOV) infection: therapeutic strategies. Biochem Pharmacol 93:1–10

Domingo E (2000) Viruses at the edge of adaptation. Virology 270:251–253

Domingo E, Brun A, Núñez JI et al (2006) Genomics of Viruses. In: Hacker J, Dobrindt U (eds) Pathogenomics: genome analysis of pathogenic microbes. Wiley-VCH Verlag GmbH & Co., KGaA, Weinheim, pp 369–388

Domingo E, Schuster P (2016) What is a quasispecies? Historical origins and current scope. Curr Top Microbiol Immunol doi:10.1007/82_2015_453

Domingo E, Sheldon J, Perales C (2012) Viral quasispecies evolution. Microbiol Mol Biol Rev 76:159–216

Domingo E (ed) (2005) Virus entry into error catastrophe as a new antiviral strategy. Virus Res 107:115–228
Drake JW, Holland JJ (1999) Mutation rates among RNA viruses. Proc Natl Acad Sci USA 96:13910–13913
Eigen M (2013) From strange simplicity to complex amiliarity. Oxford University Press, Oxford
Fischer W, Ganusov VV, Giorgi EE et al (2010) Transmission of single HIV-1 genomes and dynamics of early immune escape revealed by ultra-deep sequencing. PLoS ONE 5:e12303
Gerold G, Pietschmann T (2014) The HCV life cycle: in vitro tissue culture systems and therapeutic targets. Dig Dis 32:525–537
González-López C, Arias A, Pariente N et al (2004) Preextinction viral RNA can interfere with infectivity. J Virol 78:3319–3324
González-López C, Gómez-Mariano G, Escarmís C et al (2005) Invariant aphthovirus consensus nucleotide sequence in the transition to error catastrophe. Inf Genet Evol 5:366–374
Graci JD, Cameron CE (2008) Therapeutically targeting RNA viruses via lethal mutagenesis. Future Virol 3:553–566
Grande-Pérez A, Gómez-Mariano G, Lowenstein PR et al (2005a) Mutagenesis-induced, large fitness variations with an invariant arenavirus consensus genomic nucleotide sequence. J Virol 79:10451–10459
Grande-Pérez A, Lazaro E, Lowenstein P et al (2005b) Suppression of viral infectivity through lethal defection. Proc Natl Acad Sci USA 102:4448–4452
Grande-Perez, A, Martin V, Moreno H, de la torre JC (2016) Arenavirus quasispecies and their biological implications. Current Topics in Microbiol and immunol. doi:10.1007/82_2015_468
Holland JJ, Spindler K, Horodyski F et al (1982) Rapid evolution of RNA genomes. Science 215:1577–1585
Holland JJ, Domingo E, de la Torre JC et al (1990) Mutation frequencies at defined single codon sites in vesicular stomatitis virus and poliovirus can be increased only slightly by chemical mutagenesis. J Virol 64:3960–3962
Iranzo J, Perales C, Domingo E et al (2011) Tempo and mode of inhibitor-mutagen antiviral therapies: a multidisciplinary approach. Proc Natl Acad Sci USA 108:16008–16013
Li YP, Ramirez S, Mikkelsen L et al (2015) Efficient infectious cell culture systems of the hepatitis C virus (HCV) prototype strains HCV-1 and H77. J Virol 89:811–823
Lindenbach BD, Evans MJ, Syder AJ et al (2005) Complete replication of hepatitis C virus in cell culture. Science 309:623–626
Loeb LA, Essigmann JM, Kazazi F et al (1999) Lethal mutagenesis of HIV with mutagenic nucleoside analogs. Proc Natl Acad Sci USA 96:1492–1497
Lucas-Hourani M, Dauzonne D, Jorda P et al (2013) Inhibition of pyrimidine biosynthesis pathway suppresses viral growth through innate immunity. PLoS Pathog 9:e1003678
Moreno H, Grande-Perez A, Domingo E et al (2012) Arenaviruses and lethal mutagenesis. Prospects for new ribavirin-based interventions. Viruses 4:2786–2805
Mullins JI, Heath L, Hughes JP et al (2011) Mutation of HIV-1 genomes in a clinical population treated with the mutagenic nucleoside KP1461. PLoS ONE 6:e15135
Nájera I, Holguín A, Quiñones-Mateu ME et al (1995) Pol gene quasispecies of human immunodeficiency virus: mutations associated with drug resistance in virus from patients undergoing no drug therapy. J Virol 69:23–31
Nijhuis M, van Maarseveen NM, Boucher CA (2009) Antiviral resistance and impact on viral replication capacity: evolution of viruses under antiviral pressure occurs in three phases. Handb Exp Pharmacol 299–320
Oestereich L, Ludtke A, Wurr S et al (2014) Successful treatment of advanced Ebola virus infection with T-705 (favipiravir) in a small animal model. Antiviral Res 105:17–21
Orgel LE (1963) The maintenance of the accuracy of protein synthesis and its relevance to ageing. Proc Natl Acad Sci USA 49:517–521
Orgel LE (1973) Ageing of clones of mammalian cells. Nature 243:441–445
Ortega-Prieto AM, Sheldon J, Grande-Perez A et al (2013) Extinction of hepatitis C virus by ribavirin in hepatoma cells involves lethal mutagenesis. PLoS ONE 8:e71039

Ortiz-Riano E, Ngo N, Devito S et al (2014) Inhibition of arenavirus by A3, a pyrimidine biosynthesis inhibitor. J Virol 88:878–889
Padmanabhan P, Dixit NM (2016) Models of viral population dynamics. Curr Top Microbiol Immunol. doi:10.1007/82_2015_458
Pariente N, Sierra S, Lowenstein PR et al (2001) Efficient virus extinction by combinations of a mutagen and antiviral inhibitors. J Virol 75:9723–9730
Pariente N, Airaksinen A, Domingo E (2003) Mutagenesis versus inhibition in the efficiency of extinction of foot-and-mouth disease virus. J Virol 77:7131–7138
Perales C, Mateo R, Mateu MG et al (2007) Insights into RNA virus mutant spectrum and lethal mutagenesis events: replicative interference and complementation by multiple point mutants. J Mol Biol 369:985–1000
Perales C, Agudo R, Tejero H et al (2009) Potential benefits of sequential inhibitor-mutagen treatments of RNA virus infections. PLoS Pathog 5:e1000658
Perales C, Agudo R, Manrubia SC et al (2011a) Influence of mutagenesis and viral load on the sustained low-level replication of an RNA virus. J Mol Biol 407:60–78
Perales C, Henry M, Domingo E et al (2011b) Lethal mutagenesis of foot-and-mouth disease virus involves shifts in sequence space. J Virol 85:12227–12240
Perales C, Iranzo J, Manrubia SC et al (2012) The impact of quasispecies dynamics on the use of therapeutics. Trends Microbiol 20:595–603
Perales C, Beach NM, Gallego I et al (2013) Response of hepatitis C virus to long-term passage in the presence of alpha interferon: multiple mutations and a common phenotype. J Virol 87:7593–7607
Perales C, Beach NM, Sheldon J et al (2014) Molecular basis of interferon resistance in hepatitis C virus. Curr Opin Virol 8C:38–44
Perales C, Iranzo J, Sheldon J et al (2015) Impact of fitness and inhibition in the response of hepatitis C to lethal mutagenesis (Manuscript in preparation)
Richman DD (1996) Antiviral drug resistance. Wiley, New York
Ruiz-Jarabo CM, Ly C, Domingo E et al (2003) Lethal mutagenesis of the prototypic arenavirus lymphocytic choriomeningitis virus (LCMV). Virology 308:37–47
Schuster P (2016) Quasispecies on fitness landscapes. Curr Top Microbiol Immunol. doi:10.1007/82_2015_469
Sheldon J, Beach NM, Moreno E et al (2014) Increased replicative fitness can lead to decreased drug sensitivity of hepatitis C virus. J Virol 88:12098–12111
Sierra S, Dávila M, Lowenstein PR et al (2000) Response of foot-and-mouth disease virus to increased mutagenesis. Influence of viral load and fitness in loss of infectivity. J Virol 74:8316–8323
Smither SJ, Eastaugh LS, Steward JA et al (2014) Post-exposure efficacy of oral T-705 (Favipiravir) against inhalational Ebola virus infection in a mouse model. Antiviral Res 104:153–155
Steinmeyer SH, Wilke CO (2009) Lethal mutagenesis in a structured environment. J Theor Biol 261:67–73
Tapia N, Fernandez G, Parera M et al (2005) Combination of a mutagenic agent with a reverse transcriptase inhibitor results in systematic inhibition of HIV-1 infection. Virology 338:1–8
Tejero H, Montero F, Nuño JC (2016) Theories of lethal mutagenesis: from error catastrophe to lethal defection. Curr top Microbiol immunol. doi:10.1007/82_2015_463
Tsibris AM, Korber B, Arnaout R et al (2009) Quantitative deep sequencing reveals dynamic HIV-1 escape and large population shifts during CCR5 antagonist therapy in vivo. PLoS ONE 4:e5683
Wakita T, Pietschmann T, Kato T et al (2005) Production of infectious hepatitis C virus in tissue culture from a cloned viral genome. Nat Med 11:791–796
Zhong J, Gastaminza P, Cheng G et al (2005) Robust hepatitis C virus infection in vitro. Proc Natl Acad Sci U S A 102:9294–9299

Author Index

A
Aaskov J, 220, 227
Abraham J, 247
Abram ME, 282
Acevedo A, 49, 192, 194, 198, 210
Adiwijaya BS, 293
Aebischer T, 243
Agudo R, 205–206, 256, 306, 333
Aguirre J, 203
Ahmed R, 234, 250–251, 253, 260
Aita T, 48–49
Albarino CG, 239–241, 244, 248
Alexander HK, 282
Alizon S, 289
Altenberg L, 68
Althaus CL, 285
Alves D, 14, 122
Ancliff M, 135, 137
Anderson JP, 328
Anderson PW, 73
Andino R, 48–49, 220
Andrei G, 255
Appleby TC, 309
Arbiza J, 220
Archer AM, 241, 244–245, 249
Arias A, 14, 205–206, 311, 317, 330, 334
Armstrong KL, 208
Arnold JJ, 5, 305, 307, 309–312
Arora P, 285
Arribas M, 205–206
Arslan E, 82
Ashkenasy G, 149
Asquith B, 289
Astrovskaya I, 189
Athavale SS, 49, 52, 75
Austin DJ, 286
Avetisyan Zh, 137

B
Baake E, 70, 76–77, 110, 122, 124, 126–128, 137
Babajide A, 49
Baccam P, 294–295
Backofen R, 53
Baglole DJ, 233
Bagnoli F, 136–137
Bakhanashvili M, 304
Balagam R, 284, 289
Ballana E, 290
Baranovich T, 334
Baranowski E, 251, 253
Barber DL, 234
Barouch DH, 290
Barrera Oro JG, 233, 258
Barria MA, 17
Bartel DP, 52
Bass BL, 246
Bateman DA, 17
Batorsky R, 284
Batschelet E, 11
Beauchemin CA, 294–295
Beaucourt S, 250, 305
Beerenwinkel N, 68, 183–184, 210
Bergthaler A, 251
Bernacki JP, 17
Bernard LC, 304
Bernhart SH, 53
Betancourt AJ, 66
Beyer WR, 235
Bezzi M, 136–137
Biebricher CK, 4–5, 11, 13, 18, 46, 67, 70, 163, 169, 204
Billeter MA, 11, 246
Binder M, 293
Blasdell KR, 249

Current Topics in Microbiology and Immunology (2016) 392: 341–357
DOI 10.1007/978-3-319-23898-2

Blows MV, 64
Bocharov G, 284
Bodewes R, 241–242, 245
Boerlijst MC, 284
Bolken TC, 255
Bollback JP, 66
Bonhoeffer S, 208, 282–283, 285, 290
Bonnac LF, 255
Bonnaz D, 164
Borden KL, 237
Borenstein E, 211
Bornberg-Bauer E, 49
Borrow P, 251
Botten J, 259
Boulay F, 227
Bowen MD, 241, 247, 249, 258–259
Bratus AS, 77
Bray M, 233
Bressanelli S, 309
Bretscher MT, 284–285
Brown AJ, 284
Brown RJ, 250
Brumer Y, 142–143, 145
Brunotte L, 237, 239
Buchmeier MJ, 232, 234–236
Buckheit RW Jr, 208
Buesa-Gomez J, 251–252
Bull JJ, 163–169, 205, 208
Burch CL, 208
Bürger R, 76
Buss LW, 51, 55
Butcher SJ, 309

C
Cabot B, 250
Cajimat MN, 242, 244
Cale EM, 324
Cameron CE, 5, 163, 256, 306, 309–312, 328
Campbell Dwyer EJ, 237
Campbell KP, 249
Candurra NA, 255
Cann AJ, 315
Cao W, 251
Carr J, 13
Carrasco P, 207
Carrion R Jr, 259
Carvajal-Rodriguez A, 285
Casals J, 258
Cascales E, 147
Cases-González C, 205
Castilla J, 17
Castro C, 5, 163, 309, 311–312
Cattaneo R, 238, 246
Cen S, 289
Chaitin GJ, 34
Chan HS, 49
Chang DB, 294
Chao L, 202, 208
Charleston MA, 247
Charlesworth B, 70, 110
Charrel RN, 241, 244–245, 249
Chatterjee A, 291
Chen C, 309
Chen IA, 148
Chen M, 240
Chen P, 166, 168
Cheng-Mayer C, 250
Cheung PPH, 306, 314, 317
Childs JE, 247
Choe H, 247–248
Choi KH, 309
Chou H-H, 68
Christiansen FB, 285
Chun TW, 284
Ciota AT, 220–221
Ciurea A, 243
Clark AG, 284
Clavel F, 281
Codoñer FM, 174, 211
Coffey LL, 205, 208, 306, 312, 314, 317
Coffin JM, 284
Combe M, 308
Coombs D, 295
Cordo SM, 255
Cornu TI, 237, 239, 242
Coto CE, 233, 255
Coulibaly-N'Golo D, 247
Covacci A, 195
Covert AW, 208
Cowperthwaite MC, 164
Crick FHC, 75
Crotty S, 205, 329
Crow JF, 2, 76, 122
Cuesta JA, 203
Cupples CG, 329

D
Dadon Z, 148
Dahari H, 291, 293
Dahlberg JE, 223, 227
Dalldorf G, 248
Damonte EB, 233, 244, 255
Dapp MJ, 205, 253, 288–289, 304, 312, 328
Das SR, 208
De Boer RJ, 289–290
De Clercq E, 255, 334
de la Torre JC, 171, 237, 239, 242–243, 249
de Lamballerie X, 241, 249

de Visser JAGM, 211
Deeks SG, 281, 290
Deem MW, 122, 138
Deforges S, 250
Deisboeck TS, 16, 175
Delgado S, 244
Demetrius L, 83
Demogines A, 247–248
Denison MR, 254
Derrida B, 10
Di Giallonardo F, 186
Dimitrov RA, 53
Dixit NM, 284–286, 289, 291, 293, 324, 326
Djavani M, 237
Dobzhansky T, 25
Domingo E, 11–12, 14–16, 163, 171, 195, 205–206, 220, 243, 249–250, 257, 316, 324–329, 332, 335–336
Domingo-Calap P, 207
Downs WG, 247
Doyon L, 286
Drake JW, 11, 76, 206, 243, 249, 304, 329
Drossel B, 122, 136
Duchêne S, 76
Duffy S, 220

E
Eckerle LD, 308–309, 312, 317
Edwards SF, 73
Eigen M, 2, 4, 6, 10–11, 13–14, 26, 28, 30–31, 38–40, 45–46, 53–54, 76–77, 86–87, 90–92, 122–123, 162–163, 169, 204–205, 220, 252, 257, 283, 288, 316, 329
Ejima T, 289
Elemans M, 289
Elena SF, 66, 173, 208
Ellenberg P, 242–245
Ellington AD, 47
Emery VC, 291
Emmerich P, 259
Emonet SF, 239–240, 247, 249
Enns RH, 6
Enria DA, 233, 258
Erdös P, 110
Erlich HA, 47
Escarmís C, 204
Esté J, 290
Evans CF, 251, 253

F
Fahy E, 47
Falugi P, 195
Falzarano D, 233, 258
Feldman MW, 173
Feldmann H, 233, 258
Fellay J, 290
Ferré-D'Amaré AR, 48, 75
Ferrer-Orta C, 309–311
Ferretti AC, 54
Fichet-Calvet E, 233
Fischer W, 324
Fisher RA, 62
Flamm C, 45
Flanagan ML, 247–248
Flanegan JB, 11
Flatz L, 239
Flavell RA, 11
Flury F, 304
Fontana W, 51, 55, 73, 75
Fontanari JF, 14, 122, 126, 149–150
Forst CV, 49
Fox EJ, 16
Franz S, 122
Fraser C, 285, 290
Freedman DO, 233
Frey E, 148, 163
Frieden BR, 16, 18
Froissart R, 172
Fulhorst CF, 244, 249, 258
Fullerton SWB, 309
Furió V, 312

G
Gabriel W, 77, 122
Gadhamsetty S, 284, 290
Gago S, 8, 14, 76, 206
Galluccio S, 77
Galstyan V, 122, 138
Galtier N, 209
Gandhi N, 156
Gandon S, 167–168
Gansterer WN, 98
Ganusov VV, 289
Gao H, 173
Garcia JB, 249, 258
García-Arriaza J, 202
Gardiner WC Jr, 4
Gatenby RA, 16–18
Gavrilets S, 64
Geisbert TW, 233
Geleziunas R, 242
Gerland U, 136–137
Gerold G, 326
Ghaemmaghami S, 17
Ghany MG, 291, 293
Gheorghiu-Svirschevski S, 284
Giarré L, 195
Gilbert W, 49

Gillespie DT, 82–84, 168
Gillin FD, 304
Gilmore JB, 286
Gladkih I, 47
Glémin S, 209
Gnädig NF, 307–308, 312, 314
Gohara DW, 310–11
Gold L, 47
Gong P, 307, 309, 311
Gonzalez-Lopez C, 171–172, 249, 253, 330, 334
Good BH, 210
Gorodetsky P, 146
Gorodkin J, 49–50
Graci JD, 174, 206, 253, 255–256, 315, 328
Graham RL, 312, 314–315
Grande-Pérez A, 171–172, 203, 205–206, 243, 246, 249, 253–254, 257, 329–330, 332, 334
Greene WC, 283, 288
Greenwood AG, 248
Gross MD, 304
Gruener W, 51
Gruez A, 309
Grüner W, 110
Guedj J, 293

H

Hall JD, 304
Hall JS, 250
Hamming RW, 64
Hance AJ, 281
Hancioglu B, 294
Hansen JL, 309
Happel R, 45
Harki DA, 255
Harris KS, 253, 255, 288–289
Harris RS, 206
Harrison DN, 308
Hartl DL, 284
Hashiguchi T, 221–222
Hass M, 239
Hastie KM, 237
Hayashi Y, 48
Haydon DT, 250
He X, 309
Heim MH, 291–292
Heldt FS, 295
Hermisson J, 122–123, 125, 163
Herrmann E, 195
Herz AV, 286
Hetzel U, 241–242, 245
Hicks C, 255
Hietpas RT, 48
Higgs PG, 122, 128
Hinkley T, 184
Ho DD, 279
Ho SYW, 76
Hoetelmans RM, 283
Hofacker IL, 73
Hofbauer J, 54
Hogeweg P, 14, 163–164, 205
Holder BP, 295
Holland JJ, 11–12, 163, 171, 205–206, 220, 243, 249, 252, 304, 328–329, 336
Holmes EC, 207
Holtz CM, 206
Hopfield JJ, 312
Hordijk W, 55
Horga MA, 242
Hosaka Y, 223, 227
Hotchin J, 250
Howard CR, 235
Hu C-K, 14, 77, 122, 125–127, 135, 137–138, 205, 288
Huang IC, 242
Huggins JW, 233
Hugot JP, 247
Hull R, 202
Hundley HA, 246
Huynen MA, 10, 52, 211
Hwa T, 136–137

I

Iranzo J, 171–172, 174, 203, 205–206, 335
Irwin NR, 247
Isaacson M, 233
Ishii A, 242
Itan E, 146–147

J

Jabara CB, 187
Jackson AP, 247
Jahrling PB, 233, 258
Jain K, 64
Janet A, 62
Jay MT, 249
Jefferson T, 294
Jelcic I, 250
Jilek BL, 288
Jimenez JI, 48–49
Jiménez JI, 75
Johnson VA, 281
Jones BL, 6, 77
Josefsson L, 284
Joyce GF, 54
Jridi C, 250
Julias JG, 206
Jung A, 284

Jyssum K, 304

K
Kama A, 146
Kaneko K, 126, 137
Kang Y-G, 77
Kapheim KM, 220–221
Katz JM, 238
Kauffman SA, 55, 68, 69
Kawaoka Y, 238
Ke R, 227
Kessler D, 146
Keulen W, 304
Kiedrowski G, 47
Kilgore PE, 233
Kimura M, 2, 32, 52, 76, 110, 122, 166, 209
King AMQ, 242
Kingman JFC, 69
Kirakosyan Z, 122–123, 125, 134
Kirkegaard K, 205–206, 250, 256, 305, 312–313
Kirkpatrick S, 73
Klavinskis LS, 251
Kleiman M, 149, 153
Knöppel A, 147
Koch AJ, 164
Koelle K, 211
Koonin EV, 311
Korneeva VS, 306
Kosmrlj A, 290
Kouyos RD, 2, 19, 49, 67–68, 208, 210–211, 284–285
Krall P, 163
Kramer FR, 27, 30, 46
Kranzusch PJ, 237, 242
Krug J, 64
Kunz S, 236–237, 251
Küppers B-O, 24–26, 28, 30–31, 33–36, 40
Kwang J, 305, 314

L
Lalić J, 208, 209
Lamb RA, 221, 223
Lan S, 239–240
Lanfear R, 76
Laurenzi IJ, 82
Lauring AS, 48–49, 211, 220, 315
Lázaro E, 204, 206, 208
LeClerc JE, 304
Lecompte E, 247
Lee AM, 256
Lee B, 149, 151
Lee CH, 205, 252
Lee DH, 46
Lee KJ, 239
Leitner T, 284
Lelke M, 239
Lenz O, 235
Lesburg CA, 309
Leuthausser I, 76, 122
Levi LI, 305, 307, 312, 316
Levin S, 68
Levine H, 146
Levine HA, 48
Levy DN, 284
Lewicki H, 243
Li J, 17
Li T, 47
Li YP, 326
Liang Y, 240
Lifson S, 88
Lincoln TA, 54
Lindenbach BD, 326
Lipsitch M, 146
Little SJ, 279
Litwin S, 163, 288
Liu X, 307–308, 311–312, 314–315
Lobkovsky AE, 49
Loeb LA, 16, 163, 205, 252, 288–289, 328–329
Lopez N, 239
Lorenz R, 49–51, 73
Lou DI, 187, 192
Loureiro ME, 242
Lourenço J, 209
Love RA, 309
Lu G, 309
Lucas-Hourani M, 336
Luce R, 46
Lukashevich IS, 233, 244–245, 250
Luo J, 16
Luque D, 227
Luthra R, 47

M
Magnus C, 289
Mahal SP, 17
Maldarelli F, 281
Malet H, 309
Malim MH, 289
Mallela A, 246
Manrubia SC, 171–172, 203–206, 253
Mansky LM, 206, 282, 304
Marcotte LL, 310
Marin A, 19
Markowitz M, 281
Martin G, 167–168
Martín V, 174, 246, 249–250, 254

Martínez JP, 208
Martinez-Sobrido L, 237, 240
Martin-Hernandez AM, 306
Maruyama T, 166, 209
Mas A, 15, 249
Mathews DH, 49
Matloubian M, 250–251
May R, 167, 279
Maynard Smith J, 211
McBride JL, 6, 77, 122, 126
McCaskill J, 6
McCormick JB, 233
McCoy JW, 62
McGhee GR Jr, 64
McGinnes LW, 242
McKee KT Jr, 233
McLean AR, 289
McMinn PC, 314
Medeiros LJ, 47
Melikyan A, 130
Meng T, 305, 314
Merkler D, 240
Messer PW, 190–191
Mets MB, 233
Meyer BJ, 236
Miao H, 294
Miller JH, 329
Mills DR, 10, 16, 26–27, 30, 37, 67
Mills JN, 244
Minoche AE, 186
Mohanty U, 286
Mohri H, 291
Mollison D, 79
Monath TP, 258
Moreno E, 203
Moreno H, 173, 205, 242–245, 249, 253–258, 335
Morens DM, 294
Morimoto K, 250
Morin B, 236, 239
Morrison TG, 242
Moshkoff DA, 245
Mostowy R, 289
Moya A, 208
Mühlebach MD, 221
Muller G, 235
Muller HJ, 204
Mullins JI, 288–289, 328
Mullis KB, 46
Murillo LN, 291
Murphy DG, 246
Murphy RM, 17
Musso F, 193
Muzyczka N, 304

N
Nájera I, 325
Nakashima M, 221
Nåsell I, 80
Nathans R, 289
Nee S, 202
Neher RA, 190–191, 284
Neuman BW, 238
Neumann AU, 291
Neumann G, 238
Neves AGM, 135
Ng K, 309
Nicolaou KC, 47
Nicolson GL, 16
Niederbrucker G, 98
Nijhuis M, 257, 284, 324
Nilsen-Hamilton M, 48
Nilsson M, 146
Nishikura K, 245–246
Nonacs P, 220–221
Nossal NG, 304
Novella IS, 173, 249
Nowak MA, 14, 16, 87, 148, 167, 279, 285–286, 289, 291
Nowell P, 16
Noyce RS, 221
Nunberg JH, 237
Núñez JI, 208

O
O'Dea EB, 174
O'Farrell D, 309
Obermayer B, 148, 163
Ochoa G, 14
Oelschlegel AM, 17
Oestereich L, 334
Ojosnegros S, 15, 17, 203, 206
Oldstone MB, 234, 248–251, 253
Orgel LE, 328, 330
Orr HA, 209
Ortega-Prieto AM, 253, 333–334
Ortiz-Riano E, 336
Otwinowski J, 48

P
Padmanabhan P, 292–293, 324, 326
Palacios G, 233, 245
Palmer ME, 146
Palmer S, 281
Pan J, 309
Pariente N, 205, 257, 335
Park JM, 14, 135, 137
Park J-M, 77, 122, 138
Parks GD, 221, 223

Pasqual G, 236
Pathak VK, 206
Paul N, 54
Pawelek KA, 294
Pawlotsky JM, 293
Peersen OB, 307, 309, 311
Peliti L, 10, 122–124
Peng W, 136–137
Pennings PS, 284–285
Perales C, 172, 174, 205–206, 220, 249, 253, 257, 324, 326, 330–331, 333–336
Perelson AS, 279, 281, 286, 289–291
Perez M, 235, 237–239
Peters CJ, 233, 247–248, 258
Pfau CJ, 250
Pfeiffer JK, 205–206, 250, 256, 305, 312–313
Phillips AN, 279
Phillips PC, 207
Pietschmann T, 326
Pillai S, 174
Pinschewer DD, 235–237, 239–240
Pircher H, 243
Pita JS, 206
Pitt JN, 48, 75
Plattet P, 221
Plemper RK, 221
Plöger TA, 47
Plotkin JB, 48
Poch O, 237
Poelwijk FJ, 210–211
Polson AG, 246
Prabhakaran S, 188
Prince GA, 250
Prosperi MC, 189
Provine WB, 62
Pulkkinen AJ, 250

Q
Qi X, 237

R
Rabi SA, 287
Radford AD, 210
Radoshitzky SR, 247
Rager M, 223, 227
Ramratnam B, 281
Rangnekar SS, 6
Rappuoli R, 195
Rasmussen S, 47
Raz Y, 147–148
Reetz MT, 48
Regoes RR, 289
Reha-Krantz LJ, 304
Reidys C, 51, 64, 110
Reifman J, 48–49, 211
Remold SK, 208
Rényi A, 110
Ribeiro RM, 279, 283–285, 289, 291, 293
Richman DD, 324
Richmond JK, 233
Rico-Hesse R, 241, 244–245, 249
Rima BK, 246
Riviere Y, 244–245, 249, 251
Robertson MP, 54
Rodrigo AG, 284
Rodrigo WW, 240
Rogers DJ, 233
Rojek JM, 236, 240
Rokyta DR, 208
Romero PA, 48
Rong L, 293
Rosenbloom DI, 286, 288
Rouzine IM, 137, 284
Rowe W, 48–49
Rozen-Gagnon K, 307–308, 314, 317
Rueda P, 246
Ruiz-Jarabo CM, 243, 254, 256, 334
Ruppin E, 211
Ruse M, 62
Ruzzo WL, 49–50

S
Saakian DB, 14, 77, 122–123, 125–126, 128–129, 133–138, 205, 288
Sabeti PC, 236
Sadeghipour S, 305, 314
Saenz RA, 294
Salazar-Bravo J, 247–248
Salemi M, 189
Salgado PS, 309
Salvato MS, 241, 248–251
Sampah ME, 287
Sanchez AB, 239
Sanchez S, 248
Sánchez-Navarro JA, 203
Sanchis J, 48
Sanjuán R, 11, 66, 183, 206–208, 211, 250, 308
Sanz-Ramos M, 254
Sardanyés J, 164, 166, 173–174
Sato K, 126, 137
Saunders AA, 237
Schaaper RM, 304
Scheidel LM, 256
Schlub TE, 282, 284
Schmidt LD, 78
Schrödinger E, 36
Schultes EA, 52

Schuster P, 2, 6, 9–10, 14, 19, 26, 38–40, 45, 51, 53–54, 68–69, 71, 73, 83, 86–88, 90–92, 94, 102, 109–111, 122–123, 163, 169, 288, 324–328, 336
Schwarz G, 89
Sedaghat AR, 286
Segel LA, 47
Seifert D, 195
Seneta E, 77, 86
Seo TK, 284
Seronello S, 206
Severson WE, 205
Sevilla N, 243, 249, 251
Shakhnovich EI, 141–145, 166–168, 173
Sheldon J, 326–327
Shen L, 287
Sherrington D, 73
Sheward DJ, 187
Shimomaye EM, 251
Shirogane Y, 172, 220, 223–226
Sicard A, 203
Sidwell RW, 256
Siegel EC, 304
Sierra M, 174, 306
Sierra S, 205, 257, 329
Sigmund K, 54, 83
Sikora E, 250
Siliciano RF, 283, 288
Simek MD, 290
Simon EH, 223, 227
Skipper RA Jr, 62
Slemrod M, 47
Smith AM, 289
Smith EC, 254, 256
Smith HC, 291, 294
Smith JI, 55
Smith MA, 52
Smith RJ, 286
Smither SJ, 334
Sniegowski PD, 304, 308
Snoad N, 146
Sobrino F, 12
Sogoba N, 233
Solé RV, 15–16, 175
Southern PJ, 236
Spiegelman S, 27, 30, 67
Spiess EB, 12
Stadler BMR, 54–55, 148
Stadler PF, 45, 54–55, 69, 110, 148
Stafford MA, 279, 282
Steinhauer DA, 11, 195
Steinmeyer SH, 173, 334
Steitz TA, 309
Stenglein MD, 241, 245
Stephan-Otto Attolini C, 55
Stephenson KE, 290
Stiegler P, 49–50
Strecker T, 235, 237–238
Streeter DG, 256
Strogatz SH, 80
Suárez P, 306, 317
Subbarao K, 238
Sullivan BM, 251
Summers J, 163, 288
Sumper M, 37
Suryavanshi GW, 284–285
Swetina J, 87–88, 90, 102, 111, 122–123
Szathmáry E, 47
Szendro IG, 210
Szostak JW, 47

T
Taddei F, 304
Takeuchi N, 14, 163–164, 205
Tamura K, 242
Tannenbaum E, 141–143, 145–147, 149–157
Tao Y, 309
Tapia N, 257, 335
Tarazona P, 77, 89, 122
Tatsuo H, 221
Taubenberger JK, 294
Tebas P, 288
Tejero H, 92, 163, 164, 169, 173, 329, 333
Temin HM, 282
Teng MN, 252
Thangavelu PU, 289
Thomas E, 291
Thompson AA, 309
Thompson CJ, 6, 77, 122, 126
Tishon A, 251, 253
Töpfer A, 189
Torarinsson E, 52
Tortorici MA, 236
Toulouse G, 73
Tripathi K, 289
Trivedi P, 250
Tsetsarkin KA, 208
Tsibris AM, 324
Tsimring LS, 136–137
Tuerk C, 47
Turner DH, 49
Turner PE, 208

U
Urata S, 237–238, 240

V
Vaidya NK, 291
Valsamakis A, 251
van Kampen NG, 82
Van Slyke GA, 306, 308, 314, 317
Vanni I, 17
Varga S, 47
Vasilakis N, 205
Vazquez-Calvo A, 255
Vignuzzi M, 205, 208, 220–221, 250, 305, 313, 315
Vijay NN, 284, 289
Villarreal LP, 220
Vives-Adrian L, 309
Volberding PA, 281
Volkenstein MV, 38
Volpon L, 237
von Kiedrowski G, 46, 148
von Messling V, 238

W
Wachsman MB, 255
Wagner A, 211
Wagner GP, 163
Wagner H, 70, 76–77, 110, 122, 127–128, 136–137
Wagner N, 148, 149, 155
Wahl LM, 286
Wainberg MA, 304
Wakita T, 326
Walker BD, 290
Walsh B, 64
Wang C, 185
Ward CD, 11
Ward SV, 246
Watson JD, 75
Weaver SC, 208, 244, 248–249, 258
Wei X, 279
Weinberger ED, 68
Weinreich DM, 68
Weiss JN, 287
Weissmann C, 10, 17, 18
Whelan SP, 237, 242
Wickner RB, 17
Wiehe T, 70, 94
Wilke CO, 13–14, 102, 143, 163–164, 173, 183, 288–289, 334
Wills PR, 47
Withlock MC, 210
Witzany G, 220
Wolf JB, 184
Woo HJ, 48–49, 211
Woodall J, 233
Woodcock H, 122, 128
Wright CF, 250
Wright S, 62–63, 183, 209
Wu B, 167
Wu H, 286
Wu-Hsieh B, 251, 253
Wylie CS, 166–167, 173

X
Xie X, 307, 314, 317

Y
Yang X, 311–312
Yap TL, 309
Yates A, 289
York J, 237
Young CS, 294
Young KC, 256–257
Young PR, 235

Z
Zagordi O, 186, 188, 210
Zahn RC, 245–246
Zapata JC, 241, 248–249
Zeng J, 305–306, 312, 314
Zhang J, 291, 326
Zimm BH, 89
Zinkernagel RM, 234
Zuker M, 49–50, 53, 73

Subject Index

A
Adaptation, 202, 205
Adaptive MCMC, 197
Adaptive peaks, 210
ADAR1-L, 246
Aenome, mutation rates, 76
Alfalfa mosaic virus, 203
Algorithm, Gillespie, 84
Alpha-dystroglycan (αDG), 236
Ambisense coding strategy, 234
Analogue, 328
  mutagenic, 328
Animate, 156
Antagonistic pleiotropy, 208
Antibiotic drug resistance, 141, 142, 147
Antibiotic resistance, 147
Antiviral activity, broad-spectrum, 336, 337
Antiviral agents, 18
Antiviral designs, mutagenesis-based, 333
Antiviral inhibitors, 324
Antiviral interventions, 19
Antiviral therapies, 205
Antiviral treatments, 336
Argentine HF (AHF), 233
Artificial chemistry, 55
Asexual replication, 152
Asexual reproduction, 153
  unicellular organisms, 150
Associative learning, 142
Auasi-equilibrium, 13
Autocatalysis, 5, 78, 82
Autocatalytic chemical reaction, 44

B
Back mutation, 28
Bacteriophage, 205
Bacteriophage Φ6, 208
Bacteriophage Qβ, 10, 67
Baker's yeast, 152, 153
Base pair distance, 72
Bifurcation, transcritical, 80
Bimodality, bimodal, 82
Bipartite viruses, 202
Branching process, multi-type, 83
Broad-spectrum antiviral drug, 256
Budding, 237

C
Cancer, 141
Cancer cell, 15, 16, 18
  dynamics, 16
  mitosis, 18
  proliferation, 16
Candid1, 233
Catalytic networks, 142, 148
Cell-based minireplicon (MR), 236, 239
Center manifold, 13, 14
  reduction, 13
Changing environments, 205
Chemical mutagens, 156
Chikungunya virus, 208
Chromosomal instability, 141, 142
Chronic infections, 232
CIN, 147
CIN tumors, 145
Circadian rhythms, 155
Class mergence, complementary, 89, 96, 106, 109
Clonal evolution, 16
Coevolution hypothesis, 247
Cognition, 142
Combination therapy, 257, 335
Compensatory mutations, 204, 207, 208
Competition dynamics, 15
  among cells, 15
Complementation, 13, 249

Current Topics in Microbiology and Immunology (2016) 392: 341–357
DOI 10.1007/978-3-319-23898-2

Consensus, 335
sequence, 4, 113, 326
Conservative replication, 142, 144
Constant environments, 205
Constant organization, 45
Cooperative interactions, 206
Cooperative transition, 89
Cross-catalysis, 149
Crow-Kimura model, 2, 124
CTL escape mutants, 243

D
Darwinian evolution, 26–27, 44
Deep sequencing, 12, 14
Defective genome, 203
Defectors, 254, 335, 170–171
genomes, 330
Degree of independence (DI), 288
Deleterious mutations, 204
Dendritic cells (DCs), 251
Derepression, 142
Diploid organisms, 152
Diploids, 152
Direct acting antivirals (DAAs), 293
Discrete-Time Eigen Model, 124
Distribution of beneficial effects, 209
Division of labor, 142, 154, 155
DNA proofreading, 141
Drug pharmacokinetics, 286–288
Drug resistance, 282–286
during treatment, 285
mutation-selection balance, 283–284
preexistence of, 283–285
Drug resistant subpopulations, 282
Dynamic environments, 147
Dynamic landscape, 141, 148

E
Ebola hemorrhagic disease virus, 334
Effects of mutations, 207
Eigen model, 123
Eigenvalues, 78, 86
Eigenvector, 78, 86
Endocytosis, 235
Environment, 208
Environmental stress, 147
Epigenetic mechanisms, 18
Epistasis, 184, 207, 209, 210
epistatic interactions, 68
Error-prone replication, 249
Error cascade, 143
Error catastrophe, 16, 143, 162–165, 169–170, 254, 328
in cancer, 16
limits of, 163–165
Error rate, 7, 205, 206
critical, 92
uniform, 7, 84, 86
Error threshold, 8, 18, 76, 86, 89, 90, 93, 95, 98, 106, 110, 114, 149, 162–165, 204, 288, 328, 329
violation, 333
Evolution
adaptive, 67
experimental, 67
forces influence, 284
reactor, 26–27
Evolutionary innovations, 211
Evolutionary optimisation of information, 30–33
Evolutionary trajectories, 211
3′-5′ Exoribonucleases, 237
Extinction, 169–170, 203, 255, 329
mutagenesis-driven, 329
Extinction of the unfittest, 47

F
F-plasmid, 148
Faba bean necrotic stunt virus, 203
Favipiravir, 334
Features, 156
Fidelity variants, 308
high-fidelity variants, 305
low-fidelity variants, 306
in vitro, 311
in vivo, 312
Fitness, 2–4, 7, 79, 208, 325–327
cost, 325, 326
drug-resistant determinant, 327
effects of mutations, 208
factor, 147
highest, 2
increase, 327
landscape, 2
mean, 2, 4
optimization, 3, 4
recovery, 326
replicative, 327
viral, 333
Fitness landscape, 14, 19, 45, 86, 87, 183, 205, 209, 324
fully resolved, 66
HIV, 67
Nk, 75
rugged, 324
simple, 64, 65, 86, 98

single-peak, 89
tunable, 68
variable, 14
Flow rate, 79
Flow reactor, 78, 82, 84
Fluctuating environments, 146
Fluctuations, 204
Fluorouracil (FU), 329, 333, 334
Folding, free energy, 74, 75
Foot-and-mouth disease virus (FMDV), 204, 206, 208, 230
Fujiyama-like landscape, 209

G
Genetic diversity, 205
Genetic drift, random, 62
Genetic information, stability, 333
Genetic instability, 147
Genetic mismatch repair, 146
Genetic repair, 141, 146, 150
Genome segmentation, 203
Genome space, 211
Genotype-phenotype maps, 51, 70
Genotype, fittest, 85
Genotype space, 62
Global fitness maximum, 209
Graphs, random, 110
Growth hormone disease syndrome, 251

H
Hamilton-Jacobi equation, 128
Hamming distance, 4, 7, 10, 63, 64, 66, 71, 87, 93, 95, 104, 110, 111
Haploid, 151, 152
fusion, 153
Haplotype inference, 186
Hemorrhagic fever, 233
Hepatitis B virus (HBV), 326
Hepatitis C virus (HCV), 291–293, 326
Heterooligomer, 221–227
Highly mutating environments, 149
Horizontal gene transfer (HGT), 141, 147, 148
Host, 208
Host cell, 206
Host switching, 247
Human immunodeficiency virus (HIV), 149, 208, 278
quasispecies theory, 288–289
type 1, 326
Human transferrin receptor, 236
Hypermutated LCMV, 246

I
Immortal strand co-segregation, 145
Immune suppression, 234
Immunosuppressive variants, 250–251
Imperfect lesion repair, 143
Inclusion body disease (IBD), 245
Infectivity, specific, 329
Infinitely large population, 203
Inflow, 80, 83
Influenza A virus (IAV), 294
Influenza virus, 334
Information, 2
genetic, 2
Inhibitor escape mutants, 257
Inhibitor resistance, 325, 335
Instantaneous inhibitory potential (IIP), 287
Interference, 13, 172–173
Intersection theorem, 51
Intra-host viral variability, 250
Intraspecific competition, 203

J
Junin virus (JUNV), 233

K
Kinetics, 4
autocatalytic, 4

L
Labor, 153
Landscape
adaptive, 62
bacterial, 68
Nk, 68
realistic, 68, 98
simple, 89, 94
single-peak, 65, 66, 70, 84, 102
Lassa fever (LF), 233
Lassa virus (LASV), 233
Late (L) domain motifs, 238
Lethal defection, 170–173, 253, 330, 331, 334
complementation, 172–173
interference, 172–173
stochastic extinction model, 171–172
Lethal defective particles, 206
Lethality, 169–170
Lethal mutagenesis, 8, 161–176, 205, 206, 252, 316, 328, 329, 334
hypothesis, 205
theories. *See* Theories of lethal mutagenesis
Level crossing, 89, 96, 100, 102, 106, 109

Like-acetylglucosaminyltransferase (LARGE), 236
Live-attenuated Candid1 strain, 258
Living matter, 24–26
Lymphocytic choriomeningitis virus (LCMV), 233

M
Malthusian fitness, 167
Mappings, sequence, 71
Marginal fitness effects, 192
Master, 7
  superiority, 7
Master cluster, 114
Master equation, 80, 83
Master genotype, 64
Master sequence, 4, 8, 9, 18, 87, 90, 110, 202, 328
  superiority, 8, 333
Matrix
  adjacency, 114
  mutation, 86
  stochastic, 78
  value, 77, 86
Matrix (M) protein, 238
Measles virus
  F protein, 223
  membrane entry, 221–222
  membrane fusion, 221–222
  mixed genomes, 226
Metabolic pathways, 154
Metabolic replicators, 155
Metabolism, 142, 155
Micro-RNAs, 211
MIN, 147
MIN tumors, 145
Mismatch repair, 143
ML29, 233
Model, 209
  2D Ising, 76
  mutation, 76
  paramuse, 76, 77
  quasispecies, 76, 77
  selection-mutation, 76
Molecular clock, 76
Move set, 62, 65
Muller's ratchet, 150, 204
Multidrug resistance, 326, 327
Multiplicity of infection, 202
Multivesicular body (MVB), 236
Mutability, 29
Mutagen, 205
Mutagenic agent, 257
Mutagens and inhibitors
  interplay, 335
Mutant
  cloud, 6, 7
  distribution, stationary, 86
  mutagen-resistant, 335
Mutation-selection balance, 283–284
Mutation-selection-based models, 165–170
Mutants, 324
  inhibitor-escape, 324
Mutation, 2, 44
  rate, 2
Mutational backflow, 6–9, 86, 90
  zero, 90
  zero assumption, 6, 7, 9
Mutational flow, 93, 113
Mutation class, 64
Mutation flow, 108
Mutation matrix, 77, 87
Mutation mechanism, 76
Mutation rate, 4, 7, 8, 70, 85, 86, 206, 304, 332
  critical, 87
  single nucleotide, 7
Mutant spectra, 324, 335
  dynamic, 324
Mutant spectrum, 325, 327
  broadening, 327
Mutation-selection equilibrium, 212
Mutations, 141, 325, 326
  compensatory, 326
  mutations, 325
  resistance, 326
Mutator bacteria, 15
Mutators, 143

N
Natural fitness landscapes, 48
Nucleotide Excision Repair (NER), 146
Neutral drift, 13
Neutral evolution, 110
Neutral network, 51, 64, 110, 111, 211
Neutral paths, 52
Neutral selection models, 32
Neutral theory, 111
Neutrality, 67, 69, 70, 110, 114
  degree, 110
Next-generation sequencing (NGS), 182, 210, 324
Non-living matter, 24
Norovirus, 334
Nucleotide alphabet
  alphabet, 64

Nucleotide analogue, 11, 336
mutagenic, 11

O
Optimization, 79
Organ-specific LCMV variants, 250
Origin of life, 155
Oscillatory dynamics, 155
Outflow, 83

P
Panhandle structure, 239
Perfect lesion repair, 143
Phase transitions, 77
Phenomenological approach, 6, 8, 9, 86, 88, 91, 93
Phenotype, 49
Pituitary, 251
Plasmids, 141, 142
Point mutations, 64, 65
Poliovirus (PV), 328
Poliovirus polymerase, 5
Polymorphism, 12
genetic, 12
Polyploidy, 223
prebiotic matter, nucleation of, 23–41
Polysomic quasispecies model, 146
Population, 10
clonal, 10
Population bottlenecks, 204, 206
Potential surface, 62
Preextinction populations, 254
Prion, 17, 18
replicative fitness, 17
strains, 17
Product inhibition, 47, 54
Protein
multifunctional, 332
trans-acting, 333
trans-networks, 331
Punctuated-equilibrium, 52

Q
Qβ, 46
Qβ replicase, 10, 67
Qβ RNA, 10, 11
synthesis, 10
Quantum chain, Ising, 77
Quasi-equilibrium, 13, 14
theories, 13
Quasispecies, 13, 15, 18, 45, 70, 86, 87, 98, 202, 220, 252
definitions, 15
distribution, 29
dynamics, 83
equations, 142
limitations and strengths, 18
models, 204, 211
strong, 103, 106, 110
theory, 204, 288–289
transition, 100, 103, 106
as a unit of selection, 13
'Quasi-steady state' approximation, 47
Quorum sensing, 17
in bacteria, 17

R
Random landscape, 209
Random scatter, 69, 70, 100, 102, 106, 107, 109, 110
Random segregation, 143, 145
Random selection, 110
Rapid evolution, 249
RdRp structure, 308
Reassortment events, 241
Reciprocal sign epistasis, 207
Recombinant arenaviruses, 239
Recombination, 212, 244
Reductionistic research, 24
REM, 155
Repair catastrophe, 143
Repairers, 143
Replication, 2–4, 7, 44, 325
error-free, 2, 4, 7
error-prone, 325
kinetics, 3
Replication-mutation, 3–6, 8, 18, 19
kinetics, 5
mechanism, 6
Replicator, 53
equation, 54
Repressed state, 147
Repression, 142
Reptilian arenaviruses, 241
Resistance, 325
genotypic barrier, 325
phenotypic barrier to, 325
Reverse genetics, 10, 11, 238
Ribavirin, 206, 233, 329, 333
Ribonucleoprotein (RNP), 235
RNA evolution, 10
in vitro, 10
RNA folding, 49
RNA landscapes, 49
RNA ligase ribozyme, 54
RNA networks, 142
RNA polymerase, 4
RNA replicase ribozyme, 54

RNA retrovirus
human immunodeficiency, 67
RNA-RNA interaction, 53
RNA viruses, 11, 149, 211, 324, 336
as moving targets, 324
mutation rate, 11
RNA virus mutant spectra, 219–228
RNAcofold, 55
Robustness, 211
Rugged fitness landscapes, 210
Ruggedness, 67, 70, 100, 110, 114

S
Segregation, 145
Selective pathways, 324
transient, 324
Selective sweep, 190
Self-awareness, 157
Self-fertilization, 153
Self-replicating ribozyme, 54
Self-replication, 149
first-order replication, 149
second-order catalysis, 149
Self-reproduction, 28
Semantic code of evolution, 40–41
Semantic information, 23–41
context-dependence, 33–37
evolutionary optimisation, 30–33
information barriers, 37–40
living matter, 24–26
metabolism, 28
mutability, 29
natural selection of, 26–30
neutral selection models, 32
in prebiotic matter, 23–41
quasi-species distribution, 29
reaction kinetics, 28
self-reproduction, 28
semantic code of evolution, 40–41
Semiconservative replication, 141–144, 148
Set-point viral load (SPVL), 279, 290
Sequence, 335
Sequence space, 7, 10, 13–15, 62, 63, 72, 75, 110, 204, 325
connectivity, 13
drift in, 333
exploration, 15
movements, 14
occupation of, 333
size, 10
Sequential treatment, 335, 336
Sexual replication, 152
Sexual reproduction, 142, 149, 150, 153
Sexually reproducing organisms, 150
Shape space, 72
Signaling lymphocyte activation molecule (SLAM), 221, 223
Sign epistasis, 207
Single-fitness-peak approximation, 152
Single-fitness peak, 143
Site-directed mutagenesis, 11
Sleep, 155
SOS response, 146
Space of genotypes, 211
Spin glass, 77, 73
Spores, 151
Sporulation, 142, 151
State
quasistationary, 80, 82, 85
stationary, 79
Static environments, 147
Stem cells, 141
Stochastic extinction model, 171–172
Stochastic models, 18
group-specific, 18
Structure
distance, 71
minimum free energy, 73
secondary, 70, 73, 110
Sublethal mutagenesis, 174–175
Subpopulation, 13, 14
FMDV, 333
genome, 14
minority, 13
Superinfection inhibition, 242
Superiority, 90
Survival of the fittest, 47, 143
Survival of the flattest, 143, 164, 173–174
Susceptible cells, 203
Synergistic epistasis, antagonistic epistasis, 207
Systems, dynamical, 62
Systems chemistry, 148

T
Terminal complementarity, 235
Theorem
Perron-Frobenius, 86
Theoretical modeling, 141
steady-state solutions, 141
stochastic simulations, 141
Theories of lethal mutagenesis, 161–176. *See also* Lethal defection
defectors, 170
error catastrophe, 162–165, 169–170
error threshold, 162–165
extinction, 169–170
lethality, 169–170
mutation-selection-based models, 165–170

resistance problem, 173–174
sublethal mutagenesis, 174–175
Theories of viral evolution, 207
Tobacco etch virus (TEV), 207, 208
Transferring receptor 1, 247
Tri-segmented rLCMV, 240
Tumor cell, 16, 141
heterogeneity, 16
Two-strain model, 282
Type I interferon (IFN-I), 237

U
Uniform distribution, 69, 87, 95
stationary distribution, 85
Unit of selection, 14
'Universal' LASV vaccine, 259
Unspecific outflow, 45

V
Value matrix, 87
Vesicular stomatitis virus (VSV), 205, 207, 328
Viral disease, 324
control, 324
Viral ecology, 202
Viral evolution, 212
Viral extinction, 205, 328
Viral fitness landscapes, 210
Viral genomes, defective, 334
Viral load, 327
Viral persistence, 234
Viral population, 277–295
basic model, 279–282
drug pharmacokinetics, 286–288
hepatitis C virus, 291–293
and immune response, 289–290
influenza A virus (IAV), 294
quasispecies theory, 288–289
Viroids, 8, 211
Virus, migration, 334

W
Walk, adaptive, 62
Wild type subpopulations, 282
Winter Seminar, 12
Max Planck, 12
Wright-Fisher model, 13
mutation-selection, 13
Wrightian terms, 165–166